Gas Phase Chemical Physics Program

DOE Principal Investigators'
Abstracts

June 2 – 4, 2021

Chemical Sciences, Geosciences, and Biosciences Division
Office of Basic Energy Sciences
Office of Science
U.S. Department of Energy

The research grants and contracts described in this document are supported by the U.S. DOE Office of Science, Office of Basic Energy Sciences, Chemical Sciences, Geosciences and Biosciences Division.

Foreword

The Gas Phase Chemical Physics program has continued to evolve over the past year. This program, which has traditionally focused on combustion, has now expanded to focus on fundamental gas phase chemical physics research that explores chemical reactivity, kinetics and dynamics in the gas phase at the level of electrons, atoms, molecules and nanoparticles. This program evolution has resulted in the program being defined by the following five thrust areas: *Light-Matter Interactions*, *Chemical Reactivity, Gas-Particle Interconversions, Gas-Surface Chemical Physics, and Ultrafast Imaging/Spectroscopy.*

Despite the challenges posed by the pandemic over the past year, the Gas Phase Chemical Physics program continues to move forward thanks to your tireless efforts in submitting progress reports, submitting research highlights, and reviewing proposals. Your continued commitment to carrying out scientific research under these challenging conditions is very much appreciated. We also extend a special thanks to Teresa Crockett, Kerry Hochberger, and Gwen Johnson of BES Operations and Tammy Click and Paul Hudson of the Oak Ridge Institute for Science and Education (ORISE) for working behind-the-scenes to ensure smooth operation of the GPCP program. We look forward to gathering in-person in 2022 for our 41st annual meeting.

Jeff Krause
Wade Sisk

Table of Contents

Molecular Reactivity in Complex Systems

Musahid Ahmed (mahmed@lbl.gov), Daniel Neumark (dneumark@berkeley.edu), Kevin Wilson (krwilson@lbl.gov)

MS 6R 2100, Chemical Sciences Division, LBNL, Berkeley, CA-94720

Background and Significance

Our effort in molecular reactivity in complex systems targets complex multistep and multiphase chemical transformations built from isolated elementary bimolecular reactions to gas-surface reaction dynamics. The gas phase is central for controlling the multiphase chemistry with additional kinetic processes, playing a key role in governing the overall reactive outcome. Cross-cutting themes of *Chemistry at Complex Interfaces* and *Reaction Pathways in Diverse Environments* are explored, providing valuable insight into microscopic processes relevant to energy generation, storage, and thermal science. Activities in this Subtask drive new theory and simulation, to enrich the molecular level interpretation of experiments. The Gas Phase Chemical Physics program at Berkeley Lab is uniquely placed to conduct this research, with theory and experiment coupled with extensive use of DOE national user facilities such as the Advanced Light Source and NERSC.

Recent Progress:

Molecular Cluster Chemistry and Hydrogen-Bonding Networks.[1-3] We have explored the behavior of gas-phase argon-acetylene clusters formed via weak van der Waals interactions and extracted their structural features to shed light on mechanisms of electronic excitation and concomitant energy transfer leading to ionization.[2] The resemblance between the photoionization efficiency (PIE) curves of the $(C_2H_2)Ar_n$ (n = 1 – 7) clusters and the excitation spectra of Ar_n clusters is explained by Penning ionization. To probe hydrophilic interactions, we chose to work with naphthalene water clusters. $N_x(H_2O)_y$ (N = naphthalene) clusters reveal that, at photon energy below 11 eV, the naphthalene moiety is ionized without proton transfer from N^+ to water sub-cluster, where $(NOH)[(H_2O)_xH]^+$ are generated above 11 eV. These findings suggest that water sub-clusters dominate the dynamics at high photon energies. *Ab initio* calculations are performed (Head-Gordon group), as the energetics of the neutral structures $N(H_2O)_{1\text{-}4}$ and their photo-ionized counterparts are calculated, and energy decomposition analysis is performed to understand trends in the binding between the naphthalene and the water sub-cluster in the ionized species.[3]

Molecular Chemistry of Polycyclic Aromatic Hydrocarbon Growth.[4-18] The growth of polycyclic aromatic hydrocarbons (PAHs) has been explored in collaboration with Ralf Kaiser (Hawaii), and Alex Mebel (FIU). This project was performed using a resistively-heated pyrolytic silicon carbide micro-reactor coupled to synchrotron-based TOF-MS, complemented by electronic structure calculations and kinetic modeling. The growth from 4-phenanthryl and acetylene has been elucidated, with the formation of pyrene confirmed via the Hydrogen Abstraction Acetylene Elimination (HACA) mechanism.[4] Corannulene ($C_{20}H_{10}$) was conceptualized as a fragment of fullerenes as it exhibits an out-of-plane carbon backbone. The synthesis of corannulene via the reactions of 7-fluorathenyl ($C_{16}H_9^{\bullet}$) and benzo[*ghi*]fluoranthen-5-yl ($C_{18}H_9^{\bullet}$) radicals with acetylene (C_2H_2) was observed and confirmed.[5] Beyond HACA, we have examined and confirmed the HAVA (Hydrogen Abstraction/Vinylacetylene Addition) mechanism which bears no activation barrier and leads to products via exoergic pathways. Guided by the HAVA mechanism, naphthalene was synthesized from the reaction of phenyl radical and vinylacetylene (C_4H_4).[6] Successively, the reaction between 1- and 2-naphthyl and C_4H_4 gives anthracene and phenanthrene ($C_{14}H_{10}$) as products,[7] whose further reaction with C_4H_4 produces multiple 4-fused-ring PAH isomers ($C_{18}H_{12}$) depending on the structure of the radical precursor.[8-10] As the molecular mass grows, the synthesis of even larger PAH is challenging due to the difficult vaporization and low reaction cross section. Only pentacene ($C_{22}H_{14}$) from tetracenyl + C_4H_4,[11] and [5]helicene ($C_{22}H_{14}$) from [4]helicenyl ($C_{18}H_{12}$) + C_4H_4 were achieved. On the

other hand, not all additions of C_2H_2 and C_4H_4 lead to ring closure. 1-Indenyl ($C_9H_7^{\bullet}$) has the radical located on the five-membered ring and it does not follow a ring closure due to the reaction barriers,[12] whereas 5- and 6-indenyl have C on the six-membered ring radicalized and their reactions with C_2H_2 and C_4H_4 undergo ring closure into benzindene ($C_{13}H_{10}$) isomers.[13] Similar to the HACA and HAVA mechanisms, a C3 addition pathway was attained from PAH radicals via hydrogen abstraction followed by propyne or allene (C_3H_4) addition. The reactions between 1- and 2-naphthyl with propyne or allene were examined.[14, 15] The elementary reactions between two free hydrocarbon radicals leading to PAHs at high temperatures have been realized experimentally using the hot nozzle. Methyl insertion to the 5-membered ring moiety of 1-indenyl leading to naphthalene was realized for the first time.[16] Self-combination reactions of propargyls ($C_3H_3^{\bullet}$) to benzene isomers[17] and cyclopentadienyls ($C_5H_5^{\bullet}$) to naphthalene were investigated. By exploring the reaction mechanism of the phenyl radical with biphenyl/naphthalene, another novel phenyl-addition/dehydrocyclization (PAC) mechanism leading to triphenylene and fluoranthene was proposed. PAC operates efficiently at high temperatures through rapid molecular mass growth processes leading to complex aromatic structures, which are difficult to synthesize by traditional pathways such as HACA.[18]

Evaporation and scattering from flat liquid jets:[19] Gas-liquid interfaces are a common chemical environment in nature and play a major role in atmospheric chemistry, such as acid rain formation and aerosol pollution. Molecular-level studies of these interfaces have been hindered by the difficulties of introducing high vapor pressure liquids into the vacuum conditions required by many analytical techniques. Neumark has converted an apparatus previously used for gas phase photodissociation to a flat jet molecular beam scattering experiment. On this instrument, one can differentiate different gas-liquid pathways, such as inelastic scattering and desorption, using a rotatable mass spectrometer to collect time-of-flight (TOF) spectra.

The evaporation of particles from flat jets of water and dodecane, $C_{12}H_{26}$ has been investigated. Specifically, angular-resolved TOF spectra yield the first measurements of the coupled angular and translational energy distributions of molecules evaporating from a liquid flat jet. Along the surface normal a super-Maxwellian TOF spectrum is seen. The TOF distribution becomes more Maxwellian as one moves away from normal incidence. The 0° spectrum deviates more from a Maxwellian distribution than for the cylindrical jet, but this trend reverses at larger scattering angles. The extent to which this trend reflects vapor sheath collisions, which are expected to be more pronounced for a flat jet, as opposed to surface tension effects is an open area of investigation. A polar plot of the integrated scattering signal at each angle shows that the data are well matched to the cosine distribution expected for thermal desorption from a flat surface.

For liquid water, the high vapor pressure (6-9 Torr at 278-283 K) generates a much denser vapor cloud surrounding the liquid sheet. This vapor sheath contributes to an increase in the collision number of the evaporating molecules before they reach the detector. This effect is reflected in the TOF spectra of HDO and Ar, which show a much narrower distribution than expected from Maxwell-Boltzmann simulations. This deviation is significantly reduced by placing a skimmer between the detector and the liquid surface, altering the geometry of the expanding gas. The skimmed TOF spectra are broader and slower than the non-skimmed spectra, and more closely resemble Maxwellian distributions. The TOF spectra of evaporating dissolved argon appear more Maxwellian than the HDO data. This effect reflects the smaller Ar-H_2O collision cross section (vs. that of H_2O-H_2O), leading to fewer collisions during evaporation and a reduced discrepancy between the TOF spectra and Maxwellian distribution for Ar. a polar plot shows good agreement with a cosine distribution for the Ar data. The HDO polar plot does not agree as well, showing a more isotropic distribution that may reflect more collisions in the vapor sheath.

In preliminary flat jet scattering experiments, a supersonic beam of He atoms was scattered off a water flat jet at an incident angle of 45° with respect to the water surface normal and collected at the

specular scattering angle. The TOF spectrum for He shows at least two features, a fast peak attributed to impulse scattering and a slower peak whose assignment is still under consideration.

Multiphase chemistry of Criegee Intermediates (CI) and peroxy radicals:[20-26] In the environment, the two most important oxidants are ozone (O_3) and the hydroxyl radical (OH) that together, for example, account for the majority of oxidative transformations of organic molecules in the troposphere. Oxidation proceeds through networks of many elementary reactions involving highly reactive intermediates. With few exceptions, O_3 and OH reactions proceed by distinct mechanisms involving different intermediates. O_3 reactions produce Criegee intermediates (CI), while OH oxidation involve elementary reactions of peroxy and alkoxy free radicals. We reported[27] compelling evidence, for a variety of alkene systems, that there are pathways that produce CI from β-hydroxyl peroxyl radicals (β-RO_2); a result which is consistent with recent reports from the Beauchamp group (Caltech).

This mechanism contrasts with the traditional autoxidation mechanism of lipids, established since the 1940's, where radical chain cycling proceeds via RO_2 and a subsequent H-atom transfer to form peroxides (ROOH) ultimately reforming another RO_2. This mechanism was thought to be the main autocatalytic free radical chain reaction responsible for the oxidative destruction of organic molecules in biological cells, foods, plastics, petrochemicals, fuels and the environment. Our results point to an additional, and previously unknown, autoxidation pathway.

We have examined the coupling of CI with β-RO_2 from an another perspective,[28] by first generating CI via the ozonolysis and watching whether free radical cycling occurs via the β-RO_2 intermediate. Using a kinetic model, we find, during multiphase ozonolysis, that only ~ 30% of the alkene is actually consumed directly by O_3, while the remaining ~ 70% is consumed by free radicals that cycle through pathways involving CI and β-RO_2. What remains unknown in these studies, is the exact mechanism (unimolecular or bimolecular) by which the β-RO_2 forms CI. This work is ongoing together with the Head-Gordon group. While Beauchamp and coworkers suggested a unimolecular pathway facilitated by H_2O and O_2, preliminary work detailed below from the Head-Gordon group, as well as a recent publication by Wagner, suggest a more complex bimolecular mechanism.

Future Plans:

Photoionization Dynamics and Hydrogen Bonding in Clusters: We continue the study of photon-induced reactivity of non-covalent-bonded water-containing clusters at the molecular level due to the unquestioned importance, coupled with collaboration with the Head-Gordon group. We will extend our studies using alcohol-water clusters, from which we learned about ionic hydrogen bonds, towards deep eutectic solvents (DES). DES are commonly viewed as molten mixtures of at least one hydrogen bond donor and one hydrogen bond acceptor which possess a melting point that is less than the melting points of the individual compounds of the mixture. These "designer solvents" have many applications and the task-specific nature of these solvents requires a molecular-level understanding. We will extend our glycerol+water study to other sugar alcohols such as ethylene glycol and propylene glycol. Contrary to ethylene glycol and glycerol, propylene glycol has been controversial for its non-colligative behavior. Its two isomers, 1,2- and 1,3-propylene glycol, give an additional dimension where one can study the effects of adjoining hydroxyl groups *vs*. non-adjoining hydroxyl groups in cluster formation and hydrogen bonding. Therefore, one would expect different cluster formations and hydrogen bonding networks in these two isomers.

Small neutral molecules and ions can act as nucleating species, which typically play key roles in molecular growth. We have recently developed an experimental strategy for characterizing neutral *vs*. ion-induced growth using in-source ionization of molecular beams with VUV synchrotron radiation. This method in collaboration with MHG allowed us to probe systems that are relevant to atmospheric chemistry and to develop a framework in which to understand novel hydrogen bonding and non-covalent interactions. We propose to study growth processes in pure water clusters to act as a

bridge from the gas phase to condensed phase dynamics. Previously we had studied neutral induced growth processes of protonated water clusters formed in supersonic expansions. Mass spectra (6-mm distance from the nozzle) show magic numbers (at 11.5 eV) of water cluster peaks below the 21, and 30 typically observed in the literature. It is found that at a closer distance, ion-induced growth dominates the cluster distribution since the molecular density is greater. The spectral distributions are representative of a non-equilibrium frozen state and calculations from the MHG group are being used to assign structure and energetics for these new magic numbers.

Water Dynamics in Confined Spaces: A future program goal is to identify the molecular mechanisms of evaporation of water from within confined volumes, and in mixtures. Solid–liquid–vapor (SLV) interfaces are highly dynamic and can lead to far from equilibrium conditions because of significant temperature gradients. SLV interfaces are widely used in applications such as refrigeration and solar desalination. However, the complex chemical and structural properties of the SLV interface under non-equilibrium conditions make molecular level modeling and experimentation very challenging. Recently, in collaboration with Xiao-Ying Yu (PNNL) we have incorporated a microfluidic device, System for Analysis of Liquid Interfaces (SALVI) to VUV-TOF-MS to probe phase transitions, electrochemistry, and photochemistry on environmental and energy-related processes.[29-31] Liquids are sealed in between Si_3N_4 membranes in a microchannel with 2 – 3 μm apertures and surface tension across the aperture holds the liquid in high vacuum. The molecules evaporating from the liquid surface are interrogated by VUV photons and then detected by TOF-MS. We propose to physically chop the emanating vapor to measure its time-of-flight to obtain velocities and hence translational dynamics. Our group has broad experience in probing dynamics using synchrotron-based velocity measurements. We have the distinct advantage that our methodology can be used to probe evaporative processes from an SLV interface and the microfluidic nature of the device allows to probe phase transitions, evaporation, electro- and photo-chemistry. We also envision incorporating high repetition lasers (IR, THz, UV) to dynamically probe the interface in the future. A second apparatus in the proposed experiment program is to couple a broadly tunable plasma-based UV light source to perform velocity map imaging photoelectron spectroscopy of the liquid interface and also allow access to IR and THz laser radiation. Our initial focus will be to probe the evaporation of water from confined spaces (both hydrophobic and hydrophilic) and also phase changes and reactions upon electric field. Recently we have demonstrated the ability to model and probe the effects of condensation upon application of an electric field to bulk water and water embedded in carbon nanotubes and silica nanopores. We can incorporate this methodology within the SALVI device and follow aspects of evaporation.

Flat Jets and Evaporation Dynamics: Flat jet evaporation experiments aim to untangle the different evaporation pathways at the liquid interface. Previous molecular dynamics simulations have identified distinct interactions at the interface for He evaporating from dodecane that lead to kinetic energy and angular distributions that deviate in different ways from thermal expectations. It should be possible to disentangle these mechanisms using translational energy and angular resolved experiments. Experiments on water will explore the extent to which the temperature needs to be lowered in order to minimize interactions of evaporating solutes such as He or Ar with the vapor sheath. Experiments involving closed shell molecules will provide further insights into interactions at the gas-liquid interface. For example, scattering experiments will be carried out on both water and hydrocarbon flat jets with molecules such as CO_2, CH_3OH or NH_3 in order to explore the relationship between bulk solubility and interfacial scattering. Based on the bulk solubilities, one might expect more impulsive scattering and less thermal desorption from hydrocarbons, but whether these effects will be evident in interfacial scattering experiments remains an open question.

Multiphase Chemistry: Ongoing theoretical work with Head-Gordon, will focus on developing a robust understanding of the reaction pathways that connect CI and β-RO_2. We are currently explored

a number of candidate bimolecular mechanisms. Once the theoretical description of the coupling of CI and β-RO_2 is complete we will revise our kinetic models accordingly to test against our previous experimental results. A key touchpoint between theory and experiment is to be able to describe the scaling of the effective reaction probability vs. [OH]. The effective uptake coefficient increases with decreasing [OH] providing a stringent test for a kinetic model to accurately predict. We currently have an unpublished kinetic model that is constrained by previous literature. However, the largest uncertainty resides in the steps (rate coefficient and mechanism) that link CI with β-RO_2, which we expect the theoretical results provided by the Head-Gordon group to better constrain. Based upon these and any further theoretical insight we will design new experiments to test and validate these theoretical predictions.

Non-covalent Interaction and Heterogeneous reaction probabilities: It is well-known that in the field of enzyme catalysis that weak interactions (e.g. hydrogen and halogen bonds) can play an important role in altering the energetics of a reaction. Less well know is how these weak interactions can enhance reactivity at the gas-liquid interfaces. In ongoing work, we have observed an increase in the apparent reaction probability for the reaction of Cl_2 gas at an alkene aerosol interface. The reaction of Cl_2 with condensed phase alkenes is fairly well-known and there is increased interest in heterogeneous sinks of halogenated species on indoor surfaces. Preliminary results indicate that the Cl_2 reaction with aerosol alkenes, although slow, is sequential; adding two Cl functional groups per C=C site. However, when the particle is doped with species (an additive) that contains an alcohol or carbonyl functional group (which are inert towards Cl_2) the apparent reaction rate is accelerated by ~10-20X. In contrast, doping with alkanes or molecules with ester groups either does not change the reactivity or decreases it by a factors of ~3. Although work is ongoing, we hypothesize that the presence of dopants at the interface that can form halogen bonds with Cl_2 can alter the adsorption/desorption kinetics in such a way as to promote the reaction between the alkenes and Cl_2. We will continue these studies by developing a quantitative kinetic description of the catalytic mechanism in this model system. Furthermore, we plan to examine if small gas phase oxygenated molecules (such as ethanol, acetic acid) can play a similar catalytic role at the interface during heterogeneous chlorination. As these experiments progress, we anticipate theoretical support from the Head-Gordon group, whose experience in halogen bonding will prove invaluable in providing deeper insights into the catalytic mechanism controlling this heterogeneous system.

Multiphase reactions at solid and liquid interfaces: Previous collaborative computational studies with Frances Houle (LBNL) revealed that overall net reaction mechanisms can be substantially altered when molecular diffusion to and from an interface is slow compared to surface reaction timescales. We will continue these studies examining the role that diffusively confined CI play at the surface of solid alkenes. We hypothesize that diffusive confinement will introduce a dynamic interplay between CI bimolecular reactions and unimolecular decomposition. For example, one could imagine that diffusive confinement would promote CI + CI reactions. In this case, the free radical cycling observed above for the liquid alkene would effectively be suppressed. To explore these ideas, we will use two model aerosol systems: oleic and elaidic acid. Oleic acid, a liquid at room temperature is the cis isomer of elaidic acid (a solid at room temperature). Thus these two molecules are expected to exhibit nearly the same reactivity towards OH or O_3, given that they differ only in isomeric structure (this will be verified experimentally). By changing the reactor temperature, we can melt elaidic acid and freeze oleic acid. Additionally, mixtures of oleic and elaidic acids form complex phases. Thus these model systems provide tremendous flexibility in exploring how ozone reactions (and the chemistry of CI) change with phase state. For example, a study by Finlayson-Pitts found evidence that the surface reaction of ozone on self-assembled monolayers proceeded via a much different mechanism than what is observed in well-mixed liquids.

Publications: (2018 to present)

1. M. Ahmed and O. Kostko, PCCP **22** (5), 2713-2737 (2020).
2. W. Lu, R. B. Metz, T. P. Troy, O. Kostko and M. Ahmed, PCCP **22** (25), 14284-14292 (2020).
3. B. Xu, T. Stein, U. Ablikim, L. Jiang, J. Hendrix, M. Head-Gordon and M. Ahmed, Faraday Discuss **217**, 414-433 (2019).
4. L. Zhao, R. I. Kaiser, B. Xu, U. Ablikim, M. Ahmed, D. Joshi, G. Veber, F. R. Fischer and A. M. Mebel, Nat. Astron. **2** (5), 413-419 (2018).
5. L. Zhao, R. I. Kaiser, W. Lu, O. Kostko, M. Ahmed, L. Tuli, A. N. Morozov, A. H. Howlader, S. F. Wnuk, A. M. Mebel, V. N. Azyazov, R. K. Mohamed and F. R. Fischer, PCCP. **23**, 5740-5749 (2021).
6. L. Zhao, R. I. Kaiser, B. Xu, U. Ablikim, M. Ahmed, M. V. Zagidullin, V. N. Azyazov, A. H. Howlader, S. F. Wnuk and A. M. Mebel, J. Phys. Chem. Lett. **9** (10), 2620-2626 (2018).
7. L. Zhao, R. I. Kaiser, B. Xu, U. Ablikim, M. Ahmed, M. M. Evseev, E. K. Bashkirov, V. N. Azyazov and A. M. Mebel, Nat. Astron. **2** (12), 973-979 (2018).
8. L. Zhao, M. Prendergast, R. I. Kaiser, B. Xu, U. Ablikim, W. Lu, M. Ahmed, A. D. Oleinikov, V. N. Azyazov, A. H. Howlader, S. F. Wnuk and A. M. Mebel, PCCP **21** (30), 16737-16750 (2019).
9. L. Zhao, R. I. Kaiser, B. Xu, U. Ablikim, W. Lu, M. Ahmed, M. M. Evseev, E. K. Bashkirov, V. N. Azyazov, M. V. Zagidullin, A. N. Morozov, A. H. Howlader, S. F. Wnuk, A. M. Mebel, D. Joshi, G. Veber and F. R. Fischer, Nat. Commun. **10** (1), 1510 (2019).
10. L. Zhao, R. I. Kaiser, B. Xu, U. Ablikim, M. Ahmed, M. M. Evseev, E. K. Bashkirov, V. N. Azyazov and A. M. Mebel, Angew. Chem. Int. Ed. **59** (10), 4051-4058 (2020).
11. L. Zhao, R. I. Kaiser, W. Lu, M. Ahmed, M. M. Evseev, E. K. Bashkirov, V. N. Azyazov, C. Tönshoff, F. Reicherter, H. F. Bettinger and A. M. Mebel, Angew. Chem. Int. Ed. **59** (28), 11334-11338 (2020).
12. L. Zhao, M. B. Prendergast, R. I. Kaiser, B. Xu, W. Lu, U. Ablikim, M. Ahmed, A. D. Oleinikov, V. N. Azyazov, A. M. Mebel, A. H. Howlader and S. F. Wnuk, ChemPhysChem **20** (11), 1437-1447 (2019).
13. L. Zhao, R. I. Kaiser, W. Lu, O. Kostko, M. Ahmed, M. M. Evseev, E. K. Bashkirov, A. D. Oleinikov, V. N. Azyazov, A. M. Mebel, A. H. Howlader and S. F. Wnuk, PCCP **22** (39), 22493-22500 (2020).
14. L. Zhao, R. I. Kaiser, W. Lu, B. Xu, M. Ahmed, A. N. Morozov, A. M. Mebel, A. H. Howlader and S. F. Wnuk, Nature Commun. **10** (1), 3689 (2019).
15. L. Zhao, R. I. Kaiser, W. Lu, M. Ahmed, A. D. Oleinikov, V. N. Azyazov, A. M. Mebel, A. H. Howlader and S. F. Wnuk, PCCP **22** (27), 15381-15388 (2020).
16. L. Zhao, R. I. Kaiser, W. Lu, B. Xu, M. Ahmed, A. N. Morozov, A. M. Mebel, A. H. Howlader and S. F. Wnuk, Nat. Commun. **10** (1), 3689 (2019).
17. L. Zhao, W. Lu, M. Ahmed, M. V. Zagidullin, V. N. Azyazov, A. N. Morozov, A. M. Mebel and R. I. Kaiser, Sci. Adv. In press (2021).
18. L. Zhao, M. B. Prendergast, R. I. Kaiser, B. Xu, U. Ablikim, M. Ahmed, B.-J. Sun, Y.-L. Chen, A. H. H. Chang, R. K. Mohamed and F. R. Fischer, Angew. Chem. Int. Ed. **58** (48), 17442-17450 (2019).
19. S. Malerz, F. Trinter, U. Hergenhahn, A. Ghrist, H. Ali, C. Nicolas, C.-M. Saak, C. Richter, S. Hartweg, L. Nahon, C. Lee, C. Goy, D. M. Neumark, G. Meijer, I. Wilkinson, B. Winter and S. Thürmer, PCCP (2021).
20. M. Zeng and K. R. Wilson, J. PHys. Chem. Lett. **11** (16), 6580-6585 (2020).
21. M. Zeng, N. Heine and K. R. Wilson, PNAS **117** (9), 4486-4490 (2020).
22. M. I. Jacobs, B. Xu, O. Kostko, A. A. Wiegel, F. A. Houle, M. Ahmed and K. R. Wilson, J. Phys. Chem. A (2019).
23. C. Arata, N. Heine, N. Wang, P. K. Misztal, P. Wargocki, G. Bekö, J. Williams, W. W. Nazaroff, K. R. Wilson and A. H. Goldstein, Environmental Science & Technology **53** (24), 14441-14448 (2019).
24. F. A. Houle, A. A. Wiegel and K. R. Wilson, J. Phys. Chem. Lett. **9** (5), 1053-1057 (2018).
25. F. A. Houle, A. A. Wiegel and K. R. Wilson, Environmental Science & Technology **52** (23), 13774-13781 (2018).
26. N. Heine, C. Arata, A. H. Goldstein, F. A. Houle and K. R. Wilson, J. Phys. Chem. Lett. **9**, 3504-3510 (2018).
27. M. Zeng, N. Heine and K. R. Wilson, PNAS **117** (9), 4486-4490 (2020).
28. M. Zeng and K. R. Wilson, J. Phys. Chem. Lett. **11** (16), 6580-6585 (2020).
29. R. Komorek, B. Xu, J. Yao, U. Ablikim, T. P. Troy, O. Kostko, M. Ahmed and X. Y. Yu, Rev Sci Instrum **89** (11), 115105 (2018).
30. R. Komorek, B. Xu, J. Yao, O. Kostko, M. Ahmed and X. Y. Yu, PCCP **22** (26), 14449-14453 (2020).
31. X. Sui, B. Xu, J. Yao, O. Kostko, M. Ahmed and X. Y. Yu, J Phys Chem Lett **12** (1), 324-329 (2021).

Nanoparticle Surface Kinetics and Dynamics by Single Nanoparticle Mass Spectrometry

Scott L. Anderson, Chemistry Department, University of Utah
315 S. 1400 E. Salt Lake City, UT 84112 anderson@chem.utah.edu

Program Scope

This project is focused on developing and using single nanoparticle mass spectrometry (NPMS) to measure reaction kinetics and emission spectroscopy for individual carbon nanoparticles (NPs) at high temperatures. The focus is on high temperature chemistry of different types of carbon NPs, and in the past year we have worked on sublimation, O_2 oxidation, and NP growth in reactions with C_2H_2. Because NPMS is a new tool for measuring surface reaction kinetics at high and ultra-high temperatures, significant effort continues in method development. In addition to providing temperature-dependent reaction kinetics of interest for modeling purposes, we are probing the effects of two different kinds of heterogeneity on NP kinetics and spectroscopy: 1. NPs are inherently heterogeneous, with significant NP-to-NP variation in size, shape, and structure, all of which can affect reaction kinetics and spectroscopy. 2. *Individual NPs* also have distributions of surface sites that react differently, and the site distributions and resulting reaction kinetics change as the NP *evolves* at high temperatures. In particular, we have observed dramatic evolution of the reactivity of all types of carbon NPs, signaling a major structural transformation that makes them nearly inert to oxidation and growth. This process depends strongly on both the NP starting structure and on the presence of O_2, which enhances the transformation.

Methodology

The instrument used in the experiments,[1-2] and the optical system needed to record emission spectra for NP temperature (T_{NP}) determination,[3-4] have been described previously. Details of the operating procedures are in previous reports of graphite and graphene sublimation[1] and oxidation kinetics.[2] In essence, a single NP of the material of interest is trapped in the gas phase, laser heated with T_{NP} determined by fitting the blackbody-like emission spectrum, and the NP mass is measured as a function of time as the NP sublimes or reacts with gaseous reactants like O_2 or C_2H_2. The mass change vs. time can be analyzed to extract kinetics and evolution of the kinetics over time.

The single NP approach avoids ensemble averaging, thus providing unique insights into heterogeneity and structure-reactivity relationships, but it is a slow method. To enable study of statistically meaningful numbers of NPs we have devoted considerable effort to automating the experiment, aiming at eventually at 24/7 unattended operation. Currently, most aspects of the experiment are automated, and the major effort in this area is currently on automating analysis of the large data sets generated in each experiment. One benefit of this automation effort is that the main experiment can be run remotely, which allowed our main instrument to operate throughout the COVID shutdown of the university. COVID has, however, affected the effort to bring a second instrument online, intended as a test machine for continuing development of the method. This test instrument is mostly operational, and integration of the spectroscopy hardware and testing of a new approach to NP charge determination is underway.

Results in the past year

During the past year we focused on studies of oxidation by O_2, and growth by addition of C_2H_2, for a variety of structurally distinct carbon NP types. We had previously reported a study of emission spectra, and how they change after heating, for graphite, graphene, carbon black, nanodiamond, and carbon dot NPs.[4] During the past year we finished and published studies of the kinetics for sublimation[1] and O_2 oxidation[2] of graphite and graphene NPs. Both studies reported reaction rates as a function of T_{NP}, time, and P_{O2} in the oxidation study. Time is an interesting variable because the NPs were found evolve significantly during reaction. In the high T_{NP} range where sublimation is significant (>1800 K), the evolution effects are modest. Sublimation rates (C atoms lost/nm^2) are far higher for the NPs than for bulk graphite, and show large NP-to-NP variations. Over the course of time, the sublimation rates slow by factors of 5 to 10, but remain above the bulk sublimation rate.

More dramatic NP evolution is observed under oxidizing conditions, as shown in Fig. 1. The top frame shows the oxidation and sublimation ("baseline") rates measured during two sequential T_{NP} ramps, for a single graphite NP with initial mass of 55.4 MDa. Initially, the oxidation rate was relatively large

and peaked at ~1600K, but in the 2nd ramp the rate was much lower and peaked at ~2000 K, indicating that the NP had become much less reactive to O_2. Note that sublimation ("baseline") is only significant at high T_{NP}, and the slowing of the sublimation rate is modest.

The middle frame shows a constant T_{NP} and P_{O2} oxidation experiment for a different graphite NP of similar size. Note that when O_2 was first introduced (green-shaded background), the NP lost mass rapidly due to reaction with O_2. This etching reaction continued for ~4000 seconds, with fluctuating rates indicating that the number of reactive, under-coordinated surface sites fluctuated as the NP was etched. There were also interesting changes in the emissivity of the NP. Then at ~8000 seconds, the rate slowed dramatically, eventually dropping nearly 2 orders of magnitude below the maximum rate. Such a low rate is inconsistent with a graphitic NP structure, which would always have reactive under-coordinated atoms at exposed basal plane edges. The very low rate indicates that the surface had very few reactive sites, and we proposed that the NP had undergone massive isomerization to a fullerene-like (carbon nano-onion) structure, at least for the surface layer.

A further interesting aspect of the isomerization ("onionization") process is that it is substantially faster in the presence of O_2, than in inert atmosphere. This effect can be seen by comparing the middle and bottom frames of Fig. 1. Under oxidizing conditions (middle) the transition to near inertness occurred after a little over one hour, as ~27% of the initial mass was oxidized away. In the bottom frame, a graphite NP was briefly oxidized to probe its reactivity (1st green shaded area), then held at 1500 K for ~24 hours to allow annealing/isomerization to occur (along with ~3.5% mass loss), before being again exposed to O_2 (2nd green shaded area) to probe its reactivity. It can be seen that the reactivity was still high after the long annealing period. We have a number of such experiments, for graphite, carbon black, and nanodiamond NPs, and in all cases, the transition to inertness which we attribute to onionization, is much faster in O_2 than in inert atmosphere. In this example, the reactivity was also probed at the end by measuring the NP growth upon exposure to C_2H_2.

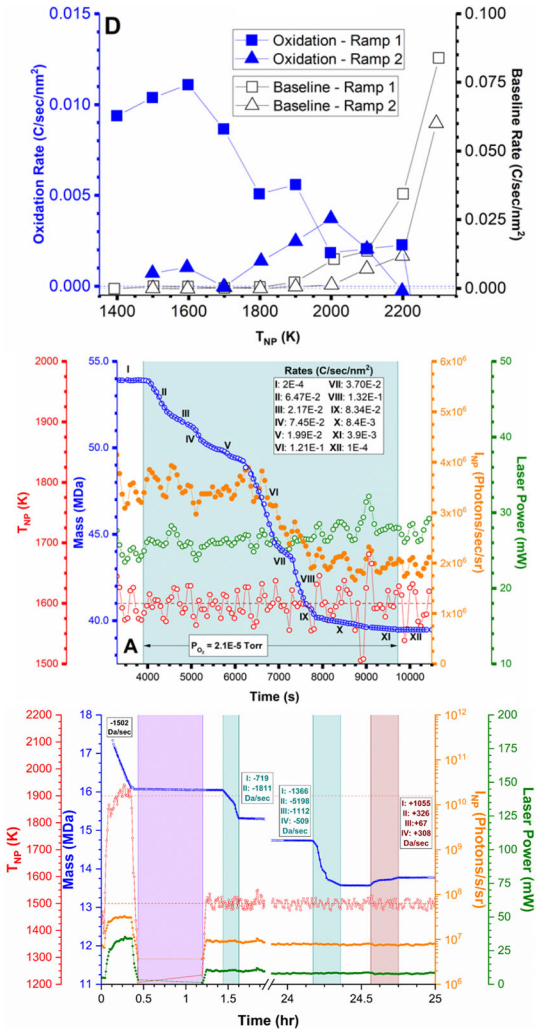

Fig.1. Top: Oxidation rate as f(T_{NP}) for a 55.4 MDa graphite NP. Middle: Constant T_{NP} & P_{O2} oxidation of a graphite NP. Bottom: Graphite NP briefly oxidized, held at 1500 K for ~24 hours, then oxidized and finally grown in C_2H_2.

Characterizing growth of carbon NPs at high T_{NP} by addition reaction with C_2H_2 and C_2H_4 has been another major effort in the past year. Our interest is both in probing the kinetics of the addition reactions, which are reminiscent of chemistry responsible for growth of soot particles, and in using the growth reaction as another probe of the availability of reactive sites on the surfaces of different NPs, at different stages of evolution. In the growth reactions with C_2H_2, the typical behavior is to observe an initial period of fast mass gain, which slows by an order of magnitude or more after growth corresponding to a fraction of a monolayer. We attribute the initial fast growth to C_2H_2 adding to under-coordinated sites on the NP surface. As shown below, the growth rate is proportional to other measures of NP reactivity, such as oxidation rate. In many cases the NP continues to grow slowly after the initial fast growth, presumably because the T_{NP} range studied (typically ~1200 – 1500 K) is high enough that C-H

bonds are unstable, resulting in continual creation of new under-coordinated sites. For some NPs, the growth eventually stops completely. Given the high temperatures, this can't be due to C-H termination of the surface, and we tentatively propose that for these NPs, the addition reactions eventually lead to onionization, i.e., they grow a fullerene-like surface layer that is thermally stable, and unreactive with C_2H_2. Some of these results are summarized below.

To explore the effects of heterogeneous NP structure on reactivity, and to further investigate the apparent isomerization to nano-onions, we studied sublimation, O_2 oxidation, and growth by reaction with C_2H_2 for a large number of carbon NPs with different initial structures, including graphite, multilayer graphene, graphene oxide, carbon black, nano-diamonds, and carbon nano-onions. The nano-onions are from the Yushin group at Georgia Tech, prepared in bulk by annealing nanodiamonds. [5]

Fig. 2 shows a representative experiment, in this case for a single carbon black NP of initial mass 57.75 MDa. This NP was trapped, then "cleaned" of surface contaminants by heating to ~1900 K (cleaning at T_{NP} up to 2600 K was tested), during which time the NP lost ~5% of its initial mass. During the purple shaded time period the NP was held at ~1200 K for charge determination, then at ~4000 sec., T_{NP} was set to 1500 K. The baseline rate of mass loss was measured (~zero), then at ~5000 sec., O_2 was added (green shading), leading to rapid oxidative etching of ~0.5 MDa. In this case, oxidation was terminated before significant rate evolution had occurred, and the O_2 was replaced by C_2H_2, which led to immediate growth of the NP, which can be seen to slow significantly over time. The NPs was then oxidized again, showing a reduced rate.

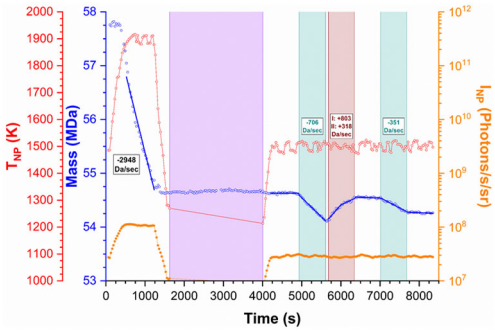

Fig. 2. A typical oxidation and growth experiment for a carbon black NP

Many experiments with multiple oxidation/growth cycles at different temperatures, pressures, etc., have been carried out. Experiments examining the onionization process for all the carbon NP types were also done. To summarize, graphitic and carbon black NPs have broadly similar oxidation and growth properties, although the graphitic NPs are significantly more reactive (see below) and there are factor-of-five NP-to-NP variations for both materials. Both are initially quite reactive with both O_2 and C_2H_2, and both evolve to inertness (onionization) on similar time scales.

In contrast, nanodiamonds undergo such fast evolution that it is difficult to catch them while they are still reactive except at very low T_{NP} (≤1400 K). Even very brief heating above 1500 K causes a ~two-order-of-magnitude drop in reactivity toward both O_2 and C_2H_2. We were expecting that the nano-onion NPs provided by our collaborators would be quite inert even when first introduced to the trap. Instead, they have initial reactivities in the range observed for graphite or carbon black NPs, but they do transition to inertness more rapidly. The origin of the unexpectedly high initial reactivity is still under investigation, however, it seems like that cause is the presence of some carbon on the NP surfaces that is not onionized, and which must be oxidized away or converted to onion structure to reach the inert state. The final state of the NPs after prolonged oxidation in our trap, regardless of NP type, has considerably fewer reactive sites than onions produced by annealing bulk samples of nano-diamonds.

Fig. 3 compares the 1500 K O_2 oxidation rates and the *initial* C_2H_2 growth rates for a set of different types of NPs with sizes ranging from ~10 to ~100 MDa. Both sets of rates are given as mass change *per* reactant collision, therefore they are approximately corrected for the variation in the NP surface areas. There are several interesting points. It is clear that the initial growth rate

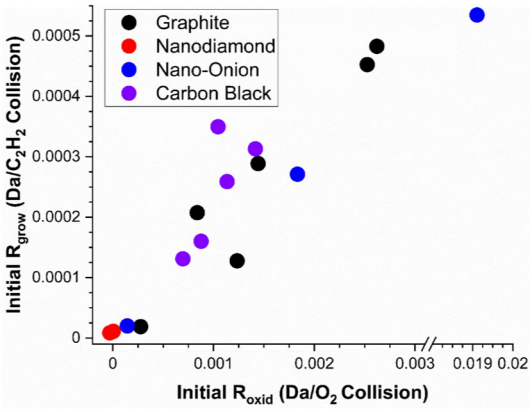

Fig. 3. 1500 K C_2H_2 growth rates plotted against O_2 oxidation rates showing correlation.

is highly correlated with the oxidation rate, and the correlation holds across several orders of magnitude, and for four different types of carbon NPs. The strong correlation suggests that O_2 attacks and etches at sites that are similar to the attachment sites in C_2H_2 addition. Given the low reactivity of graphitic basal planes and fullerenes, these reactive sites are identified as basal plane edges, defects, and other under-coordinated carbon centers. Note that the nanodiamond NPs are essentially inert. This reflects the fact, noted above, that nano-diamonds undergo very rapid onionization for $T_{NP} \geq 1500$ K, which was the T_{NP} in these experiments.

Fig. 4 compares the absolute C_2H_2-addition rates (Da/sec) for a large number of carbon NPs, showing that the initial growth rate varies significantly for different kinds of NPs, scales with the NP mass, and also is affected by how the NP was treated prior to C_2H_2 exposure. The NPs with the fastest initial growth (i.e., with the largest number of exposed reactive sites) have graphitic structures, comprising graphite NPs that were exposed to C_2H_2 either immediately, or after just short periods of oxidation. Note that for these graphitic NPs, the rate is roughly proportional to the NP mass, i.e., larger particles have more reactive sites, as expected. That is also true for the carbon black NPs, which have the next highest reactivity. The fact that for both classes of NPs, the rate is proportional to mass, rather than mass$^{2/3}$ is unsurprising because the larger NPs are probably aggregates.

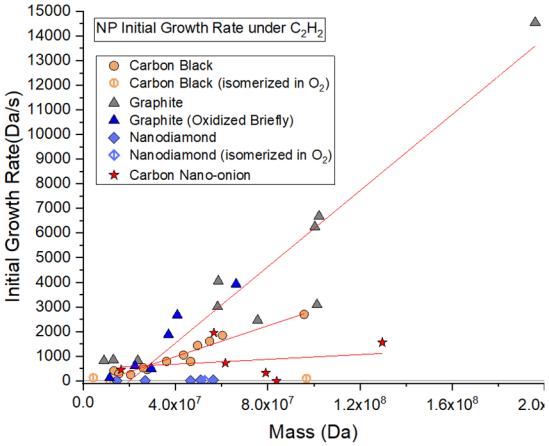

Fig. 4. Summary of C_2H_2 *initial* addition reaction rates for different carbon NPs

Growth rates are also shown for carbon black NPs that were oxidized for extended periods, allowing them to isomerize to onion surface structures which have essentially zero growth rate, independent of NP mass. The same is true for nanodiamonds, and nanodiamonds isomerized in O_2. With or without O_2, nanodiamonds onionize so rapidly that the inherent diamond reactivity can be observed only at very low temperatures. Again it can be seen that the reactivity of NPs from a bulk nano-onion sample is higher than that of the NPs isomerized in our trap.

Plans for the coming year: I expect to implement a radical source that will allow us to measure reactions rates/probabilities for species such as O, OH, H, etc. with carbon NPs in various states of evolution. I also plan to continue development of the methodology to enable kinetic studies at ultra-high temperatures, greater than 3000 K, where other methods are lacking.

References (1 – 4 acknowledge support from DOE GPCP program)

1. Long, B. A.; Lau, C. Y.; Rodriguez, D. J.; Tang, S. A.; Anderson, S. L., Sublimation Kinetics for Individual Graphite and Graphene Nano-particles (NPs): NP-to-NP Variations and Evolving Structure-Kinetics and Structure-Emissivity Relationships. *J. Am. Chem. Soc.* **2020,** *(on line 7/22/2020)*.
2. Rodriguez, D. J.; Lau, C. Y.; Long, B. A.; Tang, S. A.; Friese, A. M.; Anderson, S. L., O_2-oxidation of individual graphite and graphene nanoparticles in the 1200–2200 K range: Particle-to-particle variations and the evolution of the reaction rates and optical properties. *Carbon* **2021,** *173*, 286-300.
3. Long, B. A.; Rodriguez, D. J.; Lau, C. Y.; Anderson, S. L., Thermal emission spectroscopy for single NP temperature measurement: optical system design and calibration. *Appl. Opt.* **2019,** *58* (3), 642-649.
4. Long, B. A.; Rodriguez, D. J.; Lau, C. Y.; Schultz, M.; Anderson, S. L., Thermal Emission Spectroscopy of Single, Isolated Carbon Nanoparticles: Effects of Particle Size, Material, Charge, Excitation Wavelength, and Thermal History. *J. Phys. Chem. C* **2020,** *124*, 1704-1716.
5. Kovalenko, I.; Bucknall, D. G.; Yushin, G., Detonation Nanodiamond and Onion-Like-Carbon-Embedded Polyaniline for Supercapacitors. *Advanced Functional Materials* **2010,** *20* (22), 3979-3986.

Predictive Large-Eddy Simulation of Supercritical-Pressure Reactive Flows in the Cold Ignition Regime

Josette Bellan
Mechanical and Civil Engineering Department, California Institute of Technology
Pasadena, CA 91125
Josette.Bellan@jpl.nasa.gov
DOE Award Number: **02_GR-ER16107-14-00**
STRIPES award number: **SC0002679/0009**

I. Program Scope

This study addresses issues highlighted in the Basic Energy Needs for Clean and Efficient Combustion of 21st Century Transportation Fuels (DOE BES, 2006) under the topic of Combustion under Extreme Pressure. It is there noted that "the most basic concepts of thermal autoignition" are "based on experience and theory at near atmospheric pressures" and that "as pressure increases significantly…, many of these conceptual pictures begin to change or disappear". It is also stated "A better description of the coupling and interaction of high pressure flow and molecular transport processes with chemistry is also necessary", particularly because "Ignition and flame propagation of alternative and renewable fuels, as well as of the changing feed stocks of conventional fossil-based fuels, are very likely to be much different at very high pressures than under the more familiar, lower pressure conditions of current engines." Recognizing that "Under such *(increasing pressure)* conditions distinctions between gas and liquid phases become moot, new equations of state must be used…", it is immediately apparent that there must be "a re-examination of the basic assumptions that govern the physics and chemistry related to combustion; and the need for this type of re-examination increases as the combustion pressure increases." This recognition is also stated under the topic of Multiscale Modeling since due to the new equations of state "The combination of unexplored thermodynamic environments and new physical and chemical fuel properties results in complex interactions among multiphase *(according to the above, the multiphase distinction becomes moot with increasing pressure)* fluid dynamics, thermodynamic properties, heat transfer, and chemical kinetics that are not understood even at a fundamental level." From the theoretical viewpoint for "systems at high pressure, fluid dynamic time scales can be comparable to chemical time scales." and therefore "completely diffusion-controlled reactions … can become important".

Thus, the objective of this study is the investigation of the coupling among thermodynamics, transport properties, intrinsic kinetics and turbulence under the high-pressure and the relatively (with respect to combustion) low-temperature conditions typical of the auto-ignition regime, with particular emphasis on the manifestation of this coupling on the effective kinetic rate.

II. Recent Progress

This report contains results obtained during the previous year of funding. This previous year the attention was turned towards the effect of the chemical species distribution in high-pressure turbulent flows in the presence of strong temperature gradients as would occur during reactions in realistic flows. The prime example of such flows are boundary layers in which the wall is at a lower temperature than that of the fluid, as would be the case in Diesel engines. Previous DOE BES work in the program further highlighted the importance of the boundary layer as a configuration for fundamental studies: (1) soot formation in boundary layers is still a

problem poorly understood and depends on the availability of particular chemical species at that location, and (2) when boundary layer Large Eddy Simulations results were compared with measurements, the agreement was unfavorable, showing that this important 'unit' problem is not well understood. In turbulent flows, chemical species location depends on convective fluxes and on diffusive fluxes. Small-scale convective fluxes are well understood, but small-scale diffusive fluxes are still a subject of active research. If the effect of pressure gradients is small in the species mass flux, as it is usually the case, **Fig. 1** shows a diagram of the types of diffusion type of events that can be expected. In that figure, the diagonal corresponds to null species mass diffusion flux, as the Soret effect representing the temperature gradient, $J_{sor,y}$, precisely counteracts the species diffusional process proportional to the gradient of the species mass fraction, $J_{mol,y}$. The process of regular diffusion has been extensively studied, but uphill diffusion has received less attention. To study the species distribution in the boundary layer, we performed a suite of Direct Numerical Simulations (**DNS**) for both single species, N_2, and binary-species, N2-CH_4, where N_2 was initially separated from the wall by a layer of CH_4. DNS were typically performed at 60 atm, and for the binary-species case also at 80 atm. The DNS for the single species situation provided the baseline understanding for the binary species case. An instantaneous profile of the CH_4 normalized mass fraction is shown in Fig. 2 at the time when the boundary layer reached conditions with turbulent characteristics. To analyze the interactions between $J_{sor,y}$ and $J_{mol,y}$ at different boundary layer heights, the joint probability density function (**JPDF**) of $J_{mol,y}$ and $J_{sor,y}$ for the **Fig. 2** binary-species mixing layer at boundary layer coordinates y^+=0.3, 10, 30 and 50 is illustrated in **Fig. 3**. The line $J_{sor,y}$ = - $J_{mol,y}$ is shown in each figure to locate the JPDF with respect to this crucial boundary between regular and uphill diffusion. The JPDFs are computed using (x,z) plane data at each location. At y^+=0.3, the JPDF shows that the probability density is concentrated near the $J_{sor,y}$ = - $J_{mol,y}$ line. The concentration near the line indicates that $J_{mol,y}$ and $J_{sor,y}$ are balanced and the total species-mass flux is approximately 0 in almost the entire area. A peak of the JPDF at y^+=10 is located at ($J_{mol,y}$, $J_{sor,y}$) = (-0.3,0.2). The different sign of $J_{mol,y}$ and $J_{sor,y}$ indicates that the Soret effect flux is primarily preventing the species-mass diffusion. At y^+=10, $J_{mol,y}$ extends over a wide region of values from -2.0 to 0.5, while $J_{sor,y}$ concentrates in a narrow band between 0.2 and

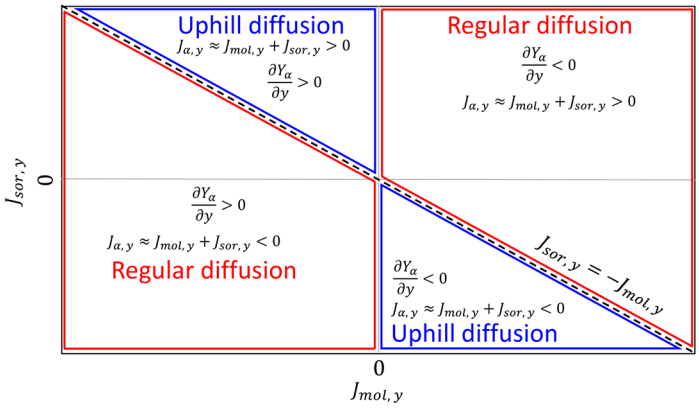

Figure 1. Diagram illustrating the classification of diffusion events which may affect chemical species distribution in the presence of a temperature gradient.

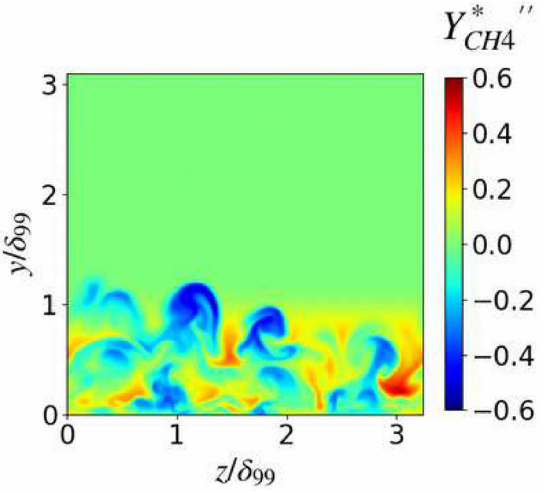

Figure 2. Normalized methane mass fraction instantaneous snapshot in the x/δ_{99}=3.25 plane for a N_2-CH_4 boundary layer at 60 atm in which the wall temperature is 300 K and the free stream fluid temperature is 600 K.

0.5. Significantly, the JPDF overlaps with the upper uphill diffusion region. This result clearly shows that Soret-induced uphill diffusion occurs at y^+=10. Soret-induced uphill diffusion inevitably makes Fick's law invalid for the species-mass diffusion for binary-species systems, and the similarity law between the thermal and species-mass diffusions also becomes invalid. At y^+=30 and 50, the JPDFs show that the regions of significant values are located near the null axis of the $J_{sor,y}$ because the temperature gradient decreases further away from the wall. As $J_{sor,y}$ becomes smaller, Soret-induced uphill diffusion occurs less frequently. In addition, when $J_{sor,y}$ is sufficiently small to be negligible, the mass flux $J_{\alpha,y}$ in a binary-species flow can be approximated as Fick's law and the similarity law between the mass and thermal diffusions is recovered. A quadrant analysis [i] shows that parcels of small CH_4-concentration near the wall are ejected by a Q2 motion. The ejected parcels mix with the surrounding fluid having a larger CH_4 concentration, and the CH_4 concentration of these parcels would tend to increase due to the molecular diffusion. However, the Soret effect flux opposes molecular species-mass diffusion due to the high temperature gradient near the wall and reduces the total species-mass flux. Therefore, the ejected fluid maintains a small CH_4 concentration. The fluid parcel related to the Q3 motion comes from the formerly ejected parcel, and thus this fluid parcel maintains small CH_4. When the small CH_4-concentration parcel is pushed back towards the wall, it generates the large negative flux contribution. The opposite occurs for the Q4 sweep and Q1 motion. Thus, parcels having small species-concentration tend to be trapped near the wall. We have thus found a new effect – Soret-induced uphill diffusion – which may trap chemical species near the wall, and these chemical species could be responsible for soot formation.

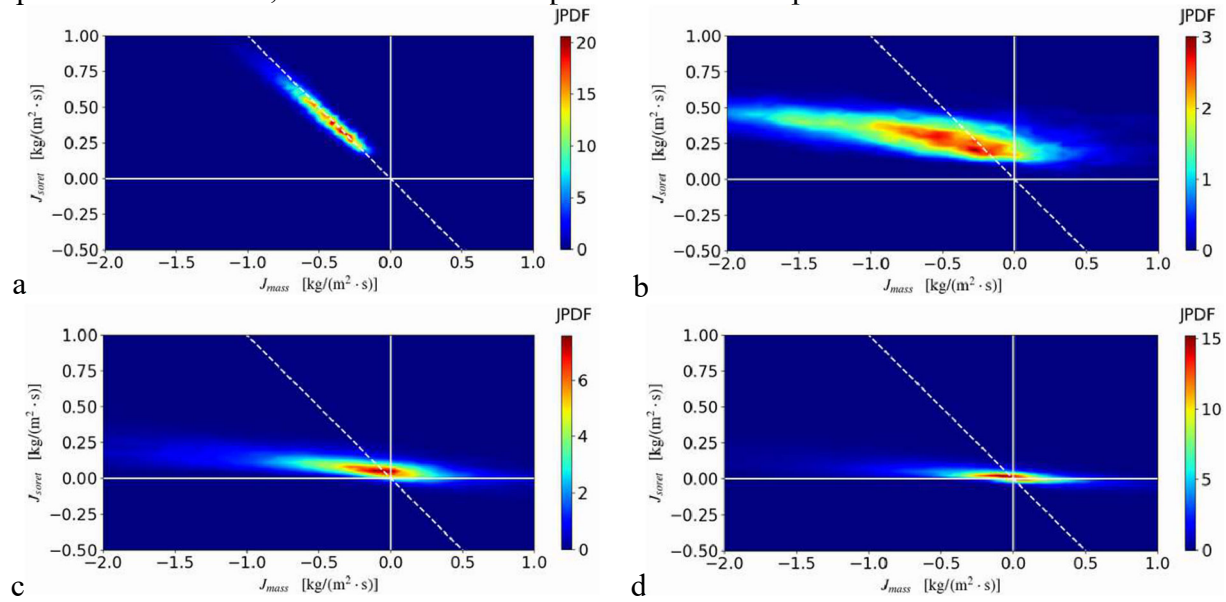

Figure 3. Joint probability density function of $J_{mol,y}$ and $J_{sor,y}$ for a N_2-CH_4 boundary layer at 60 atm where the wall temperature is 300 K and the free stream fluid temperature is 600 K: (a) at y^+=0.3, (b) y^+=10, (c) y^+=30 and (d) y^+=50. The solid white lines are null axes, and the white dashed line is given by $J_{sor,y} = -J_{mol,y}$.

III. References

i. Wallace, J. M., Eckelmann, H., Brodkey, R. S.. *J. Fluid Mech.* **1972** *54* 39.

IV. Publications and presentations supported by this project (only 2017- 2021 are listed)

[1] Bellan, J., Direct Numerical Simulation of a high-pressure turbulent reacting mixing layer, *Combust. Flame,* 176, 245-262, 2017

[2] Gnanaskandan, A.; Bellan, J., Numerical Simulation of jet injection and species mixing under high-pressure conditions, *Journal of Physics*, Institute of Physics Conference Series: Materials Science and Engineering, 821, 012020, 2017
[3] Bellan, J., Evaluation of mixture-fraction-based turbulent-reaction-rate model assumptions for high-pressure reactive flows, *Combust. Flame,* 179, 253-266, 2017
[4] Gnanaskandan, A.; Bellan, J., Side-jet effects in high-pressure turbulent flows: Direct Numerical Simulation of nitrogen injected into carbon dioxide, *J. Supercritical Fluids*, 140, 165-181, 2018
[5] Sciacovelli, L.; Bellan, J., The influence of the chemical composition representation according to the number of species during mixing in high-pressure turbulent flows, *Journal of Fluid Mechanics*, 863, 293-340, 2019
[6] Devaud, C.; Bushe, W.K; and J. Bellan, J., The modeling of the turbulent reaction rate under high-pressure conditions: *a priori* evaluation of the Conditional Source-term Estimate concept, *Combustion and Flame*, 207, 205–221, 2019
[7] Gnanaskandan, A.; Bellan, J., Large Eddy Simulations of high pressure jets : Effect of subgrid scale modeling, Chapter 11, 461-481, *AIAA Progress Series* book titled *High Pressure Flows for Propulsion Applications* (Ed. J. Bellan), 2020
[8] Bushe, W.K.; Devaud, C.; Bellan, J., Turbulent high-pressure reaction-rate modelling using the Double-conditioned Conditional Source-term Estimation method: a priori investigation of modelling elements and numerical aspects, *Combustion and Flame,* 217, 131-151, 2020
[9] Toki, T.; Bellan, J. Investigation of species-mass diffusion in binary-species boundary layers at high pressure using direct numerical simulations, submitted.
[10] Bellan, J., Modeling and numerical simulations of multi-species high-pressure reactive flows, **Invited Plenary Lecture**, Summer Program of the SFBTRR40, Institute of Aerodynamics and Fluid Mechanics Technische Universität München, Garching, Germany, August 3, 2015
[11] Bellan, J., Modeling and numerical simulations of multi-species high-pressure reactive flows, **Invited Seminar**, Purdue University, West Lafayette, IN., October 22, 2015
[12] Bellan, J., Reduced models for the simulation of multi-scale problems in physics and chemistry, **Invited Seminar**, Cornell University, Ithaca, NY., November 17, 2015
[13] Bellan, J., Modeling and Numerical Simulations of Multi-Species High-Pressure Turbulent Mixing and Combustion, **Invited Seminar,** SpaceX, Hawthorne, CA., 12/14/2016
[14] Gnanaskandan, A.; Bellan, J., Large Eddy Simulations of high pressure jets: Effect of subgrid scale modeling, paper 2017-1105 presented at the 55th Aerospace Sciences Meeting, Grapevine, TX, January 9-13, 2017
[15] Sciacovelli, L.; Bellan, J., Mixing in high pressure flows: the influence of the number of species, paper 2018-1189, presented at the 56th Aerospace Sciences Meeting, Kissimmee, FL., January 8-12, 2018
[16] Devaud, C.; Bushe, W.K.; Bellan, J., Assessment of Conditional Source-term Estimation for High-Pressure Turbulent Combustion Modeling, presented at SciTech 2019, January 7-11, 2019, San Diego, FL; also presented at the 11th US. National Meeting of the Combustion Institute, March 24-27, 2019, Pasadena, CA.
[17] Banuti, D.; Bellan, J., Influence of the real-gas equation-of-state binary interaction coefficients on the turbulent mixing of many species at diesel-engine high-pressure conditions, presented at the 11th US. National Meeting of the Combustion Institute, March 24-27, 2019, Pasadena, CA
[18] Bushe, W.K.; Devaud, C.; Bellan, J., Turbulent high-pressure reaction rate modeling using the Double-conditioned Conditional Source-term Estimation method, paper AIAA-2020-1153 presented at SciTech 2020, January 6-10, Orlando, Fl.
[19] Banuti, D.; Bellan, J., Inter-species molecular attraction effect in the development of a two-species mixing layer, paper 2020-1155 presented at SciTech 2020, January 6-10, Orlando, Fl.
[20] Toki, T.; Bellan, J. Direct numerical simulation of single-species and binary-species boundary layers at high pressure, paper 2021-0682 presented at SciTech 2021, January 11–15 & 19–21, 2021, virtual meeting.

Chemical Kinetic Data of Benchmark Accuracy through Multi-Scale Informatics Strategies

Michael P. Burke

Department of Mechanical Engineering, Department of Chemical Engineering, & Data Science Institute
Columbia University, New York, NY 10027
mpburke@columbia.edu

Program Scope

The reliability of predictive simulations for advanced energy conversion devices depends on the availability of accurate data for thermochemistry, chemical kinetics, and transport. In that regard, accurate data are critically important for both their direct use in predictive simulations and for benchmarking improved theoretical methodologies that can similarly produce accurate data for predictive simulations. The use of informatics-based strategies for the determination of accurate thermochemical data with well-defined uncertainties, i.e. the Active Thermochemical Tables (ATcT),[1] has revolutionized the field of thermochemistry – ATcT provides thermochemical data of unprecedented accuracy for direct use in predictive simulation and has served as a key enabler of *ab initio* electronic structure methodologies of equally impressive accuracy. The goal of this program is to develop an active database for chemical kinetics, akin to that for thermochemistry, to establish high-accuracy kinetic data for predictive simulation and to evaluate emerging *ab initio*-based theoretical kinetics methods, using our multi-scale informatics approach. We are particularly interested in reaction systems where non-thermal kinetic sequences arise and/or where combining theoretical and experimental data is necessary to unravel complex reaction data into chemical information.

Recent Progress

There are several significant challenges in deriving high-accuracy kinetic data of relevance to the complex reactions encountered in combustion, planetary atmospheres, and interstellar environments. First, even the most "direct" experimental rate constant determinations are often influenced by uncertainties in secondary reactions – leading to a complex web of interdependences among kinetic parameters for many reactions (and an opportunity to gain more information than has been attained previously, since uncertainties are seldom at the noise floor of the measurements). Second, there is rarely enough experimental data to constrain the full temperature, pressure, and composition ($T/P/\underline{X}$) dependence of many rate constants – rendering usual rate-parameter-based uncertainty quantification approaches ineffective. Third, many reactions of interest to various application domains and gas-phase theoretical chemistry involve non-thermal kinetic sequences[1-7,iv] – posing an additional problem for rate-parameter-based approaches.

During the past several years, we have been developing a multi-scale uncertainty quantification approach, MultiScale Informatics (MSI),[8-10,i-ii] to address the challenges involved in 1) unraveling the complex web of interdependences among reactions in complex systems data (by reinterpreting the raw data from multi-reaction systems used to determine rate constants experimentally), 2) sufficiently constraining the $T/P/\underline{X}$ dependence of rate constants (by incorporating theoretical calculations to extrapolate constraints imposed by limited data), and 3) analyzing data from reaction systems involving non-thermal kinetic sequences (by leveraging the physics-based framework to account for such processes). In this program, we are applying and expanding MSI to develop a high-accuracy kinetics database through carefully chosen reaction systems that serve to both anchor the database and grow it in ways leveraging its anchored foundations.

$CH_3 + HO_2 = products$. Our analysis of the $CH_3 + HO_2$ reaction,[i,ii] which leveraged our earlier MSI model of the H_2O_2 decomposition system,[8,10] had served to expand the MSI database to include an important

reaction to combustion and to interpretations of experimental data for other reactions. A key feature of this analysis was the inclusion of the *raw* experimental data previously used to derive rate constants – to enable MSI to identify alternative interpretations of the data that are consistent with all other data. Indeed, the resulting MSI model was consistent with both theoretical calculations[11] and the *raw* experimental data[12,13] for $CH_3 + HO_2$. By contrast, rate-parameter-based UQ[14] derives a temperature dependence inconsistent with *ab initio* theory – demonstrating the advantages of including theory directly within the UQ approach.[ii]

$HO_2 + HO_2$ = products. For several decades, OH + $HO_2 = H_2O + O_2$ (R1) and $HO_2 + HO_2 = H_2O_2 + O_2$ (R2) had been topics of significant attention and, frequently, debate. For both reactions, early experimental determinations suggested unusually deep minima at 1000-1200 K followed by a sharp rise with increasing temperature.[15-16] In 2013, our MSI analysis[8] of previous data and multi-species measurements of shock-heated H_2O_2 decomposition by Hong et al.[17] both yielded rate constants with a local minimum, albeit with much milder temperature dependence, thereby resolving the previous apparent anomalies – at least for R1. For R2, the determinations by Hong et al.[17] instead supported the earlier interpretations.[15-16]

Recent theory calculations[18-19] reveal consistent values at lower intermediate temperatures but instead show a milder temperature dependence – suggesting that inconsistencies among theoretical and experimental data still remain for R2. Furthermore, calculations of Klippenstein et al.[19] indicate a previously unknown channel $HO_2 + HO_2 = OH + OH + O_2$ (R3), which may confound all earlier analyses, and likewise reveal additional theory uncertainties of relevance.

Our present MSI results[iii] (in blue in Figs. 1-2) indicate that the theoretical calculations for R2 and R3 near their nominal values (in red in Fig. 1) exhibit no systematic inconsistencies with the *raw* experimental data, including at the lowest and highest experimental temperatures of Hong et al.[17] (e.g. Fig. 2), despite the apparent disagreement among reported rate constants.

$H + O_2 = OH + O$, $OH + H_2 = H_2O + H$, $O + H_2 = OH + O$. We have continued analysis on these three (commonly entangled) chain-branching/carrying reactions important to combustion. This MSI analysis has made use of a procedure (similar in spirit to that of Najm and co-workers[20]) for simulating the raw data from experimental studies, where the raw data were not reported, from information reported in those studies. Our results thus far suggest the importance of rate constants for H + HO_2 reactions and we have therefore been investigating these sets of reactions simultaneously.

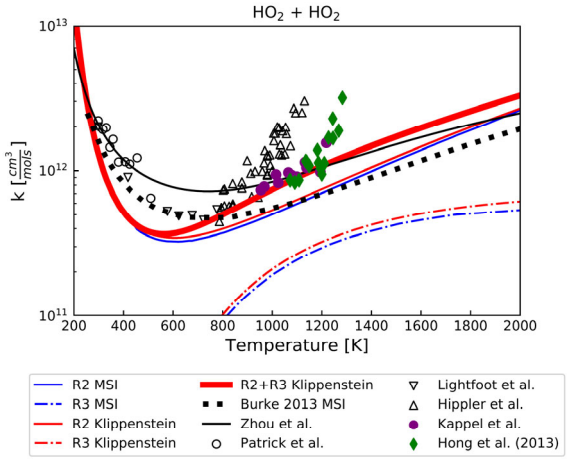

Fig. 1. Rate constants for $HO_2 + HO_2$ (R2, R3). Lines represent prior model rate constants (from Klippenstein et al.[19]) and MSI model rate constants. Symbols represent experimental determinations.[8,15-17] Solid symbols represent experimental determinations[16,17] for which the MSI model reproduces the *raw* experimental data[16,17] (e.g. see Fig. 2) with the MSI rate constants.

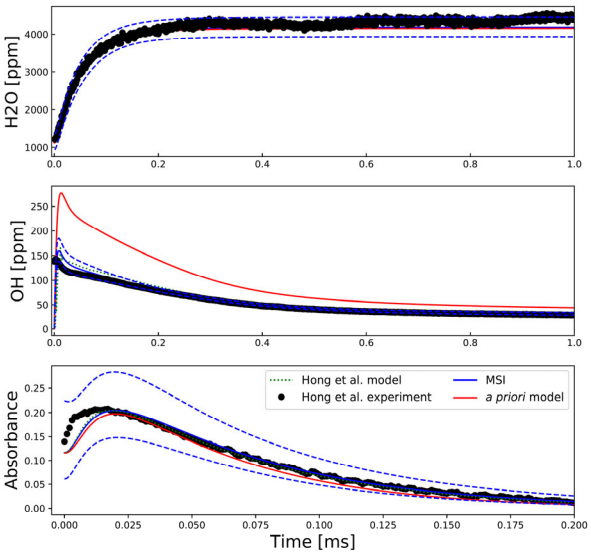

Fig. 2. Time profiles for H_2O, OH, and absorbance at 227 nm in shock-heated $H_2O_2/H_2O/O_2/Ar$ mixtures near 1283 K and 1.635 atm. Symbols denote experimental data from Hong et al.;[17] lines denote the original model interpretations of Hong et al.[17] and predictions of the prior and MSI models.

H + HO₂ = products. Our early results for the two main product channels in the H + HO_2 reaction are shown in Fig. 3, which compares rate constants from various experimental determinations, *a priori* theoretical calculations, MSI model predictions, and a previous (static) evaluation by Baulch et al. For context, Baldwin and Walker derived values for the H + HO_2 reaction rate constants at 773 K using experimentally determined ratios of rate constants for H + HO_2 relative to H + O_2 = OH + O and HO_2 + HO_2 = H_2O_2 + O_2 along with contemporary rate constant values for the latter two reactions in 1979. In 2005, Baulch et al. recommended a rate constant expression based on the values reported in the experimental studies at 298 and 773 K and assigned uncertainties of a factor of two. However, later theoretical calculations suggest rate constants that are lower by a factor of four or more (outside the error bounds from the previous evaluation). The predicted rate constants with the MSI model, which agree quite closely with the 298 K determinations and the deduced ratios (rather than the originally derived H + HO_2 rate constants) at 773 K, are also consistent with the theoretical calculations. For reference, Fig. 3 also shows the H + HO_2 rate constants determined if the experimentally derived ratios at 773 K are reinterpreted using the MSI model rate constants for H + O_2 = OH + O and HO_2 + HO_2.

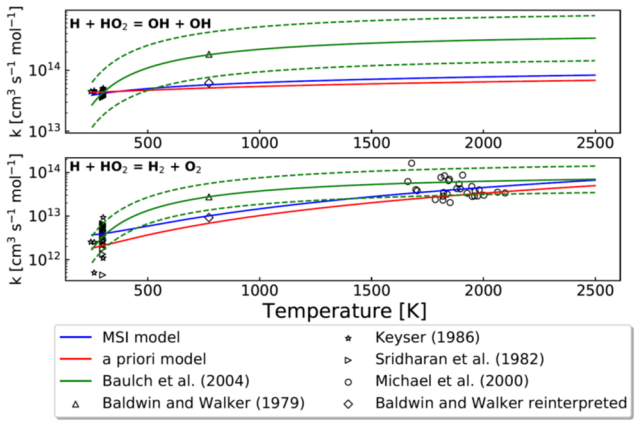

Fig. 3. Rate constants for H + HO_2 as discussed in the text.

Methodological improvements. We have also written a general-purpose wrapper for the MESS code for automated calculations of non-Boltzmann sequences spanning multiple potential energy surfaces.[iv,v] Our current automated procedure[iv,v] goes beyond previous procedures[6] for calculating rate constants for non-equilibrium kinetic sequences by (1) accounting for the energy contributed by co-reactants, (2) accounting for the energy dependence of the bimolecular rates, (3) accounting for prompt bimolecular reactions and isomerizations of rovibrationally excited fragments in bimolecular product channels, (4) reordering the implementation steps to enable recursive application to an arbitrary number of potential energy surfaces, and (5) automating the entire workflow from coupled master equations to phenomenological kinetic modeling. Altogether, the code enables rate constant calculations for non-Boltzmann kinetic sequences spanning an arbitrary number of potential energy surfaces. An example sequence spanning three potential energy surfaces is shown in Fig. 4. Of note, this methodology enables automated rate constant calculations for chemically termolecular reactions and prompt dissociation reactions as well as more complex non-Boltzmann kinetic sequences involving yet-to-be-studied phenomena such as higher order chemical reactions (with more than 3 reactants, e.g. A + B + $X^{(2)}$ + $X^{(3)}$ in Fig. 4) and prompt bimolecular reactions of rovibrationally excited fragments in bimolecular product channels (e.g. $P_{2,1}^{(2)*}$ + $X^{(3)}$ in Fig. 4).

We have been interacting with the Automech team led by Stephen Klippenstein to integrate this procedure into their suite of automated theoretical kinetics calculation codes. We are also now integrating it into MSI for rigorous evaluations of data from reaction systems involving non-equilibrium kinetic sequences, which will be important to

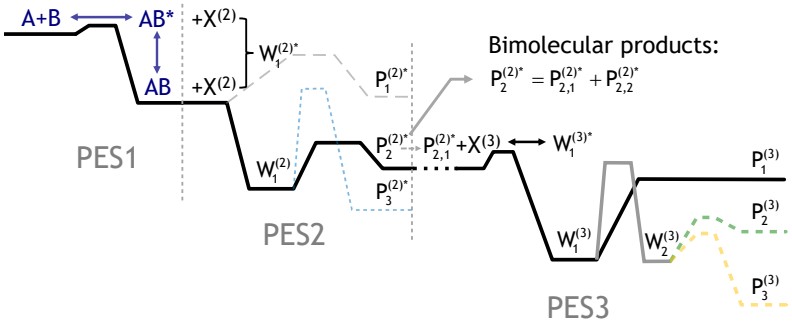

Fig. 4. An example of a non-Boltzmann kinetic sequence spanning three distinct potential energy surfaces (PES1, PES2, PES3).

understanding of and testing methodologies for non-equilibrium kinetics.

Future Plans

We plan to complete our analyses of $HO_2 + HO_2$, $H + O_2 = OH + O$, $OH + H_2 = H + H_2O$, and $O + H_2 = H + OH$, and $H + HO_2$ = products (discussed above) and continue venturing into less characterized and difficult-to-isolate subsystems, such as those involving CH_3, CH_2OH, and HCO where the anchored database can be leveraged for the analysis, and associated non-equilibrium kinetic sequences, where the new capabilities above will be invaluable. Along the way, we plan to continue methodological improvements to the MSI approach that allow data for collisional energy transfer kernels, product energy distributions, microcanonical rate constants, and photolysis quantum yields, among others, to be included as targets. We anticipate that these data types will allow a greater degree of data redundancy and allow more rigorous evaluations of theoretical methodologies for calculating non-equilibrium kinetic sequences.

References

1. B. Ruscic, et al. *J Phys Chem A* 108 (2004) 9979–9997.
2. M.P. Burke, S.J. Klippenstein. *Nature Chemistry* 9 (2017) 1078-1082.
3. D.R. Glowacki, et al. *Science* 337 (2012) 1066.
4. N.J. Labbe, R. Sivaramakrishnan, C.F. Goldsmith, Y. Georgievskii, J.A. Miller, S.J. Klippenstein. *J. Phys. Chem. Lett.* 7 (2015) 85–89.
5. M.C. Barbet, K. McCullough, M.P. Burke. *Proc Combust Inst* 37 (2019) 347-354.
6. M.P. Burke, C.F. Goldsmith, Y. Georgievskii, S.J. Klippenstein. *Proc Combust Inst* 35 (2015) 205–213.
7. R.E. Cornell, M.C. Barbet, M.P. Burke. *Proc Combust Inst* 38 (2021) 787-794.
8. M.P. Burke, S.J. Klippenstein, and L.B. Harding. *Proc Combust Inst* 34 (2013) 547–555.
9. M.P. Burke, et al. *J Phys Chem A* 119 (2015) 7095–7115.
10. M.P. Burke. *International Journal of Chemical Kinetics* 48 (2016) 212–235.
11. A.W. Jasper, S.J. Klippenstein, L.B. Harding. *Proc Combust Inst* 32 (2009) 279–286.
12. Z. Hong, D.F. Davidson, K.-Y. Lam, R.K. Hanson. *Combust Flame* 159 (2012) 3007–3013.
13. N.K. Srinivasan, J.V. Michael, L.B. Harding, S.J. Klippenstein. *Combust Flame* 149 (2007) 104–111.
14. C. Olm, T. Varga , É. Valkó, H.J. Curran , T. Turányi. *Combust Flame* 186 (2017) 45–64.
15. H. Hippler, H. Neunaber, J. Troe. *J Chem Phys* 103 (1995) 3510–3516.
16. C. Kappel, K. Luther, J. Troe. *Phys Chem Chem Phys* 4 (2002) 4392–4398.
17. Z. Hong, K.-Y. Lam, R. Sur, S. Wang, D.F. Davidson, R.K. Hanson. *Proc Combust Inst* 34 (2013) 565–571.
18. D. D. Zhou, K. Han, P. Zhang, L. B. Harding, M. J. Davis, R. T. Skodje. *J Phys Chem A* 116 (2012) 2089–2100.
19. S. J. Klippenstein, et al. 11th U.S. National Combustion Meeting (2019).
20. M. Khalil, H.N. Najm. *Combust Theor Model* 22 (2018) 635–665.
21. Y. Georgievski, J.A. Miller, M.P. Burke, S.J. Klippenstein. *J Phys Chem A* 117 (2013) 12146-12154.
22. S.N. Elliott, K.B. Moore III, A.V. Copan, M. Keçeli, C. Cavallotti, Y. Georgievskii, H.F. Schaefer III, S.J. Klippenstein. *Proc Combust Inst* 38 (2021) 375-384.

BES-supported products (9/2018-present)

i. C.E. LaGrotta, M.C. Barbet, L. Lei, M.P. Burke, "Towards a High-Accuracy Kinetic Database Informed by Theoretical and Experimental Data," 11th U.S. National Combustion Meeting, March 2019, Pasadena, CA.

ii. C.E. LaGrotta, M.C. Barbet, L. Lei, M.P. Burke, "Towards a High-Accuracy Kinetic Database Informed by Theoretical and Experimental Data: $CH_3 + HO_2$ as a Case Study," *Proceedings of the Combustion Institute* 38 (2021) 1043-1051.

iii. C.E. LaGrotta, L. Lei, M.C. Barbet, Z. Hong, D.F. Davidson, R.K. Hanson, M.P. Burke, "Towards Resolution of Lingering Discrepancies in the H_2O_2 Decomposition System: $HO_2 + HO_2$," 12th U.S. National Combustion Meeting, College Station, Texas, May 2021 (virtual).

iv. L. Lei, M.P. Burke, "An Extended Methodology for Automated Calculations of Non-Boltzmann Kinetic Sequences: $H + C_2H_2 + X$ and Combustion Impact," *Proceedings of the Combustion Institute* 38 (2021) 661-669.

v. L. Lei, M.P. Burke. AutoNonBoltzmann: A Code for Automated Calculations of Non-Boltzmann Kinetic Sequences.

Kinetics and Mechanisms of Gas-Phase Reactions towards Gas-Particle Interconversion

Rebecca L. Caravan
Chemical Sciences and Engineering Division
Argonne National Laboratory
Lemont, IL 60439
caravarl@anl.gov

Program Scope

I am developing a new experimental program to study the kinetics and mechanisms of gas-phase reactions involving reactive intermediate species. Experiments will interrogate the reactivity of zwitterions and radical intermediates to understand the different roles that they play in phenomena such as gas-particle transformations in complex environments, including Earth's troposphere. Through synergistic collaborations with theoreticians the influence of, for example, zwitterion vs. radical character and chemical structure on reactivity will be explored for potential molecular-weight growth reactions. This will deduce the chemical physics driving gas-particle interconversion, and ultimately it will aid the development and validation of predictive capabilities. Interdisciplinary collaborations will address the wider implications of our work, answering questions that are both interesting at a fundamental level and that have broader implications.

Recent Progress

Laboratory renovations, experimental design and development

Over the last year, renovations of a new laser laboratory at Argonne have been ongoing with Tranter and are now in the final stages. Design and development of the first experimental apparatus that I will construct to address my research objectives is also well underway. This new capability — a broadband UV-Visible time-resolved absorption experiment — will facilitate kinetics and mechanistic studies using multiplexed species detection over a broad range of temperatures and pressures, with sub-millisecond time-resolution. This technique has been demonstrated to be a versatile and powerful approach for kinetics studies of reactive intermediates — and my new experimental setup incorporates elements from the recent successful designs of Sheps[1] and other groups[2] worldwide. The critical components for this setup have been designed and selected and are in the process of being ordered and delivered to the laboratory.

Four-carbon, resonance-stabilized Criegee intermediate chemistry

I have continued investigations of four-carbon, unsaturated Criegee intermediate reactivity with Klippenstein, Lester, Osborn, Taatjes, and our collaborators in the atmospheric chemistry community (Percival, NASA JPL and Shallcross U. Bristol). Previously, we conducted the first direct kinetic study of the *syn* conformer of methyl vinyl ketone oxide (MVK-oxide). MVK-oxide is a four-carbon, resonance stabilized Criegee intermediate formed from the ozonolysis of isoprene and is the most abundant Criegee intermediate in Earth's troposphere. Our experimental and high-level theoretical work demonstrated that, in contrast with smaller non-conjugated Criegee intermediates, the *syn* conformer of MVK oxide reacts very slowly with water, and thus will survive high humidity regions of Earth's troposphere. Other bimolecular reactions of MVK-oxide, including those postulated to play a role in gas-particle interconversion (e.g. with SO_2, organic acids), are thus able to compete in this complex environment.

We have built on our earlier work to explore the mechanisms operating in the fast reaction of MVK-oxide with formic acid. Reactions of Criegee intermediates with organic acids are a potential initial step in tropospheric gas-particle interconversion via the formation of higher molecular weight, lower volatility reaction products.[3] Using a combination of photoionization mass spectrometry and high-level theory, we identify two reaction pathways in operation for MVK-oxide + formic acid. The major pathway is operative for both *syn* and *anti* conformers of MVK-oxide: 1,4 insertion of MVK-oxide into the acid, leading to a

higher molecular weight, functionalized hydroperoxide reaction product. A second minor channel is operative for only the *syn* conformer: acid-catalyzed isomerization to a vinyl hydroperoxide species that proceeds via H-atom transfer between the acid and MVK-oxide to regenerate formic acid. In addition to characterizing the major reaction product, we capture the photoionization spectrum of the minor reaction product using deuterated formic acid.

Following the development of a new method for direct production by the Lester group,[4] we have begun investigations on the reactivity of methacrolein oxide (MACR-oxide) – the other four-carbon, resonance stabilized Criegee intermediate derived from isoprene. Through high-level theory and photoionization mass spectrometry, we observed and identified the formation of a functionalized hydroperoxide species from the reaction of MACR-oxide with formic acid via a comparable 1,4 insertion mechanism determined for MVK-oxide and smaller Criegee intermediates. Comparison of the reaction energetics for *anti*-MACR-oxide and *syn*-MVK-oxide undergoing reaction with formic acid (Fig. 1) indicated that H-bonding interactions between the terminal Criegee intermediate oxygen and the adjacent methyl group are present in *syn*-MVK-oxide that appear to influence the reaction profile. Disruption of the H-bonding interactions, in addition to steric effects from the methyl group, result in an increased barrier to reaction with formic acid, compared with *anti*-MACR-oxide. Reaction of both MVK-oxide and MACR-oxide with formic acid are highly energetically favorable, thus it is not anticipated these effects will result in significantly different rate coefficients. However, for systems that typically have larger barriers (e.g. SO_2, water), it is expected this could result could lead to more significant differences in reaction rate coefficients for these structurally similar Criegee intermediates.

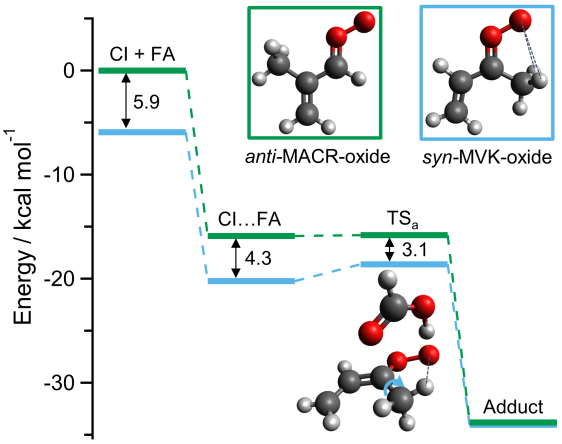

Fig. 1. Reaction coordinate comparing the absolute energies for the reaction of formic acid with *anti-trans*-MACR-oxide (green) and *syn-trans*-MVK-oxide (blue) calculated at the CCSD(T)-F12/TZF level of theory.

Oligomerization of Criegee intermediates

With Hansen, Jasper, Klippenstein, Taatjes, Osborn, and our collaborators in the atmospheric chemistry community, we have used direct and steady-state experiments and high-level theory to verify that Criegee intermediate oligomerization reactions are operative in Earth's troposphere (Fig. 2). Mass spectrometric measurements (led by Percival, NASA JPL) of the Amazonian troposphere revealed signatures, in both gas and aerosol phases, of products resulting from the sequential insertion of the CH_2OO Criegee intermediate into formic acid leading to the production of functionalized hydroperoxide reaction products. This sequence results in reaction products with sequentially higher molecular weight and lower volatility, thus has previously been proposed to contribute to atmospheric aerosol formation. Using tunable synchrotron VUV photoionization mass spectrometry, we investigated the kinetics and mechanism of the proposed reaction sequence using steady-state alkene ozonolysis experiments and direct, time-resolved Criegee intermediate experiments. Common mass spectrometric signatures in the Amazon field measurements and steady-state laboratory experiments support alkene ozonolysis as the source of the tropospheric reaction sequence. Common spectroscopic signatures and mass spectrometric features in the steady-state and direct experiments confirmed the central role of Criegee intermediates in driving this sequence. High-level theoretical work pinpointed energetically and kinetically viable reaction pathways for this potential aerosol-forming pathway that support and connect the laboratory and field measurements. Modeling work (led by Shallcross, U. Bristol) highlight that the role of Criegee intermediates in complex environments such as Earth's troposphere are currently underestimated.

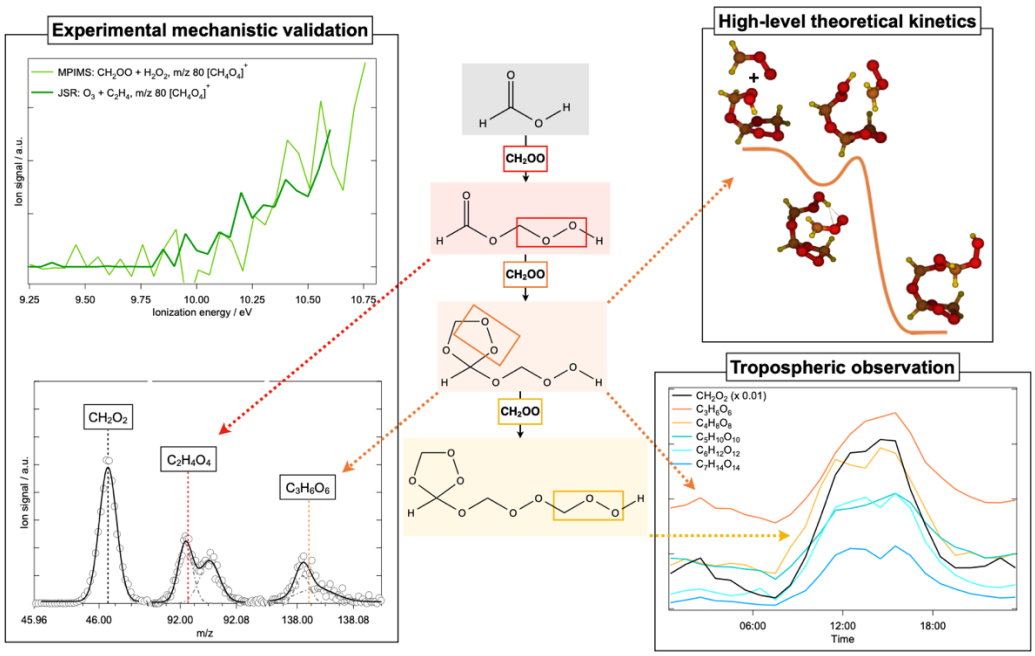

Fig. 2. Direct and steady state experiments combined with high-level theory have been utilized to validate observation of sequential Criegee intermediate insertion into formic acid in the Amazon troposphere.

Future Directions

Capability development

Final laboratory renovations will be completed for the new laser laboratory with Tranter. Construction and testing of the new broadband UV-Visible time-resolved absorption experiment will commence, after which the experiment will be utilized for kinetic and spectroscopic studies of Criegee intermediates and peroxy radicals, to support the research goals of this program.

Criegee intermediate reactivity

Investigations of Criegee intermediate reactivity will continue with Klippenstein, Lester, Osborn, Taatjes, and our collaborators outside the program, with particular focus on the influence of functional group and Criegee intermediate conjugation on reactions implicated in gas-particle interconversion. This ongoing collaboration that brings together experimental work at the Advanced Light Source and high-level theoretical kinetics will be strengthened and complemented by new insights from tabletop work at Argonne using the broadband UV-Visible time-resolved absorption experiment.

Peroxy radical-Criegee intermediate interconversion

Wilson and I are initiating direct gas-phase studies to interrogate the mechanisms operating in the facile interconversion of RO_2 to Criegee intermediates – a process observed in heterogenous environments by the groups of Beauchamp and Wilson.[5,6] Tabletop experiments at Argonne will be complemented by investigations at the Advanced Light Source in collaboration with Osborn and Taatjes.

Highly oxygenated reaction products from peroxy radical reactions

The formation of higher molecular weight, highly oxygenated, lower volatility reaction products from reactions of peroxy radicals (e.g. with OH) will be investigated with Sheps. Building on our earlier work on the reaction of OH with CH_3O_2 in which we observed the pressure-dependent stabilization of the highly oxygenated, higher molecular weight trioxide (CH_3OOOH),[7] we will explore the influence of functional group on the formation on reaction product branching, and the potential of these reactions to contribute to gas-particle interconversion.

DOE Supported Publications 2020-

1. R. L. Caravan, M. F. Vansco & M. I. Lester, Open questions on the reactivity of Criegee intermediates, *Communications Chemistry*, 2021, **4**, 44.
2. M. F. Vansco, R. L. Caravan, S. Pandit, K. Zuraski, F. A. F. Winiberg, K. Au, T. Bhagde, N. Trongsiriwat, P. J. Walsh, D. L. Osborn, C. J. Percival, S. J. Klippenstein, C. A. Taatjes & M. I. Lester, Formic acid catalyzed isomerization and adduct formation of an isoprene-derived Criegee intermediate: experiment and theory, *Physical Chemistry Chemical Physics*, 2020, **22**, 26796-26805.
3. R. L. Caravan, M. F. Vansco, K. Au, M. A. H. Khan, Y.-L. Li, F. A. F. Winiberg, K. Zuraski, Y.-H. Lin, W. Chao, N. Trongsiriwat, P. J. Walsh, D. L. Osborn, C. J. Percival, J. Jr-Min Lin, D. E. Shallcross, L. Sheps, S. J. Klippenstein, C. A. Taatjes & M. I. Lester, Direct kinetic measurements and theoretical predictions of an isoprene-derived Criegee intermediate, *Proceedings of the National Academy of Sciences*, 2020, **117** (18), 9733-9740.
4. M. F. Vansco, R. L. Caravan, K. Zuraski, F. A. F. Winiberg, K. Au, N. Trongsiriwat, P. J. Walsh, D. L. Osborn, C. J. Percival, M. A. H. Khan, D. E. Shallcross, C. A. Taatjes & M. I. Lester, Experimental evidence of dioxole unimolecular decay pathway for isoprene-derived Criegee intermediates, *Journal of Physical Chemistry A*, 2020, **124** (18), 3542-3554.

References

1. L. Sheps & D. W. Chandler, Time-resolved broadband cavity-enhanced absorption spectroscopy for chemical kinetics, SAND2013-2663, *Sandia National Laboratories*, 2013.
2. T. Lewis, D. E. Heard & M. A. Blitz, A novel multiplex absorption spectrometer for time-resolved studies, *Review of Scientific Instruments*, **89**, 024101 (2018).
3. Y. Sakamoto, S. Inomata & J. Hirokawa, *Journal of Physical Chemistry A*, **117**(48), 12912-12921 (2013).
4. M. F. Vansco, B. Marchetti, N. Trongsiriwat, G. Wang, T. Bhagde, P. J. Walsh, S. J. Klippenstein, & M. I. Lester, Synthesis, electronic spectroscopy and photochemistry of methacrolein oxide: A four carbon unsaturated Criegee intermediate from isoprene ozonolysis. *Journal of the American Chemical Society* **141**, 15058-15069 (2019
5. M. Zeng, N. Heine & K. R. Wilson, *Proceedings of the National Academy of Sciences*, **117(9)**, 4486-4490, 2020.
6. X. Zhang, K. M. Barraza, J. L. Beauchamp, Cholesterol provides nonsacrificial protection of membrane lipids from chemical damage at air–water interface. *Proceedings of the National Academy of Sciences* **115**, 3255-3260 (2018).
7. R. L. Caravan, M. A. H. Khan, J. Zádor, L. Sheps, I. O. Antonov, B. Rotavera, K. Ramasesha, K. Au, M.-W. Chen, D. Rösch, D. L. Osborn, C. Fittschen, C. Schoemaecker, M. Duncianu, A. Grira, S. Dusanter, A. Tomas, C. J. Percival, D. E. Shallcross & C. A. Taatjes, The reaction of hydroxyl and methylperoxy radicals is not a major source of atmospheric methanol. *Nature Communications* **9**, 4343 (2018)

Dynamics and Energetics of Elementary Combustion Reactions and Transient Species
Grant DE-FG03-98ER14879

Robert E. Continetti (rcontinetti@ucsd.edu)
Department of Chemistry and Biochemistry, University of California San Diego
9500 Gilman Drive, La Jolla, CA 92093-0340

I. Program Scope

This research program obtains experimental results that benchmark fundamental advances in the theoretical understanding of chemical reactions, including the development of accurate potential energy surfaces (PESs) and computational studies of the dynamics of chemical reactions. The primary focus has been on the bimolecular reactions of the hydroxyl radical,[1] the fluorine atom,[2] and oxygenated carbon radicals.[3, 4] This experimental program, often in collaboration with leading theoretical groups, has provided benchmark information on the potential energy surfaces and dynamics of important combustion systems (HOCO) and elementary reactions (F+H_2O), as well as insights into the photochemistry of negative ions, anion resonances and vibrational Feshbach resonances in neutral reactions. The program is supported by a photoelectron-photofragment coincidence (PPC) spectrometer that is equipped with a cryogenic octopole accumulator trap (COAT) that allows the preparation of anions thermalized below 20K,[5] as well as an electrostatic ion beam trap (EIBT),[6] where the PPC measurement is carried out, allowing the detection of photoelectrons, stable photoneutrals, and photofragments in coincidence. These data provide kinematically complete measurements of energy partitioning in reactions induced by photodetachment of precursor anions. During the last year, we have focused on studies that make use of the photodetachment of precursor anion complexes to probe the dynamics on the potential energy surface of hydroxyl radical reactions: $OH^-(C_2H_4)$ and the $OH + C_2H_4 \rightarrow H_2O + C_2H_3$ reaction and $CH_3O^-(H_2O)$ and the $OH + CH_3OH \rightarrow H_2O + CH_3O$ reaction. Ongoing efforts also include characterization of the photodissociation of nitrogen oxide species $N_2O_2^-$ and peroxynitrite anion $ONOO^-$ in the near-UV, as well as a study of the dissociative photodetachment of the oxyallyl anion mediated by triplet-singlet intersystem crossing in the low-lying electronic states of the oxyallyl diradical, C_3H_4O. In the following sections, recent progress will be discussed in more detail, followed by a brief review of future work including a return to IR excitation experiments[7, 8] to study the excitation and isomerization of the HOCO system. The COVID-19 pandemic has had a material impact on progress owing to laboratory shutdowns and stress on the research team that will require a no-cost extension request to complete the work under this grant.

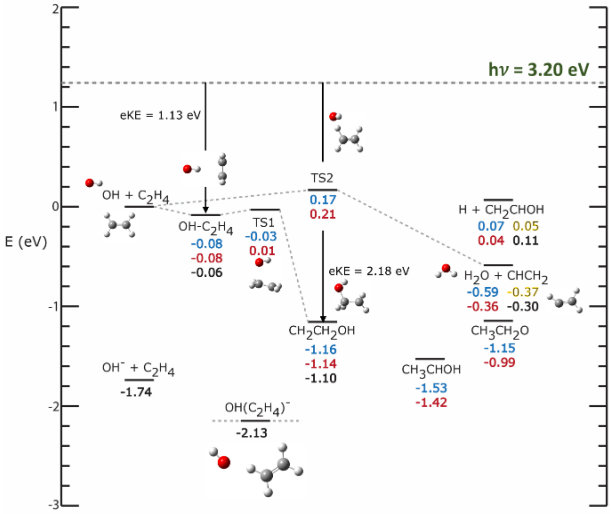

Figure 1. Energetics for the C_2H_5O system. All energies are in eV relative to the reactant asymptote $OH + C_2H_4$ with zero-point energy corrections. The energetics in blue and red correspond to previously reported theoretical values.[9,10] The values in yellow are from the Active Thermochemical Tables.[11] The energetics in black were computed in this study at the CCSD(T)/aug-cc-pVTZ level using MP2/aug-cc-pVDZ optimized geometries.

II. Recent Progress

Dissociative Photodetachment of $OH^-(C_2H_4)$ and the $OH + C_2H_4 \rightarrow H_2O + C_2H_3$ reaction

The hydroxyl radical plays a critical role in reactions involving volatile organic compounds in atmospheric and combustion processes. The reactions between OH and simple alkanes, alkenes, and alcohols have been particularly of interest in this program. A recent PPC spectroscopy study revealed key aspects of the dissociation dynamics of the OH-CH_4 system (DOE pub.4). We have now extended these studies to the OH-C_2H_4 system finding many similarities in spite of the substitution of the simple alkene for methane in the anion complex.

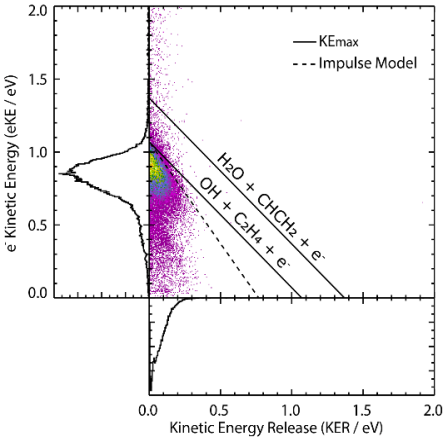

Figure 2. PPC spectrum for DPD of $OH^-(C_2H_4)$ at 3.20 eV photon energy. The KE_{max} and impulse model annotations correspond to the energetic limit for OH + C_2H_4 (v=0) + e^- channel. The KE_{max} for the H_2O + $CHCH_2$ + e^- channel is also labelled.

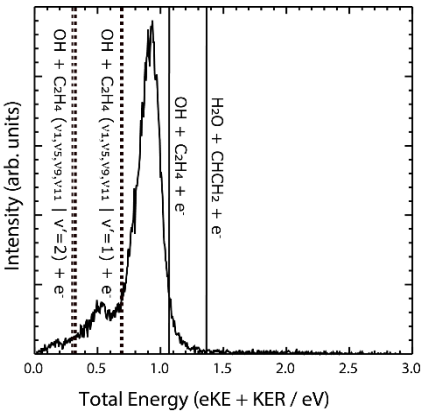

Figure 3. E_{TOT} spectrum for DPD of $OH^-(C_2H_4)$. The solid vertical lines at 1.07 and 1.37 eV correspond to KE_{max} for the OH + C_2H_4 + e^- and H_2O + $CHCH_2$ + e^- channels, respectively. The dashed vertical lines at ~0.7 and ~0.3 eV correspond to the one and two quanta of excitation, respectively, in one of the C-H stretching modes of ethylene.

PPC measurements carried out on $OH^-(C_2H_4)$ at a photon energy of 3.20 eV yielded stable, OH-C_2H_4 + e^-, and dissociative, OH + C_2H_4 + e^-, channels. The main channel formed was dissociation to the reactant channel as well as a minor channel with excitation in C-H stretching modes of C_2H_4. Similar to DPD of OH-CH_4, the weak repulsion between OH-C_2H_4 resulted in a low kinetic energy release (KER) of the dissociating fragments. The energetics diagram for this system is shown in **Figure 1**,[9-11] with the relevant energetics derived from the literature as noted in the caption. These energetics show that the OH^--C_2H_4 complex is bound by 0.06 eV more than OH^--CH_4, consistent with the increased polarizability of the electron-rich alkene. The PPC spectrum showing the correlation of electron kinetic energy (eKE) and kinetic energy release (KER) in the system is shown in **Figure 2**. The diagonal limit corresponding to formation of OH + C_2H_4 + e^- in the lowest internal states matches the data well, but it is notable that there is a deviation from the diagonal limit as KER increases. The dashed line in the figure shows that a simple impulsive model for this system, where the OH interaction with a hydrogen in C_2H_4 gives rise to significant torque and rotational excitation in the dissociation, can be used to describe the experimental results. Another way to examine the results in a PPC experiment is using the total kinetic energy spectrum, where E_{TOT} = eKE + KER for each event. This spectrum is shown in **Figure 3** and shows that in addition to the formation of OH + C_2H_4 with low vibrational excitation, there is a minor channel with excitation assigned to the C-H stretching modes in C_2H_4. This interpretation is driven by the spectator role expected for OH given the calculated anion structure.

As noted, there is a significant channel (1/3) producing complexes that are stable on the 8 μs flight time from the laser-ion-beam interaction region to the detector. The photoelectron spectrum for these stable complexes is narrower than the dissociative spectrum, however, it also shows evidence for C-H stretch excitation far exceeding the dissociation energy of the neutral entrance channel complex. This indicates that vibrational Feshbach resonances built on the weak H-bond in the entrance channel complex must play a role in this system, as previously observed in F + H_2O and F + CH_3OH systems.[2,Ray, 2016 #13] Accurate modeling of DPD using either quantum dynamics or quasiclassical trajectory calculations requires an accurate full-dimensional potential energy surface of the anion. While that remains a great challenge presently, we hope that benchmark results like this may provide an important test for efforts to predict reaction dynamics in high dimensionality systems.

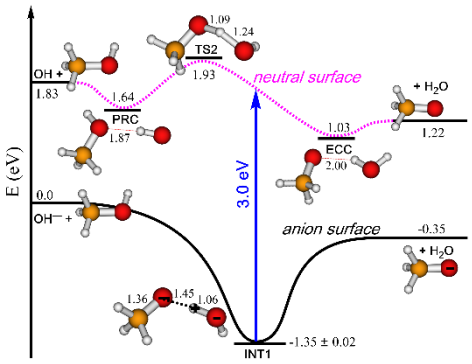

Figure 4. Relevant reaction coordinate diagram for the anion and neutral potential energy surfaces calculated using the mHEAT-345(Q) method.[13]

Photodetachment of $CH_3O^-(H_2O)$: Probing the Exit Channel of OH + CH_3OH → H_2O + CH_3O

We sought to expand our studies of OH radical reactions using anion precursors to the OH + CH_3OH system by synthesizing an appropriate anion precursor. Formation of the 49 amu precursor anion was straightforward in a pulsed discharge ion source, however the spectra observed were very different from the OH – alkane/alkene systems previously studied. To

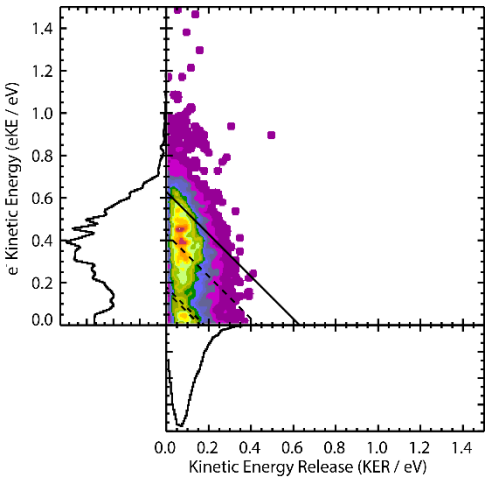

Figure 5. PPC spectrum of $CH_3O^-(H_2O)$ at 3.20 eV photon energy. The solid diagonal line is the KE_{max} for $H_2O + CH_3O + e^-$ product channel. The dashed diagonal lines at 0.43, 0.18, and 0.16 eV are KE_{max} for dissociation resulting in one quantum of excitation in the water bend, symmetric stretch, and asymmetric stretching modes, respectively.

examine this problem, a collaboration was initiated with John Stanton's group that showed via high-level m-HEAT calculations that the initial precursor anion is $CH_3O^-(H_2O)$, meaning that photodetachment of this system has Franck-Condon overlap with the exit channel for this exothermic reaction in a manner reminiscent of the $F + H_2O$ and $F + CH_3OH$ systems previously studied.[2, 12] The reaction coordinate diagram is shown in **Figure 4**,[13] and shows that the anion complex, INT1, has a structure along the path between TS2 and the exit channel complex (ECC). The energetics calculated using the mHEAT method match the experimental results well, as shown in the PPC spectrum in **Figure 5**, where the solid diagonal line corresponds to the formation of $CH_3O + H_2O + e^-$ in the ground vibrational levels, with the dashed line limits corresponding to bending and stretch excitation in the H_2O product as described in the figure caption.

The PPC spectrum in **Figure 5** provides a measure of the internal state distribution of the $CH_3O + H_2O$ products and shows that most are produced with limited internal excitation. However there is a significant fraction below the limit for excitation of the water bend as well as some evidence for stretch excitation. Again, in this system, there is significant production of stable complexes, ~30% are stable over the 7.8 μs flight time to the neutral particle detector. The stable photoelectron spectrum (not shown here) is dominated by excitation in the H_2O bend in the complex, and the majority of the events lie above the energetic limit for formation of the $CH_3O + H_2O + e^-$ products. This shows that also in this system vibrational Feshbach resonances built on the H-bonded exit channel complex well play a role. The ubiquity of these resonances in these increasingly complex systems is an interesting observation from the studies of the DPD of $OH^-(C_2H_4)$ and $CH_3O^-(H_2O)$. These results will be described in a forthcoming manuscript.[14]

Other Work in Progress

In addition to the work highlighted above, reports on our studies of the photodissociation of the nitrogen-oxide-based anions $N_2O_2^-$ and peroxynitrite anion $ONOO^-$ are in preparation. These studies have yielded state-resolved data on the autodetachment of highly vibrationally and rotationally excited NO^- photoproducts in both systems induced by near-UV photolysis. We are also finalizing our report on the single photon DPD of the oxyallyl anion, $C_3H_4O^-$, at 3.20 eV. This work extends our previous study of the photodetachment forming the stable C_3H_4O oxyallyl diradical that resulted in the reassignment of the photoelectron spectrum of ethylenedione (OCCO)[15] to the oxyallyl diradical (C_3H_4O),[16] as reported in DOE pub. [1]. We also studied the two-photon DPD yielding $CO + C_2H_4 +$ e- products (at 1.60 eV photon energy) of the oxyallyl anion mediated by a dipole-bound anion resonance significantly below the photodetachment threshold as reported in DOE pub. [2].[17] What is unique about the one-photon DPD at 3.20 eV is that the KER is completely distinct from the anion resonance-mediated two-photon DPD process, and the distinct dynamics for the three low-lying triplet and singlet states is revealed directly in the PPC spectrum for this system. This work will be submitted for publication before the end of the current project period.

III. Future Work – Impacts of COVID-19

Progress in the laboratory was impacted considerably by COVID-19, with the lab being entirely shutdown from mid-March to mid-June 2020, and only usable under strict social distancing limits through March 2021. In addition, during this period, in October 2020, the cryopump and cold head system for the EIBT failed and required major maintenance that was only completed by the vendor and returned to the laboratory in March 2021. We are now reassembling the EIBT and hope to be back online in June 2021 to resume experiments. Following calibration experiments, we plan on resuming the effort to expand on our earlier studies of the effects of infrared excitation in the $F^-(H_2O)$ system.[8] The initial experiments as previously proposed will be to promote the *cis*-$HOCO^-$/*trans*-$HOCO^-$ and $HCO_2^-/HOCO^-$ isomerizations

using vibrational excitation, and then to pursue examination of mode-specific effects on the dissociation dynamics of HOCO by the DPD of vibrationally excited $HOCO^-$ anions.

In the coming months, we will finish analysis of the DPD of hydroxide and methoxide clusters mentioned above as well as the pump-probe studies on the oxyallyl system. The important priority for later in 2020, however, is to resume studies of the IR excitation of precursor anions, with the goal of controlling product branching ratios. These will be the first IR excitation studies conducted on the PPC spectrometer since the implementation of COAT, allowing for greater control of precursor anion starting conditions given the ability to generate anions cooled to less than 20K.[18] This work will create a blueprint for future studies of transient species with controlled internal excitation, providing benchmark data for understanding important chemical phenomena relevant to atmospheric and combustion processes.

IV. DOE-supported publications by this project 2018-2021

1. K. G. Lunny, Y. Benitez, Y. Albeck, D. Strasser, J. F. Stanton, R. E. Continetti, *Spectroscopy of Ethylenedione and Ethynediolide: A Reinvestigation,* Angew. Chemie. Int. Ed. **57**, 5394-5397 (2018). https://doi.org/10.1002/anie.201801848
2. Y. Albeck, K. G. Lunny, Y. Benitez, A. J. Shin, D. Strasser and R. E. Continetti, *Resonance-Mediated Below-Threshold Delayed Photoemission and Non-Franck-Condon Photodissociation of Cold Oxyallyl Anions* Angew. Chem. Int. Ed. **58**, 5312-5315 (2019). https://doi.org/10.1002/anie.201900386
3. B. Shen, K. G. Lunny, Y. Benitez, R. E. Continetti, *Photoelectron-Photofragment Coincidence Spectroscopy with Ions Prepared in a Cryogenic Octopole Accumulation Trap: Collisional Excitation and Buffer Gas Cooling,* Front. Chem. **7**, 295 (2019). https://doi.org/10.3389/fchem.2019.00295
4. Y. Benitez, D. Lu, K. G. Lunny, J. Li, H. Guo, R. E. Continetti, *Photoelectron-Photofragment Coincidence Studies on the Dissociation Dynamics of the OH-CH_4 Complex*, J. Phys. Chem. A. **123**, 4825-4833 (2019). https://doi.org/10.1021/acs.jpca.9b02441
5. Y. Benitez, A.J. Parsons, K.G. Lunny and R.E. Continetti, *Dissociative Photodetachment Dynamics of the $OH^-(C_2H_4)$ Anion Complex*, J. Phys. Chem. A. (in revision, 2021).

References

1. C. J. Johnson, R. Otto and R. E. Continetti, Physical Chemistry Chemical Physics **16**, 19091-19105 (2014).
2. R. Otto, J. Ma, A. W. Ray, J. S. Daluz, J. Li, H. Guo and R. E. Continetti, Science **343**, 396-399 (2014).
3. A. W. Ray, B. B. Shen, B. L. J. Poad and R. E. Continetti, Chemical Physics Letters **592**, 30-35 (2014).
4. B. L. J. Poad, A. W. Ray and R. E. Continetti, Journal of Physical Chemistry A **117**, 12035-12041 (2013).
5. B. B. Shen, K. G. Lunny, Y. Benitez and R. E. Continetti, Front. Chem. **7**, 295 (2019).
6. C. Johnson, B. Shen, B. Poad and R. Continetti, Rev. Sci. Instrum. **82**, 105105 (2011).
7. R. Otto, A. W. Ray, J. S. Daluz and R. E. Continetti, EPJ Techniques and Instrumentation **1**, 3 (2014).
8. A. W. Ray, J. Ma, R. Otto, J. Li, H. Guo and R. E. Continetti, Chem. Sci. **8**, 7821-7833 (2017).
9. E. Kamarchik, L. Koziol, H. Reisler, J. M. Bowman and A. I. Krylov, J. Phys. Chem. Lett. **1** (20), 3058-3065 (2010).
10. J. P. Senosiain, S. J. Klippenstein and J. A. Miller, J. Phys. Chem. A **110**, 6960-6970 (2006).
11. B. Ruscic and D. H. Bross, (ATcT.anl.gov, 2019).
12. A. W. Ray, J. Agarwal, B. B. Shen, H. F. Schaefer and R. E. Continetti, Phys. Chem. Chem. Phys. **18**, 30612-30621 (2016).
13. J. H. Thorpe, C. A. Lopez, T. L. Nguyen, J. H. Baraban, D. H. Bross, B. Ruscic and J. F. Stanton, Journal of Chemical Physics **150**, 224102 (2019).
14. Y. Benitez, T. L. Nguyen, A. J. Parsons, J. F. Stanton and R. E. Continetti, To be submitted (2021).
15. A. R. Dixon, T. Xue and A. Sanov, J. Chem. Phys. **144**, 234305 (2016).
16. K. G. Lunny, Y. Benitez, Y. Albeck, D. Strasser, J. F. Stanton and R. E. Continetti, Angew. Chem. Int. Ed. **57**, 5394-5397 (2018).
17. Y. Albeck, K. G. Lunny, Y. Benitez, A. J. Shin, D. Strasser and R. E. Continetti, Angew. Chem. Int. Ed. **7**, 5312-5315 (2019).
18. B. B. Shen, Y. Benitez, K. G. Lunny and R. E. Continetti, J. Chem. Phys. **147**, 094307 (2017).

Dynamics of Combustion Reactions

H. Floyd Davis
Dept. of Chem. & Chem. Bio., Cornell University, Ithaca, NY 14853-1301
hfd1@cornell.edu

I. Program Scope:

Bimolecular or photochemical reactions of organic radicals can yield high-energy isomers of stable molecules. Notable examples include methyl carbene (ethylidene-CH_3CH) and dimethylcarbene (methylethylidene – CH_3CCH_3), lying about 300 kJ/mol (3 eV) above ethene and propene, respectively. Recently, we prepared these carbenes by photolysis of stable molecular precursors and free radicals, and measured product kinetic energy and angular distributions. We aim to gain insight into the topography of the potential energy surfaces for unimolecular and bimolecular reactions of radicals and carbenes.

II. Recent Progress:

Our DOE-supported research employs Endstation 1 (ES1), a rotatable source crossed molecular beams apparatus originally utilizing synchrotron radiation for photoionization detection. At Cornell, it has been combined with a high intensity VUV beamline in the 8.8-11.9 eV range employing tabletop pulsed lasers.[1,2]

a) Direct Observation of Ethylidene (CH_3CH)- the Elusive High-Energy Isomer of Ethylene[3]

Among the most elusive organic molecules is ethylidene (CH_3CH). Despite many experiments over eight decades, there has been no direct observation of ethylidene in the gas, liquid or solid phases. Ethylidene holds special importance as a prototypical short-lived species in organic chemistry. It is thought to be produced from reactions of oxygen atoms with unsaturated hydrocarbons,[4] and is initially formed by insertion of $C(^1D)$ into CH_4. Ethylidene has also been observed as a chemically-bound species in surface chemistry experiments, and as a ligand in transition metal complexes.

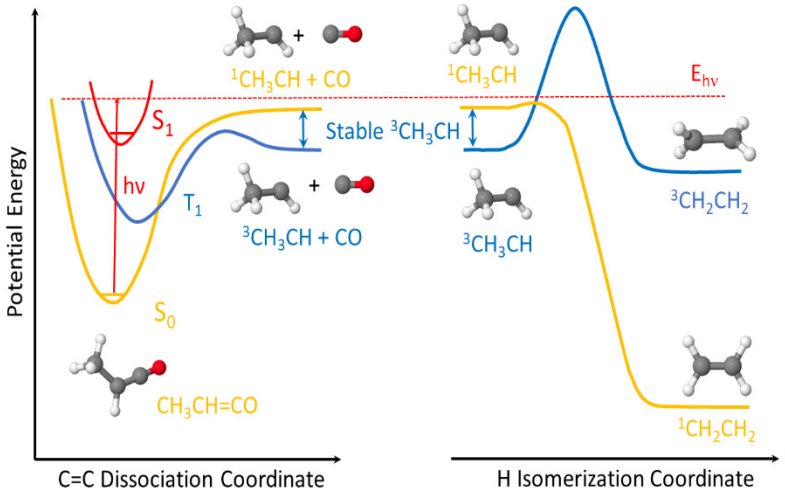

Fig. 1. *Methylketene photodissociation produces ethylidene + carbon monoxide. Triplet ethylidene ($^3CH_3CH$) is stable to intersystem crossing and isomerization if produced with internal energies below the singlet electronically excited state ($^1CH_3CH$).*

Although early theoretical studies suggested an isomerization barrier of 0 kJ/mol, *i.e.,* that singlet ethylidene is a transition state for hydrogen scrambling in ethylene, some subsequent studies indicated that ethylidene represents a true local minimum on the singlet C_2H_4 potential energy surface.[5] Here, we report that ethylidene is indefinitely stable in the absence of collisions if produced in the triplet ground state at energies below threshold for intersystem crossing. Our observations are consistent with a high potential energy barrier for isomerization on the triplet surface.[5,6] Near-UV photolysis of gaseous methylketene, or its isomer propenal (acrolein), leads to CO loss producing triplet ethylidene, which is detected by photoionization mass spectrometry. Electronically excited singlet ethylidene is also produced, rapidly undergoing isomerization by a 1,2-hydrogen atom shift *after*

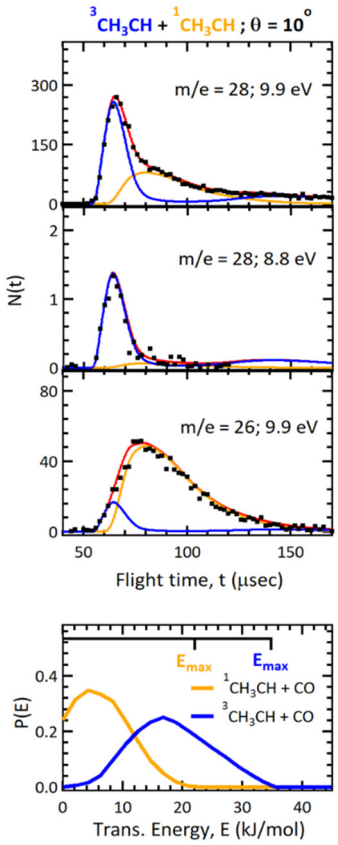

Fig. 2. *Upper: TOF spectra from 355.1 nm photodissociation of methylketene. Black dots are experimental data; blue lines are calculated TOFs for $^3CH_3CH$ + CO and orange lines for $^1CH_3CH$ + CO.*

for dimethylcarbene formation via C=C bond fission. Possible mechanisms for propene elimination via *RIES* are discussed in light of the observed energy dependence for the competing pathways.

In contrast to our observations for methylketene and acrolein, which have nearly identical UV photochemistry (due to rapid isomerization via a 1,3-H atom shift), we have found that the photochemistry of methacrolein is quite different from that of its isomer, dimethylketene.

departure of the CO, producing highly vibrationally excited ethylene. The measured product translational energy distributions verify the theoretically calculated enthalpy of formation of triplet ethylidene, and are consistent with a singlet-triplet energy gap of about 12.5 kJ/mol.

b) Dimethylcarbene vs. Direct Propene Formation in Dimethylketene Photodissociation[7]

Highly reactive carbenes are usually produced by photolysis of stable precursors. *Sequential* kinetic pathways for deactivation of nascent carbenes usually involve bimolecular reactions in competition with isomerization producing stable products such as alkenes. However, the *direct* photolytic production of stable products, effectively bypassing formation of free carbenes, has been postulated for over 50 years, but remains very poorly understood. Often termed "reaction in excited state", *RIES*, examples include 1,2-hydrogen migration within photoexcited carbene precursors yielding alkenes, and the Wolff rearrangement in photogenerated carbonyl-substituted carbenes producing ketenes.[8]

In this study, the two competing CO elimination channels from photoexcited gaseous dimethylketene, producing dimethylcarbene and propene, were studied as a function of electronic excitation energy. A significant fraction of the dimethylcarbene → propene isomerization exothermicity (~300 kJ/mol) was released as propene + CO translational energy, indicating that *propene is formed prior to, or concurrent with, CO elimination*. An increase in the propene yield with increasing excitation energy suggests that the effective potential energy barrier for this channel lies ~ 24 kJ/mol *above* the energetic threshold

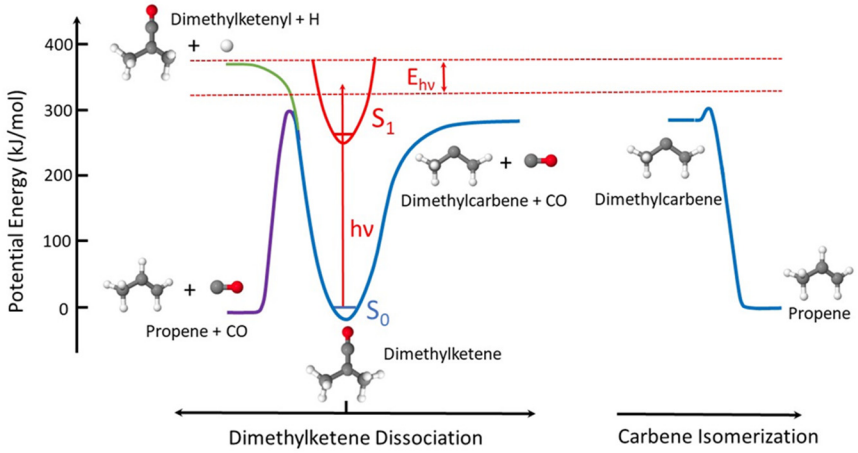

Fig. 3: *Dimethylketene photodissociation produces dimethylcarbene + carbon monoxide. Alternatively, propene + carbon monoxide can be produced via a direct reaction mechanism effectively bypassing formation of free dimethylcarbene (RIES).*

c) Isomer-Specific C-C Bond Fission in the 248 nm Photodissociation of Propyl Radicals[9]

Although the chemical kinetics and thermodynamics of alkyl radicals on their ground potential energy surfaces are relatively well understood, many questions remain unanswered regarding the dynamics of the electronically excited Rydberg states of alkyl radicals accessed by near-UV excitation.

Over the past decades, numerous experimental studies of the photodissociation of alkyl radicals, ranging from the simplest, methyl (CH_3), to larger branched and cyclic C_6 species, have been carried out using complimentary methods. With the exception of one study,[10] only the C-H bond fission channels have been characterized. The lack of knowledge pertaining to C-C bond fission is remarkable because it is energetically open for UV excitation of *all* C_2 and larger alkyl radicals, including ethyl radicals (C_2H_5) excited near their lowest lying absorption maximum near 245 nm.

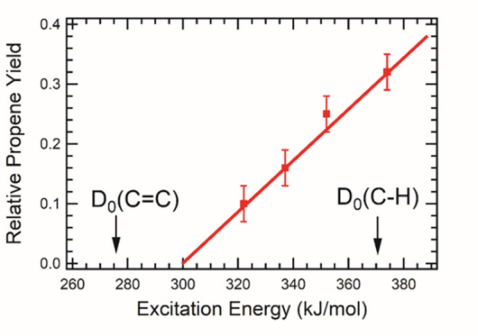

Fig. 4: *Plot of relative propene yields vs. dimethylketene excitation energy suggests an effective potential barrier for direct propene formation near 300 kJ/mol.*

In this work, the C-C bond fission channels in 1- and 2-propyl radicals following electronic excitation at 248 nm were studied with single photon ionization of nascent products. The radicals were produced in a molecular beam by flash pyrolysis of azo-1-propane and azo-2-propane. For comparison, the photolysis of 1-nitropropane and 2-nitropropane at 213 nm was also employed for generation of the radicals.

For 1-propyl radicals, C-C bond fission led primarily to formation of methylene (CH_2) and ethyl radicals (C_2H_5). In contrast, C-C bond fission in 2-propyl radicals produced methyl radicals (CH_3) plus ethylidene ($CHCH_3$). This study confirms that C-C bond fission plays an important role in alkyl radical photodissociation. The observation of *isomer-specific* dissociation dynamics in a system where isomerization is expected to proceed readily on the ground state PES demonstrates that C-C bond fission is likely dominated by *direct* dissociation from the excited state, rather than from ground state dynamics following internal conversion.

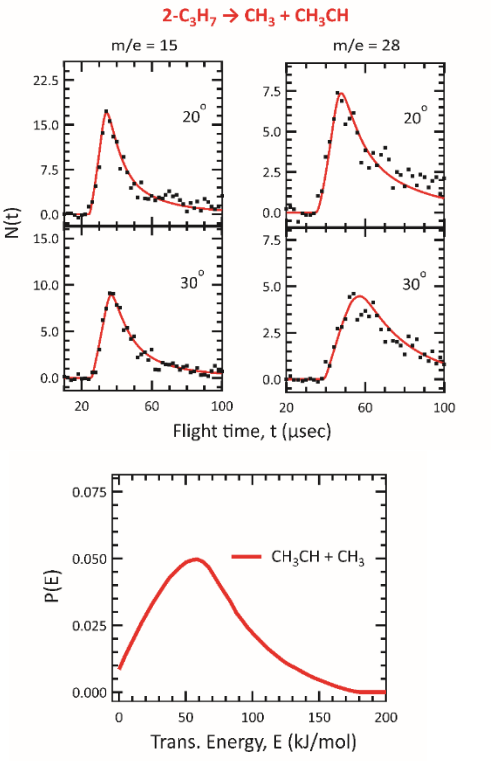

Fig. 5. Upper: *TOF spectra for momentum-matched CH_3 (m/e = 15) and CH_3CH (m/e = 28) products from 248 nm photodissociation of 2-propyl radicals.* ***Lower:*** *Corresponding translational energy distribution.*

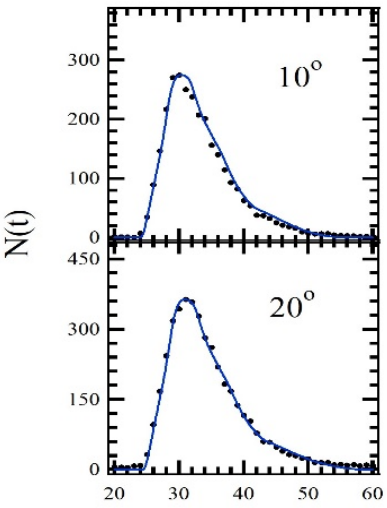

Fig. 6: *Time-of-flight spectra for CH_2 (m/e=14) from UV photolysis of 3-H diazirine*

d) Photochemistry of 3-H Diazirine (c-CH_2N_2)[11]

First discovered in the 1960s, diazirines are the cyclic isomers of diazoalkanes. Consisting of a three-member ring, the simplest example is 3-H diazirine, c-CH_2N_2. As a proof of principle towards the use of

diazirines as carbene precursors in upcoming studies, we synthesized 3-H diazirine and studied its primary photochemistry at two wavelengths. In agreement with expectations, the photodissociation products are $^1CH_2$ + N_2. Figure 6 shows the TOF spectra for CH_2 products from 314.8 nm photolysis detected using 9.9 eV photoionization, where only singlet electronically excited CH_2 is ionized. The P(E) is shown in Fig. 7; the product angular distributions are characterized by a highly negative anisotropy (β) parameters, as expected for the perpendicular nature of the electronic transition.

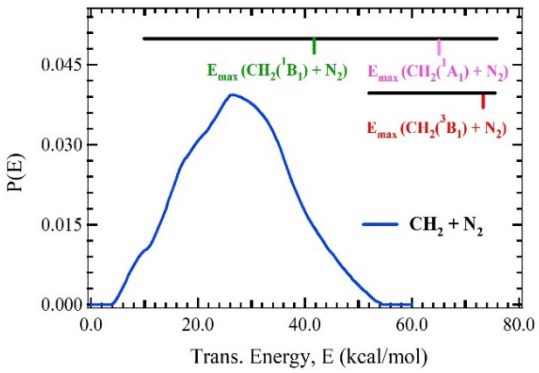

Fig. 7: *Translational energy distribution for singlet CH_2 + N_2 from diazirine UV photolysis*

III. Future Plans:

As noted above, ketenes and diazirines can be used for direct production of highly reactive carbenes. We plan to continue work on these systems, initially focusing on photochemical reactions. Our immediate primary focus will be on methylcarbene ($CHCH_3$), ethylcarbene (C_2H_5CH), and dimethylcarbene (CH_3CCH_3). Whereas the ground states of methylcarbene and ethylcarbene are of triplet multiplicity, for dimethylcarbene the ground state is singlet, leading to interesting dynamical consequences.

We also plan to study bimolecular reactions of organic radicals and carbenes. Very intense beams of methylene (CH_2) can be produced by photolysis or pyrolysis of diazirine. We will also conduct studies of reactions of hydroxyl radicals (OH) with alkenes, with our primary focus on the channels forming enols. Our recent development of an intense 8.8 eV light source for pulsed photoionization detection allows selective photoionization detection of enols without interference by their aldehyde and ketone isomers, which have higher ionization energies. We have also made some progress recently in studies of bimolecular reactions involving organic radicals such as 1- and 2- C_3H_7 and t-C_4H_9 with small molecules such as O_2 and C_2H_4. These studies are ongoing.

IV. References (* denotes recent publications supported by this DOE grant):

1. D.R. Albert and H.F. Davis "Experimental Studies of Bimolecular Reaction Dynamics Using Pulsed Tabletop VUV Photoionization Detection", *Phys. Chem. Chem. Phys.* **15**, 14566-14580 (2013).
2*. M. A. Todt, S. Datta, A. Rose, K. Leung, and H. F. Davis, "Subpicosecond HI Elimination in the 266 nm Photodissociation of Branched Iodoalkanes", *Phys. Chem. Chem. Phys.,* **22**, 27338-27347 (2020).
3*.S. Datta and H.F. Davis, "Direct observation of ethylidene, the elusive high-energy isomer of ethylene", *J. Phys. Chem. Lett.*, 11, 10476-10481 (2020).
4. Cavallotti C.; Leonori F.; Balucani N.; Nevrly V.; Bergeat A.; Falcinelli S.; Vanuzzo G.; Casavecchia P. "Relevance of the Channel Leading to Formaldehyde + Triplet Ethylidene in the O(^{3}P) + Propene Reaction under Combusion Conditions." *J. Phys. Chem. Lett.* **2014**, *5*, 4213-4218.
5. M. T. Nguyen, M.H. Matus, W.A. Lester, and D.A. Dixon, "Heats of Formation of Triplet Ethylene, Ethylidene, and Acetylene", *J. Phys. Chem. A*. **112**, 2082-2087 (2008).
6. L.B. Harding, "Ab Initio Studies of 1, 2-H Migration in Open Shell Hydrocarbons". *J. Am. Chem. Soc.* **1981**, *103*, 7469-7475.
7*.S. Datta and H.F. Davis, "Dimethylcarbene vs. Direct Propene Formation in Dimethylketene Photodissociation", submitted for publication in *J. Phys. Chem. A.*
8. M.S. Platz, "A Perspective on Physical Organic Chemistry", *J. Org. Chem.* **79**, 2341-2353 (2014).
9*.S. Datta, M.A. Todt, and H. F. Davis, "Isomer-Specific C-C Bond Fission in the 248 nm Photodissociation of Propyl Radicals", manuscript in preparation.
10. B. Negru, G.M.P. Just, D. Park, and D.M. Neumark, "Photodissociation dynamics of the t-butyl radical via photofragment translational energy spectroscopy at 248 nm.", *Phys. Chem. Chem. Phys.,* **13**, 8180 (2011).
11*. S. Datta and H.F. Davis, "Photodissociation Dynamics of 3-H diazirine", manuscript in preparation.

Exploration of chemical-kinetic mechanisms, chemical reactivity, and molecular spectroscopy using novel numerical analysis

Michael J. Davis
Chemical Sciences and Engineering Division
Argonne National Laboratory
Lemont, IL 60439
Email: davis@tcg.anl.gov

The work explores chemically reactive systems using novel numerical analyses. One focus of the work is exploration and theoretical validation of chemical-kinetic mechanisms, using global sensitivity analysis. An effort on reaction pathway analysis has been underway. The expertise developed in the earlier work has led to the implementation of these techniques for studying problems in chemical reactivity, including isolated chemical kinetics and dynamics. There is a major effort underway for using such techniques for fitting potential energy surfaces. Another major effort underway is the application of computational optimal transport to molecular spectroscopy and dynamics. This effort includes studies of the mixing of probability densities using optimal transport and related methods. The mixing includes geodesics along positive semidefinite matrices and density matrices, which may have quantum-information applications.

Recent Progress

Work on fitting potential energy surfaces has continued. It is a collaboration with Jasper and Moberg (ANL). The main focus of the work in the last year has been the development of methods for scalable basis set expansions. Scalability means that the number of basis functions scales favorably with the number of degrees of freedom. The basis sets used are permutationally invariant polynomial (PIP) expansions. When constrained by order, these expansions scale poorly as shown in Fig. 1 for the abstraction reaction H + H_2O. Because our goal in developing potential energy surfaces is to use them for chemical dynamics, any excess number of basis functions that are not essential is unwanted.

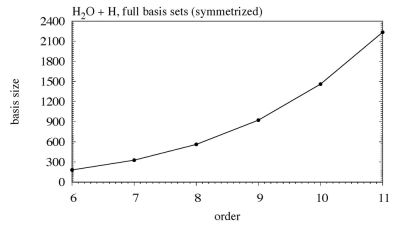

Fig. 1. Full basis sets as a function of order.

Reduced basis sets are achieved based on the notion of sparsity, a key concept that has developed in the fields of statistics, signal processing, and machine learning over the last 25 years. Sparsity implies that most of the behavior of functions can be reproduced by a limited number of basis function and many methods have been developed to leverage the sparsity for pruning basis sets used in fits of functions. In the present work we use greedy methods to achieve the pruning of the PIP basis sets. The pruning is called "subset selection" in the statistics literature and "feature selection" in the machine learning literature.

Greedy methods add or subtract functions one at a time. Forward greedy methods start with an empty set of functions and at each step add the basis function which lowers the rms fitting error the most. Backward greedy methods start with the full basis set and remove functions one at a time based on which function raises the rms error least when removed. Forward methods are preferred over the backward methods, as they never need to generate the full basis set expansion. An alternative to using rms error as a criterion for addition of functions for forward greedy methods is to add functions based on how they align with the residual error vector. There are a large number of methods that use versions of this strategy, which is called "matching pursuit", including the very popular method orthogonal matching pursuit (omp). Matching pursuit algorithms for basis-set selection are faster than the regression-based (i.e., rms-based selection), but we have not found them to be nearly as good at pruning the PIP basis sets.

In some presentations of forward selection methods, backward steps are included, usually based on a well-defined criterion. We developed a novel alternative to this idea, a multi-pass greedy approach. A series of forward steps are followed by a series of backward steps. The number of steps is varied randomly based on an average number of steps. As the method sweeps back and forth, each possible subset size is visited several times and the one that has the lowest rms fitting error is retained. We run multiple versions of this procedure, changing the average step size over a range of a few to a few hundred and once again retain the subset of a particular size that has the lowest rms error. We also calculate an out-of-sample error as the procedure is run using the leave-one-out cross-validation (loocv) error calculated with the hat matrix. A loocv error which is too large, for example, 20% larger than the rms error, can indicate overfitting and our program may reject this fit. Although the multi-pass method is complex, the computer resources necessary to implement it are a small fraction of most of the other parts of the calculations of the surfaces.

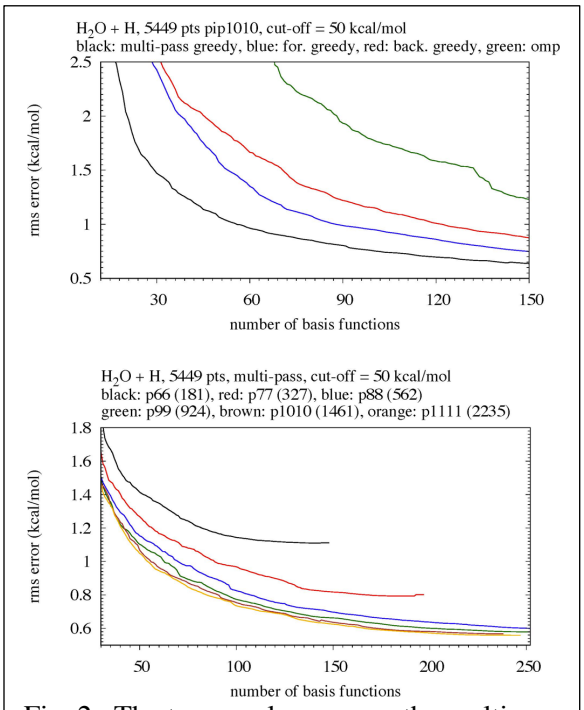

Fig. 2. The top panel compares the multi-pass algorithm with several other greedy methods. The bottom panel shows how the multi-pass method converges with the order.

The multi-pass greedy method is compared to the forward greedy method, the backward greedy method, and orthogonal matching pursuit (omp) in the top panel of Fig. 2, showing how the rms error changes with the size of the subsets of the full basis set of size 1461. This panel indicates that the multi-pass method is superior to the others, as the fitting errors are significantly lower. The multi-pass method takes considerably more computer time than the two forward methods, so they might be preferred under some circumstances. The bottom panel of Fig. 2 shows how the multi-pass greedy error changes with order, with the largest case being 11th order, whose full basis set size is 2235 (see the heading).

Figure 3 shows a different view of the convergence. Here the convergence is shown with respect to specific rms errors. The saddle point for this reaction is at 21.9 kcal/mol and thus the cases shown in Fig. 3 start slightly above 5% of this energy and are as low as 3% of it. Figure 3 shows an important result, because it indicates that the subsets actually get smaller with order, eventually converging to a size that is much smaller than the full basis set, which is growing rapidly, as demonstrated in Fig. 1. This type of result suggests that the subset selection leads to favorable scaling with the number of atoms. Because the potential energy surfaces we generate will be used to study chemical reactions, it is important to have fits that are as parsimonious as possible. In addition, PIP fits can be automated even for reactive systems and if they can compete in size with other, less automatic methods for fitting reactive potential energy surfaces, that is very useful.

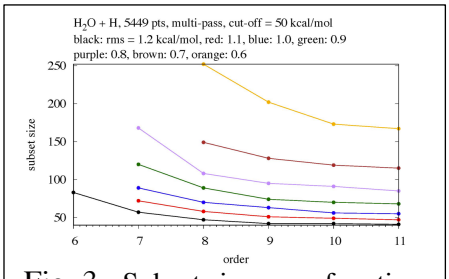

Fig. 3. Subset sizes as a function of order,

We have fit three reactive and three non-reactive potential energy surfaces with the methods described above and in Figs. 1-3. Figure 4 shows

results for four of these. This figure shows rms error vs. the size of the subset as a fraction of the full set. The systems studied in Fig. 4 are the reactive cases H + H_2O, H + CH_4, and H + C_2H_6 and the non-reactive case CH_4 + NH_3. Each curve has a point on it which indicates 1 kcal/mol error for the three reactive cases and 10 cm^{-1} for the non-reactive case. These plots demonstrate that only a small fraction of the full basis set is needed for good fits, and this fraction can be quite small if the indicated rms error matches the dots. In the top row the fractions are 0.04 and 0.024, and in the bottom row they are 0.057, and 0.005.

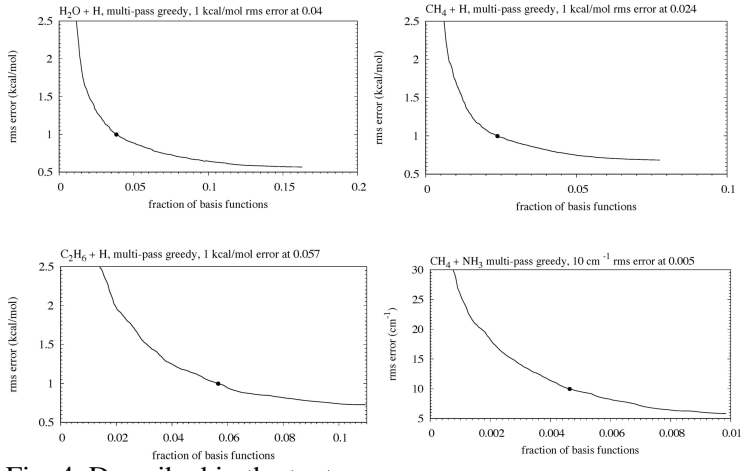

Fig. 4. Described in the text.

Table 1 summarizes some of the results for Fig. 4 and adds results for the two other surfaces fit using the subsets calculated from the multi-pass greedy algorithm. The rms error can be compared to the "reference energy" listed in the last column of the table which is the energy of the saddle point for the first three cases and the binding energy for the last three cases.

Table 1. Selected Results for the fitting of six potential energy surfaces

System[a]	Order	Full	Subset	Fraction	RMS Error	Ref. Energy
H + H_2O	10	1461	56	0.04	1 kcal/mol	21.9 kcal/mol
H + CH_4	7	1933	46	0.024	1 kcal/mol	14.9 kcal/mol
H + C_2H_6	6	2455	139	0.057	1 kcal/mol	12 kcal/mol
Ar + NH_3	6	1408	7	0.005	9.7 cm^{-1}	94 cm^{-1}
N_2 + NH_3	5	1638	67	0.04	9.9 cm^{-1}	238 cm^{-1}
CH_4 + NH_3	5	14,222	66	0.005	10 cm^{-1}	244 cm^{-1}

[a] The first three systems are abstraction reactions and the next three are intermolecular energy transfer systems.

We have continued our work on applying computational optimal transport to the study of molecular spectroscopy. This is a collaboration with Prozument and Seifert (ANL) motivated by the earlier work at Argonne by Zaleski and Prozument, where molecular rotational spectra were classified and fit using neural networks. In that earlier study comparisons between spectra were made based only on line positions, while the optimal transport compares spectra based on line positions and intensities.

We use computational optimal transport to compare two discrete spectra, a continuous and a discrete spectrum, and two continuous spectra. A distance is defined between the spectra which is based on representing spectra as probability density functions and the distance is well-defined even when the two spectra have different numbers of lines or features, as well as different levels of resolution. A key component of the analysis is the study of cumulative distribution functions generated from the spectra.

The transportation distance defined between two spectra relies on using geometry that is non-Euclidean. The utility of such an approach can be understood by examining the synthetic

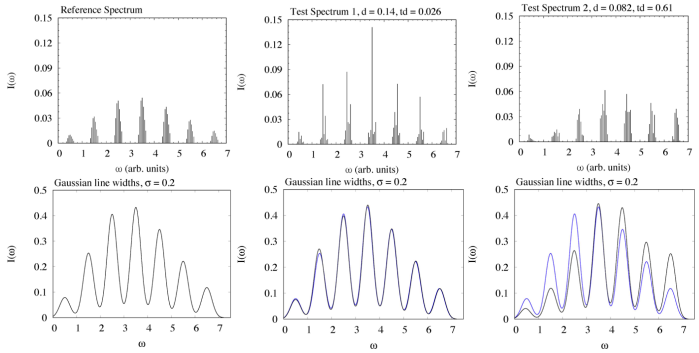

Fig. 5. The Euclidean distance on the top of the two spectra suggests that the spectrum in the middle panel (d =0.14) is farther from spectrum at the top left than the one on the top right (d = 0.082), but the lower resolution versions of the spectra in the bottom indicate that the spectrum in the middle is much closer than the one in the right panel. The transport distance, td, in fact indicates that to be true (0.026 vs. 0.62).

spectra presented in Fig. 5. All spectra have the same line positions, but the intensities differ. The standard Euclidean distance for this case is:

$$d = \sqrt{\sum_1^n (A_i - B_i)^2},$$

where the A_i's and B_i's are intensities. This distance does not take into account the overall structure of the spectrum that the transport distances does.

Future Plans

The work on fitting potential energy surfaces will continue. We plan on making the algorithm more efficient so that much larger systems can be fit. We also intend on using unsupervised learning to reduce the size of the basis set before the multi-pass algorithm is used. We also plan on studying the types of terms that are included in the subsets, which we expect will add significant physical insight into the work. We expect that the work on computational optimal transport will lead to ways of doing the molecular inversion problem, that is extracting specific structural information from the rotational spectra generated by Prozument and co-workers. There has been promising work done along these lines for Raman spectra of materials using Euclidean neural networks and such techniques will be examined. We also intend on investigating the use of dictionary learning to help in this project. We also want to use optimal transport to define geodesics as part of a quantum design process, that is the mixing of states based on the geometry of wavefunctions and density matrices. Unlike the original use of optimal transport to molecular spectra which are all positive quantities, the wavefunction problem requires a transformation of the data. A convenient and practical way of doing this has been suggested in the seismology literature.

Publications

1. G. M. Magnotti, Z. Wang, W. Liu, R. Sivaramakrishnan, S. Som, and M. J. Davis, "Sparsity Facilitates Chemical Reaction Selection for Engine Simulations", J. Phys. Chem. A **122**, 7227-7237 (2018).
2. S. Bai, R. Sivaramakrishnan, M. J. Davis, and R. T. Skodje, "A Chemical Pathway Perspective on the Kinetics of Low-Temperature Ignition of Propane", Combustion and Flame **202**, 154-178 (2019).
3. A. W. Jasper and M. J. Davis, "Parameterization Strategies for Intermolecular Potentials for Trajectory-Based Collision Parameters", J. Phys. Chem. A **123**, 3464-3480 (2019).
4. A. Mannodi-Kanakkithodi, M. Y. Toriyama, F. G. Sen, M. J. Davis, R. F. Klie, and M. K. Y. Chan, "Machine-Learned Impurity Level Prediction for Semiconductors: The Example of Cd-Based Chalcogenides", NPJ Comput. Mater. **6**, Article 39 (2020).
5. N. A. Seifert, K. Prozument, and M. J. Davis "Computational Optimal Transport for Molecular Spectra: The Fully Discrete Case", to be submitted (2021).
6. N. A. Seifert, K. Prozument, and M. J. Davis "Computational Optimal Transport for Molecular Spectra: The Semi-Discrete and Continuous Cases", preprint (2021).
7. D. R. Moberg, A. W. Jasper, and M. J. Davis. "Potential Energy Surface Expansions with Improved Scaling Using Dictionary Learning Based on Multi-Pass Subset Selection", to be submitted to J. Phys. Chem Lett. (2021).
8. C. L. Cortes, P. Lefebvre, N. Lauk, M. J. Davis, S. K. Gray, N. Sinclair and D. Oblak,"Adaptive Calibration of Photon Indistinguishability in Quantum Networks Using Bayesian Optimization", to be submitted.

Electronic structure methods and protocols with application to dynamics, kinetics and thermochemistry

Richard Dawes, dawesr@mst.edu
Missouri University of Science and Technology
400 W. 11th street, Rolla, MO 65409

I. Program Scope:

(NOTE – this project is supported jointly through the CTC and GPCP programs and this report will be submitted to both programs)

Hydrocarbon combustion involves the reaction dynamics of a tremendous number of species beginning with many-component fuel mixtures and proceeding via a complex system of intermediates to form primary and secondary products. Combustion conditions corresponding to new advanced engines and/or alternative fuels rely increasingly on autoignition and low-temperature-combustion chemistry. In these regimes various transient radical species such as HO_2, ROO·, ·QOOH, HCO, NO_2, HOCO, and Criegee intermediates play important roles in determining the detailed as well as more general dynamics. A clear understanding and accurate representation of these processes is needed for effective modeling. Given the difficulties associated with making reliable experimental measurements of these systems, computation can play an important role in developing these energy technologies.

Accurate calculations have their own challenges since even within the simplest dynamical approximations such as transition state theory, the rates depend exponentially on critical barrier heights and these may be sensitive to the level of quantum chemistry. Moreover, it is well-known that in many cases it is necessary to go beyond statistical theories and consider the dynamics. Quantum tunneling, resonances, radiative transitions, and non-adiabatic effects governed by spin-orbit or derivative coupling can be determining factors in those dynamics.

Building upon progress made during a period of prior support through the *DOE Early Career Program*, this project combines developments in the areas of potential energy surface (PES) fitting and multistate multireference quantum chemistry to allow spectroscopically and dynamically/kinetically accurate investigations of key molecular systems (such as those mentioned above), many of which are radicals with strong multireference character and have the possibility of multiple electronic states contributing to the observed dynamics.

An ongoing area of investigation is to develop general strategies for robustly convergent electronic structure theory for global multichannel reactive surfaces including diabatization of energy and other relevant surfaces such as dipole transition. Combining advances in *ab initio* methods with automated interpolative PES fitting allows the construction of high-quality PESs (incorporating thousands of high-level data) to be done rapidly through parallel processing on high-performance computing (HPC) clusters.

In addition, new methods and approaches to electronic structure theory will be developed and tested through applications. This project will explore limitations in traditional multireference calculations (*e.g.*, MRCI) such as those imposed by internal contraction, lack of high-order correlation treatment and poor scaling. Methods such as DMRG-based extended active-space CASSCF and various Quantum Monte Carlo (QMC) methods will be applied (including VMC/DMC and FCIQMC). Insight into the relative significance of different orbital spaces and the robustness of application of these approaches on leadership class computing architectures will be gained. A computational thermochemistry project recently conducted through support by the DOE SCGSR student fellowship program and collaboration with Branko Ruscic (Argonne National Labs) will be extended. A workflow framework that allows community driven expansion of the ATcT thermochemical database will be further developed. Synergy with other components of this research program such as automated PES fitting and multireference quantum chemistry will be used to address challenges encountered by the standard approaches to computational thermochemistry (those being single-reference quantum chemistry and perturbative treatments of the anharmonic vibrational

energy, which break down for some cases of electronic structure or floppy strongly coupled vibrational modes).

Recent Progress: This section describes recent progress achieved along various directions of the project occurring over the past 12 months since the last abstract was provided in May 2020 (start date of this project was 03-01-2019).

Nine new articles citing DOE support have appeared so far since 2020 including one in PNAS.[1-9] Several other papers are in prep, and a review for *Ann. Rev. of Phys. Chem.* Has been released. These have mostly been further developments and application of our code to automatically generate PESs suitable for quantum dynamics or spectroscopic studies.

The thermochemistry project spearheaded by graduate student Bradley Welch and in collaboration with Branko Ruscic and David Bross (both from ANL) has resulted in a family of user-friendly scripts implementing the thermochemistry protocol on parallel HPC clusters. This was initially reported in a publication focused on a family of methylperoxy species and has since been extended to general benchmarks on over 200 small molecules.[10] These scripts have already been extended to other projects by myself and by undergraduate students. Bradley Welch continues to develop these methods under the guidance of Angela Wilson at Michigan State University.

A main thrust mentioned above has been on robust calculation and fitting of energy and property surfaces for strongly coupled and intersecting excited electronic states. We have made some excellent progress in this area and recently reported fitting 20 different states and property surfaces in the notoriously tricky NO_2 system.[11] Success was achieved with a much greater challenge in NO_2, that of diabatization and fitting of a number of strongly coupled and intersecting excited state energy and property surfaces. Some Figures from the paper are given below that highlight the good behavior obtained by our procedures. We have now used the surfaces to predict absorption spectra including full geometry dependent transition moment surfaces.

The absorption spectra were computed using the MCTDH time dependent quantum dynamics method and the coupled PESs. A high-quality experimental spectrum recorded at 294 K is used for comparison. Spectra for J=0 were computed from a large number (125) of initial vibrational states. This allows the temperature dependence of the spectra envelope to be determined (up to 2200 K). In addition, the effect of J>0 was assessed by explicitly including the lowest 306 rotational states up to J=20, which due to the high density of states only covers thermally populated states up to 70 K. Predicted spectra are shown in Figure 4 including the lower panel which shows that detailed features in the experimental spectrum are matched by the simulation.

We are close to releasing our general 3, 4, and 5 atom code that automatically generates and refines reactive PESs for one or more electronic states. The code is interpolative and thus can reach arbitrary accuracy targets, while also employing PIP bases to properly treat all symmetry cases.

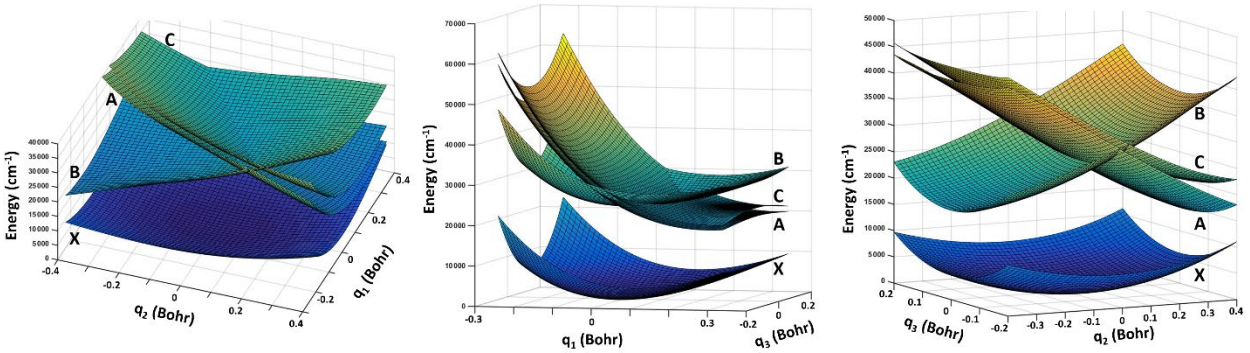

Figure 1: The lowest 4 PESs (X, A, B, and C) are plotted in the FC region as a function of pairs of normal coordinates: (left) symmetric stretch and bend (q1and q2), (middle) symmetric stretch and asymmetric stretch (q1 and q3), and (right) bend and asymmetric stretch (q2and q3). In each plot the third coordinate is fixed at the X state equilibrium.

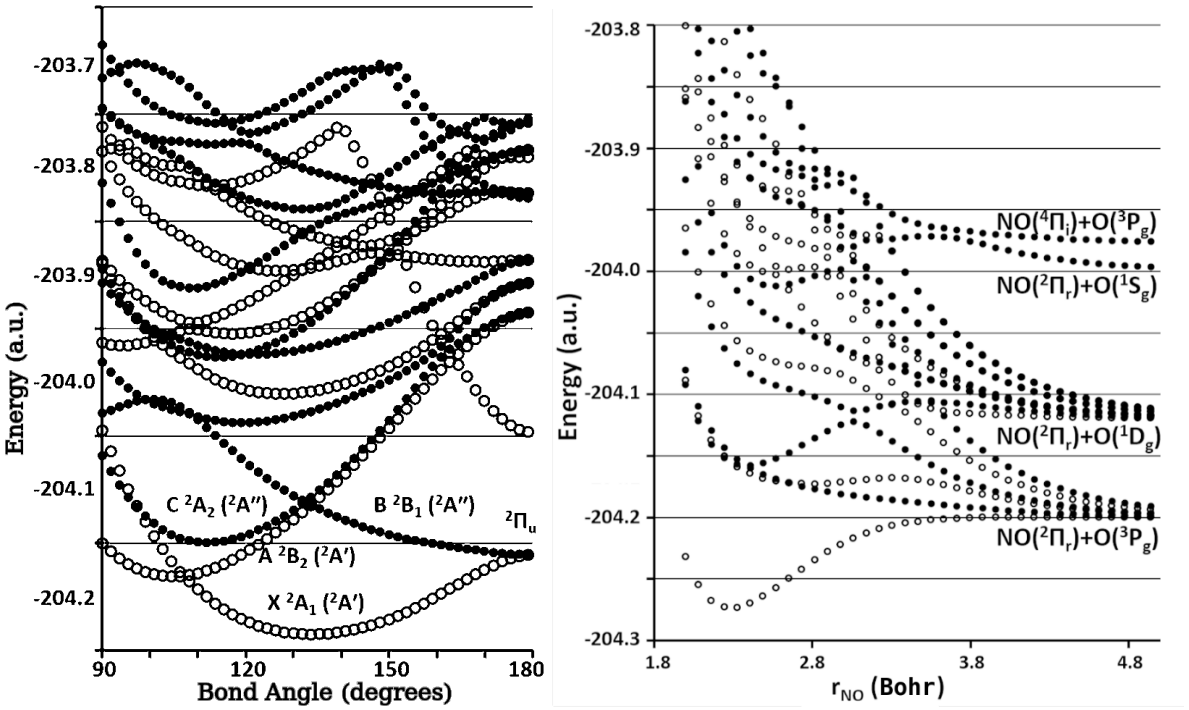

Figure 2: (left) The lowest eight ^{2}A′ states (open circles) and the lowest ten ^{2}A″ states (filled circles) are shown as a function of the bond angle (the bond distances are fixed at the X-state equilibrium). States were calculated using an 18-GDW-SA-CASSCF(13e,10o)/VDZ-F12 procedure. The lowest four states are labeled in C2v(CS) symmetry. (right) The same 18 states are plotted as a function of stretching one bond distance (the bond angle and the other bond distance are fixed at equilibrium).

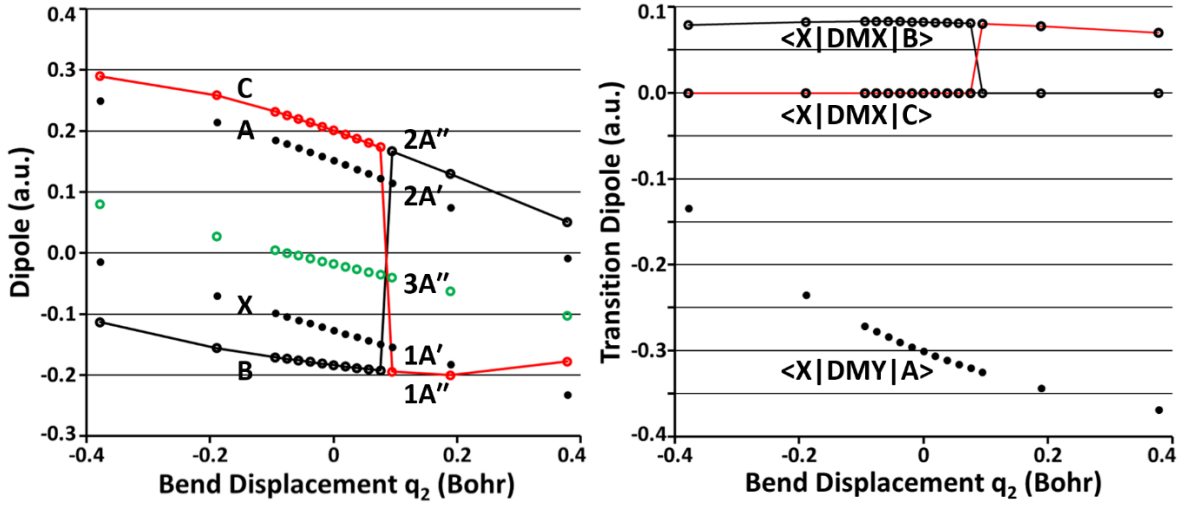

Figure 3: (left) The dipole moments of the lowest 4 states (X, A, B, and C) and one additional state of ^{2}A″symmetry computed at the MRCI-F12/VTZ-F12 level are plotted as a function of the bend normal coordinate (q2) in the adiabatic representation. The other coordinates are fixed at equilibrium so the system has C2v symmetry along this cut and only one non-zero component of the dipole. The dipoles of the B- and C-states are seen to switch abruptly due to the state crossing shown in Figure 2. (right) Transition dipoles also illustrate the abrupt state crossing behavior.

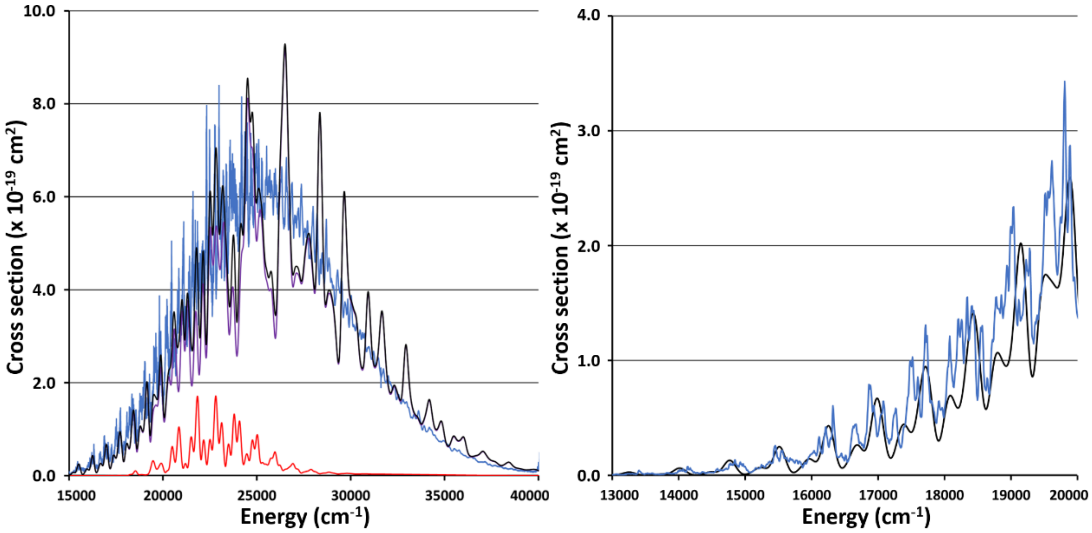

Figure 4: (left) The high-resolution experimental electronic absorption spectrum recorded by Vandaele at 294K (blue) is compared with calculations from the ground initial ro-vibrational state (0K). The contributions from absorption to the A-state (purple), B/C-states (red), and total (black) are plotted separately. The calculated spectrum was produced from a 200fs wavepacket propagation. The calculations are neither scaled nor shifted along either axis. (right) Zoom of low-energy wing of spectrum.

Grant Number and Title: Grant No. DE-SC0019740; Electronic structure methods and protocols with application to dynamics, kinetics and thermochemistry.

[1] Bop, Cheikh T., François Lique, Alexandre Faure, Ernesto Quintas-Sánchez, and Richard Dawes. "Non-LTE modelling of cyanoacetylene: evidence for isomer-specific excitation." *Monthly Notices of the Royal Astronomical Society* 501, no. 2 (**2021**): 1911-1919.
[2] Desrousseaux, Benjamin, François Lique, Javier R. Goicoechea, Ernesto Quintas-Sánchez, and Richard Dawes. "CF+ excitation in the interstellar medium." *Astronomy & Astrophysics* 645 (**2021**): A8.
[3] Endres, Eric S., Steve Ndengue, Olga Lakhmanskaya, Seunghyun Lee, Francesco A. Gianturco, Richard Dawes, and Roland Wester. "Temperature-dependent rotationally inelastic collisions of OH-and He." *Phys. Rev. A* **2021**.
[4] Han, Shanyu, Carolyn E. Gunthardt, Richard Dawes, Daiqian Xie, Simon W. North, and Hua Guo. "Origin of the "odd" behavior in the ultraviolet photochemistry of ozone." *PNAS* 117, no. 35 (**2020**): 21065-21069.
[5] Quintas-Sánchez, Ernesto, Richard Dawes, Kelvin Lee, and Michael C. McCarthy. "Automated Construction of Potential Energy Surfaces Suitable to Describe van der Waals Complexes With Highly-Excited Nascent Molecules: The Rotational Spectra of Ar–CS (v) and Ar–SiS (v)." *The Journal of Physical Chemistry A* (**2020**).
[6] Yang, Dongzheng, Junxiang Zuo, Jing Huang, Xixi Hu, Richard Dawes, Daiqian Xie, and Hua Guo. "A Global Full-Dimensional Potential Energy Surface for the K2Rb2 Complex and Its Lifetime." *The Journal of Physical Chemistry Letters* 11, no. 7 (**2020**): 2605-2610.
[7] E. Q. Sanchez, R. Dawes. "Spectroscopy and Scattering Studies Using Interpolated Ab Initio Potentials" Annu. Rev. Phys. Chem. **2021** 72:1–24, https://doi.org/10.1146/annurev-physchem-090519-051837.
[8] Bop, Cheikh T., Ernesto Quintas-Sánchez, Sangeeta Sur, Mathurin Robin, François Lique, and Richard Dawes. "Inelastic scattering in isotopologues of O_2–Ar: the effects of mass, symmetry, and density of states." *Physical Chemistry Chemical Physics* 23, no. 10 (**2021**): 5945-5955.
[9] Desrousseaux, Benjamin, Ernesto Quintas-Sánchez, Richard Dawes, Sarantos Marinakis, and François Lique. "Collisional excitation of interstellar PN by H2: New interaction potential and scattering calculations." *The Journal of Chemical Physics* 154, no. 3 (**2021**): 034304.
[10] Welch, Bradley K., Richard Dawes, David H. Bross, and Branko Ruscic. (in prep)
[11] Steve Ndengué, Ernesto Quintas-Sánchez, Richard Dawes,David Osborn, The low-lying electronic states of NO_2: potential energy and dipole surfaces, bound states, and electronic absorption spectrum, (submitted to *JPC A*, **2021**).

Theoretical and Experimental Studies of Elementary Hydrocarbon Species and Their Reactions (DE-SC0018412)

Gary E. Douberly and Henry F. Schaefer III
University of Georgia, Center for Computational Quantum Chemistry and Department of Chemistry, 1004 Cedar St., Athens, GA 30602-1546
douberly@uga.edu

Program Scope

New theoretical and experimental methods in chemical physics being developed by the PIs provide great opportunities for the study of molecular species and chemical reactions of fundamental importance in combustion processes. In this research, high level quantum mechanical formalisms are a significant source of critical predictions concerning molecular systems that may be challenging for experiments. Moreover, our helium droplet experiments have opened whole new vistas for the spectroscopic study of molecular species relevant to combustion environments. Theoretical developments proposed herein include a focus on obtaining highly accurate energetics for species pertinent to combustion reactions. Experimental developments focus on strategies to characterize transient combustion intermediates associated with low-temperature hydrocarbon oxidation processes, which have been difficult to probe with other methodologies. The combination of theory and experiment to solve problems inaccessible to either alone is a hallmark of this research.

Nearly all of the proposed non-methodological experimental research will benefit from state-of-the-art molecular electronic structure theory. In some cases, the experimental group needs theoretical predictions prior to beginning a new set of experiments. In other cases, experimental findings are puzzling and need theory for interpretation. We have an abundance of experiences with both sets of problems, and the PIs have already collaborated in several such situations. Some situations where theory-experiment interaction will be particularly important include: (i) the C_nH_m + O(^3P) reactions, where predictions of structures, energetics, and spectroscopic properties of complexes and adducts on both singlet and triplet potential energy surfaces will be required; (ii) the spectroscopic studies of $(NH_2)_2$, NH-(NH_2), and other pre-reactive radical-radical complexes, where an interpretation will require computations of structures, energetics, and intersystem crossing rates; (iii) the near-IR and mid-IR studies of HOO-alkene complexes and related QOOH species, where computations of the excited state potential energy surface in the vicinity of the exit-channel complex will be essential; and (iv) the mid-IR studies of $\cdot C_nH_{2n+1}$ radicals, where the spectra are complicated by anharmonic and Coriolis resonances to an extent that the interpretation of these spectra will only be achievable through comparisons to effective Hamiltonian computations that employ highly accurate quartic force fields and Coriolis parameters.

Recent Projects

Infrared Spectroscopy of Alkyl and Alkyl Peroxy Radicals in Solid para-Hydrogen

We have continued our collaboration with Yuan-Pern Lee's group at the National Chiao Tung University in Taiwan. We continue to analyze spectra of alkyl radicals and alkyl peroxy radicals isolated in solid *para*-H_2, and we have recently published a paper in the *Journal of Molecular Spectroscopy* that reports the comprehensive assignment of the mid-IR spectra of *n*- and *i*-propyl radicals. In these studies, we are employing both normal mode and local mode effective Hamiltonian models to help assign spectra. We are studying the transferability of local mode Hamiltonian coupling parameters over a range of alkyl radical systems. We have recently recorded spectra of all four butyl radicals in helium droplets. These spectra are compared directly to those recorded for the solid-para hydrogen matrix environment. We are finding that the local mode anharmonic vibrational model is working for the more complicated butyl radical systems. Papers describing the butyl radical spectra are in preparation with an anticipated submission date this summer.

We have published a lengthy, invited review article on the theoretical methods and associated comparisons to experiment for the novel computational anharmonic vibrational spectroscopy models employed in this work. Theoretical background, equations, and recommendations have been given for the use of the Second-Order Vibrational Perturbation Theory with Resonances (VPT2+K) anharmonic model. Many examples were given of its successful application to molecules with varying severity of anharmonic resonance. Particular attention was paid to setting up effective Hamiltonians for systems with multiple, interacting anharmonic resonances. Analytic expressions for VPT2 transition moments between the ground state and 3-quanta states were reported together, in their correct form, for the first time. The 1-quantum and 2-quanta formulas were reproduced alongside them. In modeling the CH stretch regions of hydrocarbons with large effective Hamiltonian simulations, the significance of Darling-Dennison couplings could be explored. Their contribution was found to be minimal in the CH stretching region. Although a detailed benchmarking study has not been performed, it is expected that theoretical models which neglect Darling-Dennison coupling will still be very successful here. The intensities in these hydrocarbon systems were derived from both linear harmonic oscillator transition moments and VPT2 transition moments. The agreement with experiment is sufficiently good to facilitate spectral assignment with the simpler harmonic oscillator transition moments. The far more complicated deperturbed VPT2 transition moments do not appear to be necessary for simulations of CH stretches. It may even be the case that large effective Hamiltonian simulations using harmonic oscillator transition moments provide superior predictions to small effective Hamiltonian simulations based on more rigorous transition moments, which appears to be the more prevalent choice in the literature.

Peter R. Franke, John F. Stanton, Gary E. Douberly, "How to VPT2: Accurate and Intuitive Simulations of CH Stretching Infrared Spectra Using VPT2+K with Large Effective Hamiltonian Resonance Treatments" *Journal of Physical Chemistry A* (Invited Review), **125**, 1301-1324 (2021).

Selection of Theory Projects (no experimental contribution to the work).

A. S. Abbott, B. Z. Abbott, J. M. Turney, and H. F. Schaefer, "Arbitrary-Order Derivatives of Quantum Chemical Methods via Automatic Differentiation," *J. Phys. Chem. Lett.* **12**, 3232 (2021).

In this work, we presented for the first time a general methodology for obtaining arbitrary-order nuclear coordinate derivatives of electronic energies derived from quantum chemistry methods. Through leveraging modern advances in automatic differentiation software, we demonstrated that exact derivatives can be obtained for any method. This innovation completely bypasses the issues associated with the computational stability of applying numerical differentiation methods and dispenses the need to derive challenging formulae for analytic energy derivatives. We described a freely available and open-source software implementation of our scheme and demonstrate its use in obtaining exact nuclear derivatives of energies from Hartree-Fock theory, second-order Møller-Plesset perturbation theory (MP2), and coupled cluster theory with single, double, and perturbative triple excitations [CCSD(T)]. Our sample computations included up to sextic derivatives and spanned a variety of test systems with up to 100 basis functions, confirming the viability of this scheme for a wide range of applications. Many of the results obtained have hitherto been unobtainable by exact means due to a lack of higher-order derivative formulae. The details of our implementation and possible further developments were discussed.

J. D. Weidman, J.M. Turney, and H. F. Schaefer, "Energetics and Mechanisms for the Acetonyl Radical + O_2 Reaction: An Important System for Atmospheric and Combustion Chemistry," *J. Chem. Phys.* **152** 114301 (2020).

The acetonyl radical ($\bullet CH_2COCH_3$) is relevant to atmospheric and combustion chemistry due to its prevalence in many important reaction mechanisms. One such reaction mechanism is the decomposition of Criegee intermediates in the atmosphere that can produce acetonyl radical and OH. In order to understand the fate of the acetonyl radical in these environments and to create more accurate kinetics models, we have examined the reaction system of the acetonyl radical with O_2 using highly reliable theoretical methods. Structures were optimized using coupled cluster theory with singles, doubles, and perturbative triples [CCSD(T)] with an atomic natural orbital (ANO0) basis set. Energetics were computed to chemical accuracy using the focal point approach involving perturbative treatment of quadruple excitations [CCSDT(Q)] and basis sets as large as cc-pV5Z. The addition of O_2 to the acetonyl radical produces the acetonylperoxy radical, and multireference computations on this reaction suggest it to be barrierless. No submerged pathways were found for the unimolecular isomerization of the acetonylperoxy radical. Besides dissociation to reactants, the lowest energy pathway available for the acetonylperoxy radical is a 1-5 H shift from the methyl group to the peroxy group through a transition state that is 3.3 kcal mol−1 higher in energy than acetonyl radical + O_2. The ultimate products from this pathway are the enol tautomer of the acetonyl radical along with O_2. Multiple pathways that lead to OH formation was considered; however, all of these pathways are predicted to be energetically inaccessible, except at high temperatures.

Ongoing Experimental Work and Future Plans

Sequential Capture of O(^{3}P) and Alkenes by Helium Nanodroplets: Infrared Spectroscopy and Ab Initio Computations of the Triplet Biradical Intermediates

According to Smith *et al*. [Smith, I. W. M.; Sage, A. M.; Donahue, N. M.; Herbst, E.; Quan, D. *Faraday Discuss.* **2006**, 133, 137.], for molecule + radical reactions, the energetic difference between the molecule's ionization energy (IE) and the radical's electron affinity (EA) can provide insight into the nature of the reaction barrier, either *above* or *below* the reactant asymptote. They propose that a difference (IE − EA) greater than 8.75 eV indicates a real barrier above the asymptotic limit, whereas a value below 8.75 eV indicates a submerged barrier. Indeed, this difference for the O(^{3}P) + HCN system is 12.2 eV. Accordingly, the barrier to oxygen insertion into the CN π system is ~10 kcal/mol above the reactant asymptote, and a van der Waals complex is observed when these species are brought together in a 0.4 K helium nanodroplet. However, O(^{3}P) reactions with *alkenes* are predicted to cross the postulated 8.75 eV threshold as the alkene substitution pattern evolves from ethene (no substitution) to propene (methyl group substitution) to butene (dimethyl substitution, of which there are four different isomers), and this trend was tested by Sabbah *et al.* [Sabbah, H.; Biennier, L.; Sims, I.R.; Georgievskii, Y.; Klippenstein, S.J.; Smith, I. W. *Science* **2007**, 317, 102.]. Their findings corroborated the behavior predicted by Smith *et al.* The HCN + O(^{3}P) results presented recently by us demonstrate the feasibility for analogous alkene + O(^{3}P) spectroscopic studies, in which O(^{3}P) and alkenes of varying substitution are combined in helium droplets *via* the sequential capture scheme. As the *real* reaction barrier (*i.e.* for the ethene and propene reactions) evolves to being *submerged* below the asymptotic limit (*i.e*. for the butene reactions), one might expect that strongly bound reaction intermediates, such as triplet biradicals, will be observed in helium droplets, rather than van der Waals complexes. Given the fact that a 10,000 atom helium droplet can dissipate 140 kcal/mol, it should be possible to quench the internal energy of these reaction intermediates and probe them for the first time spectroscopically.

Joseph T. Brice, Peter R. Franke, Gary E. Douberly "Sequential Capture of O(^{3}P) and HCN by Helium Nanodroplets: Infrared Spectroscopy and Ab Initio Computations of the $^3\mathbf{\Sigma}$ O-HCN Complex" *Journal of Physical Chemistry A*, **121**, 9466-9473 (2017). Published: November 2017.

Selected Publications acknowledging DOE support (2018-2021):

1. Peter R. Franke, Joseph T. Brice, Christopher P. Moradi, Henry F. Schaefer, Gary E. Douberly, "Ethyl + O_2 in Helium Nanodroplets: Infrared Spectroscopy of the Ethylperoxy Radical" *Journal of Physical Chemistry A*, **123**, 3558-3568 (2019). DOI: 10.1039/c9cp01476d. Published: April 2019.

2. Alaina R. Brown, Joseph T. Brice, Peter R. Franke, Gary E. Douberly, "Infrared Spectrum of Fulvenallene and Fulvenallenyl in Helium Droplets" *Journal of Physical Chemistry A*, **123**, 3782-3792 (2019). DOI: 10.1021/acs.jpca.9b01661. Published: April 2019.

3. Peter R. Franke, Kevin B. Moore, Henry F. Schaefer, Gary E. Douberly, "*tert*-Butyl Peroxy Radical: Ground and First Excited State Energetics and Fundamental Frequencies" *Physical Chemistry Chemical Physics*, **21**, 9747-9758 (2019). DOI: 10.1039/C9CP01476D. Published: April 2019.

4. Michael C. Bowman, Gary E. Douberly, Henry F. Schaefer, "Convergent Energies and Anharmonic Vibrational Spectra of Ca_2H_2 and Ca_2H_4 Constitutional Isomers" *Physical Chemistry Chemical Physics*, **21**, 10914-10922 (2019). DOI: 10.1039/c9cp01643k. Published: May 2019.

5. Gregory T. Pullen, Peter R. Franke, Karolina A. Haupa, Yuan-Pern Lee, Gary E. Douberly, "Infrared Spectroscopy of *n*-Propyl and *i*-Propyl Radicals in Solid *para*-Hydrogen" *Journal of Molecular Spectroscop*y, **363**, 111170 (2019). DOI: 10.1016/j.jms.2019.07.001. Published September 2019.

6. Mathew M. Davis, Jared D. Weidman, Adam S. Abbott, Gary E. Douberly, Justin M. Turney, Henry F. Schaefer, "Characterization of the 2-Methylvinoxy Radical + O_2 Reaction: A Focal Point Analysis and Composite Multireference Study" *Journal of Chemical Physics*, (2019), 151, 124302. DOI: 10.1063/1.5113800. Published: September 2019.

7. Jonathon P. Misiewicz, Kevin B. Moore, Peter R. Franke, W. James Morgan, Justin M. Turney, Gary E. Douberly, and Henry F. Schaefer, "Sulfurous and Sulfonic Acids: Predicting the Infrared Spectrum and Setting the Surface Straight" *Journal of Chemical Physics*, **152**, 024302 (2020). DOI: 10.1063/1.5133954. Published January 2020.

8. Jared D. Weidman, Justin M. Turney, Henry F. Schaefer, "Energetics and Mechanisms for the Acetonyl + O_2 Reaction: An Important System for Atmospheric and Combustion Chemistry" Journal of Chemical Physics, 152, 114301 (2020). DOI: 10.1063/1.514859. Published: March 2020.

9. Michael C. Bowman, Alexandra D. Burke, Justin M. Turney, Henry F. Schaefer, "Conclusive Determination of Ethynyl Radical Hydrogen Abstraction Energetics and Kinetics" Molecular Physics, 118 (2020). DOI: 10.1080/00268976.2020.1769214. Published: June 2020.

10. Peter R. Franke, John F. Stanton, Gary E. Douberly, "How to VPT2: Accurate and Intuitive Simulations of CH Stretching Infrared Spectra Using VPT2+K with Large Effective Hamiltonian Resonance Treatments" *Journal of Physical Chemistry A* (Invited Review), **125**, 1301-1324 (2021). DOI: 10.1021/acs.jpca.0c09526. Published January 2021.

11. Matthew G. Christianson, Anna C. Doner, Matthew M. Davis, Alanna L. Koritzke, Justin M. Turney, Henry F. Schaefer, Leonid Sheps, David L. Osborn, Craig A. Taatjes, and Brandon Rotavera. "Reaction Mechanisms of a Cyclic Ether Intermediate: Ethyloxirane" *Int. J. Chem. Kinet.* **53**, 43-59 (2021). DOI: 10.1002/kin.21423. Published: January 2021.

12. Anna C. Doner, Matthew M. Davis, Alanna L. Koritzke, Matthew G. Christianson, Justin M. Turney, Henry F. Schaefer, Leonid Sheps, David L. Osborn, Craig A. Taatjes, Brandon Rotavera, "Isomer-Dependent Reaction Mechanisms of Cyclic Ether Intermediates: cis-2,3-dimethyloxirane and trans-2,3-dimethyloxirane" *Int. J. Chem. Kinet.* **53**, 127-145 (2021). DOI: 10.1002/kin.21429. Published: January 2021.

13. Adam S. Abbott, Boyi Z. Abbott, Justin M. Turney, Henry F. Schaefer, "Arbitrary-Order Derivatives of Quantum Chemical Methods via Automatic Differentiation" *J. Phys. Chem. Lett.* **12**, 3232-3239 (2021). DOI: 10.1021/acs.jpclett.1c00607. Published: March 2021.

Coordination and Solvation of Actinide Cations Studied with Selected-Ion Infrared Spectroscopy

DOE Award No. DE-SC0018835

Michael A. Duncan
Department of Chemistry, University of Georgia, Athens, Georgia 30602

maduncan@uga.edu

Program Scope

Actinide metal and metal oxide cation-molecular complexes are studied in the gas phase to investigate their bonding, ligand coordination and solvation. Cation-molecular complexes of the form $M^{n+}(L)_y$, where M = U or Th in singly- or doubly-charged states, and L = small molecules such as H_2O, CO, N_2, CO_2, O_2, or CH_3CN, are produced in a molecular beam by pulsed laser vaporization of solid metal targets. Similar methods are used to produce metal oxide complexes. Complexes containing a metal or oxide core ion with a specific number of ligand or solvent molecules are cooled by a supersonic expansion, size-selected in a time-of-flight mass spectrometer, and studied with infrared laser photodissociation spectroscopy. The resulting vibrational spectra reveal the shifts that occur for ligand/solvent vibrations upon binding to these metals and how these vary with the charge state, the number of ligands or solvent molecules present, the geometric and electronic structures of complexes, and the possible occurrence of ligand reactions mediated by the metal center. Additional experiments employ photofragment imaging technology to further investigate cation-molecular bond energies, and photodissociation experiments on larger metal oxide clusters. The experimental work is complemented by computational chemistry, with careful attention to relativistic and spin-orbit effects. The goal of these studies is an increased understanding of the fundamental interactions and electronic structure involved in actinide bonding, coordination and solvation.

Recent Progress

In recent work on this project, we used laser vaporization to produce ion-molecule complexes of uranium-acetone, and both uranium and thorium cation complexes with cyclo-octatetraene (COT). These systems were investigated with mass spectrometry and ion photodissociation to investigate coordination behavior and possible photochemical reactions that might occur upon ultraviolet excitation. We studied uranium-acetone ion-molecule complexes during a collaborative visit to our lab by Prof. Michael Van Stipdonk (Duquesne U.). Van Stipdonk had previously studied $UO_2^{2+}(acetone)_n$ ions produced with an electrospray source using collision-induced dissociation (CID). In our lab, laser vaporization of uranium in an expansion containing acetone vapor produced primarily singly-charged $UO_2^{+}(acetone)_n$ complexes (Figure 1), with only weak intensity mass peaks for U^+ or UO^+ complexes. It is not clear whether the di-oxide ion formed from residual surface oxides on the sample rod or from a

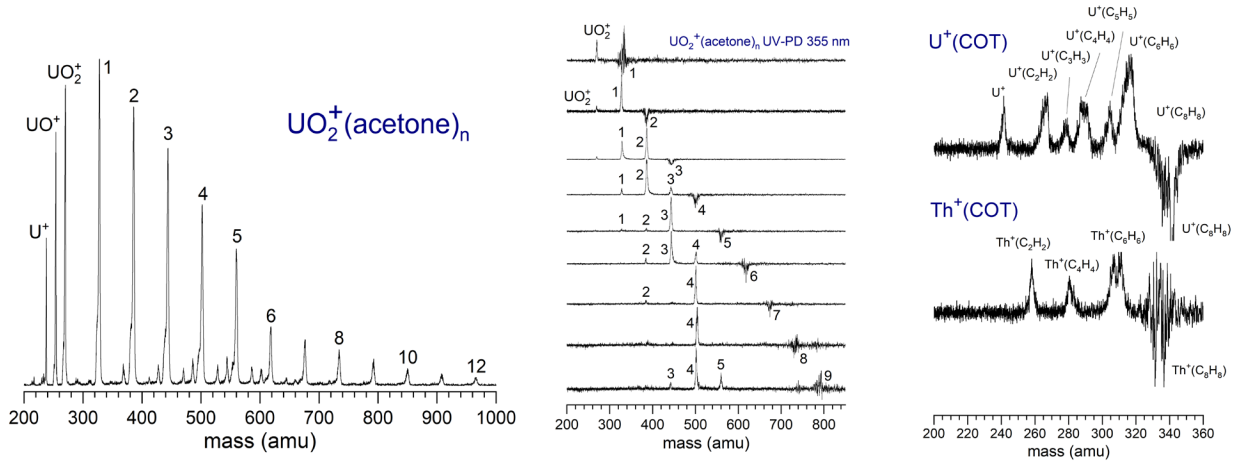

Figure 1. a) Mass spectrum of $UO_2^+(acetone)_n$ complexes (left). b) Photodissociation mass spectra of $UO_2^+(acetone)_n$ complexes at 355 nm. c) Photodissociation mass spectra of $M^+(COT)$ complexes, showing different ligand fragmentation processes for uranium vs thorium complexes.

reaction with acetone in the laser plasma. UV laser (355 nm) photodissociation of these complexes caused elimination of intact acetone molecules (Figure 1b). These complexes dissociated at very low laser powers, indicating single-photon absorption. In the larger complexes, the n = 4 complex survived preferentially, suggesting that the $UO_2^+(acetone)_4$ ion has a filled coordination. A similar coordination of four acetone ligands was found in the CID experiments on the uranyl dications. Other studies in our lab produced uranium and thorium cation-molecular complexes with cyclo-octatetraene (C_8H_8; aka, COT). In the dissociation of these complexes, intact ligand elimination was detected, but also the loss of C_2H_2 (presumed to be acetylene) via a photochemical reaction (Figure 1c). A similar reaction was seen previously for transition-metal or lanthanide cation-COT complexes. $U^+(C_5H_5)$ and $U^+(C_3H_3)$ fragment ions were also detected, which we found previously to be fragments from U^+(benzene). These unexpected reaction products were missing for thorium ions.

We have continued our studies on the infrared spectroscopy of $U^+(L)_x$ and $UO_n(L)_x^+$ complexes. In the past, we examined the carbonyl complexes of uranium and uranium oxide cations. In more recent work, we have extended these studies to complexes with L = CO_2, N_2, and water. The $U^+(H_2O)$ cation (Figure 2c) has three vibrational bands in the O–H stretching region, consistent with the formation of both a weakly bond cation-water complex and an H-U-OH^+ metal-hydroxy complex. The N–N stretches of the nitrogen complexes were shifted to lower frequencies compared to the free-N_2 stretch (Figure 2a), and the mass spectrum indicated a strong preference for an eight-coordinate complex. The spectrum of the $U^+(N_2)_8$ complex had a single vibrational band, indicating a high-symmetry structure. Uranium-CO_2 complexes had complex vibrational structure, indicating the possibility of both metal-CO_2 electrostatic complexes and the formation of O-U^+-CO reaction products. We were able to obtain infrared spectra for both singly and doubly charged complexes, e.g., $UO^{2+}(CO_2)_{7,8,9}$ in Figure 2b. Computational studies to explain these infrared spectra are ongoing. We have also continued

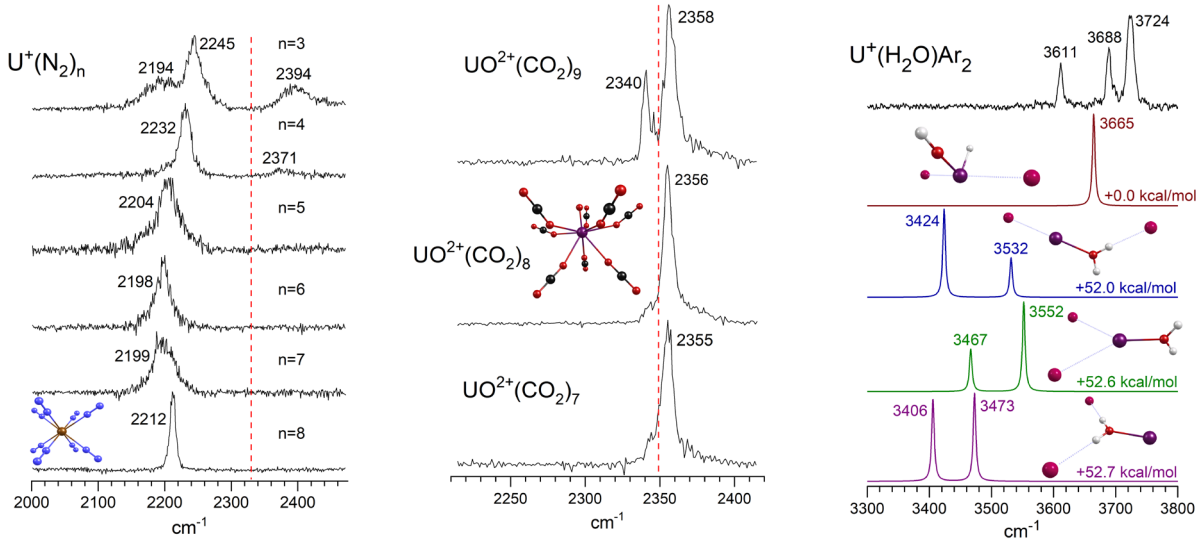

Figure 2. a) (left) IR-PD spectra for $U^+(N_2)_n$ complexes measured via the elimination of N_2. b) IR-PD spectra of $UO^{2+}(CO_2)_{7,8,9}$ showing the appearance of an un-shifted CO_2 vibration at n = 9 after the coordination is filled at n = 8. c) (right) IR-PD spectra of $U^+(H_2O)Ar_2$ compared to the predictions of theory for different isomers.

work begun under a previous DOE grant on transition metal chemistry, and have studied the complexes of several transition metal cations with acetylene. In the case of vanadium cations, single atom catalysis was observed leading to the cyclotrimerization of acetylene to form benzene. In the case of zinc cations, acetylene complexes formed a pre-reactive structure containing three acetylenes, and then the fourth acetylene was activated to form a metal-vinyl structure with a remote radical site on the distal carbon. Addition of a fifth acetylene led to a vinyl dimerization reaction.

Future Plans

We will continue the infrared spectroscopy experiments by examining uranium-acetylene and uranium-benzene complexes as well as small uranium and thorium carbonyls. Uranium cations have been suggested previously to catalyze the cyclo-trimerization reaction to form benzene, but there is no spectroscopic evidence to confirm this. An additional candidate for photodissocation studies is uranium carbide clusters. In a recent experiment with residual benzene in the gas lines, we inadvertently produced relatively large $U_xC_y^+$ clusters up to x, y values of 6,15. In future work we will optimize the production of these clusters, and use fixed-frequency photodissociation to study their stable stoichiometries.

BES Supported Publications (2018 – 2021)

1. M. A. Duncan, "Metal Cation Coordination and Solvation Studied with Infrared Spectroscopy in the Gas Phase," in *Physical Chemistry of Cold Gas Phase Functional Molecules and Clusters*, T. Ebata and M. Fujii, eds., Springer, Berlin, 2019, p. 157.

2. J. H. Marks, T. B. Ward, A. D. Brathwaite, *S. Ferguson*, M. A. Duncan, "Cyclotrimerization of Acetylene in Gas Phase $V^+(C_2H_2)_n$ Complexes: Detection of Intermediates and Products with Infrared Spectroscopy," *J. Phys. Chem. A* **123**, 6733−6743 (2019). DOI: 10.1021/acs.jpca.9b04962.

3. P. D. Carnegie, J. H. Marks, A. D. Brathwaite, T. B. Ward, M. A. Duncan, "Microsolvation in $V^+(H_2O)_n$ Clusters Studied with Selected-Ion Infrared Spectroscopy," *J. Phys. Chem. A* **124**, 1093−1103 (2020). DOI: 10.1021/acs.jpca.9b11275.

4. J. H. Marks, P. Kahn, M. Vasiliu, D. A. Dixon, M. A. Duncan, "Photodissociation and Theory to Investigate Uranium Oxide Cluster Cations," *J. Phys. Chem. A* **124**, 1940−1953 (2020). DOI: 10.1021/acs.jpca.0c00453.

5. J. H. Marks, T. B. Ward, A. D. Brathwaite, M. A. Duncan, "Infrared Spectroscopy of $Zn(Acetylene)_n^+$ Complexes: Ligand Activation and Nascent Polymerization," *J. Phys. Chem. A* **124**, 4764−4776 (2020). DOI: 10.1021/acs.jpca.0c03358.

6. A. D. Brathwaite, T. B. Ward, J. H. Marks, M. A. Duncan, "Coordination and Solvation in Gas Phase $Ag^+(C_2H_2)_n$ Complexes Studied with Selected-Ion Infrared Spectroscopy," *J. Phys. Chem. A* **124**, 8562−8573 (2020). DOI: 10.1021/acs.jpca.0c08081.

7. B. M. Rittgers, D. Leicht, M. A. Duncan, "Cation-π Complexes of Silver Studied with Photodissociation and Velocity-Map Imaging," *J. Phys. Chem. A* **124**, 9166−9176 (2020). DOI: 10.1021/acs.jpca.0c08498.

8. J. H. Marks, E. Miliordos, M. A. Duncan, "Infrared Spectroscopy of RG-$Co^+(H_2O)$ Complexes (RG = Ar, Ne, He): The Role of Rare Gas "Tag" Atoms," *J. Chem. Phys.* **154**, 064306 (2021). DOI: 10.1063/5.0041069.

Signatures of Reaction Mechanisms in the Vibrational Level Population Distribution of Reaction Products

Robert W. Field
Massachusetts Institute of Technology
Cambridge, MA 02139
rwfield@mit.edu

I. Introduction

The transition state and reaction pathway are core concepts of Chemistry, but direct *spectroscopic* characterization of a transition state has been considered to be impossible. What information could eigenstate-based frequency domain spectroscopy possibly provide about a dynamical event, such as isomerization, that occurs on a few-femtosecond time-scale?

Our project is based on the expectation that spectroscopic observation of the Vibrational Population Distributions (VPD) of photofragment molecules will convey information about the transition state at which the fragment molecules were born. This VPD information is conveniently encoded as the relative intensities of "vibrational satellites" on selected $J \leftrightarrow J+1$ rotational transitions in the Chirped Pulse millimeter-Wave (CPmmW) spectrum of the fragment molecules. CPmmW spectroscopy is a multiplexed technique in which *all* of the vibrational satellites are simultaneously sampled in *each* chirped mm-wave pulse.

Since the photofragment molecules are born distributed over many rotational levels, it is necessary to cool the rotational population distribution so that there are large population differences between the lowest few rotational levels. Rotational cooling in a supersonic molecular beam or in a cryogenic buffer gas source is very efficient and widely utilized. It is widely believed that vibrational cooling is on the order of 1000 times slower than rotational cooling. But is this true? What is the relationship between the VPDs inferred from the relative intensities of the vibrational satellite transitions and the nascent, collision-free VPD? Will this relationship be irremediably corrupted by E_{vib}-dependent and mode-specific collision-induced vibrational relaxation?

Our ultimate target is symmetric-triazine, which is known to fragment into three HCN molecules. Is this fragmentation sequential or simultaneous ("Triple Whammy")? However, in order to extract the uncorrupted nascent VPD from the CPmmW spectrum, it will be necessary to examine the propensity rules and relative rates of vibrational relaxation in molecular beams from a cryogenic buffer gas source and from a supersonic molecular beam. We have chosen the permanent gas, SO_2, as the target molecule for these preliminary studies.

The most convenient way to obtain an *a priori* known VPD in a rotationally cold molecule is to use a pulsed tunable laser to populate a single low-J vibration-rotation level of an electronically excited state. Fluorescence from this selected state will populate a Franck-Condon distribution of vibrational levels of the electronic ground state. Franck-Condon factors are routinely calculated from knowledge of the potential energy surfaces of the upper and lower energy electronic states,

even for polyatomic molecules. At high vibrational excitation in the electronic ground state, it is necessary to transform the set of normal mode Franck-Condon factors into the vibrational eigenstate representation in order to take into account inter-mode vibrational anharmonicity and Coriolis effects. For SO_2, calculations of these transformed Franck-Condon factors were completed in a previous DOE-supported program.[1–4]

II. Recent Progress

The present state of the SO_2 experiment is that an experimental apparatus has been constructed for combining the laser excitation and CPmmW beams with the SO_2 molecular beam in various geometries. The systematic effects of the extent of cooling along the direction of supersonic flow (downstream distance from the nozzle orifice) may be sampled either spatially or temporally. SO_2 is a bent triatomic molecule with only a nonzero b-axis dipole moment component. The microwave transitions are ΔK_a=odd, ΔK_c=odd, J=0, ±1. The vibrational dependence of the b-dipole transition frequency is small for modes 1 (symmetric stretch) and 3 (antisymmetric stretch), and large for mode 2 (bend). Therefore it is possible, within the bandwidth of a single chirped pulse, to sample the populations in many vibrational levels with excitations in the symmetric and antisymmetric stretching modes 1 and 3 but in only a few vibrational levels with excitations in the bending mode 2. The $\tilde{C}\leftarrow\tilde{X}$ $1_0^1 2_0^1 3_0^0$ electronic transition of SO_2 populates the (v_1=1,v_2=1,v_3=0) level of the $\tilde{C}$ state, which has a lifetime of ~50 ns. Fluorescence from this laser-populated level populates several vibrational levels of modes 1 and 2 in the $\tilde{X}$ electronic ground state. There is a long Franck-Condon progression in vibrational modes 1 and 2, as observed previously in studies of dispersed fluorescence.[5] Our CPmmW experiments in the 145-155 GHz region show that the 1_{11}-0_{00} rotational transition, which lies in the E-band, will yield several mode-1 vibrational satellites, which are expected to lie within 300 MHz of the corresponding rotation transition in the (0,0,0) and the (0,1,0) vibrational states.

Our E-band Chirped Pulse mm-wave sources and detection electronics have been tested and optimized. Experiments combining the laser excitation with CPmmW detection are in initial stages. We have been performing millimeter wave optical double resonance experiments to optimize the experimental scheme, which is sensitive to the relative polarizations of the optical and mm-wave beams. The millimeter wave radiation is polarized transverse to the molecular beam and the laser beam counter-propagates along the molecular beam axis. This arrangement will allow us to observe collision-induced vibrational relaxation at various points along the molecular beam, ranging from close to the nozzle orifice (maximum downstream collisional relaxation) to 20 cm downstream (negligible collisional relaxation). Several operating conditions of the General Valve, including backing pressure and orifice diameter, have been varied in order to optimize our study of the vibrational mode-specific relaxation dynamics of SO_2.

Its large polarizability (3.9 $Å^3$) and dipole moment (1.6 D) makes SO_2 prone to clustering. The existence of clusters has the potential to distort the observed VPD from what is expected for laser excited fluorescence from a non-clustered SO_2 molecule. Clustering is severe in a 5 bar expansion from a General Valve, but it is claimed to be negligible in a 50 Bar expansion from an Even-Lavie type valve.[6] Clustering will certainly be negligible in the expansion from a cryogenic buffer gas cell (Ne@20K, 100 mBar). Cryogenic Buffer Gas Beam (CBGB) experiments will begin after the completion of the General Valve experiments.

III. Future Work

We expect to begin CPmmW measurements of the VPD that results from laser photolysis of symmetric triazine before the end of the first year of this grant.

IV. Publications supported by this grant

1. D. P. Zaleski, R Sivaramakrishnan, H. R. Weller, N. A, Seifert, D. H. Bross, B Ruscik, K. B. Moore III, S. N. Elliott, L. B. Harding, S. J. Klippenstein, R. W. Field, and K. Prozument, "Substitution Reactions in the Pyrolysis of Acetone Revealed through a Modeling, Experiment, Theory Paradigm," J. Am. Chem. Soc. **148**, 3124/1-19 (2021).
2. Tutunnikov, L. Xu, R. W. Field, K. A. Nelson, Y. Prior, and I. Sh. Averbukh, "Enantioselective orientation of chiral molecules induced by terahertz pulses with twisted polarization, " Phys. Rev. Research **3**, 013249/1-9 (2021).

References

1. Park, G. B., Jiang, J., Saladrigas, C. A. and Field, R. W. Observation of b_2 symmetry vibrational levels of the SO_2 $\tilde{C}$ $^1B_2$ state: Vibrational level staggering, Coriolis interactions, and rotation-vibration constants. *J. Chem. Phys.* **144**, 144311/1-13 (2016).
2. Jiang, J., Park, G. B. and Field, R. W. The rotation-vibration structure of the SO_2 $\tilde{C}$ ^{1} B_2 state explained by a new internal coordinate force field. *J. Chem. Phys.* **144**, 144312/1-20 (2016).
3. Park, G. B., Jiang, J. and Field, R. W. The origin of unequal bond lengths in the $\tilde{C}$ $^1B_2$ state of SO_2: Signatures of high-lying potential energy surface crossings in the low-lying vibrational structure. *J. Chem. Phys.* **144**, 144313/1-7 (2016).
4. G. Barratt Park, "Full Dimensional Franck-Condon Factors for the Acetylene Transition. I. Method for Calculating Polyatomic Linear—Bent Vibrational Intensity Factors and Evaluation of Calculated Intensities for the gerade Vibrational Modes in Acetylene", *J. Chem. Phys*. **141**, 134304/1-18 (2014).
5. Yamanouchi, K., Takeuchi, S.and Tsuchiya, S. Vibrational level structure of highly excited SO_2 in the electronic ground state. II. Vibrational assignment by dispersed fluorescence and stimulated emission pumping spectroscopy. *J. Chem. Phys.* **92**, 4044–4054 (1990).
6. Even, U., Jortner, J., Noy, D., Lavie, N. and Cossart-Magos, C. Cooling of large molecules below 1 K and He clusters formation. *J. Chem. Phys.* **112**, 8068/1-4 (2000).

TOWARDS MACHINE LEARNING MOLECULAR DYNAMICS: PREDICTING METHANE EQUATION OF STATE

C. Franklin Goldsmith, PI
Brown University

Program Scope

One of the grand challenges for the Department of Energy is the ability to simulate the complex interactions between fluid mechanics and chemical kinetics for gases at high pressures (e.g. 100 bar). Under these conditions, the ideal gas equation of state is not valid. Although considerable advances have been made regarding real-gas equations of state for thermodynamic properties, the same cannot be said of chemical kinetics under extreme pressures. The standard approach in computational kinetics assumes that reactions occur under isolated conditions. Real-gas behavior can have a profound effect on the chemical source terms in reactive flow simulations. These many-body interactions can change both the rate constants and the product branching fractions.

In this project, we are investigating different methodologies to quantify many-body effects on transition states and thence high-pressure effects on rate constants. The specific aims are: (i) develop chemically accurate surrogate potential energy surfaces for computational kinetics with explicit solvent molecules, and use this surrogate model within molecular dynamics simulations; (ii) quantify the effects of high pressures on rate constants for different reaction families; (iii) determine the pressure at which solvent cage effects will cause the branching fractions in bond-fission reactions to favor molecular elimination products; and (iv) analyze the results for possible trends that can be applied heuristically.

Recent Progress

The past year has focused exclusively on the development of a machine learning molecular dynamics (MLMD) methodology. The goal is to develop a platform, as close to black box as possible, that will enable us to go from electronic structure calculations to a full-dimensional force-field model for use in molecular dynamics for arbitrary systems.

In order to develop a potential model suitable for MD, we need to provide sufficient sampling in both intramolecular and intermolecular interactions. Our current work uses density functional theory (DFT) to provide the required training data. Preliminary work focused on random sampling within internal-coordinate space as a way of exploring in intramolecular interactions. This approach, while computationally advantageous, did a poor job of covering the regions of phase space that were explored during the MD simulations. Instead, we used ab initio molecular dynamics (AIMD) to generate the training data.

The primary focus on the past year has been on developing a potential for methane. The advantages to beginning with methane are straightforward: it is computationally affordable, and well-validated equations of state already exist. The first step was to determine how many CH_4 are required for the AIMD. The CH_4-CH_4 interaction potential

decreases from 0.15 kJ/mol at 6 Å to 0.10 kJ/mol at 8 Å. The change in intermolecular forces was similarly negligible. At the most extreme density considered, corresponding to 1000 bar and 100 K, the average C-C coordination number was ~12 at 6 Å and ~30 at 8 Å. Thus, we considered 12 to be a suitable number of CH_4 molecules in the AIMD training simulations, since it would effectively sample a broad swath of intra- and intermolecular interactions within the first solvation shell for the high-density cases.

After different feasibility studies, we settled on the ωB97M-D3(BJ)/def2-TZVP(-f) functional and basis set, as implemented in ORCA. In order to cover a range of temperatures and pressures, we settled on the following strategy. 80 unique initial configurations were generated using Packmol. For each configuration, AIMD simulations within the *NVT* ensemble were performed with T = 1000 K, 2000 K, and 3000 K. Each simulation was run for 500 fs, with a timestep of 0.5 fs. The volume was set to have a repulsive wall to maintain an approximate density. Within each simulation, this volume was expanded every 100 fs, so as to sample different densities at a given temperature. Collectively, this approach generated 80,000 unique configurations spanning a broad range of (non-reactive) phase space.

Artificial neural networks (NN) were used for the machine learning. The package N2P2 was used, in part because it already has an established link to the LAMMPS MD package. The N2P2 code utilizes a multistream Kalman filter optimizer to facilitate the training process especially when the data set is large and forces are included in the training. The short-range local atomic environments were described within a cutoff value of 12 Bohr (6.35 Å) using a set of many-body atom-centered radial and angular symmetry function consisting 60 and 50 functions for H and C atoms, respectively. Different combinations of nodes and hidden layers were considered, as well as the impact of different random number seeds and force update criteria, resulting in 30 different NN models.

To evaluate the 30 distinct NN models, we considered how well they could predict the mass density. 512 CH_4 molecules were simulated with periodic boundary conditions using the LAMMPS/ N2P2 interface. The initial configurations were generated using the VMD TopoTools plugin. The system was first equilibrated for 25 ps in the *NPH* ensemble coupled to a Langevin thermostat to keep the temperature constant. The equilibrated system was then used for a 0.5 ns production run in the *NPT* ensemble. Preliminary studies confirmed that 0.5 ns is enough for obtaining the equilibrated mass density. The timestep of 0.5 fs was applied to all simulations and the configurations were collected every 100 fs. The resulting dataset was sufficient to predict the mass density as a function of time. The average mass density (after the initial equilibration) was then recorded.

Next, we considered the following six conditions representing approximately the extrema of our conditions: 100 K and 1 atm (liquid), 100 K and 1000 atm (liquid), 300 K and 1 atm (gas), 300 K and 1000 atm (gas), 1200 K and 1 atm (gas), and 1200 K and 1000 atm (gas). The mass density from each of the 30 NN models was computed for each of these six conditions. The NN model that was closed to the normalized mean was selected as the

most likely candidate. This $\rho(T, p)$ was then compared against the CH_4 equation of state included in CANTERA. The results are summarized below.

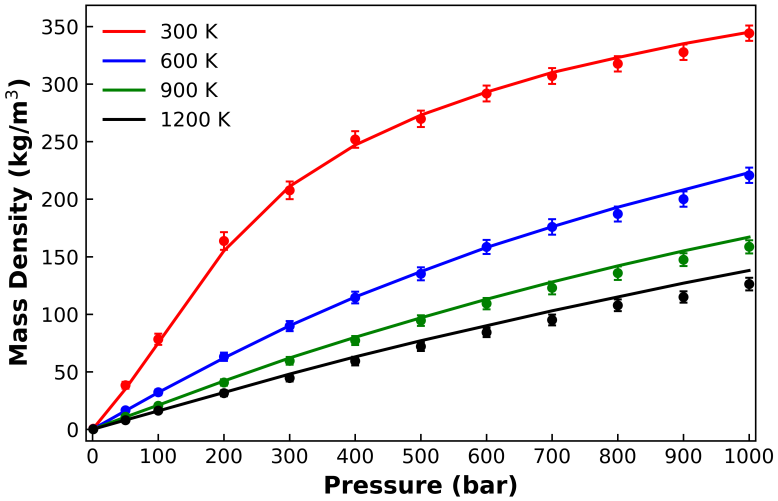

Figure 1: predicted mass density in the gas phase. The solid lines are the reference equation of state in CANTERA. The symbols are the results from our MLMD approach.

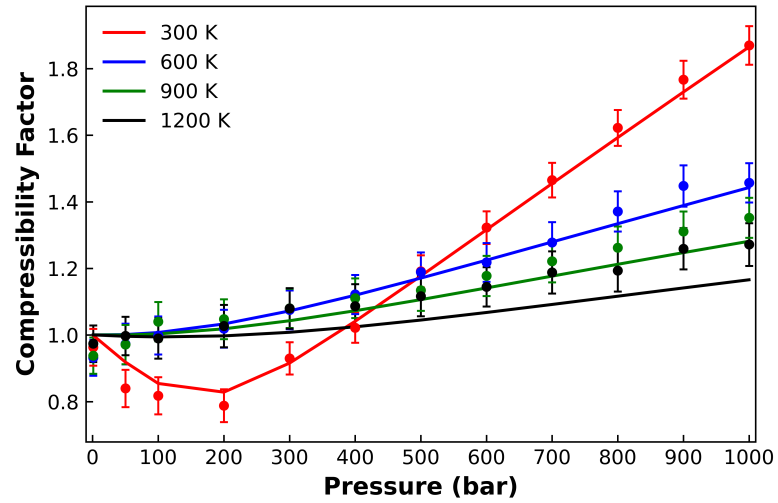

Figure 2: same data as Figure 1, but presented in terms of compressibility factor, *Z*.

Figures 1 and 2 summarize the results for the gas phase. The MLMD potential quantitatively captures the real-gas behavior of methane for the highest density configurations (*e.g.* the red line in Figures 1-2). The model is less accurate at the highest temperatures, corresponding to the lowest densities. Presumably this is due to our inability to capture some long-range interactions, given the current cut-off radius. We considered possible strategies to overcome this problem.

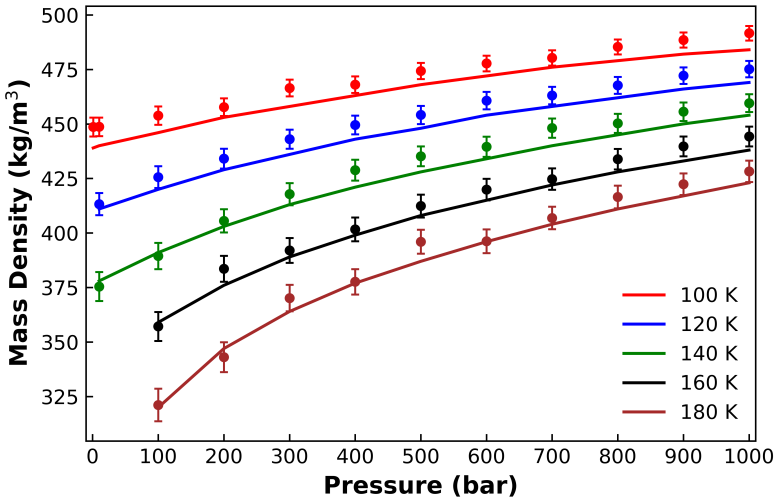

Figure 3: liquid phase mass density.

Figure 3 presents the MLMD results for the liquid state. As before, the MLMD approach is in quantitative agreement with the literature equation of state.

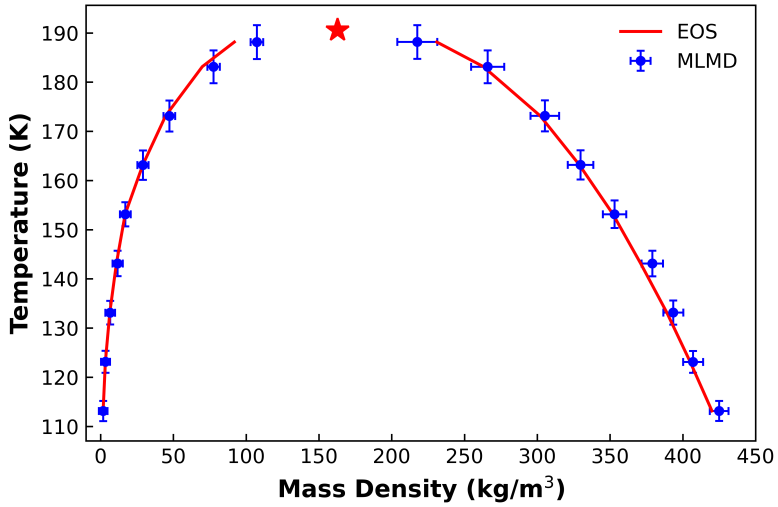

Figure 4: liquid-vapor coexistence curve.

Figure 4 demonstrates that we can correctly predict the vapor-liquid curve, suggesting that this new approach can be used for MD simulations for phase change.

Future Plans

This work will go in two directions. The next step will be to focus on kinetics. Specifically, we will use the present MLMD work to compute the change in volume of activation, $\Delta V^{\ddagger}$, as a function of temperature and pressure. This $\Delta V^{\ddagger}(T, p)$ will enable us to compute real-gas corrections for rate constants. The second direction will be to look at

the equation of state properties for real-gas mixtures – something which is currently a major theoretical challenge for novel mixtures.

BES Supported Products

- This grant supported Dr. Mostafa Abedi. We will submit the CH_4 material in the spring of 2021 for publication. (Due to the pandemic, Dr. Abedi was unable to travel to any conferences and present the work.)
- Three publications in the Proceedings of the Combustion Institute:
    [1] A. D. Danilack and C. F. Goldsmith "A statistical model for the product energy distribution in reactions leading to prompt dissociation" *Proceedings of the Combustion Institute*, 38 (2021), 507-514
    [2] A. D. Danilack, S. J. Klippenstein, Y. Georgievskii, and C. F. Goldsmith "Low-temperature oxidation of diethyl ether: Reactions of hot radicals across coupled potential energy surfaces" *Proceedings of the Combustion Institute*, 38 (2021), 671-679
    [3] T. Sikes, K. B. Burdett, R. L. Speth, C. F. Goldsmith, R. Sivaramakrishnan, and R. S. Tranter "Ring opening in cycloheptane and dissociation of 1-heptene at high temperatures" *Proceedings of the Combustion Institute*, 38 (2021), 929-937

DE-SC0021206: Langevin Dynamics modeling of gas-phase ion-ion recombination

Principal Investigator: Ranganathan Gopalakrishnan, Ph. D.

Mailing Address: 310D Engineering Science, University of Memphis, Memphis, TN 38152.
E-mail: rgplkrsh@memphis.edu

Program Scope: The recombination of ions in the gas-phase plays an important role in the chemical composition, energy and charge balance of partially ionized gas environments such as flames, plasmas, inter-planetary gas clouds and ultra-cold (~few K) systems like cryogenics and quantum computers. Motivated by the lack of robust theoretical models of gas-phase ion-ion recombination, a data-driven approach to modeling the recombination rate constant β_r by analyzing trajectories calculated (using Langevin Dynamics (LD) at pressures $\geq 1\ kPa$ and Molecular Dynamics (MD) at pressures $\leq 1\ kPa$) taking into account the ion-ion electrostatic interactions, ion-neutral gas molecule collisions and ion number concentration is pursued in this project. The recombination rate constant β_r will be parameterized by calculating the average collision time between cation and anion in the presence of neutral gas molecules for a wide range of gas pressure p and temperature T of interest to aforesaid applications ($p \geq 10^2 Pa, T \geq 1\ K$). In this framework, various chemical physics that include the effect of ionic structure, molecular rotation, ion number concentration, electron transfer kinetics will be systematically explored to develop regression expressions. An exhaustive set of experimental data for β_r obtained using FALP-VENDAMS method (mostly from Albert Viggiano's group at AFRL and a few other groups) is used to evaluate the accuracy of the developed expressions and the % difference between prediction and measurement will be used as feedback to revise the modeling assumptions. To provide accurate inputs to the Langevin/ab initio Molecular Dynamics calculation of β_r, the ionic structures will be determined using the Gaussian16® commercial package. The ion mobility or diffusion coefficient will be obtained from published experimental data or calculated using the IMoS ion mobility calculation package (developed by Prof. Carlos Larriba, IUPUI).

Recent Progress: Ion recombination or mutual neutralization is modeled within the framework of classical physics and thus does not explicitly model the quantum nature of electron transfer kinetics from the anion to the cation (proton exchange reactions are not considered). This requires a precise, universal definition of what constitutes collision recombination that may thought of to happen in two steps: transport driven by ion-ion potential interaction φ_{i-i} and ion thermal energy $k_B T$, followed by electron transfer when the ions are "sufficiently" close.

$$\varphi_{i-i}(\vec{r}_{\pm}, \vec{\theta}_{\pm}) = \sum_{i=1}^{N_+} \sum_{j=1}^{N_-} \left(4\varepsilon_{ij} \left[\left(\frac{\sigma_{ij}}{r_{ij}} \right)^{12} - \left(\frac{\sigma_{ij}}{r_{ij}} \right)^{6} \right] + \frac{\delta_i \delta_j e^2}{4\pi\varepsilon_o r_{ij}} \right) \ldots (1)$$

Here, σ_{ij} can be understood as the distance between two atoms at which the potential energy (due to van der Waals or polarization interaction) between the ions is zero. Two atoms, as they get

closer, feel a strong repulsion $\sim r^{-12}$ due to electron degeneracy pressure. For low energy ions, overcoming this repulsion is not feasible and so the ions scatter off of each other at a distance of closest approach that is of the same order of magnitude as σ_{ij}. We hypothesized that electron transfer takes place with near certainty when two atoms (one part of the cation and the other part of the anion) when their separation r_{ij} is less than or equal to σ_{ij}: $r_{ij} \leq \sigma_{ij}$. To test this hypothesis, we carried out Langevin Dynamics simulations of the following ion pairs:

- $Xe^+ + F^-$ in He gas, 300 K, 20 – 80 kPa
  - Source: Lee and Johnsen (1990)
- $SF_6^+ + SF_6^-$ in SF_6 gas, 300 K, 1 – 3000 kPa
  - Source: Jungblut et al. (1989)
- $(H_2O)_2H_3O^+ + NO_3^-, (H_2O)_3H_3O^+ + NO_3^-$ in He, Ar gas, 300 K, 20 – 80 kPa
  - Source: Lee and Johnsen (1989)

The computed β_r are compared with experimental data and the % the difference is used to assess the accuracy of the modeling assumptions. **Figures 1** presents comparisons for $SF_6^+ + SF_6^-$ in SF_6 and $Xe^+ + F^-$ in He. The presented LD calculations at high pressures ($\geq 1\ kPa$) reveal excellent agreement to support the hypothesis that σ_{ij} is an excellent approximation for the electron tunneling distance of the modeled ion recombination reactions involving both monoatomic and polyatomic ions.

Future Plans: One publication is under preparation on these results for recombination at high pressures and is expected to set the tone for future studies to address various complexities. Much work remains to be done to test this hypothesis at pressures < 1 kPa and to see what effect ion rotation plays in the recombination process. For < 1 kPa, MD simulations (using our own code as well using LAMMPS) will be used to derive β_r values. The overarching goal is to develop regressions for β_r (specific to each ion pair) that will 1) depend only on well-defined quantities such as the ion mass, chemical structure, friction or low-field electrical mobility tensor and fully resolved ion-ion potential (of the form of eq. 1) and 2) will be valid for a wide range of pressure all the way from $p \to 0$ (vacuum limit, $< 1\ kPa$) to the $p \to \infty$ (liquid limit, $> 1\ MPa$).

References to publications of DOE sponsored research:

1. Suresh*,#, V., Li*,#, L., Redmond Go Felipe*, J. and **Gopalakrishnan, R.**, Modeling nanoparticle charge distribution in the afterglow of non-thermal plasmas and comparison with measurements (*accepted* for publication in J. Physics D: Applied Physics, #equal contribution)
   https://doi.org/10.1088/1361-6463/abf70c
2. Suresh*, V. and **Gopalakrishnan, R.** (***invited*** methods article), Tutorial: Langevin Dynamics methods for aerosol particle trajectory simulations and collision rate constant modeling. *Journal of Aerosol Science* 155: 105476.
   https://doi.org/10.1016/j.jaerosci.2021.105746

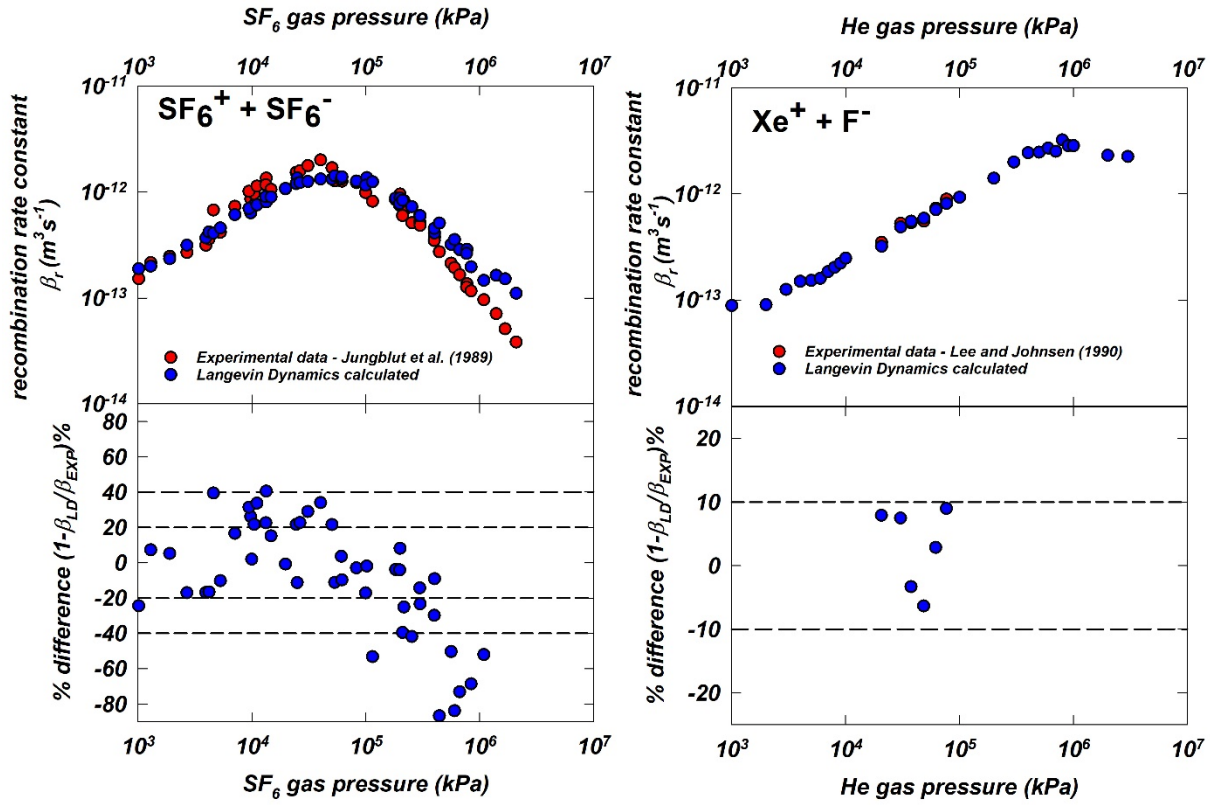

Figure 1: Comparison of experimentally measured and Langevin Dynamics computed values of the recombination rate constant β_r as a function of gas pressure at 300 K (for both data sets).

Key references

1. Jungblut, H., D. Hansen and W. F. Schmidt (1989). "Ion-ion recombination in electronegative gases." Ieee Transactions on Electrical Insulation **24**(2): 343-348.

2. Lee, H. S. and R. Johnsen (1989). "Ion–ion recombination studies in ambient helium and argon at atmospheric densities." The Journal of Chemical Physics **90**(11): 6328-6334.

3. Lee, H. S. and R. Johnsen (1990). "Recombination of Xe+ with F− ions in ambient helium." The Journal of Chemical Physics **93**(7): 4868-4873.

Computer-Aided Construction of Chemical Kinetic Models

William H. Green
Department of Chemical Engineering
Massachusetts Institute of Technology
Cambridge, MA 02139
whgreen@mit.edu

I. Program Scope

The chemistry of even simple molecules can be extremely complex, involving hundreds or thousands of kinetically significant species. To deal with this, we use the computer to both construct and solve the kinetic model. Because these large models contain so many parameters (e.g. k's, Keq's) one never has sufficient data to determine them all experimentally. Instead one must work in "predictive" mode, using theoretical values for many of the numbers in the model, and refining the most sensitive numbers through experiments. Typically there are several numerical values for each rate parameter: estimates, numbers from detailed quantum chemistry calculations, and values derived from experiments. Since there are multiple values, with various uncertainties, for hundreds of reactions, this line of research connects fundamental studies of individual reactions with data science and uncertainty quantification.

Predictive chemical kinetics is exactly what is needed for computer-aided design of combustion systems based on proposed alternative fuels, particularly for early assessment of the value and viability of proposed new fuels. It is also helpful in many other important chemistry problems, for designing and interpreting experiments, and in understanding emissions and environmental chemistry. However, making accurate predictions is hard, particularly for complicated systems where the predictions are most needed.

Our research effort is aimed at making accurate predictive chemical kinetics practical, testing the accuracy of our predictions, and then using our new modeling capability to help solve outstanding scientific and technological problems. We start from quantum chemical calculations on individual molecules and elementary-step reactions, develop improved rate/thermo estimation and calculation procedures, and create algorithms and software for constructing and solving kinetic simulations. We also develop methods for quantifying uncertainties, and for model-reduction. The models are tested with experimental data measured in our lab or in collaboration with others.

II. Recent Results

A. Chemistry of Cyclics & Polycyclics, esp. Polycyclic Aromatics

The formation of aromatics, particularly polycyclic aromatics, is a major problem in many systems, leading to particulate air pollution, fouling of equipment and engines, and emissions of carcinogens. While this topic has been heavily studied, many basic issues are still unresolved and we are still far from having models which are simultaneously consistent with experimental observations, rate theory, and the laws of thermodynamics. There are several modeling challenges: the chemistry is surprisingly complicated, with a large number of distinct polycyclic radicals, many of them with multiple resonance forms.[3,21] Also, the properties of these fused-ring species are not as systematic as the acyclic and monocyclic molecules, leading to larger errors in estimates of thermochemistry and reaction rates.

To try to fill in the gaps in existing knowledge, my group has experimentally measured several different ring-forming reactions [12-14]. We have also computed many rate and thermochemical parameters using quantum chemistry.[1,2,9,15-20] We have also developed improved methods for estimating the relevant thermochemistry.[22,23] We have also created detailed kinetic models starting from various small molecules through the formation of the second and third aromatic rings at a variety of reaction conditions.[24,25]

We recently resolved an important discrepancy. It has long been assumed that the C10H7 radicals formed by extracting an H atom from naphthalene would react sequentially with C2H2 to form

phenanthrene and anthracene (the C14H10 polycyclic aromatics with 3 fused benzene rings) via various HACA pathways. Indeed phenanthrene and anthracene are frequently measured as final products in pyrolysis and fuel-rich combustion under circumstances that suggest this reaction sequence. However, direct photoionization mass spec measurements at the ALS by Parker et al. [26] following pyrolysis of radical precursors in acetylene in a Chen-type nozzle did not detect phenanthrene or anthracene at all. Instead Parker et al. observed that one of the isomers of naphthalenyl radical primarily formed acenaphthylene (C12H8, naphthalene capped with a 5-membered ring), while the other isomer primarily formed ethynylnaphthalene (a 2-ring C12H8 species).

We therefore did a series of direct experiments, forming each naphthalene radical by flash photolysis, and then measuring the products by VUV photoionization mass spectrometry. Like Parker et al., we observe acenaphthylene from one radical isomer, formed from the initial adduct via the sequence of unimolecular reactions predicted by the quantum chemistry. From the other isomer we observe ethynylnaphthalene, same as Parker et al., but we also detect a clear C14H10 peak. Our kinetic model [27] based on quantum chemistry calculations [28-29] explains the discrepancy: at our lower-temperature (800 K) conditions the formation of phenanthrene and anthracene by the low-temperature Bittner-Howard reaction mechanism runs efficiently through a thermalized C12H9 intermediate. At the higher temperatures (e.g. 1200 K) where Parker et al. made most of their measurements, the initially-formed C12H9 intermediate does not live long enough to react with the second acetylene. At lower temperatures, Parker et al. were not able to see much signal, since the thermal decomposition of the precursor to form radicals in the nozzle was too slow to make much product. But in our experiments, we formed the radicals by flash photolysis, so we could measure products at the lower temperature where the Bittner-Howard route is important.

B. Tracking isotopes, correcting symmetry factors in TST calculations

We have added the capability to automatically track isotopic enrichment and specific isotopomers to the RMG software suite. RMG can now very reliably predict the relative yields of isotopomers in the reaction products, or vice-versa infer the original site-specific isotope enrichment from those measured in the final products.[30] This avoids the need to synthesize authentic standards of specific isotopomers.

When predicting isotopomer yields initially, we noticed that the predictions for systems where symmetrical X + X reactions are important were much less accurate than for other systems. Investigation revealed a factor of 2 error in the published formulae for k's for X+X reactions. This small error is often much larger than the small differences in reactivity of different isotopomers, so for isotope analysis it is crucial to get it right. We have carefully explained the whole issue in recent papers.[6,7]

C. Improvements to the Overall Mechanism Construction Process

We have developed an improved overall workflow, where we iterate between adding additional reactions to the mechanism (e.g. using RMG) and improving the values of uncertain rate and thermo parmeters in the existing model (e.g. by automatically spawning quantum chemistry calculations and using the results to improve rate and thermo estimates [1,17]. Adding reactions reduces the mechanism truncation error [4], i.e. it improves the structure of the model, while the second step reduces the error in the model parameters. We recently published a Perspective [10] discussing the overall kinetic model construction procedure at a high level, and a book chapter giving more technical detail.[4]

We are collaborating with Stephen Klippenstein and Judit Zador on automating the whole process of building a kinetic model including all the needed quantum chemistry calculations. We have made advances in speeding these calculations [5] and in quantifying the uncertainties in the final kinetic model predictions, accounting for the often highly-correlated errors in the parameters.[8] Many of the advances reported here have been incorporated into the open-source RMG software as version 3.0 [11]. The individual rate and thermochemical parameter estimates are also available in human-friendly form on our popular (~1,000 unique visitors per month) website (rmg.mit.edu).

A key challenge for this field has been the difficulty of computing reaction rates, largely due to the difficulty of (i) identifying which reactions have low enough barriers that they are worth computing and (ii) providing a good enough guess at the transition state geometry so that the computation will converge. Currently both of these key steps depend on human experts. We would like to automate the steps, to allow us to build models with thousands of reactions and also to make it practical for non-experts to make good kinetic models for their systems of interest. We recently succeeded to compute the transition state geometries and barrier heights for more than 10,000 reactions [31] using (expensive) Growing String methods. We used those as training data for Machine Learning methods for estimating Ea's [32] and for providing good guess TS geometries [33].

III. Future Plans

Upgrading Estimators and Automatic Quantum in RMG. As discussed above, we have recently developed much better ways to estimate reaction barriers, thermochemistry, etc., and ways to automatically spawn quantum chemistry calculations to improve the numerical values. Next step is to integrate these into RMG to rapidly and automatically improve the kinetic models.

Benzyne-driven formation of polycyclics. We are currently experimentally studying the chemically-activated reaction of ortho-benzyne (C6H4) with benzene: C6H4 + C6H6 → C10H8 + C2H2. Comandini et al. computed that this reaction would be fast, but no one has studied it experimentally, and it is not included in existing soot-formation models. In our initial flash photolysis VUV PIMS experiments, we observe a strong m/z=128 (C10H8) signal, suggesting the theoretical prediction is correct. After determining the rate coefficient, we will include this reaction and its analogues in RMG so it will automatically be included in future kinetic models.

Models for Alternative Fuels. We are in the process of developing kinetic models for the combustion of several proposed biofuels, to understand their unusual performance at engine conditions.

IV. Publications and submitted journal articles supported by DOE BES 2019-2021

1. Murat Keceli et al. Automated Computational Thermochemistry for Butane Oxidation: A Prelude to Predictive Automated Combustion Kinetics. *Proc. Combust. Inst.* **37**, 363-371 (2019).
2. Alon Grinberg Dana et al. Large Intermediates in Hydrazine Decomposition: A Theoretical Study of the N_3H_5 and N_4H_6 Potential Energy Surfaces. *J. Phys. Chem. A* **123**, 4679-4692 (2019).
3. Alon Grinberg Dana, Mengjie Liu, William H. Green. Automated Chemical Resonance Generation and Structure Filtration for Kinetic Modeling. *Int. J. Chem. Kinet.* **51**, 760–776 (2019).
4. William H. Green, Automatic Generation of Reaction Mechanisms. *Computer-Aided Chemical Engineering* **45**, 259-294 (2019).
5. Agnes Jocher et al. Scalability strategies for automated reaction mechanism generation", *Computers & Chemical Engineering* **131**, 106578 (2019).
6. Mark J. Goldman, Shuhei Ono, William H. Green. Accepted method for computing X+X rates is incorrect, causes large errors in isotope analysis. *J. Phys. Chem. A* **123,** 2320–2324 (2019).
7. Mark J. Goldman, Shuhei Ono, William H. Green. Addition to 'Accepted method for computing X+X rates is incorrect, causes large errors in isotope analysis'. *J. Phys. Chem. A* **124,** 257 (2020).
8. Connie W. Gao, Mengjie Liu, William H. Green. Uncertainty Analysis of Correlated Parameters in Automated Reaction Mechanism Generation. *Int. J. Chem. Kinet.* **52**, 266-282 (2020).
9. Ryan J. Gillis, William H. Green. Thermochemistry Prediction and Automatic Mechanism Generation for Oxygenated Sulfur Systems: A Case Study of Dimethyl Sulfide Oxidation. *ChemSystemsChem* **2**, e1900051 (2020). http://dx.doi.org/10.1002/syst.201900051
10. William H. Green. Moving from Postdictive to Predictive Kinetics in Reaction Engineering. *AIChE J.* **66**, e17059 (2020). https://doi.org/10.1002/aic.17059

11. Mengjie Liu et al. RMG 3.0: Advances in Automatic Mechanism Generation. *J. Chem. Inf. Model* (submitted)

Other Literature Cited

12. M.C. Smith et al. Direct Measurement of Radical-Catalyzed C_6H_6 Formation from Acetylene. *J. Phys. Chem. A* **124**, 2871-2884 (2020).
13. T.-C. Chu et al. From Benzene to Naphthalene, Direct Measurement of Reactions and Intermediates of Phenyl Radical and Acetylene. *Physical Chemistry Chemical Physics* **21**, 22248 (2019).
14. L. Lai, H.-W. Pang, W.H. Green. Formation of Two-Ring Aromatics in Hexylbenzene Pyrolysis. *Energy & Fuels* **34**, 1365-1377 (2020).
15. S. Khanniche, L. Lai, W.H. Green. Kinetics of intramolecular Phenyl Migration and Fused Ring Formation in Hexylbenzene Radicals. *J. Phys. Chem. A* **122**, 9778–9791 (2018).
16. K. Zhang et al. An experimental, theoretical, and modeling study of the ignition behavior of cyclopentanone. *Proceedings of the Combustion Institute* **37**, 657-665 (2019).
17. L. Lai, W.H. Green. Thermochemistry and Kinetics of Intermolecular Addition of Radicals to Toluene and Alkylaromatics. *J. Phys. Chem. A* **123**, 3176-3184 (2019).
18. L. Lai, S. Khanniche, W.H. Green. Thermochemistry and Group Additivity Values for Fused Two Ring Aromatic Species and Radicals, *J. Phys. Chem. A* **123**, 3418 (2019).
19. M.J. Goldman et al. Pressure-dependent kinetics of peroxy radicals formed in isobutanol combustion. *Phys. Chem. Chem. Phys.* **22**, 19802-19815 (2020).
20. X. Dong et al. Revealing the critical role of radical-involved pathways in high temperature cyclopentanone pyrolysis. *Combustion & Flame* **216**, 280-292 (2020).
21. M. Liu, W.H. Green. Capturing Aromaticity in Automated Mechanism Generation Software. *Proceedings of the Combustion Institute* **37**, 575-581 (2019).
22. Yi-Pei Li et al. *J. Phys. Chem. A* **123**, 2142-2152 (2019).
23. C.M. Grambow, Y.-P. Li, W. H. Green. Accurate Thermochemistry with Small Datasets: A Bond Additivity Correction and Transfer Learning Approach. *J. Phys. Chem. A* 123, 5826 (2019).
24. Te-Chun Chu et al. Modeling of aromatics formation in fuel-rich methane oxy-combustion with an automatically generated pressure-dependent mechanism. *Phys. Chem. Chem. Phys.* **21**, 813 (2019).
25. Mengjie Liu et al. Predicting polycyclic aromatic hydrocarbon formation with an automatically generated mechanism for acetylene pyrolysis. *Int. J. Chem. Kinet.* **53**, 27-42 (2021).
26. Dorian S.N. Parker et al. Unexpected Chemistry from the Reaction of Naphthyl and Acetylene at Combustion-Like Temperatures. *Angew. Chemie Intl. Ed.* **54**, 5421-5424 (2015).
27. Te-Chun Chu et al. Theoretical Study on the HACA Chemistry of Naphthalenyl Radicals and Acetylene: the formation of $C_{12}H_8$, $C_{14}H_8$, and $C_{14}H_{10}$ species. *Int. J. Chem. Kinet.* **52**, 752 (2020).
28. P. Liu et al. *Combust. Flame* **199**, 54-68 (2019).
29. Kislov, V. V.; Sadovnikov, A. I.; Mebel, A. M. *J. Phys. Chem. A* **117**, 4794-4816 (2013).
30. Mark J. Goldman et al. Computer Generated Isotope Model Achieves Experiment-Level Accuracy of Fidelity for Position-Specific Isotope Analysis. *Chem. Geo.* **514**, 1-9 (2019).
31. Colin Grambow, Lagnajit Pattanaik, William H. Green. Reactants, products, and transition states of elementary chemical reactions based on quantum chemistry. *Scientific Data* **7**, 137 (2020).
32. Colin Grambow, Lagnajit Pattanaik, William H. Green. Deep Learning of Activation Energies. *J. Phys. Chem. Lett.* **11**, 2992-2997 (2020).
33. Lagnajit Pattanaik, John B. Ingraham, Colin A. Grambow, William H. Green. Generating Transition States with Deep Learning. *Phys. Chem. Chem. Phys.* **22**, 23618-23626 (2020).

Nonadiabatic Photochemistry
DE-SC0015997

Hua Guo[1], Donald G. Truhlar,[2] and David R. Yarkony[3]
[1]*Department of Chemistry and Chemical Biology, University of New Mexico, Albuquerque, New Mexico 87131.*[2]*Department of Chemistry, University of Minnesota, Minneapolis, Minnesota 55455.* [3]*Department of Chemistry, Johns Hopkins University, Baltimore, Maryland 21218*
e-mail: hguo@unm.edu; truhlar@umn.edu; yarkony@jhu.edu

PROGRAM SCOPE

This project involves the development and application of methods for treating electronically nonadiabatic processes both with fitted diabatic potential energy matrices (DPEMs) and by direct dynamics in the adiabatic representation. The project includes both electronic structure theory and dynamics, and the dynamics involves both fully quantal calculations and semiclassical calculations.

The rationale for our emphasis on DPEMs is as follows. Direct dynamics calculations of electronically nonadiabatic processes are usually carried out in the adiabatic basis because the energy, force, and state coupling can be evaluated directly by many electronic structure methods. However, although its straightforwardness is appealing, direct dynamics is expensive when combined with quantitatively accurate electronic structure theories. Furthermore, direct dynamics is impractical for fully quantal dynamics. This generates interest in analytically fitted surfaces to cut the expense, but the cuspidal ridges of the potentials and the singularities and vector nature of the couplings at high-dimensional, non-symmetry-determined intersections in the adiabatic representation make accurate fitting almost impossible. This then motivates using diabatic representations, where the surfaces are smooth and the couplings are also smooth and – importantly– scalar.

RECENT PROGRESS

Hua Guo

(a) Fitting of diabatic potential energy matrices

In collaboration with Yarkony, we have explored various machine learning approaches to constructing high accuracy diabatic potential energy matrices and property matrices for the H_3O,[1] H_2CO,[2] and NH_3 systems.[3] These global analytical expressions open the door to accurate dynamics calculations.

(b) Product state distribution in phenol photodissociation

Phenol has served as a prototype for nonadiabatic photodissociation dynamics. However, there are many details that have been misunderstood. In one recent study, we have carried out reduced dimensional wave packet calculations using an accurate diabatic potential energy matrix (DPEM) developed by Yarkony, and identified the key vibrational mode involved in the dissociation.[4] Our results revealed the flaws in the literature concerning the vibrational excitation in the phenoxyl product, and we presented a reinterpretation of the experiment.

(c) Photodissociation of ozone

In collaboration with North at Texas A&M and Dawes at MUST, we have elucidated the origin of the even-odd propensity in the O_2 product from photodissociation of O_3,[5] which has been a

mystery for 30 years. This propensity was traced to an interference feature in the Λ-doublet of the $^{16}O_2$ product, made possible by the nuclear spin of the two oxygens.

(d) Collision dynamics

With our collaborators, we have been continuing our investigations of dynamics of bimolecular scattering and reactions. These studies include the nonadiabatic quenching dynamics of the spin-orbit excited $I(^2P_{3/2})$ by $O_2(a^1D_g)$,[6] the vibration enhanced OH + HO_2 reaction,[7] the H + O_3 reaction,[8] the N_2 + N_2 collision,[9] and Cl + CH_3OH reaction.[10] We have also published two perspectives on the development of high-dimensional potential energy surfaces using machine learning techniques[11] and on the recent advances and challenges in bimolecular reaction dynamics.[12]

Donald G. Truhlar

(e) Intersystem crossing in thioformaldehyde

This project considered two key issues – the choice of electronic structure method and the treatment of electronic decoherence. The results are very interesting in both respects.[13] We found that the results are very sensitive – not just quantitatively but also qualitatively – to the selection of the active space in the electronic structure calculations. We carried out direct dynamics calculations with the coherent switching with decay of mixing (CSDM) method, and we found that inclusion of decoherence has a dramatic effect on the buildup of triplet state populations.

(f) Conservation of angular momentum

We pointed out an angular momentum conservation problem that exists in widely used mixed quantum classical nonadiabatic dynamics algorithms, including trajectory surface hopping (TSH), semiclassical Ehrenfest (SE), and CSDM.[14] We found by using the nonadiabatic coupling vectors (NAC) directly computed from electronic structure theory codes, which are usually employed in on-the-fly nonadiabatic dynamics, none of the TSH, SE nor CSDM dynamics conserves angular momentum. We proposed a projection operator to apply to the NAC, which projects out the translational and rotational contributions, and we demonstrated that the projected NAC conserves angular momentum very well for TSH, SE, and CSDM dynamics.

(g) CSDM and time-derivative CSDM in SHARC

SHARC has become the leading computer program for direct dynamics calculations of photochemical processes. We implemented CSDM into into SHARC.[15, 16] This is a significant enhancement of the SHARC code because this code has not previously included decoherence. Then we presented a new algorithm for CSDM based on replacing NAC-based coupling by time-derivative coupling, and we also implemented that in SHARC.

(h) DPEM for methylamine

We developed a DPEM for methylamine. It was created using extended versions of techniques of general interest, namely DQ diabatization and the anchor points reactive potential method with a 2D grid of anchor points.[17] The success of the DQ method for this diabatization provides physical insight into the characters of the excited electronic states, and the use of the potential energy matrix for semiclassical simulations in future work will provide insight into the dynamics.

(i) Diabatization by deep neural network

Diabatization of electronic states is well recognized as a key tool allowing for realistic simulations of photochemical processes. More and more we see the community appreciating the usefulness of diabatic states for photochemical and charge transfer simulations. However, diabatization is very subtle and labor intensive, and therefore we have developed more user-

friendly methods. In particular we developed a new kind of architecture for a deep neural network, and we showed that it can successfully achieve diabatization.[18, 19] The method presented here is quite different from anything already in the literature. It goes beyond surface fitting and employs machine intelligence to discover the smooth diabatic surfaces lurking beneath the nonsmooth adiabatic energies. It is very convenient because it uses adiabatic energies without inputting gradient or nonadiabatic coupling vectors. In subsequent work, we showed how to use a restraint to practically make enforce permutational invariance.

(j) Potential energy surfaces for N + O_2 collisions

Potential energy surfaces for high-energy collisions between oxygen molecules and atoms and nitrogen molecules and atoms are useful for modeling chemical dynamics in shock waves. We have used both neural networks and permutationally invariant polynomials to develop potential energy surfaces for collisions of N atoms with O_2 molecules.[20]

(k) Other work

Other work supported in part by this grant in the past year[21-27] is not summarized here due to space limitations.

David R. Yarkony

(l) OH(A)+H_2

The reaction of OH(A) with H_2 includes 2 possible channels and 3 electronic states:

$$OH(A\ ^2\Sigma^+) + H_2 \rightarrow H_2O + H \qquad \text{reactive quenching} \qquad (1a)$$
$$\rightarrow OH(X\ ^2\Pi) + H_2 \qquad \text{nonreactive quenching} \qquad (1b)$$
$$\rightarrow OH(A\ ^2\Sigma^+) + H_2 \qquad \text{(in)elastic scattering} \qquad (1c)$$

is an archetypical reaction for the study of nonadiabatic reactive (1a) and nonreactive (1b) quenching. The process includes the possibility of Renner-Teller coupling impacting the production of the Λ -doublets in the entrance channel, intersystem crossing in a D_{3h} region due to spin-orbit coupling, and internal conversion.

In this initial project, we concentrated our efforts on the internal conversion, the spin-conserving nonadiabatic process which is driven by conical intersections.[1] There are several challenges here. In the first place there are two relevant seams of conical intersections the 1,2 ^{2}A and 2,3 ^{2}A seams, whose relative position and energetics must be accurately described if the nonadiabatic journey from the 3^2A state to the 1^2A state is to be correctly described. It is this requisite accuracy that has lead us to use multireference with single and double excitation configuration interaction wave functions and a fitting procedure designed to handle the seams conical intersection.

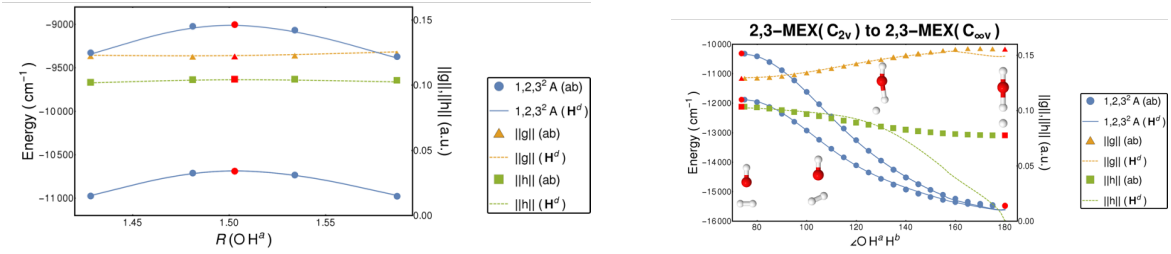

Figure:1,2^2A and 2,3^2A seams of conical intersection

Above are reported a portion of the 1,2 ^{2}A seam near its minimum energy crossing and a mapping of the energetically accessible portion of the 2,3 ^{2}A conical intersection seam extending

from the colinear $C\infty v$ region through the planar C_s region to the C_{2v} region. So a large portion of the seam must be fit. Figure 1 evinces excellent agreement for the energies and the magnitudes of the conical parameters $\mathbf{g}^{I,J}$ energy difference gradient and $\mathbf{h}^{I,J}$ the interstate coupling gradient the exception being $\| \mathbf{h}^{I,J} \|$ for I=2, J=3, the I,J^2A conical intersection for $\angle OH^2H^3$ between140˚ and 180˚.

A second essential aspect of reaction (1) is the entrance channel on the 3^2A PES, where there have been questions about the stereochemistry of the inelastic scattering.. Using our coupled diabatic` surfaces we were able to reliably quantify the entrance-channel dynamics and provide the resolution and explanation of a decades old discrepancy between experimentally inferred and computationally determined branching ratios .

(m) Diabatization by the NN_SURFGEN code

The H_3O coupled diabatic surfaces were described using SURFGEN which simultaneously fits and diabatizes *ab initio* adiabatic electronic structure data (ESD) using functions of bond distances, bond angles, and dihedral angles. The formaldehyde project described below uses NN-SURFGEN which replaces the molecular functions of SURGEN with feed forward neural network (NN) functions. This algorithm (NN-SURFGEN) employs permutationally invariant polynomials (PIPs) which – unlike molecular functions of SURFGEN– can be easily CNPI symmetry adapted.[2]

(n) Photochemical branching: H_2CO (A) + hυ → HCO + H, H_2 + CO

Developing a computational method that is both affordable and accurate for intersystem crossing is major challenge. Depending on the potential surface topography, intersystem crossing can successfully compete with internal conversion even for molecules composed of light atoms. The electronic structure of the S_0 and S_1 states of formaldehyde have been investigated by many groups. The discovery of roaming following photoexcitation has further expanded interest in this system. We have calculated the S_1 and S_0 surfaces and their derivative couplings and fit them using NN_SURFGEN.[2] Initial tests of the DPEM are quite encouraging. We will extend this approach to include thioformaldehyde. This will enable us to compare our DPEM-based dynamics with the direct dynamics simulation described next

FUTURE PLANS

Hua Guo

We will be focusing on the nonadiabatic dynamics for the OH(A) + H_2 reaction, which includes the reactive and nonreactive quenching channels, using the newly developed DPEMs from both the Yarkony and Truhlar groups. The initial phase of the work will deal with the non-reactive quenching channels for J=0, but extensions to higher partial waves will be performed subsequently. The treatment of the reactive channel will be much more challenging because of the polyatomic products and the large energy release. The comparison of the two DPEMs will shed light on the differences in the electronic structure methods and fitting algorithms. We plan to further investigate the nonadiabatic predissociation of the H_2-HO(A) complex in the entrance channel and determine the energies and lifetimes. The mode specificity of the predissociation lifetimes sheds insight into the effect of the conical intersection on nonadiabatic transitions.

In addition, we will explore the internal conversion and intersystem crossing in H_2CO using the recent DPEM from Yarkony. This is an interesting system because of the two possible nonadiabatic routes, via internal conversion to the S_0 state and intersystem crossing to the T_1 state.

The calculated energies and lifetimes can be compared with a large set of experimental data. These nonadiabatic processes are also at the center of the roaming dynamics on the S_0 state.

Finally, we plan to implement the multi-configuration time-dependent Hartree approach to high-dimensional nonadiabatic photodissociation dynamics, using the DPEMs developed by both groups. This is necessary because of the limitations of grid based methods which scales exponentially with the size. We hope to address first the 9-dimensional photodissociation of hydroxymethyl radical.

Donald G, Truhlar

We will carry out further studies of photochemical processes in the singlet manifold, and in particular we propose to study substituent effects on the photodissociation of 2-fluorothiophenol. For this purpose, we are developing a new version of our diabatization by deep neural networks approach in which we use internal coordinates. The dynamics will be carried out by CSDM.

We also plan to develop a specific-reaction-parameters approach to photochemical surface generation based on an orthogonalization-corrected OMx semiempirical molecular orbital configuration interaction method.

David R. Yarkony

In the next period we will complete our study of the intersystem crossing in formaldehyde and perform similar calculations for the isovalent thioformaldehyde. In order to perform spin non-conserving nonadiabatic dynamics the spin-orbit coupling must be available at each geometry sampled. For on-the-fly direct dynamics this is readily accomplished since the electronic wave function is available at each geometry. For our DPEM based methods we will diabatize the spin-orbit coupling and then fit the spin-orbit-interaction and DPEM to NN forms. We can include spin-orbit coupling in the adiabatic representation as in Truhlar's direct dynamics. We plan to compare with Truhlar's adiabatic surfaces and CSDM dynamics.

CITED PUBLICATIONS

1. Malbon, C. L.; Zhao, B.; Guo, H.; Yarkony, D. R. On the nonadiabatic collisional quenching of OH(A) by H_2: a four coupled quasi-diabatic state description, *Phys. Chem. Chem. Phys.* **2020,** *22*, 13516-13527.
2. Guan, Y.; Xie, C.; Guo, H.; Yarkony, D. R. Neural network based quasi-diabatic representation for S_0 and S_1 states of formaldehyde, *J. Phys. Chem. A* **2020,** *124*, 10132-10142.
3. Guan, Y.; Guo, H.; Yarkony, D. R. Extending the representation of multistate coupled potential energy surfaces to include properties operators using neural networks: Application to the $1,2^1A$ states of ammonia, *J. Chem. Theo. Comput.* **2020,** *16*, 302-313.
4. Xie, C.; Zhao, B.; Malbon, C. L.; Yarkony, D. R.; Xie, D.; Guo, H. Insights into the mechanism of nonadiabatic photodissociation from product vibrational distributions. The remarkable case of phenol, *J. Phys. Chem. Lett.* **2020,** *11*, 191-198.
5. Han, S.; Gunthardt, C. E.; Dawes, R.; Xie, D.; North, S. W.; Guo, H. Origin of the "odd" behavior in the ultraviolet photochemistry of ozone, *Proc. Natl. Acad. Sci. U. S. A.* **2020,** *117*, 21065-21069.
6. An, F.; Chen, J.; Hu, X.; Guo, H.; Xie, D. Nonadiabatic electronic energy transfer in the chemical oxygen–iodine laser: Powered by derivative coupling or spin–orbit coupling?, *J. Phys. Chem. Lett.* **2020,** *11*, 4768-4773.
7. Liu, Y.; Song, H.; Xie, D.; Li, J.; Guo, H. Mode specificity in the $OH + HO_2 \rightarrow H_2O + O_2$ reaction: Enhancement of reactivity by exciting a spectator mode, *J. Am. Chem. Soc.* **2020,** *142*, 3331-3335.

8. Zuo, J.; Chen, Q.; Hu, X.; Guo, H.; Xie, D. Theoretical investigations of rate coefficients for H + O_3 and HO_2 + O reactions on a full-dimensional potential energy surface, *J. Phys. Chem. A* **2020,** *124*, 6427-6437.
9. Li, J.; Varga, Z.; Truhlar, D. G.; Guo, H. Many-body permutationally invariant polynomial neural network potential energy surface for N_4, *J. Chem. Theo. Comput.* **2020,** *16*, 4822-4832.
10. Lu, D.; Li, J.; Guo, H. Comprehensive dynamical investigations on the Cl + $CH_3OH \rightarrow$ HCl + CH_3O/CH_2OH reaction: Validation of experiment and dynamical insights, *CCS Chem.* **2020,** *2*, 882-894.
11. Jiang, B.; Li, J.; Guo, H. High-fidelity potential energy surfaces for gas phase and gas-surface scattering processes from machine learning, *J. Phys. Chem. Lett.* **2020,** *11*, 5120-5131.
12. Li, J.; Zhao, B.; Xie, D.; Guo, H. Advances and new challenges to bimolecular reaction dynamics theory, *J. Phys. Chem. Lett.* **2020,** *11*, 8844-8860.
13. Zhang, L.; Shu, Y.; Sun, S.; Truhlar, D. G. Direct coherent switching with decay of mixing for intersystem crossing dynamics of thioformaldehyde: The effect of decoherence, *J. Chem. Phys.* **2021,** *154*, 094310.
14. Shu, Y.; Zhang, L.; Varga, Z.; Parker, K. A.; Kanchanakungwankul, S.; Sun, S.; Truhlar, D. G. Conservation of angular momentum in direct nonadiabatic dynamics, *J. Phys. Chem. Lett.* **2020,** *11*, 1135-1140.
15. Shu, Y.; Zhang, L.; Mai, S.; Sun, S.; González, L.; Truhlar, D. G. Implementation of coherent switching with decay of mixing into the SHARC program, *J. Chem. Theo. Comput.* **2020,** *16*, 3464-3475.
16. Shu, Y.; Zhang, L.; Sun, S.; Truhlar, D. G. Time-derivative couplings for self-consistent electronically nonadiabatic dynamics, *J. Chem. Theo. Comput.* **2020,** *16*, 4098-4106.
17. Parker, K. A.; Truhlar, D. G. Semiglobal diabatic potential energy matrix for the N–H photodissociation of methylamine, *J. Chem. Phys.* **2020,** *152*, 244309.
18. Shu, Y.; Truhlar, D. G. Diabatization by machine intelligence, *J. Chem. Theo. Comput.* **2020,** *16*, 6456-6464.
19. Shu, Y.; Varga, Z.; Sampaio de Oliveira-Filho, A. G.; Truhlar, D. G. Permutationally restrained diabatization by machine intelligence, *J. Chem. Theo. Comput.* **2021,** *17*, 1106-1116.
20. Varga, Z.; Liu, Y.; Li, J.; Paukku, Y.; Guo, H.; Truhlar, D. G. Potential energy surfaces for high-energy N + O_2 collisions, *J. Chem. Phys.* **2021,** *154*, 084304.
21. Zhang, L.; Truhlar, D. G.; Sun, S. Association of Cl with C_2H_2 by unified variable-reaction-coordinate and reaction-path variational transition-state theory, *Proc. Natl. Acad. Sci. U. S. A.* **2020,** *117*, 5610-5616.
22. Wu, J.; Gao, L. G.; Ren, W.; Truhlar, D. G. Anharmonic kinetics of the cyclopentane reaction with hydroxyl radical, *Chem. Sci.* **2020,** *11*, 2511-2523.
23. Wu, J.; Gao, L. G.; Ning, H.; Ren, W.; Truhlar, D. G. Direct dynamics of a large complex hydrocarbon reaction system: The reaction of OH with exo-tricyclodecane (the main component of Jet Propellant-10), *Combus. Flame* **2020,** *216*, 82-91.
24. Wu, J.; Gao, L. G.; Varga, Z.; Xu, X.; Ren, W.; Truhlar, D. G. Water catalysis of the reaction of methanol with OH radical in the atmosphere is negligible, *Angew. Chem. Int. Ed.* **2020,** *59*, 10826-10830.
25. Pilgrim, J. S.; McIlroy, A.; Taatjes, C. A. Kinetics of Cl atom reactions with methane, ethane, and propane from 292 to 800 K, *J. Phys. Chem. A* **1997,** *101*, 1873-1880.
26. Zhang, R. M.; Xu, X.; Truhlar, D. G. Low-pressure limit of competitive unimolecular reactions, *J. Am. Chem. Soc.* **2020,** *142*, 16064-16071.
27. Truhlar, D. G., Semiclassical Multidimensional Tunneling Calculations. In *Tunnelling in Molecules: Nuclear Quantum Effects from Bio to Physical Chemistry*, Kaestner, J.; Kozuch, S., Eds. RSC Publishing: Cambridge, 2021; pp 261-282.

Theory of Electronic Structure and Chemical Dynamics

Martin Head-Gordon, Eric Neuscamman, David Prendergast
Chemical Sciences Division, Lawrence Berkeley National Laboratory, Berkeley, California 94720.
mhg@cchem.berkeley.edu, eneuscamman@berkeley.edu, dgprendergast@lbl.gov

Scope of the Project: To expand knowledge of transient species such as radicals relevant to combustion chemistry, atmospheric photochemistry, and other areas including catalysis, new theoretical methods are needed for reliable computer-based prediction of their properties. In electronic structure theory, focus centers on the development of new density functional theory methods and new wave function theories. Newly developed theoretical methods, as well as existing approaches, are employed to study prototype radical reactions, often in collaboration with experimental efforts in the related subtasks (see separate LBNL abstracts). These studies help to deepen understanding of the role of reactive intermediates in diverse areas of chemistry. They also sometimes reveal frontiers where new theoretical developments are needed in order to permit better calculations in the future.

Recent Progress

Due to length limitations, only a selection of projects can be summarized here.

High Accuracy Excited States and Monte Carlo Optimization. Neuscamman and co-workers have continued to develop excited-state-specific methodologies in both quantum chemistry and quantum Monte Carlo (QMC) and to improve QMC wave function optimization techniques. Our most exciting development this year has been to extend our state-specific work into core excited states. One interesting finding here is that, despite straightforwardly neglecting electron correlation, excited state mean field theory predicts oxygen, nitrogen, and carbon K-edges with an accuracy against experiment better than 1 eV. Upon adding second order perturbation theory (much as MP2 improves Hartree-Fock), the mean unsigned error for these K-edges drops to 0.3 eV, which is competitive with the best density functionals (and better than most!) used in the ROKS approach (e.g. as developed by Head-Gordon and co-workers). This finding shows us that the similarities in accuracy between MP2 and DFT extend into core states. In the course of this work, we also developed a corrected core-valence separation scheme that helps account for the bias in the number of electrons that are correlated in ground and excited state calculations. We have also extended our excited-state-specific variational Monte Carlo (VMC) methodology in order to handle core states and found that it offers accuracies for K-edges in water, ammonia, and methane of about 0.2 eV, and peak separations within 0.07 eV. Although this is a preliminary test set, when we compare to experiment, we find that VMC peak separations are more accurate than other available methods, and that the K-edge accuracies are on par with the best available methods. In our ongoing work to expand the power of VMC to optimize more sophisticated wave functions, we have shown that a low-memory approach that hybridizes the best features of the long-standard linear method with newer accelerated descent methods outperforms both. The new approach achieves an accuracy in optimization better than accelerated descent techniques and on par with the linear method, requires far less memory than the linear method, and requires less sampling and thus computational time.

Density functionals. Head-Gordon and co-workers have been interested in seeking the limit of transferable accuracy that can be achieved with current forms for density functionals. This has resulted in the "survival of the most transferable" (SOMT) procedure to design new density functionals. This approach has been used to create very accurate new density functionals, such as the ωB97X-V and ωB97M-V hybrids, and the ωB97M(2) double hybrid. Recently, they have explored how these and other functionals perform for bond-breaking, and have discovered that a class of multiconfigurational open shell singlet states can be accurately treated by DFT using a single determiment of complex molecular orbitals. Their functionals were employed in collaboration with Musa Ahmed to model photoionization-induced reactivity in complexes of naphthalene and water.

Electron correlation methods: Head-Gordon and co-workers are developing wavefunction-based electron correlation methods for problems where DFT suffers from self-interaction and/or strong

correlation errors. The simplest such approach is a regularized orbital optimized MP2 method (κ-OOMP2) that removes strong correlation contributions associated with small gaps. κ-OOMP2 can remove artificial spin symmetry-breaking associated with Hartree-Fock, while retaining "essential symmetry-breaking" as a signature of strong correlations because of its single reference character. κ-OOMP2 has been applied to fullerenes to address debate over whether C60 is strongly correlated (we conclude it is not). We have shown that biradicals can be well treated by κ-OOMP2 with the aid of Yamaguchi spin projection, or complex orbitals when such solutions exist. Another recent advance is an efficient implementation of the adaptive sampling CI (ASCI) method, that approximates full CI at dramatically reduced cost by exhibiting soft instead of hard exponential scaling. ASCI has been applied to explore limitations of conventional coupled cluster methods for some small strongly correlated transition metal diatomics (hydrides, halides, oxides, carbides and nitrides), as well as in a competition between selected CI methods to predict the ground state energy of benzene. Finally, a generalized coupled cluster method that is promising for quantum computing purposes has been suggested, and preliminary results reported based on simulations on classical computers.

Excited-state dynamics and transient inner-shell spectroscopy: Prendergast and co-workers are applying both linear response time-dependent DFT and wave-function methods in the context of fewest-switches surface hopping to explore excited-state dynamics of various small molecules. To provide interpretation of ultrafast pump-probe inner-shell transient spectroscopy, we have demonstrated how to effectively interpret such spectra from a physical perspective – separating peaks by species and explaining peaks shifts in terms of orbital character and localization, and exciton binding. We have also successfully extended the application of RASSCF to mixed core-valence excited states, as accessed in pump-probe experiments, and further employed RAS state interaction to include spin-orbit interactions for heavier atoms and to calculate transition amplitudes for transient absorption spectra that probe excited states with nontrivial angular momentum (l=2 here), with application to methyl iodide. A collaboration with the Neumark and Leone groups led to new insights into the dynamics associated with passage through a spin-orbit coupling induced conical intersection in the iso-propyl iodide and tert-butyl iodide molecules (i-C3H7I and t-C4H9I).

Future Plans:

(i) *Multi-configurational core excitations and accelerated optimization:* Current efforts focus on further improving wave function optimization and on extending our success with core excitations into radical and diradical systems whose core states are multi-configurational due to spin recoupling. Our VMC approach, which uses a selected-CI-like wave function as its initial guess, is naturally able to handle this multi-configurational structure, even in cases where the picture is more complicated than spin recoupling alone. Indeed, key issues our VMC approach is expected to resolve are (a) qualitatively, to what degree is spin recoupling responsible for diradical species' complexity and to what degree is more involved multi-reference mixing present, and (b) quantitatively, what are the correct core excitation peak positions and assignments in diradical species for which experimental data is lacking or unclear. Answers to these questions will provide benchmarks that help the wider theoretical community make headway with these states while at the same time assisting experimental investigations. In wave function optimization, we will leverage our group's development of excited-state-specific complete active space self-consistent field techniques to allow VMC to start from orbitals that have already been relaxed for the excited state. Our initial data indicate that no further orbital relaxation is needed in most systems, even when charge transfer or doubly excited states are in play, which will dramatically reduce VMC optimization costs and thus expand the range of systems in which it can offer its highly accurate and systematically improvable predictions.

(ii) *Assessment and further development of density functionals:* Additional tests of density functionals on transition metal systems are underway, to explore the nature of electron correlation in the organometallic complexes where there are long-standing debates about the extent of strong correlations. Are strong correlations far more common in TM complexes than in main group molecules and radicals, and if so why? This work will complement the evaluations of density

functional performance for main group containing molecules, and should help set the stage for further density functional developments in the future.

(iii) Electron correlation and orbital optimization. Further tests of the regularized orbital optimized MP2 method (κ-OOMP2) are underway, to assess its performance, as well as the performance of MP3 extensions using those orbitals for non-bonded interactions. The question is whether or not the promising results reported very recently by Rettig et al (2020) are transferable to broader classes of problems, where conventional MP2 is known to fail. Additionally, tests of the performance of κ-OOMP2 for transition metal complexes will be performed, since conventional MP2 is also known to perform very poorly for ligand binding energies. The results of these studies will either validate the approach, which is free of the delocalization error of DFT, or inspire new ideas for better ways to provide wavefunction-based alternatives to DFT.

(iv) Collaborative applications to photoionized clusters of glycerol and water are underway (with Musa Ahmed), and oxidative chemistry in aerosols of long-chain hydrocarbons (with Kevin Wilson), and combustion related reactions of unsaturated radicals (with Hope Michelson). The new core excited tools developed by Neuscamman will be applied to problems of interest in the Leone and Neumark groups, to complement the ROKS-based approaches developed by the Head-Gordon group.

Recent Publications Citing DOE Support (2018-2021)

- Bertels, L.W.; J. Lee, and M. Head-Gordon, "Polishing the Gold Standard: The Role of Orbital Choice in CCSD(T) Vibrational Frequency Prediction", J. Chem. Theory Comput. 17, 742-755 (2021); doi: 10.1021/acs.jctc.0c00746
- Blunt, N. S.; Neuscamman, E., Excited-state diffusion Monte Carlo calculations: a simple and efficient two-determinant ansatz. *J. Chem. Theory Comput.* **2019**, 15, 178. DOI: 10.1021/acs.jctc.8b00879
- Chang, K.F.; M. Reduzzi, H. Wang, S.M. Poullain, Y. Kobayashi, L. Barreau, D. Prendergast, D.M. Neumark, and S.R. Leone, "Revealing electronic state-switching at conical intersections in alkyl iodides by ultrafast XUV transient absorption spectroscopy", Nat. Commun. 11, 4042 (2020); doi: 10.1038/s41467-020-17745-w
- Eriksen, J.; T.A. Anderson, J.E. Deustua, K. Ghanem, D. Hait, M.R. Hoffmann, S. Lee, D. Levine, I. Magoulas, J. Shen, N. Tubman, K.B. Whaley, E. Xu, Y. Yao, N. Zhang, A. Alavi, G. Chan, M. Head-Gordon, W. Liu, P. Piecuch, S. Sharma, S. Ten-no, C. Umrigar, J. Gauss, "The Ground State Electronic Energy of Benzene", J. Phys. Chem. Lett. 11, 8922−8929 (2020); doi: 10.1021/acs.jpclett.0c02621
- Fang, J.; D. Hait, M. Head-Gordon, and M.C.Y. Chang, "Chemoenzymatic Platform for Synthesis of Chiral Organofluorines Based on Type II Aldolases", Ang. Chem. 131, 11967 –11971 (2019); doi: 10.1002/ange.201906805
- Garner, S. M.; Neuscamman, E., A variational Monte Carlo approach for core excitations, *J. Chem. Phys.*, **2020**, 153, 144108; doi:
- Garner, S. M.; Neuscamman, E., Core Excitations with Excited State Mean Field and Perturbation Theory. *J. Chem. Phys.* **2020**, 153, 154102; doi:
- Hait, D. and M. Head-Gordon, "How accurate is density functional theory at predicting dipole moments? An assessment using a new database of 200 benchmark values." *J. Chem. Theory Comput.* 14, 1969−1981 (2018); doi: 10.1021/acs.jctc.7b01252
- Hait, D. and M. Head-Gordon, "xDH double hybrid functionals can be qualitatively incorrect for non-equilibrium geometries: Dipole moment inversion and barriers to radical-radical association using XYG3 and XYGJ-OS", *J. Chem. Phys.* 148, 171102 (2018); doi: 10.1063/1.5031027
- Hait, D. and M. Head-Gordon, "Delocalization errors in density functional theory are essentially quadratic in fractional occupation number", *J. Phys. Chem. Lett.* 9, 6280−6288 (2018); doi: 10.1021/acs.jpclett.8b02417
- Hait, D.; A. Rettig, and M. Head-Gordon, "Well-behaved versus ill-behaved density functionals for single bond dissociation: Separating success from disaster functional by functional for stretched H_2", *J. Chem. Phys.* 150, 094115 (2019); doi: 10.1063/1.5080122
- Hait, D.; N.M. Tubman, D.S. Levine, K.B. Whaley, and M. Head-Gordon, "What levels of coupled cluster theory are appropriate for transition metal systems? A study using near exact quantum chemical values for 3d transition metal binary compounds" J. Chem. Theory Comput. 15, 5370−5385 (2019); doi: 10.1021/acs.jctc.9b00674

- Hait, D.; Y.H. Liang, and M. Head-Gordon, "Too big, too small or just right? A benchmark assessment of density functional theory for predicting the spatial extent of the electron density of small chemical systems", J. Chem. Phys. 154, 074109 (2021); doi: 10.1063/5.0038694
- Johansson, K.O.; M. P. Head-Gordon, P.E. Schrader, K.R. Wilson, and H.A. Michelsen, "Resonance-stabilized hydrocarbon- radical chain reactions may explain soot inception and growth", *Science* 361, 997–1000 (2018); doi: 10.1126/science.aat3417
- Lee, J.; D.W. Small, and M. Head-Gordon, "Open-shell coupled-cluster valence-bond theory augmented with an independent amplitude approximation for 3-pair correlations: Application to a model oxygen-evolving complex and single molecular magnet", *J. Chem. Phys.* 149, 244121 (2018); doi: 10.1063/1.5052667
- Lee, J.; W. Huggins, M. Head-Gordon, and K.B. Whaley, "Generalized unitary coupled cluster wavefunctions for quantum computation", *J. Chem. Theory Comput.* 15, 311-324 (2019); doi: 10.1021/acs.jctc.8b01004
- Lee, J. and M. Head-Gordon, "Distinguishing Artificial and Essential Symmetry Breaking in a Single Determinant: Approach and Application to the C60, C36, and C20 Fullerenes", *Phys. Chem. Chem. Phys.* 21, 4763-4778 (2019); doi: 10.1039/c8cp07613h
- Lee, J. and M. Head-Gordon, "Two Single-Reference Approaches to Singlet Biradicaloid Problems: Complex, Restricted Orbitals and Approximate Spin-Projection Combined With Regularized Orbital-Optimized Møller-Plesset Perturbation Theory", J. Chem. Phys. 150, 244106 (2019); doi: 10.1063/1.5097613
- Lee, J.; L.W. Bertels, D.W. Small, and M. Head-Gordon, "Kohn-Sham density functional theory with complex, spin-restricted orbitals: Accessing a new class of densities without the symmetry dilemma", Phys. Rev. Lett. 123, 113001 (2019); doi: 10.1103/PhysRevLett.123.113001
- Lehtola, S., J.A. Parkhill and M. Head-Gordon, "Orbital optimization in the perfect pairing hierarchy. Applications to full-valence calculations on linear polyacenes", *Mol. Phys.* 116, 547-560 (2018); doi: 10.1080/00268976.2017.1342009
- Lucas, M.; A.M. Thomas, T. Yang, R.I. Kaiser, A.M. Mebel, D. Hait, M. Head-Gordon, "Exotic Chemistry in the Phenyl - Silane System: Exploring the Prototype of a Radical Substitution Mechanism," *J. Phys. Chem. Lett.* 9, 5135−5142 (2018); 10.1021/acs.jpclett.8b02303
- Mardirossian, N. and M. Head-Gordon, "Survival of the most transferable at the top of Jacob's Ladder: Defining and testing the ωB97M(2) double hybrid density functional", *J. Chem. Phys.* 148, 241736 (2018); doi: 10.1063/1.5025226
- Otis, L.; Neuscamman, E., "Complementary First and Second Derivative Methods for Ansatz Optimization in Variational Monte Carlo" *Phys. Chem. Chem. Phys.* **2019**, 21, 14491; doi: 10.1039/C9CP02269D
- Pineda Flores, S. D. and E. Neuscamman, Excited State Specific Multi-Slater Jastrow Wave Functions. *J. Phys. Chem. A* **2019**, 123, 1487. DOI: 10.1021/acs.jpca.8b10671
- Rettig, A.; D. Hait, and M. Head-Gordon, "Third order Moller-Plesset theory made more useful? The role of density functional theory orbitals", J. Chem. Theory Comput. 16, 7473-7489 (2020); doi: 10.1021/acs.jctc.0c00986
- Small, D. W. and M. Head-Gordon, "Independent amplitude approximations in coupled cluster valence bond theory: Incorporation of 3-electron-pair correlation and application to spin frustration in the low-lying excited states of a ferredoxin-type tetrametallic iron-sulfur cluster", *J. Chem. Phys.* 149, 144103 (2018); doi: 10.1063/1.5046318.
- Toulson, B. W.; Borgwardt, M.; Wang, H.; Lackner, F.; Chatterley, A. S.; Pemmaraju, C. D.; Neumark, D. M.; Leone, S. R.; Prendergast, D.; Gessner, O.; Probing ultrafast C–Br bond fission in the UV photochemistry of bromoform with core-to-valence transient absorption spectroscopy, *Structural Dynamics* **2019**, 6, 054304; doi: 10.1063/1.5113798
- Tubman, N.M., C.D. Freeman, D.S. Levine, D. Hait, M. Head-Gordon, K.B. Whaley, "Modern Approaches to Exact Diagonalization and Selected Configuration Interaction with the Adaptive Sampling CI Method", J. Chem. Theory Comput. 16, 2139-2159 (2020); doi: 10.1021/acs.jctc.8b00536
- Wang, H.; Odelius, M.; Prendergast, D., A combined multi-reference pump-probe simulation method with application to XUV signatures of ultrafast methyl iodide photodissociation, *J. Chem. Phys.* **2019**, 151, 124106-; doi: 10.1063/1.5116816
- Xu, B.; T. Stein, U. Ablikim, L. Jiang, J. Hendrix, M. Head-Gordon, and M. Ahmed, "Probing solvation and reactivity in ionized polycyclic aromatic hydrocarbon-water clusters with photoionization mass spectrometry and electronic structure calculations", Faraday Disc. 217, 414-433 (2019); doi: 10.1039/c8fd00229k

Probing Supercritical Phase Transition using Ultrafast X-ray Diagnostics

Principal Investigator: Matthias Ihme
Department of Mechanical Engineering
Stanford University,
488 Escondido Mall, Stanford, CA 94305
email: mihme@stanford.edu

Co-Investigator Dimosthenis Sokaras
SLAC National Accelerator Laboratory,
2575 Sand Hill Road, Menlo Park, California 94025
email: dsokaras@slac.stanford.edu

Program Scope

The objective of this research is to probe dynamical processes within supercritical fluids that are associated with the thermal motion, molecular diffusion, and intermolecular cluster transition at supercritical conditions. Of particular interest is hereby to examine the ultrafast timescales of the cluster transfer and intermolecular cluster-exchange processes across the structural transition line. To this end, X-ray Photon Correlation Spectroscopy (XPCS) at the Linac Coherent Light Source (LCLS) will be utilized to measure equilibrium and non-equilibrium processes by continuously scanning the delay range of two X-ray pulses up to few picoseconds with better than 20 femtosecond temporal resolution.

Over recent years, several hypotheses have been put forward to elucidate supercritical transition states. Despite significant progress on the fundamental understanding of fluids at these supercritical conditions, important questions concerning the microstructure and dynamical processes remain [1-5]. A particular research issue is hereby the fundamental understanding of the morphology of the molecular microstructure and its effect on the macroscopic behavior and thermodynamic response functions. It is widely believed that the supercritical state is homogeneous without structural and dynamic observables to distinguish between a liquid and a vapor. However, recent investigations have identified regions of distinct liquid-like or vapor-like properties even under supercritical conditions [1,5]. Specifically, it was shown that the transition between liquid-like and vapor-like states occurs across an extension to the coexistence line (see red "Widom line" in Fig. 1a), marked by almost discontinuous changes in fluid properties. This transition was first identified experimentally by Nishikawa and Tanaka [6] and stands in contrast to the classical presentation of the supercritical state space as a featureless, homogeneous domain.

Structurally, the most important properties of supercritical fluids are the dynamic heterogeneities and local density fluctuations that are present within the fluid state at the microscopic level. These inhomogeneities are associated with the formation of molecular clusters of various sizes with liquid-like properties separated by voids of unbound gas-phase molecules (see Fig. 1b) which continuously restructure itself at picosecond timescales.

By utilizing ultrafast X-ray Photon Correlation Spectroscopy (XPCS) at the Linac Coherent Light Source (LCLS) as an experimental probe of these structural changes at the molecular level we seek to elucidate the higher-order phase transition from a liquid-like to a vapor-like state in the region extending the critical point. Open questions we seek to address particularly with XPCS are: (i) the underlying mechanisms responsible for the density fluctuations at supercritical conditions and how these dynamical processes at the molecular level affect the thermodynamic response functions and (ii) on what timescales do dynamical

processes evolve that are associated with thermalization, molecular diffusion, and intermolecular cluster transfer.

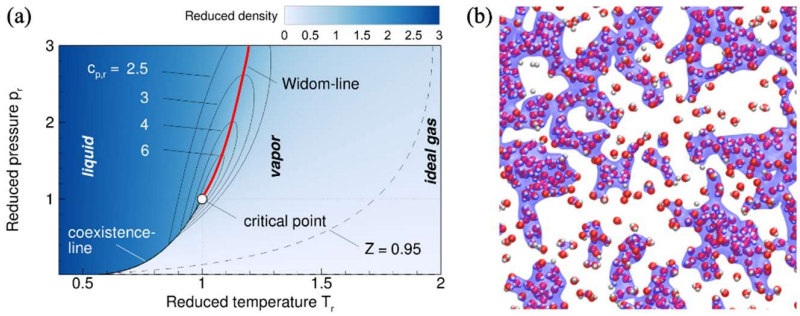

Figure 1: *(a) Reduced p-T diagram with transition between liquid-like and vapor-like states as an extension to the coexistence line into the supercritical region. The reduced pressure and temperature are defined with respect to the critical state, i.e., $p_r=p/p_c$ and $T_r=T/T_c$. (b) Cluster formation during liquid-vapor transition.*

Recent Progress

Experimental Setup: As part of our work, we have built and implemented a pressure cell and flow-system for Small-Angle X-ray Scattering (SAXS) and X-ray Photon Correlation Spectroscopy (XPCS) experiments. This pressure-cell provides direct control over *p/T*-operating conditions, excellent repeatability, and operation with different fluids and mixtures. A schematic of the pressure-cell is shown in Fig. 2. The pressure cell and flow system are fully operational and have be utilized for SAXS and XPCS measurements, as discussed in the following sections. This pressure cell is able to operate at pressures up to 1000 bars and the cartridge heaters allows to achieve temperatures of up to 750 K. For adaptation to the XPCS-facility, optimization of the single-crystal diamond windows (100 µm thickness) and the sample thickness (100 – 2000 µm) have been characterized to maximize speckle contrast and optimize for accessible range of scattering momentum transfer, *Q*.

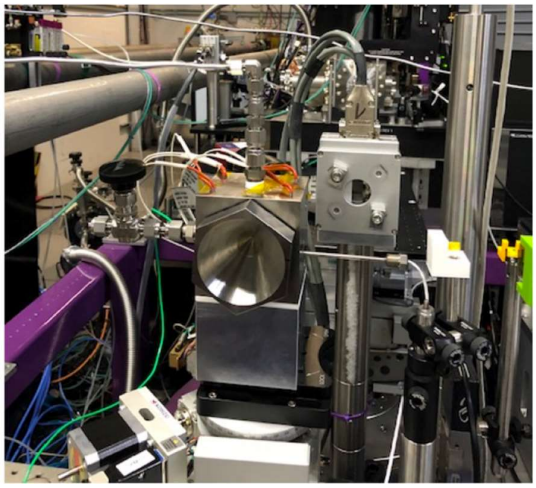

Figure 2: *High-pressure cell suitable for SAXS and XPCS developed for this project, utilized at the XPCS measurement at the XCS instrument at LCLS; image shows the instrumented pressure cell in XCS instrument.*

The pressure cell and flow system have been utilized successfully for both, SAXS experiments at beamline 4.2 at SSRL as well as XPCS experiments at the XCS instrument at the LCLS XCS-instrument. The pressure cell and fluid system have been proven reliable with single component fluids such as CO_2, H_2O and Xe. The pressure cell is currently updated to apply fluid mixtures.

Small Angle X-ray Scattering (SAXS): X-ray scattering techniques are commonly applied to resolve the molecular structure with atomic scale resolution. In particular, SAXS has demonstrated its capability to observe molecular structures on intermolecular length scales and its relevance to study the cluster formation of supercritical pure fluids and their mixtures [6-8].

We performed SAXS measurements at BL-4.2 at SSRL with 15 keV photon energy covering a Q-range from 0.01 – 0.5 Å^{-1}. Figure 3a shows high-quality SAXS scattering intensities from a CO_2 sample measured with our setup at SSRL close to the critical point. Ornstein-Zernike analysis has been applied to extract correlation length (ξ) from the increase in scattering intensity $I(Q)$ at low momentum transfer Q, by $I(Q) = I(0)/(1 + \xi^2 Q^2)$. The correlation length is shown in Fig. 3b with an increase of the correlation length, reflecting the growth of clusters in proximity of the critical point of CO_2, i.e., 31 °C and 74 bar.

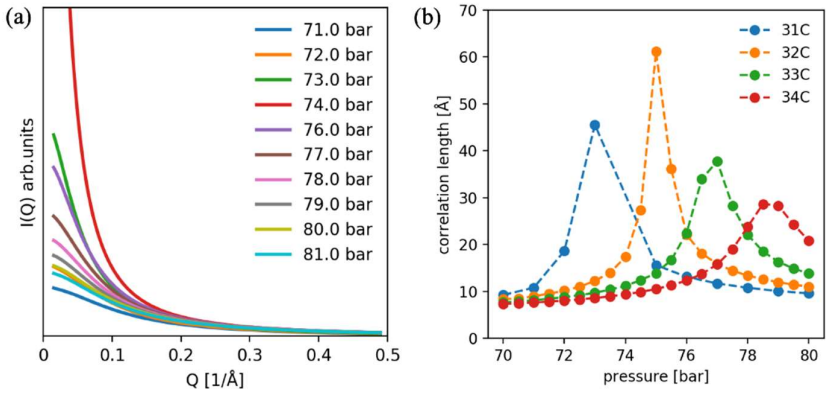

Figure 3: *(a) SAXS scattering intensity for CO_2 at 31°C. (b) Correlation length for CO_2 close to its critical point.*

X-ray Photon Correlation Spectroscopy (XPCS): XPCS utilizes the high intensity (~mJ) and ultrashort (≤ 30 fs) XFEL-pulses and their transverse coherence to produce scattering speckle pattern which reveal the sample's electron density distribution. The XCS-instrument at LCLS operates in the split-pulse version of the XPCS technique, providing two x-ray pulses with variable delays ranging up to few picoseconds with ~20 fs time resolution [9,10]. Fluctuations within the sample cause this speckle pattern to fluctuate accordingly and the experimentally measured quantity is the intensity autocorrelation function. Figure 4a shows a speckle pattern of a SiO_2 nanoparticles measured during our experiment. SiO_2 nanoparticles have been used as a reference sample due to its increased speckle contrast and scattering intensity compared to a supercritical CO_2 sample. The speckle pattern exhibits a spatial correlation along the vertical direction due to the geometry of the XPCS setup. Figure 4b shows the autocorrelation of the SiO_2 speckle pattern with a sideband occurring at ~12 pixels along the vertical displacement. We can relate the amplitude of the autocorrelation sideband to the speckle contrast and obtain a value of the speckle contrast of $\beta \approx 0.01$ [9]. These results show the successful implementation of our setup and the possibility to provide XPCS measurements in the supercritical phase for future experiments.

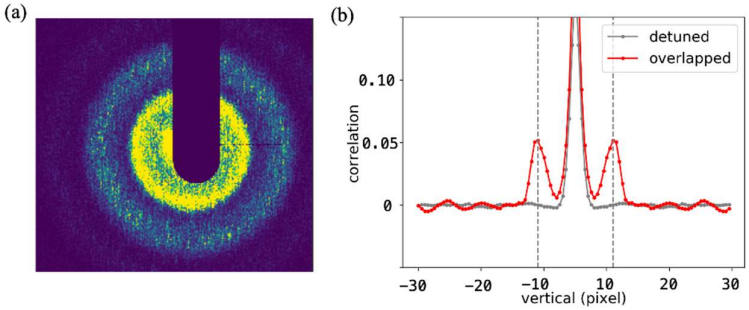

Figure 4*: (a) SiO_2 X-ray speckle pattern recorded by EPIX100 detector at the XCS instrument at LCLS. (b) Autocorrelation of the 2D-detector image shown in (a). A correlation of ≈5% is obtained in case of overlapped x-ray pulses (red line).*

Future Plans

Next steps in this project are the continuation of the XPCS experiments at LCLS in July 2021 by considering supercritical CO_2 and H_2O. Furthermore, the pressure cell and flow system will be upgraded to allow for mixtures in particular CO_2/H_2O as well as other fluids. In preparation of the next experiment, we performed MD simulations on supercritical CO_2 (Fig. 5) in order to estimate the speckle contrast decay as a function of the time delay between the two X-ray pulses. For the experiment, we are planning to probe the cluster dynamics at $Q \approx 0.1\text{Å}^{-1}$, which are predicted to be on the order of 1-10 ps.

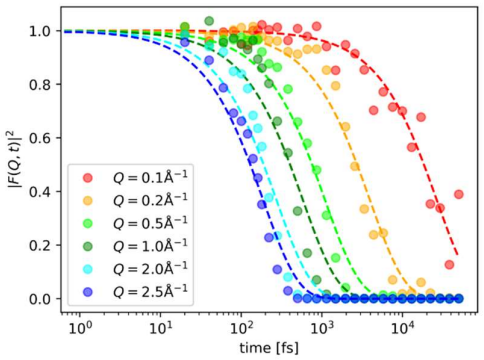

Figure 5: *Speckle contrast obtained by MD simulation on supercritical CO_2.*

References

[1] G. G. Simeoni, et al. The Widom line as the crossover between liquid-like and gas-like behaviour in supercritical fluids. *Nat. Phys.* 6.7 (2010): 503-507

[2] P. F. McMillan and H. E. Stanley. Going supercritical. *Nat. Phys.* 6.7 (2010): 479-480.

[3] J. Frenkel. *Kinetic Theory of Liquids*. Dover, 1955.

[4] H. E. Stanley. *Introduction to Phase Transitions and Critical Phenomena*. International Series of Monographs on Physics. Oxford University Press, 1971.

[5] F. Gorelli, M. Santoro, T. Scopigno, M. Krisch, and G. Ruocco. Liquidlike behavior of supercritical fluids. *Phys. Rev. Lett.*, 97(24):245702, 2006.

[6] K. Nishikawa and I. Tanaka. Correlation lengths and density fluctuations in supercritical states of carbon dioxide. *Chem. Phys. Lett.* 244.1-2 (1995): 149-152

[7] T. Morita, K. Nishikawa, M. Takematsu, H. Iida, and S. Furutaka. Structure study of super-critical CO2 near higher-order phase transition line by X-ray diffraction. *J. Phys. Chem. B*, 101(36):7158–7162, 1997.

[8] K. Nishikawa, A. A. Arai, and T. Morita. Density fluctuation of supercritical fluids obtained from small-angle X-ray scattering experiment and thermodynamic calculation. *J. Supercrit. Fluids*, 30(3):249–257, 2004.

[9] Y. Sun, et al. Compact hard X-ray split-delay system based on variable- gap channel-cut crystals. *Opt. Lett.*, 44(10):2582–2585, 2019.

[10] G. Grübel, A. Madsen, and A. Robert, X-ray Photon Correlation Spectroscopy (XPCS) in Soft Matter Characterization in X-ray and Neutron Techniques for Nanomaterials Characterization, edited by R. Borsali and B. Pecora, pp. 54–195, 2008.

Semiclassical Methods for Pressure Dependent Kinetics and Electronically Nonadiabatic Chemistry

Ahren W. Jasper
Chemical Sciences and Engineering Division
Argonne National Laboratory
ajasper@anl.gov

Program Scope

The outcome of a gas phase chemical reaction results from the competition of a variety of underlying microscopic processes, including collisional energy transfer, internal energy redistribution, bonding rearrangements, and inherently quantum mechanical events like electronic transitions. These same phenomena govern reactivity in more complex environments, and a major goal of the project is to develop a comprehensive set of semiclassical approaches for describing the fundamental chemical physics of elementary phenomena with high accuracy and that are broadly applicable throughout chemistry.

The improvement of first-principles theories via the construction of more and more detailed physical models benefits from the increasing impact of large-scale computing in chemistry, including Argonne's leadership-class resources. Our focus on the development of methods and codes for dynamics and kinetics recognizes that these approaches are now poised to take advantage of the tremendous advances made in electronic structure theory in recent decades. We pursue the development of semiclassical strategies, where the term is used here to describe approaches that incorporate one or more quantum effects into simulations involving classical or nearly classical nuclear motion. Semiclassical methods offer a scalable balance of computational cost and accuracy and are well suited for high performance computing. We focus on the advancement of first principles semiclassical approaches, i.e., methods that are systematically improvable and that may be assigned a priori error bars. We have demonstrated in a variety of contexts that our most detailed semiclassical models have accuracies that match and sometimes even exceed what is possible experimentally and approach the semiclassical accuracy limit of ~20%.

The increased accuracy of a priori theory and its use alongside experiment as an independent source of quantitative chemical and physical information may be anticipated to have a transformative effect in chemical modeling. Recent work supported by this project has continued the development of methods and codes for nonadiabatic dynamics and intersystem crossing, collisional energy transfer and transport, potential energy surface fitting, nonequilibrium reactivity, and rovibrational anharmonicity at high energies and temperatures.

Recent Progress

A general strategy was developed for constructing and validating permutationally invariant polynomial (PIP) expansions for chemical systems of any stoichiometry. Demonstrations were made for three applications: collisional energy transfer trajectories for predicting pressure dependent kinetics, three-body collisions for describing transient van der Waals adducts relevant to atmospheric chemistry, and nonthermal reactivity via quasiclassical trajectories. Systems with up to 15 atoms and 39 degrees of freedom were considered, and permutational invariance was enforced in PIP expansions with more than 30 million terms and as many as 13 permutationally-distinct atom types by taking advantage of petascale computational resources. The quality of the PIP expansions was demonstrated through the systematic convergence of in-sample and out-of-sample errors, and these errors were shown to predict errors in the dynamics for both reactive and nonreactive applications (Fig. 1).

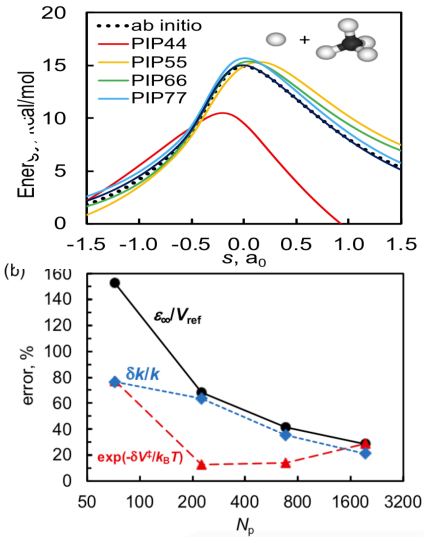

Fig. 1. (a) Minimum energy paths for H + CH4 for four PIP expansions. (b) The relative fitting error (black) predicts the relative dynamical errors (blue), whereas the error in the barrier height alone (red) does not.

With Davis, we demonstrated a strategy for reducing the number of terms required for accurate PIP expansions. In conventional total-

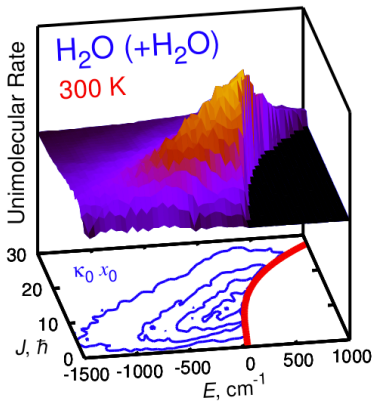

Fig. 2. Contribution to the low-pressure limit rate constant k_0 for H_2O ($+H_2O$) shown as a function of the initial state of H_2O.

order PIP expansions, the number of terms scales unfavorably with system size ($\sim n^{2o}$, where n is the number of atoms and o is the order of the PIP), and this limiting drawback was addressed using minimal basis sets optimized using multi-pass greedy subset selection, a strategy borrowed from forward and backward subset selection methods developed in the statistics and signal processing literature. Notably, the sizes of the minimal optimized basis sets scale ~linearly with dimensionality, in line with chemical intuition.

Low-pressure-limit microcanonical rate constants, $\kappa_0(E,J)$, describe the rate of activating bath gas collisions in a unimolecular reaction as a function of the initial internal state (E,J) of the reactant. We showed that κ_0 can be calculated using classical trajectories and quantized thresholds for reaction. The resulting semiclassical rate constants are two-dimensional (in total energy E and total angular momentum J) and are intermediate in complexity between the more-familiar four-dimensional state-to-state collisional energy and angular momentum transfer rate constant, $R(E',J';E,J)$, and the highly-averaged thermal rate constant, k_0. We generated results for CH_4 (+M), C_2H_x (+M), x = 3–6, and H_2O (+M) and showed that $\kappa_0(E,J)$ is a sensitive function of the bath gas, temperature, and initial state of the unimolecular reactant (Fig. 2). Strong variations in κ_0 with respect to E and J lead to complex trends in relative microcanonical bath gas efficiencies, complicating the search for simple explanations for observed trends in relative thermal bath gas efficiencies. A new measure of the microcanonical collision efficiency that describes the energy range of activating collisions was introduced to support the empirical decomposition of collisional activation into separable translational-to-vibrational and rotational-to-vibrational activation mechanisms. The two mechanisms depend differently on mass, temperature, and the J-dependence of the threshold energy for reaction, with rotational-to-vibrational activation favored for heavier baths and for reactions with rigid transition states.

Using potential energy surfaces developed by Harding and Georgievskii, Monte Carlo phase space integration (MCPSI) was used to compute full dimensional and fully anharmonic—but classical—rovibrational partition functions for 22 small- and medium-sized molecules and radicals. Several of the species featured multiple minima and low-frequency nonlocal motions, and efficiently sampling these systems was facilitated using curvilinear (stretch, bend, and torsion) coordinates. The curvilinear coordinate MCPSI method was demonstrated to be applicable to the treatment of fluxional species with complex rovibrational structures and as many as 21 fully coupled rovibrational degrees of freedom. Trends in the computed anharmonicity corrections were identified and discussed. In a follow-up study, we implemented our curvilinear coordinate MCPSI code "at scale" on Argonne's petascale machine, Theta. There, we calculated semiclassical rovibrational state counts and partition functions for systems with two and three coupled torsions and as many as 30 rotational and vibrational modes. These results were used as benchmarks to quantify the accuracy of simpler reduced-dimensional approaches and analyzed for general physical insights about the nature of fluxional mode coupling at high temperatures and energies. For example, we identified and quantified the effect of low-frequency heavy-atom bends coupling to torsions.

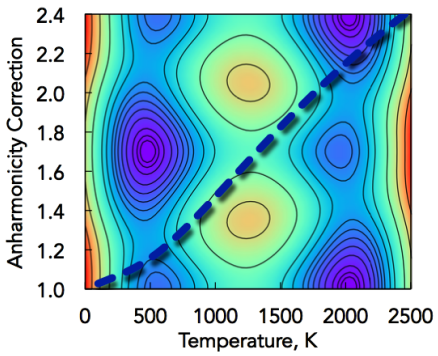

Fig. 3. Correction to the harmonic state count for NH_2OH overlaid over a contour plot of the PES as a function of the $-NH_2$ inversion and N–O torsion coordinates.

Future Work

We will continue to develop and apply our semiclassical dynamics code, DiNT, which includes

theories for nonadiabatic dynamics with detailed and validated treatments of (de)coherence and classically forbidden transitions, e.g., as in the Coherent Switching with Decay of Mixing (CSDM) and Fewest-Switches with Time Uncertainty (FSTU) methods. This code uses Argonne's petascale machines to facilitate direct dynamics applications and high-order PIP expansions. Preliminary results have been obtained for the ultrafast internal conversion in alkenes, with the goal of testing the impact of improved semiclassical treatments of decoherence as well as to improve the performance of tight-binding models for describing coupled potential energy surfaces relevant to multistate alkene chemistry. These models provide efficient enough representations to study photon capture, charge separation, and energy storage in supramolecular molecules (aromatic hydrocarbons with ~100 atoms) relevant to artificial photosynthesis.

We propose to continue to advance the applicability of MCPSI to include systems where the accuracy of existing anharmonicity approaches has not been well characterized, such as transition states and species involving constrained torsions and rings. In earlier work, we approximated the high-dimensional MCPSI integrals via a hierarchy of expressions based on so-called "*n*-mode intrinsic" state densities. The 2-mode (pairwise) intrinsic state density Δ_{ij}, for example, is defined for each pair of coordinates i and j as the state density for those modes not represented by the convolution of the one-dimensional densities ρ_i. The full-dimensional density of states is then approximated through second order via convolutions of Δ_{ij} and ρ_k. Intractable high-dimensional integrals are thus computed from convolutions of readily obtained one- and two-dimensional ones. This 2nd-order result can be systematically improved via 3rd- and higher-order corrections. Despite the significant computational savings of this approach, the number of convolutions required can become cumbersome. We will explore approximations where terms are eliminated based on their order and with respect to the number of intrinsics in the term. Preliminary studies for CH_4 show that retaining terms with just one 2nd-order intrinsic speeds up the calculation by two orders of magnitude with a negligible (2%) loss of accuracy. This strategy provides a route toward practical applications of MCPSI for very large molecular systems.

To support ongoing investigations into nonthermal and nonequilibrium kinetics, we will test the accuracy of studying these processes using transition state theory (TST). The TST expression for the rate constant can be written very generally as $k = \frac{1}{2}\int dxdpf^{\ddagger}v/\Pi_R\int dxdpf_R$, i.e., as ½ the ratio of a phase space integral of the flux through the transition state dividing surfaces and phase space integrals for the reactants. To evaluate this expression, one must *choose* the functions $f^{\ddagger}$ and f_R, which describe the population distributions at the transition state and for the reactants including relative coordinates, respectively. When either microcanonical or thermal equilibration choices are consistently made, the familiar TST expressions result. We will consider alternate choices, including choices appropriate for nonthermal reactions of recent interest like $H_2O^* + H \rightarrow H_2 + O_2$, where, in this example, we wish to employ mixed equilibration assumptions with f_{H2O*} described microcanonically with an internal energy E close to its dissociation threshold while f_{rel} for the relative translational coordinates are described thermally by a local temperature T. The corresponding choice for $f^{\ddagger}$ is not at all obvious (other than it should be some function of E and T), as, of course, unambiguous 1-to-1 relationships between the degrees of freedom at the transition state and those for the reactants do not exist. Quasiclassical trajectories will be used to test and improve the accuracy of competing schemes for choosing $f^{\ddagger}$. These studies will benefit from recent developments of our MCPSI sampling work, which can be incorporated to explore the effects of anharmonicity as well as the use of generalized (momentum- or energy-dependent) transition state dividing surfaces.

Publications supported by this project since 2019

1. D. R. Moberg and A. W. Jasper, Permutationally invariant polynomial expansions with unrestricted complexity, submitted (2021).

2. D. R. Moberg, A. W. Jasper, and M. J. Davis, Potential energy surface expansions with improved scaling using dictionary learning based on multi-pass greedy selection, submitted (2021).

3. P. Glarborg, H. Hashemi, S. Cheskis, and A. W. Jasper, On the rate constant for $NH_2 + HO_2$ and third

body collision efficiencies for NH_2 + H (+M) and NH_2 + NH_2 (+M), *J. Phys. Chem. A* 125, 1505–1516 (2021).

4. A. C. Rousso, A. W. Jasper, Y. Ju, and N. Hansen, Extreme low temperature combustion chemistry: Ozone-initiated oxidation of methyl hexanoate, *J. Phys. Chem. A* 124, 9897–9914 (2020).

5. J. B. Randazzo, A. W. Jasper, R. Sivaramakrishnan, T. Sikes, P. T. Lynch, and R. S. Tranter, An experimental and theoretical study of the high temperature reactions of four butyl radical isomers, *Phys. Chem. Chem. Phys.* 22, 18304–18319 (2020).

6. J. A. Miller, R. Sivaramakrishnan, C. F. Goldsmith, M. P. Burke, A. W. Jasper, J. Zádor, N. Hansen, N. J. Labbe, and P. Glarborg, Combustion chemistry in the twenty-first century: Developing theory-informed chemical kinetics models. *Prog. Energy Combust. Sci.* 83, 100886 (2020).

7. Z. Wang, N. Hansen, A. W. Jasper, B. Chen, S. M. Popolan-Vaida, K. K. Yalamanchi, A. Najjar, P. Dagaut, and S. M. Sarathy, Cool flame chemistry of diesel surrogate compounds: n-decane, 2-methylnonane, 2,7-dimethyloctane, and n-butylcyclohexane. *Combust. Flame* 219, 384–392 (2020).

8. Y. Tao, A. W. Jasper, Y. Georgievskii, S. J. Klippenstein, and R. Sivaramakrishnan, Termolecular chemistry facilitated by radical-radical recombinations and its impact on flame speed predictions. *Proc. Combust. Inst*., in press (2020).

9. N. Hansen, G. Kukkadapu, B. Chen, S. Dong, H. J. Curran, C. A. Taatjes, A. J. Eskola, D. L. Osborn, L. Sheps, W. J. Pitz, K. Moshammer, A. W. Jasper, W. Chen, J. Yang, and Z. Wang, The impact of the third O_2 addition reaction network on ignition delay times of neo-pentane. *Proc. Combust. Inst*., in press (2020).

10. A. W. Jasper, "Third-body" collision parameters for hydrocarbons, alcohols, and peroxides and an effective internal rotor approach for estimating them. *Int. J. Chem. Kinet.* 52, 387–402 (2020).

11. A. W. Jasper, Microcanonical rate constants for unimolecular reactions in the low-pressure limit. *J. Phys. Chem. A* 124, 1205–1226 (2020).

12. N. Hansen, K. Moshammer, and A. W. Jasper, Isomer-selective detection of keto-hydroperoxides in the low-temperature oxidation of tetrahydrofuran. *J. Phys. Chem. A* 123, 8274–8284 (2019).

13. A. W. Jasper, L. B. Harding, C. Knight, and Y. Georgievskii, Anharmonic rovibrational partition functions at high temperatures: Tests of reduced-dimensional models for systems with up to three fluxional modes. *J. Phys. Chem. A* 123, 6210–6228 (2019).

14. A. G. Dana, K. B. Moore III, A. W. Jasper, and W. H. Green, Large intermediates in hydrazine decomposition: A theoretical study of the N_3H_5 and N_4H_6 potential energy surfaces. *J. Phys. Chem. A* 4679–4692 (2019).

15. A. W. Jasper and M. J. Davis, Parameterization strategies for intermolecular potentials for predicting trajectory-based collision parameters. *J. Phys. Chem. A* 123, 3464–3480 (2019).

16. A. C. Rousso, N. Hansen, A. W. Jasper, and Y. Ju, Identification of the Criegee intermediate reaction network in ethylene ozonolysis: Impact on energy conversion strategies and atmospheric chemistry. *Phys. Chem. Chem. Phys.* 21, 7341–7357 (2019).

17. A. W. Jasper, R. Sivaramakrishnan, and S. J. Klippenstein, Nonthermal rate constants for CH_4* + X = CH_3 + HX, X = H, O, OH, and O_2. *J. Chem. Phys.* 150, 114112 (2019).

18. D. H. Bross, A. W. Jasper, B. Ruscic, and A. F. Wagner, Toward accurate high temperature anharmonic partition functions. *Proc. Combust. Inst.* 37, 315–322 (2019).

19. S. Elliott, Y.-P. Li, M. S. Johnson, C. Cavallotti, Y. Georgievskii, W. H. Green, M. Pelucchi, J. M. Wozniak, A. W. Jasper, and S. J. Klippenstein, Automated computational thermochemistry for butane oxidation: A prelude to predictive automated combustion kinetics. M. Keçeli, *Proc. Combust. Inst.*, 37, 363–371 (2019).

Studies of non-equilibrium high pressure kinetics at supercritical H_2O/CO_2 conditions using a new supercritical jet stirred reactor (SP-JSR)

Yiguang Ju, PI

Dept. of Mechanical and Aerospace Engineering, Princeton University, Princeton, NJ 08540,
Email: yju@princeton.edu

Program Scope

The goal of this work is to advance fundamental understanding of non-equilibrium chemical kinetics via the real gas effects with strong intermolecular force, multi-body collisional reactions, and non-equilibrium energy distribution on low temperature combustion as well as HO_2 chemistry at pressures up to 100-300 atm with CO_2 and H_2O dilutions. Specifically, a new, supercritical pressure jet stirred reactor (SP-JSR) operating up to 100-300 atm will be developed to obtain important kinetic data of low and intermediate temperature combustion chemistry, species dependence on pressure and bath gas colliders at supercritical CO_2 and H_2O conditions for hydrogen and C_1-C_4 hydrocarbons and alcohols. Non-equilibrium effects via real gas intermolecular force, reactive termolecular reactions involving HO_2 and OH, vibrational non-equilibrium energy distribution, and collisional energy broadening at high pressure will be examined. Key HO_2 reactions with fuels and radicals will be studied by using microsecond time-resolved mid-IR Faraday rotation spectroscopy (FRS) and high level quantum chemistry calculations. The obtained high pressure data and the newly measured and computed reaction rates will be used to develop and validate new high pressure combustion models by including non-equilibrium chemical kinetic effects. The present studies will advance the fundamental understanding of non-equilibrium chemical kinetics and HO_2 chemistry at extreme pressures.

Recent Progress

a. Development of SP-JSR

We have developed and tested a SP-JSR up to 200 atm between 300-1300 K. The schematic and direct image of SP-JSR are shown in Fig. 1 [1]. The spherical JSR has an internal volume of 0.5 cm^3. To improve the mixing, SP-JSR has 8 nozzles with 0.2 mm inner diameter to generate intense turbulence for homogenous mixing. Numerical simulations were performed to show that the present SP-JSR design has a narrower flow residence time distribution than the conventional JSR with four nozzles [2-4]. The quartz reactor is placed inside a stainless-steel pressure-resistant jacket. The gas or vaporized liquid fuel vapor flow rates were controlled by high-pressure mass flow controllers. Pressure balancing inside and outside the reactor is enabled by using a pressure regulator. The axial temperature distribution

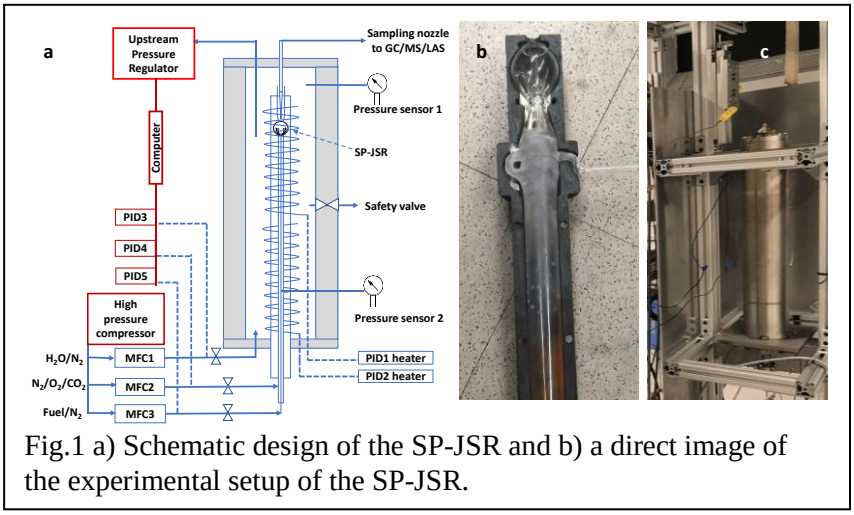

Fig.1 a) Schematic design of the SP-JSR and b) a direct image of the experimental setup of the SP-JSR.

under the experimental flow conditions were measured and the temperature variation was within ± 3 K between 300-1000 K. The exhaust gases from the JSR exit are sampled by a quartz sonic nozzle with rapid expansion quenching using vacuum generated by a dry pump. The gas samples were quantified by using a micro gas chromatograph (μ-GC).

b. Kinetic studies of the oxidation of hydrogen and small hydrocarbons at 100 atm

The HP-JSR was employed to study the high pressure oxidation of hydrogen, methane, and n-butane at 100 atm with and without H_2O and CO_2 dilution. Fig. 2(a) and 2(b) show the dependence of H_2 mole fraction on the temperature of SP-JSR for a lean H_2-O_2-N_2 mixture at equivalence ratio of 0.34 and pressure of 100 atm, respectively, without and with 10% H_2O (a) and 20% CO_2 (b) dilutions. The experimental data are compared with different model predictions. It is seen that without H_2O and CO_2 dilutions, models predict the fuel oxidation reasonable well between 800 and 900 K, but under-predict the experimental results above 1000 K. However, with H_2O and CO_2 dilutions, the experimental data show clearly that the onset of H_2 oxidation is slowed down and shifted to higher temperature. In addition, at a higher temperature above 950 K, Fig. 2(a) shows that H_2O dilution accelerates the fuel oxidation. However, all of the models fail to capture the effects of H_2O and CO_2 dilution on the fuel oxidation. Therefore, the HO_2 and H_2O_2 reaction kinetics involving the third-body collision reactions such as HO_2+M and H_2O_2+M need to be re-examined at high pressure. In addition, the real gas effect on reaction kinetics modeling will also need to be studied.

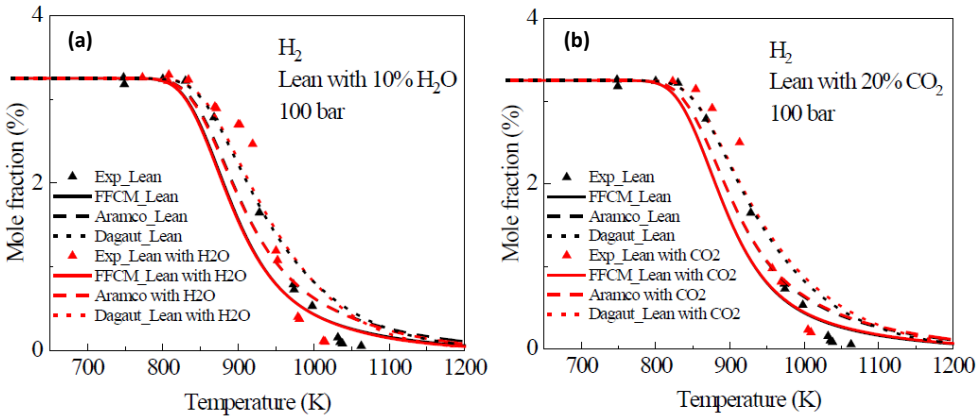

Fig.2 Dependence of H_2 mole fraction on the temperature of SP-JSR at equivalence ratio of 0.34 and 100 atm. Lines are predictions and solid triangles are experimental data.(a) with/without 10% H_2O dilution, (b) with/without 20% CO_2 dilution.

Fig.3 shows the dependence of CH_4 mole fraction on the temperature of SP-JSR at 100 atm for CH_4-O_2-N_2 mixtures with equivalence ratios of 0.24 (black markers) and 1.83 (red makers), respectively. For the fuel lean mixture, Fig.3 shows that all of the models fail to predict the fuel oxidation above 900 K. The discrepancy between the experimental results and model predictions increases with the temperature. This large difference shows that the models may have missing reaction pathways at very high pressure. At fuel rich conditions, the experimental data show that there is a clear negative temperature coefficient (NTC) effect between 900 and 1025 K. However, only the AramcoMech 3.0 [5] can capture the onset temperature of the NTC effect but still under predicts the fuel oxidation at temperature above 1025 K. Therefore, both low temperature kinetics and the thermochemistry of methane oxidation at high pressure need to be revisited.

Fig.4 shows the dependence of n-butane mole fraction on the temperature of SP-JSR at equivalence ratio of 0.1, respectively, for 10 atm (green) and 100 atm with (red) and without (black) 20% CO_2 dilution. At 10 atm without CO_2 addition, experimental data show a typical low temperature fuel oxidation from 600 K to 780 K and a clear NTC behavior. However, at 100 atm, a much weaker NTC behavior is observed and the intermediate temperature oxidation is shifted to lower temperatures with and without CO_2 addition. Therefore, the NTC effect is strongly dependent on the pressure due to the competition between the multi-oxygen addition processes, which are more favored at high pressure, and the decomposition of QOOH and O_2QOOH. It is also seen that supercritical CO_2 has limited effect on the onset of low temperature oxidation of n-butane, but slows down the intermediate temperature fuel oxidation. This may be because of the impact of CO_2 addition on the HO_2 chemistry.

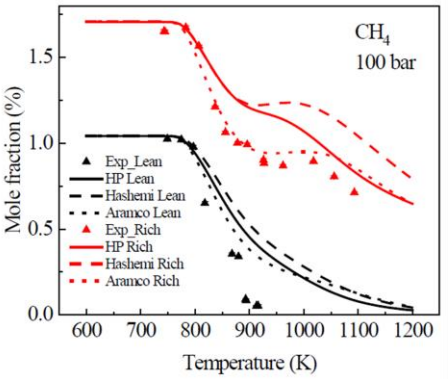

Fig.3 Dependence of CH_4 mole fraction on the temperature of SP-JSR at 100 atm with equivalence ratio of 0.24 (black) and 1.83 (red), respectively, for CH_4-O_2-N_2 mixtures.

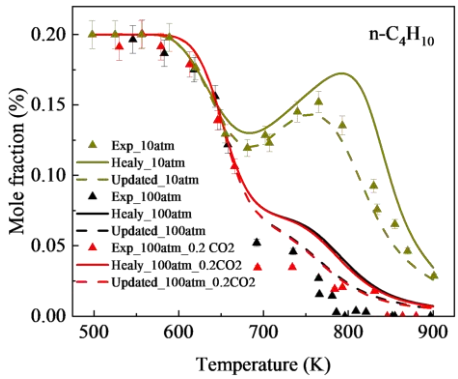

Fig.4 Dependence of n-butane mole fraction on the temperature of SP-JSR at equivalence ratio of 0.1, respectively, at 10 atm (green) and 100 atm with (red) and without (black) 20% CO_2 dilution.

Future Plans

In the 2nd year, we will continue to collaborate with Drs. Ahren Jasper and Stephen Klippenstein at Argonne National Laboratory to update the HO_2+M and H_2O_2+M chemistry for hydrogen oxidation. In addition, we will examine the effect of the real gas equation of states on model prediction at supercritical conditions. Moreover, we will examine the effect of high pressure stabilization of CH_3O_2 on low temperature methane oxidation. Furthermore, the high pressure experiments will be extended to oxygenated fuels such as methanol and ethanol.

Journal publications supported by this BES project (2020-2021)

[1] H. Zhao, C. Yan, T. Zhang, G. Ma, M.J. Souza, C.-W. Zhou, Y. Ju, Studies of high-pressure n-butane oxidation with CO2 dilution up to 100 atm using a supercritical-pressure jet-stirred reactor, **Proceedings of Combustion Insittute** 38 (2021) 279–287.

[2] Mengni Zhou, Omar R. Yehia Wenbin Xu, Christopher B. Reuter, Ziyu Wang, Chao Yan, Bo Jiang, Yiguang Ju, The radical index and the effect of oxygen concentration on non-premixed cool flame extinction of large n-alkanes, **Combustion and Flame**, 2021, accepted.

Acknowledgement: The PI would like to thank Drs. Ahren Jasper and Stephen Klippenstein at Argonne National Laboratory for collaborations in quantum chemistry calculations

References

[1] H. Zhao, C. Yan, T. Zhang, G. Ma, M.J. Souza, C.-W. Zhou, Y. Ju, Studies of high-pressure n-butane oxidation with CO2 dilution up to 100 atm using a supercritical-pressure jet-stirred reactor, Proceedings of Combustion Insittute 38 (2021) 279–287.

[2] P. Dagaut, M. Reuillon, M. Cathonnet, Experimental study of the oxidation of n-heptane in a jet stirred reactor from low to high temperature and pressures up to 40 atm, Combustion and flame 101 (1995) 132-140.

[3] A.C. Rousso, N. Hansen, A.W. Jasper, Y. Ju, Low-Temperature Oxidation of Ethylene by Ozone in a Jet-Stirred Reactor, The Journal of Physical Chemistry A 122 (2018) 8674-8685.

[4] H. Zhao, L. Wu, C. Patrick, Z. Zhang, Y. Rezgui, X. Yang, G. Wysocki, Y. Ju, Studies of low temperature oxidation of n-pentane with nitric oxide addition in a jet stirred reactor, Combustion and Flame 197 (2018) 78-87.

[5] C.-W. Zhou, Y. Li, U. Burke, C. Banyon, K.P. Somers, S. Ding, S. Khan, J.W. Hargis, T. Sikes, O. Mathieu, An experimental and chemical kinetic modeling study of 1, 3-butadiene combustion: Ignition delay time and laminar flame speed measurements, Combustion and Flame 197 (2018) 423-438.

Probing the Reaction Dynamics of Hydrogen-Deficient Hydrocarbon Molecules and Radical Intermediates via Crossed Molecular Beams

Ralf I. Kaiser
Department of Chemistry, University of Hawai'i at Manoa, Honolulu, HI 96822
ralfk@hawaii.edu

1. Program Scope

The major goals of this project are to explore experimentally by exploiting molecular beams to study the fundamental reaction dynamics and underlying potential energy surfaces (PESs) of hydrocarbon molecules and their corresponding (resonantly free stabilized and aromatic) radical precursors, which are relevant to the formation and molecular growth of polycyclic aromatic hydrocarbons (PAHs). First, reactions are initiated in a crossed molecular beams machine under single collision conditions by crossing two supersonic reactant beams containing radicals and/or closed shell species under a well-defined collision energy and intersection angle. By recording angular-resolved time of flight (TOF) spectra, we obtain information on the reaction products, intermediates involved, branching ratios of competing reaction channels, reaction energetics, and on the underlying reaction mechanisms. Second, in collaboration with Dr. Musahid Ahmed (Chemical Sciences Division, Lawrence Berkeley Laboratory), reactions are carried out in a chemical reactor at well characterized pressure and temperature distributions with reaction products interrogated isomer-selectively by tunable vacuum ultraviolet light (VUV) via photoionization (PI) coupled with a reflectron time of flight mass spectrometer (ReTOFMS). Merged with electronic structure calculations (Prof. Alexander M. Mebel, Florida International University), these data are of fundamental importance to comprehend the underlying formation mechanisms of two key classes of molecules involved in molecular mass-growth processes leading to carbonaceous nanostructures from the bottom up: resonantly stabilized free radicals (RSFRs) and polycyclic aromatic hydrocarbons.

2. Recent Progress

We elucidated fundamental low- and high-temperature reaction mechanisms leading to the formation of PAHs carrying up to five rings via neutral-neutral involving five key reaction mechanisms: **H**ydrogen **A**bstraction – **C**$_2$H$_2$ (acetylene) **A**ddition (**HACA**), **H**ydrogen **A**bstraction – **V**inylacetylene **A**ddition (**HAVA**), **P**henyl **A**ddition – Dehydro**C**yclization (**PAC**), **R**adical-**R**adical **R**eactions (**RRR**), and **M**ethylidyne **A**ddition - **C**yclization - **A**romatization (**MACA**) (**P32**). *First*, a unified low-temperature reaction mechanism on the formation of acenes, phenacenes, and helicenes –PAHs that are distinct via the linear, zigzag, and ortho-condensed arrangements of fused benzene rings - was revealed. This mechanism is mediated through a barrierless, vinylacetylene mediated gas-phase chemistry (HAVA) utilizing tetracene, pentacene, [4]-phenacene, and [4]-helicene ($C_{18}H_{12}$) as benchmarks challenging established ideas that molecular mass growth processes to PAHs only transpire at elevated temperatures (**P22, P24**). This mechanism can be also expanded to PAHs carrying five-membered rings such as benzindenes (**P26**). *Second*, we provided testimony on a facile formation of benzene (C_6H_6) and naphthalene ($C_{10}H_8$) via Radical-Radical Reactions (RRR) involving aromatic (indenyl) and resonantly stabilized free radicals (propargyl) (**P15**, **P33**), *Third*, crossed molecular beam studies combined with electronic structure calculations exposed low temperature pathways to indene (C_9H_8) via the newly elucidated **M**ethylidyne **A**ddition - **C**yclization - **A**romatization (**MACA**) mechanism; this pathways essentially converts a vinyl sidechain attached to an aromatic, six-membered ring via reaction with methylidyne radicals to a five-membered ring (**P29**, **P32**). Finally, a combination of HACA/HAVA with PAC and HACA revealed to be essential in the first directed, high temperature gas phase preparation of corannulene (**P31**).

3. Future Plans

Having established synthetic pathways to PAHs carrying up to five six-membered rings such as pentacene and corannulene, we will elevate our studies to the formation of more complex PAHs like coronene and annulated corannnulenes as fundamental molecular building blocks to two- and three-dimensional carbon nanostructures, respectively. Further, we are expanding our radical – radical reactions beyond the formation of benzene and naphthalene to prepare aromatic systems with up to three six-membered rings

(anthracene, phenanthrene). Finally, we will work toward a better understanding of fundamental reaction mechanisms beyond HACA, HAVA, PAC, RRR, and MACA leading to aromatic molecules thus defining the role and complementary nature of key reaction mechanisms in PAH growth. Electronic structure calculations will be conducted by Prof. Mebel (Florida International University).

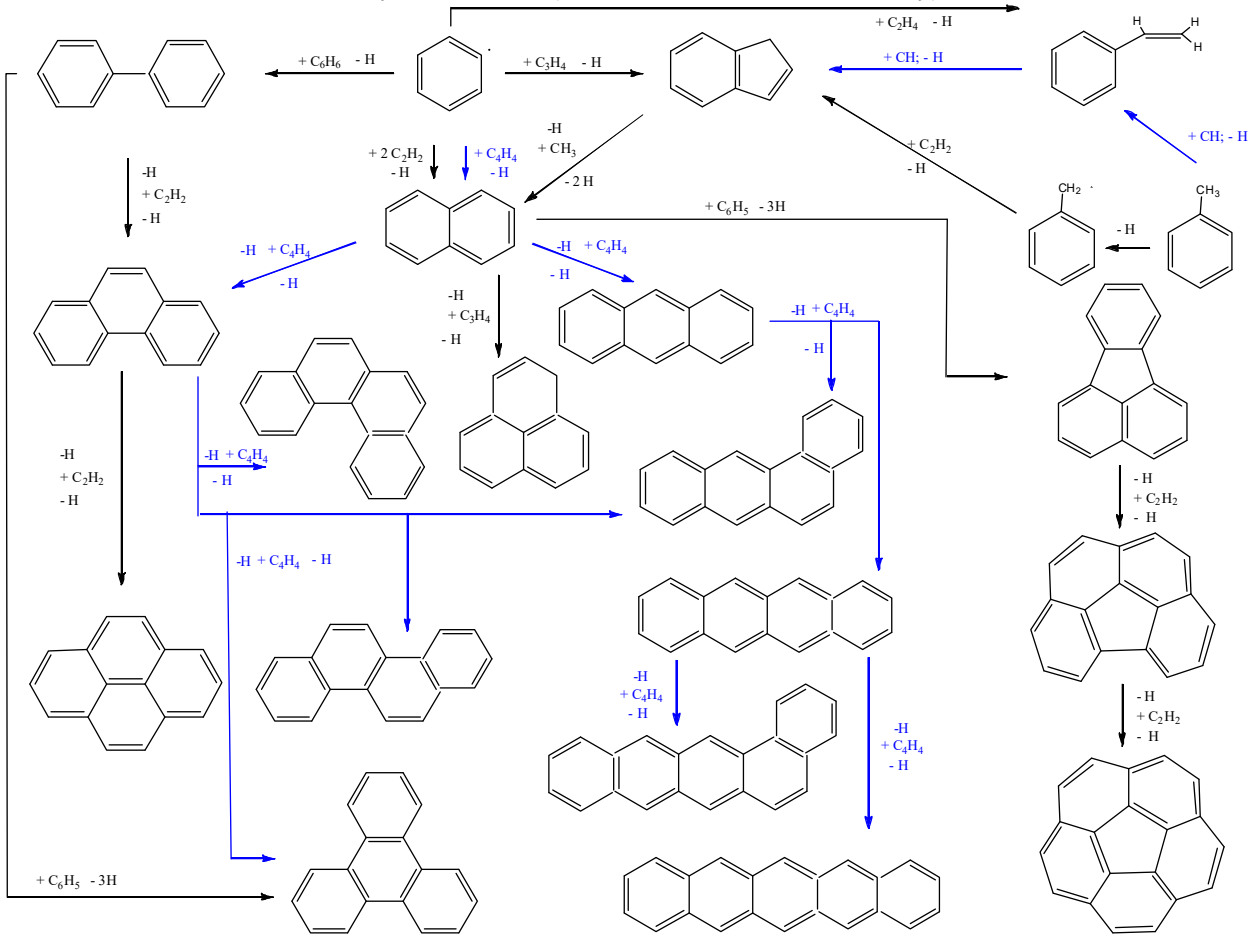

Fig. 1: Pathways to aromatic systems via HACA, HAVA, RRR, PAC, and MACA elucidated through molecular beams experiments; blue arrows represent barrierless pathways; adapted from **P32**.

4. Acknowledgements

This work is supported by US Department of Energy (Basic Energy Sciences; DE-FG02-03-ER15411).

5. Publications Acknowledging DE-FG02-03ER15411 (6/2018 – now)

1 M. Lucas, A.M. Thomas, R. I. Kaiser, E.K. Bashkirov, V.N. Azyazov, A.M. Mebel, Combined Experimental and Computational Investigation of the Elementary Reaction of Ground State Atomic Carbon (C; ^3P_j) with Pyridine (C_5H_5N; X^1A_1) via Ring Expansion and Ring Degradation Pathways. J. Phys. Chem A. 122, 3128-3139 (2018).

2 A.M. Thomas, M. Lucas, L. Zhao, J. Liddiard, R.I. Kaiser, A.M. Mebel, A Combined Crossed Molecular Beams and Computational Study on the Formation of Distinct Resonantly Stabilized C_5H_3 Radicals via Chemically Activated C_5H_4 and C_6H_6 Intermediates. Phys. Chem. Chem. Phys. 20, 10906-10925 (2018).

3 L. Zhao, R.I. Kaiser, B. Xu, U. Ablikim, M. Ahmed, D. Joshi, G. Veber, F.R. Fischer, A.M. Mebel, Pyrene Synthesis in Circumstellar Envelopes and its Role in the Formation of 2D Nanostructures. Nature Astron. 2, 413-419 (2018).

4 L. Zhao, R.I. Kaiser, B. Xu, U. Ablikim, M. Ahmed, M.V. Zagidullin, V.N. Azyazov, A.H. Howlader, S.F. Wnuk, A.M. Mebel, VUV Photoionization Study of the Formation of the Simplest Polycyclic Aromatic Hydrocarbon: Naphthalene ($C_{10}H_8$). J. Phys. Chem. Lett. 9, 2620–2626 (2018).

5 A.M. Thomas, L. Zhao, C. He, A.M. Mebel, R. Kaiser, A Combined Experimental and Computational Study on the Reaction Dynamics of the 1-Propynyl (CH_3CC)—Acetylene (HCCH) System and the Formation of Methyldiacetylene (CH_3CCCCH). J. Phys. Chem. A (W.M. Jackson Special Issue) 122, 6663-6672 (2018).

6 L. Zhao, R.I. Kaiser, B Xu, U. Ablikim, M. Ahmed, M. Evseev, E.K. Bashkirov, V.N. Azyazov, A.M. Mebel, Low-Temperature Formation of Polycyclic Aromatic Hydrocarbons in Titan's Atmosphere. Nature Aston. 2, 973-979 (2018).

7 M.V. Zagidullin, R.I. Kaiser, D.P. Porfiriev, I.P. Zavershinskiy, M. Ahmed, V.N. Azyazov, A.M. Mebel, Functional Relationships between Kinetic, Flow, and Geometrical Parameters in a High-Temperature Chemical Microreactor. J. Phys. Chem. A 122, 8819–8827 (2018).

8 L. Zhao, B. Xu, U. Ablikim, W. Lu, M. Ahmed, M.M. Evseev, E.K. Bashkirov, V.N. Azyazov, A.H. Howlader, S.F. Wnuk, A.M. Mebel, R.I. Kaiser, Gas-Phase Synthesis of Triphenylene ($C_{18}H_{12}$). ChemPhysChem. 20, 791-797 (2019).

9 L. Zhao, R.I. Kaiser, B. Xu, U. Ablikim, W. Lu, M. Ahmed, M. Evseev, E. K. Bashkirov, V.N. Azyazov, M.V. Zagidullin, A.N. Morozov, A.H. Howlader, S.F. Wnuk, A.M. Mebel, D. Joshi, G. Veber, F. R. Fischer, Gas Phase Synthesis of [4]-Helicene. Nature Commun. 10, 1510 (2019).

10 A.M. Thomas, C. He, L. Zhao, G.R. Galimova, A.M. Mebel, R.I. Kaiser, Combined Experimental and Computational Study on the Reaction Dynamics of the 1-Propynyl (CH_3CC)—1,3-Butadiene ($CH_2CHCHCH_2$) System and the Formation of Toluene under Single Collision Conditions. J. Phys. Chem. A (H. Reisler Special Issue) 123, 4104-4118 (2019).

11. L. Zhao, M.B. Prendergast, R.I. Kaiser, B. Xu, W. Lu, U. Ablikim, M. Ahmed, A.D. Oleinikov, V.N. Azyazov, A.M. Mebel, A.H. Howlader, S.F. Wnuk, Reactivity of the Indenyl Radical (C_9H_7) with Acetylene (C_2H_2) and Vinylacetylene (C_4H_4). ChemPhysChem 20, 1437-1447 (2019).

12 C. He, L. Zhao, A.M. Thomas, A.N. Morozov, A.M. Mebel, R.I. Kaiser, Elucidating the Chemical Dynamics of the Elementary Reactions of the 1-Propynyl Radical (CH_3CC; X^2A_1) with Methylacetylene (H_3CCCH; X^1A_1) and Allene (H_2CCCH_2; X^1A_1). J. Phys. Chem. A. 123, 5446-5462 (2019).

13 L. Zhao, M. Prendergast, R. I. Kaiser, B. Xu, U. Ablikim, W. Lu, M. Ahmed, A.D. Oleinikov, V.N. Azyazov, A.H. Howlader, S.F. Wnuk, A.M. Mebel, How to Add a Five-Membered Ring to Polycyclic Aromatic Hydrocarbons (PAHs) – Molecular Mass Growth of the 2-Naphthyl Radical ($C_{10}H_7$) to Benzindenes ($C_{13}H_{10}$) as a Case Study. Phys. Chem. Chem. Phys. 21**,** 16737-16750 (2019).

14 C. He, A. M. Thomas, G. R. Galimova, A.M. Mebel, R.I. Kaiser, Gas Phase Formation of the Interstellar Molecule Methyltriacetylene. ChemPhysChem, 20, 1912-1917 (2019).

15 L. Zhao, R.I. Kaiser, W. Lu, B. Xu, M. Ahmed, A.N. Morozov, A.M. Mebel, A.H. Howlader, S.F. Wnuk, Molecular Mass Growth through Ring Expansion in Polycyclic Aromatic Hydrocarbons via Radical-Radical Reactions. Nature Commun. 10, 3689 (2019).

16 A.M. Thomas, C. He, L. Zhao, A.M. Mebel, R.I. Kaiser, Directed Gas Phase Synthesis of Triafulvene under Single Collision Conditions. Angewandte Chemie – International Edition 58, 15488 (2019).

17 C. He, L. Zhao, A. M. Thomas, A.M. Mebel, R.I. Kaiser, A Combined Experimental and Computational Study on the Reaction Dynamics of the 1-Propynyl Radical (CH_3CC; X^2A_1) with Ethylene (H_2CCH_2; X^1A_{1g}) and the Formation of 1-Penten-3-yne ($CH_2CHCCCH_3$; X^1A'). Physical Chemistry Chemical Physics 21, 22308 (2019).

18 L. Zhao, M. Prendergast, R.I. Kaiser, B. Xu, U. Ablikim, M. Ahmed, B.-J. Sun, AH.H. Chang, R.K Mohamed, F.R. Fischer, Phenyl Addition - Dehydrocyclization Triggered Synthesis of Polycyclic Aromatic Hydrocarbons - The Third Way. Angewandte Chemie – International Edition 58, 17442 (2019).

19 A.M. Thomas, S. Doddipatla, R.I. Kaiser, A.M. Mebel, A Barrierless Pathway Accessing the C_9H_9 and C_9H_8 Potential Energy Surfaces via the Elementary Reaction of Benzene with 1-Propynyl. Scientific Reports (Special Issue Molecular Reaction Dynamics) 9, 17595 (2019).

20 C. He, A.M. Thomas, G.R. Galimova, A.M. Mebel, R.I. Kaiser, Gas-phase Formation of 1-Methylcyclo-propene and 3-Methylcyclopropene via the Reaction of the Methylidyne Radical (CH; $X^2\Pi$) with Propylene (CH_3CHCH_2; X^1A'). The Journal of Physical Chemistry A 123, 10543-10555 (2019).

21 C. He, A.M. Thomas, G.R. Galimova, A.M. Mebel, R.I. Kaiser, Gas-Phase Formation of Fulvenallene (C_7H_6) via the Jahn-Teller Distorted Tropyl (C_7H_7) Radical Intermediate under Single-Collision Conditions. The Journal of the American Chemical Society 142, 3205-3213 (2020).

22 L. Zhao, B. Xu, M. Ahmed, A.M. Mebel, R.I. Kaiser, A Unified Mechanism on the Formation of Acenes, Helicenes, and Phenacenes in the Gas Phase. Angewandte Chemie – International Edition 59, 4051-4056 (2020).

23 C. He, L. Zhao, S. Doddipatla, A.M. Thomas, A. Anatoliy, A. Nikolayev, G.R. Galimova, Valeriy N. Azyazov, A.M. Mebel, R.I. Kaiser, Gas-Phase Synthesis of 3-Vinylcyclopropene via the Crossed Beam Reaction of the Methylidyne Radical (CH; $X^2\Pi$) with 1,3-Butadiene ($CH_2CHCHCH_2$; X^1A_g). Chem. Phys. Chem 21, 1295-1309 (2020).

24 L. Zhao, R.I. Kaiser, W. Lu, M. Ahmed, M. M. Evseev, E.K. Bashkirov, Valeriy N. Azyazov, C. Tönshoff, F. Reicherter, H.F. Bettinger, A.M. Mebel, A Free Radical Prompted Barrierless Gas Phase Synthesis of Pentacene. Angewandte Chemie – International Edition 59, 11334-11338 (2020).

25 L. Zhao, R.I. Kaiser, W. Lu, M. Ahmed, A.D. Oleinikov, V.N. Azyazov, A.M. Mebel, A. Hasan Howladere, S. F. Wnuk, Gas Phase Formation of Phenalene via 10π Aromatic Resonantly Stabilized Free Radical Intermediates. Physical Chemistry Chemical Physics, 22, 15381-15388 (2020).

26 L. Zhao, R. I. Kaiser, W. Lu, O. Kostko, M. Ahmed, M. M. Evseev, E. K. Bashikirov, A. D. Oleinikov, V. N. Azyazov, A. M. Mebel, A. H. Howlader, S. F. Wnuk, Gas phase formation of cyclo-pentanaphthalene (benzindene) isomers via reactions of 5- and 6-indenyl radicals with vinylacetylene, Phys. Chem. Chem. Phys. 22, 22493-22500 (2020).

27 A. H. Howlader, K. Diaz, A. M. Mebel, R. I. Kaiser, S. F. Wnuk Iodoindenes: Synthesis and application to cross-coupling, Tetrahedron Lett., 61, 152427 (2020).

28 C. He, G. R. Galimova, Y. Luo, L. Zhao, A. K. Eckhardt, R. Sun, A. M. Mebel, R. I. Kaiser, A Chemical Dynamics Study on the Gas-phase Formation of Triplet and Singlet C_5H_2 Carbenes, Proc. Natl. Acad. Sci. U.S.A. 117, 30142-30150 (2020).

29 S. Doddipatla, G. R. Galimova, H. Wei, A. M. Thomas, C. He, Z. Yang, A. N. Morozov, C. N. Shingledecker, A. M. Mebel, R. I. Kaiser, Low-temperature Gas-phase Formation of Indene in the Interstellar Medium, Science Advances, 7, eabd4044 (2021).

30 C. He, A. A. Nikolayev, L. Zhao, A. M. Thomas, S. Doddipatla, G. R. Galimova, V. N. Azyazov, A. M. Mebel, R. I. Kaiser, Gas-Phase Formation of C_5H_6 Isomers via the Crossed Molecular Beam Reaction of the Methylidyne Radical (CH; $X^2\Pi$) with 1,2-Butadiene (CH_3CHCCH_2; X^1A'), J. Phys. Chem. A 125, 126-138 (2021).

31 L. Zhao, S. Doddipatla, R. I. Kaiser, W. Lu, O. Kostko, M. Ahmed, L. B. Tuli, A. N. Morozov, A. H. Howlader, S. F. Wnuk, A. M. Mebel, V. N. Azyazov, R. K. Mohamed, F. R. Fischer, Gas-phase synthesis of corannulene - a molecular building block of fullerenes, Phys. Chem. Chem. Phys., 23, 5740-5749 (2021).

32 R.I. Kaiser, N. Hansen, An Aromatic Universe – A Physical Chemistry Perspective, The Journal of Physical Chemistry A, Invited Perspective (in press 2021).

33 L. Zhao, W. Lu, M.A. Ahmed, M. V. Zagidullin, V.N. Azyazov, A.M. Mebel, R.I. Kaiser, Gas Phase Synthesis of Benzene via the Propargyl Radical Self Reaction. Science Advances (in press 2021).

THEORETICAL CHEMICAL KINETICS

Stephen J. Klippenstein
Chemical Sciences and Engineering Division
Argonne National Laboratory
Lemont, IL, 60439
sjk@anl.gov

Program Scope

The focus of this program is the development and application of theoretical methods for exploring gas phase chemical kinetics. The research involves a combination of *ab initio* electronic structure calculations, variational transition state theory (TST), classical trajectory simulations, and master equation (ME) calculations. Detailed applications, including careful comparisons with experiment as feasible, are used to (i) develop a deeper understanding of the applicability of various foundational principles of gas phase chemical kinetics, (ii) motivate improvements in theoretical chemical kinetics methodologies, and (iii) enhance our understanding of various aspects of combustion, atmospheric, and interstellar chemistry. The specific reactions studied are generally motivated by global modeling efforts and state-of-the-art experimental observations.

Recent Progress

Tunneling: In work led by Yuri Georgievskii, we explored various physical aspects of tunneling. In particular, we obtained a closed-form rate expression for the tunneling rate constant that is a direct analog of the rigid-rotor-harmonic-oscillator expression. This expression introduces a novel "entanglement factor" that modulates the reaction rate. Furthermore, we extended this expression, which is valid for non-separable systems at low temperatures, to properly account for the conservation of angular momentum. In contrast, previous calculations have considered only vibrational transverse modes and so effectively employ a decoupled rotational partition function for the orientational modes. We also suggest a simple theoretical model to describe the tunneling effects in the vicinity of the crossover temperature (the temperature where tunneling becomes the dominating mechanism). This model allows one to naturally classify, interpret, and predict experimental data and explore the relative contributions from different transverse modes. Among other things, it quantitatively explains in simple terms the so-called "quantum bobsled" effect, also known as the negative centrifugal effect, which is related to curvature of the reaction path. Taken together, the expressions obtained here allow one to predict the thermal and E-resolved rate constants over broad ranges of temperatures and energies.

Automated Kinetics: Our automated kinetics effort (github.com/Auto-Mech) was focused this past year on demonstration calculations for a dual fuel combination of *n*-dodecane and isooctane. The reasonably large size of these fuels, and the sheer number of species (~2000) and reactions (~2000) studied presented various challenges. To address these challenges we (i) developed a novel scheme for extending the master equation solution for temperatures beyond that at which a given species is kinetically stable, (ii) developed scaling relations that allow us to use rigid torsional scans in approximately mapping the hindered rotor partition functions, and (iii) implemented the connectivity based hierarchy scheme of Raghavachari as a means for obtaining high accuracy thermochemistry from relatively modest computational effort (i.e., via DFT

calculations for large species coupled with ANL0 calculations for a set of core species). These calculations demonstrate the feasibility of employing ab initio kinetics to map essentially a complete mechanism for a large complex fuel of practical relevance.

QOOH Dissociation Kinetics: In a ground-breaking experimental effort, Marsha Lester's group synthesized, isolated, identified, and studied the dissociation kinetics of a prototypical hydroperoxyalkyl radical via time-resolved IR activation coupled with LIF detection of the OH coproduct. In addition to providing valuable information for the key chain branching process in low temperature oxidation, the observed dissociation rates also provide an exquisite test of the validity of RRKM theory, which provides the foundation stone for much of gas phase kinetic theory. Notably, such tests are essentially non-existent for unimolecular reactions of radicals. Our first principles RRKM calculations, which implement high level ab initio methods and advanced state counting procedures, yield quantitative agreement with Lester's observed decay rates. Coupling with novel first principles energy transfer simulations of Ahren Jasper, allow us to convert the microcanonical rates into thermal rate predictions of importance to chemical modeling.

Oligomerization of Criegee Intermediates: In a large multi group collaboration led by Rebecca Caravan, we explored a possible role for oligomerization of Criegee intermediates in the formation of secondary organic aerosols. The work involved a combination of field observations of a sequence of species that correlates well with successive steps in the oligomerization, experimental measurements of rate constants for key reactions that are representative of the oligomerization steps, theoretical calculations of a similar set of key reactions, and global atmospheric modeling of the ramifications of such reactions. The theoretical analysis focused on studies of the reaction of the smallest Criegee intermediate, CH_2OO, with hydrogen peroxide, t-butylhydroperoxide, hydroperoxymethylformate (HPMF), and with the secondary ozonide formed as a product in the CH_2OO + HPMF reaction. The theoretical analysis indicates the presence of submerged barriers, with corresponding reasonably large rate constants, for each of these reactions. It also indicates that such barrierless reactions should persist for ever larger oligomers.

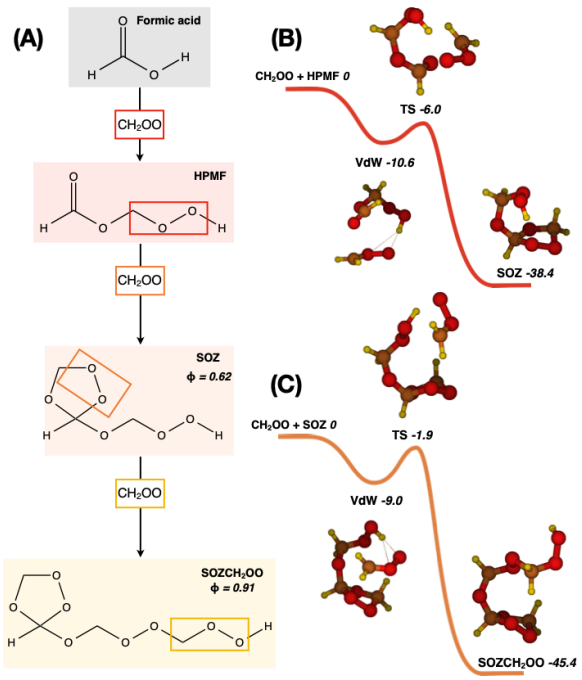

NH_3 Oxidation: Recent modeling studies of NH_3 oxidation, which are motivated by the prospective role of ammonia as a zero-carbon fuel, have indicated significant discrepancies between existing literature mechanisms. In collaboration with Glarborg, we performed high level theoretical kinetics analyses for the reaction of NH_2 with HO_2, which has previously been highlighted as an important reaction with high sensitivity and high uncertainty. The potential energy surface was explored with coupled cluster calculations including large basis sets and high-level corrections to yield high accuracy (~0.2 kcal/mol) estimates of the stationary point energies.

Variational transition state theory was used to predict the microcanonical rate constants, which were then incorporated in master equation treatments of the temperature and pressure dependent kinetics. For the radical-radical channels, the microcanonical rates were obtained from variable reaction coordinate transition state theory implementing directly evaluated multireference electronic energies. The analysis yields predictions for the total rate constant as well as the branching to the $NH_3 + O_2$, $H_2NO + OH$, and $HNO + H_2O$ channels. Rate constants are also reported for the $H_2NO + OH$ reaction as they arise naturally from the analysis. The rate constant and branching fraction determined for the $NH_2 + HO_2$ reaction deviate significantly from values used in most previous modeling studies. The fact that the main product channel is chain terminating, rather than propagating, has strong implications for modeling NH_3 ignition and oxidation, in particular at intermediate temperatures and elevated pressure.

Future Directions

We continue to work toward implementing automated high-level theoretical thermochemical kinetics as a means to improving our understanding of classic combustion mechanisms. Currently, we are interested in applying this methodology to the generation of a high-fidelity mechanism consisting solely of a priori theory determined rate parameters. One important outcome of such an analysis is an expected highlighting of various shortcomings in standard kinetic modeling procedures.

We are currently preparing a publication providing a well documented release version of our AutoMech suite of codes. In further AutoMech developmental work, we will focus on completing our implementation of advanced TST treatments, such as our variable reaction coordinate approach, and Monte Carlo sampling based partition function evaluations.

We plan to further collaborate with Marsha Lester's group in enumerating the kinetics of QOOH dissociations. We are also currently interested in further mapping out the kinetics of key reactions of relevance to NH_3 oxidation.

DOE Supported Publications, 2019-Present

1. **Automated Computational Thermochemistry for Butane Oxidation: A Prelude to Predictive Automated Combustion Kinetics,** M. Keceli, S. Elliott, Y.-P. Li, M. S. Johnson, C. Cavallotti, Y. Georgievskii, W. H. Green, M. Pelucchi, J. M. Wozniak, A. W. Jasper, S. J. Klippenstein**,** *Proc. Combust. Inst*. **37**, 363-371 (2019).
2. **Small Ester Combustion Chemistry: Computational Kinetics and Experimental Study of Methyl Acetate and Ethyl Acetate,** A. Ahmed, W. J. Pitz, C. Cavallotti, M. Mehl, N. Lokachari, E. J. K. Nilsson, J.-Y. Wang, A. A. Konnov, S. W. Wagnon, B. Chen, Z. Wang, H. J. Curran, S. J. Klippenstein, W. J. Roberts, S. M. Sarathy, *Proc. Combust. Inst.* **37**, 419-428 (2019).
3. **Simulating the Density of Organic Species in the Atmosphere of Titan with a Coupled Ion-Neutral Photochemical Model,** V. Vuitton, R. V. Yelle, S. J. Klippenstein, P. Lavvas, S. M. Horst, *Icarus* **324**, 120-197 (2019).
4. **EStokTP: Electronic Structure to Temperature- and Pressure-Dependent Rate Constants – A code for Automatically Predicting the Thermal Kinetics of Reactions,** C.

Cavallotti, M. Pelucchi, Y. Georgievskii, S. J. Klippenstein, *J. Chem. Theory Comp*. **15**, 1122-1145 (2019).

5. **Ab Initio Kinetics for Pyrolysis and Combustion Systems,** S. J. Klippenstein, C. Cavallotti; in: Mathematical Modeling of Complex Reaction Systems: Pyrolysis and Combustion, T. Faravelli, F. Manenti, and E. M. Ranzi, Eds. Computer Aided Chemical Engineering Series, Elsevier: New York, (2019).
6. **Propane Clusters in Titan's Lower Atmosphere: Insights from a Combined Theory/Laboratory Study,** J. Bourgalais, O. Durif, S. D. Le Picard, P. Lavvas, F. Calvo, S. J. Klippenstein, L. Biennier, *Mon. Not. Roy. Ast. Soc*. **488**, 676-684 (2019).
7. **Synthesis, Electronic Spectroscopy, and Photochemistry of Methacrolein Oxide: A Four-Carbon Unsaturated Criegee Intermediate from Isoprene Ozonolysis,** M. F. Vansco, B. Marchetti, N. Tronsiriwat, T. Bhagde, G. Wang, P. J. Walsh, S. J. Klippenstein, M. I. Lester, *J. Am. Chem. Soc.* **141,** 15058-15069 (2019).
8. **Photodissociation Transition States Characterized by Chirped Pulse Millimeter Wave Spectroscopy,** K. Prozument, J. H. Baraban, P. B. Changala, G. B. Park, R. G. Shaver, J. S. Muenter, S. J. Klippenstein, V. Y. Chernyak, R. W. Field, *Proc. Nat. Acad. Sci*. **117**, 146-151 (2020).
9. **Reaction Profiles and Kinetics for Radical-Radical Hydrogen Abstraction via Multireference Coupled Cluster Theory,** C.-H. Wu, D. B. Magers, L. B. Harding, S. J. Klippenstein, W. D. Allen, *J. Chem. Theory Comp.* **16***,* 1511-1525 (2020).
10. **Experimental and Theoretical Studies of the Doubly-Substituted Methyl-Ethyl Criegee Intermediate: Infrared Action Spectroscopy and Unimolecuar Decay to OH Radical Products,** V. P. Barber, A. S. Hansen, S. J. Klippenstein, M. I. Lester**,** *J. Chem. Phys.* **152***, 094301* (2020).
11. **Direct Kinetic Measurements and Theoretical Predictions of an Isoprene-Derived Criegee Intermediate,** R. L. Caravan, M. F. Vansco, K. Au, M. A. H. Khan, Y.-L. Li, F. A. F. Winiberg, K. Zuraski, Y.-H. Lin, W. Chao, N. Trongsiriwat, P. J. Walsh, D. L. Osborn, C. J. Percival, J. Jr-M. Lin, D. E. Shallcross, L. Sheps, S. J. Klippenstein, C. A. Taatjes, M. I. Lester**,** *Proc. Nat. Acad. Sci.* **117**, 9733-9740 (2020).
12. **Formic Acid Catalyzed Isomerization and Adduct Formation of an Isoprene-Derived Criegee Intermediate: Experiment and Theory,** M. F. Vansco, R. L. Caravan, S. Pandit, K. Zuraski, F. A. F. Winiberg, K. Au, T. Bhagde, N. Trongsiriwat, P. J. Walsh, D. L. Osborn, C. J. Percival, S. J. Klippenstein, C. A. Taatjes, M. I. Lester**,** *Phys. Chem. Chem. Phys*. **22***,* 26796-26805 (2020).
13. **Automated Theoretical Chemical Kinetics: Exploring the Initial Stages of Pyrolysis,** S. N. Elliott, K. B. Moore, A. V. Copan, M. Keceli, C. Cavallotti, Y. Georgievskii, H. F. Schaefer III, S. J. Klippenstein**,** *Proc. Combust. Inst.* **38**, 375-384 (2021).

ARGONNE-SANDIA CONSORTIUM ON HIGH-PRESSURE COMBUSTION CHEMISTRY

Ahren W. Jasper, Stephen J. Klippenstein (PI), Raghu Sivaramakrishnan, Robert S. Tranter
*Chemical Sciences and Engineering Division, Argonne National Laboratory, Lemont, IL, 60439

Leonid Sheps, Nils Hansen, Craig A. Taatjes (PI)
#Combustion Research Facility, MS 9055, Sandia National Laboratories Livermore, CA 94551-0969
sjk@anl.gov; cataatj@sandia.gov

Program Scope

The goal of this project is to explore the fundamental effects of pressure on chemical kinetics and to employ that knowledge in the development of accurate models for combustion chemistry at the high pressures of current and future combustion devices. We design and implement novel experiments, theory, and modeling to probe high-pressure combustion kinetics from elementary reactions, to submechanisms, and ultimately to flames. We continue to invest in the development of sensitive time-resolved experimental probes of reaction intermediates, which enable direct pressure-dependent studies of chemical systems of interest to high-pressure combustion chemistry and other DOE energy missions. We are applying novel master equation and stochastic simulation methods to accurately predict the kinetics of key processes. The theoretical predictions and experimental observations are employed in non-empirical modeling that provides high fidelity chemical models for combustion processes, and, more importantly, identifies departures from standard chemical kinetics assumptions. Recently, we have been pursuing detailed understandings of non-equilibrium effects and of radical oxidation chemistry. We are currently integrating modeling, experiment, and theory (MET) through feedback loops at all levels of chemical complexity for small alkanes, alcohols, and ethers (including cyclic variants) as key prototype fuels. The consortium expands and enhances collaborations between Argonne's Chemical Dynamics in the Gas Phase Group and the Combustion Chemistry Group in Sandia's Combustion Research Facility.

Recent Progress

***HRRST*:** The high repetition rate shock tube (HRRST) has enabled studies of a variety of chemical systems at pressures up to 15 bar and temperatures from 700 to 2400 K. Three versions of the HRRST based on the original design have recently been constructed in the US, France, and Japan, with the first two through extensive collaboration with the HPCC. The various HRRSTs have now been applied to studies of gas-phase chemical kinetics, dynamic physical properties in shock tubes, laser absorption, and ignition delays. These studied relied on the high repetition rate (up to 2 Hz) and the very good reproducibility of reaction conditions, permitting the efficient collection of data over long periods. Additionally, the reproducibility enables signal averaging and observations at multiple experimental points (e.g. different ionization energies, physical locations in the shock tube) in essentially the same reaction environment.

In collaboration with Comandini and Chaumeix (CNRS-Orleans), the first shock tube/I^{2}PEPICO experiments were performed at the SOLEIL synchrotron. These experiments studied the pyrolysis of ethanol at reaction conditions under non-sooting and sooting conditions to target early stages of

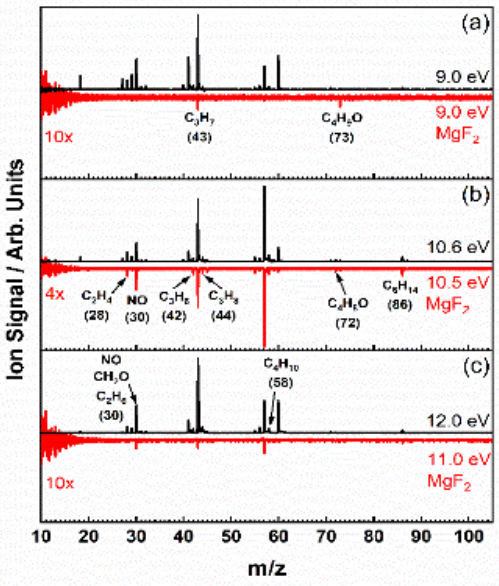

Figure 1: Post shock mass spectra at selected photon energies for 0.25% n-butyl nitrite/argon. Upward pointing black lines no MgF_2 filter, T_5=670 K, P_5=6.4 bar. Downward pointing red lines with MgF_2 filter T_5=682 K, P_5=6.3 bar.

pyrolysis and the transition to forming PAH. The mass and photoelectron spectra obtained allowed positive identification of a number of species. This was the first experiment conducted with the SOLEIL I^{2}PEPICO apparatus that operated in a pulsed fashion with species concentrations changing rapidly during the pulse. As well as 'static' spectra, time resolved data was also recovered yielding the time histories of key species. Further experiments are planned for Sept. 2021.

During the last year, interpretation of previously obtained data has been ongoing. Areas of particular focus have been alkyl radical reactions, aromatic pyrolysis, and the chemistry of silicon nanoparticle precursors. These projects leverage the MET paradigm that is core to the HPCC methodology and complement efforts in the Chemical Dynamics in the Gas Phase Program and the Fundamental Chemical Kinetics of Siloxane and Silicon Compounds Program. For example, for *n*-propyl and *i*-propyl radicals we applied a similar analysis to that discussed earlier for butyl radicals. In particular, from photoionization mass spectra obtained at the ALS, the radical and stable species involved in decomposition, self-reaction and addition reactions of the two radicals were mapped over 700 – 900 K and pressures of ~6 bar. Example mass spectra are shown in Fig. 1. As well as unambiguously identifying products and elucidating reaction paths, branching ratios for key reactions were obtained. Notably, the HPCCs combined MET expertise facilitated the investigation of non-thermal reactions arising from the addition of H and CH_3 to propyl.

Theory for Diethyl Ether Oxidation: As part of the MET effort for diethyl ether (DEE) oxidation, ab initio transition state theory based master equation calculations were implemented for the initial abstractions, the first two O_2 additions, and the dissociation of the keto-hydroperoxides. One novel aspect of this analysis was an indication of the importance of diastereomeric effects on the reaction kinetics. These master equations are now playing a key role in our exploration of non-thermal effects for this system.

High-Pressure Autoignition Chemistry: We completed our first experimental study of DEE oxidation chemistry at pressures 10 – 7500 Torr and temperatures 400 – 650 K, using our recently-built high-pressure laser photolysis reactor (HPLPR) and photoionization mass spectrometry (PIMS) apparatus. A major part of this work was to identify key autoignition intermediates ROO, OOQOOH, and ketohydroperoxide (KHP). All three molecules underwent complete dissociative ionization, significantly complicating the analysis of the observed mass spectra. However, with the aid of quantum chemical calculations of photoionization dynamics, we assigned the main daughter ion channels, determined the absolute photoionization cross-sections (PIXS), and quantified the time-dependent concentrations of ROO, OOQOOH, and KHP directly from the complex oxidation reaction of DEE. The experimental dataset provides the basis for an ongoing modeling effort that implements the theory results as described above.

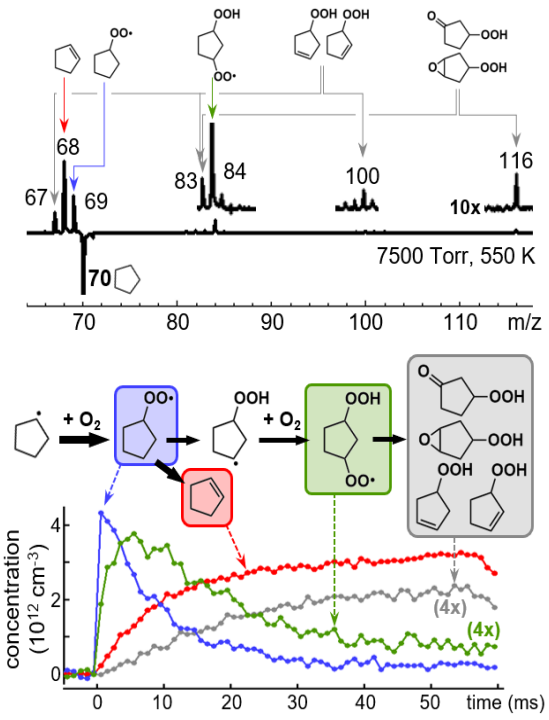

Figure 2: Typical results of high-pressure PIMS probing of Cl-initiated cyclopentane oxidation. Top: transient mass spectrum with ion peak assignments; Bottom: quantified chemical species concentrations

We extended our HPLPR-PIMS approach to probing of the oxidation chemistry of cyclopentane, as shown in Fig. 2, as part of our ongoing exploration of the molecular structure effects on reactivity in the low-*T* combustion regime (*J. Phys. Chem. A*, in press). We reported the PIXS of ROO and OOQOOH and quantified their time-dependent concentrations at *P*

up to 7500 Torr and T up to 700 K. We supported the experimental results with PES calculations in collaboration with J. Zador (under core BES funding). Interestingly, we found that in addition to KHP + OH, OOQOOH dissociates to HO_2 + unsaturated hydroperoxide. This result differs from the linear ether DEE but is in line with our findings for the cyclic ether THF (*J. Phys. Chem. A*, 120 (2016), 6582), suggesting that HO_2 elimination from OOQOOH is a general feature of cyclic molecules. Together with our study of DEE, the cyclopentane results demonstrate the broad applicability of our experimental approach to directly probe and quantify reactive intermediates, which was not possible previously.

Acetone Pyrolysis: The application of the MET paradigm to the pyrolysis of acetone revealed an unexpected importance for substitution reactions in this well studied system. The theory component of this study was performed with the AutoMech code (github.com/Auto-Mech) as part of the HPCC project, while the experimental and modeling efforts were part of Argonne's core program in GPCP. The ability to efficiently generate large sets of rate constants facilitated the exploration of the newly proposed substitution reactions.

Review of Theoretical Kinetics Methods: We reviewed in detail theoretical methods for accurately describing the kinetics of reactions relevant to gas phase combustion chemistry. This review deals with the theoretical precepts relevant to multiple-well master equations, non-thermal effects (prompt dissociations, chemically termolecular reactions), non-adiabatic reactions, collisional energy transfer, transport properties and also with methods to handle the complexity induced by the hundreds of species and coupled reactions necessary for a complete description of chemical reactivity in combustion.

Collision Parameters for Kinetics and Modeling: Collision parameters describing pressure-dependent kinetics and transport (the Lennard–Jones parameters σ, ε and the collision efficiency range parameter $\alpha = \langle\Delta E_d\rangle$, etc.) are typically poorly known. By analyzing a large data set of trajectory-based collision parameters for more than 300 alkanes, alcohols, and hydroperoxides, we showed that we can reliably estimate σ and ε based on the number of heavy atoms and α based on an effective number of heavy atoms N_{eff} related to internal rotor types. As part of our comprehensive theory-based modeling efforts, this approach was generalized to include radicals, ethers, esters, expoxides, and peroxides. A new intermolecular surface fitting strategy was developed that enabled high-accuracy trajectory-based collision efficiency calculations for several small-molecule reactions. The predicted collision efficiencies are in quantitative agreement with literature experimental values from Glen MacDonald (e.g., NH_3(+M) at 300 K, CH_4:N_2 = 3.15 vs 2.60 ± 1.14) and Joe Michael (e.g., HO_2(+M), H_2O:Ar = 24 vs 23 ± 2 at 300 K).

Future Work

HRRST*:* The chemistry of aromatic species continues to be an area of considerable interest. Building on our studies of styrene we will investigate the high temperature and high pressure chemistry of alkylbenzenes which form a significant fraction of fuels. Styrene is an important intermediate in pyrolysis of alkylbenzenes and our recent mechanism for styrene decomposition will form a core part of an alkylbenzene mechanism. Initial, studies have been conducted on ethylbenzene, which leveraged the high reproducibility of the HRRST to conduct shock tube/TOF-MS experiments with low energy electron impact (EI) ionization in the laboratory. This was a new style of experiment inspired in part by the lack of access to the ALS in 2020. These experiments would not be possible with a conventional shock tube as the S/N is far too small for a single shot experiment. However, signal averaging techniques allowed the EI experiments to be conducted at low reagent concentrations, while suppressing signal due to the bath gas which often dominates shock tube/TOF-MS work. We will also begin a comprehensive study of benzyne isomers as part of an effort to explore the isomerization, addition and self-reactions of benzyne isomers that utilizes the complete suite of experimental tools in the HPCC.

Experimental Development: We recently developed (under LDRD funding) a high-P laminar flow reactor (HPFR) that uses a new gas injector, capable of mixing separate gas flows in only a few ms, even at P of 10s of bar. This rapid mixing enables well-defined reactor residence times, from milliseconds to seconds. We are now coupling the HPFR to high-P PIMS detection. Reactions are initiated thermally in this setup,

making it a versatile complement to our laser photolysis-PIMS studies by allowing a greater selection of reactive precursors and wider range of *T*. We have also interfaced the HPFR with a Fluorescence Assay by Gas Expansion (FAGE) detector, built under LDRD funding, and are now calibrating the HPFR-FAGE to provide quantitative detection of OH and HO_2 radicals. OH and HO_2 are difficult to detect by PIMS, and thus the HPFR-FAGE is an important new addition to our suite of experimental probe methods. Lastly, we are incorporating the new rapid mixer into the existing laser photolysis reactor so that the fuel, O_2, photolytic precursor, and buffer gas are combined into a reactive mixture just before being photolyzed, rather than ahead of time. This will delay spontaneous thermal decomposition of the mixture and allow operation at higher temperatures than before.

Thermal and Prompt Dissociations of Weakly Bound Radicals: We are progressing towards a comprehensive model of the reactivity of $\cdot CH_2OC(O)H$ (R1) and $CH_3OC(O)\cdot$ (R2) radicals, which are prototypical weakly-bound oxygenated species that easily decompose even at low temperatures. We have obtained a high-quality experimental dataset at $P = 10$ Torr and $T = 400 – 700$ K, in which Cl atoms, formed via photolysis of Cl_2, were used to produce R1 and R2 by H abstraction from methyl formate. Preliminary modeling of our experiments showed sensitivity not only to the primary decomposition of R1 → CH_2O + HCO and R2 → $CH_3 + CO_2$ but also to secondary reactions of these radicals with Cl_2 and other species, as well as to initial branching into R1 and R2 from Cl + methyl formate. To fully describe this complex system, we are now incorporating quantum-chemical calculations of key reaction kinetics into our chemical model to reliably constrain the decomposition rates of R1 and R2 and the relevant secondary chemistry. This work includes a high-level analysis of the Cl abstraction reaction to determine the initial concentrations of R1 and R2.

Prompt Dissociations of Resonance Stabilized Free Radicals: Prompt dissociations are ubiquitous in free radical dissociations, and we have hypothesized that its relevance to global combustion observables such as flame speeds depends on satisfying specific criteria. Two criteria that motivate the present study are that the free radicals must play a central role in the oxidation mechanism and that their thermal dissociation rate coefficients should be small enough. Resonance stabilized radicals (RSR) have bond strengths of ~50 kcal/mol (or larger) and consequently are known to dissociate slowly and persist even in high temperature environments. Therefore, we have initiated studies to calculate prompt dissociation probabilities for some simple allylic (allyl, methyl allyl, and dimethyl allyl) radicals. Flame simulations will be performed to quantify the relevance of including prompt dissociations of these RSR's.

Absolute Photoionization Spectra of Combustion Radicals: We continue to pursue spectroscopic studies of reactive intermediates with the goal of directly probing these species in complex reactions. We have recently measured the absolute PI spectra of 1- and 2-propyl, 1-, 2-, sec-, and *tert*-butyl radicals, formed by the photolysis of corresponding iodoalkanes. In addition, we have measured the absolute PI spectra of ethyl peroxy, 1- and 2-propyl peroxy. These results are being prepared for publication. We anticipate that knowledge of isomer-specific cross-sections will be critical to quantitative probing of radical self-reactions, in which *T*- and *P*-dependent competition between disproportionation and stabilization channels is predicted.

Low Temperature Autoignition Chemistry: Building on recent success in applying high-pressure PIMS probing, we will continue our survey of the autoignition reactions of representative hydrocarbon and oxygenated fuels, in close collaboration with theory and modeling efforts. We have recently detected OOQOOH and KHP in the oxidation of propane (the smallest typical alkane fuel), for which HPCC has developed theory-based reaction mechanisms. We are also nearing completion on the autoignition study of dimethyl ether (the smallest typical ether) and neo-pentane (2,2-dimethylpropane). Neo-pentane is a model compound with all primary C-H bonds; its molecular symmetry results in a simplified oxidation reaction sequence, proceeding through a single QOOH isomer. This simplified chemistry will enable reliable experimental quantification of 1st and 2nd O_2 addition products and allow detailed comparisons with chemical model predictions.

Diethyl Ether Oxidation: We are currently in the process of applying the full MET paradigm to the low temperature oxidation of diethyl ether. The focus of this effort involves comparisons with the novel HPLPR-PIMS time-resolved species profiles for key intermediates. Interestingly, preliminary results suggest that acetic acid acts as a key marker for non-thermal effects. This realization, which was missed in prior modeling studies, naturally arises from the current state-of-the-art implementation of all aspects of the MET paradigm.

Chemically Termolecular Reactions and Their Impact in Flames and DNS Simulations: Nonthermal reactivity relevant to two important association reactions in hydrogen oxidation ($H + O_2 + M$, $H + OH + M$) were revisited. Special attention was paid to understanding the role of branching induced as a result of this nonthermal reactivity, which mainly consists of two aspects. The first involves the competition among back-dissociation, collisional stabilization, and reactive collisions of the energized complexes (HO_2* and H_2O*). The potential energy surface, lifetimes of collision complexes involved, and the range of internal energies all have a role to play in determining this branching. The second aspect involves potential channel switching between the various product channels in the HO_2* + H reaction. Flame simulations were performed to quantify the impact of the uncertainties in product branching in this important reaction. These discussed examples serve to illustrate the intriguing role of nonthermal chemistry in understanding the simple hydrogen-oxidation combustion mechanism.

In collaboration with J. H. Chen (CRF-Sandia) and T. F. Lu (U. Conn.) we have initiated studies to identify and quantify the effects of including chemically termolecular nonthermal reactions on the evolution of an initial deflagration front to a developing detonation in H_2/CH_4-air mixtures under boosted internal combustion (IC) engine conditions. In preliminary studies, direct numerical simulations (DNS), with and without non-thermal reactivity, are performed for a constant volume reactor containing stoichiometric H_2/CH_4-air mixture. It is found that inclusion of termolecular chemistry facilitated by radical-radical recombinations results in a delayed onset of end-gas auto-ignition. Concurrently, the developing detonation intensity is also observed to be significantly lower. Chemical explosive mode analysis (CEMA) has been performed to identify the dominant species/reactions responsible for the observed variation in the results.

Stochastic Dynamics: We propose to extend our stochastic sampling approach for describing elementary chemical events in complex reactive mixtures. These computations are enabled by Argonne's high-performance computing resources and combine stochastic sampling of binary and higher-order collision events with high-level dynamics and kinetics descriptions of these events. Sampled events include both reactive and nonreactive (thermalizing) collisions, and global properties emerge via their competition. Preliminary studies of nonthermal systems resolve ambiguities in analytic collision models that find more practical use in master equations. The stochastic approach will be used to quantify and improve our 2DME collision kernel, to characterize the influence of collisions on threshold reactivity of the two-channel CH_2O (+M), and to study the reactivity of transient van der Waals complexes at high pressures. The stochastic approach provides a means of modeling these complex many-body chemistries *a priori*.

Publications acknowledging support from this program, 2019-Present

1. **Direct Measurements of Channel Specific Rate Constants in OH + C_3H_8 Illuminates Prompt Dissociations of Propyl Radicals,** R. Sivaramakrishnan, C. F. Goldsmith, S. L. Peukert, J. V. Michael, *Proc. Combust. Inst.* 37**,** 231-238 (2019).
2. **High-Pressure Oxidation of Propane**, H. Hashemi, J. M. Christensen, L. B. Harding, S. J. Klippenstein, P. Glarborg, *Proc. Combust. Inst*. 37, 461-468 (2019).
3. **Influence of Ether Functional Group on Ketohydroperoxide Formation in Cyclic Hydrocarbons: Tetrahydropyran and Cyclohexane,** J. C. Davis, A. L. Koritzke, R. L. Caravan, I. O. Antonov, M. G. Christianson, A. C. Doner, D. L. Osborn, L. Sheps, C. A. Taatjes, B. Rotavera, *J. Phys. Chem. A* 123, 3634-3646 (2019).
4. **Kinetics of 1-Butyl and 2-Butyl Radical Reactions with Molecular Oxygen: Experiment and Theory**, A. J. Eskola, T. T. Pekkanen, S. P. Joshi, R. S. Timonen, S. J. Klippenstein, *Proc. Combust. Inst*. 37, 291-298 (2019).

5. **Nonthermal Rate Constants for CH_4* + X → CH_3 + HX, X = H, O, OH, and O_2**. A. W. Jasper, R. Sivaramakrishnan, S. J. Klippenstein, *J. Chem. Phys.* 150, 114112 (2019).
6. **Reference Natural Gas Flames at Nominally Autoignitive Engine-Relevant Conditions**, A. Krisman, C. Mounaim-Rouselle, R. Sivaramakrishnan, J. A. Miller, J. H. Chen, *Proc. Combust. Inst.* 37, 1631-1638 (2019).
7. **Sensitive Mass Spectrometer for Time-Resolved Gas-Phase Studies at High Pressures**, L. Sheps, I. Antonov, K. Au, *J. Phys. Chem. A* 123, 10804-10814 (2019).
8. **Comment on "Influence of Multiple Conformations and Paths on Rate Constants and Product Branching Ratios. Thermal Decomposition of 1-Propanol Radicals"**, J. Zador, J. A. Miller, *J. Phys. Chem. A*, 123, 1129-1130 (2019).
9. **An Experimental and Theoretical Study of the High Temperature Reactions of Four Butyl Radical Isomers**, J. B. Randazzo, A. W. Jasper, R. Sivaramakrishnan, T. Sikes, P. T. Lynch, R. S. Tranter, *Phys. Chem. Chem. Phys.* **22**, 18304-18319 (2020).
10. **Direct Time-Resolved Detection and Quantification of Key Reactive Intermediates in Diethyl Ether Oxidation at T = 450 – 600 K**, M. Demireva, K. Au, L. Sheps, *Phys. Chem. Chem. Phys.* 22, 24649-24661 (2020).
11. **Isomer-Dependent Reaction Mechanisms of Cyclic Ether Intermediates: Cis-2,3-Dimethyloxirane and Trans-2,3-Dimethyloxirane.** A. C. Doner, M. M. Davis, A. L. Koritzke, M. G. Christianson, J. M. Turney, H. F. Schaefer III, L. Sheps, D. L. Osborn, C. A. Taatjes, B. Rotavera, *Int. J. Chem. Kinet.* (2020).
12. **Low Temperature Oxidation of Diethyl Ether: Reactions of Hot Radicals Across Coupled Potential Energy Surfaces**, A. D. Danilack, S. J. Klippenstein, Y. Georgievskii, C. F. Goldsmith, *Proc. Combust. Inst.* 38, 671-679 (2020).
13. **Solenoid Actuated Driver Valve for High Repetition Rate Shock Tubes**, R. S. Tranter, T. Sikes, *Rev. Sci. Instrum.* 91, 056101 (2020).
14. **Temporally and Spatially Resolved X-Ray Densitometry in a Shock Tube**, R. A. Shaik, A. L. Kastengren, R. S. Tranter, P. T. Lynch, *Combust. Flame* 224, 136-149 (2020).
15. **Termolecular Chemistry Facilitated by Radical-Radical Recombinations and Its Impact on Flame Speed Predictions**, Y. Tao, A. W. Jasper, Y. Georgievskii, S. J. Klippenstein, R. Sivaramakrishnan, *Proc. Combust. Inst.* 38, 515-522 (2020).
16. **"Third-Body" Collision Parameters for Hydrocarbons, Alcohols, and Peroxides and an Effective Internal Rotor Approach for Estimating Them**, A. W. Jasper, *Int. J. Chem. Kinet.* **52**, 387-402 (2020).
17. **Combustion Chemistry in the Twenty-First Century: Developing Theory-Informed Chemical Kinetics Models**, J. A. Miller, R. Sivaramakrishnan, Y. Tao, C. F. Goldsmith, M. P. Burke, A. W. Jasper, N. Hansen, N. J. Labbe, P. Glarborg, J. Zádor, *Prog. Energy Combust. Sci.* **83**, 100886 (2021).
18. **Reaction Mechanisms of a Cyclic Ether Intermediate: Ethyloxirane**. M. G. Christianson, A. C. Doner, M. M. Davis, A. L. Koritzke, J. M. Turney, H. F. Schaefer III, L. Sheps, D. L. Osborn, C. A. Taatjes, B. Rotavera, *Int. J. Chem. Kinet.* 53, 127-145 (2021).
19. **Reactions of Propyl Radicals: A Shock Tube–VUV Photoionization Mass Spectrometry Study** C. K. Banyon, T. Sikes, R. S. Tranter, *Combust. Flame*, 224, 14-23 (2021).
20. **Pyrolysis of Ethanol Studied in a New High-Repetition-Rate Shock Tube Coupled to Synchrotron-Based Double Imaging Photoelectron/Photoion Coincidence Spectroscopy**, S. Nagaraju, R. S. Tranter, F. E. Cano Ardila, S. Abida, P. T. Lynch, G. A. Garcia, J. F. Gil, L. Nahon, N. Chaumeix, A. Comandini, *Combust. Flame* 226, 53-68 (2021).
21. **Substitution Reactions in the Pyrolysis of Acetone Revealed through a Modeling, Experiment, Theory Paradigm,** D. P. Zaleski, R. Sivaramakrishnan, H. R. Weller, N. A. Seifert, D. H. Bross, B. Ruscic, K. B. Moore III, S. N. Elliott, A. V. Copan, L. B. Harding, S. J. Klippenstein, R. W. Field, K. Prozument, *J. Am. Chem. Soc.* 143, 3124-3142 (2021).

DEVELOPING NEW MECHANISTIC INSIGHTS INTO OXIDATIVE COUPLING OF METHANE THROUGH COMBINED GAS-PHASE AND SURFACE-SENSITIVE SPECTROSCOPIES WITH SITE-ISOLATED CATALYSTS

Coleman Kronawitter and Ambarish Kulkarni

Department of Chemical Engineering, University of California, Davis

One Shields Ave, Davis, CA 95616

ckrona@ucdavis.edu, arkulkarni@ucdavis.edu

PROGRAM SCOPE

In heterogeneous catalytic systems for chemical synthesis and energy conversion, the solid surface plays an essential role in controlling reaction kinetics, and as a result, the vast majority of mechanistic investigation in this field is dedicated to the characterization of surface events. However, it is known that for many reaction classes and system conditions, gas phase events critically influence reaction outcomes, as well as dictate the nature of events occurring on surfaces through gas-surface species exchange.

A core objective of this project is to develop and implement an integrated experiment-theory approach to provide new insights into the interconnected roles of the surface and the near-surface gas phase in heterogeneous catalytic oxidative coupling reactions. This work is enabled by use of:

(1) New research technologies, originally developed for the field of combustion science, which through recent adaptation now facilitate interrogation of the local, near-surface gas phase above catalyst surfaces in *operando* conditions.

(2) Site-isolated supported metal catalysts (often atomically dispersed), comprehensively characterized to define active sites and minimize site heterogeneity over length scales of experimental interrogation.

(3) DFT-derived microkinetic models to interpret reaction and materials characterization results from (1) and (2), deriving relationships between specific active site structures and local reaction outcomes.

Efforts aim to develop a deeper understanding of the efficient oxidative coupling of methane (OCM), a high-temperature reaction known to rely heavily on the gas-phase coupling of radicals for ethylene production. It is also known, however, that during this reaction a dynamic exchange of species between the gas phase and surface occurs, resulting in both homogeneous and surface-mediated oxidations and dehydrogenations that influence conversion-selectivity optimization.

This project strives to bring clarity to the relationship between active site structures on surfaces and the composition of species in the near-surface gas phase during OCM. Catalysts with low levels of site heterogeneity are critical to connect specific sites with product/intermediate distributions. For this reason, we develop new atomically-dispersed supported metal catalysts, which are comprehensively characterized through spectroscopy, microscopy, and computational modeling. Preliminary work toward this goal involves understanding the lower-temperature oxidative coupling of methanol-derived oxygenates, which facilitates experimental development as well as computational work toward DFT-derived microkinetic modeling of oxidative coupling events in complex C-H-O-containing systems.

RECENT PROGRESS

Oxidative conversion of methanol toward understanding gas-surface coupling reactions

Operando universal detection of near-surface species

Through collaboration with Sandia National Laboratories' Combustion Research Facility (SNL-CRF), this project utilizes near-surface MBMS as a primary tool for interrogation of gas phase composition above working catalysts.

To date, we have measured the composition of the near-surface gas phase during methanol oxidation for multiple catalysts with the goal of developing structure-function relationships for straightforward metal and

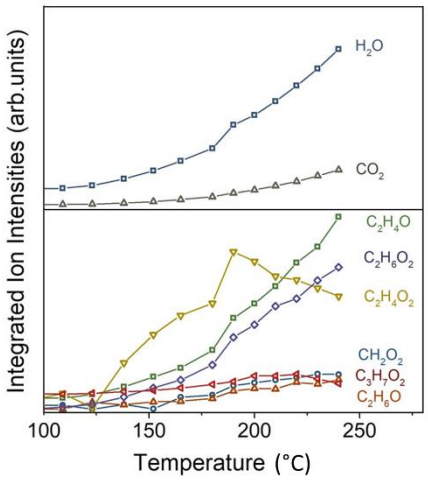

Figure 1. Representative curves showing temperature dependence of methanol oxidation products detected 500 μm above a catalyst (Pd) surface.

metal alloy systems, which provided a valuable materials platform to examine how MBMS can be used to characterize reactions. Specifically, we have measured the near-surface gas phase composition as a function of temperature during methanol oxidation for Pd, Au, AuPd, Au_2Pd, and $AuPd_2$ catalysts. The Au_xPd_y alloy system was used in the initial stages of our work because it allows for continuous composition tuning with associated varied adsorbate binding strengths, and because it has been previously investigated for methanol oxidation through conventional catalysis studies, providing valuable benchmarks. Figure 1 shows results from a typical MBMS temperature scan.

For Pd, we have expanded this work to include local product analysis with eight different feed ratios and as a function of distance from the catalyst surface. Figure 1 shows the methanol:O_2 feed ratio dependence of product composition 500 μm above a Pd surface. Similar data was recorded for the Au_xPd_y alloy system.

One important outcome of these results that has guided our work in understanding C-H-O coupling reactions involves the species $C_2H_5O_2^+$ in Figures 1 and 2. This species (corresponding to m/z 61) is the primary signal obtained (a cracking fragment) and a clear fingerprint for methoxymethanol (CH_3OCH_2OH). This molecule is thermodynamically unstable and very reactive, and it eludes detection through traditional product measurement tools (such as gas chromatography) – only a few instances of its detection are reported in the heterogeneous catalysis literature. However, methoxymethanol has been proposed to be a critically important intermediate species in the conversion pathway between adsorbed formaldehyde and methoxy and value-added products such as methyl formate and dimethoxymethane ($C_2H_4O_2$ and $C_3H_7O_2$, both also present in Figures 1 and 2). We also record MBMS at fixed temperatures as a function of distance from the catalyst surface, which has proven to be useful to understand the steady-state balance of generation (local products) and consumption (local reactants) of species at surfaces (not shown). We are in the process of completing two studies that analyze the role of methoxymethanol, detected with unprecedented sensitivity in a range of conditions (especially temperature and feed composition), in dictating the branching ratios for methyl formate and dimethoxymethane production.

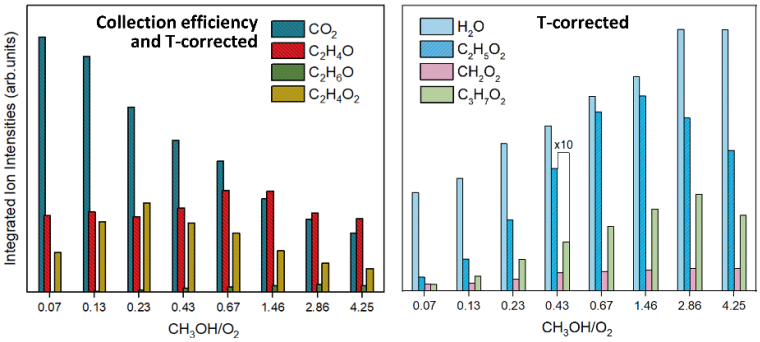

Figure 2. Near-surface (500 μm above surface) MBMS results showing the methanol/O_2 feed ratio dependence of product distributions from oxidative methanol conversion over Pd catalysts at 160 ºC and 800 mbar (90% N_2).

<u>Development of a DFT-derived microkinetic model for reactions with combined surface-mediated and gas phase steps</u>

We have made progress in developing a DFT-derived microkinetic model that works in concert with our universal detection of near-surface gas-phase species as well as detection of stable surface-bound species through spectroscopy.

Building on prior methanol partial oxidation models that predict *CH_3, *OCH_3, *CO, *H, and H_2CO* as the dominant surface species (here, * refers to surface-bound species), we have used we have used DFT

calculations (RPBE functional, D3(BJ) van der Waals corrections, Vienna Ab-initio Simulation Package) to determine the mechanism of formation of various C_2 products over Ag(111) (chosen for its relevance to catalysis in our first published work with SNL, *ACS Catalysis*, 2021, 11, 155−168). Figure 3 shows the transition states for: (1) a coupling reaction of formaldehyde and methoxy to form a hemiacetal intermediate (E_a = 0.29 eV), which is subsequently (2) dehydrogenated to from methyl formate.

As expected, our calculations show that the dehydrogenation barriers are lower for the *O-assisted (E_a = 0.34 eV) and *OH-assisted (E_a = 0.65 eV) pathways, compared to the "clean" Ag surface (E_a = 0.8 eV). Our DFT-calculations also show that formation of methoxymethanol (via hydrogenation of the hemiacetal intermediate) is feasible with a low energy barrier (E_a < 0.5 eV). Analogous pathways for the formation of other observed C_2 products (i.e. dimethyl ether and acetaldehyde, also present in the experiment results of Figs. 1,2) have also been determined (not shown). Note that these results were obtained using the "standard" nudged-elastic band (NEB) and dimer methods to determine the transition state. These calculations are significantly more expensive compared to simply calculating the binding energies of various intermediates.

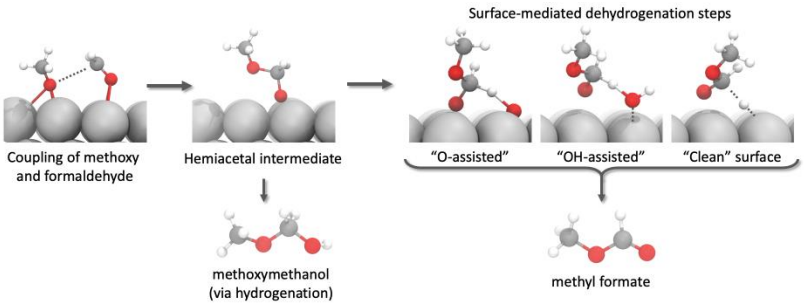

Figure 3. DFT-calculated transition states for the surface-mediated coupling of formaldehyde and methoxy to form the hemiacetal intermediate over Ag(111), which is the precursor for the formation of methyl formate (via dehydrogenation) and methoxymethanol (via hydrogenation).

<u>*Operando* imaging of the near-surface, multicomponent gas phase above a catalyst surface</u>

In addition to MBMS, to characterize the near-surface gas phase during catalysis we also work with our SNL-CRF collaborators to use planar laser induced fluorescence (PLIF) and 1-D Raman spectroscopy imaging to resolve species distributions. We continue to work together to bring new capabilities, notably epi-illumination reflection for probing surface oxidation/coking and a transition to high-temperature reactions, which will enhance research in this project.

<u>*Operando* detection of surface-bound species</u>

We have begun using *operando* diffuse reflectance FTIR (DRIFTS) to probe the steady-state composition of surface-bound species during reaction. We have so far recorded measurements of adsorbates associated with methanol oxidation over Pd, to complement the gas-phase data shown above. We are the process of interpreting these data. The goal here is to correlate the identity of surface-bound species with the near-surface gas phase composition measured by MBMS.

Atomically dispersed catalysts and development of a comprehensive characterization protocol

To develop new structure-function relationships for coupling reactions (especially OCM) that directly connect the near-surface gas phase composition to specific reaction centers, we use MgO-supported transition metal (TM) catalysts with highly dispersed (often atomically dispersed), active sites.

Supported by this project, we have developed a systematic, theory-led workflow for characterization of atomically dispersed catalysts. Our approach combines state-of-the-art characterization techniques (e.g., microscopy – high-angle annular dark field scanning transmission electron microscopy (HAADF-STEM) and X-ray absorption spectroscopy – extended X-ray absorption fine structure (EXAFS) and high-energy resolution fluorescence detection (HERFD-XANES) with large-scale DFT calculations and automated analyses to positively identify the local environment for atomically dispersed catalysts. The work in this aspect of the project has been conducted in collaboration with Bruce Gates (UC Davis) and Simon Bare (SLAC National Accelerator Lab). We focused initially on atomically dispersed Pt cations supported by

MgO. To the best of our knowledge, this study represents the first example of a well-characterized sub-surface platinum cation stabilized within an MgO lattice.

Atomically dispersed Pt/MgO catalysts (~ 0.05 wt%, confirmed by ICP-MS) are prepared by reacting a K_2PtCl_4 precursor with MgO powder in an ethanol solvent, followed by a high-temperature calcination at 700 °C. Figure 4a,b shows a HAADF-STEM images of Pt/MgO. The image of Fig 4b suggest that the Pt atoms are isolated, as shown by intensity profiles (Fig. 4c) along the line X-Y line in the image of Fig. 4b.

We use a theory-guided characterization approach to elucidate the local Pt bonding environment. Specifically, we used DFT calculations (PBESol functional, implemented in VASP) to create a comprehensive library of all catalytically relevant Pt/MgO structures. As summarized in Fig. 4d-e, we consider three representative facets (terrace sites: [100], Mg vacancy terrace sites: $[100]^{Mg\text{-}vac}$, step sites: [310]), various adsorbates (i.e., *O, $*O_2$), vacancy sites (i.e, O_{vac}, Mg_{vac}), and sub-surface Pt locations. Our calculations show that surface Pt ([100]/sub/$*O_2$) and leading step edge ([310]/pos1/$*O_2$) sites are favored at experimental conditions for CO oxidation (our probe reaction), respectively for the stoichiometric surfaces. While surface Pt sites are preferred for the [100] facet, Pt substitution is favorable in the first sub-surface layer (denoted as $[100]^{Mg\text{-}vac}$/sub1) for the vacancy sites.

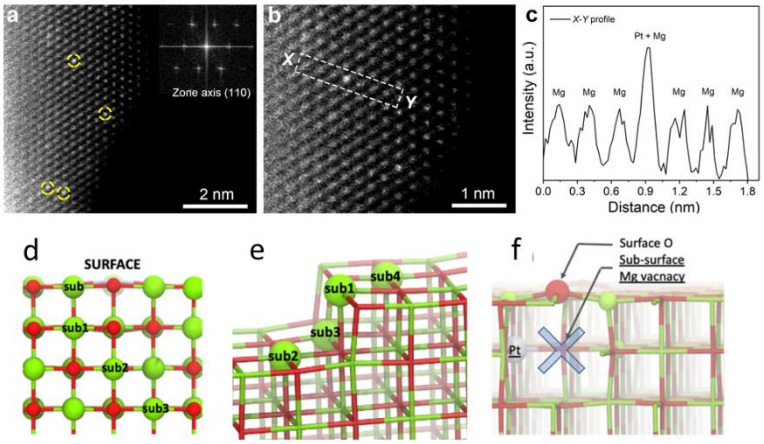

Figure 4. (a) HAADF-STEM image (along the (110) zone axis) showing that the MgO-supported Pt atoms (yellow circles) are atomically dispersed. (b) Higher magnification showing an isolated Pt atom. (c) The intensity profile from corresponding to the X-Y line scan in (b). Atomistic models for the (d) [100], (e) [100]Mg-vac and (f) [310] facets considered in this study.

We have used the open-source X-ray Larch package to perform unbiased EXAFS analysis of 47 DFT-optimized structures. The histogram in Fig. 5a shows the Fréchet distance (δ_F), which measures similarity between the experimental and simulated EXAFS spectra (lower number is better), corresponding to each structure. In general, we observe that the $[100]_{Mg\text{-}vac}$ structures (blue bars in Fig. 5a) are in better agreement with the experimental measurements ($\delta_F < 2$, $\delta_{area} < 2$). While some of the [100] and [310] Pt configurations show reasonable agreement with experimental EXAFS ($\delta_F < 4.5$ and $\delta_{area} < 6.0$), our DFT calculations show these configurations as being highly unstable (> 1 eV unstable). To further understand the structure of Pt/MgO catalysts, the experimental HERFD-XANES data were compared by FEFF-simulated XANES spectra based on various DFT structures (not shown). Of all the stable structures, both [100]/sub/$*O_2$ and $[100]^{Mg\text{-}vac}$/sub1 show good agreement with the experimental XANES data; however, by comparing the corresponding EXAFS spectra in Fig. 5c, the Mg-vacancy is a noticeable improvement over [100]/sub/$*O_2$.

Building on the above microscopy, synchrotron experiments, and theoretical analysis of the Pt bonding environment, we investigated the catalytic activity of Pt/MgO catalyst using CO oxidation as a probe reaction. The light-off curves (Figure 6a), indicate that CO oxidation on Pt/MgO becomes readily measurable at approximately 180 °C, with the CO conversion reaching nearly 100% at 280 °C. Separate experiments were carried out to determine reaction rates (turnover frequencies, TOF – rates per Pt atom, assuming all atoms are catalytically active) at low conversions (not shown), which were determined to be differential by the linear dependence of conversion on inverse space velocity for data determined in a temperature range of 180–200 °C (Figure 6b). An Arrhenius plot indicates an apparent activation energy of 79.1± 2.2 kJ mol^{-1} (not shown). The DFT calculated mechanism via the carbonate pathway for the $[100]^{Mg\text{-}vac}$/sub1 site is consistent with experimental kinetics (now shown).

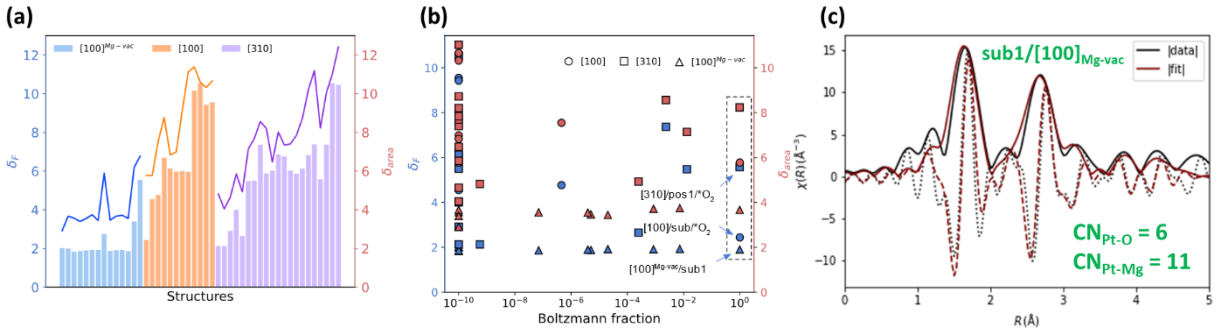

Figure 5. (a) Frechet distance and area of EXAFS plots for all DFT optimized structures. (b) Identifying the structures with favorable Boltzmann fractions and EXAFS fit. (c) EXAFS spectra of Mg-vac on [100].

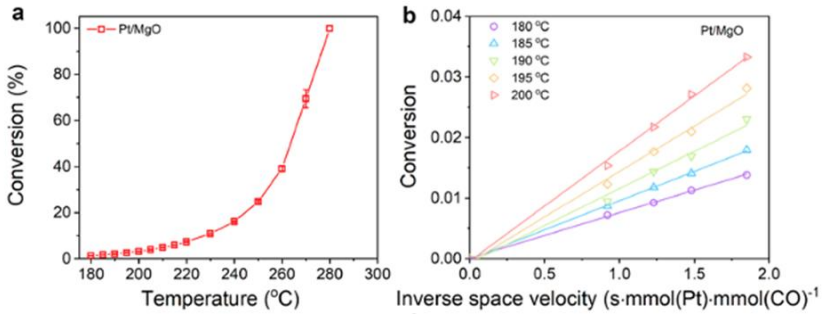

Figure 6. (a) Light-off curve for CO oxidation. Error bars represent standard deviation from three independent measurements. 5.0% CO in He 4.0 mL/min + 5.0% O_2 in He flowing at 16.0 mL/min. (b) Demonstration of differential conversion at various temperatures.

This work has demonstrated an integrated methodology that combines a suite of experimental characterization tools (HAADF-STEM, EXAFS, and HERFD-XANES) with theoretical calculations (DFT, FEFF simulations) to identify the local coordination environment of atomically dispersed catalysts. In contrast to existing approaches, which involve finding the active site model that is consistent we experimental measurements, here, we examine a large library of possible structures (initially motivated by microscopy) and identify the most likely sites. This also allows us to unequivocally see if the site changes after reactions. We are in the process of applying this approach to investigate the dynamics of the TM and lay the foundation for *in situ* EXAFS studies that track the changes in the nature of the atomically dispersed sites as the catalyst evolves.

FUTURE WORK

Apply integrated experiment-theory approach to derive new insights into specific coupling reactions

In the next steps of this work, we will apply the methodology illustrated through results in our Progress Report to gain new mechanistic information into specific coupling reactions with both surface-mediated and gas-phase reaction steps. We also aim to answer specific questions related to the approach itself: What at are the signatures in MBMS, PLIF, 1-D Raman results for surface-dominant coupling mechanisms versus those with gas-phase-dominant mechanisms? Leveraging the mechanistic insights from DFT-derived microkinetic models, how do we interpret/analyze these data?

Work on these systems will utilize a materials platform based on monometallic oxides and oxide-supported metals. In addition to the atomically dispersed materials described above, supported PdO and Pd, MgO, and Li-modified MgO have been identified to be especially helpful for mechanistic studies. This is because Pd/PdO is known to execute both methanol coupling and methane coupling reactions with dominantly surface-mediated steps. (Li)MgO, in contrast, is known (especially for OCM at high temperature) to effect coupling reactions through gas-phase dominant events. We are working closely with our SNL-CRF collaborators to obtain near-surface gas phase PLIF, 1-D Raman, and MBMS data for OCM at high

temperatures (> 650 ºC). We currently are synthesizing, and testing with SNL, Li/MgO catalysts that we have shown to be active for OCM, consistent with the literature.

The spectroscopic imaging tools will yield spatial distributions of species involved in coupling events, complementing MBMS, and will inform mechanistic interpretation. A combination of *operando* DRIFTS and reflectance spectroscopy will reveal the steady-state composition of adsorbates and *in situ* oxidation to inform mechanistic claims. Temperature-programmed reactions using a downflow packed bed reactor with GC/MS analysis will generate light-off curves for methanol (methane) and O_2 conversions and stable products. We also believe that separate PLIF and 1-D Raman experiments, with flow and temperature conditions matched to the reactor conditions, will reveal aspects of the spatial distribution of key products to further refine mechanistic deductions for OCM.

Integration of site-isolated catalysts into workflow for examining coupled gas-surface steps

Another important transition planned for the near future is to combine the approaches that are outlined in the Progress Report above. That is, we will apply our integrated experiment-theory approach for studying coupling reactions with gas- and surface-mediated steps with the use of highly characterized catalysts with well-defined active sites.

We are specifically interested in investigating two main aspects:

(1) Driven by the hypothesis that C_2 production through OCM over atomically dispersed TM/MgO is dominated by gas-phase events (i.e., similar to the proposed Li/MgO mechanisms), we will correlate the trends in catalytic activity of OCM and the speciation of intermediates in the gas phase with the structure of the active site across different transition metals.

(2) Building on preliminary experimental results that show formation of metal nanoparticles at higher metal loadings, we will quantify the relative contributions of gas-phase and surface-mediated reactions for a subset of MgO-supported TM catalysts.

The goal of this work is to derive relationships between local composition/structure of (uniform) active sites and the local gas-phase universal speciation during reaction.

Publications from September 2019 - Present

1. **Near-Surface Imaging of the Multi-Component Gas Phase above a Silver Catalyst During Partial Oxidation of Methanol**

   B. Zhou, E. Huang, R. Almeida, S. Gurses, A. Ungar, J. Zetterberg, A.R. Kulkarni, C.X. Kronawitter, D.L. Osborn, N. Hansen, J. Frank

   ACS Catalysis, **2021**, 11, 155−168.

2. **Supported Metal Pair-Site Catalysts**

   E. Guan, J. Ciston, S.R. Bare, R.C. Runnebaum, A. Katz, A.R. Kulkarni, C.X. Kronawitter, B.C. Gates

   ACS Catalysis, **2020**, 10, 9065–9085.

A Coupled Theoretical and Experimental Approach to Elucidating the Mechanisms of Methyl Esters

Nicole J. Labbe,[1] G. Barney Ellison,[2] John W. Daily[1]
[1]Department of Mechanical Engineering
[2]Department of Chemistry
University of Colorado Boulder
UCB 427, 1111 Engineering Drive, Boulder, CO 80301-0427
Nicole.Labbe@colorado.edu, John.Daily@colorado.edu, Barney@jila.colorado.edu

Program Scope

The goal of our program is to probe fundamental kinetics questions regarding the gas phase reactive behavior of oxygenates. In order to succeed, our program involves both an experimental component and a theoretical component. In short, the microreactor experiment at CU Boulder combined with advanced diagnostics allows for resolution of the very short-time thermal decomposition and abstraction chemistry of molecules of interest. The reactors feature a small (1mm ID x ~3cm long) silicon carbide tube that can be heated to 1700 K. The residence time in the reactor is short, 50-200 μsec, allowing study of the earliest reaction processes. A powerful advantage of our microreactor is the use of two complimentary diagnostic tools to detect products: time-of-flight photoionization mass spectrometry (PIMS) and matrix-isolated infrared spectroscopy (IR). PIMS and IR are universal, multiplexed, and sensitive; all atoms or molecules can be ionized and all polyatomic molecules are IR active, and therefore detectable. The results of our experimental work are compared directly to our theoretical thrust of our program. Electronic structure theory, including QM/DFT, is a powerful tool for calculating energetics of molecules and transition structures at high accuracies. These techniques allow for reliable rate constants and thermochemistry to be calculated, helping to further clarify the mechanistic insights from the experimental work.

In this program, we specifically aim to understand the fundamental chemistry of esters, which are of particular interest due to their use as biofuels and drop-in fuel replacements. In the prior year, our work has focused on three primary thrusts, improving our experimental capabilities with the addition of a partially tunable VUV light source for our PIMS experiments, understand the role of acids for the pyrolysis of a ethyl propanoate (an ethyl ester), and to create and test new kinetic models that accurately reflect the chemistry of two model methyl esters, methyl hexanoate ($CH_3CH_2CH_2CH_2COOCH3$), and methyl 5- hexenoate (CH_2=$CHCH_2CH_2COOCH_3$) to address uncertainties regarding unsaturation in methyl esters, as well as other select oxygenates such as the propanols (iso-propanol and n-propanol).

Recent Progress

Development of Novel Microreactors for Gas Phase Kinetics Experiments: Recently, the Labbe Lab has developed a new method for manufacturing silicon carbide tubes with custom internal geometries using a hybrid traditional and additive manufacturing approach. The result is a new reactor with comparable ceramic properties to the silicon carbide tubes used previously in our

research group and others based on the Chen Nozzle. However, two critical differences exist: 1) the reactors are constructed in a way as to reduce internal defects and pores, creating a smooth internal service which reduces the potential for wall reactions, and 2) custom geometries can now be created such as the inclusion of a tapered nozzle at the end, which effectively chokes flow and stabilizes pressure throughout the reactor body.

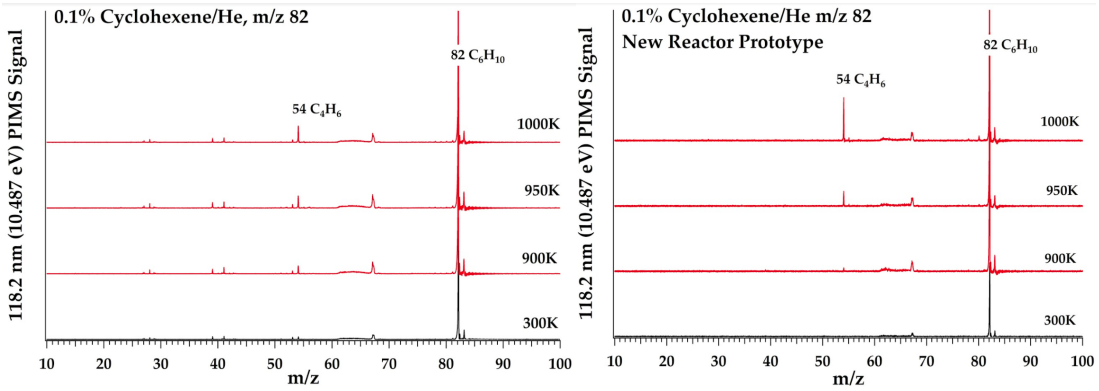

Figure 1: Initial comparison of the original reactor (Left) to the new tapered reactor (Right) for the decomposition of cyclohexene. The original reactor experiments highlight the appearance of stronger secondary product signals relative to main product butadiene, while the new reactor reduce secondary product signal strength compared to butadiene.

To highlight the changes in behavior of the two reactors, Figure 1 shows a direct comparison between the original Chen-style reactor (Left) and the new reactors (Right). 0.1% cyclohexene was diluted in helium and flown through each reactor. The previous reactors showed low signal height of the dominant decomposition product, 1,3-butadiene. Due to the smaller signal strengths overall, we observe several more secondary product signals. Alternatively, the signal strength for the new reactor for the same experimental mixture highlights a much cleaner experimental signal due largely to the increased signal strength of the 1,3-butadiene. These reactors will become our primary reactors in the future.

Double Bond Effects in Methyl Ester Decomposition: Work on the reactions of methyl hexanoate, has continued with a new focus on two of its unsaturated isomers, methyl 3 hexenoate and methyl 5 hexenoate. Methyl hexanoate is relatively low sooting, as highlighted in Table 1 for measured and estimated sooting tendencies as reported in Ref. 1 & 2. As expected, YSI indicates that the inclusion of a double bond into the C_5 tail of the methyl ester can increase soot tendency. However, where the double bond is located can have a stronger effect on sooting.

Table 1: YSI reported from the NREL YSI Estimator [1,2] for methyl hexanoate and two of its unsaturated isomers

Molecule	YSI Reported	YSI Estimated
methyl hexanoate	26.7 +/- 2.4	32.9 +/- 8.5
methyl 3 hexenoate		48.0 +/- 8.9
methyl 5 hexenoate	39.2 +/- 2.1	42.1. +/- 8.8

To explore this, we have conducted a combined theoretical and experimental campaign on these 3 methyl esters to understand their reactive differences. The pyrolysis of these molecules highlights the fundamental differences between these three molecules. For methyl hexanoate, weakened C-C bond homolytic fissions dominate the pyrolysis, as seen in Reactions 1-4, with Reaction 2 dominating at ~32% of the high pressure limit unimolecular flux.

$CH_3CH_2CH_2CH_2CH_2C(=O)OCH_3 \rightarrow CH_3 + CH_2CH_2CH_2CH_2C(=O)OCH_3$ (~16%) (1)
$CH_3CH_2CH_2CH_2CH_2C(=O)OCH_3 \rightarrow CH_3CH_2 + CH_2CH_2CH_2C(=O)OCH_3$ (~38%) (2)
$CH_3CH_2CH_2CH_2CH_2C(=O)OCH_3 \rightarrow CH_3CH_2CH_2 + CH_2CH_2C(=O)OCH_3$ (~22%) (3)
$CH_3CH_2CH_2CH_2CH_2C(=O)OCH_3 \rightarrow CH_3CH_2CH_2CH_2 + CH_2C(=O)OCH_3$ (~14%) (4)

The hexenoates tend to have just one dominate reaction. Methyl 5 hexenoate has a similar reaction trend, with C_3H_5 fission dominating (Reaction 5), while methyl 3 hexenoate cleaves the methyl group (Reaction 6).

$CH_2=CHCH_2CH_2CH_2C(=O)OCH_3 \rightarrow CH_2=CHCH_2 + CH_2CH_2C(=O)OCH_3$ (~94%) (5)
$CH_3CH_2CH=CHCH_2C(=O)OCH_3 \rightarrow CH_3 + CH_2CH=CHCH_2C(=O)OCH_3$ (~95%) (6)

The resultant radicals are what differentiate the two. Methyl 5 hexenoate produces similar products to Reaction 3, though the production of C_3H5, which ultimately forms allene. However methyl 3 hexenoate preferentially forms methyl and a resonantly stabilized radical, which tends to add to itself to form ring structures rather than decompose via β-scission.

Low Temperature Ignition Kinetics for Other Oxygenates: Recently we have developed a collaboration with Nils Hansen to answer some recently revealed questions regarding the low-temperature oxidation mechanism of tetrahydrofuran (THF) concerning the formation of keto-hydroperoxides from his experimental study [3]. In particular, keto-hydroperoxides originating from the THF-β radical were not captured accurately by current literature models, motivating this work to calculate the energetics of the first and second O_2-addition pathways for THF radicals. Electronic structure calculations at the CCSD(T)/cc-pV∞Z//M06-2X/cc-pVTZ level of theory were used to generate potential energy surfaces for the α-C and β-C THF radicals and subsequent pathways to the formation of the keto-hydroperoxide isomers. These are the first theoretical calculations of the second O_2-addition radical pathways for the THF-β radical. Results from the theorical work provided further insight into the low-temperature oxidation of THF, including identifying the pathways most likely to form the keto-hydroperoxide isomers observed in prior experimental work and detecting that the shortcomings in prior models are likely due to uncertainties in R + THF abstraction reaction rates. A comparison of our work compared to other published theoretical work on the low temperature oxidation of THF is highlighted in Figure 2.

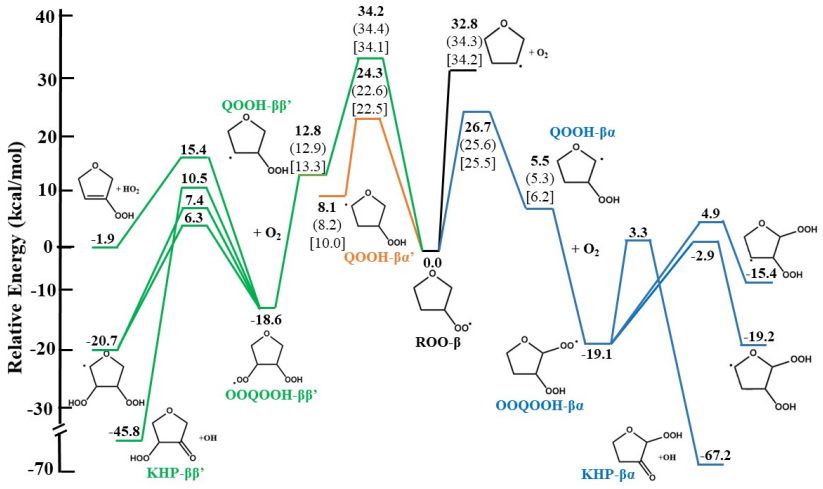

Figure 2: PES at the CCSD(T)/cc-pV∞Z//M06-2X/cc-pVTZ level of theory of the THF ROO-β radical pathways leading to the formation of KHP-ββ' and KHP-βα species. Competing reactions from the unimolecular

decomposition of the OOQOOH-ββ' and OOQOOH-βα radicals are also shown. Corresponding calculated energies from Fenard et al. [4] (parentheses) and Antonov et al. [5] [brackets] are included when available.

This same approach has been extended to studying the unimolecular decomposition and low temperature oxidation of two small alcohols, n-propanol and iso-propanol. Work on these two alcohols is ongoing.

Future Plans

We are wrapping up our work on methyl hexanoate and the two methyl hexenoates, with plans to publish on these molecules this year. We are also wrapping up our work on the publications on n-propanol and iso-propanol. As this work moves forward, we hope to continue testing of the new microreactors and fully adopt these in the future, including through a collaboration with Rob Tranter and Alan Kastengren to image these reactors at the APS. Eventually, we hope to use this information to support other groups within the GPCP program who use the original Chen reactors. We also hope to continue active collaborations with Nils Hansen and Bill Pitz on the low temperature oxidation chemistry of furans and alcohols.

References

[1] D. D. Das, P. C. St. John, C. S. McEnally, S. Kim, L. D. Pfefferle, "*Measuring and predicting sooting tendencies of oxygenates, alkanes, alkenes, cycloalkanes, and aromatics on a unified scale"* Combust. Flame 190 (2018) 349-364.

[2] P. C. St. John, M. Bartlett, S. Kim. "*Group-Contribution Predictions of Yield Sooting Index (YSI).*" *YSI Estimator*, ysi.ml.nrel.gov/.

[3] N. Hansen, K. Moshammer, A. W. Jasper, "*Isomer-Selective Detection of Keto-Hydroperoxides in the Low-Temperature Oxidation of Tetrahydrofuran,*" J. Phys. Chem. A. 123 (38) (2019) 8274-8284.

[4] Y. Fenard, A. Gil, V. G., H. Carstensen, K. M. Van Geem, P. R. Westmoreland, O. Herbinet, F. Battin-Leclerc, *A model of tetrahydrofuran low-temperature oxidation based on theoretically calculated rate constants*, Combustion and Flame 191 (2018) 252-269.

[5] I. O. Antonov, J. Zádor, B. Rotavera, E. Papajak, D. L. Osborn, C. A. Taatjes, L. Sheps, *Pressure-Dependent Competition among Reaction Pathways from First- and Second-O2 Additions in the Low-Temperature Oxidation of Tetrahydrofuran*, J. Phys. Chem. A 120 (33) (2016) 6582-6595.

Publications, Presentations, and Submitted Articles Acknowledging This Grant (2018-present)

1. D. E. Couch, Q. L. Nguyen, D. D. Hickstein, H. C. Kapteyn, M. M. Murnane, and N. J. Labbe, "*Detection of the Keto- Enol Tautomerization in Acetaldehyde, Acetone, Cyclohexanone, and Methyl Vinyl Ketone with a Novel VUV Light Source*". Proc. Combust. Inst. (2020), 1737-1744.
2. C. O. Rogers, K. S. Lockwood, Q. L. Nguyen, and N. J. Labbe*, "Diol Isomer Revealed as the Source of Methyl Ketene from Propionic Acid". Int. J. Chem. Kinetics (2021), Under Review*
3. C. O. Rogers, D. Kaczmarek, T. Kasper, and N. J. Labbe, "*Probing the Low-Temperature Chemistry of Methyl Hexanoate: Insights from Oxygenate Intermediates*". Proc. Combust. Inst. 38 (2020), 621-629.
4. K. Lockwood, N. J. Labbe*, "Insights on Keto-Hydroperoxide Formation from O2 Addition to the Beta-Tetrahydrofuran Radical"* Proc. Combust. Inst. (2020), 533-541.
5. C. Rogers, K. Cummins, J. Porterfield, J. W. Daily, G. B. Ellison, N. J. Labbe, *"The Pyrolysis Chemistry of Propionic Acid and Ethyl Propionate in a Microreactor"* Oral Presentation at the US National Combustion Meeting, Pasadena, CA, March 2019
6. C. Rogers, K. Cummins, J. Porterfield, J.W. Daily, G.B. Ellison, N.J. Labbe *"The Pyrolysis Chemistry of Propionic Acid and Ethyl Propionate Revealed,"* International Conference on Chemical Kinetics, Orleans, France, June 2019. [Invited Talk]
7. C. Rogers, J.P. Porterfield, J.W. Daily, G.B. Ellison, N.J. Labbe. *"Pyrolysis of Ethyl Esters in a Micro-Reactor*," International Symposium on Molecular Spectroscopy, Champaign-Urbana, Illinois, June 2019.

SPECTROSCOPY AND DYNAMICS OF REACTION INTERMEDIATES IN COMBUSTION CHEMISTRY

Marsha I. Lester
Department of Chemistry
University of Pennsylvania
Philadelphia, PA 19104-6323
milester@sas.upenn.edu

I. Program Scope

Our research aims to characterize important, yet often elusive, reaction intermediates in combustion chemistry using novel spectroscopic and dynamical methods. A new thrust is focused on characterizing hydroperoxyalkyl radical intermediates (•QOOH) containing a carbon radical center (•Q), which are important intermediates in low temperature combustion of hydrocarbon fuels and atmospheric oxidation of volatile organic compounds.[1-3] In addition, our research continues to focus on carbonyl oxides (Criegee intermediates, $R_1R_2C{=}O^+O^-$) with novel zwitterionic character, which are important intermediates in tropospheric hydrocarbon oxidation and some combustion reactions.

II. Recent Progress

A. Electronic spectroscopy and photoinitiated dynamics

We have continued our investigation of the photodissociation dynamics of the simplest Criegee intermediate CH_2OO.[4] UV excitation of CH_2OO across most of the broad span of the (B $^1A'$) – (X $^1A'$) spectrum results in prompt dissociation to two energetically accessible asymptotes: O (^1D) + H_2CO (X $^1A_1$) and O (^3P) + H_2CO (a $^3A''$). Dissociation proceeds on multiple singlet potential energy surfaces that are coupled by two regions of conical intersection (CoIn).[5, 6] Velocity map imaging (VMI) experiments reveal a bimodal total kinetic energy (TKER) distribution for the O (^1D) + H_2CO (X $^1A_1$) products with the major and minor components accounting for ca. 40% and ca. 15% on average of the available energy (E_{avl}), respectively. The unexpected low TKER component corresponds to highly internally excited H_2CO (X $^1A_1$) products accommodating ca. 85% of E_{avl}. Full dimensional trajectory calculations suggest that the bimodal TKER distribution originates from two different dynamical pathways to the O (^1D) + H_2CO (X $^1A_1$) products: a primary pathway (69%) evolving through one CoIn region to products and a smaller component (20%) sampling both CoIn regions enroute to products. Those that access both CoIn regions likely give rise to the more highly internally excited H_2CO (X $^1A_1$) products. The remaining trajectories (11%) dissociate to O (^3P) + H_2CO (a $^3A''$) products after traversing through both CoIn regions. The complementary experimental and theoretical investigation provides insight on the photodissociation of CH_2OO via multiple dissociation pathways through two regions of CoIn that control the branching and energy distributions of products.[7]

B. Photoionization mass spectrometry studies of bimolecular chemistry

We have examined two active mechanisms for reaction of methyl vinyl ketone oxide (MVK-oxide), a four-carbon unsaturated Criegee intermediate generated from isoprene ozonolysis, with formic acid: (1) bimolecular reaction of formic acid with both *syn*- and *anti*-conformers of MVK-oxide via a 1,4-insertion mechanism that generates a functionalized hydroperoxide[8] and (2) formic acid catalyzed isomerization of *syn*-MVK-oxide via a barrierless double H-atom transfer mechanism to form vinyl hydroperoxide (HPBD) with regeneration of formic acid,[9] which have been predicted theoretically.

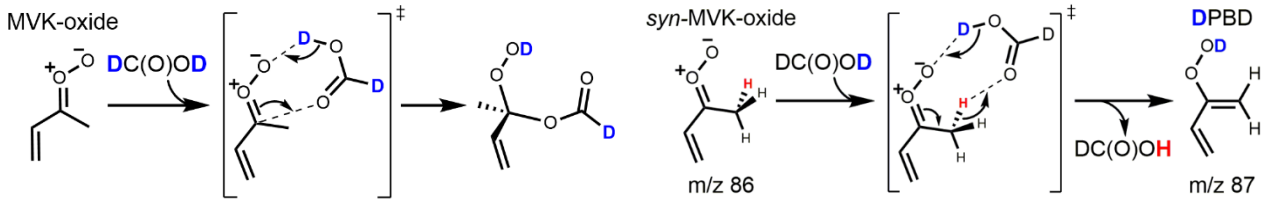

Scheme 1. Reaction mechanisms for MVK-oxide with deuterated formic acid: adduct formation (left) and acid-catalyzed isomerization (right).

We have demonstrated that reaction of deuterated formic acid with MVK-oxide in a flow cell (298 K, 10 Torr) with photoionization (MPIMS) detection at the Advanced Light Source (ALS) enables identification of both the adduct formation and acid catalyzed reaction pathways.[10] Previously, the HPBF adduct was shown to be a primary product of the reaction of MVK-oxide with formic acid.[8] Specifically, dissociative photoionization of the HPBF adduct was observed by identification of fragment ions associated with $-HCO_2$ and $-HO_2$ loss processes. Here, the partially deuterated HPBF adduct from reaction of MVK-oxide with D_2-formic acid is observed through analogous fragment ions ($-DCO_2$ at m/z 88 and $-DO_2$ at m/z 100) associated with dissociative photoionization. The photoionization efficiency curves for the fragment ions from reaction with D_2-formic acid agree with those reported previously for reaction with formic acid,[8] providing further support for the formation of the partially deuterated HPBF adduct in the MVK-oxide + D_2-formic acid reaction.

In addition, the formic acid catalyzed isomerization pathway is revealed using D_2-formic acid, which is identified for the first time. D-atom transfer from the acid to *syn*-MVK-oxide yields a partially deuterated vinyl hydroperoxide (DPBD), which is identified through MPIMS by its distinct mass (m/z 87) and photoionization threshold. The analogous pathway with normal formic acid would appear at the same m/z as MVK-oxide, which makes it difficult to observe. The onset energy at ca. 8.7 eV observed for photoionization of the DPBD products (m/z 87) from the acid catalyzed isomerization of *syn*-MVK-oxide is in good accord with a prior high-level theoretical calculation of the adiabatic ionization energy of HPBD (8.7 eV).[11] The product branching is estimated from the magnitude of the ionization signals (assuming similar photoionization cross sections). This indicates that the HPBF adduct is the dominant product channel (94%) and the acid catalyzed isomerization to DPBD is a minor channel (6%), assuming equal populations of *syn* and *anti*-MVK-oxide are generated under the present experimental conditions and equal photoionization cross sections. High-level *ab initio* calculations indicate HPBF adduct formation is strongly favored compared to acid catalyzed isomerization, consistent with the experimental results.[10]

An analogous study of the bimolecular reaction of methacrolein oxide (MACR-oxide), the other four-carbon resonantly-stabilized Criegee intermediate derived from isoprene ozonolysis, has shown that its reaction with formic acid also forms a functionalized hydroperoxide adduct.[12] Again, this study was carried out in a flow cell (298 K, 10 Torr) with MPIMS detection at the ALS. Electronic structure calculations indicate the reaction proceeds via an energetically favorable 1,4-addition mechanism. The formation of the product is observed by the rapid appearance of a fragment ion at m/z 99, consistent with the proposed mechanism and characteristic loss of HO_2 upon photoionization of functional hydroperoxides.

C. Infrared spectroscopy and unimolecular dissociation dynamics of •QOOH

A new thrust of our research is centered on the infrared (IR) spectroscopy and unimolecular dissociation dynamics of a prototypical hydroperoxyalkyl radical (•QOOH) intermediate, specifically the carbon-centered •QOOH radical formed in isobutane oxidation.[13, 14] The •QOOH radical is generated in a quartz capillary reactor tube, building on previously developed methods,[15, 16] where it is collisionally stabilized and rapidly cooled in a pulsed supersonic expansion. The structure, stability, and dissociation dynamics of •QOOH are examined using IR action spectroscopy,[17, 18] in which the OH radical products

are selectively detected by UV laser-induced fluorescence. Our recent work has yielded an IR fingerprint of the •QOOH radical intermediate, along with •QOOH unimolecular dissociation rates through energy-resolved and time-dependent appearance of OH products. The •QOOH unimolecular decay rates are in excellent accord with those predicted theoretically utilizing state-of-the-art electronic structure characterizations of the transition state barrier region,[19, 20] which advance beyond a prior high-level focal point analysis.[13]

III. Ongoing and Future Work

An initial report on the dissociation dynamics of a prototypical •QOOH radical intermediate has been prepared for publication with extensive theoretical calculations, analysis, and insights from Stephen Klippenstein and Argonne collaborators.[20] Ongoing work is focused on unraveling the IR spectroscopic signature of the •QOOH radical as well as examining the changes in the IR action spectrum and dissociation dynamics upon deuteration.

Other work underway at Penn includes characterizing the second $\pi^* \leftarrow \pi$ transition of MVK-oxide involving primarily the vinyl group. We are also examining the UV photochemistry of the four-carbon unsaturated Criegee intermediate via velocity map imaging of the spin-allowed dissociation to O ^{1}D (or O ^{3}P) products, where we observe bimodal total kinetic energy distributions. Of great interest is the nonadiabatic coupling in two regions of conical intersection that give rise to multichannel decay dynamics.

We plan continued collaboration on ALS experiments with Rebecca Caravan (Argonne) and Craig Taatjes (Sandia), which are focused on the bimolecular chemistry of the MVK-oxide and MACR-oxide Criegee intermediates derived from isoprene ozonolysis. In particular, we are interested in changes in bimolecular reaction rates and/or mechanisms that arise from disruption of the extended conjugation in these resonantly-stabilized, four-carbon Criegee intermediates.

Our Penn laboratory research was halted in mid-March 2020 for 3 months due to COVID-19, followed by periods of low and higher density occupation of the laboratory that enabled resumption of research. In addition, our ALS beamtime was lost due to COVID-19 (May 2020, Fall 2020, Spring 2021) and wildfires (October 2019). Nevertheless, our DOE research has continued with the team engaged in writing papers, carrying out theoretical calculations, and planning future research.

IV. References

1. D. R. Glowacki and M. J. Pilling, ChemPhysChem **11**, 3836 (2010).
2. D. L. Osborn, Annu. Rev. Phys. Chem. **68**, 233 (2017).
3. J. Zádor, C. A. Taatjes and R. X. Fernandes, Prog. Energy Combust. Sci. **37**, 371 (2011).
4. M. F. Vansco, H. Li and M. I. Lester, J. Chem. Phys **147**, 013907 (2017).
5. R. Dawes, B. Jiang and H. Guo, J. Am. Chem. Soc. **137**, 50 (2015).
6. K. Samanta, J. M. Beames, M. I. Lester and J. E. Subotnik, J. Chem. Phys. **141**, 134303 (2014).
7. V. J. Esposito, T. Liu, G. Wang, A. Caracciolo, M. F. Vansco, B. Marchetti, T. Karsili and M. I. Lester, submitted (2021).
8. R. L. Caravan, M. F. Vansco, K. Au, M. A. H. Khan, Y.-L. Li, F. A. F. Winiberg, K. Zuraski, Y.-H. Lin, W. Chao, N. Trongsiriwat, P. J. Walsh, D. L. Osborn, C. J. Percival, J. J.-M. Lin, D. E. Shallcross, L. Sheps, S. J. Klippenstein, C. A. Taatjes and M. I. Lester, Proc. Natl. Acad. Sci. **117**, 9733 (2020).
9. M. Kumar, D. H. Busch, B. Subramaniam and W. H. Thompson, Phys. Chem. Chem. Phys. **16**, 22968 (2014).
10. M. F. Vansco, R. L. Caravan, S. Pandit, K. Zuraski, F. A. F. Winiberg, K. Au, T. Bhagde, N. Trongsiriwat, P. J. Walsh, D. L. Osborn, C. J. Percival, S. J. Klippenstein, C. A. Taatjes and M. I. Lester, Phys. Chem. Chem. Phys. **22**, 26796 (2020).

11. V. P. Barber, S. Pandit, A. M. Green, N. Trongsiriwat, P. J. Walsh, S. J. Klippenstein and M. I. Lester, J. Am. Chem. Soc. **140**, 10866 (2018).
12. M. F. Vansco, K. Zuraski, F. A. F. Winiberg, K. Au, N. Trongsiriwat, P. J. Walsh, D. L. Osborn, C. J. Percival, S. J. Klippenstein, C. A. Taatjes, M. I. Lester and R. L. Caravan, submitted (2021).
13. K. B. Moore, J. M. Turney and H. F. Schaefer, J. Chem. Phys. **146**, 194304 (2017).
14. J. Bugler, J. Power and H. J. Curran, Proc. Combust. Inst. **36**, 161 (2017).
15. J. Zádor, H. Huang, O. Welz, J. Zetterberg, D. L. Osborn and C. A. Taatjes, Phys. Chem. Chem. Phys. **15**, 10753 (2013).
16. C. A. Whelan, M. A. Blitz, R. Shannon, L. Onel, J. P. Lockhart, P. W. Seakins and D. Stone, J. Phys. Chem. A **123**, 10254 (2019).
17. F. Liu, J. M. Beames, A. S. Petit, A. B. McCoy and M. I. Lester, Science **345**, 1596 (2014).
18. Y. Fang, F. Liu, S. J. Klippenstein and M. I. Lester, J. Chem. Phys. **145**, 044312 (2016).
19. S. J. Klippenstein, L. B. Harding and B. Ruscic, J. Phys. Chem. A **121**, 6580 (2017).
20. A. S. Hansen, T. Bhagde, K. B. Moore, D. R. Moberg, A. W. Jasper, Y. Georgievskii, M. F. Vansco, S. J. Klippenstein and M. I. Lester, submitted (2021).

V. Publications supported by this DOE project (2019-present)

1. M. F. Vansco, B. Marchetti, and M. I. Lester, "Electronic spectroscopy of methyl vinyl ketone oxide: A four-carbon unsaturated Criegee intermediate from isoprene ozonolysis", *J. Chem. Phys.* 149, 244309 (2018). https://doi.org/10.1063/1.5064716
2. M. F. Vansco, B. Marchetti, N. Trongsiriwat, G. Wang, T. Bhagde, P. J. Walsh, S. J. Klippenstein, and M. I. Lester, "Synthesis, electronic spectroscopy and photochemistry of methacrolein oxide: A four carbon unsaturated Criegee intermediate from isoprene ozonolysis", *J. Am. Chem. Soc.* **141**, 15058−15069 (2019). http://dx.doi.org/10.1021/jacs.9b05193
3. R. L. Caravan, M. F. Vansco, K. Au, M. A. H. Khan, Y.-L. Li, F. A. F. Winiberg, K. Zuraski, Y.-H. Lin, W. Chao, N. Trongsiriwat, P. J. Walsh, D. L. Osborn, C. J. Percival, J. Jr-M. Lin, D. E. Shallcross, L. Sheps, S. J. Klippenstein, C. A. Taatjes, and M. I. Lester, "Direct kinetic measurements and theoretical predictions of an isoprene-derived Criegee intermediate", *Proc. Natl. Acad. Sci.* **117**, 9733-9740 (2020). https://doi.org/10.1073/pnas.1916711117
4. M. F. Vansco, R. L. Caravan, K. Zuraski, F. A. F. Winiberg, K. Au, N. Trongsiriwat, P. J. Walsh, D. L. Osborn, C. J. Percival, M. A. H. Khan, D. E. Shallcross, C. A. Taatjes, and M. I. Lester, "Experimental evidence of dioxole unimolecular decay pathway for isoprene-derived Criegee intermediates", *J. Phys. Chem. A* **124**, 3542-3554 (2020). https://doi.org/10.1021/acs.jpca.0c02138
5. M. F. Vansco, R. L. Caravan, S. Pandit, K. Zuraski, F. A. F. Winiberg, K. Au, T. Bhagde, N. Trongsiriwat, P. J. Walsh, D. L. Osborn, C. J. Percival, S. J. Klippenstein, C. A. Taatjes, and M. I. Lester, "Formic Acid Catalyzed Isomerization and Adduct Formation of an Isoprene-Derived Criegee Intermediate: Experiment and Theory", *Phys. Chem. Chem. Phys* **22,** 26796-26805 (2020). https://doi.org/10.1039/D0CP05018K
6. R. L. Caravan, M. F. Vansco, and M. I. Lester, "Open questions on the reactivity of Criegee intermediates", *Commun. Chem*. **4**, 44 (2021). https://rdcu.be/chswf

Advanced Nonlinear Optical Methods for Quantitative Measurements in Flames

Robert P. Lucht
School of Mechanical Engineering, Purdue University
West Lafayette, IN 47907-2088
Lucht@purdue.edu

I. Program Scope

Nonlinear optical techniques such as laser-induced polarization spectroscopy (PS), resonant wave mixing (RWM), and ultrafast coherent anti-Stokes Raman scattering (CARS) are techniques that show great promise for high-repetition-rate temperature measurements and sensitive measurements of transient gas-phase species, and diagnostic applications of these techniques are being pursued actively at laboratories throughout the world. The objective of this research program is to develop and test strategies for quantitative concentration and temperature measurements using nonlinear optical techniques in flames and plasmas. We have continued our fundamental theoretical and experimental investigations of these techniques. In recent years our theoretical and experimental efforts have been focused on investigating the potential of femtosecond (fs) laser systems for sensitive and accurate CARS measurements in gas-phase media. In the last few years we have demonstrated the acquisition of single-shot temperature measurements at data rates of 5 kHz in highly turbulent, swirl-stabilized methane-air flames and then in pilot-stabilized jet flames with both gaseous and liquid fuels (these measurements are described in Papers P2-P4) using N_2 chirped-probe-pulse (CPP) fs CARS. Our recent efforts have focused on the CPP fs CARS spectroscopy of other species such as CO_2 and O_2. We have also performed measurements on these species in a high-pressure, high-temperature gas cell and have observed very significant self-phase modulation of the pump and Stokes beams, with consequent significant impact on the CPP fs CARS spectra.

We are investigating the physics of both fs CARS and two-color PS by direct numerical integration (DNI) of the time-dependent density matrix equations for the resonant interaction. Significantly fewer restrictive assumptions are required using this DNI approach compared with the assumptions required to obtain analytical solutions. We are concentrating on the accurate simulation of two-photon processes, including Raman transitions, where numerous intermediate electronic levels contribute to the two-photon transition strength. Recent progress has been much more rapid in our modeling efforts after my PhD student Mingming Gu parallelized the time-dependent density matrix code with the assistance of my faculty colleague Prof. Carlo Scalo. Using this parallelized computer code, we have investigated the in detail the effects of chirp in the pump and Stokes beams on the Raman excitation efficiency and on signal generation for chirped-probe-pulse (CPP) fs CARS.

We also have performed theoretical analysis of Raman transitions for molecules with non-$^1\Sigma$ ground electronic levels, in particular pure rotational Raman transitions for NO and O_2. The theoretical analysis is based on the use of irreducible spherical tensors and Hund's case (a) basis states. The theoretical results for NO were compared with pure rotational CARS measurements performed several years ago on this project, and we have determined a new value for the anisotropic molecule-fixed tensor invariant that gives rise to the electronic Raman transition at 121 cm^{-1} between the spin split $^2\Pi_{1/2}$ and $^2\Pi_{3/2}$ ground electronic levels. We are also starting to perform pure rotation O_2 CPP fs CARS spectroscopy, and the modeling of the $^3\Sigma$ ground electronic level is necessary to model the spectra that we obtain.

We are continuing our investigation of two-color polarization spectroscopy. In particular, we are investigating collision-induced resonances in NO using this technique.

II. Recent Progress

A. Advances in CPP Fs CARS

Fs CARS offers several major potential advantages compared with nanosecond (ns) CARS; i.e., CARS as usually performed with nanosecond pump and Stokes lasers. These potential advantages include an elimination of collisional effects in the signal generation and the capability of performing real-time temperature and species measurements at data rates of 1 kHz or greater as compared to 10-50 Hz for ns CARS. Our Coherent ultrafast laser system operates at 5 kHz with a fundamental pulse width of 55-60 fs and pulse energy of over 2 mJ.

We have completed an investigation of the effects of moderate chirp in the pump and Stokes beams on the Raman excitation efficiency and signal generation for CPP fs CARS. The results are discussed in detail in Paper P6. The key result of our study of pump and Stokes chirp effects is that as long as the sign and magnitudes of the chirp are nearly equal for the pump and Stokes beams, the bandwidth of Raman excitation efficiency envelope decreases only slightly. We were able to model the decrease in the bandwidth of the Raman excitation efficiency using our parallelized time-dependent density matrix code. Our results indicate that inducing moderate levels of chirp appears to actually enhance slightly the temperature accuracy and precision of the CPP fs CARS technique.

In our most recent work we are exploring the potential for measuring temperature and concentrations from CPP fs CARS for species such as CO_2 and O_2. These studies are significant for future measurements in oxy-fuel flames or in pressure gain combustion devices where N_2 may not be present in high concentrations for CARS temperature measurements. The spectral models for both O_2 and CO_2 are much more complicated than for N_2, although the O_2 model is much more tractable than for CO_2. Some results of our initial experimental and theoretical results for combined O_2/CO_2 CPP fs CARS are shown in Fig. 1 from Paper P9. The CO_2 signal remains strong at much longer probe delays compared to O_2, as shown in Fig. 1c, due to the narrow bandwidth of the vibrational modes in the CO2 Raman spectrum. Consequently CO_2 spectra can be obtained without interference from O_2, even in regions with high O_2 concentrations.

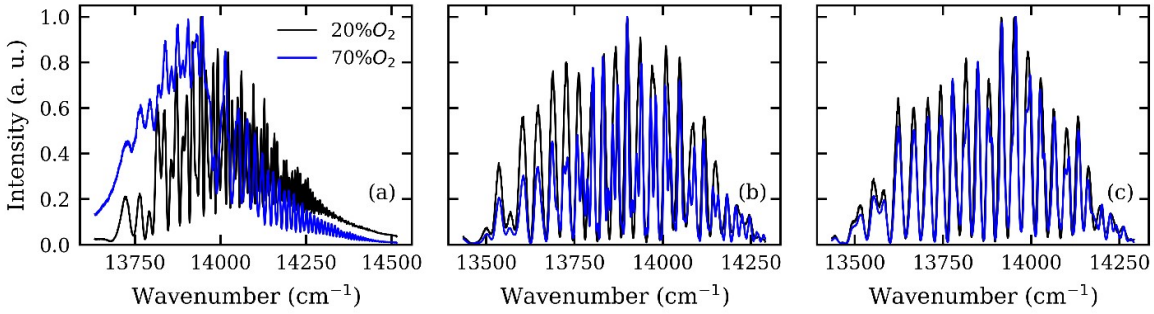

Fig. 1. CPP fs CARS spectra of O_2/CO_2 mixtures at room temperature and pressure at different probe time delays of (a) 0 ps, (b) 2 ps, and (c) 9 ps.

B. Self-Phase Modulation Effects in Femtosecond CARS

Several years ago we measured the CPP fs CARS spectra of methane and ethylene at room temperature and at pressures ranging from 1 to 7 bar. The methane spectrum was essentially unchanged as a function of pressure, but the ethylene spectrum changed drastically as the pressure was increased from 1 to 7 bar. We were not able to explain this effect at that time, but in 2018 we again started to investigate high-pressure effects for N_2, CO_2, O_2, CH_4 and C_2H_4 in a new high-pressure, high-temperature cell at pressures from 1 to 10 bar. We observed that at high pulse energies that the spectra of all of these species were very pressure dependent, even though the characteristic collisional times were much longer than the chirped probe pulse time duration of ~3 ps. We measured the spectra of the pump and Stokes beams before and after the cell and observed a drastic change in the spectrum

for high cell pressures due to self-phase modulation (SPM). We have been able to model these effects and to determine the nonlinear phase induced on the pump and Stokes beam as they traverse the gas cell. Using the nonlinear phase calculated at the probe volume, we are able to obtain good fits even for spectra that are affected significantly by SPM. The results are described in detail in Paper P5.

C. Pure Rotational Raman Spectroscopy of Nitric Oxide and Oxygen

Several years ago, we performed pure rotational CARS measurements mixture of nitric oxide and nitrogen at room temperature. The simultaneous acquisition of pure rotational CARS spectra from known mixtures of these two species will enable us to determine with excellent accuracy the pure rotational Raman cross section for nitric oxide, given that the pure rotational Raman cross section of nitrogen is so well known. The theoretical analysis of the pure rotational Raman process in nitric oxide is complicated because the ground electronic level is a $^2\Pi$ level rather than a $^1\Sigma$ level. This analysis is described in detail in Paper P7. The analysis of the O_2 pure rotational Raman transitions is proceeding in support of our investigation of pure rotational CPP fs CARS spectroscopy of O_2.

D. Collision-Induced Resonances in Two-Color Polarization Spectroscopy of Nitric Oxide

We have continued our experimental and theoretical investigation of two-color polarization spectroscopy (TCPS) of the NO molecule. An energy level diagram and a comparison of theory and experiment are shown in Fig. 2. The circularly polarized pump beam for the TCPS process is tuned to the $R_{11}(11.5)$ transition. In the absence of transfer of Zeeman state anisotropy during rotational transfer collisions, only the $P_{11}(11.5)$ and $P_{11}(13.5)$ transitions, which share common lower and upper levels with the pump transition would be observed as the linearly polarized probe beam is scanned over the P-branch resonances. However, we observe significant signals from P-branch resonances that do not share the same levels with the pump transition, indicating that the pump-induced anisotropy is preserved to some extent during rotational transfer collisions. We are able to model the result using our time-dependent density matrix equation after incorporation of a detailed model for rotational transfer collisions. We found that for high-J levels collisional transfer between F1 and F2 levels was essentially forbidden.

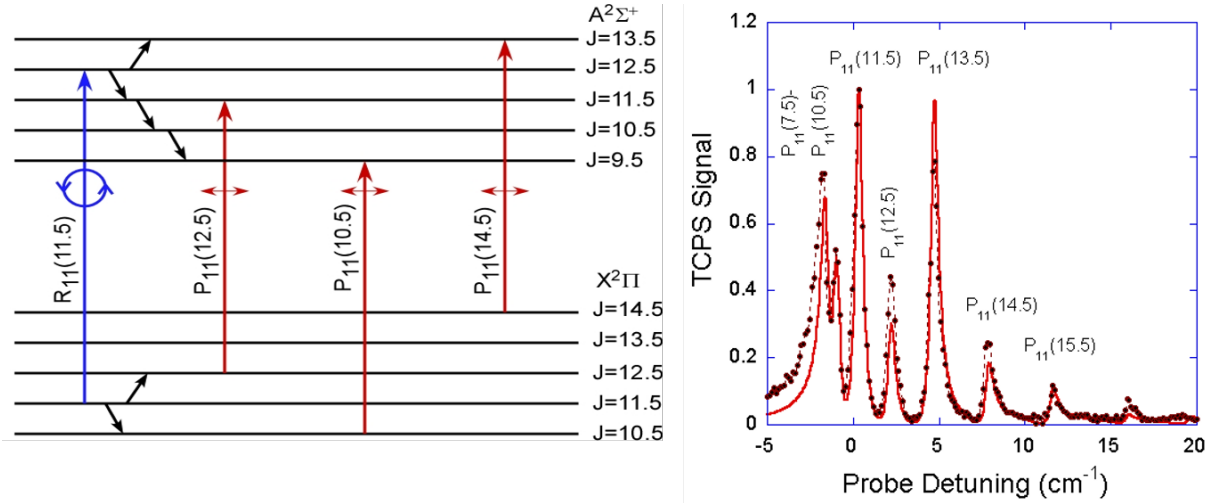

Figure 2. Generation and detection of collision-induced resonances for two-color NO polarization spectroscopy. The mixture was 1% NO in He buffer gas. The pump beam is tuned to the $R_{11}(11.5)$ transition as shown in the energy level diagram (left panel). The TCPS spectrum is shown in the right panel (experiment – filled symbols, dashed line; theory – solid red line).

III. Future Work

We will continue to perform fs CARS experiments using the Coherent ultrafast laser system. Our studies of temperature measurements using CPP fs CARS will continue. We continue to

investigate the effect of laser system parameters on the CPP fs CARS spectrum to improve the temperature accuracy of the technique. We will explore the potential for using CPP fs CARS for accurate concentration measurements for polyatomic species such as CO_2 and hydrocarbons. We will make full use of the high-temperature, high-pressure gas cell that we have fabricated for fundamental studies of the effects of temperature and pressure on CPP fs CARS spectra. We will explore further the effects of soot and droplets on the CPP fs CARS process, and use a Pockels cell between crossed polarizers as a fast electronic shutter for the 5 kHz fs CARS measurements.

Our investigation of two-color PS and 6WM for species such as NO will continue. We will continue to explore collisional effects on the PS and 6WM processes in much more detail using a two-dye laser system. We will explore further the effects of buffer gas collisions on collision-induced resonances in single-photon, two-color PS of NO. We will continue to use the density matrix code to gain insight into the physics of the PS and 6WM processes.

Our theoretical studies of the physics of two-photon and Raman resonances will also continue. We will also initiate an investigation of ultrafast two-photon-induced fluorescence for species such as NO. The broadband excitation provide by fs pulses will be a significant advantage for these measurements. Although our initial ultrafast spectroscopy efforts have been focused on fs CARS, ultrafast laser systems will be useful for a wide range of future diagnostic techniques involving two-photon-induced processes including fluorescence, PS, and RWM.

IV. Refereed publications and submitted journal articles supported by this project 2019-2021

P1. A. Lowe, L. M. Thomas, A. Satija, R.P. Lucht, and A.R. Masri, "Chirped-Probe-Pulse Femtosecond CARS Thermometry in Turbulent Spray Flames," *Proceedings of the Combustion Institute* **37**, 1383-1391 (2019). DOI: 10.1016/j.proci.2018.06.149

P2. L. M. Thomas, A. Lowe, A. Satija, A.R. Masri, and R.P. Lucht, "5 kHz Thermometry in Turbulent Spray Flames Using Chirped-Probe-Pulse Femtosecond Coherent Anti-Stokes Raman Scattering, Part I: Processing and Interference Analysis," *Combustion and Flame* **200**, 405-416 (2019). DOI: 10.1016/j.combustflame.2018.11.004

P3. A. Lowe, L. M. Thomas, A. Satija, R.P. Lucht, and A.R. Masri, "Chirped-Probe-Pulse Femtosecond CARS Thermometry in Turbulent Spray Flames," *Proceedings of the Combustion Institute* **37**, 1383-1391 (2019). DOI: 10.1016/j.proci.2018.06.149

P4. A. Satija, Z. Chang, A. Lowe, L. M. Thomas, A. Masri, and R. P. Lucht, "CARS Thermometry in Laminar Sooting Ethylene-Air Co-Flow Diffusion Flames with Nitrogen Dilution," *Combustion and Flame* **208**, 37-44 (2019). DOI: 10.1016/j.combustflame.2019.06.025

P5. M. Gu, A. Satija, and R. P. Lucht, "Effects of Self-Phase Modulation (SPM) on Femtosecond Coherent Anti-Stokes Raman Scattering Spectroscopy," *Optics Express* **27**, 33955-33967 (2019). DOI: 10.1364/OE.27.033954

P6. M. Gu, A. Satija, and R. P. Lucht, "Impact of Moderate Pump-Stokes Chirp on Femtosecond Coherent Anti-Stokes Raman Scattering Spectra," *Journal of Raman Spectroscopy* **51**, 115-124 (2020). DOI: 10.1002/jrs.5754

P7. A. Satija, N. Chai, M. T. Arendt, and R. P. Lucht, "Pure Rotational Coherent Anti-Stokes Raman Scattering Spectroscopy of Nitric Oxide: Determination of Raman Tensor Invariants," *Journal of Raman Spectroscopy* **51**, 807-828 (2020). DOI: 10.1002/jrs.5836

P8. M. Gu, A. Satija, and R. P. Lucht, "CO_2 Chirped-Probe-Pulse Femtosecond CARS for Thermometry," *Proceedings of the Combustion Institute* **38**, 1599-1606 (2021). DOI: 10.1016/j.proci.2020.06.134

Chemistry of Ammonia-Based Fuels

Paul Marshall
Department of Chemistry and Center for Advanced Scientific Computing and Modeling
University of North Texas, 1155 Union Circle #305070, Denton, TX 76203
E-mail marshall@unt.edu

Program Scope

Ammonia can serve as a carbon-free energy transfer fuel when it is synthesized from green sources of energy such as wind, solar or hydroelectric. Liquid ammonia is relatively easily transported (by comparison to liquid hydrogen) and can be catalytically decomposed to release hydrogen for use in fuel cells, or directly burned for energy release, for example, as a substitute for diesel fuel. There are indications that ammonia's ignition and engine properties are improved by mixing with conventional fuel. This study is aimed at understanding the combustion chemistry of ammonia alone and in conjunction with hydrocarbons, so that with a reliable chemical mechanism, engines can be modified or designed intelligently.

Species to be considered are ammonia (NH_3) and the primary product of radical attack, amino radicals (NH_2). Recombination of a pair of NH_2 radicals leads to hydrazine (N_2H_4). Oxidation of NH_2 leads to nitrogen oxide intermediates and species such as NH_2O and NH_3O. Cross reactions with hydrocarbons, such as recombination of NH_2 and CH_3, will form amines (and perhaps unsaturated imines) and subsequent chemistry of the exemplar methylamine (CH_3NH_2) and related species will be investigated. Key radicals in high-temperature combustion are H and OH, where the rapid diffusion of atomic hydrogen in particular influences flame speed. In the ignition regime, below 1000 K, hydroperoxy (HO_2) radicals have important roles in determining ignition delay. Reactions with O_2 allow for initial attack on fuel molecules and radical formation, and can provide chain-branching at high temperatures. These systems will be studied both by theory and experiments, in the context of isolated elementary reactions and in multireaction systems, to gain fundamental insight into nitrogen chemistry, to permit detailed comparisons with theory, and to create a quantitative mechanism for combustion of ammonia/hydrocarbon mixtures.

Recent progress

Laser-photolysis laser-induced fluorescence is applied to measure radical kinetics under conditions (low concentration and short time) where single elementary reactions dominate the measured species profiles. Exploration of NH_2 chemistry is the first experimental target, and initial results have been obtained for

$$NH_2 + N_2H_4 \rightarrow \text{products} \qquad (1)$$

at room temperature. The results are compared with published computed rate constants k_1 [Li and Zhang, J. Chem. Phys. 125, 064304 (2006)] in Fig. 1. There is a large discrepancy, with theory too low by a

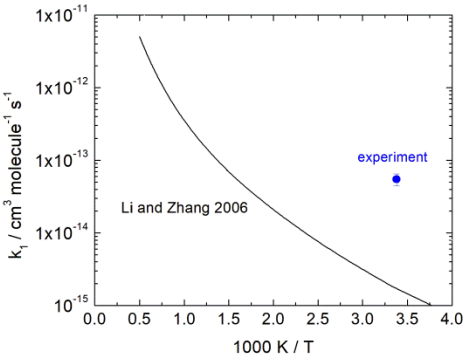

Figure 1. LP-LIF measurements for $NH_2 + N_2H_4$ and literature calculation for abstraction.

factor of ~30. This might reflect computational errors (too high a barrier for abstraction) or a role for a product channel other than direct abstraction. Our own computational analysis is underway.

Quantum chemical methods have been applied to several systems, typically with the M06-2X density functional and the 6-311++G(2df,2p) basis set for geometries and, after scaling, for zero-point vibrational energy and for fundamental frequencies used in partition functions. Direct extrapolation of coupled cluster CCSD(T) energies to the complete basis set limit, and the CBS-APNO approximation, both yield reaction enthalpies with an rms error of less than 2 kJ mol^{-1} when compared to data from the Active Thermochemical Tables.

Potential energy surfaces for the reaction of CH_3NH_3, and it subsequent products, with molecular O_2 have been investigated (see Figure 2 for an example), and rate constants derived with simple transition state theory for the following processes:

$CH_3NH_2 + O_2 \rightarrow HO_2 + CH_2NH_2$ and CH_3NH

CH_2NH_2 and $CH_3NH + O_2 \rightarrow HO_2 + CH_2NH$

$CH_2NH + O_2 \rightarrow HO_2 + HCNH$ and H_2CN

The associated process

$CH_2NH_2 \rightleftarrows CH_3NH$ (high-pressure limit)

was also characterized. Some of these reactions have been investigated before in the context of atmospheric chemistry. Thermochemistry and kinetics were derived for high-temperatures, and incorporated into a mechanism that successfully rationalized explosion limits for CH_3NH_2 and its oxidation in a fast flow reactor. Work remains to reach quantitative agreement with flame speeds and oxidation in the presence of high NO concentrations.

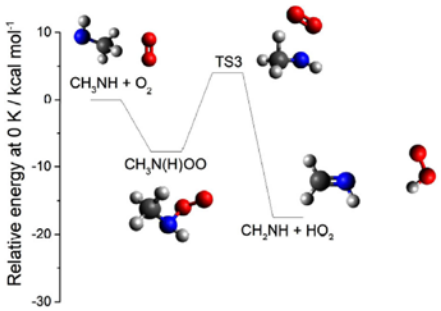

Figure 2. Potential energy diagram for $CH_3NH + O_2$. Literature aimed at atmospheric conditions focused on the initial fast addition to make a peroxy radical. This will not be stable at high temperatures where TS3 becomes the bottleneck.

A contribution was made to mechanistic interpretation of dimethyl ether (DME, CH_3OCH_3) co-combustion with NH_3, probed via measurement of ignition delays in a rapid Compression Machine at the University of Groningen. Kinetics for

$NH_2 + CH_3OCH_3 \rightarrow NH_3 + CH_2OCH_3$

and the thermochemistry and bond strengths in $CH_3OCH_2NH_2$ were computed.

The high pressures and high NH_3 concentrations that arise with use of NH_3 as a fuel, rather than as a model for a fuel-nitrogen source of NO_x, mean that diamine formation may be important. A submitted study focused on diazene (HNNH), emphasizing reactions of the Z (*cis*) isomer, as well as the more usually studied and more stable E (*trans*) isomer. There is also the higher energy *ipso* H_2NN isomer. Pathways that interconvert the isomers, and formation and consumption reactions, were addressed, and low-pressure, falloff and high-pressure behaviors were quantified. One observation is that Z HHNH dissociation to H + NNH is almost two orders of magnitude faster than for the E isomer at atmospheric pressure. There are substantial barriers to E $\rightleftarrows$ Z for both bending and twisting pathways, so at low, ignition temperatures they may need to be treated as distinct species, while at high temperatures interconversion is fast, as shown in Figure 3, and partial equilibrium may be attained.

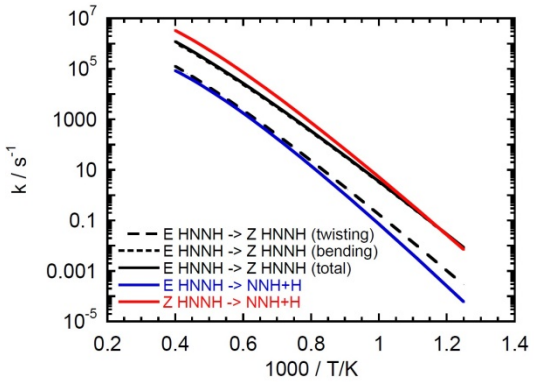

Figure 3. Arrhenius plot for dissociation and isomerization of HNNH isomers at atmospheric pressure.

Another conclusion is that H-abstraction by H-atom attack on N_2H_3 (triplet pathways) is rapid at elevated temperatures and favors formation of the least thermodynamically favorable H_2NN isomer, followed by E HNNH, then Z HNNH.

Future Plans

Computationally, the reactions of E/Z HNNH with H_2, O_2, C_2H_4 and itself will be evaluated. As noted above, $NH_2 + N_2H_4$ will be analyzed to complement experiments, and some further N_2H_4 chemistry may be addressed if the reactions appear significant in mechanisms. A conclusion from ignition delay studies of the DME/NH_3 system is that one of the most sensitive reactions is $NH_3 + O_2 \rightleftarrows HO_2 + NH_2$. By analogy with $HO_2 + OH$, a loose adduct is expected between HO_2 and NH_2 on the triplet potential surface, so that kinetic analysis will incorporate a loose transition state between $HO_2 + NH_2$ and this adduct, and a tighter transition state going on towards $NH_3 + O_2$.

Experiments will continue with NH_2 detection by LIF, and reactions with CH_2O and H_2O_2 are selected because their weak bonds to H may make abstraction feasible. This will give insight into the reverse processes, i.e., HCO and HO_2 attack on NH_3. $H + CH_3NH_2$ will be measured with resonance fluorescence detection of H atoms. Theory will help assess H-abstraction from C-H vs N-H, but also possible pathways to $CH_4 + NH_2$ and $CH_3 + NH_3$.

The photolysis cell with FT-IR detection will be modified for high-temperature photochemistry, to investigate the relative reactivity and product formation for NH_3 and CH_3NH_2 reactions, initially with O atoms.

DOE Sponsored Publications 2020-2021

1. "Oxidation of Methylamine" P. Glarborg, C.S. Andreasen, H. Hashemi, R. Qian and P. Marshall, Int. J. Chem. Kinet., 52, 893-906 (2020).
2. "Ignition Delay Times of NH_3/DME Blends at High Pressure and Low DME fraction: RCM Experiments and Simulations" L. Dai, H. Hashemi, P. Glarborg, S. Gersen, P. Marshall, A. Mokhov and H. Levinsky, Combust. Flame, 227, 120-134 (2021).
3. "New Reactions of Diazene and Related Species for Modeling Combustion of Amine Fuels" P. Marshall, G. Rawling and P. Glarborg, Mol. Phys. *submitted*.

Thermal Decomposition of Cyclic, Oxygenated Hydrocarbons

Laura R. McCunn-Jordan
Chemistry Department, Marshall University
1 John Marshall Dr.
Huntington, WV 25755
mccunn@marshall.edu

Program Scope

The objective of this project is to investigate how chemical structure affects the thermal decomposition mechanisms of cyclic, oxygenated hydrocarbons that are relevant to biofuels and combustion. The primary specific aim of the proposed experiments is to identify the thermal decomposition products of dihydro-2-furanone, dihydro-3-furanone, 2-cyclopentenone, 3-cyclopentenone, 2-pyrone, and 4-pyrone. A pulsed hyperthermal nozzle will be used to induce gas-phase pyrolysis at temperatures up to 1600 K. Product detection will be accomplished with a matrix-isolation FTIR spectrophotometer. A second specific aim of the project is to construct a mass spectrometer with tunable low-energy electron-impact ionization that can be used with the same hyperthermal nozzle. The introduction of a new detection technique will complement the FTIR experiments and provide a more complete characterization of the pyrolysis products, which is essential to the development of accurate thermal decomposition mechanisms.

The experiments are designed to probe the early steps in the pyrolysis mechanism, with the possibility of capturing radical intermediates. Two goals can be accomplished by this approach. First, the results will augment the existing body of knowledge created by shock-tube and static pyrolysis experiments, which typically probe the ultimate products of thermal decomposition on relatively long timescales. Adding to the variety of techniques in the literature will clarify pyrolysis mechanisms, which can include dozens of elementary steps. Second, identifying pyrolysis products of compounds that are intermediates or by-products in the production or combustion of new fuels will enable the prediction of pollutants from these fuels. The experimental results will contribute to the elucidation of pyrolysis mechanisms and enable the assessment of the environmental impact of various fuels. The completed research will build a foundation of knowledge for overcoming challenges to the nation's energy supply and environmental quality.

Recent Progress

Matrix-isolation FTIR experiments have been completed on several of the cyclic, oxygenated hydrocarbons targeted for study in this project. Pyrolysis was performed on five different molecules: dihydro-2-furanone; dihydro-3-furanone; 2-cyclopentenone; 3-cyclopentenone, and 4-pyrone. (Figure 1) Each molecule was mixed with argon at various dilute

concentrations (0.02-0.4%) and subject to pyrolysis at a range of temperatures (900-1500 K). Products were identified with FTIR spectroscopy following matrix isolation.

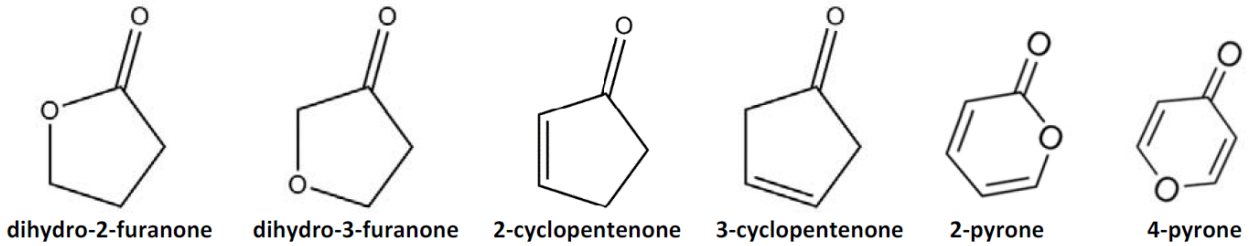

Figure 1. Cyclic, oxygenated hydrocarbons for pyrolysis studies

Pyrolysis reactions of dihydrofuranones

Dihydro-3-furanone, also known as oxolan-3-one, thermally decomposes to ketene, formaldehyde, carbon monoxide, ethylene, acetylene, water, and propyne over the employed pyrolysis temperature range of 800 to 1400 K and at concentrations of 0.1-0.4% in argon. (Figure 2) These products, excepting propyne, are consistent with unimolecular reaction pathways predicted by CBS-QB3 calculations performed by collaborators Xinli Song (Wuhan University) and Carol Parish (University of Richmond). The dominant pathway expected, based on calculated transition state energies, yields carbon monoxide, formaldehyde, and ethylene.

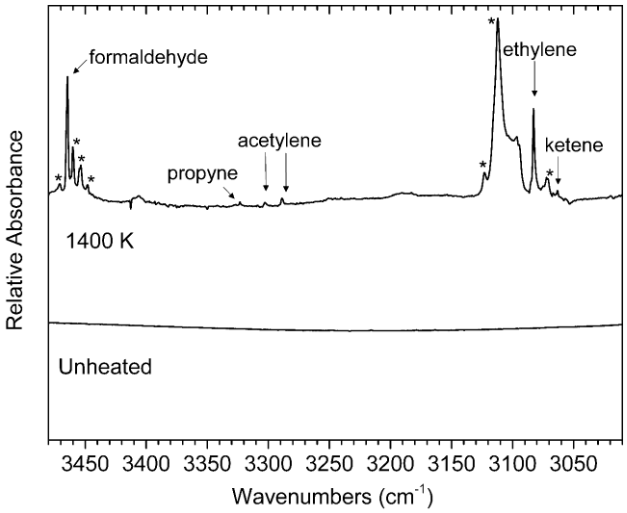

Figure 2. FTIR spectrum of pyrolysis (1400 K) products of dihydro-3-furanone isolated in an argon matrix, compared an unheated sample isolated in argon.

A small number of unassigned bands in the FTIR spectra suggest the presence of a substituted ketene, believed to be hydroxyketene. Optimization and frequency calculations of hydroxyketene at the B3LYP/6-311++G(d,p) level suggest that the experimentally observed bands at 2130 cm^{-1} and 3610 cm^{-1} belong to the C=C=O asymmetric stretch and OH stretch, respectively, of hydroxyketene. Hydroxyketene and ethylene are the products of a minor pathway of unimolecular decomposition of dihydro-3-furanone, with a CBS-QB3 transition state energy 33 kcal/mol higher than that of the carbon monoxide + formaldehyde + ethylene pathway.

Dihydro-2-furanone, more commonly known as gamma-butyrolactone, produces carbon dioxide, carbon monoxide, formaldehyde, ethylene, and ketene. Formaldehyde is noteworthy as it has not been observed in pyrolysis experiments performed with other techniques in the literature. Preliminary work has been undertaken to model the unimolecular reaction pathways of dihydro-2-furanone at the B3LYP/6-311G(d,p) level of theory.

Pyrolysis reactions of cyclopentenones

The cyclic ketone 2-cyclopentenone thermally decomposes to propene, acrolein, acetylene, ethylene, vinylacetylene, propargyl, and carbon monoxide over the employed pyrolysis temperatures of 1000 to 1400 K and at a concentrations of 0.5% in argon. (Figure 3) The presence of propargyl radicals in these experiments is particularly interesting because it indicates that 2-cyclopentenone could be a precursor to soot formation in certain high-temperature environments.

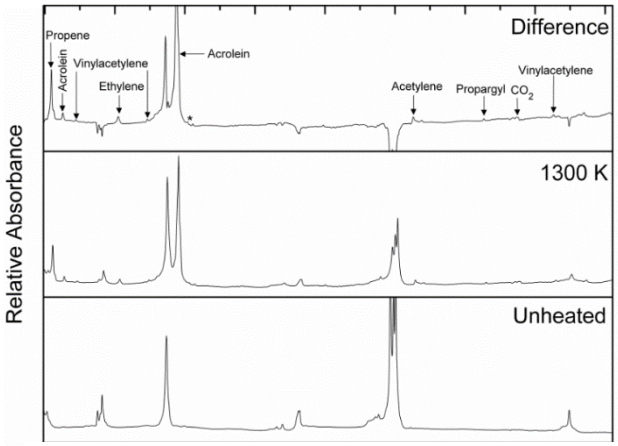

Figure 3. FTIR spectrum of pyrolysis (1300 K) products of 2-cyclopentenone isolated in an argon matrix, compared an unheated sample isolated in argon.

An unassigned band at 2128 cm^{-1} in the FTIR spectra following pyrolysis of 2-cyclopentenone suggests the presence of a substituted ketene. Preliminary calculations at the B3LYP/6-31G(d) level of theory have optimized transition states leading from 2-cyclopentenone to several substituted ketenes: prop-2-enylketene, prop-1-enylketene, and cyclopropylketene. In order to facilitate the identification of these ketenes, a comprehensive computational investigation of substituted ketenes was undertaken. Optimization and frequency calculations at the B3LYP/6-311++G(d,p) level of theory have been performed on the aforementioned substituted ketenes, as well as ketenes with existing spectroscopic benchmarks: ketene, methylketene, and ethylketene. A comparison of calculated frequencies for the C=C=O asymmetric stretch and the known experimental frequencies for matrix-isolated ketene, methylketene, and ethylketene produced a scaling factor that could be used to predict the vibrational bands of unassigned substituted ketenes in these experiments. The predicted values show that the experimentally observed band at 2128 cm^{-1} is most likely prop-2-enylketene. In order to experimentally confirm this assignment, very recent experiments have sought to establish an experimental benchmark for the vibrational bands of prop-2-enylketene. The molecule 4-pentenoic anhydride was selected as a good candidate for a clean pyrolytic precursor to prop-2-enylketene. Pyrolysis of the anhydride, 0.4% in argon, at 1000 K yielded a clear band at 2128 cm^{-1}, supporting a tentative assignment of prop-2-enylketene in the pyrolysis of 2-cyclopentenone.

The products of pyrolysis of 3-cyclopentenone are: carbon monoxide, ketene, acetylene, ethylene, propyne, allene, vinylacetylene, propargyl, and ethynol. While there are many products in common with 2-cyclopentenone, the appearance of propyne, allene, and ethynol should lead to interesting revelations about the influence of chemical structure on the pyrolysis mechanism. Work has begun to probe the energetics of the unimolecular dissociation pathways of 3-cyclopentenone. Optimization and frequency calculations at the B3LYP/6-31G(d,p) level of theory have determined energies of the transition states and products for initial reactions in the pyrolysis of 3-cyclopentenone. Initial results show that hydrogen migrations were found to have much lower transition states than ring-opening reactions.

Future Plans

The pyrolysis studies of dihydro-3-furanone and 2-cyclopentenone have revealed the prevalence of ketene formation in the pyrolysis of oxygenated hydrocarbons, and more

importantly, a need for good experimental benchmarks to identify substituted ketenes. Immediate efforts in the laboratory will focus on the pyrolysis of clean precursors to isolate and characterize hydroxyketene, prop-1-enylketene and cyclopropylketene.

Implementation of the new mass spectrometer was delayed by the COVID-19 pandemic, so much of the final year of the project will be devoted to using the newly constructed mass spectrometer to study the pyrolysis of the various cyclic, oxygenated hydrocarbons that are the focus of this project. The mass spectra will confirm the product assignments already made from the FTIR spectra and will likely reveal a few unknown products as well. The mass spectra will also be especially important in confirming the substituted ketenes observed in the matrix-isolation FTIR studies. Additionally, studies will begin of 2-pyrone (Figure 1), with both matrix-isolation FTIR and mass spectrometry detection of pyrolysis products.

Completion of the computational investigations of the thermal decomposition of the cyclic oxygenated hydrocarbons in this work will be the other major objective in the final year of the project. The collaboration with Professor Carol Parish at the University of Richmond and Xinli Song at Wuhan University, established in the first year of the project has proven fruitful in the study of dihydro-3-furanone (oxolan-3-one). All but one of the experimentally observed products are accounted for by the CBS-QB3 calculated pathways. These calculations, in concert with the experimental identification of intermediates and products will be key to understanding the pyrolysis mechanisms of the cyclic, oxygenated hydrocarbons.

Publications During Project Period (2019-present)

1. Brown, G.; Ellis, M.; Martin, T.; McCunn, L. R. Vibrational Bands of the 2-Butyn-1-yl Radical. *J. Phys. Chem. A.* **2020**, *124*, 4081–4086.

IR Spectroscopy and Dynamics of Jet-Cooled Combustion Radicals: Transient Carbenes and Oxyhydrocarbon Intermediates

David. J. Nesbitt

Our research program involves experimental and theoretical study of transient chemical species relevant to fundamental combustion and atmospheric chemical processes. The work focuses on spectroscopy and unimolecular/bimolecular dynamics of highly reactive radical intermediates, combining i) high-resolution direct IR laser absorption methods with quantum shot noise limited detection, ii) high densities (10^{12}-10^{14} #/cm^3) of jet-cooled hydrocarbon radicals and molecular ions in slit supersonic discharge expansions, accompanied by iii) high-level *ab initio* potential surface and multidimensional quantum mechanics calculations. Over the past two years, our group has explored multiple jet-cooled transients such as i) highly reactive singlet carbenes (e.g., HCF, HCBr), ii) Criegee intermediate precursor halocarbon radicals (e.g., CH_2Br), and iii) H atom radical catalyzed oxyhydrocarbon isomerization dynamics (e.g., *trans*- to *cis*-HCOOH) via high-resolution IR laser spectroscopy. Highlights from the first two topics are briefly discussed below,[1,2] with more detailed discussion in all areas to be provided at the May Contractors Meeting.

A. High-resolution infrared spectroscopy of halocarbene diradicals: HCF

Halogenated molecules are of importance in commercial product/organic synthesis, as well as in combustion, atmospheric, and interstellar chemistries.[3,4] In particular, halogen containing complex organic molecules (COMs, e.g., CH_3Cl) can be formed as the byproduct of biological activity and have been proposed as biomarkers in exoplanet atmospheres.[5] However, the recent observation of CH_3Cl towards a sun-like star forming region and in the comet 67P/Churyumov-Gerasimenko indicates that there are non-biological formation mechanisms in the interstellar medium (ISM).[6] One such mechanism is by halogen atom (X) incorporation into simple molecules and COMs in irradiated ice mantles of dust grains, including sequential H-atom addition to CX.[4,7] In order to better understand how halogenated molecules are formed in the ISM, a more complete understanding of the reaction-pathway intermediates and their relative abundances is needed. This requires gas-phase laboratory spectra with which to make unambiguous molecular assignments in astronomical observations of possible halogen containing molecules in the reaction network.

There is considerable additional interest in such halocarbene species (HCX) from an atmospheric chemistry perspective, as these simple biradical species are thought to be products in solar photolytic and OH radical decomposition of halogenated hydrocarbons commonly used in post-Montreal accord refrigerants (e.g., H-fluoro/chloro hydrocarbons) and fumigant pesticides (e.g., methyl bromide). This again provides strong motivation for detailed spectroscopic characterization of such transient HCX species, providing access to detecting trace concentrations with remote sensing instruments. Over the past year of COVID, we have pursued spectroscopy of two such biradicals, specifically HCF and HCBr.

To date, the pure rotational transitions of three fluorinated molecules have been detected in astronomical spectra: CF^+ and HF, in diffuse and translucent clouds; HF, in dense sources;[8-11] and HF and AlF, in circumstellar envelopes of carbon rich stars.[12,13] HF has also been observed in absorption in interstellar gas through its infrared rovibrational transitions, $\nu = 1 \leftarrow 0$ R(0) and R(1).[14] Since the interstellar formation mechanism for CH_3F, like CH_3Cl, is thought to be dominated by grain surface reactions starting from CF, with the

diradical halocarbene HCF as an intermediate,[4] and given that the interstellar abundance of F is comparable to Cl,[15] it is highly likely that CH_3F and its simpler radical derivatives, e.g., HCF, also exist in astronomical environments. However, detection of fluorinated molecules with more than two atoms is currently hampered by limited laboratory-based high-resolution spectroscopic data.

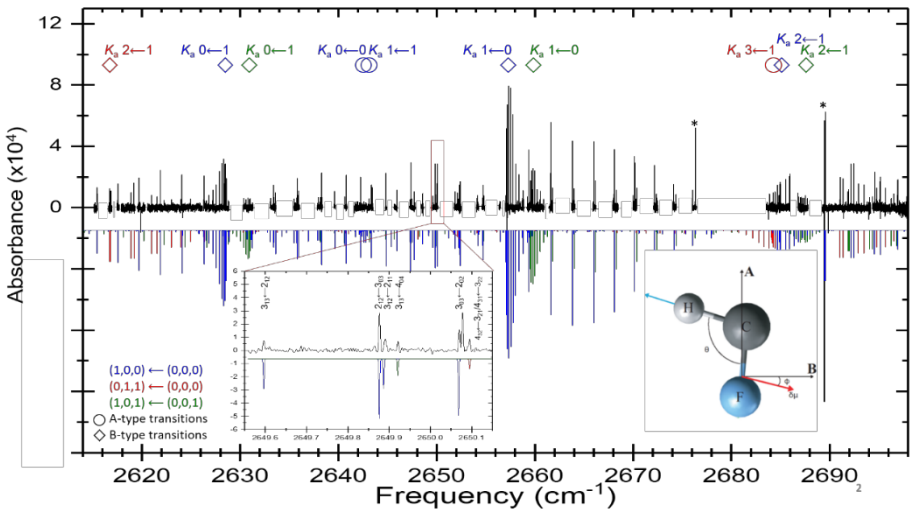

Over the past two years we have obtained results from a high-resolution infrared study of jet-cooled singlet monofluorocarbene (HCF) in the CH stretch region near 2600 cm^{-1}, with the absorption signals recorded using near quantum shot noise limited laser absorption methods (see sample spectral region above). The fully resolved absorption spectra of the CH stretch (ν_1) fundamental band and a partial progression of transitions of the HCF bend plus CF stretch ($\nu_2+\nu_3$) combination band are observed, and show clear evidence of a strong rovibrational coupling between the ν_1 $K_a^i = 2$ and $\nu_2+\nu_3$ $K_a^i = 3$ manifolds, including the observation of "dark state" transitions. A detailed perturbation analysis of a c-type Coriolis interaction is carried out for these two coupled vibrational states, providing experimental determination of precise rovibrational constants. A combined ground state combination difference fit of the transitions to the ν_1 and $\nu_2+\nu_3$ vibrational states in this study with previously reported LIF $\tilde{A}(0,0,0) \leftarrow \tilde{X}(0,0,0)$ data has been done to increase the accuracy of the ground state rotational constants. Moreover, we report for the first time hot band ($\nu_1+\nu_3 \leftarrow \nu_3$) transitions due to vibrationally excited HCF in the CF stretch mode, ν_3. The high-resolution results for all vibrational frequencies and rotational constants are in good agreement with and significantly extend the analysis of the rovibrational manifold of HCF.[16] The present ground state and ν_3 spectroscopic parameters now permit improved predictions for pure rotational and ν_3 fundamental transitions to aid spectral searches for HCF in the laboratory and the interstellar medium.

B. High-resolution infrared spectroscopy of jet cooled CH_2Br radicals:

Ever since their initial prediction over 50 years ago, the spectroscopy and quantum dynamics of diradical carbonyl oxides (so-called Criegee intermediates) have become increasingly significant topics because of their relevance to atmospheric and combustion chemistry, particularly with the recent demonstration that gas phase synthesis of Criegee intermediates R_1R_2COO can be made relatively simply by the addition of O_2 to mono-iodohydrocarbon radicals.[17] This approach has been quite recently extended to mono-bromohydrocarbon radicals by Nakajima and Endo[18] in Fourier-transform microwave spectroscopy (FTMS) measurements, based on dissociating CH_2Br_2 in a O_2 doped discharge

and collisionally stabilizing the subsequent Criegee species ($CH_2Br + O_2 \rightarrow CH_2OO + Br$) in a supersonic expansion. Given the important role of CH_2Br in the chemical formation of Criegee intermediates, we have chosen to explore the infrared rovibrational spectroscopy of the jet cooled radical CH_2Br as a first step towards spectroscopic study of CH_2OO itself.

Beyond utility in generating Criegee intermediates, the CH_2Br radical is of fundamental interest in both atmospheric and interstellar chemistry (ISC). For example, methyl bromide (CH_3Br) is known to have a relatively long residence time (roughly two years[19]) in the atmosphere, with the primary removal process by hydroxyl radical abstraction reaction to form CH_2Br, i.e.,

$$CH_3Br + OH \rightarrow CH_2Br + H_2O$$

Once the CH_2Br radical is generated, it can undergo solar photodissociation and production of free radical Br atoms, known to be a strong catalytic species in the destruction of stratospheric ozone.[20,21] Natural sources of CH_2 Br include evolution of CH_3Br from biological activity in the marine environments, with less benign anthropormorphic sources of CH_3Br due to fumigant use still permitted by the Montreal Protocol.[22] From the perspective of ISC, halogen-containing complex organic molecules (COMs) such as CH_3Br on earth are predominantly formed as the byproduct of biological activity and have therefore also been proposed as potential biomarkers in exoplanetery atmospheres.[5] However, recent observational data for halogenated organic molecules in comets and sun-like star forming regions suggests that there might also be *non-biological* formation pathways in the interstellar medium (ISM),[6] such as halogen incorporation into COMs via irradiation of ice mantles on dust grains.[23] In order to better characterize the formation of halogenated molecules in the ISM, therefore, a more complete understanding of the underlying brominated hydrocarbon reaction intermediates and their high resolution infrared (IR) spectroscopic signatures would be extremely helpful, toward which these efforts have been directed.

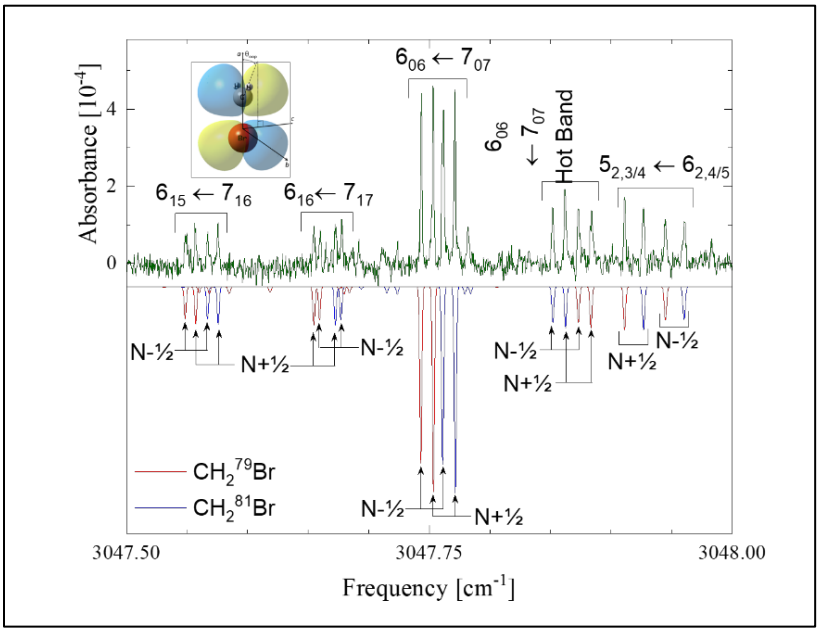

Direct laser absorption of a slit supersonic discharge expansion provides the first high-resolution spectroscopic results on symmetric CH stretch excitation (ν_1) of bromomethyl (CH_2Br) radical in the ground electronic state. Narrowband (< 1 MHz) mid-infrared radiation is produced by difference frequency generation of two visible lasers beams, with the open shell halohydrocarbon radical generated by electron associative detachment of CH_2Br_2 in a discharge and rapidly cooled to $T_{rot} = 18 \pm 1$ K in the subsequent slit-jet supersonic expansion. Rovibrational structure in the radical spectrum is fully resolved, as well as additional splittings due to spin-rotation effects and $^{79}Br/^{81}Br$ isotopologues in natural abundance. Spectroscopic constants and band origins are determined by fitting the transition

frequencies to a non-rigid Watson Hamiltonian, yielding results consistent with a vibrationally averaged planar radical and an unpaired electron in the out-of-plane p_π orbital. Additionally, extensive satellite band structure from a vibrational hot band is observed and analyzed. This hot band is compared to CFOUR/VPT2 (CCSD(T)cc-pVQZ) ab initio anharmonic predictions of the vibration rotation alpha matrix. This permits unambiguous assignment of this band to CH_2 symmetric stretch excitation built on the singly excited CH_2 out-of-plane bending mode ($\nu_1+\nu_4 \leftarrow \nu_4$). Longitudinal cooling of the Doppler width in the slit jet expansion geometry also reveals partially resolved hyperfine structure on transitions from the lowest angular momentum states which is in excellent agreement with predictions based on microwave studies. High level ab initio MOLPRO calculations (CCSD(T)-f12b/VnZ-f12 (n=3, 4, CBS) are also performed with explicitly correlated f12 electron methods for the out-of-plane CH_2 bending mode over the halogen series CH_2X (X = F, Cl, Br, I), which clearly reveals a non-planar geometry for X = F (with a $\Delta E \approx 0.3$ kcal/mol barrier) and yet planar equilibrium geometries for X = Cl, Br, and I. Finally, a detailed Boltzmann analysis of the transition intensities provides support for negligible collisional equilibration of the entangled H atom nuclear spin states on the few hundred microsecond time scale and high collision densities of a slit supersonic expansion.

1 K. D. Doney *et al.*, J. Chem. Phys. **152** 014305 (2020).
2 A. Kortyna *et al.*, J. Chem. Phys. **152**, 134305 (2020).
3 S. Elliott and F. S. Rowland, J. Chem. Educ. **64**, 387 (1987).
4 K. Acharyya and E. Herbst, Astrophys. J. **850** (2017).
5 E. W. Schwieterman *et al.*, Astrobiology **18**, 663 (2018).
6 E. C. Fayolle *et al.*, Nat. Astron. **1**, 703 (2017).
7 M. Kama *et al.*, Astron. Astrophys. **574** (2015).
8 D. A. Neufeld *et al.*, Astrophys. J. **488**, L141 (1997).
9 D. A. Neufeld *et al.*, Astron. Astrophys. **454**, L37 (2006).
10 T. G. Phillips *et al.*, Astron. Astrophys. **518** (2010).
11 P. Sonnentrucker *et al.*, Astrophys. J. **806** (2015).
12 J. Cernicharo and M. Guelin, Astron. Astrophys. **183**, L10 (1987).
13 M. Agundez *et al.*, Astron. Astrophys. **533** (2011).
14 N. Indriolo *et al.*, Astrophys. J. **764** (2013).
15 M. Asplund *et al.*, in *Annual Review of Astronomy and Astrophysics, Vol 47*, edited by R. Blandford, J. Kormendy, and E. VanDishoeck (Annual Reviews, Palo Alto, 2009), Vol. 47, pp. 481.
16 M. Kakimoto *et al.*, J. Mol. Spectrosc. **88**, 300 (1981).
17 C. A. Taatjes *et al.*, J. Am. Chem. Soc. **130**, 11883 (2008).
18 M. Nakajima and Y. Endo, J. Chem. Phys. **139**, 101103 (2013).
19 A. Mellouki *et al.*, Geophys. Res. Lett. **19**, 2059 (1992).
20 S. C. Wofsy *et al.*, Geophys. Res. Lett. **2**, 215 (1975).
21 Y. L. Yung *et al.*, J. Atmosph. Sci. **37**, 339 (1980).
22 S. W. J. Johnson, S. Gerik, in *Outlooks on Pest Management* (2012), Vol. 23, pp. 53.
23 M. Kama *et al.*, Astron. Astrophys. **574**, A107 (2015).

Fundamental Molecular Spectroscopy and Chemical Dynamics

Stephen R. Leone and Daniel M. Neumark
Lawrence Berkeley National Laboratory and Departments of Chemistry and Physics, University of California, Berkeley, California 94720 (510) 643-5467 srl@berkeley.edu, 510-642-3502
dmneumark@berkeley.edu

Scope of the Project: Decades of research into molecular dynamics, including branching fractions, dissociation dynamics, and energetics, have vastly improved our fundamental understanding of chemical processes. Measurements of radical spectroscopy, ions and excited state dynamics comprise key future goals of the effort, especially the development of new ways to probe excited-state dynamics and photoproducts by the program of Leone and Neumark. The Leone group has pioneered femtosecond time-resolved table-top x-ray spectroscopic investigations of chemical dynamics at sufficiently high photon energies to access the carbon K-edge. Ultrafast x-ray transient absorption spectroscopy based on this methodology investigates transition states and products. The Neumark program uses a suite of experimental methods aimed at the spectroscopy and photodissociation dynamics of reactive free radicals: slow electron velocity-map imaging of cryogenically cooled anions (cryo-SEVI), a high resolution variant of photoelectron spectroscopy, fast radical beam (FRBM) studies of radical photodissociation, in which a beam of radicals is generated by negative ion photodetachment, and molecular beam photodissociation of radicals (XBeam) carried out on species generated by flash pyrolysis of suitable precursors.

Recent Progress:

Femtosecond Soft X-ray Transient Absorption Experiments

The ultrafast excited state non-adiabatic dynamics of acetylacetone was studied after excitation with a 266 nm pulse using time resolved x-ray absorption spectroscopy at the carbon K-edge (284eV). At this wavelength, the predominant enol tautomer of acetylacetone was excited to the S_2 ($^1\pi\pi^*$) electronic state, which undergoes an internal conversion to the lower-lying S_1 ($^1n\pi^*$) state before finally undergoing an intersystem crossing to the triplet T_1 ($^3\pi\pi^*$) state on a 1.5 ± 0.2 ps timescale. Aided by density function theory, the evolution of the core-to-valence resonances at the carbon K-edge directly establish the electronic states involved in the photochemistry. Recently, hexafluoro-acetylacetone was similarly explored and revealed a similar photochemistry with the intersystem crossing occurring on a 1.7 ± 0.2 ps timescale. Additionally, calculations were carried out (in collaboration with the Martin Head-Gordon group) using a square gradient minimization algorithm, which obtains spin-pure restricted open-shell Kohn-Sham energies. These calculations also demonstrated rotamerization along the T_1 state, which agrees with a proposed mechanism for the primary dissociation pathway.

The sensitivity of x-ray spectroscopy to changes in molecular structure and orbital occupancy was applied to probe the excited states of cations for the first time, which are challenging to observe with UV or visible light. Two-photon ionization was used to selectively prepare the ground state of benzene radical cation. Table-top ultrafast broadband x-ray measurements at the carbon K-edge was used to measure the x-ray spectral features of benzene and its radical cation. Comparison of the x-ray absorption spectra of the neutral and the cation reveals a splitting of the two degenerate π^* orbitals as well as an appearance of a new peak due to excitation to the partially occupied π-subshell. The π^* orbital splitting of the cation is discovered to be due to both the Jahn-Teller distortion leading to a lower symmetry, and even more dominantly due to spin couplings of three unpaired electrons in the probe transition.

Carbon K edge spectroscopy sheds light on the photochemical changes in pyrazine after 266 nm excitation, providing unambiguous proof for the participation of the optically dark ^1A_u ($n\pi^*$) state and distinguishing the previously characterized $^1B_{2u}$ ($\pi\pi^*$) (S_2) and $^1B_{3u}$ ($n\pi^*$) (S_1) states. The ^1A_u ($n\pi^*$) state is populated about 200 femtoseconds after electronic excitation and plays a key role in the relaxation of pyrazine to the ground state. The nature of the excited states was established by a combination of experimental x-ray core-to-valence spectroscopy, electronic structure, nonadiabatic dynamics

simulations, and x-ray spectral computation (carried out by collaborators Sonia Coriani and Anna Krylov).

In order to access even faster electronic dynamics – such as passage through conical intersections – a new beamline has been designed for attosecond and few-femtosecond soft x-ray transient absorption experiments. In this lab, 1300 nm pulses are compressed down to 12 fs few-cycle pulses and used to generate a soft x-ray continuum up to 375 eV. The brightness of this beamline allows the measurement of absorption spectra in a few seconds, an order of magnitude improvement compared to existing apparatuses that provide photon continua in this energy range. Few-cycle pulses centered at 800 nm are simultaneously produced at a millijoule level and can be used as a pump pulse for strong-field ionization or impulsive stimulated Raman scattering. The cross-correlation between the soft x-ray pulses and near-IR pulses is measured to be 11 fs, thus opening many possibilities for the observation of ultrafast chemical dynamics on this timescale.

A vibrational wavepacket superposition of states was observed, produced by impulsive stimulated Raman scattering, in sulfur hexafluoride (SF_6). The superposition is observed through six different sulfur core-excited states of the molecule (170-240 eV). The vibrational period for the ν_1 mode (symmetric stretching of S-F bonds) of 43 fs is well resolved in the time domain. The x-ray transition energies are very sensitive to small changes in internuclear distances, here of the order of a few 0.01 Å. Each core-excited state responds differently to the same vibrational wavepacket, shifting the transition energy by a certain amount with bond length. This allows to determine experimentally the gradients of the core-excited state potential energy surfaces. Calculations of the potential energy surfaces were done by collaborator Victor Kimberg, and new methods being developed by Neuscamman, and the relative slopes of 3 core level states (energetic shift with bond elongation and compression) are found to be in good agreement with experimental results, indicating that states with significant orbital density on the central sulfur have the greatest changes with bond length.

In a related experiment, carbon dioxide (CO_2) was vibrationally excited by impulsive stimulated Raman scattering. A multimode vibrational wavepacket superposition composed of the ν_1 and $2\nu_2$ modes of the well-known CO_2 Fermi resonance is excited and observed via the C 1s electronic transitions at 293 eV. Work by theoretical collaborator John Stanton elucidated important new features of pseudo Jahn-Teller distortion in the x-ray spectra of CO_2. The temporal resolution of the experiment allows observing an ~22 fs vibrational motion in the time-domain. This result demonstrates the ability of the apparatus to resolve very short ultrafast molecular dynamics at the carbon K-edge, and the probing of such superposition states connects directly to quantum coherence properties that will be important in molecular dynamics.

Free radical spectroscopy and dynamics

Cryo-SEVI was used to obtain isomer-specific, high resolution photoelectron spectra of the *para*-, *meta*- and *ortho*-pyridinide anions, yielding electron affinities and detailed vibrational structure for the three neutral pyridyl radical isomers. The vibronic structure for each isomer is distinct, and the electron affinity of the *ortho*-pyridinyl radical was found to be 0.6 eV lower than that of the other two isomers. Strong isomeric variations in the photoelectron angular distributions were explained by a model approximating the anion orbitals from which detachment occurs as superpositions of *s*-, *p*-, and *d*-like hydrogenic wavefunctions. In ongoing work, the cryo-SEVI spectrum of the allyl anion was measured. The vibrational resolution is considerably improved over previous work and shows clear evidence for Franck-Condon forbidden transitions that occur via Herzberg-Teller coupling between the ground and first excited state of the allyl radical.

On the FRBM instrument, photodissociation of the *tert*-butyl perthiyl (*t*-BuSS) radical was investigated at 248 and 193 nm. This work is motivated by previous studies of the tert-butyl peroxy radical and at 248 nm, the dominant product channel (90%) was found to be S loss, with a product translational energy distribution that peaked close to the maximum available energy and an anisotropic photofragment angular distribution, indicating dissociation along a repulsive excited state. A minor channel (10%)

leading to the formation of S_2 + *t*-Bu was also observed. At 193 nm, both two- and three-body dissociation were observed. Formation of S_2 + *t*-Bu is the dominant two-body product channel, with multiple electronic states of the S_2 molecule produced via excited state dissociation processes. The three-body channels are S_2 + H + isobutene, S_2 + CH_3 + propene, and S + SH + isobutene.

At 248 nm, the dominant dissociation channels from the isopropoxy (*i*-C_3H_7O) radical are CH_3 + CH_3CHO and OH + C_3H_6 with some contribution from H + C_3H_6O. CH_3 and H loss are attributed to dissociation on the ground electronic state of *i*-C_3H_7O, but in a nonstatistical manner because RRKM dissociation rates exceed the rate of energy randomization. Translational energy and angular distributions for OH loss are consistent with ground state dissociation, but the branching ratio for this channel is considerably higher than predicted from RRKM rate calculations. Additionally, *i*-C_3H_7O undergoes three-body fragmentation to CH_3 + CH_3 + HCO and CH_3 + CH_4 + CO. These three-body channels are attributed to dissociation of *i*-C_3H_7O to CH_3 + CH_3CHO, followed by secondary dissociation of CH_3CHO on its ground electronic state.

The photodissociation of jet-cooled cyclohexyl on the XBeam instrument was studied by exciting the radicals to their 3p Rydberg state using 248 nm laser light and detecting photoproducts by photofragment translational spectroscopy. Both H-atom loss and dissociation to heavy fragment pairs are observed. The H-atom loss channel exhibits a two-component translational energy distribution. The fast photoproduct component is attributed to impulsive cleavage directly from an excited state, likely the Rydberg 3s state, forming cyclohexene. The slow component is due to statistical decomposition of hot cyclohexyl radicals that internally convert to the ground electronic state prior to H-atom loss. Internal conversion to the ground state also leads to ring opening followed by dissociation to 1-buten-4-yl + ethene in comparable yield to H-loss, with the C_4H_7 fragment containing enough internal energy to dissociate further to butadiene via H-atom loss. A very minor ground-state C_5H_8 + CH_3 channel is observed, attributed predominantly to 1,3-pentadiene. The ground-state branching ratios agree well with RRKM calculations, which also predict C_4H_6 + C_2H_5 and C_3H_6 + C_3H_5 channels with similar yield to C_5H_8 + CH_3. If these channels were active it was at levels too small to be observed.

Future Plans:

The UV-pump and soft x-ray-probe apparatus will continue to be used to spectroscopically investigate fundamental photochemical processes. In the future, it is planned to focus on topics such as the decomposition of ketones and diradicals, excited state proton transfer, ring puckering and ring opening dynamics, and study of cycloaddition reactions in detail. Future investigations include methyl vinyl ketone, o-nitrophenol, furanone and norbornadiene. Many of these molecules will make use of femtosecond 200 nm pump light, which offers a far wider array of possible systems and scientific questions to be studied. Future efforts will extend the soft x-ray probe in order to obtain energy-tunable pulses reaching the nitrogen K-edge (410eV) as well as the time resolution to obtain few-femtosecond timescales. The new attosecond soft X-ray apparatus will be combined with a short 267nm UV pump to provide the excellent temporal resolution necessary in order to resolve excited state dynamics through conical intersections, e.g. furfural, cyclohexadiene, and acetylacetone. The use of the attosecond setup will allow for the clear separation of electronic and structural interactions in the benzene cation providing the first ever opportunity to measure the Jahn-Teller effect using x-ray spectra. Lastly, the improved temporal resolution opens the door to explore charge migration dynamics on a molecule such as uracil. An oscillating charge distribution involving the π orbitals will allow the x-ray spectrum to probe the hole density at each carbon atom in the molecule.

Complementary high-resolution photoelectron spectroscopy and fast beam experiments will be carried out on several peroxy radicals of interest, in particular two acyl peroxy species: peroxyformyl $HC(O)CO_2$ and peroxyacetyl $CH_3C(O)CO_2$. These species represent the next level of chemical complexity with respect to the alkyl peroxy radicals previously studied with these methods, and complement planned carbon K-edge femtosecond transient absorption work on ketones. Moreover, both radicals play a key role as reactive intermediates in combustion and atmospheric chemistry. In a new research direction, cryo-SEVI experiments will be performed on anions that have been pre-excited with

an infrared laser; this experiment, which will be carried out on the allyl anion, represents a novel means to measure infrared spectra of cold, gas phase anions, and simultaneously explore neutral vibrational energy levels and regions of the neutral potential energy surface that are inaccessible via detachment from the anion ground vibrational state.

Recent Publications Acknowledging DOE GPCP Support (2018-2021):

- Chang, K. F.; Reduzzi, M.; Wang, H.; M.-Poullain, S.; Kobayashi, Y.; Barreau, L.; Prendergast, D.; Neumark, D. M.; Leone, S. R., "Revealing Electronic State-Switching at Conical Intersections in Alkyl Iodides by Ultrafast XUV Transient Absorption Spectroscopy". Nat. Commun. 11, 4042 **(2020).** DOI: 10.1038/s41467-020-17745-w.
- Epshtein, M.; Scutelnic, V.; Yang, Z.; Xue, T.; Vidal, M. L.; Krylov, A. I.; Coriani, S.; Leone, S. R. "Table-Top X-Ray Spectroscopy of Benzene Radical Cation". J. Phys. Chem. A, 124, 9524–9531 **(2020)**. DOI: 10.1021/acs.jpca.0c08736.
- Nichols, B.; Sullivan, E. N.; Neumark, D. M., "Photodissociation Dynamics of the tert-butyl perthiyl Radical". J. Chem. Phys. 152, 244301 **(2020).** DOI: 10.1063/5.0006913.
- Sullivan, E. N.; Saric, S.; Neumark, D. M., "Photodissociation of iso-Propoxy (i-C3H7O) Radical at 248 nm". Phys. Chem. Chem. Phys. 22, 17738-17748 **(2020)**. DOI: 10.1039/d0cp02493g.
- Vidal, M. L.; Epshtein, M.; Scutelnic, V.; Yang, Z.; Xue, T.; Leone, S. R.; Krylov, A. I.; Coriani, S. "Interplay of Open-Shell Spin-Coupling and Jahn–Teller Distortion in Benzene Radical Cation Probed by X-Ray Spectroscopy". J. Phys. Chem. A 124, 9532–9541 **(2020)**. DOI: 10.1021/acs.jpca.0c08732.
- Hait, D.; Haugen, E.; Yang, Z.; Oosterbaan, K.; Leone, S. R.; Head-Gordon, M., "Accurate Prediction of Core-Level Spectra of Radicals at Density Functional Theory Cost via Square Gradient Minimization and Recoupling of Mixed Configurations". J. Chem. Phys. 153, 134108 **(2020)**. DOI: 10.1063/5.0018833.
- Barreau, L.; Ross, A. D.; Garg, S.; Kraus, P. M.; Neumark, D. M.; Leone, S. R. "Efficient Table-Top Dual-Wavelength Beamline for Ultrafast Transient Absorption Spectroscopy in the Soft X-ray Region". Sci. Rep. 10, 5773 **(2020)**. DOI: 10.1038/s41598-020-62461-6
- Sullivan, E. N.; Nichols, B.; Neumark, D. M.; "Fast Beam Photofragment Translational Spectroscopy of the Phenoxy Radical at 225 nm, 290 nm, and 533 nm". Phys. Chem. Chem. Phys. 21, 14270-14277 (**2019**). DOI: 10.1039/c8cp06818f
- Ramphal, I.; Lee, C.; Neumark, D. M., "Photodissociation Dynamics of the Methylsulfinyl Radical at 248 nm". Molec. Phys. 117, 3043-3055 (**2019**). DOI: 10.1080/00268976.2019.1580781
- Schnorr, K.; Bhattacheriee, A.; Oosterbaan, K. J.; Delcey, M. G.; Yang, Z.; Xue, T.; Attar, A. R.; Chatterley, A. S.; Head-Gordon, M.; Leone, S. R., Gessner, O.; "Tracing the 267 nm-Induced Radical Formation in Dimethyl Disulfide Using Time-Resolved X-ray Absorption Spectroscopy". J. Phys. Chem. Lett. 10, 1382−1387 (**2019**). DOI: 10.1021/acs.jpclett.9b00159
- Sullivan, E. N.; Nichols, B.; Kugelgen, S. v.; Silva, G. d.; Neumark, D. M., "Multiphoton Dissociation Dynamics of the Indenyl Radical at 248 nm and 193 nm". J. Chem. Phys. 151, 174303 (**2019**). DOI: 10.1063/1.5121294.
- DeVine, J. A.; Babin, M. C.; Blackford, K.; Neumark, D. M., "High-Resolution Photoelectron Spectroscopy of the Pyridinide Isomers". J. Chem. Phys. 151, 064302 (**2019**). DOI: 10.1063/1.5115413.

- Toulson, B. W.; Borgwardt, M.; Wang, H.; Lackner, F.; Chatterley, A. S.; Pemmaraju, C. D.; Neukmark, D. M.; Leone, S. R.; Prendergast, D.; Gessner, O., "Probing Ultrafast C–Br Bond Fission in the UV Photochemistry of Bromoform with Core-to-Valence Transient Absorption Spectroscopy". Struct. Dynam. 6, 054304 (**2019**). DOI: 10.1063/1.5113798
- Geneaux, R.; Marroux, H. J. B.; Guggenmos, A.; Neumark, D. M.; Leone, S. R., "Transient Absorption Spectroscopy Using High Harmonic Generation: A Review of Ultrafast X-ray Dynamics in Molecules and Solids". Phil. Trans. R. Soc. A 377, 20170463 (**2019**). DOI: 10.1098/rsta.2017.0463
- Bhattacherjee, A.; Leone, S. R., "Ultrafast X-ray Transient Absorption Spectroscopy of Gas-Phase Photochemical Reactions - A New Universal Probe of Photoinduced Molecular Dynamics". Acc. Chem. Res. 51, 3203−3211 (**2018**). DOI: 10.1021/acs.accounts.8b00462
- Yang, Z.; Schnorr, K.; Bhattacherjee, A.; Lefebvre, P. L.; Ephstein, M.; Xue, T.; Stanton, J. F.; Leone, S. R., "Electron-Withdrawing Effects in the Photodissociation of CH_2ICl to Form CH_2Cl Radical, Simultaneously Viewed through the Carbon K and Chlorine $L_{2,3}$ X-ray Edges". J. Am. Chem. Soc. 140, 13360 (**2018**). DOI: 10.1021/jacs.8b08303
- Bhattacherjee, A.; Schnorr, K.; Oesterling, S.; Yang, Z.; Xue, T.; Vivie-Riedle, R.; Leone, S. R., "Photoinduced Heterocyclic Ring Opening of Furfural: Distinct Open-Chain Product Identification by Ultrafast X-ray Transient Absorption Spectroscopy". J. Am. Chem. Soc. 140, 12538 (**2018**). DOI: 10.1021/jacs.8b07155
- Kraus, P. M.; Zürch, M.; Cushing, S, K.; Neumark, D. M.; Leone, S. R., "The Ultrafast X-Ray Spectroscopic Revolution in Chemical Dynamics". Nat. Rev. Chem. 2, 82 **(2018)**. DOI: 10.1038/s41570-018-0008-8
- Weichman, M. L.; Neumark, D. M., "Slow Photoelectron Velocity-Map Imaging of Cryogenically-Cooled Anions". Annu. Rev. Phys. Chem. 69, 101-124 (**2018**). DOI: 10.1146/annurev-physchem-050317-020808. DOI: 10.1146/annurev-physchem-050317-020808
- Sullivan, E. N.; Nichols, B.; Neumark, D. M., "Photodissociation Dynamics of the Simplest Alkyl Peroxy Radicals, CH_3OO and C_2H_5OO, at 248 nm". J. Chem. Phys. 148, 033409 (**2018**). DOI: 10.1063/1.5011985

State-to-State Molecular Reactions in the Ultracold Regime

Kang-Kuen Ni
Department of Chemistry and Chemical Biology, Harvard University
12 Oxford St., Cambridge, MA 02138
ni@chemistry.harvard.edu

Research Scope:
We aim to gain state-to-state experimental data for both the AB + CD and AB + C types of reactions, which can be compared to advanced theoretical calculations to help elucidate the role of quantum mechanics in the processes of bond breakage and formation. Our approach is to conduct experiments with reactants that are prepared at ultracold temperatures ($< 1\mu K$) such that the quantum effects of translational motion are an important factor. Specific example reactions, including the potassium-rubidium metathesis reaction $KRb + KRb \rightarrow K_2 + Rb_2$ and the atom exchange reaction $K + KRb \rightarrow K_2 + Rb$, are chosen because the technology of quantum internal and motional state control of these types of molecules is particularly advanced. We have constructed a new quantum degenerate gas apparatus that integrates ion detection and velocity map imaging capabilities, and have begun to explore the bimolecular reaction in detail. In general, reactions in this regime will serve as sensitive probes to compare to high accuracy *ab initio* potentials and quantum scattering calculations. This work will advance our intuition about chemistry at ultracold temperatures, as well as our ability to control chemistry at the most basic quantum level.

Recent Progress:
For the funding period since last year, our efforts in studying bimolecular reactions of KRb molecules at sub-microkelvin temperatures focused on developing quantum state detection of the reaction products, and yielded two key results. 1. We observed strong parity preferences for the rotational states of the reaction product dimers, K_2 and Rb_2, which we then used to establish nuclear spin conservation throughout such a reaction [1]. 2. We developed quantum-state-resolved coincident detection of the product pairs and mapped out the complete product state distribution, which was compared to a state-counting model based on statistical theory [2]. Our results show an overall agreement with the state counting model, but also reveal several deviating state-pairs. An exact quantum calculation is beyond the current state-of-the-art.

To experimentally examine the reaction outcome with quantum state resolution, we employed resonantly-enhanced multi-photon ionization (REMPI), which is schematically illustrated in Fig. 1(left). We note that the exothermicity of the reaction is too small (10 cm^{-1}) to allow vibrational excitations, so that the detection scheme needs only to distinguish different rotational states. The complete data set for the rotational state distribution of the reaction products K_2 and Rb_2 is shown in Fig 1(right), which reveals a strong parity preference for the product dimers. We explain such a parity preference by first noting that the homonuclear dimers must respect the exchange symmetry of the indistinguishable nuclei. For $^{40}K_2$, the nuclei are bosons, and for $^{87}Rb_2$, the nuclei are

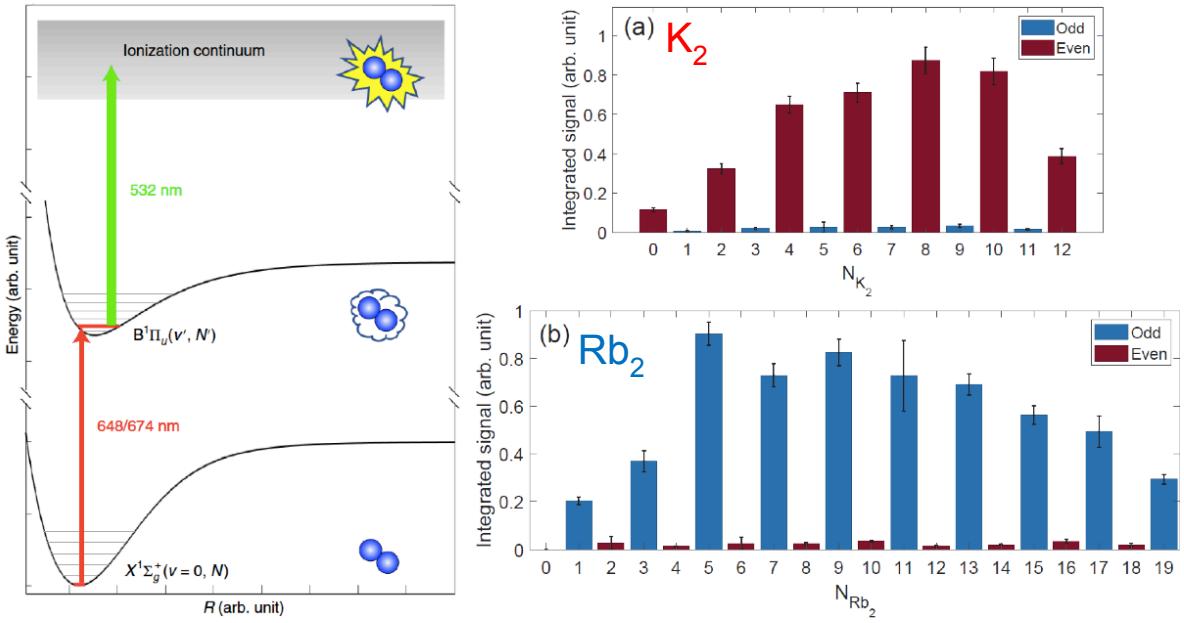

Figure 1: **Quantum state detection of reaction products via REMPI.** (**Left**) Schematic for the optical transitions used for the $1+1'$ REMPI of $^{40}K_2$ and $^{87}Rb_2$. The first photon (~ 650 nm for K_2 and ~ 670 nm for Rb_2) promotes the products from the ground $X^1\Sigma_g^+(v=0,J)$ state to the excited $B^1\Pi_u^+(v',J')$ state ($v'=1$ for K_2 and $v'=4$ for Rb_2), and the second photon (532 nm) ionizes the excited molecules, allowing them to then be detected. (**Right**) Rotational state distribution of reaction products K_2 and Rb_2, showing strong parity preferences.

fermions. Observing even rotational states for K_2 and odd rotational states for Rb_2 means the nuclear spin wavefunctions for both dimers are symmetric. Because the KRb reactants are prepared with well-defined nuclear spins, represented by the state $|I^K=4, m_I^K=-4; I^{Rb}=3/2, m_I^{Rb}=1/2\rangle$, where I and m_I denote a nucleus' spin and its projection onto a quantization magnetic field, respectively, symmetric dimer nuclear spin wavefunctions arise when the reactant nuclear spins are conserved during the reaction process. To further test this hypothesis, we experimentally varied the magnetic field between 5 and 50 Gauss to alter the initial spin composition of the reactants. We observed corresponding changes of the rotational state parity of the dimers as a function of magnetic field, in accordance with nuclear spin conservation.

The establishment of nuclear spin conservation in the reaction under study reduces the state space of all possible outcomes at 30 G. However, the data shown in Fig. 1 does not yet give the full state-to-state reaction information needed to study the underlying reaction dynamics. To gain the full picture experimentally, we need to detect the two reaction products in coincidence from the same reaction events. For this purpose, we developed a state-resolved coincidence detection scheme, which involves three main steps: simultaneous state-selective ionization of K_2 and Rb_2 via laser pulses, velocity-map imaging (VMI) of the resulting ions, and determination of the number of K_2^+ and Rb_2^+ ion pairs which are associated with the same reaction events. Each simultaneous observation of a K_2^+ and a Rb_2^+ ion is further screened by the conservation of linear momentum, which

requires $\vec{P}_{K_2} + \vec{P}_{Rb_2} = 0$ ("zero" due to the nearly zero reactant velocity at ultracold temperatures), for product pairs from the same event. In our system, the momentum components transverse to the time-of-flight (TOF) axis are mapped to spatial positions on an ion detector through VMI, while the component along this axis is encoded in the ion TOF, which allows us to screen for momentum conservation in all directions. With this technique in hand, we accumulated data for all the state-pairs that satisfy parity and angular momentum conservation, and which are positioned around or below the 10 cm^{-1} exothermicity. We found 57 state pairs with positive signals. The overall data presented in Fig. 2(A) took approximately 3 months of nearly continuous accumulation. While an exact quantum calculation of the distribution outcome is beyond the current state-of-the-art, the fact that a long-lived reaction complex (360 ns lifetime) exists suggests that the reaction could explore all possible exit channels with equal probability. We use such a statistical intuition to build a state-counting model for comparison. The main non-trivial factor is to account for the number of degenerate channels arising from a lack of detection of the orbital angular momentum of the product escape (the orbital angular momentum, along with the rotational states of K_2 and Rb_2, have to add up to 1 to conserve angular momentum.) We perform such a comparison using the likelihood ratio test and find that, once 7 deviating state-pairs (out of 57) are removed, the observed distribution agrees with the state-counting model. The completeness of our measurements provides a valuable benchmark for quantum dynamics calculations beyond the current state-of-the-art.

Future Plans:
Our efforts so far have focused on KRb molecule-molecule reactions. One reason is because

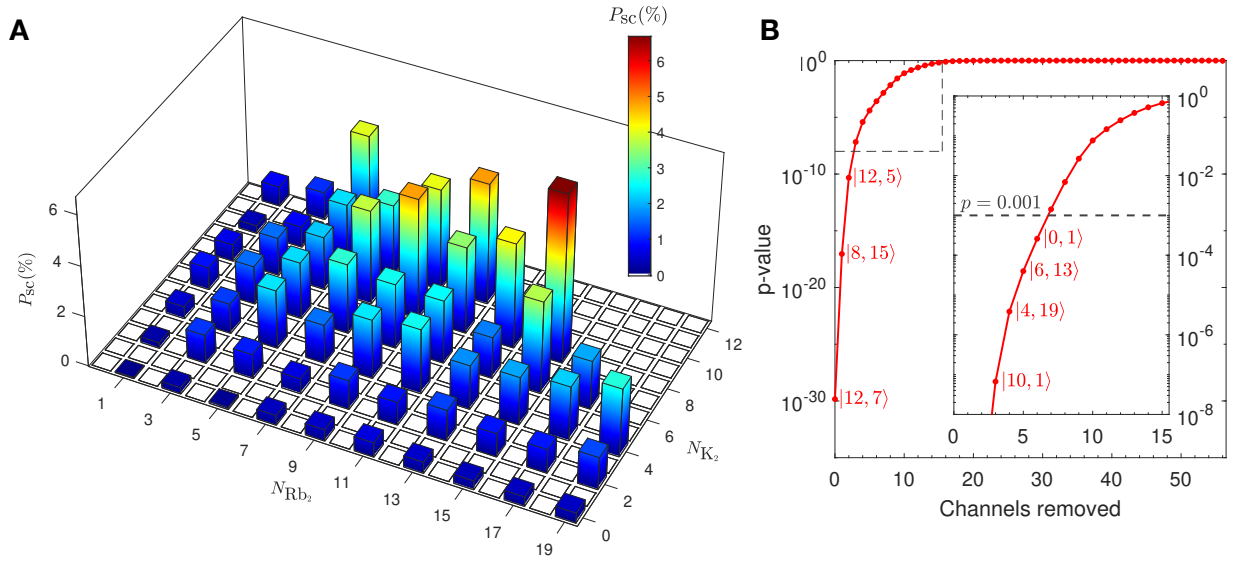

Figure 2: **Full quantum state distribution for the KRb** ($v = 0, N = 0$)**+KRb** ($v = 0, N = 0$) **reaction, and comparison to a state-counting model**. **A** Scattering probability (P_{sc}) of each quantum state-pair for the full range of rotational states of K_2 and Rb_2. P_{sc} is large for state pairs with large and similar quantum numbers. **B** p-value for the hypothesis that the measured and state-counting model distributions agree, as state-pairs that deviate most significantly from the prediction are successively removed.

the exothermicity of the reaction is small, 10 cm^{-1}, which, as we have demonstrated, makes it feasable to map out the complete product quantum state distribution. However, an exact quantum calculation for such a reaction involving 4 heavy atoms is still far beyond the current state-of-the-art. Atom-molecule reactions involving 3 atoms, on the other hand, are theoretically tractable [3]. To provide better comparisons between experiment and theory, we aim to investigate the atom-molecule reactions/collisions, K+KRb and Rb+KRb, where the reactions are exothermic and endothermic, respectively, by 100-200 cm^{-1}. A challenge is that there are vastly more possible exit channels, and mapping out the full outcome could be time consuming. To take data within a realistic time span, we aim to increase our data rate by employing a pulsed ionization laser with a faster repetition rate (from a few kHz to 10s or 100 kHz). Ultimately this will enable investigation of the reaction complex, as well as the ability to obtain state-to-state reaction resolution for the ultracold atom-molecule system.

References to publications of DOE sponsored research:

(1) M.-G. Hu*, Y. Liu*, D. D. Grimes, Y.-W. Lin, A. H. Gheorghe, R. Vexiau, N. Bouloufa-Maafa, O. Dulieu, T. Rosenband, and K.-K. Ni. Direct Observation of Bimolecular Reactions of Ultracold KRb Molecules, Science 366, 1111 (2019)

(2) Y. Liu*, D. D. Grimes*, M.-G. Hu*, K.-K. Ni Probing Ultracold Chemistry using Ion Spectrometry, Phys. Chem. Chem. Phys. 22, 4861-4874 (2020)

(3) Y. Liu*, M.-G. Hu*, M. A. Nichols, D. D. Grimes, Tijs Karman, Hua Guo, K.-K. Ni. Steering ultracold reactions through long-lived transient intermediates, Nature Physics 16, 1132-1136 (2020)

(4) M.-G. Hu*, Y. Liu*, M. A. Nichols, L. Zhu, G. Quemener, O. Dulieu, and K.-K. Ni. Nuclear spin conservation enables state-to-state control of ultracold molecular reactions, Nature Chemistry (2020) https://doi-org.ezp-prod1.hul.harvard.edu/10.1038/s41557-020-00610-0

(5)Y. Liu*, M.-G. Hu*, M. A. Nichols, D. Yang, D. Xie, H. Guo, K.-K. Ni. Precision test of statistical dynamics with state-to-state ultracold chemistry, arXiv:2012.15842 (2020)

Reference

[1] Ming-Guang Hu, Yu Liu, Matthew A Nichols, Lingbang Zhu, Goulven Quéméner, Olivier Dulieu, and Kang-Kuen Ni. Nuclear spin conservation enables state-to-state control of ultracold molecular reactions. Nature Chemistry, 2020.

[2] Yu Liu, Ming-Guang Hu, Matthew A. Nichols, Dongzheng Yang, Daiqian Xie, Hua Guo, and Kang-Kuen Ni. Precision test of statistical dynamics with state-to-state ultracold chemistry, 2020.

[3] JFE Croft, Constantinos Makrides, M Li, A Petrov, BK Kendrick, N Balakrishnan, and S Kotochigova. Universality and chaoticity in ultracold k+ krb chemical reactions. Nature communications, 8:15897, 2017.

Chemical Kinetic Modeling of Combustion Chemistry

William J. Pitz, Charles K. Westbrook
Lawrence Livermore National Laboratory, P.O. Box 808, Livermore, CA 94550
pitz1@llnl.gov

1. Program Scope

We develop chemical kinetic reaction models to describe the combustion of hydrocarbons and other related fuels, including bio-derived fuels. The models also describe reactions important for the formation of emissions such as PAHs. These models are validated through comparisons between simulated and experimental results in carefully controlled laboratory-scale facilities including shock tubes, stirred reactors, flow reactors, premixed flames, diffusion flames, and rapid compression machines. After validation, these models are then used to understand more complex combustion phenomena in practical combustion systems. We identify particularly sensitive parts of these models and provide that information to other DOE/GPCP researchers who can use theory and new experiments to refine the kinetic models. We try to anticipate kinetic modeling needs of the DOE combustion community, so other researchers can have accurate models to assist in their own research projects. Our kinetic models are freely available at https://combustion.llnl.gov/ and provide a valuable service to the combustion community.

2. Recent Progress

We participated in four papers for a special journal issue in honor of Joe Michael. The first study was a chemical kinetic and experimental study on n-butylcyclohexane which is a surrogate compound to represent cycloalkanes in jet and diesel fuels [1]. This compound was examined in shock tube and rapid compression machine experiments for ignition delay times (IDTs). Based on the chemical kinetic simulations with a new kinetic model, it was identified that quantum chemistry calculations are needed to compute RO_2 isomerizations between the ring and the alkyl chain to further reduce the uncertainty in these rate constants and increase the accuracy of the IDT simulations. The second paper [2] investigated the pyrolysis of four straight-chain and branched C3-C4 alkenes (that contain allylic C-H bonds in a single-pulse shock tube. The experiments were simulated with a recently updated chemical kinetic mechanism NUIGMech1.0. The kinetic analyses in the study identified the important reactions for formation of first aromatic ring. The main pathways were found to be propargyl self-recombination, and the recombination of cyclopentadienyl and methyl radicals followed by ring enlargement reactions. The third paper [3] was on shock tube measurements of 1-pentene and 3-methyl-1-butene (3M1B) oxidation in a shock tube at three different equivalence ratios at about 1.4 atm over a temperature range of 1330 to 1880 K, with spectroscopic measurement of water time histories. It was found that 3M1B is more reactive than 1-pentene particularly due to the weak allylic C-H bond in 3M1B which allows for faster H-atom abstraction by active radicals including H, OH, O, HO_2, and CH_3. The fourth paper [4] investigated four large iso-alkanes (iso-octane, iso-nonane, iso-dodecane, and iso-cetane) that are used to represent an alcohol-to-jet-fuel in a high-pressure shock tube over a temperature range of 800 to 1300 K, at an equivalence ratio of ~1.3 and pressures of 4 and 50 bar. The iso-alkanes are blended with n-heptane, a well-characterized fuel. Speciation measurements are compared to a new chemical kinetic model for iso-nonane (2,2,4,4, tetramethylpentane) and iso-dodecane (2,2,4,6,6-pentamethyl heptane), and an updated one for iso-cetane (2,2,4,4,6,8,8 heptamethylnonane). The kinetic model did a good job of representing the experimental data

except for some minor discrepancies for CO and CO_2. To further increase the accuracy of these kinetic models, pressure-dependent rate-constants for their fuel decomposition reactions are needed.

Another area our work focused on developing and improving the chemical kinetic model for formation of PAHs which are important precursors in the formation of soot emissions. Recently, we have developed a reduced mechanism of 43 species for the formation of PAHs that was based on a reaction network derived from our recently improved detailed chemical kinetic PAH model [5]. The reaction network uses repetitive methyl, acetylene, propargyl and radical-radical recombination reactions for describing molecular growth. The arrows in red in Fig. 1 are reaction

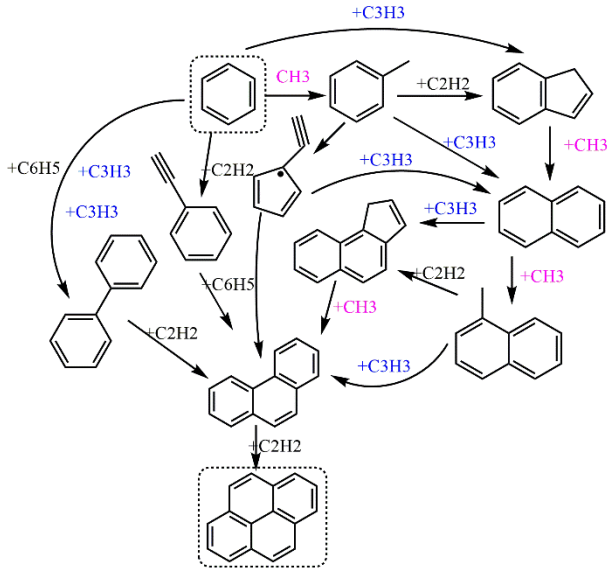

Fig. 1: Formation of pyrene from benzene through the reaction with C1 to C3 species.

paths missing from reduced mechanisms in the literature but included in the present reduced mechanism. With the availability of this updated reduced PAH mechanism, the accuracy of predicting PAH formation in multidimensional reacting flow simulations is enhanced.

We have also recently been updating and improving the chemical kinetic mechanism for n-pentanol which is an interesting fuel component that can be made from biomass and has an intermediate reactivity attractive for use in advanced compression ignition engines. We have updated the thermochemistry of n-pentanol-related species, its reaction rate with OH by analogy recent literature studies on n-butanol and updated other rate constants. We have improved the treatment of its low-temperature chemistry in collaboration with Prof. Labbe at University of Colorado, Boulder. This collaboration allowed the inclusion of pressure-dependent rate constants and of low-temperature paths not present in previous literature mechanisms of n-pentanol. The simulations using the new mechanism are being compared to new experimental IDTs from the rapid compression machine of Prof. Henry Curran's group at the National University of Ireland and to other literature data with favorable results.

We have been investigating the role of NO and NO_2 in promoting or inhibiting autoignition. We updated the Glarborg NOx mechanism [6] with the latest thermodynamic parameters and rate

constants from the literature. To simulate fuel effects, reactions between fuel species and NOx species were added to the updated mechanism. Reactions such as $R\dot{O}_2+NO \Leftrightarrow R\dot{O}+NO_2$ can redirect $R\dot{O}_2$ from a low temperature chain branching path to a chain propagation path and inhibition autoignition. However, the rate constant of this reaction currently is only available when R is a methyl radical, highlighting a need for rate constants for other hydrocarbon radicals. The mechanism also includes recent rate constants for the reaction of $\dot{R}+NO_2 \Leftrightarrow R\dot{O}+NO$ where R = 3-heptyl radical from Prof. Goldsmith's group [7]. Figure 2 compares the simulated and experimental profiles of n-pentane in a jet stirred reactor with NO addition where the inhibiting effect can be seen at low temperatures less than 675K [8].

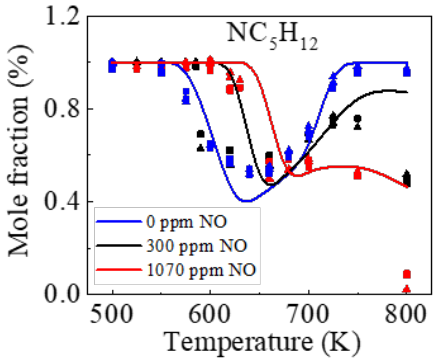

Figure 2: Measured (symbols) and predicted (lines) mole fractions of n-pentane as a function of temperature at 1 atm, equivalence ratio of Φ=0.5 and 1% initial mole fraction of n-pentane [8].

3. Future Plans

In the future, we plan to continue our development of chemical kinetic models for fuel components present in gasoline, diesel and alternative fuels. We also will continue our work on the development of an accurate PAH kinetic model and soot model, and we plan to focus on the oxidation reactions of PAHs.

Acknowledgements

This work was performed under the auspices of the U.S. Department of Energy by Lawrence Livermore National Laboratory under Contract DE-AC52-07NA27344.

References

1-5: See publications 1-5 below.

6. C. A. Almodovar and C. F. Goldsmith, "Laser schlieren study of the thermal decomposition of 2-ethylhexyl-nitrate," Proc. Combust. Inst. 38, 997-1005 (2021).
7. P. Glarborg, J. A. Miller, B. Ruscic and S. J. Klippenstein, "Modeling nitrogen chemistry in combustion," 8. Progress in Energy and Combustion Science 67, 31-68 (2018).
9. H. Zhao, L. Wu, C. Patrick, Z. Zhang, Y. Rezgui, X. Yang, G. Wysocki and Y. Ju, "Studies of low temperature oxidation of n-pentane with nitric oxide addition in a jet stirred reactor," Combust. Flame 197, 78-87 (2018).

Published papers in 2019 to 2021

1. W. J. Pitz, J. Liang, G. Kukkadapu, K. Zhang, C. Conroy, J. Bugler and H. J. Curran, "A detailed chemical kinetic modeling and experimental investigation of the low- and high-temperature chemistry of n-butylcyclohexane," Int. J. Chem. Kinet. 53, 465-475 (2021). **Special issue for Joe Michael.**
2. S. S. Nagaraja, G. Kukkadapu, S. Panigrahy, J. Liang, H. Lu, W. J. Pitz and H. J. Curran, "A pyrolysis study of allylic hydrocarbon fuels," Int. J. Chem. Kinet. 52, 964-978 (2020). **Special issue for Joe Michael.**
3. C. M. Grégoire, C. K. Westbrook, S. A. Alturaifi, O. Mathieu and E. L. Petersen, "Shock-tube spectroscopic water measurements and detailed kinetics modeling of 1-pentene and 3-methyl-1-butene," Int. J. Chem. Kinet. 53, 67-83 (2021). **Special issue for Joe Michael.**
4. J. Guzman, G. Kukkadapu, K. Brezinsky and C. K. Westbrook, "Oxidation of an iso-paraffinic alcohol-to-jet fuel and heptane mixture: an experimental and modelling study," Int. J. Chem. Kinetics, accepted (2021). **Special issue for Joe Michael.**
5. G. Kukkadapu, S. W. Wagnon, W. J. Pitz and N. Hansen, "Identification of the Molecular-Weight Growth Reaction Network in Counterflow Flames of the C_3H_4 Isomers Allene and Propyne," Proc. Combust. Inst. 38, 479-488 (2021).
6. N. Hansen, G. Kukkadapu, B. Chen, S. Dong, H. J. Curran, C. A. Taatjes, A. J. Eskola, D. L. Osborn, L. Sheps, W. J. Pitz, K. Moshammer, A. W. Jasper, W. Chen, J. Yang and Z. Wang, "The Impact of the Third O_2 Addition Reaction Network on Ignition Delay Times of neo-Pentane," Proc. Combust. Inst. 38, 299-307 (2021).
7. S. Panigrahy, J. Liang, S. S. Nagaraja, Z. Zuo, G. Kim, S. Dong, G. Kukkadapu, W. J. Pitz, S. S. Vasu and H. J. Curran, "A comprehensive experimental and improved kinetic modeling study on the pyrolysis and oxidation of propyne," Proc. Combust. Inst. 38, 479-488 (2021).
8. S. S. Nagaraja, J. Liang, S. Dong, S. Panigrahy, A. Sahu, G. Kukkadapu, S. W. Wagnon, W. J. Pitz and H. J. Curran, "A hierarchical single-pulse shock tube pyrolysis study of C2–C6 1-alkenes," Combust. Flame 219, 456-466 (2020).
9. S. S. Nagaraja, J. Power, G. Kukkadapu, S. Dong, S. W. Wagnon, W. J. Pitz and H. J. Curran, "A single pulse shock tube study of pentene isomer pyrolysis," Proc. Combust. Inst. 38, 881-889 (2021).
10. S. Dong, K. Zhang, E. M. Ninnemann, A. Najjar, G. Kukkadapu, J. Baker, F. Arafin, Z. Wang, W. J. Pitz, S. S. Vasu, S. M. Sarathy, P. K. Senecal and H. J. Curran, "A comprehensive experimental and kinetic modeling study of 1- and 2-pentene," Combust. Flame 223, 166-180 (2021).
11. S. Dong, C. Aul, C. Gregoire, S. P. Cooper, O. Mathieu, E. L. Petersen, J. Rodriguez, F. Mauss, S. W. Wagnon, G. Kukkadapu, W. J. Pitz and H. J. Curran, "A comprehensive experimental and kinetic modeling study of 1-hexene," Combust. Flame, accepted, (2021).
12. A. R. Laich, E. Ninnemann, S. Neupane, R. Rahman, S. Barak, W. J. Pitz, S. S. Goldsborough and S. S. Vasu, "High-pressure shock tube study of ethanol oxidation: Ignition delay time and CO time-history measurements," Combust. Flame 212, 486-499 (2020).
13. C. Saggese, C. M. Thomas, S. W. Wagnon, G. Kukkadapu, S. Cheng, D. Kang, S. S. Goldsborough and W. J. Pitz, "An improved detailed chemical kinetic model for C3-C4 linear and iso-alcohols and their blends with gasoline at engine-relevant conditions," Proc. Combust. Inst. 38, 415-423 (2021).
14. S. Cheng, D. Kang, S. S. Goldsborough, C. Saggese, S. Wagnon and W. J. Pitz, "Experimental and modeling study of C2-C4 alcohol autoignition at intermediate temperature conditions," Proc. Combust. Inst. 38, 611-619 (2021).
15. S. Dong, K. Zhang, P. K. Senecal, G. Kukkadapu, S. W. Wagnon, S. Barrett, N. Lokachari, S. Panigaphy, W. J. Pitz and H. J. Curran, "A comparative reactivity study of 1-alkene fuels from ethylene to 1-heptene," Proc. Combust. Inst. 38, 611-619 (2021).
16. N. Lokachari, S. Panigrahy, G. Kukkadapu, G. Kim, S. S. Vasu, W. J. Pitz and H. J. Curran, "The influence of iso-butene kinetics on the reactivity of di-isobutylene and iso-octane," Combust. Flame 222, 186-195 (2020).
17. C. S. Mergulhão, H.-H. Carstensen, H. Song, S. W. Wagnon, W. J. Pitz and G. Vanhove, "Probing the antiknock effect of anisole through an ignition, speciation and modeling study of its blends with isooctane," Proc. Combust. Inst. 38, 739-748 (2021).

OPTICAL PROBES OF ATOMIC AND MOLECULAR DECAY PROCESSES

S.T. Pratt
Building 200, B-125
Argonne National Laboratory
9700 South Cass Avenue
Lemont, Illinois 60439
E-mail: stpratt@anl.gov

PROGRAM SCOPE

Molecular photoabsorption, photoionization, and photodissociation dynamics can reveal how energy and angular momentum flow among the electronic, vibrational, and rotational degrees of freedom in isolated, highly energized molecules. This project is focused on these dynamics in small molecules, with the goal of determining the mechanisms of these decay processes and their product branching distributions. With the growing interest in using high-harmonic sources and free-electron lasers to probe inner-valence and core-shell processes, we are increasingly focusing on interactions among multiple electronic states and electronic autoionization processes. A second aspect of this work involves the determination of absolute photoabsorption and photoionization cross sections, as well as the general principles that determine them. The experimental approach uses both laboratory-based laser techniques for single- and multiphoton excitation of valence-shell processes, and facilities-based vacuum-ultraviolet (VUV) and x-ray techniques for the excitation of both valence-shell and inner-shell processes. The detection methods include mass spectrometry, photoion- and photoelectron-imaging, high-resolution photoelectron spectroscopy, photoelectron-photoion coincidence techniques, and VUV Fourier-transform absorption spectroscopy. Time-domain experiments enabled by new VUV and x-ray free electron laser (FEL) sources are being performed to complement ongoing frequency-domain work.

RECENT PROGRESS

The current effort is focused on three general areas: the photoabsorption and photoionization of molecular nitrogen; inner-valence and inner-shell spectroscopy of small polyatomic molecules; and the photoabsorption and photoionization of acetylene, larger alkynes, and their fragments. While new experimental work has been hindered in the past year, particularly with the loss of several expected beamtimes, some new experiments have been performed virtually, and a significant effort has been made is analyzing data from earlier experiments. I have also expanded my research into areas involving time-resolved photoionization and photodissociation studies.

Photoionization of Molecular Nitrogen

I continue to work on the comprehensive analysis of the valence-shell photoabsorption and photoionization of molecular nitrogen. This work combines data from double-resonance studies in my laboratory at Argonne, synchrotron studies using photoabsorption and photoelectron-photoion coincidence techniques, and theoretical studies in collaboration with Ch. Jungen (Orsay). In collaboration with Ubachs (Amsterdam) and Jungen, experiments were scheduled to use the VUV Fourier Transform Spectrometer at SOLEIL to record the absorption spectrum of isotopically substituted $^{15}N_2$ across a broad energy range spanning the Rydberg manifold below the first ionization threshold and extending to above the N_2^+ B $^2\Sigma_u$ threshold. This beamtime was cancelled but, with the help of Nelson de Oliveira (SOLEIL), we were able to record the desired spectra during a virtual beamtime. We now have comprehensive spectra available for the $^{14}N_2$, $^{15}N_2$, and $^{14}N^{15}N$ isotopes. Comparison of these very high-resolution spectra should be a significant help in providing a more detailed assignment of the VUV spectra of this important molecule.

The analysis of an existing time-resolved dataset on the photoionization of N_2 from a previous beamtime at the FERMI FEL with K. Ueda et al. was completed. I helped complete this analysis and wrote the manuscript for publication. In these experiments, the FEL was used to coherently excite a group of Rydberg

and valence states near 15.6 eV, and an infrared laser was used to ionize this group of states as a function of the time delay between the two pulses. The photoelectrons from the ionization process were imaged using a velocity map imaging spectrometer, which provided information on both the energy distributions and angular distributions of the photoelectrons. The states within the initial wavepacket included Rydberg states based on multiple vibrational levels of both the $X\ ^2\Sigma_g^+$ and $A\ ^2\Pi_u$ states of the ion, as well as several vibrational levels of the $b'\ ^1S_u^+$ valence state. Ionization of the wavepacket resulted in oscillating signals in the vibrationally resolved photoelectron spectra, as well as in the angular distributions of those photoelectrons. Examination of the phase and frequency of the oscillations allowed the determination of which states were interacting with each other, and which states were being ionized into the same ionization continuum. Fourier transforms of the transient oscillations provided additional insight into which states were connected to each other. The decay of the oscillating signal also provided insight into the lifetimes of the intermediate states. Unfortunately, the experiments were limited in the time-window that could be accessed for the decay, so that only vibrational and electronic energy spacing were accessible. This work was recently published in the Journal of Chemical Physics. Future experiments with longer time windows could provide much more detailed information on the intermediate states, and the experience gained through these experiments was quite valuable for the experiments on acetylene described below.

Inner-shell and inner-valence processes in methyl iodide and xenon difluoride

I have continued my collaboration with D. Holland (STFC, UK) and R. Forbes (SLAC) on the photoelectron spectroscopy of the inner-shell and inner-valence shells of methyl iodide. New complementary experiments on the ionization of the 4d subshell of CF_3I were postponed because of facility shutdowns. It will be particularly interesting to see how the electronegativity of the F atoms affects both the resonant structure below the 4d thresholds, and the resonant and nonresonant Auger decay processes that follow excitation. In a closely related study, I am currently analyzing our recent data on the photoionization of the Xe 4d shell of XeF_2, which shows remarkable similarities to the corresponding CH_3I structure. Because the 4d photoionization of atomic Xe is so well-studied, the details of how the F atoms influence the electronic structure and decay processes can be readily assessed. We also have detailed information on the shake-up and shake-off structure in the photoionization spectrum. I am currently preparing a manuscript describing this work.

Photoabsorption and Photoionization of Alkynes and Alkynyl Radicals

I have been working on a systematic study of the photoabsorption and photoionization spectra of small alkynes and alkynyl radicals for several years. These efforts continue to focus on the analysis of trends in the VUV absorption spectra of butylacetylene isomers, as well as the analogous pentyl- and hexyl- systems. I am working with L. Harding (Argonne) to see if theoretical calculations can reproduce the observations and provide an understanding of the trends that are observed in the spectra. I am also continuing to work on the photoionization of the C_4H_5 radical isomers and related species. Finally, as discussed below, I am also working on the photoabsorption and photoionization spectra of acetylene. The focus of this work is on the elucidating electronic and vibrational relaxation processes in excited states.

FUTURE PLANS

Recently, I led a virtual beamtime at the FERMI free-electron laser (FEL) to perform pump-probe experiments on acetylene using a 200-nm pulse to excite the trans-bent A state, and a 15.6 eV or 20.8 eV pulse from the FEL to probe the time-resolved dynamics on the 200 fs to 600 ps timescale. A magnetic bottle electron spectrometer was used to collect the resulting photoelectron spectra and mass spectra. The goal was to see if we could observe and characterize the time-dependent behavior leading to time-dependent ionization dynamics within the A state, internal conversion to high vibrational levels of the electronic ground state, intersystem crossing into the triplet manifold, or isomerization to the vinylidene structure. The use of a 16 eV probe enabled by the FEL should allow the observation of all of these potential decay channels, and provide new insight into the dynamics of this fundamental molecule. The preliminary analysis of the data has only just begun, clear time-dependent features are observed in both the photoelectron spectra

and the mass spectra, and the spectra show different behaviors with the two different FEL energies. We are optimistic about this potential of this approach to provide additional insight into excited state dynamics, and the more complete analysis of the data will continue in the coming year. I am also participating in a beamtime proposals to XFEL to study dissociation dynamics in methyl iodide, and to the LCLS to study the dynamics of two-site double-core excitation in N_2O. The former experiments will make use of the data generated in our earlier studies of inner-valence excitation of methyl iodide. The latter experiments on the characterization of the doubly excited states of N_2O is closely connected to the understanding of shake-up processes in resonant Auger decay that is being addressed in the experiments on XeF_2.

A number of synchrotron beamtimes originally scheduled for 2020 have optimistically been rescheduled for late 2021. First, we have two beamtimes on the PLEIADES beamline at SOLEIL to characterize the inner-valence spectroscopy of CF_3I, CH_3Br, and CH_3Cl, and to use these with our existing data on CH_3I to provide a systematic description of how the structure and dynamics depends on the nature of the halogen atom and substitution on the methyl site. Second, we have beamtime at the MAX IV synchrotron to extend our initial experiments on the inner- and outer-valence-shell ionization of imidazole to the methylimidazole isomers. This work is an attempt to see how feasible it is to extend the methods and approach to biologically relevant molecules. Third, we have beamtime scheduled on the DESIRS beamline to attempt to make an accurate determination of the absolute photoionization cross section of the iodine atom just above threshold. This cross section has been used in the determination of photoionization cross sections for a number of radicals because it is straightforward to photodissociate the precursor iodide molecules and photoionize both fragments. The absolute cross section for iodine atom then allows the determination of the radical cross section. We plan to perform new laboratory measurements on the photodissociation of the four butyl iodide molecules to obtain absolute photoionization cross sections for the four butyl radical isomers. In this case, even a determination of the relative photoionization cross sections of the butyl radicals would be useful for the analysis of some kinetics measurements. We also hope to extend these measurements to larger alkyl radicals, as well as to unsaturated radicals.

I will continue to work on a more comprehensive analysis of the photoabsorption and photoionization spectra of molecular nitrogen, bringing together results from laser-based double-resonance spectroscopy, synchrotron studies, and theory. Comparison of the new data on the absorption spectra of $^{15}N_2$ and $^{14}N^{15}N$ and our existing data on $^{14}N_2$ should be of considerable help for the assignment of all three spectra. At this time, my collaboration with Jungen should be particularly valuable, as his multichannel quantum defect theory calculations will ultimately be essential for a global assignment of the data.

Finally, I will continue to work on the analysis of existing absorption data on a series of butyl-acetylene molecules and related molecules, as well as on the analysis of more detailed high-resolution photoabsorption datasets on acetylene, ammonia, and nitric oxide.

ACKNOWLEDGEMENTS

I have been fortunate to collaborate with several teams of people on the experiments at SOLEIL, MAX IV, and FERMI. Work at Soleil was performed in collaboration with S. Boyé-Péronne and B. Gans (ISMO, Orsay), J. -C. Loison (Bordeaux), D. M. P. Holland (STFC, Daresbury), R. Forbes (SLAC), I. Powis (Nottingham), and J. Bozek, G. Garcia, L. Nahon, and N. de Oliveira (all from SOLEIL). Work at MAX IV was performed with Holland, Powis, and M. Patanen (University of Oulu). The previous work at FERMI on He and N_2 was performed in collaboration with a large international group of researchers led by K. Ueda (Tohoku University, Japan). New work at FERMI was performed in collaboration with Holland, Powis, K. Reid (Nottingham), R. Minns (Southampton), and C. Vozzi (Milano). Theoretical work on N_2 was performed in collaboration with Ch. Jungen (Laboratoire Aimé Cotton). This work was supported by the U.S. Department of Energy, Office of Science, Office of Basic Energy Sciences, Division of Chemical Sciences, Geosciences, and Biological Sciences under contract No. DE-AC02-06CH11357.

DOE-SPONSORED PUBLICATIONS SINCE 2019

1. A. Sen and S. T. Pratt, Double-resonance studies of electronically autoionizing states of molecular nitrogen, Mol. Phys. **117**, 2930-2940 (2019). DOI: 10.1080/00268976.2018.1544672

2. H. R. Hrodmarsson, J.-C. Loison, U. Jacovella, D. M. P. Holland, S. Boyé-Péronne, B. Gans, G. A. Garcia, L. Nahon, and S. T. Pratt, Valence-shell photoionization of the C_4H_5 radical, J. Phys. Chem. A **123**, 1521-1528 (2019).

3. B. Gans, G. A. Garcia, S. Boyé-Péronne, S. T. Pratt, J.-C. Guillemin, A. Aguado, O. Roncero, and J.-C. Loison, Origin band of the first photoionizing transition of hydrogen isocyanide, Phys. Chem. Chem. Phys. **21**, 2337-2344 (2019).

4. O. J. Harper, M. Hassenfratz, J.-C. Loison, G. A. Garcia, N. de Oliveira, H.R. Hrodmarsson, S. T. Pratt, S. Boyé-Péronne, and B. Gans, Quantifying the photoionization cross section of the hydroxyl radical, J. Chem. Phys. **150**, 141103 (2019) DOI: 10.1063/1.5091966

5. A. B. Trofimov, A. M. Belogolova, S. A. Serebrennikova, R. Forbes, S. T. Pratt, and D. M. P. Holland, An experimental and theoretical study of the C 1s ionization satellites in CH_3I, J. Chem. Phys., **150**, 224303 (2019).

6. V. Makhija, K. Véyrinas, A. E. Boguslavskiy, R. Forbes, I. Wilkinson, R. Lausten, S. P. Neville, S. T. Pratt, M. S. Schuurman, and A. Stolow, Ultrafast molecular frame electronic coherences from lab frame scattering anisotropies, J. Phys. B **53**, 114001 (2020).

7. R. Forbes, S. T. Pratt, A. De Fanis, A. R. Milosavljević, C. Nicolas, J. D. Bozek, N. A. Besley, and D. M. P. Holland, Photoabsorption, photoionization, and auger processes at the carbon K-edge in CH_3I, Phys. Rev. A **101**, 023408 (2020).

8. R. Forbes, A. De Fanis, D. Rolles, S. T. Pratt, I. Powis, N. A. Besley, A. R. Milosavljević, C. Nicolas, J. D. Bozek, and D. M. P. Holland, Photoionization of the I 4d and valence orbitals of methyl iodide, J. Phys. B **53**, 155101 (2020).

9. S. Hartweg, J. -C. Loison, S. Boyé-Péronne, B. Gans, D. M. P. Holland, G. A. Garcia, L. Nahon, and S. T. Pratt, Photoionization of the C_4H_5 isomers, J. Phys. Chem. A **124**, 6050-6060 (2020).

10. H. R. Hrodmarsson, B. Gans, S. Boyé-Péronne, G. A. Garcia, L. Nahon, S. T. Pratt, D. M. P. Holland, The effect of autoionization on the HBr^+ $^2\Pi_{3/2,1/2}$ state photoelectron angular distributions, Chem. Phys. **539**, 110961 (2020).

11. M. Fushitani, S. T. Pratt, D. You, S. Saito, Y. Luo, K. Ueda, H. Fujise, A. Hishikawa, H. Ibrahim, F. Légaré, P. Johnsson, J. Peschel, E. R. Simpson, A. Olofsson, J. Mauritsson, P. A. Carpeggiani, P. K. Maroju, M. Moioli, D. Ertel, R. Shah, G. Sansone, T. Csizmadia, M. Dumergue, N. G. Harshitha, S. Kühn, C. Callegari, O. Plekan, M. Di Fraia, M. Danailov, L. Giannessi, L. Raimondi, M. Zangrando, G. De Ninno, P. R. Ribic, and K. C. Prince, Time-resolved photoelectron imaging of complex resonances in molecular nitrogen, J. Chem. Phys. **154**, 144305 (2021).

Reaction Mechanisms Studied with Chirped-Pulse Rotational Spectroscopy

Kirill Prozument
Argonne National Laboratory
Chemical Sciences and Engineering Division
Lemont, IL 60439
prozument@anl.gov

1. Scope of the Program

The goal of the Program is to gain detailed understanding of the dynamical processes that govern chemical reactivity. Oftentimes, the rates predicted for even simple reactions are in disagreement with experimental observations. The discrepancy may arise because such effects as roaming dynamics, tunneling reaction mechanism, lack of thermal equilibration of reaction intermediates and others are often neglected in kinetics models. We investigate the pyrolysis and photolysis reactions that help us reveal these mechanisms. We aim at generalizing our findings to broad classes of reactions. The experimental approach in this Program is based on chirped-pulse Fourier transform millimeter-wave (CP-FTmmW) spectroscopy. The reaction products are detected non-destructively, with quantum state specificity and time resolution. Because CP-FTmmW spectroscopy is also quantitative, branching ratios are measured and can be compared with theoretical models. The versatility of the CP-FTmmW technique is sufficient for its application to a wide range of experiments in reaction dynamics and kinetics in the gas phase. The program is currently focused of two experimental directions: i) investigation of pyrolysis chemistry in the microtubular reactor at 1000–1800 K, and ii) *in situ* time-resolved chirped-pulse spectroscopy of photoproducts at room temperature. The third direction of the Program is development of the Artificial Intelligence (AI) methods for automation of spectroscopic assignment. The need for that component is pressing as vast amounts of potentially useful spectroscopic data are generated in broadband rotational experiments, but rarely are fully analyzed. The goal of the AI thrust is that vast amounts of *spectroscopic* data becomes the *chemical* information, ready for reaction mechanisms discovery.

2. Recent Progress

MET: Modeling, Experiment, Theory paradigm

With colleagues at the Gas-Phase Chemical Dynamics group, we have demonstrated the power of the joint Modeling (Sivaramakrishnan), Experiment (Prozument), Theory (Klippenstein) approach to discovering the chemical dynamics phenomena.[1] The case study was the pyrolysis of acetone. Although the thermal decomposition of acetone had been studied for about 90 years, our MET approach has revealed the new mechanisms of substitution by H-atom and settled disagreements about the role of the enol form of acetone that existed in the literature. Active Thermochemical Tables (ATcT) by Ruscic provided the accurate equilibrium constant for the keto/enol concentration. Experimental observation of acetaldehyde as a product was a surprise that spurred

the theoretical and modeling efforts. Our hypothesis was that the substitution reaction H + $CH_3C(O)CH_3 \rightarrow CH_3CHO + CH_3$ was responsible for the observed CH_3CHO product.

The substitution reactions are known, but often overlooked mechanisms in the gas-phase chemistry. The theory by Klippenstein proposed the "well-skipping" homolytic substitution mechanism in which an H-atom is added to the carbonyl carbon atom of acetone to form a transient complex $CH_3CH(O)CH_3$* (< 1 ps lifetime) that cannot stabilize in its potential well, but immediately proceeds to form the $CH_3CHO + CH_3$ products. The kinetic model by Sivaramakrishnan with incorporated substitution mechanism correctly predicts the $[CH_3CHO]:[CH_2CO] = 0.03$ branching ratio measured by the CP-FTmmW spectroscopy (CH_2CO is a major product of the abstraction reaction in the pyrolysis of acetone). Well-skipping is apparently a ubiquitous but underappreciated phenomenon in gas-phase chemical physics, and this MET work elucidates an important class of these reactions – the well-skipping homolytic substitution.

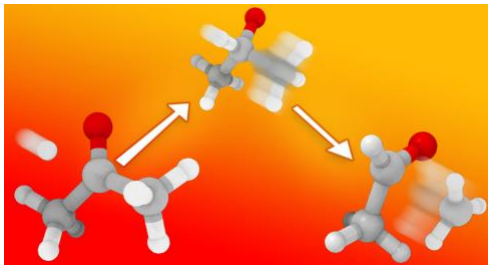

Our theory shows that keto-enol tautomerization $CH_3C(O)CH_3 \leftrightarrow CH_2C(OH)CH_3$ with the 65 kcal/mol barrier is significantly more accessible in the 1500–1800 K pyrolysis than the next pathway, which is a simple bond fission to $CH_3 + CH_3CO$ at 83 kcal/mol. Based on that, the model predicts the central role of the enol form of acetone in its pyrolysis, confirmed by the CP-FTmmW detection of the corresponding products propene, propyne, and water.

Time-Resolved Kinetic Chirped-Pulse (TReK-CP) spectroscopy

Our new 260 – 290 GHz CP-FTmmW spectrometer has demonstrated a remarkable improvement in sensitivity in the TReK-CP experiments compared to the previously employed[2] 75 – 110 GHz band spectrometer. It has been shown in our previous work, that HCCCN product of CH_2CHCN photodissociation at 193 nm results in sequential loss of two hydrogen atoms. The system has just enough energy for the second step $CH_2CCN \rightarrow H + HCCCN$, thus yielding relatively cold HCCCN. We are now able to detect HCCCN in multiple vibrational states *immediately* after the laser pulse while collisions with the bath gas are normally required to rotationally cool reaction products. We believe this is the first time when truly nascent reaction products, prior to any collisions, are sampled with rotational spectroscopy.

Automated Identification of Molecules in Broadband Rotational Spectra

Previously, the PI and his postdoctoral associate Daniel Zaleski have demonstrated the potential of using machine learning to extract the rotational constants from broadband rotational spectra.[3] The next challenge is to find an efficient way of predicting the likely chemical identity from those constants. One of the ways of solving this inverse problem is to compare, using machine learning methods, the results of the prediction of the rotational constants to the database of molecules labeled with their structures and rotational constants. To that end, we have developed a tool that converts the SMILES codes for molecules used in many databases to molecular geometries. Because rotational spectroscopy is uniquely sensitive to molecular conformers the developed program searches the conformational landscape of each SMILES and calculates the geometry and electronic structure of each conformer. Another way of identifying the molecules by their spectra is to directly

compare a spectrum of an unknown molecule to the database of molecules labeled with spectra. In order to facilitate that, an efficient way of comparing rotational spectra is required. In collaboration with Davis, we have been developing the method of comparing spectra using the computational optimal transport (OT). OT proved to be a versatile approach suitable for quantifying the closeness between theoretical stick spectra (with the same or different number of lines), and between a stick spectrum and a broadened experimental spectrum.

3. Future Plans

The next direction in the pyrolysis experiments is to approach oxidation chemistry. Modifications to the pyrolysis microreactor are underway to prevent its decomposition at elevated temperatures by O_2. Preliminary experiments show that oxidation of ethylene gives rich distribution of reaction products. We plan to apply the MET paradigm to study that chemistry. The nascent HCCCN photoproducts will be explored with the upgraded TReK-CP experiment. Is it possible to measure the kinetic energy of HCCCN by accurately measuring Doppler broadening? We plan to continue building the molecular database labeled with spectroscopic parameters to implement AI-assisted identification of molecules in collaboration with Balaprakash from MCS Division at Argonne.

References

1. Zaleski, D. P.; Sivaramakrishnan, R.; Weller, H. R.; Seifert, N. A.; Bross, D. H.; Ruscic, B.; Moore, K. B.; Elliott, S. N.; Copan, A. V.; Harding, L. B.; Klippenstein, S. J.; Field, R. W.; Prozument, K., Substitution Reactions in the Pyrolysis of Acetone Revealed through a Modeling, Experiment, Theory Paradigm. *J. Am. Chem. Soc.* 143, 3124–3142 (2021)

2. Zaleski, D. P.; Harding, L. B.; Klippenstein, S. J.; Ruscic, B.; Prozument, K., Time-Resolved Kinetic Chirped-Pulse Rotational Spectroscopy in a Room-Temperature Flow Reactor. *J. Phys. Chem. Lett.* 8, 6180−6188 (2017)

3. Zaleski, D. P.; Prozument, K., Automated assignment of rotational spectra using artificial neural networks. *J. Chem. Phys.* 149, 104106 (2018)

DOE-Sponsored Publications Since 2019

K. Prozument, J. H. Baraban, P. B. Changala, G. B. Park, R. G. Shaver, J. S. Muenter, S. J. Klippenstein, V. Y. Chernyak, and R. W. Field. “Photodissociation transition states characterized by chirped pulse millimeter wave spectroscopy”, *Proc. Natl. Acad. Sci. U.S.A.* 117, 146−151 (2020)

K. Prozument, B. G. Sartakov, and A. F. Vilesov. “Mixed ortho-H_2 and para-H_2 clusters studied by vibrational coherent anti-Stokes Raman spectroscopy”, *Phys. Rev. B* 101, 184507 (2020)

D. P. Zaleski, R. Sivaramakrishnan, H. R. Weller, N. A. Seifert, D. H. Bross, B. Ruscic, K. B. Moore III, S. N. Elliott, A. V. Copan, L. B. Harding, S. J. Klippenstein, R. W. Field, and K. Prozument, “Substitution Reactions in the Pyrolysis of Acetone Revealed through a Modeling, Experiment, Theory Paradigm”, *J. Am. Chem. Soc.* 143, 3124–3142 (2021)

Ultrafast Transient Absorption Spectroscopy of Hydrocarbon Radicals

Melanie Reber
Department of Chemistry
University of Georgia, Athens, GA 30602
mreber@uga.edu

Project Scope

We aim to i) complete an ultrafast cavity-enhanced transient absorption spectrometer and incorporate two sources of radicals in molecular beams and ii) study the excited state dynamics of vinyl radical and allyl radical. The spectrometer consists of a home-built Ytterbium fiber laser frequency comb and Ytterbium fiber chirped-pulse amplification system that generates ultrafast (about 100 fs pulse duration) pulses across much of the visible region. This light is split into pump and probe beams and coupled into enhancement cavities housed in a vacuum chamber. Lock-in detection and noise subtraction techniques are used for noise suppression. With the increase in signal-to-noise with these techniques, it will be possible to perform ultrafast transient absorption spectroscopy in the visible and near-IR spectral regions of radical intermediates in molecular beams. The first goal is to demonstrate the ability to take ultrafast transient absorption spectroscopy of the electronically excited states of radical intermediates.

The second goal is to study the excited state dynamics of vinyl, C_2H_3, and allyl, C_3H_5, radicals. The first excited state of allyl radical exhibits a broad absorption and is thought to connect to the ground state through several conical intersections. The upper state lifetime is less than 5 ps and excitation of this state results in the release of a hydrogen atom through an unknown mechanism. Direct, time-resolved absorption spectroscopy could elucidate this mechanism. Similarly, the first excited state of vinyl radical has picosecond lifetimes, with a decrease in lifetimes with higher vibrational excitation. The frequency-resolved spectroscopy has the signature of ultrafast predissociation from the ground state. We hope to gain insight into these processes in vinyl radical with ultrafast transient absorption spectroscopy. This work will advance our knowledge of excited state processes in combustion intermediates and reactive species.

Recent Progress

The cavity-enhanced transient absorption spectrometer was under construction in Fall 2019 when this project started. The major recent activities included (i) improving the cavity-enhanced transient absorption spectrometer, (ii) modeling the differential pumping system and (iii) simulating spectra and developing spectral analysis tools. These reflect the limitations imposed due to the covid-19 pandemic while still making progress on the project. All of these activities are necessary to complete the first goal of the project of building an ultrafast transient absorption spectrometer to study radicals in molecular beams.

The Ytterbium fiber laser system and chirped-pulse amplification system is operational. During the past year we were able to make improvements to the operation of the Yb:fiber oscillator that resulted in a broader spectra and decreased the pulse duration to as short as 65 fs, which is the limit of our detection. A paper and provisional patent are in progress for this project. We have frequency doubled the light and are optimizing the spectral broadening in a fiber. We therefore have the necessary visible light for first experiments on vinyl and allyl radical. The cavity-enhanced spectrometer includes two enhancement cavities, locking electronics, and the detection scheme. While the locking electronics have been tested and the cavity is set up. The cavity-

enhanced transient absorption spectrometer is nearly up and running, with the vacuum chamber and molecular beam apparatus being the last major components to finish.

The enhancement cavities require near microTorr pressure levels to prevent contamination of optics and minimize cavity dispersion. The optical region is therefore pumped by a turbomolecular pump. To accommodate the high gas flow of a molecular beam, the nozzle region will be pumped by a Roots blower. Then enhancement cavity beams must enter the molecular beam interaction region through small holes, rather than windows, to maintain the high-finesse of the optical cavity and minimize dispersion. Using COMSOL Multiphysics software and the molecular flow module, we are able to compare geometries for the differential pumping. We have run computations on layouts with simple geometries and compared them to analytical solutions. We are now running several test layouts to come up with an optimized design. The designs are then drawn up in Solidworks to check that they fit the optical layout and existing infrastructure. Once this last piece is designed, we will incorporate it into the vacuum chamber and test the entire spectrometer.

In anticipation of the completion of the cavity-enhanced transient absorption spectrometer, we also worked on simulating spectroscopic data. This included simulating transient absorption data of sample molecules with multiple states and lifetimes using Matlab. We also worked on *ab initio* calculations in Gaussian of small molecules and spectral simulations of rovibrational structure in SpecView. With so much simulated data, we developed an algorithm to sort a complex mixture of data, as might happen if a clean synthesis of radicals isn't possible. The algorithm uses spectral fitting and chemometrics techniques and the preliminary results are very promising. Further refinement of this is possible, with the goal of a publication of the algorithm.

Future Plans:

The final step before we can take transient absorption spectra of radicals is the installation of the photolysis source. We will use an excimer laser for the photolysis source, which is on order, and have designs in progress for the integration of this into the ultrafast cavity-enhanced transient absorption spectrometer. We will also implement a moveable nozzle. The nozzle actuators will be motorized to enable optimization of the molecular beam and cavity overlap while the system is under vacuum and is adjustable in the x-, y-, and z-directions.

The ultrafast cavity-enhanced transient absorption spectrometer, once coupled with a photolysis source for generating combustion radicals, will be a powerful new tool for understanding combustion intermediates. Completion of the first phase of the spectrometer is expected within the next few months. We will then start with studying the time-resolved excited state spectroscopy of vinyl and allyl radical. Experiments with a wide range of combustion radicals are planned for the future as well as increasing the spectral range of the spectrometer to include the infrared and mid-infrared region.

Photoinitiated Reactions of Molecules and Radicals in Molecular Beams

Hanna Reisler
Department of Chemistry, University of Southern California
Los Angeles, CA 90089-0482
reisler@usc.edu

Program Scope

The UV photochemistry of organic molecules is a fundamental process that governs reactions in the atmosphere, synthetic chemistry, organic aerosols, and biological damage in living tissues. The ensuing dynamics usually involve pathways that are in competition, such as direct dissociation on excited states, couplings to lower potential energy surfaces, isomerization, and secondary dissociation of products. This program is focused on detailed photochemical mechanisms of alpha-keto carboxylic acids. In the atmosphere, they are destroyed mainly by solar radiation but studying their photochemistry has been surprisingly difficult because of the complexity of their excited electronic states, the many energetically allowed dissociation pathways, and the effects of collisions and secondary reactions on final outcomes.

Recent Progress

Photodissociation of Pyruvic Acid at 351 nm and the role of methylhydroxycarbene

Pyruvic acid (PA, $CH_3COCOOH$), like other alpha-keto carboxylic acids, comprises a carbonyl, a carboxylic group, and an alkyl group, with the carbonyl serving as chromophore. It has multiple sources in Earth's atmosphere, including photo-oxidation of isoprene and direct emissions. Its most stable conformer, cis-keto, has an internal hydrogen bond that influences the evolution of its unimolecular decomposition. The solar actinic flux near the Earth's surface overlaps with the lowest energy absorption band of PA (290-380 nm), which has a maximum around 350 nm. Dissociation via this band, which accesses the S_1 excited state by a $\pi^* \leftarrow n$ transition, has attracted considerable research interest but also some controversy. The primary photoproducts are believed to be CO_2 and methylhydroxycarbene (MHC),[1] although this carbene has never been observed in PA photodissociation. Presumably, it rapidly isomerizes to its most stable isomer – acetaldehyde (Ac), which was the only observed C_2H_4O product. Most of the previous experiments were carried out in static gas cells where nascent products were subject to secondary reactions and prolonged irradiation in solar simulation chambers.

In previous publications, we reported on the photodissociation dynamics of PA initiated on the S_2 and S_3 states and observed by using a combination of velocity map imaging (VMI) and the multiplexed photoionization mass spectrometer (MPIMS) setup developed at the Sandia Combustion Research Facility. The latter technique exploits tunable narrowband VUV radiation at the Advanced Light Source (ALS). In the past year, we summarized for publication results obtained on the photodissociation of PA following excitation to the S_1 state at 351 nm. Our goal was to identify primary products and elucidate the photodissociation mechanism. In addition to $CH_3COCOOH$, we also used $CH_3COCOOD$ (denoted d_1-PA). All the work described below was done in collaboration with David Osborn and carried out at the Advanced Light Source using the MPIMS setup.

By using a combination of high-resolution multiplexed photoionization mass spectrometry and tunable VUV radiation, we achieved the first direct experimental observation of singlet methylhydroxycarbene (MHC) following 351 nm excitation of PA, supporting the decarboxylation mechanism previously proposed. The experiment was done in a flow cell at a He pressure of 4.0 Torr. We find that decarboxylation to MHC + CO_2 represents 97 – 100% of product branching at 351 nm. In addition, we observe vinyl alcohol and acetaldehyde, the two other C_2H_4O isomers, which we attribute to isomerization of the nascent MHC. We also observe a 3 ± 2% yield of the Norrish Type I photoproducts CH_3CO + DOCO, but only from d_1-PA. The possible reaction channels and their heats of reaction are summarized in Table 1. For 351 nm excitation (81.5 kcal mol^{-1}), the excess energy available to products in the lowest-energy decarboxylation pathway (R1, forming CO_2 + MHC) is 37.5 kcal mol^{-1}, which is above the isomerization

barriers connecting MHC to both the acetaldehyde and vinyl alcohol (VA) tautomers. Moreover, we present the first evidence of a bimolecular reaction of MHC in the gas phase, where MHC reacts with pyruvic acid to produce a $C_4H_8O_2$ product. This observation implies that some MHC produced from pyruvic acid in Earth's troposphere will be stabilized and participate in chemical reactions, which should be considered in atmospheric modeling.

Table 1: Possible photodissociation pathways of PA and their heats of reaction evaluated at 0 K.

Reaction		ΔH^0_{rxn} (kcal mol^{-1})	
$CH_3C(O)C(O)OH + h\nu \rightarrow$	$CH_3COH + CO_2$	44.0 ± 1.3	(R1)
	$H_2C{=}CHOH + CO_2$	3.6 ± 0.6	(R2)
	$CH_3CHO + CO_2$	-6.5 ± 0.6	(R3)
	$CH_3C(O)OH + CO$	-2.8 ± 0.6	(R4)
	$CH_3CO + HOCO$	80.4 ± 0.6	(R5)

The MPIMS instrument, which employs tunable photoionization and high mass resolution, allows the detection of products that are stable for longer than about a millisecond and enables quantitative determination of their mole fraction yields. In Figures 1 and 2 we show evidence for the formation of the three C_2H_4O isomers. Figure 1(a) depicts the photoionization of the stable products acetaldehyde and vinyl alcohol at m/z = 44.03. This is the first observation of vinyl alcohol as a photodissociation product of PA. Figure 1(b) shows the CO_2 product at m/z = 44.00. These products are separated by their mass and photoionization (PI) curves. Using the known absolute PI cross-sections of acetaldehyde and vinyl alcohol, we determine that they are formed in the ratio of 2.1 ± 0.4 (favoring acetaldehyde).

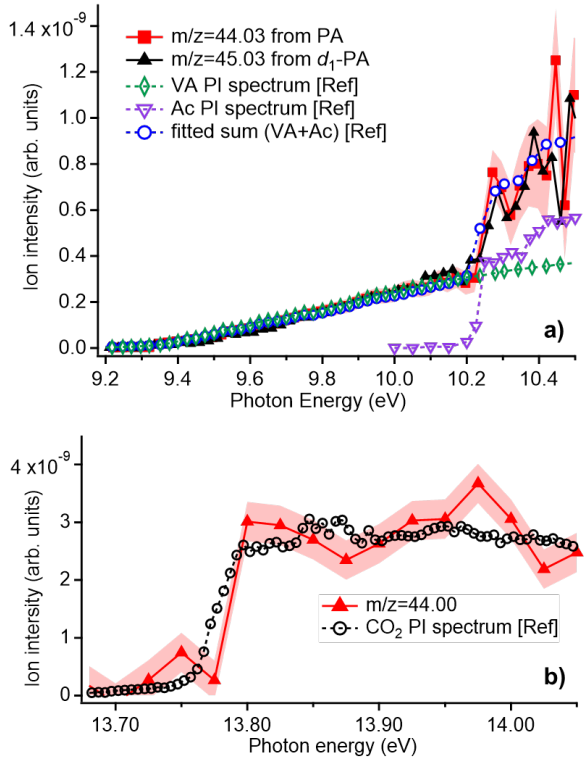

Fig. 1: Photoinization curves of (a) C_2H_4O isomers, and (b) the CO_2 product

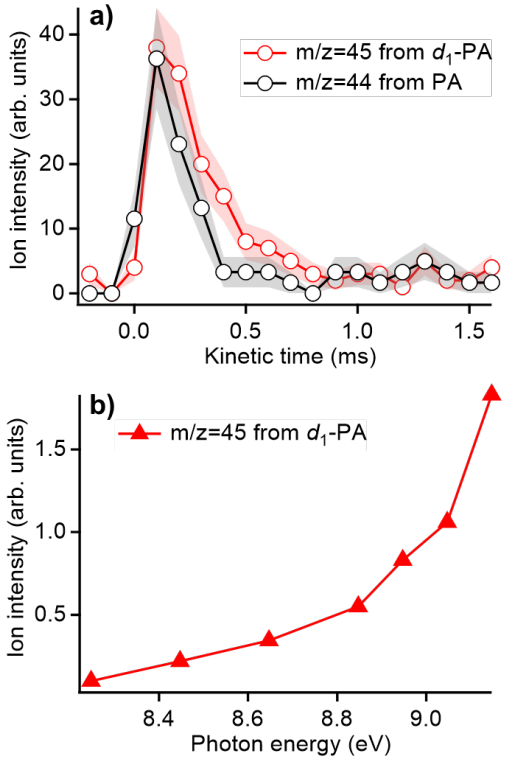

Fig. 2. MHC: (a) kinetic time plot, and (b) photoinization curve from d_1-PA.

At ionization energy IE < 9.1 eV, we observe another C_2H_4O isomer, which we assign as MHC. Whereas the time traces of m/z = 44.03 above ~ 9.2 eV rise with an instrument limited risetime to a plateau, the shape of the time trace changes dramatically at photon energies below 9.1 eV, which is below the IEs of both *syn*- and *anti*-vinyl alcohol (9.30 and 9.17 eV, respectively). Significant signal averaging (~ 1.2×10^6 laser shots) revealed a kinetic time trace with an instrument limited risetime but a fast decay (see Figure 2(a)), implying detection of a very reactive species at m/z = 44.03 for d_0-PA and m/z = 45.03 for d_1-PA. The PI spectrum shown in Figure 2(b) is assigned to d_1-MHC.[2] The nascent MHC photoproducts are likely to have a broad distribution of internal energies. As a result, MHC can decay by isomerization to the other isomers when it has sufficient internal energy to surmount the barriers, and it may also react with other species when produced in a collisional environment. We estimate that under our experimental conditions about half of the MHC product is stabilized.

We also observe small but reproducible signals of m/z = 43 (C_2H_3O) and m/z = 46 (DCO_2) in experiments with d_1-PA (but not with d_0-PA) at photon energies as low as 8.8 eV. We assign these masses to the acetyl radical (CH_3CO; IE = 7.01 eV) and the d_1-hydroxyformyl radical (DOCO; IE = 8.19 eV), respectively. Fission of a C-C bond adjacent to the carbonyl group is common in dissociation of many carbonyls (knows as Norrish Type I reaction), and has been seen in photodissociation of PA following excitation to S_2 and S_3.

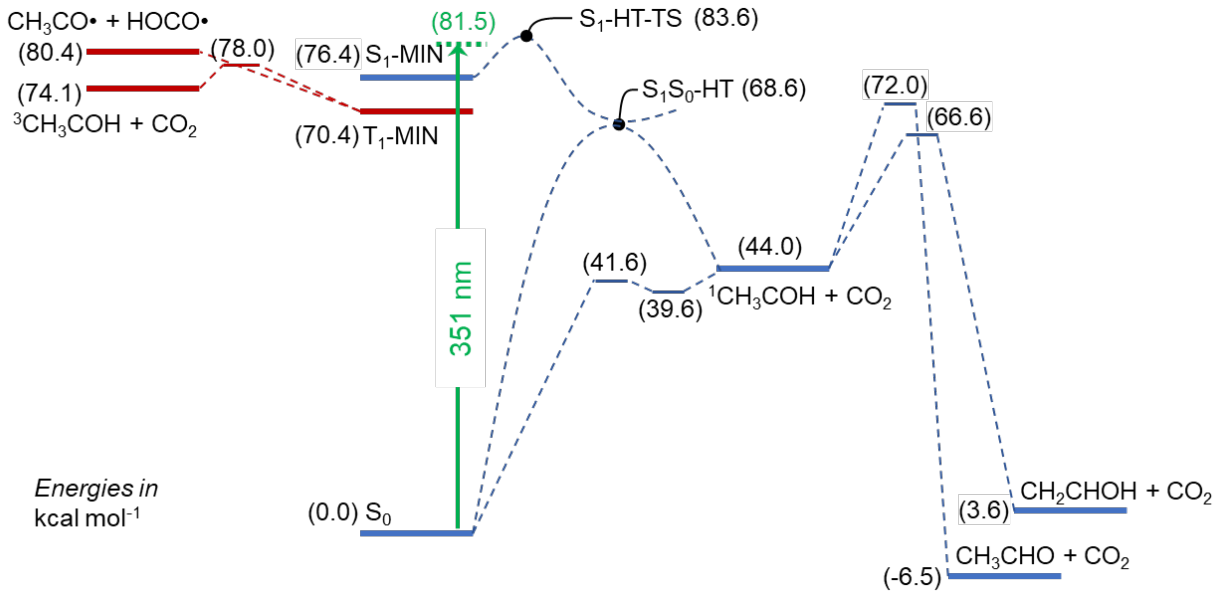

Fig. 3: Stationary points on pyruvic acid potential energy surfaces. Singlet surfaces are shown in blue, the lowest triplet surface in red, and the 351 nm photon in green, with energies in kcal mol^{-1}. S_1-HT and S_0-HT are the hydrogen-transferred isomers of S_1 and S_0, respectively. The S_1-HT energy is very close to the conical intersection with S_0, S_1S_0-HT.

A qualitative expectation of the dynamics when PA is excited to the S_1 state can be developed based upon the known hydrogen-bonded molecular structure of the cis-keto S_0 conformer and the nature of the $\pi^* \leftarrow n$ electronic excitation. The two possible dissociation pathways upon S_1 excitation are decarboxylation following hydrogen transfer from OH to the ketonic carbonyl, and intersystem crossing (ISC) from S_1 to the slightly lower-lying triplet surface (T_1). These pathways are shown in Figure 3, which is based on calculations by Chang et al.[3] Once on the T_1 surface, Norrish Type I fission of the C-C bond gives rise to CH_3CO + DOCO. The calculations attest to the complexity of the dynamics following excitation to S_1, and are in qualitative agreement with our results. Upon excitation to S_1, H-transfer takes place on S_1 over a small barrier, creating S_1-HT at a location close to a conical intersection with S_0. In addition, intersys-

tem crossing to T_1 may occur, especially when excitation reaches S_1 below the barrier to H-transfer. Thus, we expect the photodissociation product yields to depend sensitively on excitation energy.

Our analysis indicates that under our experimental conditions about half the nascent MHT isomerizes, giving rise to acetaldehyde and vinyl alcohol, whereas the other half has energies below the isomerization barriers and can survive long enough to participate in chemical reactions. Indeed, we were able to identify the first reaction of MHC in the gas phase giving a product with a molecular formula of $C_4H_8O_2$, or twice the molecular mass of MHC. The only bimolecular reaction consistent with our kinetic data is the MHC + PA reaction forming a $C_4H_8O_2$ product whose structure we cannot yet assign.

Reactions of MHC were not taken into account in previous atmospheric modelling,[4] but one should expect the presence of MHC in the troposphere from photolysis of PA by sunlight, and the fraction of stabilized MHC is likely to increase at 1 bar compared our low-pressure conditions. The effect of vinyl alcohol production from PA photodissociation should also be included in atmospheric models, and may provide a source of additional formic acid. In the troposphere, MHC is unlikely to react with PA because it will collide first with other molecules (notably N_2, O_2, and H_2O) present in much higher concentrations.

We propose that PA and related alpha-keto carboxylic acids could provide ways to create alkylhydroxycarbenes in the laboratory, enabling exploration of their kinetics and reaction products that may, in turn, inform chemical models of complex reaction systems.

Future work

The pandemic has put an unfortunate halt to our experiments, but we hope to be able to resume them in the near future. PA is known to slowly react with water, and we plan to study this reaction, as well as other collisional effects. The lifetime of the excited S_1 state as a function of excitation energy will be determined using time-resolved fluorescence detection. We also plan to continue studying the atmospheric relevant reactions of hydroxy-carbenes in the gas phase, observed for the first time in our work.

References

1. S. Yamamoto and R. Back, *Can. J. Chem.*, 1985, **63**, 549-554.

2. B. R. Samanta, S. Sutradhar, R. Fernando, A. I. Krylov and H. Reisler, *J. Phys. Chem. A*, 2018, **122**, 6176-6182.

3. X.-P. Chang, Q. Fang and G. Cui, *J. Chem. Phys.*, 2014, **141**, 154311; DOI: 10.1063/1.4898085.

4. IUPAC Task Group on Atmospheric Chemical Kinetic Data Evaluation, https://iupac-aeris.ipsl.fr/htdocs/datasheets/pdf/P37CH3(CO)C(O)OH.pdf.

Publications 2019-2021

1. S. Sutradhar, B.R. Samanta, R. Fernando, and H. Reisler, "Spectroscopy and two-photon dissociation of jet-cooled pyruvic acid", J. Phys. Chem. A **123**, 5906-5917(2019).
2. B.R. Samanta, R. Fernando, D. Rösch, H. Reisler, and D.L. Osborn, "Looking at the bigger picture: Identifying the photoproducts of pyruvic acid at 193 nm", J. Chem. Phys. **153**, 074307 (2020).
3. B. R. Samanta, R. Fernando, D. Rösch, H. Reisler, and D.L. Osborn, "Primary photodissociation mechanisms of pyruvic acid on S_1: observation of methylhydroxycarbene and its chemical reaction in the gas phase", Phys. Chem. Chem. Phys. **23**, 4107-4119 (2021).

FUNCTIONAL GROUP EFFECTS ON UNIMOLECULAR QOOH REACTIONS AT HIGH PRESSURE USING HIGH-RESOLUTION ELECTRONIC ABSORPTION SPECTROSCOPY

Brandon Rotavera
College of Engineering | Department of Chemistry
University of Georgia
Athens, GA 30602

rotavera@uga.edu | (rotavera.uga.edu)

Program Scope

The primary goal of this research program is to produce new fundamental knowledge on connections between molecular structure of hydroperoxy-substituted carbon-centered radicals (ȮOOH) and selectivity towards specific unimolecular reaction pathways (**Figure 1**). This knowledge is derived in part from combustion experiments using a jet-stirred reactor that is employed to measure isomer-resolved species concentration profiles of multi-functional intermediates derived from ȮOOH formed via oxidation of the C4 species in **Figure 2**. As a primary outcome, this research program expands gas-phase chemical kinetics knowledge on the effects of functional groups on chemical reactivity that is necessary to refine computational combustion models that support ongoing efforts to incorporate biofuels in current and future combustion systems. Additionally, owing to the complex combustion behavior of functionalized molecules, this program focuses on identifying new reaction pathways that are studied in greater detail using theoretical chemical kinetics computations, including potential energy surfaces and rate calculations.

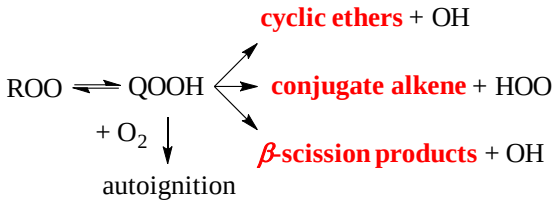

Figure 1. *Reaction mechanisms of ȮOOH radicals are central to understanding and developing modeling capabilities for hydrocarbon and biofuel oxidation. Accurately quantifying product formation from ȮOOH reflects the balance of chain-branching reactions (downward-pointing arrow) to chain-propagation and chain-inhibiting reactions (arrows pointing towards the right), each of which can produce an abundance of isomers.*

Direct measurements of such isomers, e.g. cyclic ethers, provide stringent benchmarks of ȮOOH chemistry and are therefore central to the development of robust chemical kinetics mechanisms. This program bridges knowledge gaps between molecular structure and ȮOOH reactivity for C4 molecules, namely the balance of unimolecular decomposition vs. bimolecular reaction with O_2.

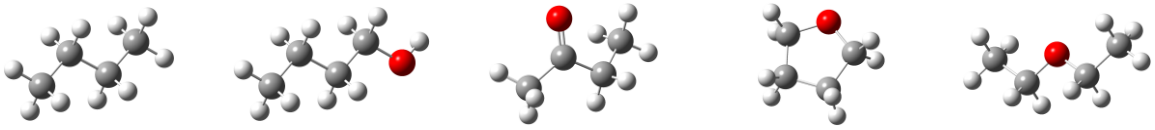

Figure 2. *Molecular structure of C4 species studied in this program (left to right): n-butane, 1-butanol, butanone, tetrahydrofuran, and diethyl ether*.

Recent Progress

Speciation experiments in a jet-stirred reactor: The jet-stirred reactor (JSR) at the University of Georgia is capable of experiments at pressures up to 50 atm and operates with a well-characterized temperature profile. Particular attention is paid to quantifying spatial temperature uncertainty in the sampling region as well as in species quantification. Complete temperature characterization was accomplished using a systematic series of experiments conducted at residence times up to 4000 ms

over a range of temperatures controlled independently in the two main heating regions of the JSR, the reactor region and the pre-heating region. In all cases, owing to a custom-built, woven Inconel and ceramic insulation heating system, 1σ deviations in temperature are < 1% of the reaction temperature (up to 1200 K) over a 3-cm sampling distance. Species quantification is accomplished with an uncertainty of < 10% in all cases and is achieved via tandem gas chromatography (GC) measurements via two independent detection schemes. The first uses electron-impact mass spectrometry and the second uses vacuum ultraviolet (VUV) absorption spectroscopy. Consistency in species quantification between these two methods is routinely within 5%. **Figure 3a** shows an example total ion count from 1-butanol oxidation at a retention time of 13.86 min. from which two different spectra are extracted. **Figure 3b** is the corresponding electron-impact mass spectrum (EI-MS) and **Figure 3c** is the absorption spectra of signal detected at 13.86 min. Both detectors are utilized in producing species concentration profiles at the conditions of interest. **Figure 3d** shows an example from 1-butanol oxidation at 800 K and 1 atm conducted from $0.28 \leq [O_2] \leq 2.20 \cdot 10^{18}$ molecules cm^{-3}. The main objective of these experiments is to provide quantitative targets for modeling ȮOOH-mediated chemistry over a range of oxygen concentration to probe the chemistry depicted in **Figure 1**, particularly species that are uniquely formed via the unimolecular step, including cyclic ethers and HOO-elimination products such as butanal (**Figure 3d**). Similar experiments were conducted for diethyl ether and *n*-butane.

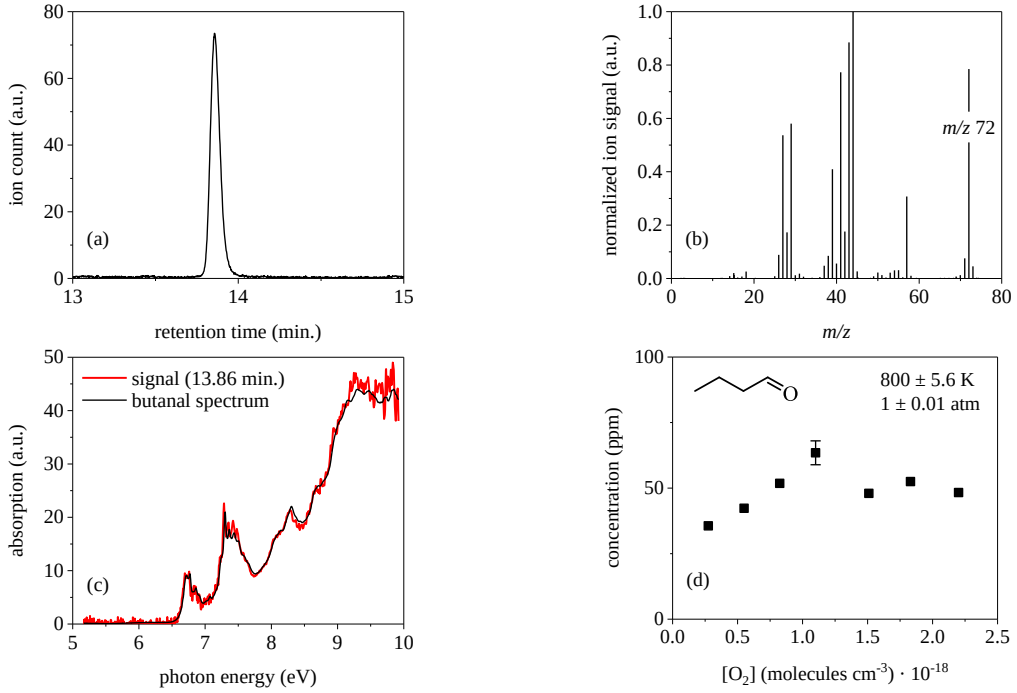

Figure 3. *Data produced from 1-butanol oxidation in the JSR at 800 K and 1 atm: (a) ion signal as a function of retention time (13.86 min.). (b) EI-MS and (c) absorption spectrum of ion signal at the retention time. (d) concentration of butanal as a function of* $[O_2]$ *from* $0.28 – 2.20 \cdot 10^{18}$ *molecules* cm^{-3}.

High-resolution absorption spectroscopy: Measurements of reference spectra and quantified absorption cross-sections are essential to achieving the goals of the program. To-date, more than 100 spectra have been measured and include multi-functional intermediates relevant to the molecules in **Figure 1**. The reference spectra are measured off-column, separate from GC measurements, using differential absorption spectroscopy in a temperature- and pressure-controlled flow cell. Time-averaged absorption signals are measured at a frequency of 91 Hz and averaged at a frequency of 4.5

Hz for a total of 20 measurements to produce a single spectrum. Each measurement is repeated 3-5 times to produce a statistical average of absorption signal. Cross-sections are quantified from 5.16 – 9.92 eV at 2-meV resolution. **Figure 4** shows absorption spectra highlighting sensitivity to stereoisomers, *cis*- and *trans*-2,3-dimethyloxirane, and to the presence of π bonds.

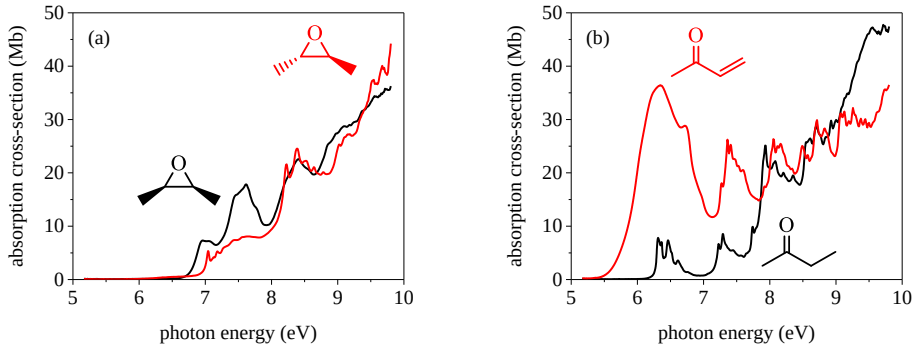

Figure 4. *Absorption spectra measured at 800 Torr and 50 °C. (a) Spectra of cyclic ether isomers produced in n-butane oxidation. (b) Spectra of carbonyl species (butanone and methyl vinyl ketone).*

Potential energy surface computations: **Figure 5** shows an example pathway included in ongoing PES computations of new reactions that may produce products in the JSR experiments. The formation of butan-1-al-4-yl via the mechanism below may be a significant contribution to 3-butenal formation (via an HOO-elimination step) in 1-butanol.

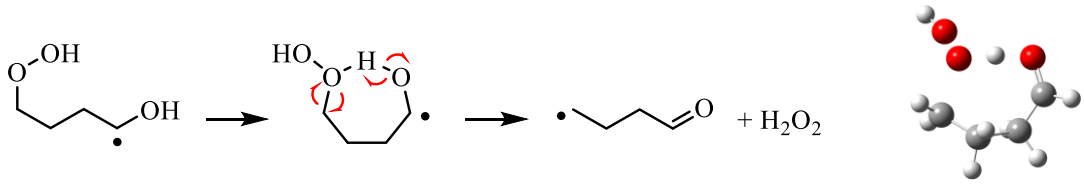

Figure 5. *(left) New reaction pathway identified for δ-Q̇OOH derived from 1-butanol oxidation forming butan-1-al-4-yl + H_2O_2 via abstraction of hydroxylic hydrogen by non-terminal oxygen. (right) Structure of optimized 7-membered transition state (ν ~1600i cm^{-1}) computed using B3LYP/cc-pVTZ.*

Future Work

High-pressure jet-stirred reactor experiments: A high-pressure control system is currently being implemented into the JSR for operation up to 50 atm. Temperature profile measurements are also being conducted to quantify temperature gradients and uncertainty as a function of reaction pressure in the combustion experiments, which is important due to changes in diffusion rates with pressure. Quantification of measurement uncertainties will be completed over the full range of experimental variables, namely temperature, pressure, and residence time. Subsequent to measurements of thermal gradients at high pressure, oxidation experiments at 20 atm are planned for all species in **Figure 1**.

Machine learning and isomer-resolved absorption spectroscopy for species identification: In order to identify spectra for which no reference data are available, machine learning techniques are under development. In such cases, machine learning will be employed to identify spectral features that correspond to functional group type, number of π bonds, and cyclic versus acyclic structure by relying on a robust training set of spectra that contains varying combinations of these motifs. **Figure 6** provides recent results for principal component 1 (PC1) and principal component 2 (PC2) scores for 89 VUV absorption cross-sections, clustered into three groups using the Fuzzy C Mean clustering method. The clusters are well-defined into three groups: (1) the teal-colored cluster (bottom left

quadrant), shows low scores for both PC1 and PC2, (2) the blue-colored cluster, shows high PC2 scores and PC1 scores near zero, and (3) the yellow cluster, which shows low PC2 scores and high PC1 scores. Large PC1 values correspond to large absorption cross-sections below ~7.5 eV, where $\pi \rightarrow \pi^*$ transitions dominate. Therefore, species with large PC1 values typically contain π bonds or conjugated π systems. Negative PC2 scores correspond to large cross-sections below ~6.5 eV or above ~8.0 eV. Large absorption cross-sections below 6.5 eV tend to correspond with oxygen-atom-containing conjugated π-systems, while large absorption cross-sections above ~8.0 eV without significant absorption below ~6.5 eV are consistent with saturated hydrocarbons. Future work is aimed at enhancing the predictive capability of the machine learning methods by, among other efforts, increasing the number and diversity of spectra in the training set.

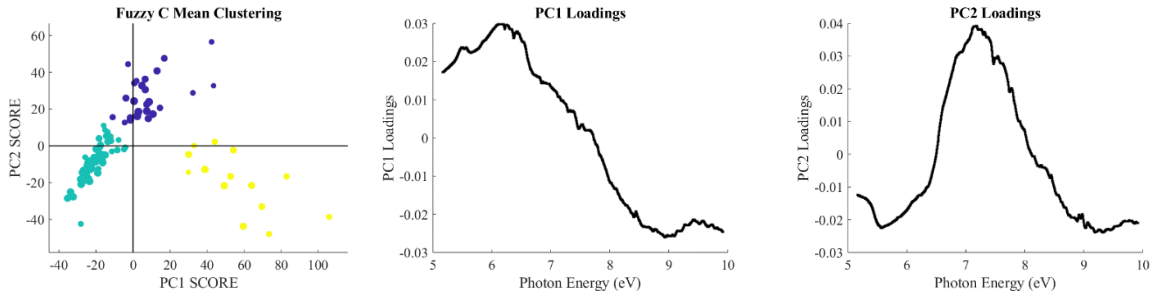

Figure 6. *Machine learning results from analysis of 89 VUV absorption cross-sections of a diverse array of species (alkanes, alkenes, ethers, carbonyls, alcohols, esters, and multi-functional intermediates).*

Rate computations: Species for which new reaction pathways are identified, such as those depicted in **Figure 5**, will require rate computations and, in some cases, thermochemistry to include in chemical kinetics mechanisms to assess the impact on combustion model predictions. This will be accomplished using KinBot software and the PAPR code in collaboration with both Sandia National Laboratories and Argonne National Laboratory.

Refining chemical kinetics mechanisms: The efforts above combine to achieve one of the primary goals of the program, which is increasing the quantitative prediction capabilities of chemical kinetics mechanisms by (i) providing new, benchmark experimental data, (ii) identifying new reaction pathways that may hold relevance to increasing the accuracy of modeling combustion, and (iii) computing rates. Future work on this topic will involve using existing mechanisms from the literature on the five species in **Figure 1** and refining via a combination of the above three sets of results.

Publications/Presentations Acknowledging Support from the Gas-Phase Chemical Physics Program, 2020-Present:

1. **Influence of Functional Groups on Low-Temperature Combustion Chemistry of Biofuels,** B. Rotavera and C. A. Taatjes, *Prog. Energy Combust. Sci.*, 1-96 (2021); https://doi.org/10.1016/j.pecs.2021.100925.
2. **Vacuum-Ultraviolet Absorption Cross-Sections of Functionalized Cyclic Hydrocarbons: Five-Membered Rings,** M. G. Christianson, A. C. Doner, A. L. Koritzke, K. Frandsen, B. Rotavera, *J. Quant. Spec. Rad. Trans.* **258**, 1-8 (2020); https://doi.org/10.1016/j.jqsrt.2020.107274
3. **Vacuum-Ultraviolet Absorption Cross-Sections of Functionalized Four-Carbon Species,** A. C. Doner, M. G. Christianson, A. L. Koritzke, A. Larsson, K. Frandsen, B. Rotavera, *J. Quant. Spec. Rad. Trans.* (submitted).
4. (invited seminar, March 6, 2021) "Influence of Functional Groups on Low-Temperature Combustion Chemistry of Biofuels", Brandon Rotavera, *Princeton/Georgia Tech Combustion Seminar Series* (**link**).

Active Thermochemical Tables

Branko Ruscic
Chemical Sciences and Engineering Division, Argonne National Laboratory,
9700 South Cass Avenue, Lemont, IL 60439
ruscic@anl.gov

Program Scope

The *spiritus movens* of this program is fueled by the need to provide the scientific community with accurate and reliable thermochemical information on chemical species that are relevant in energy-generating chemical processes or play prominent roles in subsequent environmental chemistry. Detailed knowledge of thermodynamic parameters for a broad array of both ephemeral and stable chemical species is pivotal to chemistry and essential in many industries. In particular, the availability of *accurate, reliable, and internally consistent* thermochemical values is a *conditio sine qua non* in chemical kinetics, reaction dynamics, formulation of plausible reaction mechanisms, and construction of predictive models of complex chemical environments, such as combustion, atmospheric chemistry, catalysis, astrochemistry, etc. Last, but not least, the availability of accurate thermochemical values has historically been the prime driver for steady advancements of increasingly sophisticated electronic structure theories.

The aim of this program is to develop and exploit new methodologies in the field of thermochemistry in order to systematically improve both the quality and quantity of available thermochemical data. To that end, this program has developed and introduced a novel approach that is centered on analyzing and optimally utilizing the information content of *all available* thermochemically relevant determinations, irrespective of whether these originated from experiment or from state-of-the-art theory. The aim is not only to dynamically produce the best currently possible thermochemical parameters for the targeted chemical species, but also to allow efficient updates when new knowledge becomes available, propagating properly its consequences through all affected chemical species, as well as to provide critical tests of new experimental data or theoretical methods and generate pointers to new determinations that are likely to efficiently improve the overall thermochemical knowledge base. In order to provide a broad perspective of this area of science, the effort of this program is synergistically coordinated with related experimental and theoretical efforts within the Gas-Phase Chemical Dynamics Group at Argonne.

Recent Progress

In past years, we have strived to take a balanced approach between activities that use primarily the effort of this program and those that involve extensive collaborations with other researchers. However, the pandemic has made the latter more onerous and time consuming, and, in order to make best use of the available time, we have emphasized the formed in favor of the latter. Thus, over the past year we have focused on continued development and expansion of Active Thermochemical Tables (ATcT).

Concisely, ATcT are a new paradigm for producing accurate and reliable thermochemical values. Thermochemically relevant determinations (reaction enthalpies, equilibrium constants, etc.), involve two or more chemical species, thus defining the thermochemistry of the target species *only relative* to other species in the chemical reaction, creating a network of intertwined (and frequently inconsistent) species interdependencies. In contrast to the traditional *sequential approach* of inferring enthalpies of formation, which discards information by pruning the network into a sparse tree (A begets B, B begets C, etc.), ATcT constructs the underlying thermochemical network from all relevant determinations, statistically analyzes it to identify 'optimistic' uncertainties, brings the network to self-consistency, and then finds a simultaneous solution for all species, exploiting all available knowledge.

The most significant vehicle for disseminating the ATcT results is the ATcT website, ATcT.anl.gov. During the last year, we have publicly released four (somewhat related) versions of ATcT results, 1.122h, 1.122n, 1.122o, and 1.122p, each containing successive improvements of the reported thermochemistry. Noting that all ATcT results are strictly versioned, and once publicly released, versions remain

indefinitely available on the archive of the website, the most recent public version, ATcT TN ver. 1.122p, which was released in September 2020, covers 1727 chemical species.

The ATcT website continues to grow in popularity, and is generally hyped in the literature as the most reliable source of enthalpies of formation for species relevant in combustion and atmospheric chemistry, as well as other areas. In fact, ATcT continues to emerge as the top result on several popular search engines, including Google, for searches such as 'thermochemical tables' (outranking the venerable JANAF Tables), and ranks very highly on searches such as '[XYZ] enthalpy of formation'. The number of website visitors keeps steadily growing, attracting 25,000+ monthly visitors. A scrutiny of the Apache server logs indicates that during 2020 the website had been accessed by ~280,000 *different* IP addresses (i.e. repeat visits are not counted here). Along similar lines, Google reports that during the last 12 months ~270,000 searches ended by a click landing the visitor on the ATcT website (see Fig. 1).

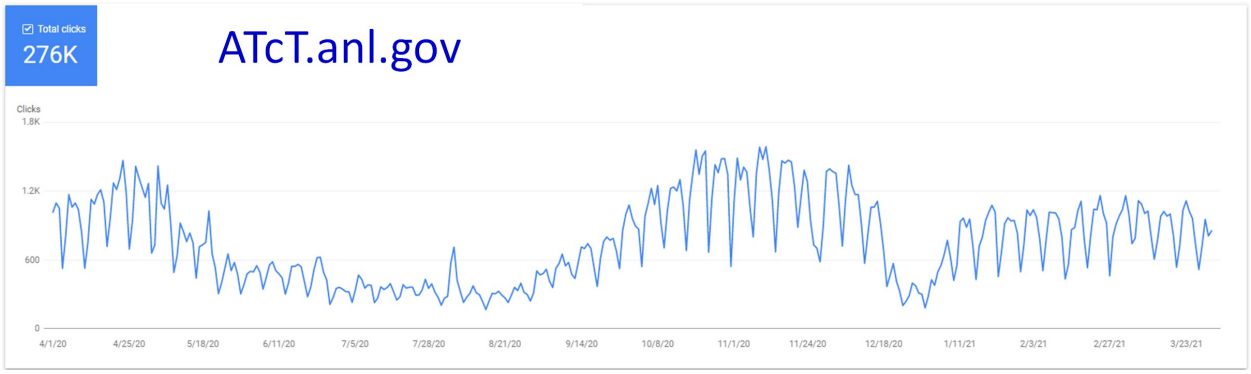

Figure 1. Google Console report for the ATcT website on access via their search engine during 2020.

As hinted to above, during the past year we have focused on expanding the coverage of the ATcT TN. The current developmental version, 1.122z, recently surpassed 2750 species, for an increase of more than 500 species with respect to the previous year (as opposed to ~150-200 species/year in earlier years). In order to define the thermochemistry of all these species, the TN now includes >29,500 active determinations (both from experiment and high-level theory), and thousands inactive determinations that have been rendered obsolescent during previous ATcT TN analyses and rounds of improvements.

In spite of the pandemic, we have continued a reasonably broad range of collaborations, both outside (nationally and internationally) and inside the Gas-Phase Chemical Dynamics Group at ANL. One of the new results particularly worth highlighting here is the publication of a paper that involves a significant fraction of PIs in our group, producing a high-fidelity mechanism of flash pyrolysis of acetone by combining rotational spectroscopy for quantitative and isomer-specific detection with advanced theory and ATcT thermochemistry (JACS **143**, 3124 (2021); DOI: 10.1021/jacs.0c11677), and revealing important roles of a number of radical substitution reactions that were previously omitted in the corresponding combustion mechanisms. The paper was highlighted in Science (DOI: 10.1126/science.372.6537.44-b) as a major breakthrough in chemical kinetic modeling.

The ATcT Task Force One (J. Stanton and T. L. Nguyen and their groups at UF, B. Ellison, UColorado, B. Changala, Harvard-Smithsonian, J. Baraban and his group at Ben-Gurion, and D. H. Bross, ANL) has remained very active, maintaining weekly teleconference meeting. One of the several ongoing projects that we would like to highlight here relates to the introduction of key sulfur species in ATcT. The project, which is in its advanced stages, combines existing experimental determinations with state-of-the-art HEAT computations performed at UF, resulting not only in the establishment of accurate thermochemistry for key sulfur-containing species such as SO, SO_2, SO_3, H_2SO_4, etc., but forcing a significant revision of the CODATA enthalpy of formation of S atom (a key quantity for electronic structure methods that utilize the route of total atomization energy to derive enthalpies of formation).

A second Task Force (collab. with K. Peterson, WSU and his group, and D. H. Bross, ANL) is aiming to expand ATcT into actinides. This project is also in its advanced stages. The thermochemistry of uranium

and other actinides is particularly relevant for the separation techniques related to generation of nuclear power. Historically, the associated thermochemistry relied on difficult and frequently inconsistent experimental determination. However, with the advent of highly improved theoretical approaches for electronic structure computation of species containing heavy and ultra-heavy elements, ATcT is now in an excellent position to synergistically combine new theoretical determination with extant experimental measurements and produce reliable values for compounds containing U and other actinides.

In another collaboration, with A. R. Ravishankara (Colorado State) and his group, A. Mellouki (ICARE-CRNS) and his group, and S. S. Brown (NOAA), we have conducted a combined experimental and theoretical study of the reactions of aromatic aldehydes with NO_3 under atmospheric conditions. Aromatic aldehydes (benzaldehyde, methylated benzaldehydes, etc.) are emitted both from anthropogenic (primarily combustion) and biogenic sources. While they are removed primarily from the atmosphere by reactions with OH, oxidation of aromatic aldehydes by NO_3, producing acyl peroxy nitrates (PANs), is important at night in NO_x-rich locations. PANs can be easily transported far from their origin, with consequences for ozone production and particle formation away from polluted regions.

In collaboration with the ECC project (led by J. Zador, Sandia CRF), we have started enabling ATcT to describe the thermochemistry of adsorbates that occur on the gas phase/solid phase interfaces. We have now developed the core systematics for these species, which parallels in a number of ways the ATcT systematics for aqueous thermochemistry (albeit with an inherently higher complexity).

Future Plans

Future plans of this program pivot around further development and expansion of the Active Thermochemical Tables approach, continuing to provide accurate thermochemistry to the scientific community, and driving targeted thermochemically-relevant theoretical and experimental investigations of radicals and transient species that are intimately related to combustion and post-combustion atmospheric processes. A significant part of the effort will be focused on continued 'finalization' and dissemination of the resulting ATcT thermochemistry, typically involving groups of related chemical species. One important component of this process, focused on their enthalpies of formation, consists of testing and analyzing the TN dependencies, using tools such as the variance/covariance decomposition approach and analyses of the influence of relevant determinations via the hat-matrix, followed by improving the connectivity within the TN and adding new high-quality results (either virtual, i.e. computational, or actual, i.e. experimental) to coerce the resulting thermochemistry toward stable, 'release quality' values. This iterative process unavoidably results in an expansion of the TN with new related chemical species, which is an added benefit. Another equally important component focuses on enhancing the accuracy of the partition functions, typically by upgrading RRHO partition functions to NRRAO partition functions, which is also a currently ongoing effort. Future plans also incorporate the expansion of the per-species data presented on our website, as well as expansion of ATcT coverage to other interesting areas of chemistry (catalysis, batteries, etc.)

This work is supported by the U.S. Department of Energy, Office of Basic Energy Sciences, Division of Chemical Sciences, Geosciences, and Biosciences, under Contract No. DE–AC02–06CH11357.

Publications resulting from DOE sponsored research (2018 – present)

- *Reactions of NO_3 with Aromatic Aldehydes: Gas Phase Kinetics and Insights into the Mechanism of the Reaction*, Y. Ren, L. Zhou, A. Mellouki, V. Daële, M. Idir, S. S. Brown, B. Ruscic, R. S. Paton, M. R. McGillen, and A. R. Ravishankara, *Atmos. Chem. Phys.* (submitted, under open review) (2021); DOI: 10.5194/acp-2021-228
- *Partition Functions via Phase Space Integration of Minima-Preserving Neural Network Potential Energy Surrogates: Quantifying the Effect of Anharmonicity on the Free Energy and Thermodynamic Properties of Hydrogen on Cu(111)*, K. Blöndal, K. Sargsyan, D. H. Bross, B. Ruscic, and C. F. Goldsmith, *J. Phys. Chem. C* (submitted) (2021)
- *Substitution Reactions in the Pyrolysis of Acetone Revealed through a Modeling, Experiment, Theory*

Paradigm, D. P. Zaleski, R. Savaramakrishnan, H. R. Weller, N. A. Seifert, D. H. Bross, B. Ruscic, K. B. Moore III, S. N. Elliott, A. V. Copan, L. B. Harding, S. J. Klippenstein, R. W. Field, and K. Prozument, *J. Am. Chem. Soc.* **143**, 3124-3142 (2021); DOI: 10.1021/jacs.0c11677

- *Active Thermochemical Tables (ATcT) Enthalpies of Formation Based on version 1.122p of the Thermochemical Network*, B. Ruscic and D. H. Bross, Argonne National Laboratory, Argonne, Ill. (2020); URL: https://atct.anl.gov/Thermochemical%20Data/version%201.112p/
- *Active Thermochemical Tables (ATcT) Enthalpies of Formation Based on version 1.122o of the Thermochemical Network*, B. Ruscic and D. H. Bross, Argonne National Laboratory, Argonne, Ill. (2020); URL: https://atct.anl.gov/Thermochemical%20Data/version%201.112o/
- *Active Thermochemical Tables (ATcT) Enthalpies of Formation Based on version 1.122n of the Thermochemical Network*, B. Ruscic and D. H. Bross, Argonne National Laboratory, Argonne, Ill. (2020); URL: https://atct.anl.gov/Thermochemical%20Data/version%201.112n/
- *Active Thermochemical Tables (ATcT) Enthalpies of Formation Based on version 1.122h of the Thermochemical Network*, B. Ruscic and D. H. Bross, Argonne National Laboratory, Argonne, Ill. (2020); URL: https://atct.anl.gov/Thermochemical%20Data/version%201.112h/
- *High-Accuracy Extrapolated ab initio Thermochemistry. IV. A Modified Recipe for Computational Efficiency*, J. H. Thorpe, C. A. Lopez, T. L. Nguyen, J. H. Baraban, D. H. Bross, B. Ruscic, and J. F. Stanton, *J. Chem. Phys.* **150***,* 224102/1-16 (2019); DOI: 10.1063/1.5095937
- *An Automated Thermochemistry Protocol Based on Explicitly Correlated Coupled-Cluster Theory: The Methyl and Ethyl Peroxy Families*, B. K. Welch, R. Dawes, D. H. Bross, and B. Ruscic, *J. Phys. Chem. A* **123**, 5673-5682 (2019); DOI: 10.1021/acs.jpca.9b04381
- *Active Thermochemical Tables (ATcT) Enthalpies of Formation Based on version 1.122g of the Thermochemical Network*, B. Ruscic and D. H. Bross, Argonne National Laboratory, Argonne, Ill. (2019); URL: https://atct.anl.gov/Thermochemical%20Data/version%201.112g/
- *Active Thermochemical Tables: The Partition Function of Hydroxymethyl (CH_2OH) Revisited*, D. H. Bross, H.-G. Yu, L. B. Harding, and B. Ruscic, *J. Phys. Chem. A* **123**, 4212-4231 (2019); DOI: 10.1021/acs.jpca.9b02295 (*Hanna Reisler Festschrift*)
- *Thermochemistry*, B. Ruscic and D. H. Bross, *Comp. Aided Chem. Eng.* **45**, 3-114 (2019); DOI: 10.1016/B978-0-444-64087-1.00001-2 (Ch. 1 in *Mathematical Modelling of Gas-Phase Complex Reaction Systems: Pyrolysis and Combustion*, T. Faravelli, F. Manenti, and E. Ranzi, Eds., Elsevier: Amsterdam 2019)
- *Active Thermochemical Tables (ATcT) Enthalpies of Formation Based on version 1.122e of the Thermochemical Network*, B. Ruscic and D. H. Bross, Argonne National Laboratory, Argonne, Ill. (2019); https://atct.anl.gov/Thermochemical%20Data/version%201.112e/
- *Enthalpy of Formation of $C_2H_2O_4$ (Oxalic Acid) from High-Level Calculations and the Active Thermochemical Tables Approach*, D. Feller, D. H. Bross, and B. Ruscic, *J. Phys. Chem. A* **123**, 3481-3496 (2019); DOI: 10.1021/acs.jpca.8b12329
- *A Master Equation Simulation for the •OH + CH_3OH Reaction*, T. L. Nguyen, B. Ruscic, and J. F. Stanton, *J. Chem. Phys.* **150**, 084105/1-8 (2019); DOI: 10.1063/1.5081827
- *Toward Accurate High Temperature Anharmonic Partition Functions*, D. H. Bross, A. W. Jasper, B. Ruscic, and A. F. Wagner, *Proc. Combust. Inst.* **37**, 315-322 (2019); DOI: 10.1016/j.proci.2018.05.028
- *Modeling Nitrogen Chemistry in Combustion*, P. Glarborg, J. A. Miller, B. Ruscic, and S. J. Klippenstein, *Progr. Energy Combust. Sci.* **67**, 31-68 (2018); DOI: 10.1016/j.pecs.2018.01.002
- *Unimolecular Reaction of Methyl Isocyanide to Acetonitrile: A High-Level Theoretical Study*, T. L. Nguyen, J. H. Thorpe, D. H. Bross, B. Ruscic, and J. F. Stanton, *J. Phys. Chem. Lett.* **9**, 2532-2538 (2018); DOI: 10.1021/acs.jpclett.8b01259
- *Active Thermochemical Tables (ATcT) Enthalpies of Formation Based on version 1.122d of the Thermochemical Network*, B. Ruscic and D. H. Bross, Argonne National Laboratory, Argonne, Ill. (2018); URL: https://atct.anl.gov/Thermochemical%20Data/version%201.112b/

Coordinated Interrogation and Modeling in Ammonia Oxidation Catalysis

William F. Schneider and Jason C. Hicks
Department of Chemical and Biomolecular Engineering, 250 Nieuwland Science Hall, Notre Dame, Indiana, 46556
wschneider@nd.edu, jhicks@nd.edu

Program Scope

The overarching goal of this project, joint between GPCP and Catalysis Science, is to establish the potential for plasma stimulation to modify the behavior of a catalytic system, through application of plasma stimulation to well-defined and well-characterized thermal catalytic systems, chosen for reaction features that are amenable to careful experimental and computational interrogation. While the theory and practice of thermal heterogeneous catalysis is well established and design rules well understood, the same cannot be said of catalysis in the presence of external stimulus. Electrocatalysis and photocatalysis are two familiar examples of stimulated catalysis, but plasma-promoted catalysis is emerging as a third, high potential alternative. Plasmas are easy to generate and have the distinctive feature of creating non-equilibrium energy distributions within the plasma phase. By appropriately coupling this non-equilibrium behavior with a catalytic surface, we hypothesize that it is possible to carry out otherwise difficult or impossible chemical transformations, to do so at high efficiency, to take advantage of renewable electricity to drive chemistry, and to do so at smaller scales than those possible thermally.

This project combines careful synthesis and interrogation of catalytic materials and chemistry under plasma stimulation with first-principles-based microkinetic modeling to both elucidate and guide experiment. Its primary output will be fundamental insights transferable across this space. The project focuses on the catalytic chemistry of nitrogen. Nitrogen reductions and oxidations are of great economic value and critical to environmental protection, thermal catalytic chemistry is well understood, and relevant reactions are simple enough to be readily probed but complex enough to provide non-trivial insights. In particular, we focus on the reduction of N_2 (ammonia synthesis) and oxidation of N_2 (an alternative to the Ostwald process).

Recent Progress

Ammonia synthesis: Ample literature evidence from our group and others indicates that ammonia can be formed at or near ambient conditions in a dielectric barrier discharge (non-thermal) plasma integrated with a catalytic surface. Our prior work (*Nature Catal.* 2018, https://doi.org/10.1038/s41929-018-0045-1) reveals that at least one mode of action of the plasma is to decrease the demands on the catalytic surface to dissociate nitrogen. To provide more clarity into the influence of the optimal catalytic material, we performed experiments at the Spallation Neutron Source at Oak Ridge National Laboratory and density functional

perturbation theory to probe the relationship between exposure of a catalytic Ni surface to N_2 and/or H_2 plasma and the formed surface species. Both experiments and models highlight the appearance of chemisorbed hydrogen and of partially to fully hydrogenated nitrogen in the N_2/H_2 plasma, in contrast to a plasma-free control. Further, we find that a sequential exposure to N_2 plasma and to H_2 without plasma leads to the same surface intermediates, highlighting the role of N_2 excitations specifically on ammonia synthesis. This work is under consideration for publication at *ACS Energy Letters*.

Nitrogen oxidation: Nitrogen oxidation to NO is an alternative route to nitrogen fixation that, owing to the fact that it is endothermic, is particularly well suited to plasma promotion. Nitrogen oxidation in thermal plasmas has a long history, and recent evidence indicates that the same is possible in non-thermal plasmas. We have developed a modeling framework to assess the potential for plasma-catalyst combinations to promote nitrogen oxidation over a Pt catalyst, based on a reduced model for plasma-phase chemistry and DFT-predicted results for surface catalytic chemistry. The models highlight the sensitivity of NO productivity to plasma conditions (radical density, vibrational temperature, and mixing ratio) and reveal plasma regimes well suited to catalytic promotion of NO production. Experiments performed by collaborators at the Dutch Institute for Fundamental Energy Research (DIFFER) agree well with model predictions. The work is particularly significant in that it demonstrates quantitatively a plasma-catalytic coupling at conditions at which intrinsic plasma and catalytic contributions alone are negligible and which produces NO at concentrations that exceed thermal equilibrium. This work is under consideration for publication at *Nature Catalysis*.

Future Plans

Work to-date is refining our understanding of how plasma properties, reactor configuration, and material selection interplay to determine the productivity of plasma-catalyst combinations. Further progress depends on improved understanding of the mechanisms of reaction at the catalyst surface. We plan to continue to exploit *in situ* spectroscopy and transient product analysis to provide these mechanistic insights across a range of metal catalysts, using ammonia synthesis and nitrogen oxidation as our two model reactions. Computational models will be extended to encompass this wider material range. Our modeling strategy will follow two streams, one aimed at capturing trends with variation in material and ambient pressure plasma and the other aimed at quantitative predictions for precisely defined and low pressure plasmas.

Publications from the Project

Bogaerts, A.; Tu, X.; Whitehead, J. C.; Centi, G.; Lefferts, L.; Guaitella, O.; Azzolina-Jury, F.; Kim, H.-H.; Murphy, A. B.; Schneider, W. F.; Nozaki, T.; Hicks, J. C.; Rousseau, A.; Thevenet, F.; Khacef, A.; Carreon, M. The 2020 Plasma Catalysis Roadmap. J. Phys. D: Appl. Phys. 2020, 53 (44), 443001. https://doi.org/10.1088/1361-6463/ab9048

SPECTROSCOPIC INVESTIGATIONS OF MOLECULAR SYMMETRY BREAKDOWN

Trevor J. Sears
Department of Chemistry, Stony Brook University, Stony Brook, NY 11794-3400
trevor.sears@stonybrook.edu

Program Scope

This project aims to make precise measurements of the spectra of small molecules to address fundamental questions in chemical physics in the realm of nuclear spin symmetries and their breakdown in molecules, and parity non-conservation caused by the weak nuclear force. Nuclear spin symmetry is intimately connected to parity in symmetrical molecules and plays a central role in the physical and chemical properties of symmetric molecules, their collisional relaxation, and the establishment of thermodynamic equilibrium in an ensemble. Such effects are present in every molecular system or process, but their small size means they are often only directly observable under special conditions. However, their measurement is of fundamental, and often practical importance, and strongly relates to the themes of coherence in light and matter in the recent Basic Energy Sciences Advisory Committee (BESAC) report "Challenges at the Frontiers of Matter and Energy: Transformative Opportunities for Discovery Science".

I. Recent Progress

Progress in the past year has of course been heavily impacted by the coronavirus pandemic which caused the complete shutdown of laboratory work for 3 months. This was followed by another 4-6 weeks of restricted activity and delays caused by problems encountered restarting the frequency comb and other equipment. On the plus side, the spectrometer has been modified and upgraded and the quality of the data produced greatly improved compared to that obtained early last year. In particular, the precision line shape measurements relating to the investigation of reported ortho-para differences in pressure-broadening coefficients in the $\nu_1+\nu_3$ band of C_2H_2 were repeated resulting in unequivocal conclusions regarding this controversial report.

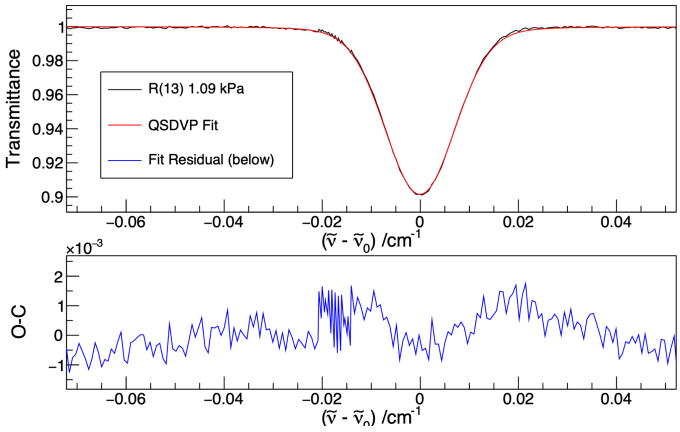

Secondly, during the enforced shutdown of experimental work, we were able to revisit some data recorded at Brookhaven National Laboratory in 2017 and we completely assigned spectroscopic data for the 1.66 μm spectrum of ethynyl radical, C_2H.

A. Precision Line Shape Measurements and Analysis

We have completely remeasured the pressure dependence of the shape and position of the series of lines, R(8)-R(13), in the $\nu_1+\nu_3$ band of pure acetylene gas using the improved comb-referenced spectrometer. An example of the data and modelling is shown above for R(13) at a pressure of 8.18 torr. The extra points around -0.02 cm^{-1} are the result of overlap between two scans and illustrate the reproducibility of the data. Iwakuni et al. [Phys. Rev. Letts. **117**, 143902 (2016); **119**, 069402 (2017)] had reported a controversial large (10%) alternation in the magnitudes of self-pressure broadening coefficients between the ortho- and para- nuclear spin states (odd and even J values) of ground state acetylene. The new data do not support this observation.

In analyzing the new measurements, it was vital to include the effects of weak background absorption lines using slightly refined line strengths from the Hitran database [I. Gordon, et al. J. Quant. Spectros. Rad. Transf. **203**, 3 – 69 (2017)] and assuming Voigt profiles. These hotband, weak overtone and low abundance isotopic lines have intensities of up to a few percent of the main lines in this region and their presence distorts the main line by amounts that vary from line to line. A suite of Python programs was written to read the data files, collate files by transition, fit the data to a normalized line shape function, and present the resulting line profile parameters. The new code was based on previously published work from our group [D. Forthomme, et al. J. Quant. Spectrosc. Rad. Transf.. **165**, 28–37 (2015)] and is publicly available in the Gitlab repository, https://gitlab.com/searssbu/rotfit. After investigating the parameter space, we found the new data were adequately fitted using a quadratic speed-dependent Voigt profile (QSDVP) which includes the broadening and shift parameters for the most probable molecular speed and quadratic (in speed) dependent corrections to these two parameters, although the speed-dependent correction to the shift was found to be negligible for these data because the pressures included in it are relatively small. Global fits of the sets of data corresponding to the same vibration-rotational transition at varying pressures and pathlengths were performed to extract the line profile parameters, in particular the broadening coefficients, to compare to the controversial report of an ortho- para- variation.

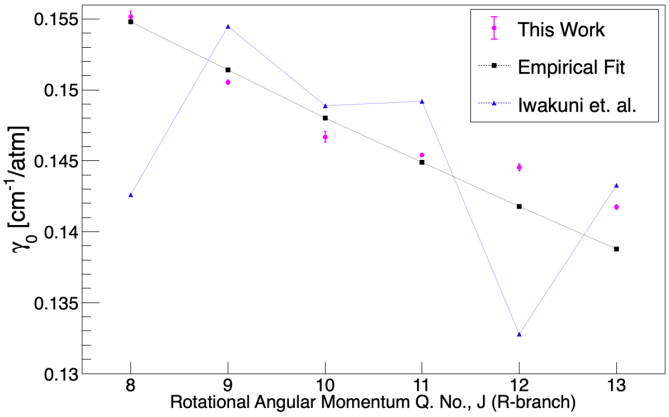

The resulting most probable speed broadening parameters for the transitions in question, in units of cm^{-1}/atm, are plotted in comparison to those reported by Iwakuni et al. in the figure to the left. The dramatic "sawtooth" variation between odd (ortho-nuclear spin symmetry) and even (para-) rotational quantum number levels is not reproduced by our data and analysis. The new results are in reasonable accord with the smooth variation of a model empirical fit of data from multiple published experimental measurements. Details are given in the very recently published paper describing this work. [*J. Chem. Phys.* **154**, 054305 (2021)]

The question arises as to how the data and/or the analysis of the original report could have led to the apparent variation in the broadening coefficient. The answer lies in the approximate line shape model used in the analysis [Hartman and Tran, *Phys. Rev. Letts.* **119**, 069401 (2017)]. As reported last year at this meeting, we have investigated the effect further by using smoothly varying QSDVP line shape parameters to simulate the data of Iwakuni et al including the exact reported pressures and path lengths used in that work and a Gaussian random noise at the level of their data, and shown how the use of the inexact model can lead to the reported results. The modeling code is also publicly available at https://gitlab.com/searssbu/htp-matlab_codes and the detailed write up available as supplementary data for the published *J. Chem. Phys.* paper.

B. The 1.66 μm spectrum of C_2H

The high resolution transient absorption spectrum of the ethynyl radical in the, previously unexplored, 1.66μm region was obtained some years ago at Brookhaven National Laboratory. During the enforced COVID shutdown in early and mid-2020, the data were assigned and shown to be due to two main band systems. A hot band originating in the first excited bending vibrational level, and a second band resulting from absorption from the zero point $X^2\mathbf{\Sigma}$ level of the radical. Both the observed bands were parallel in nature and terminated in previously unobserved levels of $^2\Pi$ and $^2\mathbf{\Sigma}$ vibronic symmetry, respectively.

The data have been analyzed in terms of effective Hamiltonians describing the rotational, fine- and hyperfine-structure of the vibronic levels and combined with all previously published high resolution data related to the ground and excited vibronic levels associated with the first and second excited bending vibrational levels of the radical. The figure below shows a section of the observed spectrum and, in the lower panel, the simulation based on the best fit molecular parameters.

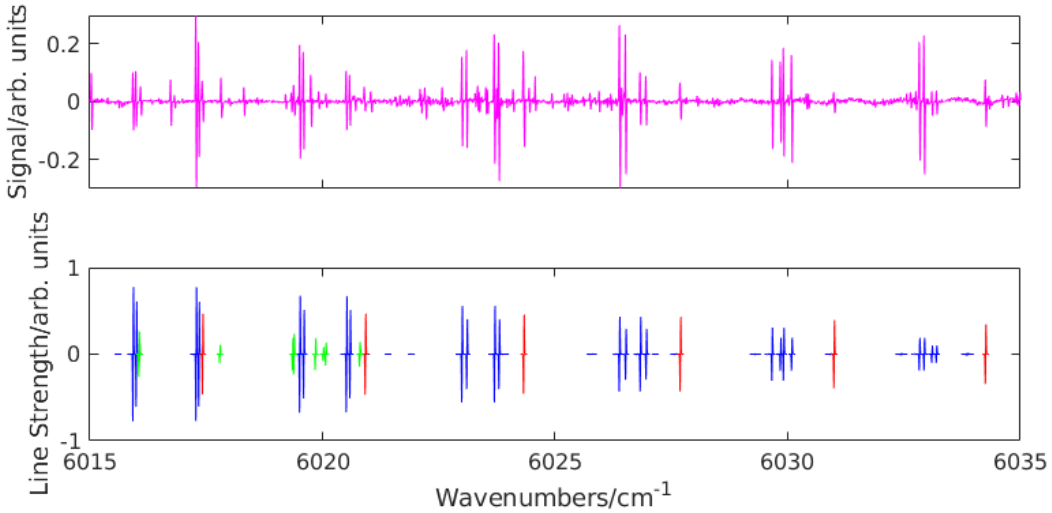

Section of the observed spectrum (upper panel) showing contributions from the $^2\Pi$(6413.5) - $^2\Pi$(010) (blue in the lower panel), $^2\Sigma$(6055.6) - $^2\Sigma$(000) (red) and $^2\Pi$(6817.9) - $^2\Sigma$(000) (green) vibronic bands. The variations in relative intensity in the observed spectrum compared to the simulations derive from accumulation of deposits on the photolysis laser window between cleanings.

This work has also recently been published in *J. Molec. Spectrosc.* 376, 111404 (2021).

II. Future Work

A. Low temperature measurements of C_2H_2 broadening and shifts

To augment the ambient temperature data measurements described above, we have begun a series of low temperature (i.e. between 160 and 240K) measurements of the same series of lines. As an example, the figure shows R(13) at 160.38K and 5.064 torr pressure. Preliminary fits to the data are very good and the variation in pressure broadening coefficients with temperature will provide additional data for modeling the astronomical observations of the atmosphere of Titan and other solar system bodies. We will complete the data set in this context by also recording the pressure broadening and shifts caused by collisions with nitrogen molecules, also at temperatures between 160K and 298K.

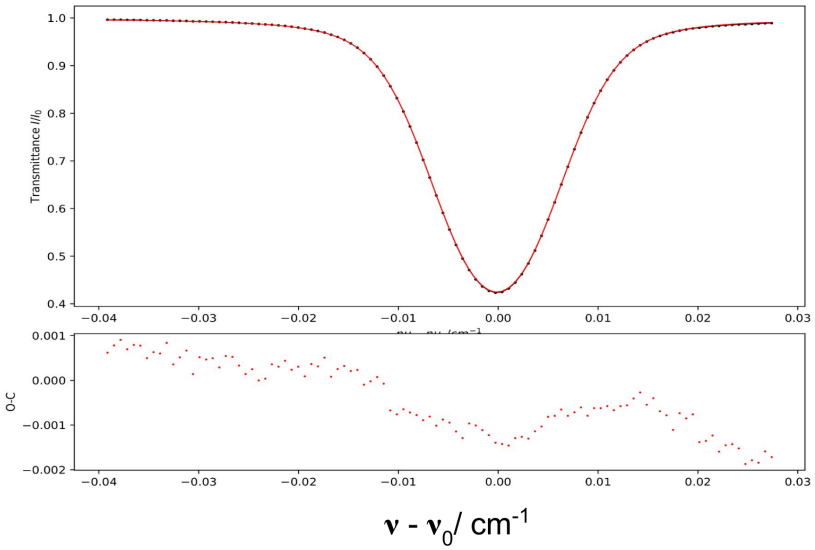

B. Nuclear Spin-Rotation-Vibration Splittings in CH_4

Due to the effects of the COVID-19 virus shutdown and consequent delays in experimental measurements, the methane measurements proposed last year have yet to be started. However, with the spectrometer and closed cycle cryogenic cell now working routinely, we anticipate the first of these measurements will be able to be completed this coming summer.

III. Publications related to this project since 2018

1. Investigating the photodissociation of H_2O_2 using frequency modulation laser absorption spectroscopy to monitor radical products, J. P. A. Lockhart, E. C. Gross, T. J. Sears and G. E. Hall, *Chem. Phys. Letts.* **711**, 148-151 (2018).
2. Frequency measurements and self-broadening of sub-Doppler transitions in the $\nu_1 + \nu_3$ band of acetylene, S. Twagirayezu, G. E. Hall and T. J. Sears, *J. Chem. Phys.*. **149**, 154308 (2018).
3. Kinetic study of the OH + ethylene reaction using frequency-modulated laser absorption spectroscopy, J. P. A. Lockhart, E. C. Gross, T. J. Sears and G. E. Hall, *Int. J. Chem. Kin.* **51**, 412-421 (2019)
4. Re-evaluation of ortho-para-dependence of self-pressure broadening in the $\nu_1 + \nu_3$ band of acetylene, E. C. Gross, K. A. Tsang, and T. J. Sears, *J. Chem Phys,* **154**, 054305 (2021).
5. The 1.66 μm spectrum of the ethynyl radical, CCH, E. C. Gross, Anh T. Le, G. E. Hall and T. J. Sears, *J. Molec. Spectrosc.* 376, 111404 (2021).
6. The electric field dependent g−factor for the lead monofluoride, PbF, ground state, V.V. Baturo, P. M. Rupasinghe, T. J. Sears, R. J. Mawhorter, J.-U. Grabow, A.N. Petrov, *Phys. Rev A*. (submitted, Feb. 2021) https://arxiv.org/abs/2102.12874

Theoretical Studies of Potential Energy Surfaces and Computational Methods

Ron Shepard
Chemical Sciences and Engineering Division,
Argonne National Laboratory, Lemont, IL 60439
[email: shepard@tcg.anl.gov]

Program Scope: This project involves the development, implementation, and application of theoretical methods for the calculation and characterization of potential energy surfaces (PES) involving molecular species that occur in combustion, atmospheric, and general gas-phase chemistry. An accurate and balanced treatment of reactants, intermediates, and products for both ground and excited electronic states is required. This difficult challenge is met with general multiconfiguration self-consistent field (MCSCF) and multireference configuration interaction (MRCI) methods [see *Chem. Rev.* **112**, 108 (2012)]. More recently, the *graphically contracted function* (GCF) method has been developed to address some of the practical limitations of the traditional MCSCF and MRCI approaches, including the number of active electrons that may be accommodated and the overall expense associated with the study of larger molecular systems [see *J. Chem. Phys.* **141**, 064105 (2014) and references therein]. These methods are developed and maintained within the COLUMBUS Program System.

Recent Progress: The COLUMBUS Program System uses extensively the Graphical Unitary Group Approach (GUGA) to specify the configuration state function (CSF) expansion space with which many-electron wave functions can be represented. The Shavitt graph, the fundamental entity of GUGA, is a compact visual and computational data structure that specifies the orbital occupation and spin coupling of each individual CSF and also the entire CSF expansion space. A single-headed Shavitt graph specifies the expansion space for a given number of orbitals *n*, a given number of electrons *N*, and a given spin multiplicity *S*. The union of several such expansion spaces with different *N* and *S* values is appropriate for computing state-averaged wave functions, orbitals, and reduced density matrices, and also for computing ground- and excited-state wave functions with spin-orbit interaction in which the total spin *S* is not a good quantum number.

Coupling coefficients within GUGA correspond to pairs of walks from the tail of the graph to a head of the graph. The nonzero coupling coefficients for one-electron $\langle m|\hat{E}_{pq}|n\rangle$ or two-electron $\langle m|\hat{e}_{pqrs}|n\rangle$ operators are sparse in the CSF indices *m* and *n* and in the spatial orbital indices *p*, *q*, *r*, and *s*. To facilitate the efficient identification, computation, and storage of the coupling coefficients, the auxiliary pair graph (APG) was introduced. The APG maps pairs of interacting nodes to a single vertex, and it maps coupling coefficients to a single path from the APG tail to an APG head. The value of a coupling coefficient is computed as products of segment values, each of which can be stored or computed on-demand as needed. Each segment value corresponds to a quartet of nodes of the Shavitt graph, or to an upper node pair and lower node pair, or to an upper and lower APG vertex connected with an APG edge. Expressions have been derived previously (see *Int. J. Quantum Chem.* **107**, 3191 (2007) and references therein) for the number of

This work was performed under the auspices of the Office of Basic Energy Sciences, Division of Chemical Sciences, Geosciences, and Biosciences, U.S. Department of Energy, under contract number DE-AC02-06CH11357.

walks in the Shavitt graph, the number of nodes in the Shavitt graph, the number of arcs in the Shavitt graph, and the number of node pairs of the Shavitt graph for both single-headed and multi-headed Shavitt graphs. We have recently extended this analysis to the computation of Shavitt graph segment counts or, equivalently, to APG edge counts. There are 208 possible segment types. Of these, 68 node pair and segment shape combinations can be ignored because they do not correspond to the ΔN and ΔS restrictions appropriate for two-electron operators. Of the 140 remaining segment types, several count expressions are related through bra-ket interchange or particle-hole interchange symmetry.

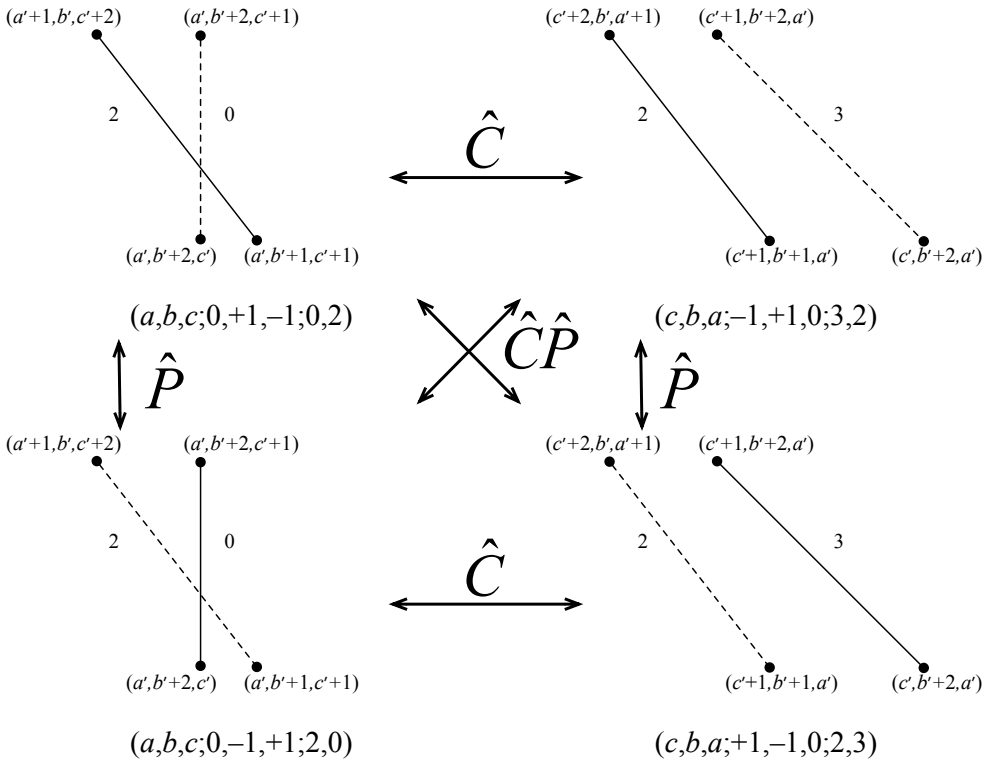

Figure 1. Symbolic representation of the $\hat{P}$ and $\hat{C}$ mappings between example segment types in Shavitt graph G with head node (a,b,c) and its dual graph $\hat{C}G$ with head node (c,b,a). For each of the four segment type diagrams, the nodes are labeled as Paldus triples, and arcs with their step values, and the diagram with its segment type notation at the bottom. The bra steps are designated with the dashed lines and the ket steps with the solid lines. All mappings are bidirectional due to the involutory nature of the operators.

A segment may be denoted in several equivalent ways. One such choice is $(a,b,c;\Delta a,\Delta b,\Delta c;d,d')$, where (a,b,c) denotes the Shavitt graph head (and thereby the entire CSF expansion space), $(\Delta a,\Delta b,\Delta c)$ denotes the lower node pair, and (d,d') denotes the 16 possible step pairs for the bra and ket steps respectively. With this convention, bra-ket interchange is denoted

$$\hat{P}\left(a,b,c;\Delta a,\Delta b,\Delta c;d,d'\right)=\left(a,b,c;-\Delta a,-\Delta b,-\Delta c;d',d\right)$$

and particle-hole interchange is denoted

$$\hat{C}\left(a,b,c;\Delta a,\Delta b,\Delta c;d,d'\right)=\left(c,b,a;\Delta c,\Delta b,\Delta a;\hat{C}d,\hat{C}d'\right)$$

with the $\hat{C}d$ mapping defined as

$$\hat{C}\{0,1,2,3\}=\{3,1,2,0\}.$$

The particle-hole interchange operator maps a segment from within the $(a,b,c)=(\alpha,b,\alpha')$ graph to a segment within its dual graph $(a,b,c)=(\alpha',b,\alpha)$ with the values of a and c interchanged. Both of these mappings are bijections (one-to-one and onto), both mappings are involutory ($\hat{P}\hat{P}=\hat{I}$ and $\hat{C}\hat{C}=\hat{I}$), and both operators commute ($\hat{P}\hat{C}=\hat{C}\hat{P}$). The mappings four related segments are shown in Fig. 1. Because these operator mappings are bijections, enumeration of the number of segments of the type in the upper left of Fig. 1 gives also the number of segments of the type in the upper right, lower left, and lower right segments. Because of the a-c interchange associated with the $\hat{C}$ operator, this also establishes a relationship between related segment types within a given graph (a,b,c). These operators reduce the 140 two-electron operator segments down to 41 unique segment types. Enumeration of these 41 symmetry-unique types is sufficient to enumerate the full 140 operator segment types. The total edge counts are given below.

$$\begin{aligned}
N_{\text{edge}}\left(a,b,c\right)=&\,140abc-172ac-19b-50\delta_{b0}+38-\left(26b-26\delta_{b0}+32\right)\left(a+c\right)\\
&+\left(44b-14\delta_{b0}-16\right)\left(a\delta_{c0}+c\delta_{a0}\right)\\
&+\left(8b+38\delta_{b0}-26\right)\left(\delta_{a0}+\delta_{c0}\right)+\left(4b-26\delta_{b0}+14\right)\delta_{a0}\delta_{c0}\\
&+2\delta_{a1}\left(\left(2c+1\right)b-\left(2-\delta_{c0}\right)\left(1-\delta_{b0}\right)\right)+2\delta_{c1}\left(\left(2a+1\right)b-\left(2-\delta_{a0}\right)\left(1-\delta_{b0}\right)\right)\\
&+2\delta_{b1}\left(a+c+\delta_{a0}+\delta_{c0}-2\right)+66Z\left(a,c\right)+37Z\left(a+1,c\right)+37Z\left(a,c+1\right)
\end{aligned}$$

$$\begin{aligned}
N_{\text{edge}}^{\text{SO}}\left(a,b,c\right)=&\,140abc-365ac-19b-44\delta_{b0}+36-\left(26b-22\delta_{b0}+43\right)\left(a+c\right)\\
&+\left(44b-10\delta_{b0}-58\right)\left(a\delta_{c0}+c\delta_{a0}\right)\\
&+8\left(b+4\delta_{b0}-2\right)\left(\delta_{a0}+\delta_{c0}\right)+4\left(b-5\delta_{b0}-1\right)\delta_{a0}\delta_{c0}\\
&+2\delta_{a1}\left(\left(2c+1\right)\left(b-1\right)-\left(2-\delta_{c0}\right)\delta_{b0}\right)+2\delta_{c1}\left(\left(2a+1\right)\left(b-1\right)-\left(2-\delta_{a0}\right)\delta_{b0}\right)\\
&+2\delta_{b1}\left(a+c+\delta_{a0}+\delta_{c0}-2\right)\\
&+132Z\left(a,c\right)+66Z\left(a+1,c\right)+66Z\left(a,c+1\right)+8Z\left(a+2,c\right)+8Z\left(a,c+2\right)
\end{aligned}$$

with

$$Z(a,c)=\sum_{a'=0}^{a}\sum_{c'=0}^{c}\min(a',c')=\tfrac{1}{2}\eta(a+1)(c+1)-\tfrac{1}{6}\eta(\eta+1)(\eta+2)$$

and η=min(a,c). These expressions, for single-headed and for multi-headed spin-orbit graphs, are both symmetrical with respect to a-c interchange. The coefficient of the abc factor is 140 in both expressions. This is because each of the 140 segment types contributes one such term. The nonspin-orbit edge count has 140 Z terms for the same reason while the spin-orbit edge count has exactly twice that number, 280, Z terms. This is because each of the spin-orbit segment types contributes two Z terms. These expressions ultimately allow the computational effort associated with various electronic structure methods to be quantified. In methods that precompute and store the segment values for later access, such as the GCF method, these expressions also determine the amount of memory required to store each nonzero segment value. In future work, these expressions will be used to determine closed-form expressions for the number of nonzero coupling coefficients.

Publications:

"On the All Configuration Mean Energy Condition," 59th Sanibel Symposium in Honor of Klaus Ruedenberg Proceedings, (2019).

"The All Configuration Mean Energy Multiconfiguration Self-Consistent-Field Method I. Equal Configuration Weights," R. Shepard and S. R. Brozell, *Mol. Phys.* **117**, 2374-2390 (2019). DOI: 10.1080/00268976.2019.1635275.

"The All Configuration Mean Energy (ACME) MCSCF Method," R. Shepard, S. R. Brozell, G. Gidofalvi, *7th Annual OpenMolcas Developers' Workshop Book of Abstracts*, 27 (2019).

"Some Recent Applications of the Graphical Unitary Group Approach," R. Shepard, S. R. Brozell, G. Gidofalvi, *The Utah Workshop on Quantum Methods in Molecular and Solid-State Theory Abstracts*, (2019).

"Representations of Shavitt Graphs Within the Graphical Unitary Group Approach," R. Shepard, S. R. Brozell, and G. Gidofalvi, *J. Computational Chem.* **41**, 129-135 (2020). DOI: 10.1002/jcc.26080.

"An Arc Density Maximum Flow Algorithm," R. Shepard, S. R. Brozell, J. Larson, P. Hovland, and S. Leyffer, 60th Sanibel Symposium Abstracts (2020).

"The Generality of the GUGA MRCI Approach in COLUMBUS for Treating Complex Quantum Chemistry," H. Lischka, R. Shepard, T. Müller, P. G. Szalay, R. M. Pitzer, A. J. A. Aquino, M. M. A. do Nascimento, M. Barbatti, L. T. Belcher, J.-P. Blaudeau, I. Borges Jr., S. R. Brozell, E. A. Carter, A. Das, G. Gidofalvi, L. Gonzalez, W. L. Hase, G. Kedziora, M. Kertesz, F. Kossoski, F. B. C. Machado, S. Matsika, S. A. do Monte, D. Nachtigallova, R. Nieman, M. Oppel, C. A. Parish, F. Plasser, R. F. K. Spada, E. A. Stahlberg, E. Ventura, D. R. Yarkony, Z. Zhang, *J. Chem. Phys.* **152**, 134110 (2020). DOI: 10.1063/1.5144267.

"Wave Function Analysis with a Maximum Flow Algorithm," R. Shepard, S. R. Brozell, J. Larson, P. Hovland, and S. Leyffer, *Mol. Phys.* (2020). DOI: 10.1080/00268976.2020.1861351.

Mechanisms and Models for Simulating Gas Phase Chemical Reactivity

Raghu Sivaramakrishnan
Chemical Dynamics Group, Chemical Sciences & Engineering Division
Argonne National Laboratory, Argonne, IL 60439
raghu@anl.gov

I. Program Scope

Mechanisms describing the chemical reactivity of small gas phase species can be complex involving a myriad of unimolecular and bimolecular elementary steps. The primary scope of this program is to develop and validate detailed chemical kinetics mechanisms and models for use in predictive simulations of high temperature gas phase reactivity. Kinetics modeling has been used predominantly as an engineering tool for making predictions for practical applications in combustion and chemical conversions. However, within the context of the chemical physics BES program we have utilized a concerted Modeling-Experiment-Theory (MET) approach in collaboration with PI's in the group and externally to highlight interesting problems pertinent to gas phase chemical reactivity. In such a context, modeling combustion chemistry provides access to a wide range of relevant physical (pressures, temperatures and gradients in these), chemical environments (small gas phase hydrocarbon species to particulate matter), internal energies, and timescales to allow us to highlight the role of quantum effects such as tunneling, anharmonic thermochemistry, and chemically activated molecules and nonthermal reactions among others.

II. Recent Progress

A. Radical-Radical Reactions at High Temperatures

In prior studies[1] we have highlighted the role of chemically activated adducts in radical-radical reactions and emphasized the role of unaccounted for pathways that can be accessed through such energized adducts to explain the evolution of species in flames. Most detailed chemical kinetics models often consider only the recombination process (and typically at its high-pressure limit) in a radical-radical reaction for C_4 and larger hydrocarbons. For H + alkyl and CH_3 + alkyl radical reactions, prior theoretical studies[2,3] have determined high-pressure limiting rate constants for the recombination processes in selected straight and branched chain alkyl radicals. However, the presumption that recombination will be the dominant process may not hold good since steric effects may dictate large contributions from disproportionation processes. Additionally, at elevated temperatures there is an increased likelihood to access higher energy channels from the chemically activated adducts formed in radical-radical reactions. In recent studies, Tranter and co-workers have performed experiments to determine rate constants for such self-reactions of all four butyl radical isomers (n, sec, iso, and tert). In collaboration with theoretical predictions for capture rates from Jasper, we have simulated these experiments[4] to determine the role of addition vs disproportionation in these bimolecular processes. In the experimental conditions accessed (700-1300K) by Tranter, these alkyl radicals also dissociate predominantly[5,6,7] via, tert-$C_4H_9 \rightarrow$ H + i-C_4H_8, iso-$C_4H_9 \rightarrow CH_3 + C_3H_6$, sec-$C_4H_9 \rightarrow CH_3 + C_3H_6$, and n-$C_4H_9 \rightarrow C_2H_5 + C_2H_4$ and lead to reactive H, CH_3, and C_2H_5 radicals in each of these radical systems. Proper interpretation of the experiments also requires consideration of reactions of these reactive atoms/radicals with the parent butyl radicals, i. e. H + tert-C_4H_9, CH_3 + iso-C_4H_9/sec-C_4H_9 and C_2H_5 + n-C_4H_9. Again, as with the self-reactions of butyl radicals, addition and disproportionation processes occur in these reaction systems. Additionally, energetically accessible addition-elimination radical products can also be accessed in these reactions. While detailed kinetics models consider recombination to be the dominant channel[8] (or the only channel[9]) for these reactions, our preliminary results indicate that even for the larger C_2H_5 + n-C_4H_9 system at T > 1000 K and P = 1 bar there is significant contribution (~20%) to addition-elimination leading to n-C_3H_7 + n-C_3H_7. At higher temperatures and lower pressures and for the other three smaller radical systems, addition-eliminations through chemically activated C_4 and C_5 alkanes are major channels.

Another area of interest in such radical-radical reactions is the role of the roaming transition state mediating direct abstraction such that this may be the dominant kinetic process at low temperatures and pressures. In collaboration with Klippenstein we plan on initiating theoretical and modeling studies to characterize this in the C_2H_5 + C_2H_5 system. This reaction also plays a crucial role in a recent low-temperature study[10] of the C_2H_5 + HBr reaction, and if disproportionation is favored over recombination, then this may lead to a re-interpretation of these very low pressure studies on R + HX that are at odds with other literature studies on the kinetics for these reactions. Lastly, we were highlighted to this problem by Ruscic and Bross who have been developing accurate thermochemical functions for C_2H_5. The R + HX (HBr and HI) kinetic equilibrium studies described above have also been used to determine heats of formation for the alkyl radicals of interest. The recent work of Leplat et al.[10] concluded from their results and a third law analysis that the heat of formation of the C_2H_5 radical needs to be lower which is inconsistent with current ATcT recommendations. Reinterpreting these very low-pressure bromination and iodination studies may also have an implication for the derived experimental thermochemistry of C_2H_5 and other alkyl radicals.

B. Ring Opening in Cycloheptane and the Subsequent Dissociation of 1-Heptene

Cycloalkanes and alkenes are important components of real fuels but there is little kinetic and mechanistic data on the dissociation of most large cyclic and olefinic molecules at elevated temperatures. Consequently, a series of systematic experimental studies on cyclopentane and cyclohexane along with their primary products, 1-pentene and 1-hexene respectively, have been performed by Kiefer et al.[11] and Tranter et al.[12] in prior shock tube studies. The present work on cycloheptane initiated by Tranter[13] is a continuation of these studies to characterize the role of size and ring-strain in the thermal dissociation of cycloalkanes. The potential energy surface (PES) for cycloheptane isomerization to 1-heptene and other potentially competing processes was characterized using electronic structure theory at the CCSD(T)/cc-pV∞Z//M06-2X/cc-pVTZ level. The lowest energy pathway in cycloheptane is ring opening leading to the formation of a diradical which has a low barrier for subsequent hydrogen transfer to form 1-heptene. The direct process for cycloheptane isomerization has a much higher barrier and therefore is not expected to be relevant to the formation of 1-heptene. VLPP studies on cycloheptane pyrolysis[14] suggest that C-H fission and formation of cycloheptene are potentially relevant channels. However, the current calculations show large barriers for these processes, thereby rendering them irrelevant to the unimolecular kinetics of cycloheptane dissociation. The present calculations provide convincing support for the diradical mechanism that is known to be the dominant kinetic process in other similar sized cycloalkanes such as cyclopentane[12,15] and cyclohexane.[11] The lowest energy bond fission process in 1-heptene leads to the formation of the resonance stabilized allyl radical and n-butyl radical. Six-center retro-ene elimination pathways[16] are known to be active in such molecules, and in 1-heptene this is the energetically most favorable pathway forming propene and 1-butene with a barrier 55.3 kcal/mol. Despite the lower barrier for the molecular process, the tight nature of the TS leads to lower A-factors and at high temperatures, T>1000 K, this process is expected to be a minor channel. Theoretical kinetics results from master equation calculations were in good agreement with the present experimental results for cycloheptane and 1-heptene dissociations.

C. Substitution and Chemically Activated Reactions in Acetone Pyrolysis

Recent studies using micro-tubular reactors[17,18] coupled with a variety of diagnostics have been used to probe the high temperature pyrolytic chemistry of organic molecules. These experiments offer access to conditions akin to those in laminar premixed flames; i. e. low-pressures and high-temperatures, which can emphasize the role of chemically activated reactions. In prior work with J. V. Michael, L. B. Harding, and S. J. Klippenstein, we have conclusively demonstrated[19] the role of keto-enol tautomerizations and radical-molecule addition-elimination reactions to explain product observations[17] from CH_3CHO pyrolysis using a micro-tubular reactor. Such reactions are also expected to play a role in acetone pyrolysis. In a recent collaboration[20] with Prozument and Klippenstein we have utilized a combined Modeling-Experiment-Theory (MET) paradigm to characterize the mechanism of acetone

decomposition at high temperatures. Acetone decomposition is known to be a prototypical example of a free-radical mechanism[21] involving chain reactions. Broadband rotational spectroscopy was used to quantify selected products from the high temperature pyrolysis of acetone. Ketene was observed as the major product, along with the minor products: acetaldehyde, propyne, propene, and H_2O (from measurements of HDO in deuterated acetone experiments). An automated theoretical kinetics code was used to rapidly calculate a priori rate constants for the numerous addition and abstraction reactions of acetone and its enol isomer (2-propenol) with H, CH_3, and OH and to model the subsequent dissociations of radicals formed by substitutions/abstractions. These results were used to assemble a kinetics model to describe the formation of the numerous intermediates observed in the present and prior studies. CH_3CHO has not previously been observed as a product in acetone pyrolysis. The present theory/modeling studies attribute its formation to a well-skipping homolytic substitution process that involves addition of an H atom to acetone followed by the loss of a CH_3 group. Keto−enol tautomerization is also shown to be an important process in acetone pyrolysis, with enol driven chemistry being the dominant source for the propene, propyne, and water observed in the present experiments. Propene is a product of another substitution reaction in which free H atoms replace OH in the enol isomer of acetone. In a broader context, this work emphasizes the importance of the radical substitution reactions that are often overlooked. The theory-aided model also was used to simulate the formation of other intermediates in high temperature shock tube studies from the literature. While the extended Rice−Herzfeld mechanism was deemed sufficient to describe acetone pyrolysis in studies to date, the present MET framework highlights the prominent role of enol driven chemistry and well-skipping reactions to advance our understanding of the pyrolysis of the simplest ketone, acetone.

D. Competition between Radical and Molecular Channels in Methylformate Decomposition

Methylformate (MF), CH_3OCHO, as a prototype simple methylester, has been the subject of numerous combustion studies. Thermal decompositions and abstractions in MF were shown to play an important role in a prior combustion modeling study.[22] However, this study was unable to reconcile the theoretically predicted[23,24] activation energies for the three major molecular decompositions in methylformate, (R1) – (R3),

$CH_3OCHO \rightarrow CH_3OH + CO$ (R1)

$CH_3OCHO \rightarrow CH_2O + CH_2O$ (R2)

$CH_3OCHO \rightarrow CH_4 + CO_2$ (R3)

A high temperature shock tube study of methylformate pyrolysis using multi-species (CO, CH_2O, CH_4) absorption diagnostics[25] concurs with the model-based estimates[22] for the activation energies and rates for reactions (R1) - (R3). The discrepancies between experimental/modeling studies[22,25] and theoretical predictions[23,24] for the thermal decompositions have motivated the present theory/modeling study on the combustion of methylformate. In collaboration with Klippenstein, the CH_3OCHO and H + CH_3OCHO potential energy surfaces were re-analyzed using high-level electronic structure theory calculations. Exploration of the CH_3OCHO PES indicates a potential role for the formation of the carbene, CH_3OCOH, not characterized in the prior theoretical studies and its subsequent decomposition to $CH_4 + CO_2$ and $CH_3 + HOCO$. Additionally, a triple-whammy channel leading to $CH_2O + H_2 + CO$ has been identified that is energetically lower than the 4-center elimination to CH_2O (R2) characterized in prior theoretical studies. Theoretical kinetics calculations have been initiated using the updated PES to characterize the competition between these molecular channels and higher energy bond-fissions at high temperatures. These theoretical results will be used to assemble the pyrolysis sub-mechanism for methylformate and to re-interpret the observations from the prior literature shock tube[24,25] studies.

III. Acknowledgements

This work was supported by the U.S. Department of Energy, Office of Science, Office of Basic Energy Sciences, Division of Chemical Sciences, Geosciences, and Biosciences under Contract No. DE-AC02-06CH11357.

IV. References

1. N. J. Labbe, R. Sivaramakrishnan, S. J. Klippenstein, Proc. Combust. Inst. 35, 447 (2015).
2. L. B. Harding, Y. Georgievskii, S. J. Klippenstein, J. Phys. Chem. A 109, 4646 (2005).
3. S. J. Klippenstein, Y. Georgievskii, L. B. Harding, Phys. Chem. Chem. Phys. 8, 1133 (2006).
4. J. B. Randazzo, R. Sivaramakrishnan, A. W. Jasper, T. Sikes, P. T. Lynch, R. S. Tranter, Phys. Chem. Chem. Phys. 22 (2020) 18304-18319.
5. V. D. Knyazev, I. A. Dubinsky, I. R. Slagle, D. Gutman, J. Phys. Chem. 98, 5279 (1994).
6. V. D. Knyazev, I. A. Dubinsky, I. R. Slagle, D. Gutman, J. Phys. Chem. 98, 11099 (1994).
7. V. D. Knyazev, I. R. Slagle, J. Phys. Chem. 100, 5318 (1996).
8. H. Wang, X. You, A.V. Joshi, S.G. Davis, A. Laskin, F. Egolfopoulos, C.K. Law, USC Mech Version II.
9. W.K. Metcalfe, S.M. Burke, S.S. Ahmed, H.J. Curran, Int. J. Chem. Kin. 45 (2013) 638-675.
10 N. Leplat, A. Wokaun, M. J. Rossi, J. Phys. Chem. A 117, 11383 (2013).
11. J.H. Kiefer, K.S. Gupte, L.B. Harding, S.J. Klippenstein, J. Phys. Chem. A. 113 (2009) 13570–13583.
12. J.B. Randazzo, C.J. Annesley, K. Bell, R.S. Tranter, Proc. Combust. Inst. 36 (2017) 273–280.
13. T. Sikes, K.B. Burdett, R.L. Speth, C.F. Goldsmith, R. Sivaramakrishnan, R.S. Tranter, Proc. Combust. Inst. 38 (2021) 929.
14. L.E. Gusel'nikov, V. V. Volkova, P.E. Ivanov, S. V. Inyushkin, L. V. Shevelkova, G. Zimmermann, U. Ziegler, B. Ondruschka, J. Anal. Appl. Pyrolysis. 21 (1991) 79–93.
15. B. Sirjean, F. Buda, H. Hakka, P.A. Glaude, R. Fournet, V. Warth, F. Battin-Leclerc, M. Ruiz-Lopez, Proc. Combust. Inst. 31 (2007) 277–284.
16. A.T. Blades, H.S. Sandhu, Int. J. Chem. Kinet. 3 (1971) 187–193.
17. A. Vasiliou, K.M. Piech, B. Reed, X. Zhang, M.R. Nimlos, M. Ahmed, A. Golan, O. Kostko, D.L. Osborn, D.E. David, K.N. Urness, J.W. Daily, J.F. Stanton, G.B.; Ellison, J. Chem. Phys. **2012**, 137, 164308.
18. K. Prozument, Y.V. Suleimanov, B. Buesser, J.M. Oldham, W.H. Green, A.G. Suits, R.W. Field, J. Phys. Chem. Lett. **2014**, 5, 3641-3648.
19. R. Sivaramakrishnan, J.V. Michael, L.B. Harding, S.J. Klippenstein, J. Phys. Chem. A **2015**, 119, 7724-7733.
20. D. P. Zaleski, R. Sivaramakrishnan, H. R. Weller, N. A. Seifert, D. H. Bross, B. Ruscic, K. B. Moore, S. N. Elliott, A. V. Copan, L. B. Harding, S. J. Klippenstein, R. W. Field, K. Prozument, J. Am. Chem. Soc. **2021**, 143, 3124-3142.
21. F. O. Rice, K. F. Herzfeld, J. Am. Chem. Soc. **1934**, 56, 284−289.
22. S. Dooley, M. P. Burke, M. Chaos, Y. Stein, F. L. Dryer, V. P. Zhukov, O. Finch, J. M. Simmie, H. J. Curran, Int. J. Chem. Kinet. **2010**, 42, 527-549.
23. W. K. Metcalfe, J. M. Simmie, H. J. Curran, J. Phys. Chem. A **2010**, 114, 5478-5484.
24. S. L. Peukert, R. Sivaramakrishnan, M.-C. Su, J. V. Michael, Comb. and Flame **2012**, 159, 2312-2323.
25. W. Ren, K.-Y. Lam, S. H. Pyun, A. Farooq, D. F. Davidson, R. K. Hanson, Proc. Combust. Inst. **2013**, 34, 453.

V. Journal articles supported by this project 2018-2021

1. P. J. Weddle, C. Karakaya, H. Zhu, R. Sivaramakrishnan, K. Prozument, R. J. Kee, "Boundary-layer Model to Predict Chemically Reacting Flow within Heated, High-Speed, Micro-tubular Reactors", Int. J. Chem. Kin. **50** (2018) 473-480.
2. G. Magnotti, Z. Wang, W. Liu, R. Sivaramakrishnan, S. Som, M. J. Davis, "Sparsity Facilitates Chemical-Reaction Selection for Engine Simulations", J. Phys. Chem. A **122** (2018) 7227-7237.
3. S. Bai, M. J. Davis, R. Sivaramakrishnan, R. T. Skodje, "A Chemical Pathway Perspective on the Kinetics of Low-Temperature Ignition of Propane", Comb. and Flame **202** (2019) 154-178.
4. J. B. Randazzo, R. Sivaramakrishnan, A. W. Jasper, T. Sikes, P. T. Lynch, R. S. Tranter, "An Experimental and Theoretical Study of the High Temperature Reactions of the Four Butyl Radical Isomers", Phys. Chem. Chem. Phys. **22** (2020) 18304-18319.
5. T. Sikes, K. B. Burdett, R. L. Speth, C. F. Goldsmith, R. Sivaramakrishnan, R. S. Tranter, "Ring Opening in Cycloheptane and Dissociation of 1-heptene at High Temperatures", Proc. Combust. Inst. **38** (2021) 929-937.
6. D. P. Zaleski, R. Sivaramakrishnan, H. R. Weller, N. A. Seifert, D. H. Bross, B. Ruscic, K. B. Moore III, S. N. Elliott, A. V. Copan, L. B. Harding, S. J. Klippenstein, R. W. Field, K. Prozument, "Substitution Reactions in the Pyrolysis of Acetone Revealed through a Modeling, Experiment, Theory Paradigm", J. Am. Chem. Soc. **143** (2021) 3124-3142.
7. T. Sikes, R. Sivaramakrishnan, C. Banyon, R. A. Schwind, P. T. Lynch, A. Comandini, R. S. Tranter, "Initiation Reactions in the High Temperature Decomposition of Styrene", In Preparation, Phys. Chem. Chem. Phys. (2021).
8. R. Sivaramakrishnan, N. J. Labbe, S. J. Klippenstein, "Molecular and Radical Channels in the High Temperature Decomposition of Methylformate", In Preparation, J. Phys. Chem. A (2021).

ADVANCED DIAGNOSTICS

David W. Chandler, Jonathan H. Frank, Nils Hansen, Christopher J. Kliewer, Habib N. Najm, David L. Osborn, Krupa Ramasesha, Leonid Sheps, Craig A. Taatjes, Timothy S. Zwier
Combustion Research Facility, Sandia National Laboratories, MS 9055, Livermore, CA 94551-0969
chand@sandia.gov, jhfrank@sandia.gov, nhansen@sandia.gov, cjkliew@sandia.gov, hnnajm@sandia.gov, dlosbor@sandia.gov, kramase@sandia.gov, lsheps@sandia.gov, cataatj@sandia.gov, tszwier@sandia.gov

PROGRAM SCOPE

A unifying theme throughout the experimental work in this task is the need for incisive advanced diagnostics that illuminate the hidden world of molecules. Over the years, our program has made many innovations that support chemical physics research in areas such as non-linear spectroscopy, ion imaging, 3-dimensional laser-induced fluorescence, multiplexed photoionization / photoelectron spectroscopy, and x-ray absorption and scattering. These approaches include *in situ* laser and light source-based techniques that directly probe reacting environments, and *ex situ* techniques that extract species from reactive environments before implementing diagnostics that would be impossible under the native conditions of the chemical reaction. We leverage these experimental innovations with theoretical advances that predict dynamics and kinetics to compare with experiment, and to inform the improvement of diagnostics. Our recent work in optimal experimental design adds a new dimension to the coupling between experiment and theory, providing a feedback loop to optimize an experiment, thereby maximizing extracted information and quantifying uncertainty. Our proposed research includes new developments in areas where we are well established, and additional ideas that broaden our work on both ends of the electromagnetic spectrum. Ultrafast non-linear spectroscopy in the soft and hard x-ray region is a new area of emphasis, as well as combining broadband microwave spectroscopy with specialized molecular sources to enable new spectroscopy of reactive intermediates. As these advanced diagnostics mature, they provide the new tools that enable deeper exploration in Gas Phase Chemical Physics

RECENT PROGRESS

Bayesian Optimal Experimental Design, Application to Time-of-Flight Mass Spectrometry We worked on further development of a Bayesian optimal experimental design (OED) construction targeting Sandia's high-pressure photoionization mass spectrometry apparatus (HP-PIMS). HP-PIMS samples reacting gas mixtures from a high-pressure laser photolysis reactor and analyzes the chemical composition of the gas in real-time using a 40 kHz pulsed reflectron time of flight (TOF) mass spectrometer with tunable synchrotron VUV photoionization. A proper representation of the instrument sensitivity, and uncertainties associated with the initial reaction conditions, as well as the sampling and detection process, is critical to the interpretation of HP-PIMS data. Over the past year, we (1) finalized construction of a probabilistic model of the experimental system in its pre-photolysis phase, accounting for noise, model error, and parametric uncertainties; and (2) demonstrated the calibration of this model using Bayesian inference relying on existing pre-photolysis data from this experiment; to arrive at a model that fits the pre-photolysis baseline data with quantified uncertainty. We have a manuscript in-progress to report these results. We have also formulated the instrument model for the post-photolysis experiment, relying on the pre-photolysis model as a baseline, and are working on the preparation of necessary algorithms and code utilities to facilitate the computational solution. Much of the effort that went into the pre-photolysis model construction had to deal with the intricacies of the representation of the uncertain peak structure in the mass spectrum signal, particularly at low signal. This construction is immediately applicable to the post-photolysis data structure, thus resolving a significant part of the necessary effort *a priori.*

Building a Time-Resolved Photoelectron Photoion Coincidence Spectrometer We have made significant progress commissioning our new PEPICO spectrometer at Sandia. Due to pandemic restrictions we have not yet been able to test the new instrument at the Chemical Dynamics Beamline of the Advanced Light

Source Synchrotron of Lawrence Berkeley National Laboratory, where tunable vacuum ultraviolet photons maximize the power of the instrument. Nevertheless, using vacuum ultraviolet radiation from discharges of Ar and Ne, we have acquired velocity mapped photoelectron and photoion spectra of noble gas atoms and small molecules, both from supersonic jet and chemical reactor tube sources. These initial results show an electron kinetic energy range of 0 – 6 eV with energy resolution of $\Delta E/E \sim 3\%$, which we believe will improve when the apparatus can take advantage of high-brightness synchrotron radiation. We have achieved mass resolution for cations of $m/\Delta m > 1000$ at present.

Broadband Microwave Spectroscopy for Isomer-specific Detection of Transient Intermediates
Over the past year, we have focused our attention on bringing on-line and optimizing the performance of our multiplexed spectrometer that combines broadband chirped-pulse Fourier transform microwave (CP-FTMW) detection with VUV photoionization time-of-flight mass spectrometry. These complementary detection schemes enable sensitive detection and spectroscopic interrogation of complex gas mixtures. There are significant opportunities for application of CP-FTMW spectroscopy to reacting mixtures that contain free radicals or other highly reactive intermediates. In its present form, the instrument incorporates a heated pulsed valve for sample introduction via supersonic expansion. A flash pyrolysis source affixed to the faceplate of the pulsed valve can be used to study the thermal decomposition of selected molecules of interest. During the past year, we have completed the analysis and published[1] a study of the pyrolysis of *trans*-3-pentenenitrile (CH_3-CH=CH-CH_2-CN, C_5H_7N, 81 amu), a molecule of interest as a possible precursor to the heteroaromatic pyridine. In collaboration with Alex Mebel (FIU), we have mapped out the decomposition pathways. Loss of two H-atoms to form a 79 amu product is proven from its microwave transitions to contain *trans*-Z-2,4-pentadienenitrile, while no pyridine is observed. Methyl loss, HCN loss, and breaking the central C(2)-C(3) bond all occur following isomerization of the position of the double bond, thereby opening up low-energy pathways to these decomposition channels. We also published[2] our exploratory investigation that combined an atmospheric pressure jet-stirred reactor (JSR) with the broadband chirped-pulse microwave spectrometer to identify key reactive intermediates in low-temperature and ozone-assisted oxidation processes.

High harmonic generation of extreme ultraviolet pulses
Core-to-valence transient absorption spectroscopy combines the element-specificity of core orbitals with the sensitivity of valence orbitals to bonding environment, making this technique a powerful, site-specific probe of non-adiabatic dynamics. Through a grant from Sandia's Laboratory-Directed Research and Development program, we have constructed an apparatus for high harmonic generation (HHG) of extreme ultraviolet pulses and core-level transient absorption spectroscopy. Using a BES GPCP-funded high-power laser system that produces 13 mJ, <40 fs pulses centered at 800 nm to drive HHG in this apparatus, we have generated XUV pulses in Ar and Ne spanning ~30 eV to >72 eV (see Figure 1) for use as a probe in core-level transient absorption spectroscopy. These XUV photon energies allow access to core-to-valence transitions in many elements such as first-row transition metals and some halogens.

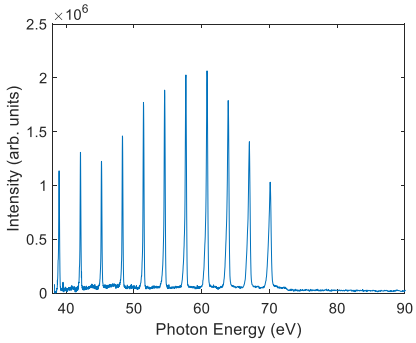

Figure 1: Extreme ultraviolet spectrum from 800 nm-driven high harmonic generation in Ne. The abrupt cut-off at ~72 eV represents the $L_{2,3}$-edge of Al due to an Al filter present in the beam path for blocking residual 800 nm.

PROPOSED WORK

Bayesian Optimal Experimental Design, Application to Time-of-Flight Mass Spectrometry We will proceed with the application of Bayesian OED to the HP-PIMS experiment. The next immediate target is the demonstration of the instrument model for the post-photolysis phase. One of the key challenges in this will be the application of Bayesian inference for the post-photolysis system model calibration. Given the

large number of parameters that need to be estimated, we are looking at using Hamiltonian Monte Carlo (HMC) methods for solving the Bayesian inference problem. HMC requires gradients of the model output observables with respect to parameters being estimated – a non-trivial requirement. We are exploring the use of TChem (https://github.com/sandialabs/TChem) for GPU-enabled kinetic computations, which has been developed under ECC BES funding, and employing automatic differentiation in this context, to facilitate this. With this construction in hand, we will then move to the Bayesian OED construction proper, where HMC/TChem GPU capabilities will be crucial to enable feasible solutions. We will explore efficient nested random sampling strategies, dealing particularly with the need for large numbers of computational samples for the marginal likelihood estimation using importance sampling. We plan to demonstrate the construction with close coupling to HP-PIMS experimental measurements, in order to provide necessary validation, and iterate towards optimal design conditions. This proposed demonstration of Bayesian OED with HP-PIMS is highly synergistic with activities under the joint Argonne-Sandia High-Pressure Combustion Chemistry program, which depend critically on continuous feedback between experiments and theory-based chemical modeling. Our OED approach strengthens the HPCC modeling-experiments link by enabling targeted, impactful experiments to maximally inform the chemical models.

Characterizing the new Photoelectron Photoion Coincidence Spectrometer Assuming that pandemic restrictions ease in the next year, allowing us to install the PEPICO spectrometer at the Chemical Dynamics Beamline, we will finalize commissioning and demonstrate Slow PhotoElectron Spectroscopy (SPES), which is a powerful extension of threshold photoelectron spectroscopy. After characterization using Ar, Kr, and Xe ionization from supersonic expansions, we will proceed to measure the molecular beam velocity distribution produced by a slow-flow quartz chemical reactor that we've been utilizing for years with Multiplexed Photoionization Mass Spectrometry. Although we initially assumed the expansion from this ~ 2 - 10 Torr source would be nearly effusive, our initial results at Sandia indicate it is a harder expansion than we expected. We will then proceed to study photolytically initiated chemically reacting systems, beginning with known reactions such as $CH_2OO + SO_2$, and progressing to reactions where the improved spectral fingerprints offered by photoelectron spectroscopy will enable new scientific understanding, such as highly unsaturated reactions important in molecular weight growth chemistry.

Ultrafast core-level transient absorption spectroscopy of chemical dynamics We will upgrade the current high-harmonic generation apparatus to generate soft X-ray pulses spanning ~150-350 eV for use in core-to-valence transient absorption spectroscopy at the sulfur L- and the carbon K-edges of gas phase molecules. Pushing the photon energies into the soft X-ray regime requires driving HHG using near-infrared pulses, because the high harmonic cut-off photon energy is proportional to the square of the wavelength of the HHG driver pulses. However, the efficiency of HHG drops precipitously with increasing wavelength of the HHG driver pulses, to the inverse sixth power of the wavelength of HHG driver pulses. This fact necessitates the use of a high-power source of near-infrared pulses to produce sufficient soft X-ray flux for use in pump-probe experiments. The new high-power laser system will pump an existing high-energy commercial OPA (HE-TOPAS-Prime Plus, Light Conversion), which generates near-infrared pulses ranging in wavelength from 1100 nm to 2600 nm. The near-infrared pulses will then be used for driving HHG in helium gas maintained at near-atmosphere pressure in a semi-infinite gas cell. The rest of the apparatus will be largely unchanged from XUV operation, except for modifications to the X-ray spectrometer to allow for higher photon energy detection.

Broadband Microwave Spectroscopy for Isomer-specific Detection of Transient Intermediates As a test of the capabilities of the instrument following improvements in the electronics, we are currently carrying out studies of a series of symmetric phenol derivatives that can undergo hindered internal rotation of the OH group. Tunneling splittings report on the height and shape of the barrier to OH internal rotation. Since the OH group differs little in mass from ^{19}F, this fascinating molecule is a near-oblate symmetric top in which the tunneling hydrogen is the major source of asymmetry.

We will soon be re-installing the flash pyrolysis nozzle on the pulsed valve as a source of specific transient intermediates of interest. In collaboration with Kyle Crabtree at UC-Davis, we plan to study the broadband microwave spectroscopy of a series of methylated phenoxy radicals, *o*-, *m*-, and *p*-methyl phenoxy. These radicals will have both methyl internal rotation and electron spin as angular momentum sources, offering a spectroscopic puzzle that has not yet been solved. When ZrO_2 rather than SiC is used as the pyrolysis tube material, O_2 can be added to the heated mixture, offering many opportunities for detecting oxygen-rich intermediates. Using a ZrO_2 flash pyrolysis source, we will target initially a series of reactions of the resonance-stabilized radicals propargyl (C_3H_3), cyclopentadienyl (C_5H_5), and benzyl (C_7H_7) with O_2.
We will also incorporate a recently developed, small-volume (~1cm^3) high-pressure laminar flow reactor (HPFR) as source. The HPFR can operate at up to 100 bar and 1000 K and was built by Sheps using LDRD funding in 2019. To demonstrate the feasibility of this idea, we will quantify the formation of several crucial early intermediates in diethyl ether oxidation.

Finally, a major task for the coming year is to design, construct, and test a cryo-cooled buffer gas cell as an alternative means of detecting transient intermediates via broadband microwave techniques. The injection of the effluent from the pyrolysis or fast mixing flow reactor into the cryo-cooled buffer gas cell offers improvements in sensitivity that we will explore. Compared to a pulsed supersonic expansion, the buffer gas cell cools the molecules and holds them in the cell for much longer interrogation times (>10 ms) before removal on the cold walls. This makes it possible to interrogate at up to 50 kHz repetition rate, with the same molecules contributing to the signal throughout their residence time in the cell.

Tandem Mass Spectrometry for Molecular-Weight Growth Reactions To complement and extend photoionization spectroscopy, PEPICO, and rotational spectroscopy, we are working towards adding tandem mass spectrometry to our array of diagnostic techniques. This technique is uniquely suited to identify complex chemical structures. Our mass spectrometer consists of an atmospheric pressure photoionization (APPI) or nanospray ionization source, a quadrupole mass filter, a collision cell filled with Ar for the collision-induced dissociation (CID) process, and a reflectron time-of-flight spectrometer to mass analyze the ions. We are in the process of modifying the interface to the APPI source to allow for sampling from flash pyrolysis sources for the investigation of radical-radical and radical-molecule reactions in high-temperature hydrocarbon rich environments (see Chemical Kinetics). The emphasis of this work will be on the detection of aliphatically bridged multi-core PAHs, and on the identification of cross-linked PAHs, which are the centerpieces in the proposed radical-radical chain reaction sequence for soot formation. Furthermore, we propose to follow low-temperature oxidation chemistry and the various O_2 addition sequences by interfacing a jet-stirred reactor with the tandem mass spectrometer. This approach is motivated by the fact that the 3rd O_2 addition reaction products have only been observed in such zero-dimensional reactors and by the opportunities tandem mass spectrometry offers for unraveling the molecular structures of the complex intermediates. The first targets include the oxidation of neo-pentane and cyclohexane.

BES-SPONSORED PUBLICATIONS (SINCE 2019)

1. J. D. Savee, B. Sztaray, O. Welz, C. A. Taatjes, D. L. Osborn, Valence Photoionization and Autoionization of the Formyl Radical, J. Phys. Chem. A **2021**, accepted.
2. J. H. Frank, Advances in imaging of chemically reacting flows, J. Chem. Phys. **2021**, 154 (4), 040901.
3. S. M. Fritz, P. Mishra, J. Wullenkord, P. G. Fugazzi, K. Kohse-Höinghaus, T. S. Zwier, N. Hansen, Detecting Combustion Intermediates Via Broadband Chirped-Pulse Microwave Spectroscopy, *Proceedings of the Combustion Institute* **2020,** *in press*. DOI: 10.1016/j.proci.2020.06.169.
4. P. Mishra, S.M. Fritz, S. Herbers, A.M. Mebel, T.S. Zwier, Gas-phase pyrolysis of *trans* 3-pentenenitrile: Competition between Direct and Isomerization-directed Dissociation, *Phys. Chem. Chem. Phys.* **2021***, in press*. DOI: 10.1039/d1cp00104c.

5. B. Zhou, T. Li, J. H. Frank, A. Dreizler, B. Bohm, Simultaneous 10 kHz three-dimensional CH2O and tomographic PIV measurements in a lifted partially-premixed jet flame, *Proceedings of the Combustion Institute* **2021,** *in press*. DOI: doi.org/10.1016/j.proci.2020.07.039
6. B. Zhou, J. H. Frank, Experimental study of vorticity-strain interactions in turbulent premixed counterflow flames, *Proceedings of the Combustion Institute* **2021,** 38 *in press*. DOI: doi.org/10.1016/j.proci.2020.06.182
7. T. Li, B. Zhou, J. H. Frank, A. Dreizler, B. Böhm, High-speed volumetric imaging of formaldehyde in a lifted turbulent jet flame using an acousto-optic deflector, *Exp. Fluids* **2020**, 61 (4), 112.
8. N. Hansen, R. S. Tranter, J. B. Randazzo, J. P. A. Lockhart, and A. L. Kastengren, Investigation of sampling-probe distorted temperature fields with X-ray fluorescence spectroscopy, *Proc. Combust. Inst.*, **2019,** 37, 1401-1408.
9. B. Zhou, A. J. Ruggles, E. Huang, J. H. Frank, Wavelet-based algorithm for correction of beam-steering artefacts in turbulent flow imaging at elevated pressures. *Exp. Fluids* **2019**, 60 (8), 136.
10. T. C. W. Lau, J. H. Frank, G. J. Nathan, Resolving the three-dimensional structure of particles that are aerodynamically clustered by a turbulent flow. *Phys. Fluids* **2019**, 31 (7), 071702.

CHEMICAL DYNAMICS METHODS AND APPLICATIONS

David W. Chandler, Laura M. McCaslin, David L. Osborn, Timothy S. Zwier
Sandia National Laboratories, MS 9051, Livermore, CA 94551-0969
chand@sandia.gov, lmmccas@sandia.gov, dlosbor@sandia.gov, tszwier@sandia.gov

PROGRAM SCOPE

This program focuses on the gas phase molecular dynamics of molecules and molecular clusters to unravel the fundamental physical chemistry of reactions, interactions, and time-resolved electronic structure. This task weaves together multiplexed experimental techniques and theoretical tools to develop a detailed picture of molecular motion as well as energy flow within and between molecules. The studies reported here are related to and interconnected with the Ultrafast Physics, Ultrafast Chemistry, and Advanced Diagnostics tasks, which encompass the study of energy flow within molecules, correlations between nuclear and electronic motion, and development of advanced optical techniques, respectively. Highlights from our program include development of molecular alignment techniques at low laser power, studies of photodissocation processes and resulting reaction channels, isomerization dynamics, and analysis tools for correlating molecular motion and IR spectral features in ab initio molecular dynamics (AIMD) calculations. Time-resolved velocity measurements of products in single and crossed molecular beam experiments is studied via velocity mapped imaging (VMI) of ions and electrons. The products and intermediates of chemical reactions are selectively probed via time-resolved multiplexed photoionization mass spectrometry (MPIMS) and photoelectron photoion coincidence spectroscopy (PEPICO). Molecular dynamics are calculated theoretically via AIMD calculations and complex IR spectra resulting from large amplitude motion are calculated via the autocorrelation function of the dipole moment. Analysis tools have been developed for an intuitive approach to IR spectral decomposition as well as temperature dependence.

RECENT PROGRESS

Alignment of the Hydrogen molecule in the electronically excited E, F state

We have finished a study of the alignment of hydrogen molecules by utilizing excited electronic states of the H_2 molecule that are mixed by the laser fields. This mixed state of the molecule possesses a very large polarization anisotropy. Polarization anisotropy is a measure of how polarizable the molecule is along the molecular axis relative to the perpendicular axis. High polarization anisotropy allows a laser field to align the H_2 molecular axis with the laser polarization direction. We accomplish this by first exciting an H_2 molecule to a single ro-vibratonal state of the E, F electronic state using ~200 nm light. This state has a lifetime of about 200 ns. We then come in with two other laser beams, a strong beam at 1064 nm that mixes the E,F state with neighboring B and C states and aligns the hydrogen molecule. The other beam is a weak beam at 532-nm frequency that excites the H_2 molecule to a repulsive electronic state, producing H (n=3) atoms upon dissociation. The 532-nm light also ionizes these H (n=3) atoms and the H^+ are imaged on a phosphor backed microchannel plate. At low laser power for the 1064-nm beam, the image of the H^+ from the H (n=3) dissociation channel is nearly isotropic with a small intensity peak perpendicular to the laser ionization direction. As the laser power is increased, the H^+ signal is seen to strongly align along the laser polarization axis. By measuring the alignment as a function of the 1064-nm laser beam power we are able to extract the laser isotropy parameter. We modelled this alignment behavior with a simple two-state model involving the Stark mixing of the initially-prepared $J = 0$ with the $J = 2$ rotational state. This model is able to reproduce all of the observed angular distribution and permits us to extract from the fit the polarizability anisotropy of H_2 (E,F) electronic state. We determine this value to be $(3.7 \pm 1.2) \times 10^3$ a.u. As this value is extremely large in comparison to what one would expect from the pure H_2 (E,F) electronic state, we hypothesize that this value comes from the 1064-nm laser beam mixing nearby electronic states with the initially laser prepared (E,F) state generating a mixed state with an extremely large polarizability anisotropy. This new technique for aligning molecules in moderate laser powers should be appropriate for any molecule with electronic states that live for a few nanoseconds.

Pyruvic Acid Photodissociation excited to S_1 and S_3

Pyruvic acid, $CH_3C(O)COOH$ is a prototypical bifunctional molecule, with properties of both ketones and carboxylic acids. In collaboration with Hanna Reisler's group at the University of Southern California, we have studied its dissociation after excitation to the S_3 surface (at 193 nm) [doi.org/10.1063/5.0018582] and the S_1 surface (at 351 nm) [DOI: 10.1039/d0cp06424f] using velocity map imaging and multiplexed photoionization mass spectrometry. At 193 nm we observe a wide variety of nascent photoproducts: CO_2, CO, H, OH, HCO, CH_2CO, CH_3CO, CH_3, CH_3CHO, and $H_2C{=}COH$. Most of the observed products arise from 3- and 4-body dissociation due to the large excess energy. Multivariate analysis of the products points to three main reaction mechanisms: (1) decarboxylation terminating in CO_2 + other primary products (~50%), (2) Norrish Type I dissociation typical of carbonyls (~ 30%), and (3) O-H and C-H bond fission reactions generating H atoms (~10%). The anisotropy parameters of H and CO fragments measured by VMI point to a fast dissociation process. However, the excited state relaxation and dissociation pathways are not clear from this work. Pyruvic acid is present in Earth's troposphere from photo-oxidation of isoprene and by direct emissions. It is one of the few organic molecules destroyed in the troposphere by solar radiation rather than reaction with OH radicals. It absorbs in the near UV via its $S_1 \leftarrow S_0$ transition of $\pi^* \leftarrow$ n character. Its photolysis has been studied many times, but primarily in chamber experiments meant to mimic Earth's atmosphere, which can obscure the fundamental photochemistry in this system. Our work supports the previous conclusion that decarboxylation, producing CO_2 + C_2H_4O is the primary product channel. Using time-resolved photoionization spectroscopy, we have observed all three isomers of C_2H_4O: acetaldehyde (CH_3CHO), vinyl alcohol ($H_2C{=}COH$), and the elusive methylhydroxycarbene (CH_3-C-OH). We observe minor amounts of the Norrish Type I products CH_3CO + DOCO, but only in the case of d_1-pyruvic acid. Our results support a mechanism in which hydrogen transfer on the S_1 excited state occurs at least partially by tunneling, in competition with intersystem crossion to the T_1 state. Finally, we observe a bimolecular reaction between CH_3-C-OH and pyruvic acid, producing a $C_4H_8O_2$ product. This observation implies that some methylhydroxycarbene from pyruvic acid photodissociation will be stabilized in Earth's troposphere, and its chemistry should be included in atmospheric modeling. This work opens the door to fundamental studies of hydroxycarbene chemistry.

Selective Conformational Isomerization using IR-population transfer spectroscopy

Conformational isomerization is a ubiquitous process in large, flexible molecules. In order to probe this process under well-controlled conditions, we have studied the process under jet-cooled conditions where isomerization is initiated by selective IR excitation of a single conformer. As a backdrop to such studies, we have carried out single-conformation IR and UV spectroscopy of the prototypical capped γ-peptide Ac-γ^4-Phe-NHMe (γ^4F), a model synthetic foldamer. We performed conformer-specific IR-UV double resonance spectroscopies and compared the results with dispersion-corrected DFT calculations to make assignments and explore the differences between the γ^2 and γ^4 substituted molecules. We found four conformers of γ^4F in our experiment. Three conformers form 9-membered hydrogen bonded rings (C9) enclosed by an NH···O=C H-bond, but differing in their phenyl ring position (*a*, *g*+, *g*-). The fourth conformer forms a strained 7-membered hydrogen bonded ring in which the amide groups lie in a nominally anti-parallel stacked arrangement with respect to one another. We used IR population transfer (IR-PT) spectroscopy to study the isomerization dynamics. By exciting with an IR pulse early in the supersonic expansion, the IR-excited conformers isomerize in competition with cooling back to the zero-point levels of the conformers. We used IR-PT to demonstrate efficient IR-induced isomerization between the three C9 phenyl rotamers and also observed interconversion of the nearly stacked to C9 and *vice versa*. We determine fractional abundances of the γ^4F conformers in the expansion. We calculated disconnectivity graphs for γ^4F that reveal separate basins associated with the C9 and amide-stacked conformational families which are separated by a barrier of about 30 kJ/mol, about 10 kJ/mol lower than the IR photon energy. The over-all shape of the potential energy surface bears a resemblance to peptides and proteins that have a misfolding pathway that competes with formation of the native structure.

Developing Analysis Tools for Understanding IR Spectra from Ab Initio Molecular Dynamics

Theoretical prediction of infrared spectra for "floppy" molecules and molecular clusters with large amplitude motion requires approaches that go beyond the harmonic approximation. In particular, systems with conformational changes such as molecules with free rotors or clusters exhibiting proton transfer have complex dynamics that are not sufficiently captured with harmonic-based approaches, including those with perturbative corrections (e.g. VPT2). One approach to capture these complex dynamics in a theoretical IR spectrum is to calculate IR intensities by taking the Fourier transform of the autocorrelation function of the dipole moment in an ab initio molecular dynamics (AIMD) trajectory. Similarly, the vibrational density of states can be computed by taking the Fourier transform of the autocorrelation function of the nuclear velocities. This powerful approach has many benefits, however, the analysis of the intensities is far more difficult than in harmonic-based approaches. Furthermore, the dependence of the intensities on temperature can be computed via changing the nuclear velocities to reflect larger kinetic energy in the molecular motion, though this is a computationally expensive approach. In light of the challenges to correlating molecular motion to peak intensities as well as the computational expense of understanding temperature dependence, we have developed a computational analysis code that works to improve analysis of IR spectra from AIMD. Understanding the correlation between molecular motion and spectral features requires different coordinate systems for different molecular systems. The recently developed code offers the choices of normal, internal, and generalized normal coordinates for determining the "weight" of a coordinate's displacement within a spectral feature. This spectral decomposition allows for an intuitive understanding of the correlation of complex spectral features and molecular motion. As for the computational expense of computing temperature dependence through explicitly performing additional AIMD trajectories at a higher temperature, we have implemented new theoretical insights from statistical mechanics that allow for calculation of temperature dependence of IR intensities in the linear response regime without additional AIMD trajectory calculations. Our new analysis code thus aids in the development of a more intuitive understanding of complex spectral features from underlying dynamics as well as their temperature dependence.

FUTURE WORK

New experiments involving electronic energy transfer between chromophores are planned for the coming year to study the mechanism of energy transfer when nearly identical chromophores span a range of separations. Unlike previous FRET experiments using two fluorescing molecules, we will study energy transfer between chromophores of a cryo-cooled ion, in which energy transfer breaks a bond adjacent to the acceptor molecule. Since ions are prepared under cryo-cooled conditions, they can selectively excited to single vibronic levels of the chromophores, and do not need donors and acceptors to absorb at very different wavelengths in order to assign fluorescence to the donor or acceptor. As a result, we will explore circumstances in which subtle energy differences between the chromophores makes vibronic coupling important. For instance, we can deuterate one ring and not deuterate another, and we can study electronic energy transfer between them after selective excitation of *either* chromophore. As the project progresses, we will build up arrays of nearly identical chromophores, much as exist in photosynthetic reaction centers, seeking to selectively excite one and watch where the energy transfers by the distribution of side chain breakage at each chromophore.

In order to develop our program's study of non-equilibrium systems, experiments involving highly rotationally excited molecules as well as collisions of vibrationally excited ephemeral species will be performed. While the effects of highly excited translational and vibrational states on chemical reactions are well-characterized, the effects of highly rotationally excited molecules are not as well understood. As described in the Ultrafast Physics task, an optical centrifuge is being developed, which will allow for highly rotationally excited N_2O to be formed. Photodissociation of these "super-rotors" will be performed at ~200 nm and N_2 and $O(^1D)$ products will be detected via velocity mapped imaging (VMI). To better understand the reactions of super-rotors and atoms, reactions of rotationally excited N_2O and $O(^1D)$ to form NO will

be monitored by VMI. On the ephemeral complexes front, studies of collisionally-stabilized association reactions of non-equilibrium vibrationally excited species and atoms will be carried out. Vibronically-excited NO_2 at ~400 nm will be optically generated in a molecular beam within 10 kcal/mol of the NO + O dissociation energy. These excited NO_2 molecules will be collided with CO to gauge production of NO via VMI.

New experiments are being developed to measure the pair correlation function with vibrational state resolution for reactive collisions and rotational resolution for inelastic scattering in crossed molecular beam scattering. These experiments will vibrationally excite molecules with an ultra high-resolution infrared quantum cascade laser down the length of the beam, preparing a narrow distribution (milliKelvin) of state-selected molecules. The second beam will be velocity-chirped by extending the distance that the molecules travel, keeping the molecular pulse short. A small crossing angle will allow for very high scattering velocity resolution as well as resolution of the quantum states of the scattering partner via the quantum state of the detected molecule. Such experiments to obtain the pair correlation function have been performed with a complicated Stark decelerator. These new experiments will allow for the detailed study of potential energy surfaces of molecule-molecule interactions, while previous measurements have only been performed for atom-molecule interactions.

BES-SPONSORED PUBLICATIONS (SINCE 2019)

1. J.L. Fischer, K.M. Blodgett, C.P. Harrilal, P.S. Walsh, S.H. Choi, and T.S. Zwier, Conformer-specific Spectroscopy and IR-induced Isomerization of a Model g-peptide: Ac-g^4-Phe-NHMe, (submitted)
2. B. R. Samanta, R. Fernando, D. Roesch, H. Reisler, and D. L. Osborn, Primary photodissociation mechanisms of pyruvic acid on S_1: observation of methylhydroxycarbene and its chemical reaction in the gas phase, Phys. Chem. Chem. Phys. DOI: 10.1039/D0CP06424F (2021).
3. B. R. Samanta, R. Fernando, D. Rösch, H. Reisler, and D. L. Osborn, Looking at the bigger picture: Identifying the photoproducts of pyruvic acid at 193nm, J. Chem. Phys. **153**, 074307 (2020).
4. M. Fournier, G.V. Lopez, A.K. Spiliotis, T.A. Casey, T.P. Rakitzis, D.W. Chandler, Alignment and Dissociation of Electronically-Excited Molecular Hydrogen With Intense Laser Fields, Mol. Phys. **119**, 1 (2020).
5. I. Antonov, K. Voronova, M. W. Chen, B. Sztaray, P. Hemberger, A. Bodi, D. L. Osborn, L. Sheps, To Boldly Look Where No One Has Looked Before: Identifying the Primary Photoproducts of Acetylacetone, J. Phys. Chem. A **123**, 5472 (2019).

ELECTRON-DRIVEN CHEMISTRY

David W. Chandler, Jonathan H. Frank, Nils Hansen, Laura M. McCaslin, Krupa Ramasesha, Leonid Sheps
Sandia National Laboratories, MS 9051, Livermore, CA 94551-0969
chand@sandia.gov, jhfrank@sandia.gov, nhansen@sandia.gov, lmmccas@sandia.gov,
kramase@sandia.gov, lsheps@sandia.gov

PROGRAM SCOPE

Electron-driven chemistry, which we define as chemical transformations driven by long-range motion of electrons or charges, underpins many areas of interest to the DOE. The goal of this program is to deepen understanding of reactivity that is driven by motion of charges. We will apply a combination of sophisticated experimental and theoretical methodologies to provide detailed time- and state-resolved views of complex charge-transfer processes. These investigations will illuminate phenomena that defy the common simplifying assumptions of the Hartree-Fock and Born-Oppenheimer approximations, and will aid in developing more sophisticated descriptions of coupled electron and molecular motion. This work extends the research we have done on neutral processes, utilizing quantum state-resolved experiments that provide detailed information about the relevant potential energy surfaces and the dynamics upon those surfaces. We pursue experiments that span from induced charge separation in an isolated molecule, to dynamics following attachment of a free electron to a neutral molecule, to coupled chemical and physical evolution of a laser-induced plasma. In each area, we apply advanced techniques, including some in development, to provide a deeper understanding of chemical physics processes than have been previously obtained. This effort complements research being performed in the Solar Photochemistry and Condensed-Phase and Interfacial Molecular Sciences programs and addresses BES Grand Challenges associated with the study of the nature of excited electronic states and the breakdown of the Born-Oppenheimer approximation. This research is closely tied to other work in our program. The study of ultrafast intramolecular charge transfer dynamics of large conjugated systems has strong connections to the ultrafast non-adiabatic dynamics studied in the "Ultrafast Chemistry" task and uses X-ray techniques from the "Advanced Diagnostics" task. Research described in this subtask extends the work performed under the "Chemical Dynamics" task to investigate inelastic collisions of electrons with molecules, and links to studies of neutral reacting systems in the "Chemical Kinetics" task.

RECENT PROGRESS

Development of new apparatus for studying electron scattering processes

In the last year, we have built and tested a new apparatus for the study of electron-driven chemical processes. This new apparatus uses laser produced electrons from resonance-enhanced multiphoton ionization (REMPI) to provide a source of electrons with specific energies between 0 and 3 eV. An atom, generally Kr, is incorporated into an atomic beam along with a molecule whose electron attachment is to be studied. The Kr is excited to a metastable state from which it is ionized with a tunable laser source. This produces electrons with tunable energy and a narrow energy distribution that can then interact with other species in the atomic/molecular beam. The electron-molecule interaction is monitored either by imaging the electrons and measuring the energy loss of the electrons that are produced by scattering from the molecule or by monitoring anions that are formed by dissociative electron attachment (DEA).

In some studies, the electron production via REMPI generates enough electrons and cations that a plasma is created within the molecular beam. In this plasma, further chemistry proceeds and the resulting products can be extracted by a pulsed electric field at a later time. We are able to measure the electron velocity distribution within the plasma using velocity-mapped imaging (VMI) of the electrons as a function of time as the plasma forms (by changing the time delay between the laser production and the pulsed electric field extraction), as shown in Fig. 1. This approach provides a new and powerful method for measuring the temperature of a thermalized plasma: one can extract time-resolved translational energy distributions of

specific ions and neutrals in the plasma by changing the polarity of the repeller, gating the detector, and/or using an additional ionizing laser pulse.

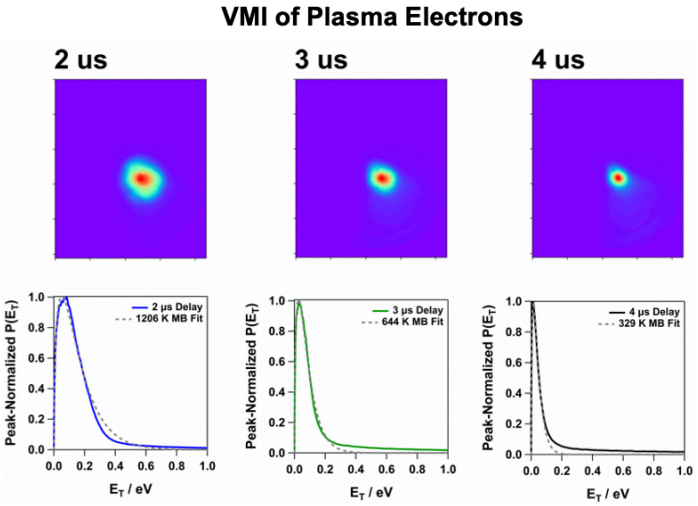

Fig. 1: Imaging the velocity distribution of a REMPI-generated plasma in a pulsed supersonic beam of pure Kr using 214.7 nm light. Top: Velocity-mapped images of electrons from the plasma at three delays from the laser excitation pulse demonstrating electron cooling from a highly non-equilibrium initial state. Bottom: At times ≥ 2 µs, the images are approximately symmetric and can be Abel inverted to extract the electron energy distributions that are well-described by Maxwell-Boltzmann distributions.

We also recently demonstrated DEA experiments on acetylene (C_2H_2), which was combined with Kr in a molecular beam. For these experiments, we developed a pulsed extraction scheme for the VMI using a sub-ns high voltage pulser to reject background interference that occurs in our colinear experimental setup (electrons, ions, and neutral metastable species). The timing diagram for this scheme is shown in Fig. 2. Our initial experiments monitored the production of C_2H^-, C_2^-, and several other lower mass-to-charge species. Figure 3 shows the portion of the mass spectrum containing C_2H^- formed by DEA as well as the anion of the parent acetylene molecule $C_2H_2^-$. Imaging experiments are underway using this timing scheme.

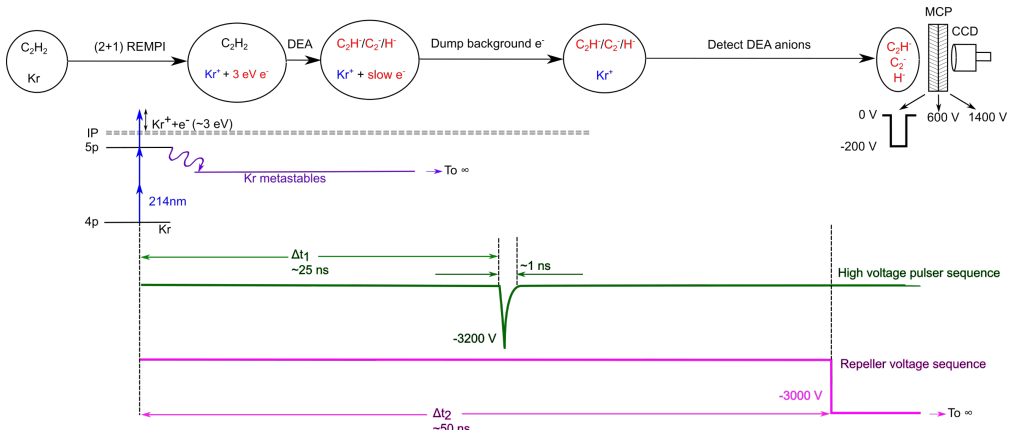

Fig. 2: Timing diagram of the pulsed lasers and electron optics voltages (not to scale). A single 214 nm laser pulse is used to generate 3.32 eV electron bursts via ionization of Kr. A second tunable laser pulse can also be used to generate tunable energy electrons via ionization of Kr metastable state. The green pulse denotes a short (~1 ns) -3.2 kV pulse applied at the mesh electrode that serves to isolate the excitation region from the time-of-flight region of the apparatus at approximately 25 ns after the laser pulse to push the background electrons away from the detector. The pink pulse denotes a long -3 kV pulse applied at the repeller plate approximately 50 ns after the laser pulse to extract the DEA anions to the detector.

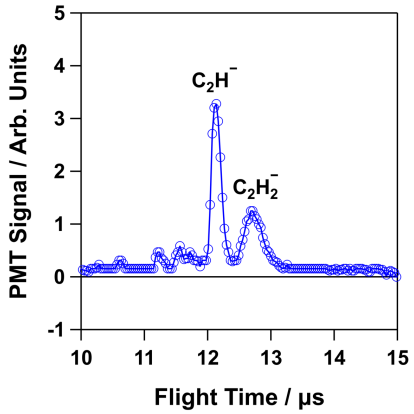

Fig. 3: Time-of-flight spectrum demonstrating the formation of C_2H^- by DEA of acetylene with 3.32 eV electrons generated by 2+1 REMPI of Kr. This spectrum was collected in a photofragment imaging spectrometer using the scheme described in Fig. 2. The parent $C_2H_2^-$ anion is also observed which may be a product of electron attachment to C_2H_2 in a cluster environment, with excess energy removed by cluster evaporation.

FUTURE WORK

Experimental studies of dissociative electron attachment

Our unique electron scattering apparatus has two characteristics that we are taking advantage of. One is the high energy resolution of the electrons dictated by the frequency spread of the laser beam. This allows us to scan the frequency of the laser and scan the energy of the electrons with approximately 0.5 cm^{-1} (0.06 meV) resolution. We will scan the energy of the electron through low energy resonances of small molecules such as NO. We will then use 1+1 REMPI to detect the vibrationally excited NO that is formed by electron attachment followed by detachment. In this manner, we will measure the natural linewidth of the resonances associated with production of vibrationally excited ground state transient ions and therefore determine the lifetime of the transient anions. The other characteristic that we will take advantage of is the time resolution of using pulsed lasers to produce the electrons. The electrons traverse the molecular beam in a time that is shorter than the laser pulse duration. Therefore, all transient anions will be formed during the 5-ns laser pulse as the electrons encounter molecules in the molecular beam. As we have control over the time of the electron generation, we can excite a molecule in the molecular beam prior to the electron production. In this manner, we will study the production of transient anions from electronically excited states of molecules. The first systems that we are planning to study involve NO(A) and excited electronic states of SO_2, CS_2, actonitrile (CH_3CN), and fluorenone ($C_{13}H_8O$).

The time resolution of our electron scattering apparatus will also allow us to measure the lifetime of transient anions that have lifetimes between 5 ns and 2 µs. We will do this by detaching the electron from the transient anion with a second laser with a unique frequency so that the electrons will be imaged to unique positions on our imaging detector. By energy analyzing the electrons, we will be able to learn about the energy loss to the molecule after electron attachment. The first systems we hope to study using this laser-initiated detachment are CH_3CN, triethylamine, and phenylamine.

The motivation for studying DEA to nitric oxide is that it exhibits significant changes in dissociative electron attachment to the ground and electronically excited states that require a more detailed understanding. Dissociative electron attachment to ground state NO requires a minimum electron energy of approximately 7.5eV. In contrast, DEA to electronically excited NO in the $A^2\Sigma^+$ state is exothermic by 0.45eV, and the DEA cross sections are three orders of magnitude larger for the electronically excited state.[1] This extraordinary enhancement in the cross section is associated with a Feshbach resonance. The dissociation channel in the excited state also differs from that of ground state NO. DEA to ground state NO

primarily produces $N(^2D) + O^-(^2P)$, and DEA to electronically excited NO(A) produces $N(^4S) + O^-(^2P)$.[2] The sensitivity of the DEA enhancement and branching of dissociation channels to varying levels of vibronic excitation are not well established. We propose to investigate the enhancement and branching ratios of DEA to excited-state NO by selective laser excitation to different vibronic states prior to electron attachment.

Electronic excitation of carbon disulfide, CS_2, and sulfur dioxide, SO_2, has profound effects on the dissociation channels following electron attachment, resulting in nearly complete suppression in the production of some ionic fragments. For CS_2 that is excited to the $^1B_2$ electronic state, the DEA cross sections for formation of S^- increases by an order of magnitude and for CS^- by a factor of three relative to DEA to the ground electronic state.[3] However, the formation of the S_2^- anion is only observed for DEA to ground state CS_2 and is absent from DEA to electronically excited $CS_2(^1B_2)$. Although some hypotheses for this suppression of S_2^- formation have been proposed, a detailed mechanistic understanding has not been established. For DEA to SO_2 in the excited electronic state ($\tilde{B}^1B_1$), the cross-sections for formation of products O^- and SO^- are enhanced by factors of 6 and 1.5, respectively, while the formation of S^- is almost entirely suppressed.[4] Previous studies of these effects of DEA to excited state CS_2 and SO_2 primarily focused on using time-of-flight mass spectrometry (TOFMS) and included limited investigation into the sensitivity of cross sections and product channels to different levels of excitation. We will conduct a series of detailed studies of DEA to both CS_2 and SO_2 using velocity-mapped imaging to provide mass selective detection of the kinetic energy and angular distribution of the DEA fragments following laser excitation of the parent molecule.

We also plan to investigate DEA to CH_3CN near the 3 eV resonance to resolve the recently reported conflict in the lower appearance energies of the anion fragments by Tian *et al.*[5] and to quantify the dissociation dynamics of the DEA process. Additionally, we intend to carry out the first velocity-mapped imaging study on the formation of dipole bound anions created by electron attachment to CH_3CN clusters. Lastly, we are interested in using REMPI electrons to monitor the change in resonant electron attachment to laser-excited fluorenone as it undergoes singlet-triplet intersystem crossing on a 10 ns timescale.[6] To accomplish this, we will modify the ion optics so that REMPI electrons pass through a plate with an aperture along the axis of the molecular beam to interact with laser-excited fluorenone on the other side before extracting any anions that are formed with a pulse on the aperture plate. This experiment is unique because most of the existing literature on excited state resonant electron attachment has targeted systems with long lived excited states (e.g., DEA of excited state SO_2).

Theoretical studies of dissociative electron attachment

We will pair experimental studies with theoretical investigations of the DEA processes in excited-state molecules. In order to probe the underlying dynamics and electronic structure involved in the vibrational- and electronic-state dependence of reactions such as $CS_2 + e^-$ and $SO_2 + e^-$, ab initio molecular dynamics (AIMD) calculations will be performed. Initial velocities will be chosen to reflect the initial vibrational state and electronically excited trajectories will be propagated on excited state surfaces. Though these are relatively small systems, the electronic structure is quite difficult to describe. Equation-of-motion coupled cluster in its electron-attachment variant (EOM-CC) will be used for a high-accuracy description of the ground and excited state potential energy surfaces.

Intramolecular charge transfer dynamics in gas phase donor-bridge-acceptor systems

We will begin a series of studies focusing on excited-state dynamics in large conjugated molecules with extended π-orbitals. These dynamics are governed by the molecular structure, the nature of participating valence orbitals, the interactions among electronic states, and the surrounding environment. Donor-bridge-acceptor (DBA) molecules are a class of π-conjugated systems, where large amplitude changes to molecular structure are coupled to intramolecular charge transfer (ICT). Given the known sensitivity of ICT to external electric fields and solvent interactions, we propose to first study the *baseline* charge transfer dynamics in

isolated gas phase DBA molecules in cold molecular beams, free from interaction with the environment. The systems we are interested in, *p*-nitroaniline (PNA) and 4-dimethylamino-4'-nitrostilbene (DANS), have an electron-acceptor $–NO_2$ group and an electron-donor $–NH_2$ or $–N(CH_3)_2$ group, respectively. Following electronic excitation of these molecules to the locally excited singlet state, excited state evolution to the twisted ICT state and to triplet states via intersystem crossing are expected to compete. Our experiments will study excited state dynamics in jet-cooled PNA or DANS using femtosecond time-resolve photoelectron spectroscopy (TRPES) and core-level X-ray absorption spectroscopy following electronic excitation to the locally excited state. In TRPES, photoelectrons will be detected in a velocity-mapped imaging apparatus in order to measure photoelectron energies and angular distributions, which report on the electronic energies and orbital character of the electronic states involved. In parallel, core-level spectroscopy at the O and N K-edges will serve as site-specific probes of ICT dynamics, and to this end, we will be writing a user proposal for beam time at the LCLS. In order to guide future X-ray absorption spectra of PNA, we recently calculated the nitrogen and oxygen K-edge transitions at the core-valence separation ADC(2) level of theory with a 6-31G* basis. The nitrogen K-edge spectrum of ground state PNA, shown in Fig. 4, demonstrates that transitions from the NH_2 and NO_2 moieties of PNA are sufficiently separated in energy to be experimentally distinguished. In the planned experiments, we will detect valence excitation and charge transfer-induced changes in the electronic structure of the NH_2 and NO_2, reflected in shifts of these energies and intensities, which will be compared with theoretical predictions of electronically excited PNA. The effects of valence excitation on oxygen K-edge spectra will also be computed for comparison.

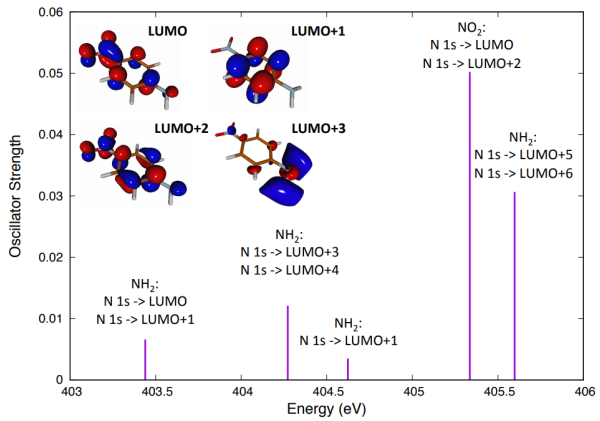

Fig. 4: The calculated lowest-energy core nitrogen K-edge transitions in ground state PNA, originating from the nitrogen atoms in the NH_2 and NO_2 moieties.

Long-range electron transfer in rare gas/large molecule clusters

In the next year, we plan to initiate a program to study the excited-state dynamics in rare gas-molecule van der Waals clusters (Rg·M). The excitation of meta-stable electronic states of Rg in these clusters is expected to lead to Penning ionization (PI, $Rg^*{\cdot}M \rightarrow Rg + M^+ + e^-$) or to charge-transferred ion-pair formation (CT, $Rg^*{\cdot}M \rightarrow Rg^+ + M^-$). Both processes are long-range electron transfers that depend on the interaction of the Rg and M electronic states with each other and on the coupling of electronic and nuclear motion of the cluster. We seek to understand how the rate of electron transfer depends on the structure of Rg and M *via* an approach that has advantages over previous (mostly crossed molecular beam) studies: i) selective initial state preparation by two-photon laser excitation of Rg*, ii) well-defined initial geometry and orbital interactions of Rg and M, and iii) using a relatively simple rare gas atom as one partner in the cluster.

We will form Rg·M clusters in a pulsed supersonic expansion at 30 Hz and excite them via allowed UV 2-photon transitions into the 5p or 6p state manifold for Rg = Kr or Xe, respectively, using tunable (212 – 256 nm) ~5-ns laser pulses. This excitation scheme is the same as depicted for Kr in Fig. 2. We hypothesize that after excitation, PI will compete with intra-cluster CT, depending on the electronic coupling of Rg* to M. The PI electrons will be ejected spontaneously and detected in the VMI spectrometer; electrons from

meta-stable Rg*·M or the charge-transferred $Rg^+ \cdot M^-$ cluster will be photodetached with a time-delayed laser pulse and also detected. Both, PI and CT processes may couple to the molecular vibrations of M or to low-frequency cluster vibrations, and the detected electron kinetic energy distributions will report on which motions become populated.

The molecular partner M will be chosen based on its ionization potential and electron affinity in order to make PI and CT either endothermic or exothermic. Initially, we will focus on small M such as NO, Br_2, and CH_3CN. Subsequently, complex M such as *para*-nitroaniline will be targeted to probe how the electronic character of its frontier orbitals (e.g. those localized on the NH_2, the benzene ring, or the NO_2 moiety) affects charge transfer rates. If initial studies are successful, we will also move on to more advanced photoelectron-photoion coincidence studies using a new double-imaging PEPICO apparatus recently built by D. Osborn. Both Penning ionization and photodetachment of a CT ion pair may result in the dissociation of the cluster cation; in this case, correlated electron/ion detection should report on the internal energy of the molecular fragment (whether it is neutral M or M^+), because the atomic co-fragment (Rg^+ or Rg) will have no internal energy. This will shed light on the coupling of long-range electron transfer to specific molecular motions in the cluster and provide new detailed benchmarks for theory.

REFERENCES

1. Kuo, C. T.; Hardwick, J. L.; Moseley, J. T., Low-energy-electron attachment to excited nitric oxide. *J. Chem. Phys.* **1994,** *101* (12), 11084-11085.
2. Kuo, C. T.; Ono, Y.; Hardwick, J. L.; Moseley, J. T., Dissociative attachment of electrons to the A $^2\Sigma^+$ state of nitric oxide. *J. Phys. Chem.* **1988,** *92* (18), 5072-5074.
3. Rangwala, S. A.; Kumar, S. V. K.; Krishnakumar, E., Dissociative electron attachment to electronically excited CS_2. *Phys. Rev. A* **2001,** *64* (1), 5.
4. Krishnakumar, E.; Kumar, S. V. K.; Rangwala, S. A.; Mitra, S. K., Dissociative-attachment cross sections for excited and ground electronic states of SO_2. *Phys. Rev. A* **1997,** *56* (3), 1945-1953.
5. Li, H.; Gao, X.-F.; Meng, X.; Tian, S. X., Dissociative Electron Attachment to Molecular Acetonitrile. *The Journal of Physical Chemistry A* **2019,** *123* (42), 9089-9095.
6. Soep, B.; Mestdagh, J.-M.; Briant, M.; Gaveau, M.-A.; Poisson, L., Direct observation of slow intersystem crossing in an aromatic ketone, fluorenone. *Physical Chemistry Chemical Physics* **2016,** *18* (33), 22914-22920.

GAS PHASE INTERACTIONS WITH OTHER PHASES

David W. Chandler, Farid El Gabaly, Nils Hansen, Christopher J. Kliewer, Laura M. McCaslin, Habib N. Najm, David L. Osborn, Leonid Sheps and Craig A. Taatjes
Combustion Research Facility, Sandia National Labs, Livermore, CA 94550
chand@sandia.gov, felgaba@sandia.gov, nhansen@sandia.gov, cjkliew@sandia.gov, lmmccas@sandia.gov, hnnajm@sandia.gov, dlosbor@sandia.gov, lsheps@sandia.gov, cataatj@sandia.gov

PROGRAM SCOPE

This research program encompasses experimental and computational investigations of a wide range of multiphase phenomena, investigating the formation of particulates in gas-phase reaction systems, measuring and modeling the gas-phase processes at reactive interfaces and probing the physical and chemical interactions between phases. Understanding reactions that lead to particle formation and calculating surface reactions draw on work in the Sandia "Chemical Kinetics for Complex Systems" task, and experiments employ innovations from the "Ultrafast Physics: Nonlinear Optical Spectroscopy and Diagnostics" and "Advanced Mass Spectrometry and X-Ray Diagnostics" tasks. Recent emphasis is on chemically controlled gas-to-particle conversion; proposed new directions will extend work into understanding the interactions of gas-phase molecules with liquid and solid surfaces. These initiatives complement the catalytic surface investigations in Sandia's "Imaging the Near-Surface Gas Phase" program.

RECENT PROGRESS

Detection of spatially resolved reaction products near a surface using REMPI and ion imaging Improved instrumentation for monitoring the location and kinetics of chemically or catalytically active domains on an arbitrary surface is an attractive and potentially transformative goal. However, any efforts to monitor the concentration of a target gas very near a surface that is producing the target gas is very dependent on the size of the reactive domains and the spatial resolution associated with sampling the target gas. We have pursued the development of an approach based upon imaging the HD during the H_2/D_2 exchange reaction over a Pt surface through resonant enhanced multiphoton ionization (REMPI). We discovered that the spatial blurring caused by translational velocity of the HD molecules degraded the spatial resolution of the product image.

Because the product molecules desorb from the surface with a significant velocity distribution, this velocity spread will be superimposed on the ion image. We have explored an idea to eliminate the velocity spread by using velocity map imaging of the cation distribution placing a small (less than 1 mm) orifice at the velocity map imaging plane (the Fourier plane of the spatial image). In this manner only ions moving in a particular direction will pass through the orifice. These ions are expanding as they move toward the imaging detector. One then records an image of the spatial distribution of the ions within the laser focus. As a first effort to asses this technique, we were able to easily expand a focused beam with a 2 mm confocal parameter to 60 mm on the detector representing a magnification of 30 and a resolution of ~65 microns at the catalyst surface, which can be increased by lengthening the distance between the pinhole and detector.

We have observed HD (v=0,1 J=0,1,2) products from the reaction of H_2 + D_2 on a patterned platinum surface. The surface had 1mm wide stripes of platinum on a gold surface. The surface temperature can be increased to 200 C^o for high catalytic turnover frequency. The catalyst surface itself acts as the repeller plate in a traditional velocity mapped ion imaging apparatus. An aperture is placed 4 cm above the velocity mapped imaging lens and lens voltages adjusted in order to focus at the plane of the orifice. This is done by minimizing the width of the image one observes on the detector. Initial results are being analyzed and show a modulation of HD product over the 2 mm length of the laser focus, but the image is not as sharply

defined as we expect. Further experiments are being planned with a smaller orifice and different surface pattern.

Particle Formation from Carbonyl Oxide Oligomerization To test the hypothesis that oligomeric hydroperoxides built from carbonyl oxides can nucleate, and to develop a framework to follow the chemistry and physics of this nucleation step, we measured the products of particle inception and mass growth. As a first step, we performed an experimental study of the chemical composition of particles generated in controlled laboratory ozonolysis experiments. This work was done with Kevin Wilson from the Lawrence Berkeley National Laboratory who has developed an aerosol mass spectrometer to probe atmospheric aerosols. Following the successful measurement of gas-phase photoionization measurements of carbonyl oxide oligomerization reactions in an atmospheric pressure jet-stirred reactor, we have performed some proof-of-principle experiments, connecting the jet-stirred reactor chamber to Wilson's aerosol mass spectrometer via a transfer line, in which the sampled particles are immediately diluted to reduce further coagulation.

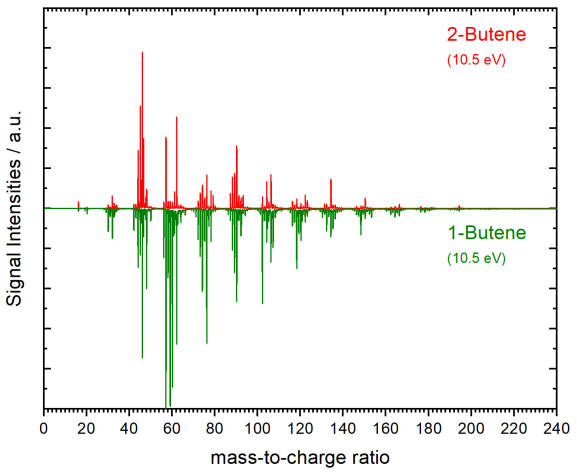

Figure 1: Comparison of mass spectra showing the composition of aerosols generated in ozonolysis of butene isomers

An example is provided in Fig. 1 which compares mass peaks following the ozonolysis of butene isomers at room temperature. Highly oxygenated species, containing 7-8 oxygen atoms, are formed. We plan to begin systematic investigations comparing with the well-understood ethene ozonolysis reaction network, which, because of its simplicity, provides a perfect test case. We anticipate that similar sequences will be observed in the gas-phase and aerosol mass spectrometer; controlling the oxidation conditions and identifying differences between the phases will enable oligomerization reaction mechanisms to be tested.

Developing Tools to Detect the Vibrational Signatures of Ice Nucleation at the Salt Water Interfaces Techniques for analyzing IR spectra, described in the Chemical Dynamics task, have been applied to study the temperature dependence of the vibrational structure of water at long-chain alcohol and carboxylic acid monolayer interfaces to investigate spectral signatures of ice nucleation. It has been found that long-chain alcohol monolayers efficiently nucleate ice, though long-chain fatty acids, short-chain fatty acids, and polysaccharides are also active in ice nucleation, which impacts atmospheric and aerosol science. In order to develop spectroscopic tools for detecting signatures of ice nucleation at interfaces, Infrared Reflection-Absorption Spectroscopy (IRRAS) performed in the group of Heather Allen (Ohio State) is performed on water surfaces covered in a monolayer of long chain alcohols and carboxylic acids at 21 °C and 0 °C. Corresponding gas phase studies of the vibrational structure of the first solvation shell around carboxylic acid and alcohol systems are performed using *ab initio* molecular dynamics (AIMD) in order to model interface behavior. Propanol + $6H_2O$ and propionic acid + $10H_2O$ are investigated in detail at the temperatures studied experimentally.

Competition between Cl^- Substitution and Hydrolysis of N_2O_5: S_N2-Type Reactions of Nitrogen Oxides Recent studies in collaboration with R. Benny Gerber's group (Hebrew University, UC Irvine) and Mark Johnson's group (Yale) indicate that nitrogen oxide species in the atmosphere, including N_2O_5 and $ONONO_2$, undergo a new class of S_N2-type substitution reactions when in contact with seawater and sea spray aerosols. In order to study the competition between halide substitution and hydrolysis of nitrogen oxides, we build theoretical model systems of the type $N_2O_5 + Cl^- + nH_2O$ (n=1-5) and study their potential

energy surfaces via electronic structure calculations and *ab initio* molecular dynamics (AIMD) simulations. In model studies of the cluster $N_2O_5 + Cl^- + H_2O$, we determine that when H_2O and Cl^- are near N_2O_5, halide substitution is a faster reaction, though the products of hydrolysis are more energetically stable. We additionally find that the barrier to hydrolysis is substantially lowered (by ~15 kcal/mol) in the presence of Cl^-. As the microhydration environment is changed via addition of water molecules, one by one, the structure of hydrogen bonding in the system substantially influences the mechanisms of the substitution and hydrolysis reactions.

Investigation of the Effects of Cations on Nitric Acid Dissociation In the reported studies of N_2O_5, the physical effects of cations, such as Na^+, are largely neglected. However, recent studies from our collaborations with R. Benny Gerber's group (Hebrew University, UC Irvine) and Mark Johnson's group (Yale) indicate that the electric field effect from a cation (Cs^+) has significant effects on the transition from intact HNO_3 in small H_2O clusters to dissociated HNO_3 in larger H_2O clusters. This water-mediated charge separation of HNO_3 in Cs^+/nH_2O clusters (n=0-11) at 20 K is studied via IR-IR double resonance action spectroscopy in concert with quantum chemistry and AIMD calculations. For n=7-9, vibrational signatures of many isomers corresponding to intermediate species between intact and dissociated HNO_3, while full dissociation is observed at n=10. These gas phase cluster studies have major implications for the reactions and interactions of acids at complex interfaces.

Kinetic Monte Carlo for surface kinetics We worked on the formulation of a time integration strategy for kinetic Monte Carlo (KMC) computations of stiff surface-kinetics chemical systems. KMC by construction ignores a range of fast processes, retaining slower time scales associated with both chemistry and transport across surface sites. Nonetheless, residual stiffness can lead to significant computational bottlenecks. We have started the formulation of a construction that extends the existing KMC-based use of Gillespie's stochastic simulation algorithm (SSA), with particular regard to stiffness detection and handling.

PROPOSED WORK

Kinetic Monte Carlo for surface kinetics Stochastic Chemical Systems We plan to work on development of an efficient KMC time-integration strategy for stiff surface-kinetic systems. One of the key challenges will be the efficient implementation of an adaptive strategy for monitoring the local system state, identification of active timescales, and the definition of the fast subspace to be appropriately modeled. Selecting a timescale for requisite modeling of fast processes in the context of SSA will translate to, in the KMC context, a corresponding spatial scale. The incorporation of this adaptive construction in the context of lattice KMC will lead to a physically informed construction that employs local dynamical features of the system response to inform means of modeling fast processes, thereby enabling accurate time integration of stiff surface-kinetic systems with large time steps.

Assessment and physicochemical properties of gasified electrocatalytical radicals We have started a new effort in the BES core program to study phenomena of electrocatalytic intermediates (electro-radicals) in the gas phase. The production of these out-of-equilibrium, efficient radicals, which have never before been observed in the gas phase, have the potential to become useful for methane and CO_2 capture and chemical conversion, directly in the gas phase. We are using custom-designed solid-state electrolyzer cells at overvoltage conditions in an electrochemical holder we have created for high-temperature electrocatalysis (Fig. 2). The experiment creates a supersaturation condition at the electrode / electrolyte interface, leading to excess electro-radicals on the surface. When a fraction of them volatilizes (given their high chemical potential / concentration) they will be identified and quantified with mass spectrometry. They can also be easily isolated and concentrated as, we predict, they may maintain their net charge after desorption. We have also fabricated the special thin-film solid-state electrolyzer cells. We are currently finalizing the assembly of all the experimental parts. As a model reaction, we use gas mixtures combining CO, CO_2 and H_2, H_2O over symmetric M/YSZ/M (M = Ni, Pt, Ce) solid oxide electrolyzers to identify if key electro-

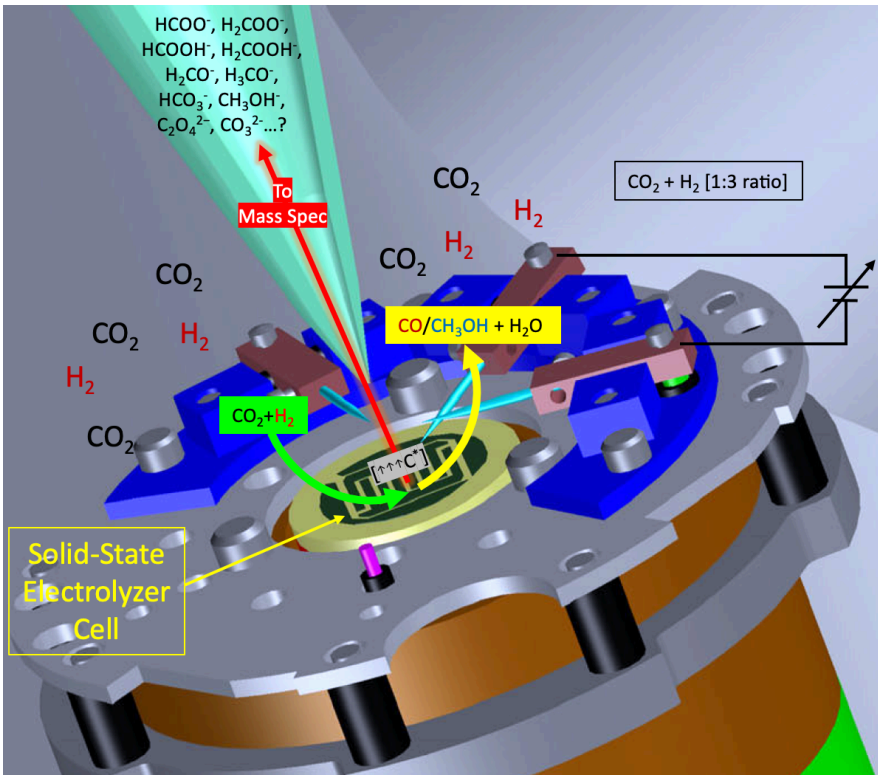

Figure 2: Experimental setup for the characterization of volatilized surface intermediates using mass spectrometry. As an example, the schematic represents the sampling of intermediates in the electrochemical CO_2 hydrogenation by a solid-state electrolyzer cell.

radicals can be volatilized and isolated for CO_2 capture, clean H_2 production, and clean methanol and syngas production. We have completed the experimental design and custom-part fabrication.

BES-SPONSORED PUBLICATIONS (SINCE 2019)

1. S. Mitra, N. Yang, L.M. McCaslin, R.B. Gerber, M.A. Johnson, "Size-Dependent Onset of Nitric Acid Dissociation in $Cs^+(HNO_3)(H_2O)_{n=0-11}$ Clusters at 20K", *J. Phys. Chem. Lett.*, 12, 3335 (2021).
2. N. Hansen, B. D. Adamson, S. A. Skeen, M. Ahmed, "Nucleation of Soot: Experimental Assessment of the Role of Polycyclic Aromatic Hydrocarbon (PAH) Dimers," *Z. Physik. Chem.* **234**, 1295-1310 (2020).
3. Q. Wang, P. Elvati, D. Kim, K. O. Johansson, P. E. Schrader, H. A. Michelsen, and A. Violi, "Spatial dependence of polycyclic aromatic compound growth in counterflow flames", *Carbon* **149**, 328-335. (2019).

CHEMICAL KINETICS FOR COMPLEX SYSTEMS

Jacqueline H. Chen, Nils Hansen, Habib N. Najm, David L. Osborn, Krupa Ramasesha,
Leonid Sheps, Craig A. Taatjes, and Judit Zádor
Sandia National Laboratories, MS 9055, Livermore, CA 94551-0969
jhchen@sandia.gov, nhansen@sandia.gov, hnnajm@sandia.gov, dlosbor@sandia.gov,
kramase@sandia.gov, lsheps@sandia.gov, cataatj@sandia.gov, jzador@sandia.gov

PROGRAM SCOPE

This program employs a unique set of experimental and theoretical studies with the goal of elucidating mechanisms of elementary chemical reactions, which impacts the research theme of Reaction Pathways in Diverse Environments. This task is linked with many other parts of the Sandia program; it extends the high-resolution view of the "Chemical Dynamics Methods and Applications" task to encompass complex interactions in collisional environments, and it provides a basis for the interface studies in the "Gas Phase Interactions with Other Phases" task. Methods developed under the "Advanced Diagnostics" task and analytical tools that use tunable vacuum ultraviolet light from the Advanced Light Source synchrotron at Lawrence Berkeley National Laboratory enable sensitive and sometimes even isomer-specific ionization of reactant and product molecules sampled from chemical reactions. These individual reaction studies are linked to controlled measurements of more complex reaction systems as found in well-defined laboratory scale zero- and one-dimensional reactors. Alongside, we use master equation (ME) frameworks to characterize the kinetics on complex potential energy surfaces (PESs), and approaches to study stochastic and nonthermal effects at the mesoscale.

RECENT PROGRESS

Stochastic Chemical Systems We continued our work on using computational singular perturbation theory for enabling stable large time-step explicit time integration of stiff stochastic mesoscale models of chemical systems, employing the chemical Langevin equation (CLE) model. We formulated a range of different approximations relying on linearization of the CLE diffusion terms to enable explicit large time step integration with controlled accuracy. We proved results concerning weak/strong error and convergence scaling for the resulting numerical constructions and illustrated the performance of the method with both linear and nonlinear systems.

Non-Thermal Reaction Systems In combustion simulations, it is usually assumed that highly-energized collision complexes (either radical or stable species) formed in exothermic reactions are always under thermal equilibrium as they evolve through competing networks of reactions. However, in practical fuel/air flames, non-trivial amounts of reactive radicals such as H, O and OH are present apart from O_2. As a result, collisions of these reactive species with the energized collision complexes have been shown in recent studies to induce non-thermal reactivity. These studies have also demonstrated that such non-thermal reactions can be suitably represented in macroscopic kinetics models as chemically termolecular reaction. In the past year, we focused on identifying and quantifying the effects of including such reactions on the evolution of an initial deflagration front to a developing detonation in H_2/CH_4-air mixtures under boosted internal combustion (IC) engine conditions. Specifically, fully resolved simulations, with and without non-thermal reactivity, were performed for a constant volume reactor containing stoichiometric H_2/CH_4-air mixture [Desai et al. 2021]. It was found that inclusion of termolecular chemistry facilitated by radical-radical recombinations resulted in a delayed onset of end-gas auto-ignition. Concurrently, the developing detonation intensity was observed to be significantly higher. Chemical explosive mode analysis (CEMA) was performed to identify the dominant species/reactions responsible for the observed variation in the results.

Direct Simulation Monte Carlo We have confirmed the validity of direct simulation Monte Carlo (DSMC) to simulate the evolution of a turbulent shear in the incompressible flow regime. We have investigated the possibility of using physics informed neural network (PINN) by inferring the equation of state from shock

tube data with DSMC in collaboration with Nathan Trask et al. (submitted to the Journal of Computational Physics, https://arxiv.org/abs/2012.05343) Lastly, we confirmed that DSMC is capable of capturing thermal nonequilibrium induced by local shocks.

Automated Kinetics In our automated kinetics code, KinBot, we implemented tools to include uncertainty estimates automatically, extended the set of reactions it can explore, improved conformation searches for cyclic species, and in general increased the robustness of the code.

Low-Temperature Oxidation of Cyclopentane We explored five PESs in the cyclopentyl + O_2 + O_2 reaction system automatically using KinBot to uncover the major pathways that cyclopentane undergoes under low-temperature oxidation conditions. We compared our theoretical results to high- and low-pressure MPIMS experimental results done under the HPCC project. We have shown that the dominant pathway is ROO (+ O_2) $\rightarrow$ γ-QOOH + O_2 $\rightarrow$ γ-OOQOOH $\rightarrow$ products. Photoionization dynamics calculations enabled the reliable quantification of the time-resolved concentrations of elusive species.

Cyclopentene + O^3P We investigated the reaction of O(^3P) with cyclopentene at 4 Torr, 298 K using MPIMS experiments. We found large yields of propylketene and 1-butene + CO products, two channels that have never been observed or described before. Our automatically explored reactive PES coupled with ME calculations provides strong evidence that crossing happens around two geometries, that of the initial triplet adduct and that of triplet propylketene. Our work shows how a cyclic alkene can fundamentally differn compared to aliphatic analogues in the alkene + O(^3P) reaction class.

Ketohydroperoxide Decomposition – Theory We calculated pressure- and temperature-dependent kinetics for the decomposition reactions of 3-hydroperoxypropanal using KinBot to explore the PES. We showed that the fraction going into the Korcek channel is negligible under most circumstance. We amended the calculations with AIMD simulations to study the dynamics of the homolytic dissociation pathway. In part supported by this program we also explored the main aspects of the kinetics of 61 ketohydroperoxide molecules, up to 12 carbon atoms.

Molecular-Weight Growth in Hydrocarbon Rich Environments We explored the role of the propargyl radical (C_3H_3) in growth of larger aromatic species. We found that C_3H_3 facilitates growth by radical+radical recombination reactions, through reactions with aliphatically substituted aromatics, and through formation of C_5 rings, which subsequently can undergo ring-enlargement reactions to C_6 rings. Following up on this work, we investigated the participation of the cyclopentadienyl (C_5H_5) radical in molecular-weight growth processes through ring-enlargement reactions in high-temperature environments. The mass-spectral data implies a direct participation of C_5H_5 in ring-enlargement reactions with CH_3, C_3H_3, C_3H_5, and C_2H_2 to produce the aromatic species benzene, styrene, ethylbenzene, and the benzyl radical, respectively.

Ozone-Initiated Oxidation Chemistry Following up on our earlier studies on the ozone-initiated chemistry and the chemistry of the Criegee Intermediate reaction network we studied the influence of ozone on the low-temperature oxidation of dimethyl ether and methyl hexanoate. A new oxidation regime was observed, dubbed the extreme low-temperature chemistry (ELTC), at temperatures below traditional low-temperature chemistry. Our results indicate that the LTC-like peroxide chemistry dominates the ELTC regime as well. However, observed differences in concentrations and the detection of distinct isomers in either LTC or ELTC regimes indicate that competing chemical pathways are active. We also studied the molecular-weight growth in ozone-initiated low-temperature oxidation of methyl crotonate. We revealed the presence of keto-hydroperoxides, their reaction network, and their importance for molecular-weight growth processes.

3rd O_2 Addition Reaction Network We studied the oxidation of neo-pentane by combining experiments, theoretical calculations, and mechanistic developments to elucidate the 3rd O_2 addition reaction network. The experiments were based on photoionization mass spectrometry in a jet-stirred reactor allowing for sensitive detection of the keto-hydroperoxide (KHP) and keto-dihydroperoxide (KDHP) intermediates. When modeling this reaction network, using the experimentally observed KHP-to-KDHP ratio as target,

we revealed uncertainties about the rate of formation of hydroperoxyl-cyclic oxiranes from the β-$P(OOH)_2$ radical. This reaction competes with the 3rd O_2 additions at low temperatures.

PROPOSED WORK

Product Branching in Peroxy Radical – Radical Reactions Peroxy radical self-reactions proceed on singlet and triplet PESs and involve competing product channels, mediated by intersystem crossing from the triplet to the singlet surface of the RO−O_2−OR' adduct: H-transfer to form closed-shell carbonyl + alcohol, dissociation to alkoxy radicals, and ^{1}ROOR' stabilization. Recent calculations by Kurten and co-workers (*J. Phys. Chem. A* **2019**, *123, 6596-6604*, *J. Phys. Chem. A*, **2020**, *124, 8305-8320*,) indicate that adduct formation is energetically accessible and is most likely the overall rate-limiting step. However, their theoretical exploration of several archetypal alkyl and oxygenated radicals could not even qualitatively predict product branching ratios and highlighted the challenges associated with applying statistical rate theories and multireference electronic structure methods to these adducts, which have 4 unpaired electrons. Similarly, ROO + OH reactions occur on singlet and triplet PESs and may form ^{1}ROOOH adducts at atmospheric pressures (*Nat. Comm.*, **2016**, *7*, *13213*). Over the past two years, we have performed experiments on ROO + ROO and ROO + OH reactions (R = CH_3, CH_3CH_2, CH_3CO) using photolytic radical production at pressures from 4 to 760 Torr. We employed multiplexed synchrotron VUV photoionization mass spectrometry to probe numerous reaction products and intermediated with sub-ms time resolution and obtained preliminary evidence of ROOR and ROOOH formation. In the coming year, we will analyze this rich experimental dataset with a special emphasis on quantifying the product branching on the triplet vs. singlet PES.

Theoretical Investigation of ROO + HO_2 Reactions ROO and HO_2 radicals can react both on the singlet and triplet surface, most likely producing alkyl hydroperoxides (ROOH) + O_2 via a barrierless entrance and a submerged barrier. We propose to characterize the ROO + HO_2 reactions in more detail using multireference electronic structure methods necessitated by the substantial multi-reference character of the critical barrier, an effective two-transition state for the accurate determination of the capture rate coefficients, and using nonadiabatic TST for calculating the branching between the singlet and the triplet surfaces.

Low-Temperature Oxidation of Cyclopentane, Cyclic Ethers, and di-n-Propyl Ether Our prior work on this system paved the way for detailed comparisons of experimental time profiles with theoretical predictions from master equation-based kinetic models. We will assemble a validated, uncertainty-quantification-driven set of kinetic description for this system. In collaboration with Brandon Rotavera (U Georgia) and using support from the SCGSR program we want to understand and quantify cyclic ether oxidation kinetics to produce new computational sub-mechanisms that will widen our understanding of how structural characteristics, such as ring size and substituents, affect the reactivity of the species that are ubiquitous in low-temperature oxidation systems. We will study the low-temperature oxidation of di-n-propyl ether experimentally using our JSR-MBMS set-up. Special emphasis will be paid to the chemistry that controls the dual-stage negative temperature coefficient behavior.

Molecular-Weight Growth in Hydrocarbon Rich Environments With benzene formation well understood under extreme high-temperature conditions, our focus shifts to two- and three-ring aromatic species. We are currently interested in the formation of indene and naphthalene through phenyl/benzyl+C_3 radicals. Another is on phenyl and benzyl reactions to form aliphatically bridged PAHs and on ring-enlargement reactions involving cyclopentadienyl radicals with allyl and propargyl. In order to investigate kinetics of resonance-stabilized radicals at high temperatures, we have developed a new resistively heated plug-flow reactor for kinetics and coupled it to our existing mass-spectrometric analysis tools. We started to work on interfacing this reactor with our uniquely powerful measurement tools of MS-MS (see the abstract on Advanced Diagnostics).

Chemically Termolecular Reactions We plan to include both chemically termolecular reactions as well as corrected recombination rate constants as a function of pressure. The corrections to the recombination rate

constants have been shown in simple atmospheric laminar flames to affect the results. We will also quantify the effects of radical-radical recombination induced termolecular chemistry over a broader range of mixture compositions and also under the influence of compression ignition.

Thermal Nonequilibrium Chemistry We will extend the thermal equilibrium direct numerical simulation (DNS) code, S3D, to predict thermal nonequilibrium in air induced by shocks (and validate against DSMC results which solve the Boltzmann equation) which is computationally more expedient than DSMC for low Knudsen number flows. We plan to perform DSMC simulations of H_2-Air reactive flows with strong thermal nonequilibrium including multiple interacting shocks. These DSMC simulations will require detailed molecular level simulations (i.e. QCT) to provide accurate collision cross sections between species. Finally, we will use the DSMC results to build simplified chemical reaction mechanisms that account for thermal nonequilibrium.

BES-SPONSORED PUBLICATIONS (SINCE 2019)

1. Baroncelli, M.; Felsmann, D.; Hansen, N.; Pitsch, H. Investigating the effect of oxy-fuel combustion and light coal volatiles interaction: A mass spectrometric study. *Combustion and Flame* **2019,** *204*, 320-330.
2. Baroncelli, M.; Mao, Q.; Galle, S.; Hansen, N.; Pitsch, H. Role of Ring-Enlargement Reactions in the Formation of Aromatic Hydrocarbons. *Physical Chemistry Chemical Physics* **2020,** *22*, 4699-4714.
3. Bierkandt, T.; Höner, M.; Gaiser, N.; Hansen, N.; Köhler, M.; Kasper, T. Experimental Flat Flame Study of Monoterpenes: Insights into the Combustion Kinetics of α-Pinene, β-pinene, and mycrene. *Proceedings of the Combustion Institute* **2020**, in press.
4. Bourgalais, J.; Caster, K. L.; Durif, O.; Osborn, D. L.; Le Picard, S. D.; Goulay, F. Product detection of the CH radical reactions with ammonia and methyl-substituted amines. *The Journal of Physical Chemistry A* **2019,** *123*, 2178-2193.
5. Braun-Unkhoff, M.; Hansen, N.; Dietrich, M.; Methling, T.; Moshammer, K.; Yang, B. Entanglement of n-Heptane and iso-Butanol Chemistries in Flames Fueled by their Mixtures. *Proceedings of the Combustion Institute* **2020**, in press.
6. Caravan, R. L.; Vansco, M. F.; Au, K.; Khan, M. A. H.; Li, Y.-L.; Winiberg, F. A.; Zuraski, K.; Lin, Y.-H.; Chao, W.; Trongsiriwat, N. Direct kinetic measurements and theoretical predictions of an isoprene-derived Criegee intermediate. *Proceedings of the National Academy of Sciences* **2020,** *117*, 9733-9740.
7. Chen, B.; Wang, H.; Wang, Z.; Han, J.; Alquaity, A. B. S.; Wang, H.; Hansen, N.; Sarathy, S. M. Ion chemistry in premixed rich methane flames. *Combustion and Flame* **2019,** *202*, 208-218.
8. Chen, B. J.; Ilies, D. B.; Hansen, N.; Pitsch, H.; Sarathy, S. M., Simultaneous production of ketohydroperoxides from low temperature oxidation of a gasoline primary reference fuel mixture. *Fuel* **2021,** *288*, 119737
9. Chen, B. J.; Kruse, S.; Schmid, R.; Cai, L. M.; Hansen, N.; Pitsch, H., Oxygenated PAH Formation Chemistry Investigation in Anisole Jet Stirred Reactor Oxidation by a Thermodynamic Approach. *Energy & Fuels* **2021,** *35*, 1535-1545
10. Chhantyal-Pun, R.; Shannon, R. J.; Tew, D. P.; Caravan, R. L.; Duchi, M.; Wong, C.; Ingham, A.; Feldman, C.; McGillen, M. R.; Khan, M. A. H. Experimental and computational studies of Criegee intermediate reactions with NH_3 and CH_3NH_2. *Physical Chemistry Chemical Physics* **2019,** *21*, 14042-14052.
11. Chhantyal-Pun, R.; Khan, M. A. H.; Taatjes, C. A.; Percival, C. J.; Orr-Ewing, A. J.; Shallcross, D. E., Criegee intermediates: production, detection and reactivity. *Int. Rev. Phys. Chem.* **2020,** *39*, 383-422
12. Christianson, M. G.; Doner, A. C.; Davis, M. M.; Koritzke, A. L.; Turney, J. M.; Schaefer III, H. F.; Sheps, L.; Osborn, D. L.; Taatjes, C. A.; Rotavera, B. Reaction mechanisms of a cyclic ether intermediate: Ethyloxirane. *Inernational Journal of Chemical Kinetics* **2021,** *53*, 43-59.
13. Davis, J. C.; Koritzke, A. L.; Caravan, R. L.; Antonov, I. O.; Christianson, M. G.; Doner, A. C.; Osborn, D. L.; Sheps, L.; Taatjes, C. A.; Rotavera, B. Influence of the Ether Functional Group on Ketohydroperoxide Formation in Cyclic Hydrocarbons: Tetrahydropyran and Cyclohexane. *The Journal of Physical Chemistry A* **2019,** *123*, 3634-3646.

14. Doner, A. C.; Davis, M. M.; Koritzke, A. L.; Christianson, M. G.; Turney, J. M.; Schaefer III, H. F.; Sheps, L.; Osborn, D. L.; Taatjes, C. A.; Rotavera, B. Isomer-dependent reaction mechanisms of cyclic ether intermediates: cis-2, 3-dimethyloxirane and trans-2, 3-dimethyloxirane. *International Journal of Chemical Kinetics* **2021,** *53*, 127-145.
15. Han, X.; Najm, H. N. Effective construction of eigenvectors for a class of singular sparse matrices. *Journal of Applied Mathematics Letters* **2019,** *97*, 121-126.
16. Han, X.; Valorani, M.; Najm, H. N. Explicit time integration of the stiff chemical Langevin equations using computational singular perturbation. *The Journal of Chemical Physics* **2019,** *150*, 194101.
17. Hansen, N.; He, X.; Griggs, R.; Moshammer, K. Knowledge generation through data research: New validation targets for the refinement of kinetic mechanisms. *Proceedings of the Combustion Institute* **2019,** *37*, 743-750.
18. Hansen, N.; Kukkadapu, G.; Chen, B.; Dong, S.; Curran, H. J.; Taatjes, C. A.; Eskola, A. J.; Osborn, D. L.; Sheps, L.; Pitz, W. J.*, et al.* The impact of the third O2 addition reaction network on ignition delay times of neo-pentane. *Proceedings of the Combustion Institute* **2020**, in press.
19. Hansen, N.; Moshammer, K.; Jasper, A. W. Isomer-Selective Detection of Keto-Hydroperoxides in the Low-Temperature Oxidation of Tetrahydrofuran. *The Journal of Physical Chemistry A* **2019,** *123*, 8274-8284.
20. He, X; Hansen, N.; Moshammer, K. Molecular-weight growth in ozone-initiated low-temperature oxidation of methyl crotonate. *J. Phys. Chem. A* **2020**, *124*, 7881–7892.
21. Holland, R.; Khan, M. A. H.; Chhantyal-Pun, R.; Orr-Ewing, A. J.; Percival, C. J.; Taatjes, C. A.; Shallcross, D. E. Investigating the Atmospheric Sources and Sinks of Perfluorooctanoic Acid Using a Global Chemistry Transport Model. *Atmosphere* **2020,** *11*, 407.
22. Holland, R.; Khan, M. A. H.; Driscoll, I.; Chhantyal-Pun, R.; Derwent, R. G.; Taatjes, C. A.; Orr-Ewing, A. J.; Percival, C. J.; Shallcross, D. E., Investigation of the Production of Trifluoroacetic Acid from Two Halocarbons, HFC-134a and HFO-1234yf and Its Fates Using a Global Three-Dimensional Chemical Transport Model. *ACS Earth Space Chem.* **2021**, doi: 10.1021/acsearthspacechem.0c00355.
23. Huang, C.; Li, S.; Tao, T.; Zhang, F.; Hansen, N.; Law, C. K.; Qi, F.; Yang, B. From inherent correlation to constrained measurement: Model-assisted calibration in MBMS experiments. *Proceedings of the Combustion Institute* **2020**, in press.
24. Koritzke, A. L.; Davis, J. C.; Caravan, R. L.; Christianson, M. G.; Osborn, D. L.; Taatjes, C. A.; Rotavera, B. QOOH-mediated reactions in cyclohexene oxidation. *Proceedings of the Combustion Institute* **2019,** *37*, 323-335.
25. Kukkadapu, G.; Wagnon, S. W.; Pitz, W. J.; Hansen, N. Identification of the Molecular-Weight Growth Reaction Network in Counterflow Flames of the C3H4 Isomers Allene and Propyne. *Proceedings of the Combustion Institute* **2020**, in press.
26. Leon, L.; Ruwe, L.; Moshammer, K.; Seidel, L.; Shrestha, K.; Wang, X.; Mauss, F.; Kohse-Höinghaus, K.; Hansen, N. Chemical insights into the larger sooting tendency of 2-methyl-2-butene compared to n-pentane. *Combustion and Flame* **2019,** *208*, 182-197.
27. Lia, H.; Shiqing, K.; Hansen, N.; Zhang, F.; Yang, B. Influence of ozone addition on the low-temperature oxidation of dimethyl ether in a jet-stirred reactor. *Combustion and Flame* **2020,** *214*, 277-286.
28. Liao, H.; Tao, T.; Sun, W.; Hansen, N.; Law, C. K.; Yang, B. Investigation of the low-temperature oxidation of n-butanal in a jet-stirred reactor. *Proceedings of the Combustion Institute* **2019,** *37*, 453-460.
29. Liao, H.; Tao, T.; Sun, W.; Hansen, N.; Yang, B. Isomer-specific speciation behaviors probed from premixed flames fueled by acetone and propanal. *Proceedings of the Combustion Institute* **2020**, in press.
30. Miller, J. A.; Sivaramakrishnan, R.; Tao, Y.; Goldsmith, C. F.; Burke, M. P.; Jasper, A. W.; Hansen, N.; Labbe, N. J.; Glarborg, P.; Zádor, J. Combustion chemistry in the twenty-first century: Developing theory-informed chemical kinetics models. *Progress in Energy and Combustion Science* **2021,** *83*, 100886.
31. Pieper, J.; Hemken, C.; Büttgen, R.; Graf, I.; Hansen, N.; Heufer, K. A.; Kohse-Höinghaus, K. A high-temperature study of 2-pentanone oxidation: experiment and kinetic modeling. *Proceedings of the Combustion Institute* **2019,** *37*, 1683-1690.
32. Prendergast, M. B.; Kirk, B. B.; Savee, J. D.; Osborn, D. L.; Taatjes, C. A.; Hemberger, P.; Blanksby, S. J.; da Silva, G.; Trevitt, A. J. Product detection study of the gas-phase oxidation of methylphenyl radicals

using synchrotron photoionisation mass spectrometry. *Physical Chemistry Chemical Physics* **2019,** *21*, 17939-17949.
33. Rousso, A.; Hansen, N.; Jasper, A.; Ju, Y. J. P. C. C. P. Identification of the Criegee intermediate reaction network in ethylene ozonolysis: Impact on energy conversion strategies and atmospheric chemistry. *Physical Chemistry Chemical Physics* **2019,** *21*, 7341-7357.
34. Ruwe, L.; Cai, L.; Moshammer, K.; Hansen, N.; Pitsch, H.; Kohse–Höinghaus, K. The C5 chemistry preceding the formation of polycyclic aromatic hydrocarbons in a premixed 1-pentene flame. *Physical Chemistry Chemical Physics* **2019,** *206*, 411-423.
35. Ruwe, L.; Cai, L.; Wullenkord, J.; Schmitt, S. C.; Felsmann, D.; Baroncelli, M.; Chen, B.; Moshammer, K.; Hansen, N.; Pitsch, H.*, et al.* n-Heptane combustion chemistry in less studied configurations: Aromatics formation and oxidation chemistry in counterflow flame and flow reactor. *Proceedings of the Combustion Institute* **2020**, in press.
36. Schmitt, S.; Wick, M.; Wouters, C.; Ruwe, L.; Graf, I.; Andert, J.; Hansen, N.; Pischinger, S.; Kohse-Höinghaus, K. Effects of water addition on the combustion of iso-octane investigated in laminar flames, low-temperature reactors, and an HCCI engine. *Combustion and Flame* **2020,** *212*, 433-447.
37. Sun, W.; Lailliau, M.; Serinyel, Z.; Dayma, G.; Moshammer, K.; Hansen, N.; Yang, B.; Dagaut, P. Insights into the oxidation kinetics of a cetane improver–1, 2-dimethoxyethane (1, 2-DME) with experimental and modeling methods. *Proceedings of the Combustion Institute* **2019,** *37*, 555-564.
38. Sun, W.; Tao, T.; Liao, H.; Hansen, N.; Yang, B. Probing fuel-specific reaction intermediates from laminar premixed flames fueled by two C5 ketones and model interpretations. *Proceedings of the Combustion Institute* **2019,** *37*, 1699-1707.
39. Sun, W.; Wang, J.; Huang, C.; Hansen, N.; Yang, B. Providing effective constraints for developing ketene combustion mechanisms: A detailed kinetic investigation of diacetyl flames. *Combustion and Flame* **2019,** *205*, 11-21.
40. Taatjes, C. A.; Khan, M. A. H.; Eskola, A. J.; Percival, C. J.; Osborn, D. L.; Wallington, T. J.; Shallcross, D. E. Reaction of perfluorooctanoic acid with Criegee intermediates and implications for the atmospheric fate of perfluorocarboxylic acids. *Environmental Science & Technology* **2018,** *53*, 1245-1251.
41. Van de Vijver, R.; Zádor, J. KinBot: Automated stationary point search on potential energy surfaces. *Computer Physics Communications* **2020,** *248*, 106947.
42. Vansco, M. F.; Caravan, R. L.; Pandit, S.; Zuraski, K.; Winiberg, F. A.; Au, K.; Bhagde, T.; Trongsiriwat, N.; Walsh, P. J.; Osborn, D. L. Formic acid catalyzed isomerization and adduct formation of an isoprene-derived Criegee intermediate: experiment and theory. *Physical Chemistry Chemical Physics* **2020,** *22*, 26796-26805.
43. Vansco, M. F.; Caravan, R. L.; Zuraski, K.; Winiberg, F. A.; Au, K.; Trongsiriwat, N.; Walsh, P. J.; Osborn, D. L.; Percival, C. J.; Khan, M. A. H. Experimental evidence of dioxole unimolecular decay pathway for isoprene-derived Criegee intermediates. *The Journal of Physical Chemistry A* **2020,** *124*, 3542-3554.
44. Wang, Z.; Hansen, N.; Jasper, A. W.; Chen, B.; Popolan-Vaida, D. M.; Yalamanchi, K. K.; Najjar, A.; Dagaut, P.; Sarathy, S. M. Cool Flame Chemistry of Diesel Surrogate Compounds: n-Decane, 2-Methylnonane, 2,7-Dimethyloctane, and n-Butylcyclohexane. *Combustion and Flame* **2020,** *219*, 384-392.
45. Wang, Z.; Herbinet, O.; Hansen, N.; Battin-Leclerc, F. Exploring hydroperoxides in combustion: History, recent advances and perspectives. *Progress in Energy and Combustion Science* **2019,** *73*, 132-181.
46. Zádor, J.; Miller, J. A. Comment on "Influence of Multiple Conformations and Paths on Rate Constants and Product Branching Ratios. Thermal Decomposition of 1-Propanol Radicals". *The Journal of Physical Chemistry A* **2019,** *123*, 1129-1130.

IMAGING THE NEAR-SURFACE GAS PHASE: A NEW APPROACH TO COUPLED GAS-SURFACE CHEMISTRY

Jonathan H. Frank, Farid El Gabaly, Nils Hansen, Christopher J. Kliewer, David L. Osborn
Sandia National Laboratories, Livermore, CA
jhfrank@sandia.gov, felgaba@sandia.gov, nhansen@sandia.gov, cjkliew@sandia.gov, dlosbor@sandia.gov
Coleman Kronawitter and Ambarish Kulkarni
Department of Chemical Engineering, University of California, Davis
ckrona@ucdavis.edu, arkulkarni@ucdavis.edu

PROGRAM SCOPE

The chemical reactivity of gases with solid surfaces is ubiquitous in natural and industrial energy transformation. Cooperative effects that couple gas phase chemistry with surface chemistry are critical for foundational understanding but challenging to probe experimentally and theoretically. Heterogeneous catalysis is an ideal field to expose and isolate the fundamental chemical physics of these cooperative effects. We have recently started a program to characterize gas-surface coupling, through chemically specific, temporally and spatially resolved probes of both reacting surfaces and the near-surface gas phase. The program combines optical spectroscopy with mass spectrometry probes of both gas phase and surface species. The long-term goal is to elucidate the fundamental mechanisms of cooperative gas-surface chemistry, influencing DOE mission research in catalysis, synthesis, and energy transformation.

This program comprises two interrelated thrusts that are distinguished by the physical mechanism of gas-surface coupling – transport or reaction – and employ differing degrees of chemical complexity and control over the model catalyst surface. The first thrust explores how molecular transport in the gas phase may mediate coupling between different domains on a surface without gas-phase chemical reactions and employs well-controlled reactions on atomically cleaned crystalline and polycrystalline surfaces prepared under ultra-high vacuum (UHV) conditions, with reactivity studied under pressures of 10^{-6} to 760 Torr. The second thrust adds the complexity of reactive coupling, with bond breaking and formation among intermediates occurring in the gas phase as well as on the surface. Thrust 2 utilizes both polycrystalline films and more complex surfaces (e.g., doped metal oxides, and bifunctional supported catalysts), with reactivity studied at elevated temperatures (700 - 1250 K) and pressures of 1 – 1500 Torr.

RECENT PROGRESS

Design and Procurement of an Optically Accessible Ambient Pressure Imaging X-Ray Photoelectron Spectrometer

We have designed a truly novel experimental system that simultaneously allows for optical spectroscopy techniques, including 2D coherent anti-Stokes Raman scattering (2D-CARS), femtosecond sum-frequency generation (SFG) and planar laser-induced fluorescence (PLIF), to be performed alongside 2D imaging ambient pressure X-ray photoelectron spectroscopy (AP-XPS). The system also includes a flexible gas handling system and a variety of surface science techniques such as LEED, Auger and sputtering. Imaging AP-XPS delivers the power of x-ray photoelectron spectroscopy to measure, via core-level transitions, spatially resolved (~10 microns) oxidation states of surface species. AP-XPS is successful even with gas pressures of 1 – 20 torr above a surface. The addition of laser spectroscopy will add simultaneous observation of near-surface gas phase molecules. This combination enables direct and detailed correlation of surface oxidation states with near-surface gas phase composition. Over the first year of this program, we worked to complete the design and procurement of this large experimental system which includes: a newly developed, fast CMOS electron detector, a state-of-the-art hemispherical analyzer, a monochromatic X-ray gun capable of operating at gas-pressures of up to 20 torr, a 5-axis motorized sample manipulator, a combination of surface science techniques in a preparation chamber, and

optical access to the sample surface during operation. This custom-designed system is being manufactured and is expected to be installed in late 2021.

Surface Science Chamber for Ultrafast Sum Frequency Generation, 2D-CARS, and PLIF Analysis of Coupled Gas-Surface Interactions The gas-surface chemical mapping reactor chamber described above will enable breakthrough understanding of the feedback between gas-phase reactants and intermediates and detailed surface chemistry, resolving, for example, the feedback mechanism in many oscillatory hydrocarbon oxidation reactions at surfaces that exhibit time-varying kinetics. The local catalytic product flux will be correlated with imaged surface oxidation. While we await installation of this chamber, we have constructed a relatively miniaturized combined UHV / high pressure reaction chamber for detailed surface (and near-surface) spectroscopy to be carried out over surfaces that have been atomically cleaned prior to gas-surface reactions. The optical chamber design enables UHV conditions (~ 10^{-9} Torr) to be reached quickly because of the small surface area. Both the manipulator and turbomolecular pump can be shut off from the chamber through pneumatic gate valves, and the chamber can be filled with reactant gases with pressure range from UHV to 1 atm. The chamber is equipped with an ion sputtering gun and Auger electron spectrometer, and the sample holder can be heated to 800C or cooled with a liquid nitrogen cold finger. This allows for an atomically clean, annealed surface as the starting point for our gas-surface experiments. Several optical access ports around the sample enable ultrafast 2D-CARS, SFG, and PLIF analysis of the reacting surface and near-surface gas phase. We have recently demonstrated initial studies of time-resolved femtosecond sum-frequency generation vibrational spectroscopy for molecules that are physisorbed to a metal surface. With funding under the final year of a DOE Early Career Award, we have investigated the adsorption, vibrational lifetime, and rotational motion of CO adsorbed on a Au(111) surface and characterized the nature of the energy transfer and bonding of these weakly adsorbed species. Under the current project we have investigated the dynamics of CH_4 during weak physisorption, as described below. In future work, this apparatus will be used to image the *local* catalytic production of HD in the H_2/D_2 exchange reaction over a patterned Pt surface using 2D-CARS where the gas phase acts as a reporter on local spatially resolved catalytic activity.

Freely rotating physisorption: a new understanding of weak molecule/surface interactions The long-held belief that physisorbed molecules on metal surfaces are rapidly thermalized to the surface temperature has recently come into question because of work from the Wodtke group demonstrating long-lived vibrational lifetimes for CO on Au(111). We have explored the time-resolved surface dynamics of CH_4 adsorbed to Au(111). Remarkably, our results demonstrate not only the methane can have exceptionally long vibrationally excited lifetimes on Au(111), but our recent results have provided the first direct evidence for adsorbed, yet freely rotating, molecules with rovibrational lifetimes of several 10's of picoseconds, as seen in Figure 1. While MD simulations have predicted rotating physisorption for years, it has never been directly observed experimentally. This follows from work sponsored under the DOE Early Career program (Kliewer) that first observed such dynamics for CO on Au(111) using temporally resolved fs/ps-SFG as a probe. The high spectral (few cm^{-1}) and temporal (few picosecond) time resolution provided by the hybrid SFG approach provided for the capability to resolve the spectral and temporal dynamics of these freely rotating physisorbed molecular species. While it has long been understood that vibrational excitation of molecules (through direct absorption of photons or by electron impact in a plasma) can often lead to enhanced reaction rates at surfaces, the mechanism has often only been speculated. The key understanding for such processes rests in the vibrational lifetime of adsorbed species when compared to the forward surface reaction rate. In this new work, we have discovered that methane can exist in a weakly bound physisorbed state in excited vibrational and rotational distributions for an extended period. As such, energy transfer processes between such bound rotors and more strongly coupled chemisorbed species are likely to have significant impact on gas-surface chemical kinetics quite broadly. These first-in-kind measurements have been summarized in a publication presently under review.

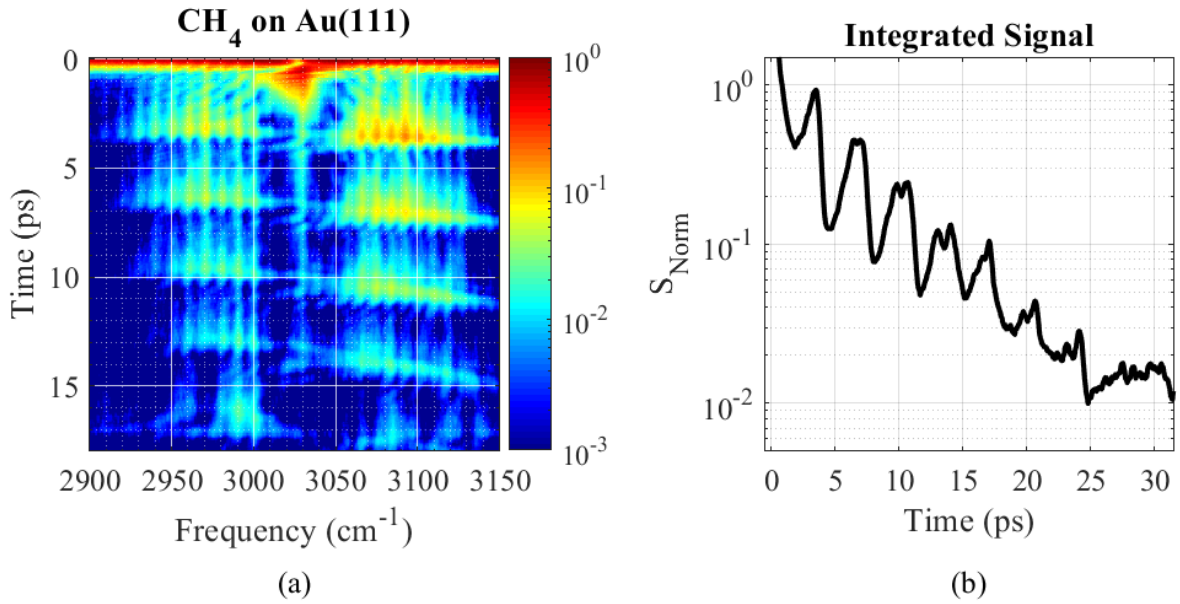

Figure 1: The SFG signal from CH_4 on a Au(111) surface at 300 K. Panel (a) displays the full spectral-temporal mapping of the rovibrational SFG decay, while panel (b) shows the time-integrated signal decay rate.

Imaging of Gas-Phase Species in Catalytic Oxidation of Methanol over Ag A great deal of catalysis research has focused on investigating surface chemistry in UHV. However, most catalysts are operated at pressures that are orders of magnitude above UHV conditions. Elevated pressures involve a different operating regime with higher surface coverage of reactants and a greater probability of gas-phase chemical reactions. Therefore, *operando* experiments are needed to provide mechanistic understanding at realistic conditions.

We recently published[1] a study of the partial oxidation of CH_3OH over polycrystalline silver (Ag) surfaces. For this study, we built two similar flow reactors for gas-phase measurements above the Ag surface and demonstrated in-situ *operando* measurements using 1D Raman scattering, 2D PLIF, and near-surface molecular beam mass spectrometry of minor species. The CH_3OH/Ag system provided a convenient testbed for developing and implementing a suite of diagnostic techniques relevant to our future work. As the Ag surface is heated to temperatures of 350-700C, catalytic production of formaldehyde progresses via two main pathways of partial oxidation: $2CH_3OH + O_2 \rightarrow 2H_2CO + 2H_2O$, and dehydrogenation $CH_3OH \rightarrow H_2CO + H_2$.

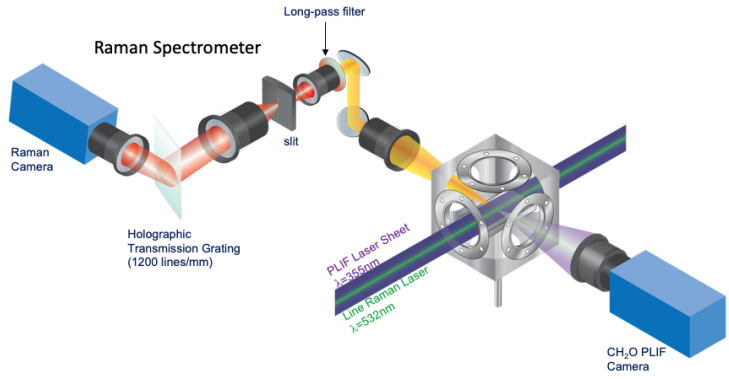

Figure 2: Optically accessible flow reactor

The experimental configuration of our optically accessible flow reactor is shown in Fig. 2. The reactor consists of a 3-inch cube with fused silica windows on opposite sides for collecting LIF and Raman signals. A mixture of reactants enters the cube forming a laminar boundary layer flow across the 150nm thick silver catalyst that is mostly Ag(111) facets. 2D PLIF imaging of formaldehyde and 1D spontaneous Raman scattering from major species are collected on opposite sides as shown.

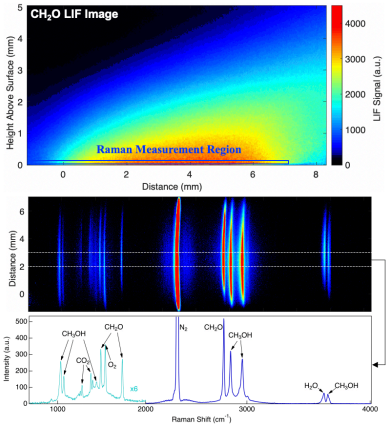

Figure 3: Optical data of the near-surface gas phase in CH_3OH partial oxidation over Ag

A representative CH_2O PLIF image and Raman spectrum from this system (the latter taken ~60 μm above the catalyst surface) are shown in Fig. 3. In addition to the dominant Raman peaks from the reactant mixture (CH_3OH, O_2, N_2), we observe peaks from H_2O, CO_2, O_2, and CH_2O. Because N_2 is unreactive, its concentration reflects total number density and is used to determine the temperature by the Ideal Gas Law. As a complement to these optical approaches, we have also developed near-surface molecular beam mass spectrometry (MBMS) to provide a global view of the species present in partial oxidation of CH_3OH over Ag (Fig. 4). Unlike conventional downstream analysis of effluent gas by mass spectrometry in previous heterogenous catalysis experiments, in our approach reaction gases are sampled immediately above the catalyst surface through a quartz nozzle with a 40° cone angle and a ~50 μm orifice diameter. The rapid expansion of gas beyond the orifice forms a molecular beam, stopping all further chemistry, which preserves both closed and open-shell species. These neutral molecules are ionized by either electrons or VUV photons, and analyzed by orthogonal acceleration time-of-flight mass spectrometry. Figure 4 shows the observation of unexpected intermediates CH_3 and CH_3O vs. height above surface. This ability to perform *operando* detection of the spatial distributions of gas-phase species above a catalyst using in-situ measurements is a significant step towards gaining insight into the complex coupling between gas-phase and surface chemistry. Our next steps will involve quantification of both the optical and mass spectrometry measurements, which will leverage our long history of developing and applying these diagnostic techniques for studies in combustion science.

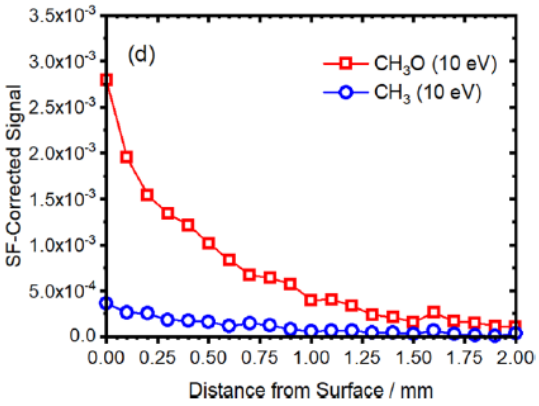

Figure 4: Electron impact near-surface molecular beam mass spectra of free radicals ejected from the surface in the CH_3OH / Ag system

FUTURE WORK

Transport-Mediated Gas-Surface Coupling and Domain-Specific Chemistry

Resolving the local reaction kinetics and mechanism during surface catalyzed reactions as they vary from one crystallographic domain to the next, under ambient pressure conditions, is a foundational but elusive measurement for understanding gas-surface catalytic reactions. We aim to accomplish this task by directly monitoring local gas-surface reactive exchange rates across the many crystallographic domains of a typical polycrystalline catalyst. These measurements will show the effects that the local crystallographic termination, structure, and oxidation state, or the local average concentration of steps and defects within a domain, have on the product formation rate for polycrystalline (nonuniform) catalysts. Gas-phase composition measurements will also determine which key species are transported via the gas-phase to other crystallographic domains.

The full imaging AP-XPS system will be installed late this year as the vendor is now producing the device, and we will prepare for the arrival of this chamber by initiating the optical portion of our first studies in the

optical surface science chamber which is currently completed. The first set of experiments in the new instrument will involve joint gas-surface measurements of H_2-D_2 exchange over patterned Pt samples to form HD. We anticipate that the local crystal structure will influence reaction rates, and that this physics could be directly measured by monitoring the gas-surface exchange and product formation rates with 2D-CARS, along with surface characterization with ambient pressure XPS to monitor oxidation state. The resulting dataset will provide a complete picture of the gas-surface chemistry for that catalytic process and will help validate microkinetic models.

Next, we will study the oxidation of H_2 over polycrystalline Rh. It is known that this reaction proceeds with time-varying, even oscillatory reactions kinetics. The unproven mechanism is believed to be a feedback between surface oxidation state, which in turn alters the dissociative adsorption rate of gas phase O_2. As the sub-surface oxide is consumed, the adsorption rate of O_2 increases. Once a high enough surface concentration of O is achieved, sub-surface O begins to form, and the sticking coefficient for O_2 again decreases allowing dissociative adsorption of H_2 to again compete. However, there is little direct proof of this postulate. By combining gas-phase imaging of the reactants and products with surface specific AP-XPS and SFG, we will directly measure whether this is the true feedback mechanism which creates oscillating kinetics for hydrogen oxidation over Rh.

Mechanistic Studies of Oxidative Coupling of Methane

In the coming year, we will study a more complex reaction – the oxidative coupling of methane (OCM) – that involves dynamic exchange of intermediates between the surface and gas phase. Although much is known about the reaction mechanism, fundamental details about the feedback between gas-phase and surface reactions remain elusive. It is generally accepted that the first C-H activation step is surface-mediated and is related to the activity of the catalyst. The overall OCM reaction on a metal-doped oxide surface involves (1) activation of the C-H bond in methane and desorption of $\bullet CH_3$, (2) coupling of $\bullet CH_3$ in the gas phase to form C_2 products, and (3) creation of surface oxygen vacancies by water desorption, which are replenished by O_2 dissociation. Although direct evidence is lacking, a wide variety of catalysts are believed to follow this mechanism. In collaboration with UC Davis, we will directly probe the near-surface reactive species and provide fundamental insights into the reaction mechanism. Specifically, we plan to begin our studies with Li-doped MgO powder, owing to the considerable available literature for Li-doped MgO catalysts. We are currently validating a laser-induced fragmentation fluorescence method for 2-D imaging of CH_3, which does not itself fluoresce. Our goal is fundamental mechanistic understanding, derived from 1) experimental probes of gas-phase species using PLIF and near-surface mass spectrometry, and 2) theoretical investigations of how the modified surface (*i.e.* the active site) controls the nature of the interaction with methane and of the subsequent binding/release of radicals. In order to facilitate comparison of our observations with numerical simulations using detailed chemical models (microkinetic modeling), we are implementing a new experimental design to provide a flow field with well-defined boundary conditions.

BES-SPONSORED PUBLICATIONS (SINCE 2019)

1. B. Zhou, E. Huang, R. Almeida, S. Gurses, A. Ungar, J. Zetterberg, A. Kulkarni, C. X. Kronawitter, D. L. Osborn, N. Hansen, and J. H. Frank, Near-Surface Imaging of the Multicomponent Gas Phase above a Silver Catalyst during Partial Oxidation of Methanol, ACS Catalysis **11**, 155 (2021).
2. B. M. Goldberg, E. D. Hermes, B. D. Patterson, P. E. Schrader, J. Zádor, and C. J. Kliewer, Direct observation of long-lived rovibrational coherence and free rotation in metal-bound molecules, under review.

ULTRAFAST PHYSICS: NONLINEAR OPTICAL SPECTROSCOPY AND DIAGNOSTICS

Christopher J. Kliewer, David W. Chandler, David L. Osborn, Krupa Ramasesha, Jonathan H. Frank
Sandia National Laboratories, MS 9051, Livermore, CA 94551-0969
cjkliew@sandia.gov, chand@sandia.gov, kramase@sandia.gov, jhfrank@sandia.gov

PROGRAM SCOPE

The interaction of intense pulsed laser fields with atoms, molecules, and surfaces induces a coherent response in the material. At especially high intensities, the material response becomes nonlinear and gives rise to a wealth of approaches to both *control* and to *probe* molecular processes in gas-phase and interfacial chemical physics, even processes very far from chemical equilibrium. In this program, our goal is to develop ultrafast optical methods to both measure and control matter at the molecular level and on molecular timescales. On the measurement side, ultrafast nonlinear approaches are advanced for the detection of transient reactive molecular species. In addition, broadband approaches enable the sampling of many spectroscopic transitions at once, allowing for the assessment of instantaneous molecular energy partitioning and energy transfer. A critical aspect of our research includes the study of fundamental spectroscopy, energy transfer, molecular dynamics, and photochemical processes. This aspect of the research is essential to the development of accurate models and quantitative application of techniques to complex environments. We are uniquely positioned to study molecular systems driven far from equilibrium, as well as relaxation rates and pathways. Time-resolved collisional dephasing measurements provide insight into the local chemical environment as well as inform spectroscopic models for quantitative interpretation.

RECENT PROGRESS

Development of a time-domain impulsive response model for CH_4

Recent work in the Ultrafast Diagnostics laboratory has led to new capabilities in the broadband impulsive excitation of all Raman-active transitions in a molecular ensemble. This was achieved through the development of a ~7 fs impulsive excitation source, coupled to a ps or ns probe pulse. We have demonstrated this approach for the simultaneous detection of CH_4, O_2, CO, CO_2, H_2, and N_2, imaging the gas-phase distribution to within 30 µm of a surface [1]. While this has proven very powerful for speciation, the full spectroscopy of each molecule contains far more information. At some pressures, the full vibrational, rotational, and translational (through the Doppler profile) energy distributions may be measured. However, to glean this information from the spectrum, a highly accurate, time and frequency resolved, spectroscopic model must be created and validated. For some simple molecules, such as N_2 and O_2 such detailed models have long been published and validated allowing for detailed state populations to be derived from the spectrum. As we move to larger important molecules, such as CH_4, such a time-domain model has not been developed, nor validated. The impact of the capability to probe the detailed spectroscopy of CH_4 with ultrafast methods extends to many

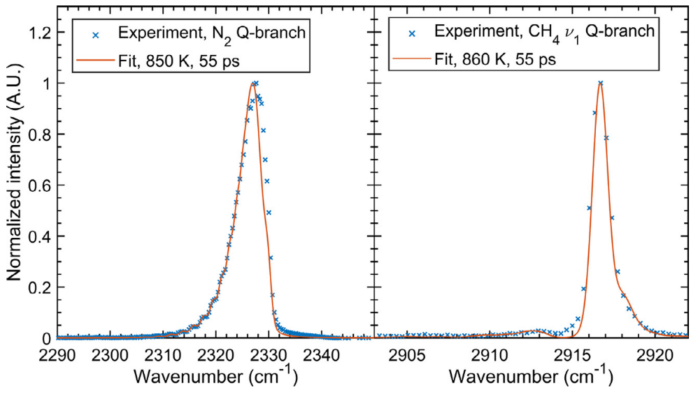

Figure 1: Simultaneously acquired signal from the N_2 (left) and CH_4 (right) vibrational Q-branch in the heated cell at 500 Torr using 7 fs excitation and 65 ps probe in an ultrabroadband CARS scheme. The well-validated N_2 spectrum serves as internal reference for the new CH_4 model.

fields of chemical physics. In gas-surface catalysis, the activation of the C-H bond in CH_4 is the most difficult step in a great many chemical valorization processes, such as during catalytic methane reforming or the partial oxidation of methane. It is currently postulated that gas-phase low temperature plasmas may be used to vibrationally excite CH_4 enhancing catalytic reaction rates at surfaces. This hypothesis remains to be validated. CH_4 is further a combustion-relevant molecule, and the capability to observe gas-surface energy exchange between rotational and vibrational degrees of freedom will provide a new understanding of flame-wall interactions.

During this past year our group has developed a time-domain spectroscopic model for CH_4 ultrafast coherent Raman scattering. Experiments in a well-controlled temperature and pressure cell were carried out from 300 k to 1000 K and from 70 Torr to atmospheric pressure. At each set of conditions, CH_4 was impulsively excited with a ~7 fs pulse from our hollow-core fiber pulse compressor, and probed with a 65 ps pulse for intermediate spectral resolution. We tested different collisional energy transfer models (such as a simple modified exponential gap model) to assess the agreement under different collisional regimes.

Tracking Molecules Far from Equilibrium

Molecular systems far from equilibrium are a grand challenge in chemical physics research, and pose a unique test for our understanding of reaction kinetics and dynamic quantum simulations. Rotation-vibration non-equilibrium and energy transfer is a key area of study for low temperature plasmas that enhances chemical reactivity in applications such as carbon nanotube synthesis[2], plasma catalysis[3], CO_2 dissociation[4], and methane reforming[5]. Therefore, it is of great interest to be able to conduct spatially resolved measurements of rotation-vibration non-equilibrium in these systems. Furthermore, as described in the future work section, we have begun development of a tailored optical centrifuge for extreme rotational excitation of molecules for use in chemical dynamics studies. Once again, the ability to follow the vibrational and rotational distributions (and transition frequencies) is of critical importance to characterizing the molecular ensemble within the optical centrifuge. We recently completed the development of a pure-rotational approach to monitor the simultaneous distribution of vibrational and rotational states in molecular N_2. Figure 2 displays a portion of the pure rotational Raman spectrum of N_2. Because higher vibrational excitation results in a slight modification of the rotational constant, a probe pulse with sufficient resolution is able to resolve higher lying vibrational level distributions from within the pure-rotational transition. We have demonstrated this approach to monitor the rotation-vibration nonequilibrium during a pin-to-pin discharge in a mixture of N_2 and CH_4.

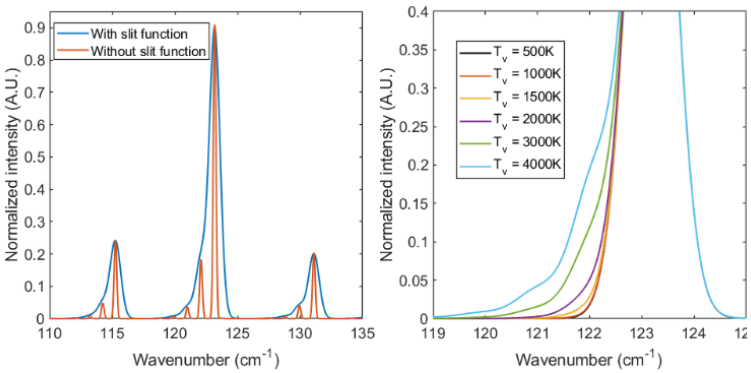

Figure 2: Modelled non-equilibrium rotational CARS spectra at T_{rot} = 500 K and T_{vib} = 4000 K, with and without convolution with the spectrometer slit function (left). Close up view of the J' = 14, 15, and 16 peaks with T_{rot} held at 500 K and T_{vib} varied from 500 K to 4000 K (right).

PROPOSED WORK

Development of the molecular optical centrifuge and novel probing methods

The selective control of population in the various degrees of freedom in molecules has opened the possibility for unprecedented understanding of reactive potential energy surfaces in gas phase chemical physics. While significant work has been dedicated to understanding, and controlling, the vibrational and translational degrees of molecular freedom, far less attention has been paid to the direct molecular control

of rotational energy. In part, this is due to the quantum mechanical selection rules that govern rotational excitation. Only small changes in angular momentum are allowed during an optical absorption or Raman process. In recent years, however, pioneering work has established a method for spinning molecules into very high angular momentum states. Like adiabatic passage methods for vibrational ladder climbing, passage up the rotational ladder has now been demonstrated on several molecules. The first experimental demonstration of the optical centrifuge technique, by Corkum and coworkers [6], was performed on Cl_2. Rotationally induced dissociation was observed through mass spectrometry for Cl_2 molecules driven to $J \sim 420$. Later work demonstrated theoretically the possibility of breaking the stronger chemical bond in HCN through tailoring of the chirp rate in an optical centrifuge [7]. Mullin and co-workers coupled a transient IR absorption spectrometer to an optical centrifuge to follow the rotational relaxation dynamics of CO_2[8], N_2O[9], and CO[10]. These works provided a wealth of new information on the collisional dynamics and energy transfer mechanisms for molecules driven to very high rotational energies.

In the long-term, our goal is to develop pulse shaping approaches within the optical centrifuge that will enable finer control over the final rotational distribution, and open the possibility for selectively climbing rotational ladders within polyatomic molecules. By spinning molecules to high rotational states along a particular rotational axis, the hypothesis of selectively weakening chemical bonds through rotation may be tested.

At present, we have begun the construction of the optical centrifuge in the ultrafast nonlinear optical diagnostics laboratory. Very strong fields are required to adiabatically trap molecules, and we have thus designed a home-built femtosecond amplifier for use in this project with low repetition rate (20 Hz) but very high power. Because the optical centrifuge follows a series of sequential impulsive Raman transitions, the resulting molecular ensemble is highly aligned along the laser polarization axis as $J \approx M_J$. The rotational wavepacket created through the excitation process will evolve coherently, and thus the distribution of rotational states created from the optical centrifuge may be probed using nonlinear scattering of a time-delayed picosecond probe pulse. This approach is analogous to the innovative hybrid femtosecond/picosecond CARS approaches we have developed in the Ultrafast Diagnostics laboratory in recent years. Initial demonstration of rotational ladder climbing in N_2 and N_2O as probed with coherent Raman scattering is planned during this next year. Pulse shaping methodologies for finer control rotational distribution will follow initial demonstration.

Direct visualization of $O_2(a^1\Delta_g)$ using nonlinear optical methods

The direct time-resolved and spatially-resolved detection and visualization of the concentration $O_2(a^1\Delta_g)$ has been a difficult goal for many years. A weak absorption cross-section for excitation to the next lowest-lying electronic state thus requires a cavity ring-down or cavity-enhanced type setup for detection. Such methods have very long effective path lengths and are line-of-sight limited and are thus not applicable to many areas of gas phase chemical physics (such as combustion and plasma assisted chemistry) where $O_2(a^1\Delta_g)$ is known or suspected to play a major kinetic role. We have recently developed a technique to directly visualize $O_2(a^1\Delta_g)$ with excellent spatial resolution based upon time-domain coherent Raman spectroscopy. In the coming months we will demonstrate this technique by measuring $O_2(a^1\Delta_g)$, quantifying the detection limits, and then applying the method in measurements of plasma generated $O_2(a^1\Delta_g)$.

Coherence Lifetime Imaging through Structured Illumination

Coherence dephasing times are often governed by intermolecular interactions. In gas-phase systems, collisional energy transfer is the dominant source of rotational and vibrational coherence dephasing. Thus measuring the coherence decay rate allows for the in-situ mapping of collisional energy transfer rates, which are highly dependent on collision partner, number density, and collision energy. In condensed phase samples, the coherence lifetime gives an indication of the coupling of individual vibrational states to the surrounding environment. In microscopy applications, coherence lifetime would provide a novel imaging contrast mechanism sensitive subtle changes in local chemical environment. In previous work, we

demonstrated the ability to measure coherence lifetimes within a single laser shot in the gas phase by separating the probe pulse into four separate weak probe pulses, each with a different phase matching angle. We propose here to develop a 2D coherence lifetime imaging approach which can have impact in both gas-phase chemistry applications as well as in condensed phase fields. Similarly to fluorescence lifetime imaging, the coherence lifetime image will provide information on the chemical coupling and energy transfer to the local environment.

In order to realize single-shot coherence lifetime imaging, we will combine our recently developed 2D-CARS approach, with the structured illumination approach developed by our colleagues at Lund University. More specifically, the probed molecules will be excited with a pump/Stokes femtosecond laser sheet. The probe beam, however, will be separated via beam-splitters into four separate beams. Each of these beams will propagate through a time-of-flight optical delay stage and then be passed through a transmission grating. These gratings will be designed to optimize the +/- 1 orders. The position of the grating will be relay imaged to the experiment. In this way, each of the four probe beams gets imprinted with a fringe pattern at a controllable angle. The CARS beams will then be recombined into a single beam and scattered from the sample. The resulting image will contain four separate probe delays, with independent spatial frequencies, which can be extracted through spatial Fourier transform. In gas phase chemistry applications such as combustion, or coupled gas-surface chemistry, such an approach would enable simultaneous speciation, measurement of energy distributions, as well as provide an assessment of the degree of coupling to other molecules or the surface.

BES-SPONSORED PUBLICATIONS (SINCE 2019)

1. T.Y. Chen, B.M. Goldberg, B.D. Patterson, E. Kolemen, Y. Ju, and C.J. Kliewer, "1-D imaging of rotation-vibration non-equilibrium from pure rotational ultrafast coherent anti-Stokes Raman scattering" Opt. Lett. **45**, 15, 4252-4255 (2020)
2. T.Y. Chen, C.J. Kliewer, B.M. Goldberg, E Kolemen, and Y Ju, "Time-domain modelling and thermometry of the CH_4 Q-branch using hybrid femtosecond/picosecond coherent anti-Stokes Raman scattering" Combustion and Flame **224**, 183-195 (2021)

REFERENCES

1. A. Bohlin, C. Jainski, B. D. Patterson, A. Dreizler, and C. J. Kliewer, Proc. Combust. Inst. **36**, 4557 (2017).
2. E. Plonjes, P. Palm, G. B. Viswanathan, V. V. Subramaniam, I. V. Adamovich, W. R. Lempert, H. L. Fraser, and J. W. Rich, Chem. Phys. Lett. **352**, 342 (2002).
3. T. Nozaki and K. Okazaki, Catal. Today **211**, 29 (2013).
4. T. Kozak and A. Bogaerts, Plasma Sources Sci. Technol. **23**, 17, 045004 (2014).
5. J. T. Sun and Q. Chen, J. Energy Chem. **39**, 188 (2019).
6. D. M. Villeneuve, S. A. Aseyev, P. Dietrich, M. Spanner, M. Y. Ivanov, and P. B. Corkum, Physical Review Letters **85**, 542 (2000).
7. R. Hasbani, B. Ostojic, P. R. Bunker, and M. Y. Ivanov, J. Chem. Phys. **116**, 10636 (2002).
8. L. W. Yuan, S. W. Teitelbaum, A. Robinson, and A. S. Mullin, Proc. Natl. Acad. Sci. U. S. A. **108**, 6872 (2011).
9. L. W. Yuan, C. Toro, M. Bell, and A. S. Mullin, Faraday Discuss. **150**, 101 (2011).
10. M. J. Murray, H. M. Ogden, C. Toro, Q. N. Liu, and A. S. Mullin, ChemPhysChem **17**, 3692 (2016).

MACHINE LEARNING FOR UNDERSTANDING HEAVY HYDROCARBON CLUSTERING

Habib Najm[1], Judit Zádor[1], Michael Eldred[2], Hope Michelsen[3]
[1]*Sandia National Laboratories, Livermore, CA*
[2]*Sandia National Laboratories, Albuquerque, NM*
[3]*University of Colorado, Boulder, CO*
hnnajm@sandia.gov, jzador@sandia.gov, mseldre@sandia.gov, Hope.Michelsen@colorado.edu

PROGRAM SCOPE

The goal of this program is to use machine learning (ML) to advance the state of the art in our understanding of reaction mechanisms in heavy hydrocarbon clustering, leading to incipient soot formation. We will do this by (1) building neural network (NN) potential energy surface (PES) representations for a class of hydrocarbon molecules, (2) using this construction to explore reaction processes among a set of initial C_mH_n molecules at concentrations typical in hydrocarbon flames, and (3) using stochastic sampling to estimate reaction probabilities and simulate growth leading to production of higher molecular weight hydrocarbons. Ultimately, our goal is to identify reactions that dominate molecular weight growth, and specifically explore the role of resonantly stabilized radicals (RSRs) in this process. Our NN training data comes from quantum chemistry computations at a range of levels of theory, and we use the information thus gained from models of different fidelities in a multilevel-multifidelity (ML/MF) formalism to efficiently attain requisite NNPES test accuracy. We also rely on an active learning strategy to identify conditions for which additional *ab initio* computations provide maximal expected information gain, thereby gaining further computational efficiency. We rely on KinBot [https://github.com/zadorlab/KinBot] for exploration of the PES for generating geometries for training, and for exploring the trained NNPES to estimate reaction rate coefficients and expand the initial pool of molecules.

RECENT PROGRESS

Generation of training data using automated kinetics:

We used KinBot, our open-source tool to discover and characterize stationary points on a reactive PES for a model RSR system. Our goal was to generate a rich initial training set for the ML framework to form the basis of proof-of-concept calculations. To this end, we explored the PES of the acetylene + propargyl reaction at the wB97XD/6-311++G** level of theory. This PES features a large number of wells and saddle points; we show the low-energy ones in Figure 1. KinBot automatically found all reaction pathways present in the literature, and several new ones.

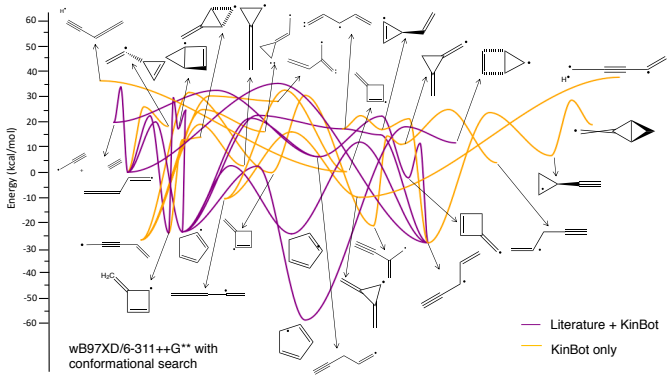

Figure 1: The acetylene + propargyl (C_5H_5) PES explored with KinBot.

We also created a code to generate data for NN training. It extracts all stationary and intrinsic reaction coordinate (IRC) points from a KinBot calculation, cleans the data (e.g., eliminates duplicates), generates SQLite databases that store displaced structures using normal mode sampling, handles the running and

storage of the corresponding energies and forces, and has diagnostic features to test the trained NN. Training data generation requires a large number of single-point calculations; to this end we are using the Balsam workflow manager to enable capability computing on HPC resources, along with our customized software for parallel database access. Working across the project team, we also laid the ground for an active learning workflow that adaptively generates data to maximize expected information gain. We are currently testing the performance of geometry optimizers, such as Sella, [https://github.com/zadorlab/sella], on the NN PES as well as the quality of harmonic frequencies, to eventually enable calculation of rate coefficients.

Machine Learning Capability Development and Demonstration:
We have continued to enhance and optimize our NN training code base. We built a flexible composite NN construction with PyTorch, and ported it to GPUs, demonstrating speedup versus CPU-based computations. Our state-of-the-art code employs the Adam optimizer with learning-rate scheduling to achieve good training performance. On the data-science angle, we developed an SQLite database code framework with associated client-server software to manage parallel database access across computational nodes. We also adopted *dvc* repository software for large-scale database storage and collaborative use. We implemented active learning via *query by committee* (QBC) methods and have used QBC to provide targeted DFT computations to provide maximal improvement in NN test accuracy. We have arrived at a demonstration of O(1kcal) accuracy of a QBC-trained 5-NN ensemble-average prediction, versus DFT test data, on a portion of the reactive PES for the C_5H_5 system, consisting of two wells, the saddle point connecting them, and the regions connecting them based on IRC calculations. For training and test data generation, we used randomized normal mode sampling at 20,000 K, i.e., extending over approximately 40 kcal/mol energies around wells, saddle and IRC points, providing a very broad description of the reactive PES.

Derivative-enhanced Training of the NNPES Construction:
As we migrate towards larger molecules and higher levels of theory, the number of *ab initio* quantum chemistry (QC) simulations that we can afford will become more limited. Particularly in these cases, it becomes important to leverage all available training data from each of these expensive simulations, and we have developed a capability to train our NNPES using both energy (value) and force (gradient) data. Since we have (*x,y,z*) tuples for each atom, inclusion of force values provides a factor of 30x more training data per simulation for our currently targeted 10-atom C_5H_5 molecule, and this factor will grow with the complexity of the target. Development of this capability has entailed derivation of chain rule relationships between the NN, atomic environment vector (AEV), and cartesian coordinates (*x,y,z*) parameterizations, extension of training loss functions and associated solver automatic differentiation support, development of a fast C++/Python analytical AEV Jacobian library, and formulation of weighting schemes for training sets that are heterogenous in data scale and volume. We are in the process of demonstrating the benefits of force-enhanced training for low data cases.

***Multilevel / Multifidelity (ML/MF) Methods*:**
We are extending ML/MF concepts to the case of NN surrogates so that we can achieve accurate NNPES models at much lower total cost by incorporating data from QC computations at different levels of theory. We approximate the target mapping from AEV into high-level theory predictions by decomposing the mapping across multiple modeling levels, where each level of QC theory adds a level to our modeling hierarchy. Starting from a NNPES for the lowest level of theory, we add NN models for each level of theory until we additively emulate the highest-level QC theory. A key component of this approach is the allocation of varying amounts of training data, commensurate with the relative cost of the QC simulations.

We have explored a number of approaches to decomposing the NN topology, notably *discrepancy-based* (each downstream NN models the difference in model predictions as a function of the AEV parameters), *sequential* (each downstream NN takes the upstream level predictions as its inputs to predict the next level of theory), and *hybrid* formulations (each downstream NN takes both the AEV inputs and the upstream level predictions as its inputs to predict the next level of theory, where these upstream/downstream

predictions can be either sequential or discrepancy-based). Moreover, training processes for the composed NN components can either be fully *independent*, in order to reduce training scale, or *all-at-once*, for which upstream network parameters can be optimized for both local and downstream accuracy. To investigate these approaches, we have explored several problems of increasing complexity, including simple algebraic test problems, elliptic PDEs for 2D advection-diffusion, and the NNPES for C_5H_5 using two levels of theory. In this last context, we used B3LYP/6-31G and wB97XD/6-311++G** for low/high theory levels. While the best architecture depends on the specific problem structure at hand, we have observed good performance in QC formulations using a *hybrid discrepancy-based* architecture with *all-at-once* training, such that we have selected this as our baseline formulation going forward.

Validation Data:

Our goal is to identify and test particle-inception mechanisms. We target the chemistry that leads to a transition from gas-phase species to condensed-phase particles. Such a transition can be identified when the properties (e.g., density, specific heat, and absorption and scattering cross sections) of the particle or cluster depart from those of the gas-phase species from which it is composed and begin to exhibit properties of a bulk material. Many of the physical properties of incipient particles are not known, but experimental results have indicated these particles have elemental carbon-to-hydrogen (C/H) ratios of 1.5- 2.5. As these particles further evolve at high temperature, they lose hydrogen, and their C/H ratios increase. To gain a better understanding of how these properties evolve, we have performed an analysis of 47 solid PAHs with C/H ratios in the range of 1.0-2.5. Using these PAHs as a proxy for incipient soot, we have analyzed measurements of density and specific heat, coupled with X-ray crystallography data, to assess the dependence of these properties on C/H ratio. The results provide estimates of the dependence of density and specific heat on C/H ratio and temperature for ranges in C/H of 1.0 to >20 and temperatures of 100 to 3000 K [1].

Multidisciplinary teams are necessary to fill some of the major gaps in the understanding of soot formation and evolution, but such teams can be hindered by an inability to communicate critical concepts at the heart of the complex scientific questions to be answered. With this perspective, we reviewed the terminology employed in the study of the production and evolution of soot and carbonaceous-particle inception and growth under high-temperature conditions [2].

PROPOSED WORK

"Identity loop":

Our immediate goal is to create a demonstration for the entire ML framework. We will modify KinBot to be able to interface with the NN PES and the optimizers we find satisfactory. Using the NN PES based on the C_5H_5 PES we will test if we can re-explore the same chemistry using the NN PES alone. We will assess the differences between the ab initio- and NN-calculation-based rate coefficients, both in terms of accuracy and timing. In the process of exploring the PES, we will also add features to KinBot to facilitate active learning strategies.

KinBot development:

KinBot does not have sufficient heuristics or other methods built into it to handle several rings or very rigid structures, and as a result, KinBot's transition-state templates tend to produce a lot of unrealistic saddle point guesses for these kinds of structures thus increasing the cost of search unnecessarily. Our preliminary calculations also indicate that already the C_7H_7 system presents a formidable challenge when it comes to the automatic enumeration of actual reaction pathways and wells using a simple energy-threshold to terminate search. We will add methods to KinBot to constrain and adjust the chemical space in a more efficient and sophisticated way. We will also enable KinBot to allow the exploration of bimolecular reactions, a development generally planned for the code. We will test and demonstrate the effectiveness of these developments on RSR systems beyond the C_5H_5 system, both uni- and bimolecular ones.

Machine Learning Capability Development and Demonstration:
We will be enhancing our AEV C++/Python pybind11 capability to include analytical AEV Hessian computations to be used in KinBot exploration of the NNPES, and will be releasing this library as an open-source utility. We will also extend our current PyTorch code to allow NN training across multiple GPUs. This will allow dealing with training on very large databases. We will also work on data subsampling to control computational costs, where we will explore the use of QBC in a subsampling strategy.

We will also extend our current work on demonstrations of NN PES accuracy to the full set of relevant species/basins in the energy landscape for C_5H_5. This will rely on the application of QBC for active learning across the full set of basins at hand, following our current proof-of-principle demonstrations with a pair of basins. It will require multiple active learning iterations, relying on training an ensemble of NN learners, and identifying structures among a large pool of candidates for which the scatter of predictive energies from the learners is large, tagging these structures as good candidates for quantum chemistry computations to provide energy/force values. This active learning loop has been most effective in improving the accuracy of our current two-basin NN, and will prove indispensable in the all-basin case. As always, independent test data based on structures that have not been used for training will be used for validation of the resulting mean-prediction from the trained learners.

Derivative-enhanced Training of the NNPES Construction:
This work is nearing completion, and we expect to energy + force training to become our standard NNPES foundation going forward (see also ML/MF proposed work below).

***Multilevel-Multifidelity (ML/MF) Methods*:**
There are several directions of algorithm enhancement for ML/MF NNPES, listed in anticipated order of exploration: (1) Integrate derivative-enhanced training across model hierarchy NN components; (2) Extend active learning approaches to the ML/MF context, competing refinements across multiple levels of theory; (3) Formalization of NNPES discrepancy-based and inter-component linkages using residual neural network (ResNet) and recurrent NN formalisms, respectively; (4) Adaptation to more general graph relationships, in particular supporting non-hierarchical model sequences that involve different model forms. In addition, we envision QC-targeted enhancements where we introduce additional levels of theory (beyond 2), likely in the direction of higher fidelity for larger molecular systems. We will work with the quantum chemistry component of the project to test these approaches also beyond the B3LYP-wB97XD or similar pair of levels, going towards coupled-cluster level accuracy.

Validation Data:
We will continue to examine the role, and evaluate the importance, of resonance-stabilized radicals (RSRs) in high-temperature hydrocarbon growth processes. To accomplish this goal, we are analyzing previously recorded measurements of particles extracted from flames and pyrolysis tubes using vacuum- ultraviolet photoionization mass spectrometry (VUV-AMS). These data provide observations of RSRs and other species produced over a wide range of high-temperature conditions that lead to soot inception.

BES-SPONSORED PUBLICATIONS (SINCE 2019)

1. H. A. Michelsen, Effects of Maturity and Temperature on Soot Density and Specific Heat, *Proc. Combust. Inst*., **38** (2020) DOI: 10.1016/j.proci.2020.06.383.
2. H. A. Michelsen, M. B. Colket, P.-E. Bengtsson, A. D'Anna, P. Desgroux, B. S. Haynes, J. H. Miller, G. J. Nathan, H. Pitsch, H. Wang, A Review of Terminology Used to Describe Soot Formation and Evolution Under Combustion and Pyrolytic Conditions, *ACS Nano*, **14** 12470-12490 (2020). DOI: 10.1021/acsnano.0c06226.

ULTRAFAST CHEMISTRY: PROBES OF NON-ADIABATIC DYNAMICS

Krupa Ramasesha, Laura M. McCaslin, Christopher J. Kliewer, Nils Hansen
Combustion Research Facility, Mail Stop 9055; Sandia National Laboratories, Livermore, CA 94550
kramase@sandia.gov, lmmcas@sandia.gov, cjkliew@sandia.gov, nhansen@sandia.gov

PROGRAM SCOPE

This program aims to apply ultrafast spectroscopy and theoretical calculations to investigate fundamental gas-phase chemical dynamics. Our research uses diverse probing techniques to follow coupled electronic and nuclear motion on femtosecond to picosecond timescales in gas-phase molecules, as well as advanced quantum chemical calculations to independently investigate these dynamics and predict experimental observables. The work in this task has strong connections to the laser spectroscopy investigated under the "Ultrafast Physics: Nonlinear Optical Spectroscopy and Diagnostics" task, and the high photon-energy techniques developed in the "Advanced Diagnostics" task. The coupling of electronic and nuclear degrees of freedom, representing a breakdown of the Born-Oppenheimer approximation, gives rise to complex pathways of non-radiative energy dissipation in electronically excited molecules, often involving participation of several electronic states. Identifying the motions that couple electronic states, the timescales and dynamics of excited state population relaxation, and the role of coupled vibrational modes of a molecule in guiding energy flow is crucial to our understanding of non-equilibrium dynamics, and it forms the mainstay of this program. This task extends the "Chemical Dynamics Methods and Applications" work down to the fundamental timescales of vibrational or electronic motion. *Ultrafast Chemistry* is one of the synergistic research themes of CSGB and this work addresses two key aspects of the Grand Challenges for Basic Energy Sciences: (1) investigating the nature of electronic excited states, and (2) exploring the breakdown of the Born-Oppenheimer approximation.

RECENT PROGRESS

Photodissociation dynamics of iron pentacarbonyl: It is well known that UV excitation of gas phase iron pentacarbonyl (IP, $Fe(CO)_5$), a prototypical organometallic system, causes rapid elimination of CO. In order to understand the mechanism of CO elimination, we performed ultrafast transient infrared absorption spectroscopy of gas phase IP following UV excitation at 265 nm and 199 nm in conjunction with advanced quantum chemical calculations at the coupled-cluster and equation-of-motion coupled cluster (EOM-CC) levels of theory. We probed the time-evolution of the C≡O stretching frequency, which reports on the coordination state of IP. Transient infrared absorption spectra at different 265 nm pump – IR probe time delays are displayed in Figure 1. Bleach at 2019 cm^{-1} and 2038 cm^{-1} appear immediately upon excitation, consistent with loss of ground state IP. An induced absorption on the low-frequency side of the bleach exhibits a frequency shift to lower frequencies with increasing pump-probe time delay. The broad line shape centered at ~1940 cm^{-1} at early times evolves to a narrow line shape centered at 1923 cm^{-1} on a 3.4 ps timescale. Calculations of harmonic frequencies, bond dissociation energies and cuts through the potential energy surfaces suggest that the species at ~1940 cm^{-1} is iron tetracarbonyl on its first singlet excited state, which then evolves to the singlet-excited iron tricarbonyl on a 3.4 ps timescale. Results from 199 nm excitation

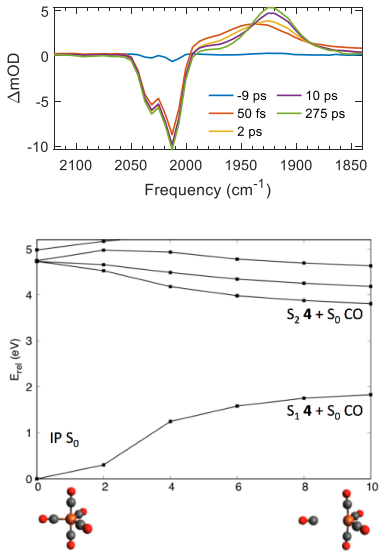

Figure 1: Transient infrared absorption spectra of IP following 265 nm excitation (top) and cuts through the potential energy surface along IP to $Fe(CO)_4$ at the EOM-CCSD(dT) level (bottom).

suggests ultrafast formation of singlet-excited $Fe(CO)_3$ which is then followed by intersystem crossing to the triplet manifold on a 15 ps timescale. This joint experimental-theoretical work has been published in the Journal of Chemical Physics.

Ultrafast photodissociation of dimethyl disulfide: Dimethyl disulfide (DMDS, CH_3SSCH_3) is a model system for the disulfide (S–S) bond, an important moiety in protein structure. Despite its central role in maintaining the structural integrity of proteins, the disulfide bond is photolabile with several electronic excited states proposed to be dissociative along the S–S and C–S bonds. Photodissociation studies on the first excited state, $S_1(n\sigma^*_{S\text{-}S})$, of DMDS have found exclusive S–S bond fission. However, relatively little work has been done on the photochemistry of the higher lying electronic excited states near the DMDS absorption maximum at 195 nm, where early nanosecond experiments suggested cleavage of C-S and S-S bonds.[1] We performed ultrafast electron diffraction (UED) at SLAC MeV-UED facility to probe the competing pathways of ultrafast photodissociation of DMDS following 200 nm and 266 nm excitation. Results show prompt appearance of differential scattering signal for both excitation wavelengths, with picosecond timescale oscillations following 200 nm excitation (Figure 2). The S-S and C-S dissociation pathways have been characterized via one-dimensional cuts through the ground and excited state potential energy surfaces with high-level EOM-CC methods. Future studies will use electronic state-sensitive ultrafast soft X-ray transient absorption spectroscopy at the S L-edge and C K-edge following 200 nm excitation, in order to monitor excited state dynamics.

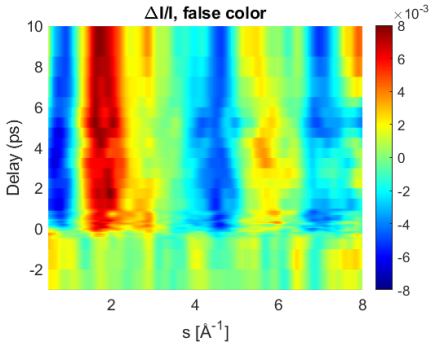

Figure 2: Differential scattering intensity of dimethyl disulfide as a function of pump-probe time delay and momentum transfer, following 200 nm excitation.

Photodissociation dynamics of nickel tetracarbonyl: Owing to a full *d* orbital, the electronic structure and excited state dynamics of nickel tetracarbonyl (NT, $Ni(CO)_4$) is expected to be quite different from that of iron pentacarbonyl described above. Excited states of NT accessible by a UV photon are predominantly of metal-to-ligand charge transfer (MLCT) character that do not effectively couple to the Ni-CO dissociation coordinate, leading to slower dynamics than seen in IP. We performed ultrafast UV pump—IR probe spectroscopy of NT, probing the evolution of the C≡O stretching frequency following 261 nm and 197 nm excitation. The transient spectra obtained from 261 nm excitation (Figure 3) suggest dynamics occurring on a few hundred femtosecond to tens of picosecond timescale. The features in the transient spectra may indicate the presence of species in different electronic and/or vibrational excited states. Results from 197 nm excitation exhibit broad featureless transient spectra at early time delays that evolve to structured spectra at longer, picosecond, time delays. Quantum chemical calculations, as performed in the studies of iron pentacarbonyl, are underway to aid in understanding the energetics of photodissociation in this system as well as frequencies and orbital character of NT and photoproducts in order to help interpret the experimental data.

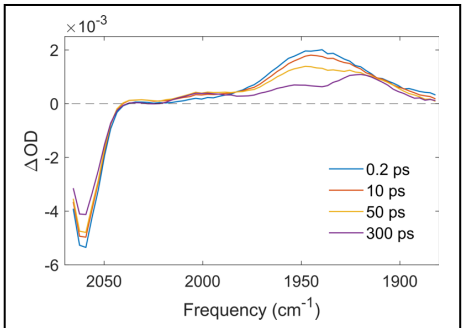

Figure 3: Transient infrared spectra of gas phase NT following 261 nm excitation.

PROPOSED WORK

Probing cyclic azide formation: The azide radical (N_3) is the smallest polynitrogen compound and its $^2\Pi_g$ ground state has been quite extensively studied experimentally and theoretically. Other stationary points

also exist on the ground doublet surface of N_3, the most remarkable being a *cyclic*-N_3 ($^2B_1$) minimum, 30.3 kcal mol^{-1} above the $X\ ^2\Pi_g$ state.[2] *cyclic*-N_3 is an interesting molecule: It is a stable isomer needing 33.1 kcal mol^{-1} of energy to dissociate into $N(^2D) + N_2$ ($X\ ^1\Sigma_g^+$) and 31.9 kcal mol^{-1} to overcome the barrier for isomerization to *linear*-N_3. There is accumulating experimental evidence concerning the formation of the *cyclic*-N_3 by photolysis of a suitable precursor.[3] Wodtke and coworkers observed the formation of N_3 products from ClN_3 photodissociation using velocity map ion imaging and photofragment translational spectroscopy. Synchrotron-based experiments revealed an ionization energy of the high-energy form of N_3 0.4-0.5 eV below the ionization of 11.06(±0.01) eV of the *linear*-N_3,[4] in agreement with *ab initio* calculations of 10.595 eV for the *cyclic*-N_3.[5] We are interested in applying ultrafast electron diffraction at SLAC MeV-UED for probing the structural evolution to *cyclic*-N_3 following UV photolysis of ClN_3, from the initial photodissociation to the isomerization of the N_3 radical to the cyclic conformation.

Three-body photodissociation of thionyl chloride: Since its observation in acetone, photo-induced three-body dissociation has been discovered in several small gas phase molecules. One example is thionyl chloride (TC, $SOCl_2$), which serves as an ideal testbed for investigating non-adiabatic processes in three-body dissociation using ultrafast electron diffraction and soft X-ray transient absorption. TC's ultraviolet absorption spectrum shows two discernable features: a strong absorption that peaks at wavelengths less than 200 nm, and a shoulder centered at 250 nm. These features are assigned to partially overlapping electronic transitions, $n_s \rightarrow \sigma^*_{SCl}$ and $n_s \rightarrow \pi^*_{SO}$ at longer wavelengths and similar transitions originating from the lone pair on the Cl atoms at shorter wavelengths. Three dissociation schemes (two-body molecular, two-body radical and three-body radical channels) have been identified for this molecule.[6-8] However, several open questions remain about this system. Particularly, is the three-body dissociation channel asynchronously concerted or sequential? How do the fragmentation mechanisms and timescales vary with excitation energy? What are the non-adiabatic pathways of the excited TC in each of these three excitation regimes? To address these questions, we are interested in performing ultrafast electron diffraction at the SLAC MeV-UED facility to follow the ultrafast dissociation process of this molecule. We will also apply high-harmonic generation based soft X-ray transient absorption spectroscopy tuned to the sulfur L-edge at ~165 eV, following valence electronic excitation at different excitation wavelengths. The sulfur 2p-to-valence transitions are expected to be particularly sensitive to the orbital occupancies and electronic energies of molecular orbitals associated with the sulfur atom (e.g. n_s, σ^*_{SCl}, π^*_{SO}), and in turn, will report effectively on the local bonding environment and electronic structure in the vicinity of the sulfur atom.

Treatment of Non-Adiabatic Effects in Ab Initio Molecular Dynamics: The difficulty of accurately treating molecular dynamics involving multiple electronic states is a well-known problem in chemical theory. When two or more electronic states are close in energy at a given molecular configuration, the Born-Oppenheimer (BO), or adiabatic, approximation breaks down, presenting many challenges for theories that rely on it. In the field of ab initio molecular dynamics (AIMD), a system's energy and nuclear forces are calculated on a single BO surface from ab initio electronic structure methods and the nuclear coordinates are propagated forward in time using Newton's equations of motion. In regions of the potential energy surface where multiple potential energy surfaces become close in energy, theories that can treat many surfaces must be used. An approach called "exact factorization" exactly separates the electronic and nuclear degrees of freedom of the wavefunction[9] without use of the BO approximation. This new formulation of the time-dependent Schrodinger equation can be approximated for semi-classical treatment of the nuclei, leading to a scalable non-adiabatic molecular dynamics approach. Proposed here is the development of a software package that uses the high-accuracy methods of equation-of-motion coupled cluster (EOM-CC) for on-the-fly AIMD,[10] which is not available in current non-adiabatic dynamics program packages. Initial studies will employ multiple spawning techniques for treatment of non-adiabatic effects due to the large computational expense of calculating derivative coupling elements. Exact factorization methods in the form of MQC-MD will be integrated into this software and employed for calculating chemical reaction mechanisms as well as quantitative reaction yields and timescales, as described in previous sections. In

order to extend the system sizes and timescales studied, neural networks will be employed to fit the energies, gradients, and couplings of the relevant potential energy surfaces. Near-future studies will focus on unsolved issues of degeneracies and high densities of electronic states in non-adiabatic dynamics calculations.

Photoinduced ring-opening in oxazole: Organic heterocycles serve as building blocks in a variety of biological systems. Ultraviolet excitation to a $\pi\pi^*$ state in these systems is typically followed either by a deformation of the ring structure (ring puckering) as the molecule relaxes back to the ground electronic state, or ring-opening via bond cleavage following non-adiabatic passage to an $n\sigma^*$ state. Ultrafast photoelectron spectroscopy and accompanying theory[11] on this system suggested <100 fs ring opening and several picosecond timescale ring puckering; however, this experiment could not detect photoproducts, and unambiguous assignment of experimental spectra to specific non-adiabatic processes was not achieved. In collaboration with Anja Roeder, Ming-Fu Lin, Sonia Coriani, Thomas Wolf, Klaus Moller, Graham Worth and Daniel Rolles, we propose to study the excited state dynamics of oxazole using near-edge X-ray absorption spectroscopy that allows site-specific probing at the N and O K-edges following 200 nm photoexcitation at SLAC/LCLS. Prior to investigating excited state dynamics, we will first characterize the ground electronic state of oxazole at the C, N, and O K-edges in X-ray absorption spectroscopy, X-ray photoelectron spectroscopy and Auger-Meitner spectroscopy at the Elletra synchrotron.

BES-SPONSORED PUBLICATIONS (SINCE 2019)

1. Cole-Filipiak, N. C.; Tross, J.; Schrader, P. E.; McCaslin, L. M.; Ramasesha, K., Ultraviolet Photodissociation of Gas-Phase Iron Pentacarbonyl Probed with Ultrafast Infrared Spectroscopy, *The Journal of Chemical Physics*, **2021**, *154* (13), *in press*.

REFERENCES

1. Nourbakhsh, S.; Liao, C. L.; Ng, C., A 193 nm laser photofragmentation time-of-flight mass spectrometric study of CH3SSCH3, SSCH3, and SCH3. *The Journal of chemical physics* **1990,** *92* (11), 6587-6593.
2. Kerkines, I. S. K.; Wang, Z.; Zhang, P.; Morokuma, K., Structures and energies of low-lying doublet excited states of N-3 from accurate configuration interaction calculations. *Molecular Physics* **2009,** *107* (8-12), 1017-1025.
3. Hansen, N.; Wodtke, A. M.; Goncher, S. J.; Robinson, J. C.; Sveum, N. E.; Neumark, D. M., Photofragment translation spectroscopy of ClN3 at 248 nm: Determination of the primary and secondary dissociation pathways. *Journal of Chemical Physics* **2005,** *123* (10).
4. Samartzis, P. C.; Lin, J. J. M.; Ching, T. T.; Chaudhuri, C.; Lee, Y. T.; Lee, S. H.; Wodtke, A. M., Two photoionization thresholds of N-3 produced by ClN3 photodissociation at 248 nm: Further evidence for cyclic N-3. *Journal of Chemical Physics* **2005,** *123* (5).
5. Mozhayskiy, V. A.; Babikov, D.; Krylov, A. I., Conical and glancing Jahn-Teller intersections in the cyclic trinitrogen cation. *Journal of Chemical Physics* **2006,** *124* (22).
6. Baum, G.; Effenhauser, C.; Felder, P.; Huber, J. R., Photofragmentation of thionyl chloride: competition between radical, molecular, and three-body dissociations. *The Journal of Physical Chemistry* **1992,** *96* (2), 756-764.
7. Chichinin, A.; Einfeld, T. S.; Gericke, K.-H.; Grunenberg, J.; Maul, C.; Schäfer, L. V., Photodissociation dynamics of SOCl 2. *Physical Chemistry Chemical Physics* **2005,** *7* (2), 301-309.
8. Abulimiti, B.; Hao, Q.-l.; Qin, C.; Xiang, M.; Zhang, B., Three-Body photodissociation of thionyl chloride. *Chinese Journal of Chemical Physics* **2018,** *31* (3), 257-262.
9. Abedi, A.; Maitra, N. T.; Gross, E. K., Exact factorization of the time-dependent electron-nuclear wave function. *Physical review letters* **2010,** *105* (12), 123002.
10. Malrieu, J. P.; Caballol, R.; Calzado, C. J.; de Graaf, C.; Guihery, N., Magnetic interactions in molecules and highly correlated materials: physical content, analytical derivation, and rigorous extraction of magnetic Hamiltonians. *Chemical reviews* **2014,** *114* (1), 429-492.
11. Geng, T.; Ehrmaier, J.; Schalk, O.; Richings, G. W.; Hansson, T.; Worth, G.; Thomas, R. D., Time-Resolved Photoelectron Spectroscopy Studies of Isoxazole and Oxazole. *The Journal of Physical Chemistry A* **2020,** *124* (20), 3984-3992.

Quantum Chemistry of Radicals and Reactive Intermediates

John F. Stanton
Quantum Theory Project
Departments of Chemistry and Physics
University of Florida
Gainesville, FL 32611
johnstanton@ufl.edu

Scope of Research

My research group works in the area of theoretical chemical physics, especially on the properties and chemistry of organic radicals and other reactive intermediates. This research follows a number of paths, including first-principles calculation of bond energies and other thermochemical information (as well as development of methodology needed for such calculations), methods for the simulation and analysis of molecular spectra (especially those relevant to experiments that can be used to glean thermochemical information), the development of *ab initio* quantum chemical methods needed for the accurate treatment of fundamental aspects of electronic structure and potential energy surfaces, and computational kinetics including semiclassical transition state theory and master equation modeling of chemical reactions.

Summary of Selected Recent Accomplishments

• In recent research done in collaboration with the Krylov group at USC, we have reported a coupled-cluster method specifically targeted towards so-called "biradical systems" (those for which the most appropriate zeroth-order state involves all configurations obtained by assigning a pair of electrons to two or more spatial orbitals) in which one begins with an $n-2$ electron state when studying an n electron molecule. In many biradical situations, and quite specifically those in which the electronic structure is well-described by two electrons outside a closed-shell core, this double electron-attachment variant of equation-of-motion coupled-cluster theory (EOMDEA-CC) offers a useful tool for quantum chemical computations. The method has been formulated and extensively benchmarked in a publication listed at the end of this document; most exciting to me is an ongoing study in which the method and the related double electron-removal approach (EOMDIP-CC) are used to study the evolution in electronic structure as ozone is transformed from its normal isoceles geometry to an equilateral triangle. This latter system involves an interesting combination of a Jahn-Teller effect (the low-lying $1E''$ state at the D_{3h} geometry, one component of which correlates diabatically to "normal" ozoen) and a profound pseudo-Jahn-Teller mixing that develops between the ground and first excited states, particularly in the region close to the ring minimum. Some recent work on the curious isotopic anomalies in exchange reactions of isotopic-substituted ozone [1] has suggested that such vibronic (Jahn-Teller and pseudo-Jahn-Teller) interactions play a potentially important role in these processes[2]. Two-electron EOM-CC models like EOMDIP-CC and the newly developed EOMDEA-CC method are ideally suited to studying the electronic structure along this

[1] See, for example, A. Teplukhin and D. Babykov *Faraday Discussions* 212, 259 (2018).
[2] S. Vasilchenko *et al. Phys. Rev. A* 102, 052804 (2020).

pathway and the subsequent process of developing appropriate vibronic Hamiltonians. Such work is currently just underway and will be summarized in our next report.

• We have continued our work on "slow" atmospheric reactions in collaboration with A.R. Ravishankara (Colorado State). This work is motivated by the fact that many atmospheric reactions occur on a timescale vastly longer than any accessible to experiment, and is epitomized by those involving atmospheric destruction processes for the N_2O molecule, which is thought to be the most important ozone-destroying molecule for the 21^{st} century[3]. Using multidimensional master-equation models that have been developed in my research group by its kinetics expert – the truly outstanding T.L. Nguyen – in combination with high-quality quantum chemistry and a multidimensional treatment of tunneling via semi-classical transition state theory (SCTST), pressure-dependent rate constants allowing for a fairly accurate prediction of atmospheric lifetime are obtained. In the last year, we have looked at the possibility that N_2O may react with carbenes and other biradicals, and have already published a study on the prototype carbene $^1CH_2$. While this reaction is vastly more efficient at destroying N_2O than OH + N_2O, it seems that N_2O is remarkably stable with respect to such loss channels (*i.e.* reaction with Criegee intermediates is unlikely to be a viable loss mechanism.

• We have carried out two studies that reveal interesting facets of quantum tunneling in chemical reactions. First, we have shown that the well-known (and perhaps unexpected) pressure dependence observed in the reaction between OH and nitric acid (to form water and NO_3) is ultimately due to quantum tunneling. That is, comparison of the fall-off curves computed with the aforementioned 2D master equation/SCTST methodology with and without tunneling showed that the tunneling factor κ depends on both temperature (as is well-known) *and* pressure. At the atmospherically relevant temperature of 250 K, the rate at ambient pressure is about three times that calculated in the absence of tunneling effects at the same temperature. In a second and related project, we have looked at tunneling effects in the well-studied decomposition of methoxy radical (CH_3O). This is an interesting study because the role of tunneling in this process at temperatures near 600 K has been controversial; some experiments have claimed that they are important, while others claim that these effects are negligible. As these conflicting opinions center about experiments done at different pressures, we investigated if a pressure effect of tunneling provides a way out of this controversy. We find again on the basis of 2D master equation studies that the answer to this is affirmative. The latter work has been submitted for publication; the former has already appeared.

• We have engaged in several projects associated with what might be termed theoretical spectroscopy. An extensive review paper on Jahn-Teller effects in molecular spectroscopy (particularly in the high-resolution regime) has been prepared; we have worked with N.J. Reilly (UMass-Boston) on the spectroscopy of a new resonance-stabilized C_7H_7 radical of relevance to both combustion and astronomy; we have studied the aqueous photochemistry of permanganate (MnO_4^-) using EOM-CC methods; we have applied vibrational perturbation theory (VPT) to compute parameters necessary to analyze the rotational spectra of benzene discharges with the particular goal to identify individual molecules in both ground and low-lying excited states. All of these works have been published, with references to be found below. Other work not yet published involves a collaboration on transition state spectroscopy with the Continetti group at UCSD, the photoelectron spectrum of the HCO_3^- radical (as well as the thermochemistry of the system comprising carbonic acid, and its neutral and charged radical decomposition products) with Ruscic at ANL, and very-high level theoretical thermochemistry calculations on selected small systems.

[3] A.R. Ravishankara *Science* 326, 123 (2009).

• Additional information about our DOE-supported research can be found in the publications listed at the end of this document.

Students and Postdoctoral Supported:
T.L. Nguyen (postdoc)
J.T. Thorpe (student)
M.B. Bentley (student)

References from 3/2019-3/2020 acknowledging BES-GPCP grant

L.T. Nguyen and J.F. Stanton Pragmatic Solution for a Fully-Resolved E,J Master Equation J. Phys. Chem. A 124, 2907 (2020).

T.L. Nguyen and J.F. Stanton Pressure-Dependent Rate Constants Caused by Tunneling: OH + Nitric Acid as an Example J. Phys. Chem. Lett. 11, 3712 (2020).

O.S. Haggag, P. Malarkar, P. Pokhilko, J.F. Stanton, A.I. Krylov, S. Ruhman, The Elusive Dynamics of Aqueous Permanganate Photochemistry Phys. Chem. Chem. Phys. 22, 10043 (2020).

D.A. Matthews, L. Cheng, M.E. Harding, F. Lipparini, S. Stopkowicz, T.-C. Jagau, P.G. Szal ay, J. Gauss and J.F. Stanton Coupled Cluster Techniques for Computational Chemistry: The CFOUR Program System 152, 214108 (2020).

N.J. Reilly, D.L. Kokkin, M.L. Ward, J. Flores, S.D. Ross, L.M. McCaslin and J.F. Stanton Gas-phase Optical Detection of 3-ethynylcyclopentenyl: A Resonance-Stabilized C_7H_7 Radical with an Embedded 1-vinylpropargyl Chromophore J. Am. Chem. Soc. 142, 10400 (2020).

T.L. Nguyen, A.R. Ravishankara and J.F. Stanton Reaction of N2O with the Prototype Singlet Biradical CH2 Chem. Phys. Lett. 749, 137446 (2020).

M.C. McCarthy, K.L.K. Lee, P.B. Carroll, J.P. Porterfield, P.B. Changala, J.H. Thorpe and J.F. Stanton Exhaustive Product Analysis of Three Benzene Discharges by Microwave Spectroscopy, J. Phys. Chem. A 124, 5170 (2020).

J.R. Barker, J.F. Stanton and T.L. Nguyen Semiclassical transition state theory/master equation kinetics of HO plus CO: Performance evaluation, Int. J. Chem. Kin. 52, 1022 (2020).

P.R. Franke, J.F. Stanton and G.E. Douberly How to VPT2: Accurate and Intuitive Simulations of CH Stretching Infrared Spectra Using VPT2+K with Large Effective Hamiltonians, J. Phys. Chem. A, 125, 1301 (2021).

S. Gulania, E.F. Kjonstad, J.F. Stanton, H. Koch and A.I. Krylov Equation-of-motion coupled-cluster method with double electron-attaching operators: Theory, implementation, and benchmarks, J. Chem. Phys. 154, 114115 (2021).

K. Sharma, T.A. Miller and J.F. Stanton Vibronically Coupled States: Computational Considerations and Characterization of Vibronic and Rovibronic Spectroscopic Parameters, Int. Rev. Phys. Chem. 40, 165 (2021).

Universal and State-Resolved Imaging Studies of Chemical Dynamics

Arthur G. Suits
Department of Chemistry, University of Missouri, Columbia MO 65211
suitsa@missouri.edu

I. Program Scope

The focus of this program is on combining universal ion imaging probes providing global insight with high-resolution state-resolved probes providing quantum mechanical detail, to develop a molecular-level understanding of chemical phenomena. Particular emphasis is placed upon elementary reactions involving transient species and in revealing new aspects of reaction mechanisms and the dynamical behavior of molecules. Much of the current effort here is in generalizing the lessons from simple systems as we investigate the behavior of larger polyatomic molecules and radical-molecule reactions. This research is conducted using state-of-the-art molecular beam machines, photodissociation, reactive scattering, and vacuum ultraviolet lasers in conjunction with velocity map ion imaging and other techniques we develop. One focus of our effort remains crossed-beam reactive scattering of polyatomic molecules. In addition, new directions in ultrafast time-resolved studies of photochemical processes are also underway.

II. Recent Progress

Crossed Beam Scattering of OH Radical Reactions

We continue our productive studies of bimolecular reaction dynamics using crossed-beam velocity map imaging with a universal 157nm probe. Following systematic studies of Cl and O(^{3}P) reactions we have recently begun to focus on OH radical reactions. Last year we reported results for reactive scattering studies of OH radical focusing on primary vs. secondary abstraction in reaction with n-butane. This work, in collaboration with Diego Troya, has since been published in *J. Chem. Phys.* Our current efforts are now focused on reaction of OH with alcohols beginning with 1- and 2-propanol. Kinetics studies suggest the OH α-H abstraction is predominant for both 1-propanol and 2-propanol as a result of their lower barriers. Theory indicates a barrier close to zero for the α-H reaction channel for 1-propanol and a submerged barrier for the 2-propanol. Every other channel produces a positive barrier, and it is the highest for the abstraction of H from the O atoms. However, a recent CRESU study on low-temperature kinetics OH radicals and 2-propanol reaction revealed a negative Arrhenius behavior and found the rate constant at 88 K is 10-fold higher than that of 298 K.

We have studied reaction of both propanol isomers with OH in crossed beams, to our knowledge the first experimental dynamics investigation of these reactions. The angular distributions obtained for both reactions at collision energies from 5-8 kcal/mol show predominantly backward scattering implying direct rebound dynamics. We observed mild translational energy release $\langle E_T \rangle \approx 2.5\text{-}3.5$ kcal mol^{-1} for both isomer reactions under all collision energies. Hydrogen atom transfer reactions exhibit acute skew angles suggesting a limiting kinematic tendency to conserve the translational energy from reactants to products. We have previously seen substantial deviations from this limiting picture, notably in the OH-butane system, suggesting kinematics alone do not account well for the dynamics. Assuming as is likely these results represent abstraction at the α-H site, this is only ~10% or the available energy. We have also seen discrepancies from kinematic predictions in our imaging dynamics study of OH + butane under similar conditions. QCT calculations in that

study showed that 70% of available energy is released into the water product and about 15% of available energy is released into the internal energy of butyl radical. We have yet not performed QCT investigations of the propanol reactions but we anticipate a similar yield of highly vibrationally excited H_2O as a major reservoir of the available energy.

Coulomb Explosion Imaging

The ability of Coulomb Explosion Imaging (CEI) to directly probe the structure of a molecule following multiple ionization by ultrafast methods has led to significant interest in both the technique itself and its application in time-resolved experiments. As described below, we have now shown that Wen Li's 3D (time and position) coincidence detection approach is capable of successful CEI experiments for structure determination, holding promise for future pump-probe studies. Our target systems are two carbonyl sulfenyl chlorides for which synchrotron studies have examined ionic decomposition products following core ionization: chlorocarbonylsulfenyl chloride (ClC(O)SCl; hereafter CCSC) and methoxycarbonylsulfenyl chloride ($CH_3OC(O)SCl$; MCSC). We focus here on CCSC to highlight the capabilities of this approach.

The mass spectrum of fragments resulting from strong field ionization of CCSC at ~7×10^{13} W/cm^2, shows that the most intense product peaks (CO+, S+, and Cl+) are those which would arise from cleavage of all the single bonds in the molecule (although other processes likely also contribute to their occurrence), while larger fragments are present in lower abundance. Three fragments show clear rings in the images, most prominently $COCl^+$ and SCl^+. The rings in the images are momentum-matched and correspond to the same peak E_T value of 6.1 eV when the features are assumed to arise from two-body fragmentation of $CCSC^{n+}$, suggesting they arise from the same process:

$$ClC(O)SCl^{2+} \rightarrow COCl^+ + SCl^+$$

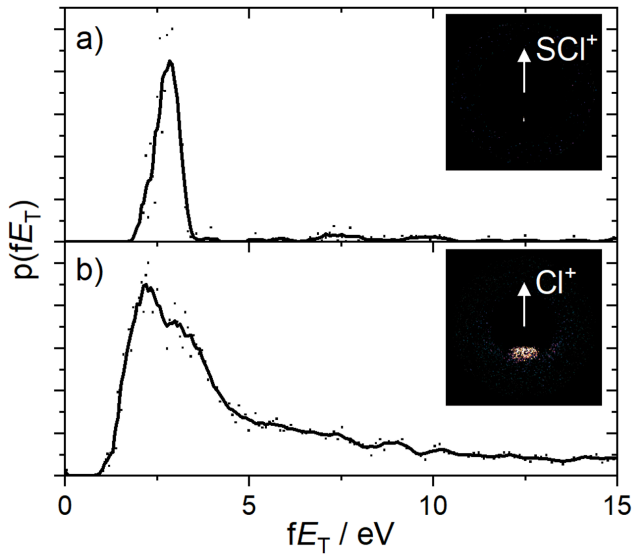

Figure 1. Fragment translational energy distributions from covariance maps of COCl+ referenced to (a) SCl+ (within angles of 176 – 183° to the reference ion vector) and (b) Cl+ (at 144 – 216° angles).

From these multimass images, we construct covariance maps (Fig. 1) to identify the relations between the observed ions. The covariance maps are calculated between pairs of 'reference' and 'plotted' ions, and show where the plotted ions are more likely to be seen in a frame in which the reference ions are oriented along a specified axis from the center (here always vertically upwards). The map for covariance of $COCl^+$ referenced to SCl^+ was calculated and is shown in Fig. 1A. A very sharp feature centered around 180° is observed in both this map and the reverse case, indicating that there exists a two-body fragmentation producing these ions. Given that these features are observed at the same radii as the rings shown in the images, this confirms that process (1), C–S bond cleavage from $CCSC^{2+}$, is responsible for these rings.

Fig. 1B shows the covariance map of $COCl^+$ referenced to Cl^+. This shows a particularly significant feature, centered around 180° but broader than those observed for the two-body dissociations described previously. Given the lack of data on the momentum of the third fragment ($S^{0/+}$), it is impossible to convert this to total E_T, but the range of angles observed in the covariance map allow for some limits to be placed on the possible values. The observed feature covers the angles 145 – 180°, so given this and equations for conservation of momentum, a lower bound can be placed on E_T of 4.1 – 8.4 eV. Here the lower bound corresponds to the slower $COCl^+$ ions at 2.1 eV with an angle to the reference vector close to 180° and the upper bound corresponds to an fE_T of 3.6 eV and angles closer to 145°.

We also showed further ionization to the trication leads to processes such as three-body fragmentation to yield $COCl^+$, S^+, and Cl^+, confirmed using three-body covariance analysis techniques, while removing further electrons leads to higher degrees of atomization where the relative trajectories of the product ions are derived from the parent molecule's starting geometry. These results demonstrate the ability of the 3D multimass coincidence technique to observe a range of Coulomb explosion dynamics while achieving excellent resolution compared to time-stamped imaging sensors. This paper is currently in revision for *J. Phys. Chem.* and a second paper on methoxycarobonysulfenyl chloride is almost ready for submission.

Time-Resolved Photodissociation Dynamics at the MeV UED Facility at LCLS

We recently completed our first experiment at the MeV-UED instrument of the LCLS User Facility. Our objective here was to examine the photodissociation dynamics of oxalyl chloride, $(ClCO)_2$ an unusual system in which UV dissociation gives rise to four fragments. The UV photodissociation of this molecule has been studied at a range of UV wavelengths with some attendant controversy. In these experiments, a femtosecond pump beam at 267nm was used to excite the system and then its time-dependent structural evolution was probed using an ultrafast relativistic electron beam. The electron diffraction patterns acquired at different pump-probe time delays is used to extract the pair distribution functions (PDF) which include the structural information. Since we suspected that the fast Cl and CO fragments are formed at much shorter delays compared to the slow fragments, we carried out two different sets of experiments at high charge state (20-30k electrons/pulse) and low charge state (5-10k electrons/pulse) to investigate kinetics at both long and short delays. Our initial analysis of the electron diffraction patterns at high charge state (Figure 2) clearly shows loss of C-C and C-Cl distances in the delay range of 0-50 ps and some recovery of the initially bonded distances in the delay range of 50-100 ps which can be indicative of vibrational excitation. These diffraction patterns show continuous loss of distances at longer delays as expected. Further offline analysis of the experimental data is being performed in order to better understand the dissociation dynamics and determine which proposed pathways (two distinct dissociative steps or the concerted four-body fragmentation) is dominant.

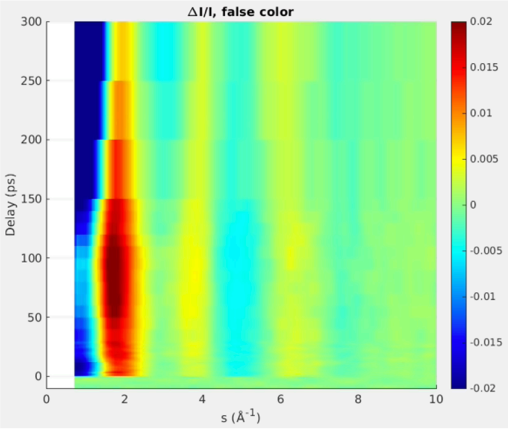

Figure 2. The experimental time resolved difference diffraction pattern following 267nm excitation of $(ClCO)_2$ at high charge state (momentum space).

III. Future Directions

<u>*Crossed-beam H atom reactions.*</u> In the next year we plan

to begin a systematic investigation of H atom reactions with polyatomic molecules. Although there has been little in the way of experimental dynamics investigation, these important reactions have been pursued by a number of theoretical groups attempting to develop reliable reduced dimensionality quantum treatments and associated semiclassical transition state theory. This is a splendid opportunity to bring the power of our single-photon ionization detection to bear to probe the reaction dynamics, including abstraction site specificity. We will then use these systems to explore conformational dependence of reaction dynamics beginning with the H-butane system. By varying the source temperature, we should be able to modulate the *gauche*-butane population by 50% while maintaining the same collision energy by varying the seed gas.

Time-resolved CEI. Our success with the Coulomb Explosion Imaging shows that we are now in a position to use this for time-dependent dynamics studies. We are currently implementing a hollow-core fiber compressor to get much shorter laser pulses for this effort. We will combine this with the tripled Ti:Sapphire fundamental in initial time-resolved studies of halomethanes and isomers of diiodobenzene (DIB). Previous Coulomb explosion work on the para-isomer observed the recoil of two iodine atoms in opposing directions after three-body fragmentation, which suggests that it should be possible to observe distinct two- and three-body covariance patterns from 1,2-DIB.

Analysis of UED results on oxalyl chloride. Our first experiment at the MeV UED facility at LCLS was clearly successful based on the high quality and consistency of the data we have obtained. This was possible despite the pandemic owing to the great support from the onsite team there for remote operation. We are gaining experience with the suite of analysis tools to understand and interpret the time-resolved diffraction data. In the coming year we will complete this analysis and prepare a paper describing the results. With this experience we will then be in a position to develop further proposals to make use of these capabilities.

IV. DOE Publications 2018-present

A. Kamasah, H. Li, J, Onvlee, A. van der Avoird, D. H. Parker, and A. G. Suits, "Imaging the inelastic scattering of vibrationally excited NO(v=1) with Ar," *Chem. Phys. Lett.* (2018) **692**, 124-128. DOI: 10.1016/j.cplett.2017.12.016

A. G. Suits, "Invited Review Article: Photofragment Imaging," (2018) 89, 111101 DOI: 10.1063/1.5045325

H. Li, A. Kamasah, S. Matsika and A. G. Suits, "Intersystem Crossing in the Exit Channel," *Nature Chem* (2018) DOI:10.1038/s41557-018-0186-5

H. Li, A. Kamasah, and A. G. Suits, "Imaging H abstraction dynamics in crossed molecular beams: O(^{3}P) + propanol isomers," *Phys Chem Chem Phys,* (2018) DOI:10.1039/CBCP06351F.

H. Li and A. G. Suits, "Universal Crossed Beam Imaging Studies of Polyatomic Reaction Dynamics," *Phys Chem Chem Phys.* (2020) (2020) **22**, 11126-11138 DOI: 10.1039/D0CP00522C.

H. Li, D. Troya and A. G. Suits, "Multichannel dynamics in the OH + n-butane reaction revealed by crossed-beam slice imaging and quasiclassical trajectory calculations," *J. Chem. Phys.* (2020) 153, 104302. DOI: 10.1063/5.0013585.

Multiscale Interaction of Turbulence, Temperature, and Soot Formation: Measurements for Critical Assessments of Chemical Kinetics and Mechanisms

Jeffrey A. Sutton
Department of Mechanical and Aerospace Engineering
Ohio State University
Columbus, OH 43210
sutton.235@osu.edu

Project Scope

This program targets an improved understanding of how turbulence affects soot formation chemistry (directly and indirectly) with a particular focus on detailing the multiscale coupling between flow turbulence, mixing, thermal transport, and soot formation kinetics in gas-phase reacting systems. There is ample evidence that soot formation and growth is strongly affected by turbulence. This is due to the fact that soot formation chemistry is characterized by slow time scales and thus surrounding fluid mechanic and mixing time scales not only influence the kinetic processes, but may dictate them. In this manner, the assessment of soot formation and the resulting chemical kinetic mechanisms for application under turbulent conditions must be benchmarked against measurements in turbulent reacting flows. This project targets simultaneous, quantitative multi-dimensional velocity, soot volume fraction, and gas-phase temperature imaging in turbulent non-premixed sooting flames to elucidate the relative effects of fluid kinematics, mixing, thermal processes, and turbulence/scalar time/length scales on soot formation chemistry and topology. The local gas-phase temperature field is critically important to further understand soot formation under turbulent conditions because of its direct linkage between turbulence (i.e., thermal and molecular mixing) and chemical kinetics (i.e., temperature-dependent reaction rates). In this program, a new implementation of filtered Rayleigh scattering (FRS) is applied for quantitative 2D temperature measurements in turbulent sooting non-premixed flames. The combined velocity (via PIV), soot volume fraction (via LII), and gas-phase temperature imaging will provide a previously unavailable database concerning turbulence-temperature-soot interaction. From these measurements, novel multi-parameter statistics will be derived that detail the coupling and importance of various kinematic and thermal parameters. This analysis is necessary for understanding relevant formation pathways, transport mechanisms, and developing soot mechanisms to be applied under turbulent conditions.

Recent Progress

Detailed Assessment of FRS Thermometry

In the last reporting period, we presented results demonstrating our proposed FRS methodology for acquiring quantitative 2D temperature measurements in turbulent sooting flames simultaneously with soot volume fraction measurements and velocity measurements from particle image velocimetry (PIV). FRS is a variant of the traditional laser Rayleigh scattering (LRS) technique which uses the combination of a spectrally narrow laser and an atomic or molecular filter (cell filled with an absorbing species such as molecular iodine, I_2) placed in front of the detector [5]. This combination rejects interference that is spectrally identical to the incident laser light (i.e., scattered light from particles), while collecting gas-phase information. In this program,

we have developed a particular fuel combination (12% C_2H_2, 45% H_2, and 43% Ar) for sooting flames such that the measured FRS signal is a known function of temperature and is not dependent on local species concentrations. This allows quantitative single-shot temperature measurements using only an FRS measurement.

During this reporting period, we assessed the temperature methodology through a hierarchy of flows to establish measurement precision and accuracy. Initial assessments in a series of heated fuel mixtures; non-sooting, near-adiabatic flat flames; and laminar non-premixed sooting flames show accuracy of the approach over a full range of expected temperatures (< 4% from known values) and high single-shot measurement precision (e.g., 65 < SNR < 80) for temperatures between 1900K and 2200K. For single-shot 2D temperature imaging, the SNR is 74 at 300K and > 60 at flame temperatures. The current FRS technique shows the highest single-shot SNR over all temperature conditions reported to date within turbulent sooting flames.

Development of Quantitative Laser-Induced Incandescence Measurements

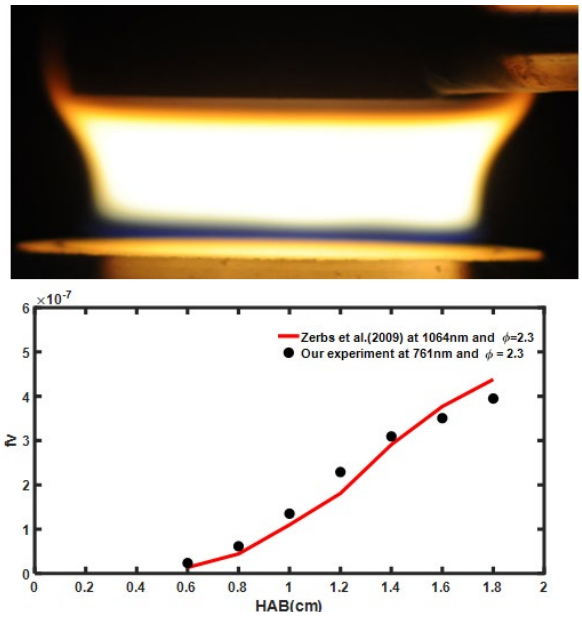

Figure 1: (Top) Photograph of premixed C2H4.air flame stabilized above the surface of a McKenna burner. (Bottom) Soot volume fraction measurements based on laser extinction as a function of height above the burner (HAB) surface.

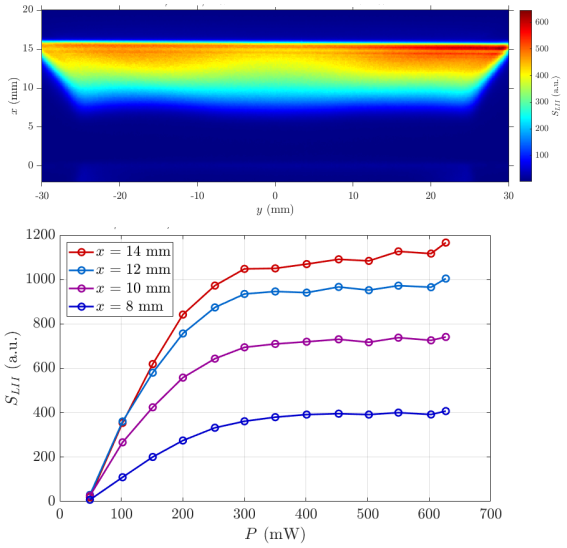

Figure 2: (Top) Average LII image from laminar, McKenna flame. (Bottom). Measurements of LII signal as a function of power (laser fluence).

During the current reporting period, we developed quantitative soot volume fraction measurements using calibrated LII. Quantification is based on line-of-sight extinction measurements in a laminar, sooting, burner-stabilized flame. Figure 1 (top) shows a visible photograph of a premixed, $\phi = 2.3$, C_2H_4/air flame, stabilized above the surface of a water-cooled McKenna burner that serves as a standard calibration flame within the International Sooting Flame Workshop [2]. The bottom of Fig. 1 shows a comparison of the current extinction measurements acquired using a 761-nm diode laser with that of Zerbs et al. [2, 3] at 1064 nm as a function of height above the burner (HAB) surface. The current laser wavelength was selected to minimize interference from water vapor in

the flame. Excellent agreement is observed between the two data sets giving confidence in our calibration approach.

The next step is determining the appropriate laser fluence to use to ensure the measurements are in the so-called "plateau" regime, where the LII signal is independent of incident laser fluence. Figure 2 (top) shows an average LII signal in the McKenna flame and Fig. 2 (bottom) shows a series of measurements characterizing LII signal as a function of incident laser power for several positions above the burner surface. The incident laser fluence (F) is related to the laser power (P) as $F = P(tA)^{-1}$, where t is time and A is the laser sheet area. From the results, a laser power of approximately 300-400 mW (F = 0.7 J/cm^2) results in an LII signal that is independent of variations in laser fluence.

Finally, Fig. 3 shows an example single-shot LII image in the Re = 11,000 turbulent flame. Laser excitation is performed at 1064 nm and emission is collected at 450 nm. The image is reasonably high signal-to-noise and shows the highly intermittent soot structure. We have now demonstrated quantitative single-shot 2D temperature and soot volume fraction imaging in a set of turbulent sooting, non-premixed flames.

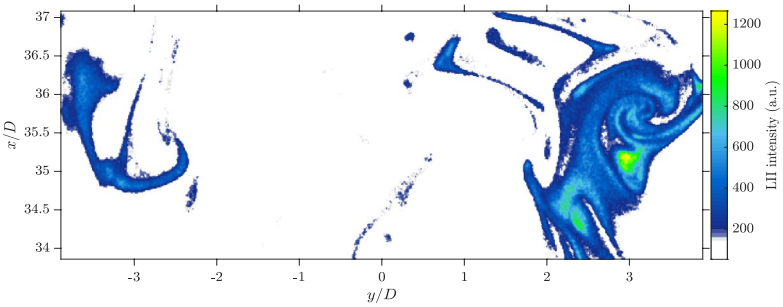

Figure 3: (Top) Example instantaneous LII (soot volume fraction) image in Re = 11,000 turbulent, sooting, non-premixed flame.

Future Plans

Current work includes the combining of FRS, PIV, and LII in turbulent non-premixed sooting flames. Previously, we have demonstrated accurate measurements of velocity and temperature using PIV and FRS in non-sooting flames [4] and the current work demonstrates accurate temperature and soot volume fraction measurements under non-premixed flame conditions. As discussed above, a series of turbulent non-premixed sooting flames have been developed for study that span a broad range of Reynolds and Damköhler numbers. A key focus of the near-term work is to characterize accuracy and precision of all measurements when combined together in order to quantify "crosstalk" effects.

With the simultaneous temperature-velocity-soot volume fraction database, longer-term work includes a detailed statistical characterization of the flames including statistical moments, integral scales, and joint statistics. A significant utility of the simultaneous LII-PIV-FRS imaging lies in the ability to formulate a set of joint statistics (including bivariate correlations, joint PDFs, conditional statistics, and multi-variate correlations) between multiple parameters with a particular focus on examining the relative roles of turbulent and thermal transport on soot formation. Finally, an investigation of the relative roles of flow kinematics and thermal variations on soot topology will be investigated. During the next year, we will also engage CFD researchers in this area to model these flames. These flames are unique in the fact that they have a multi-parameter experimental data set for assessment and use a different fuel (than typical studies) that can assess acetylene-based pathways of soot formation.

References

[1] R.B. Miles, W.R. Lempert, J.N. Forkey, *Meas. Sci.. Tech.*12.5 (2001) R33.

[2] International Sooting Flame Workshop, https://www.adelaide.edu.au/cet/isfworkshop/, accessed May 4, 2021.

[3] J. Zerbs, K.P. Geigle, O. Lammel, J. Hader, R. Stirn, R. Hadef, W. Meier, *Appl. Phys. B* 96 (2009) 683-694.

[4] T.A. McManus, J.A. Sutton, *Exp. Fluids*, 61 (2020), 1-9.

Publications Supported by this DOE Project (2018 – present)

Pu. J., Sutton, J.A., “Quantitative 2D Thermometry in Turbulent Sooting Non-Premixed Flames using Filtered Rayleigh Scattering”, submitted, Applied Optics, 2021.

Pu, J., Sutton, J.A., "Evaluation of the Tenti S6 Model for Hydrocarbon Fuels at Elevated Temperatures using Filtered Rayleigh Scattering Measurements", *Optics Letters*, 2020, 45 (19), 5579.

McManus, T.A., Sutton, J.A., "Simultaneous 2D Filtered Rayleigh Scattering Thermometry and Stereoscopic Particle Image Velocimetry Measurements in Turbulent Non-Premixed Flames", *Experiments in Fluids*, 2020, 61, 134.

Elementary Reactions of PAH Formation

Robert S. Tranter
Chemical Sciences and Engineering Division, Argonne National Laboratory Argonne, Il-60439
tranter@anl.gov

Program Scope

This program is focused on the experimental determination of kinetic and mechanistic parameters of elementary reactions, in particular those involved in the formation and destruction of the building blocks for aromatic species. The program also encompasses dissociation of novel fuels such as ethers and cyclic species and their dissociation products that are representative of intermediates in combustion mechanisms. Thermal sources of radicals are investigated and characterized for use in more complex reaction systems where secondary chemistry can be significant. Recently, the scope has been increased to include thermally initiated roaming reactions. The approach involves a diaphragmless shock tube (DFST) equipped with laser schlieren densitometry (LS) and a time-of-flight mass spectrometer (TOF-MS). The combination of these techniques accesses a wide range of reaction temperatures and pressures. Finally, x- ray diagnostics are exploited to study flows in hostile environments to provide targets for simulations and develop better understanding of the environment in common experiments.

Recent Progress

Aromatics - Pyrolysis of Styrene: The reactions of aromatic molecules and radicals and resonantly stabilized radicals (RSRs) are important in the formation of polycyclic aromatic hydrocarbons (PAH) and particulate matter. Investigations of the pyrolysis of aromatics are continuing with attention focused on styrene. Syrene is not only an important industrial species as both a reagent and a product of polymer recycling, but also as an intermediate in the combustion of alkylbenzenes that are significant constituents of fuels.

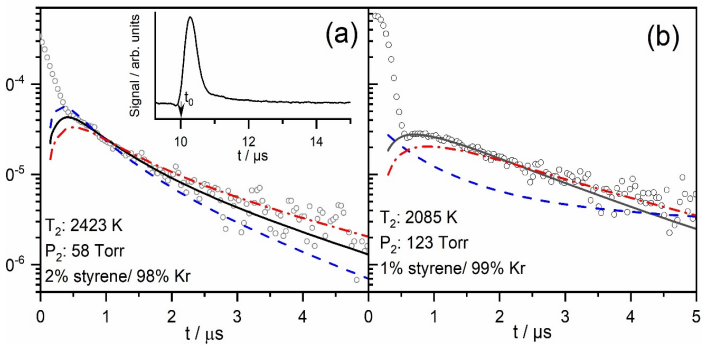

Figure 1: Semi-log plots of absolute density gradients (points) and simulations (lines). Solid black line: current model (a) Broken lines show the effect of varying k(styrene→α-styryl+H) by +/- 50%. Inset: raw LS signal. (b) Comparison of three models: Dash-dot line effect of neglecting minor channels forming styryl radical isomers; Dash line assumes styrene decomposes only to C_6H_6 + C_2H_2 per Müller-Markgraf and Troe,[1] and Grela et al.[2]

In a previous report the results of initial investigations of the pyrolysis of styrene were discussed. At that time, a mechanism had been developed that simulated a broad range of DFST/LS experiments quite well. Additionally, time dependent mass spectra had been obtained in electron impact ionization DFST/TOF-MS experiments at ~600 Torr and photoionization mass spectrometry studies in the high repetition rate shock tube (HRRST) at ~10 bar. The high pressure experiments were conducted at the Advanced Light Source under the Argonne/Sandia Consortium on High Pressure Combustion Chemistry (HPCC). While the initial model reproduced the LS r results reasonably there were discrepancies with the experimental TOF-MS results which are more influenced by the secondary chemistry. In the initial model styrene dissociated by transfer of an H-atom from the aromatic ring to the side chain subsequently forming ethylene and *o*-benzyne. This dissociation path was different to that suggested in the only other shock tube study of styrene pyrolysis[1] where C_2H_2 was eliminated leaving benzene. However, as shown in Fig. 1b a model based on C_2H_2 loss cannot simulate the LS results.

To address these issues, we have extensively reexamined the styrene pyrolysis mechanism in collaboration with Sivaramakrishnan who performed a theoretical study. The dissociation of styrene is not a simple process as previously suggested in Refs.1 and 2, but a multi-channel reaction where the most

important paths change with temperature and pressure. Multiwell master equation simulations show that a number of reaction pathways open up at the conditions of the LS and TOF-MS experiments. The most important reaction channel is H-atom elimination to form the *α*-styryl radical. This reaction accounts for roughly 50% consumption of styrene. The second most important channel is simple scission of the C-C bond between the aromatic ring and side chain. This yields a phenyl radical and a vinyl radical, accounting for around 26% of styrene. A further 20% of the styrene is consumed by C-H scissions that result in *β/o/m/p*-styryl radical isomers although each channel only consumes a few percent of the styrene. Finally, at the temperatures of the LS work dissociation to benzene and C_2H_2, favored in prior studies, only accounts for ~ 5 % of styrene. In Fig. 1 examples of the LS data are shown along with the results of simulations. In Fig. 1a the rate coefficient for the reaction forming α-styryl is varied by +/-50% and reasonable sensitivity to the reaction is found. Comparisons of various models for the initial dissociation of styrene are shown in Fig. 1b. Neglecting reactions forming the *β/o/m/p*-styryl isomers has a significant effect on the early part of the simulation. Whereas if it is assumed that styrene only forms C_6H_6 and C_2H_2 per Müller-Margraf and Troe,[1] and Grela et al.[2] then the LS results cannot be reproduced at all. The LS studies were performed at pressures of 60 to 240 Torr and temperatures of 1700 – 2400 K. These conditions are quite different to those of Grela et al., 10 mTorr and ~1400 K. The current model indicates that the H-elimination channels are insignificant at these lower T and P, and that dissociation of styrene occurs mainly by elimination of vinylidene as suggested by Grela. The temperatures from Ref. 1 are closer to those of the present work but the pressures were ~ 5 atm. Currently, we are investigating the differences between the current work and that of Ref. 1. However, the earlier study took UV absorption profiles at 200 μs reaction times over a wide wavelength range and the kinetic and mechanistic data were obtained by fitting of the complex UV profiles.

X-ray fluorescence measurements of temperatures in sooting flames: Accurate and spatially resolved measurements of temperatures are challenging to make in combustion systems, particularly in sooting regions of flames. However, such measurements are necessary for validating flame models. We have previously reported, with McEnally (Yale) and Xuan (Penn State), on measurements of temperature using x-ray fluorescence (XRF) of krypton in atmospheric pressure, sooting, co-flow methane / air flames. The experiments were performed at the 7-BM-B beamline at the Advanced Photon Source with 15 keV x-rays that allowed krypton Kα fluorescence to be measured. The fluorescence signal was proportional to the number density of Kr atoms and temperatures were obtained from the ideal gas law and Kr densities. 2D CFD simulations of the flames showed excellent agreement with the experiments which provided a rigorous benchmark for the simulations. Analysis of these data is complete and the work will shortly be submitted

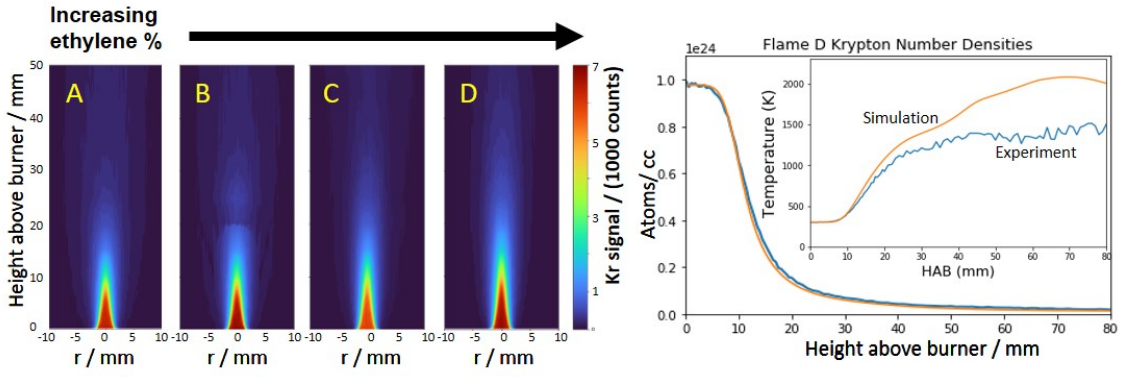

Figure 2: The left panel shows krypton x-ray fluorescence measurements in atmospheric pressure sooting ethylene/air co-flow diffusion flames Ethylene concentrations varied from 32% to 80%. Fuel flow doped with 4% Kr. Air 97.2 L/min. The right panel shows the measured and simulated Kr number densities. The excellent agreement makes the plots nearly coiincident. The inset shows the centerline flame temperature obtained from the experimental Kr densities and that from simulations.

for publication. We have recently applied the same technique to measurements in heavily sooting ethylene / air flames that are widely used by the International Sooting Flame Workshop. In these experiments, the fuel stream was doped with krypton. The measured fluorescence signals are shown in Fig. 2 for four flames with ethylene concentrations of A = 32%, B = 40%, C= 60% and D =80%. Along with the XRF data x-ray scattering data were collected and these show that the fluorescence results are not affected at all by the presence of soot, as expected. As before 2D CFD simulations are being performed and the initial results show excellent agreement with the experimental Kr number densities, Fig. 2. However, as the ethylene concentration is increased a relatively large and increasing discrepancy appears between temperatures calculated from the experimental Kr number densities and simulated flame temperatures in the regions where soot is present. The largest differences were found for flame D and are shown in Fig. 2. The source of the disagreement is not yet clear but it is possibly due to the model not including radiative cooling from soot particles.

Chemical Kinetics Code –Frhodo: A new chemical kinetic simulation program has been developed to replace the legacy FORTRAN code for simulating reactions in shock waves, particularly for LS studies that was previously used. The legacy program could not be easily modified and its limitations were hindering studies of complex systems such as styrene pyrolysis. The new program, Frhodo, is an open-source GUI-based Python application that is distributed through Github. The program uses Cantera as the chemistry solver and implements standard forms of reaction mechanisms and thermochemistry. The prior program had a unique style for describing reactions. Frhodo's extensive and easy-to-use GUI provides immediate graphical feedback about a simulation when changes are made to a mechanism. This feedback can be used to manually optimize kinetics mechanisms based on experimental observables. Alternatively, mechanisms can be optimized using built-in optimization routines. The machine learning-based optimization routines work by either minimizing normalized residuals or through Bayesian parameter estimation. In both cases, outliers are down weighted using a generalized loss function. There is currently support for high-temperature chemical kinetics experiments that can be simulated using a 0d reactor or using a custom reactor built for measurements taken behind incident shock waves. Such experiments include shock tubes, idealized rapid compression machines, etc. A tool for exploring chemical kinetics mechanisms is provided in the form of a simulation explorer, which can graph an extensive list of parameters through the course of a given simulation. One of the guiding principles of Frhodo has been to elevate researcher capabilities by minimizing repetitive tasks. The program has been used to date to develop mechanisms for several systems. The automated optimization routines were very useful for screening candidate mechanisms for styrene pyrolysis.

Methods: A new driver section has been installed on the DFST. The new section has a number of benefits including: an increase in shock velocity of about 18% for a standard experiment (equivalent to an increase in incident shock temperature of about 350 K); simplifies maintenance and alignment of the fast acting valve that is crucial to reproducibility and operation of the DFTS; the wider driver chamber also permits alternative configurations of the driver/driven section interface that will be useful for future experiments.

Upgrades have been made to the data acquisition system for the DFST/LS and TOF-MS experiments and a large update to the software is nearing completion. The software upgrade will provide a uniform platform for several current and planned apparatuses, simplify future upgrades and implements a number of features that have been developed as standalone programs during the last few years.

Under the HPCC low energy electron impact ionization was successfully tested with the HRRST/TOF-MS. The same technique has now been successfully tested with the DFST/TOF-MS. In this case, the electron energy was 21.0 eV rather than 12.0 – 16 eV used in the HRRST work. However, even averaging over less than 10 shocks, good S/N was obtained in experiments with 0.5% styrene dilute in neon and 0.25% difluoromethane dilute in neon. The low energy electron approach combined with the reproducibility of reaction conditions in the DFST has been particularly beneficial for obtaining well-defined mass spectra with minimal signal from the bath gas, at reaction pressures close to those of the LS studies, allowing more direct comparison of the experiments.

Future work

An investigation of the pyrolysis of difluoromethane has been started. Cobos et al.[3] and Matsugi[4] have studied dissociation of difluoromethane in shock tubes by different methods at similar conditions and obtained disparate results. The mechanisms proposed by Matsugi and Cobos agree on the initial dissociation reaction being elimination of HF yielding the CHF radical, but they are quite different in the secondary chemistry. To investigate these differences preliminary LS and TOF-MS studies on difluoroethane pyrolysis have been conducted. The LS experiments cannot be simulated at all with either Cobos's or Matsugi's mechanisms. Furthermore, the mass spectra showed that both HCCF and HCCH are the main secondary products. Master equation calculations by Matsugi suggest that HCCF + HF is the product of CHF + CHF and provides no route to HCCH. Preliminary simulations that incorporate branching between HCCF + HF and HCCCH + F2 from CHF + CHF simulate the LS data reasonably well. The study is still in early stages and will form an immediate focus going forward particularly to understand the branching in the reaction between CHF + CHF radicals.

The DFST/TOF-MS/LS studies of aromatics and resonantly stabilized radicals are ongoing. Investigations of alkylbenzenes have been started. These build on the studies of styrene which is an important intermediate in the pyrolysis of alkylbenzenes. The low pressure LS and TOF-MS studies will be combined with high pressure one under the HPCC. Organonitrites will be exploited as sources of a broad range of radicals including unsaturated ones, resonantly stabilized and aromatic radicals. These will allow key processes in formation of polyaromatic hydrocarbons to be tested and characterized. Michael's high purity shock tube is being converted to a DFST and optical diagnostics including ARAS and UV-OH absorption will be implemented to complement the DFST/TOF-MS/LS experiments.

References

1) W. Müller-Markgraf and J. Troe, J. Phys. Chem. **1988** 92, 4914–4922.
2) Grela, M. A. Amorebieta V. T. and Colussi,.A. J. Phys. Chem., **1992** 96, 9861–9865.
3) Cobos C. J., Knight G., Sölter L., Tellbach E. Troe J., J. Phys. Chem. A **2017**, 121, 7820-7826
4) Matsugi A., Chem. Phys. Lett. 2018, 707, 140-143.

Publications supported by this project 2019-2021

1) Tranter R. S., Chaumeix N., Wooldridge M. S. 'Editorial Joe V. Michael Memorial Issue', Int. J. Chem. Kinet., **2021** https://doi.org/10.1002/kin.21481
2) Sikes T, Bell Burdett K., Speth R. L., Goldsmith C. F., Sivaramakrishnan R., Tranter R. S., 'Ring opening in cycloheptane and dissociation of 1-heptene at high temperatures' Proc. Combust. Inst. **2021,** 38, 929-937.
3) Sikes T., Tranter R. S., "Frhodo v1.2.5', https://github.com/Argonne-National-Laboratory/Frhodo, **2020** (6 Nov).
4) Randazzo J.B., Sivaramakrishnan R., Jasper A. W., Sikes T., Lynch P. T., and Tranter R. S., 'An Experimental and Theoretical Study of the High Temperature Reactions of All Four Butyl Radical Isomers' Phys. Chem. Chem. Phys. **2020,** 22, 18304 -18319.
5) Fuller M. E., Skowron M., Tranter R. S. and Goldsmith C. F. 'A modular, multi diagnostic, automated shock tube for gas-phase chemistry' Rev. Sci. Instrum. **2019**, 90, 064104
6) Randazzo J. B., Fuller M. E., Goldsmith C. F. and Tranter R. S. 'Thermal Dissociation Of Alkyl Nitrites And Recombination Of Alkyl Radicals' Proc. Combust. Inst. **2019**, 37,703-710.
7) Hansen N., Tranter R. S., Randazzo J. B., Lockhart J. P. A., and Kastengren A. L. 'Investigation of Sampling-Probe Distorted Temperature Fields with X-Ray Fluorescence Spectroscopy' Proc. Combust. Inst. **2019**, 37, 1401-1408.

Experimental Identification and Atomistic Simulations of Active Sites, Rates and Reaction Extent in Thermo-Catalytic Decomposition and Regeneration Towards Maintaining Autocatalytic Activity

Randy Vander Wal, Adri van Duin
ruv12@psu.edu, acv13@psu.edu
Departments of Energy and Mineral Engineering, Mechanical Engineering,
The Pennsylvania State University
University Park PA 16802

Program Scope

The abundance of US shale gas has changed the energy landscape and outlook. Natural gas has displaced coal for electricity generation with renewed interests as a transportation fuel. Whether in gas turbines or IC engines, soot as a combustion byproduct is produced. The present US and worldwide natural gas abundance also prompts interest in the H_2 economy wherein decarbonization of natural gas decarbonization could serve as a bridge while also mitigating CO_2. In fact, generating solid carbon by thermo-catalytic decomposition (TCD) is not only an ideal form of carbon capture compared to gaseous CO_2 but also, given its purity, be utilized for renewable energy storage in batteries.

Thermo-catalytic decomposition of methane is an attractive alternative to conventional steam reforming because the process does not generate CO/CO_2 byproducts or consume water resources, so the need for water-gas-shift and CO_2 removal stages, along with stock desulphurization and steam generation are eliminated. The energy requirement for methane cracking process (37.8 kJ/mole of H_2) is less than that for steam reforming (74.8 kJ/mole of CH_4) [1].

Despite these advantages, carbon as a catalyst also problematically deactivates [2]. Ideally the deposited carbon would be autocatalytic but studies consistently find that the deposited carbon is not as active a catalyst as the original carbon. Regeneration, by partial oxidation (gasification) may offer a solution by creating new active sites. Significantly these are also knowledge gaps in contemporary soot models, parallel to needs in TCD and regeneration.

Analogously, the two processes dominating soot mass and emission are growth and oxidation whose rates are determined by active sites and mediated by nanostructure. Surface reactivity of soot particles is an important factor for both processes. As soot particles grow and mature their structure and composition changes, resulting in a decline in soot surface reactivity – otherwise referred to as “aging”. Oppositely during oxidation rates often increase – reflecting a combined contribution of increased surface area and potential gain in active sites.

Nanostructure evolution during growth mirrors TCD while oxidation dependence on nanostructure mirrors regeneration. The non-reactive aging (for soot) refers to an additional well-known phenomenon generally associated with loss of active sites by thermal aging but lacks substantive quantification along with nanostructure dependence. Although unaddressed in TCD studies, thermal aging is likely is a contributing factor to TCD activity decline.

Future Plans

TCD rates will be measured for varied time durations and parametrically with temperature to calculate an activation energy. Reactant concentration will be varied to identify reaction order while reactant identity will test specific chemistries associated with natural gas components and other hydrocarbon fuels.

Analogously, regeneration rates will be measured as a function of reaction progress with parametric variation of oxidant, concentration and temperature. At selected stages in both TCD and regeneration, active sites will be measured and compared to rates to evaluate their correspondence. The correspondence of active site number to underlying nanostructure will also be evaluated. Dependence of TCD carbon nanostructure upon that of the initial carbon catalyst and its evolution will be assessed. Postulated is that lamellae curvature controls the reactivity of basal sites and formation of interior active sites during regeneration [3].

Atomistic scale simulations will identify type and concentration of active sites in relation to nanostructure, guided by experimental measurements of surface chemistry. These simulations will also provide the rates of increase in regeneration and decrease of active sites during deposition at different temperatures with varied reactants, as well as the relationship between the surface density of active sites and global measures of the carbon structure, such as C/H ratio and C5/C6 ring ratio [4]. Figure 1 outlines the connections between experimental and simulations.

As the goal, the outcome of this study will be predictive model for TCD grounded in active sites and benchmarked against comparative nanostructures. Furthermore, definition of TCD-relevant parameters and mechanistic insights by simulations will advance our understanding of soot growth and oxidation towards integrated soot models.

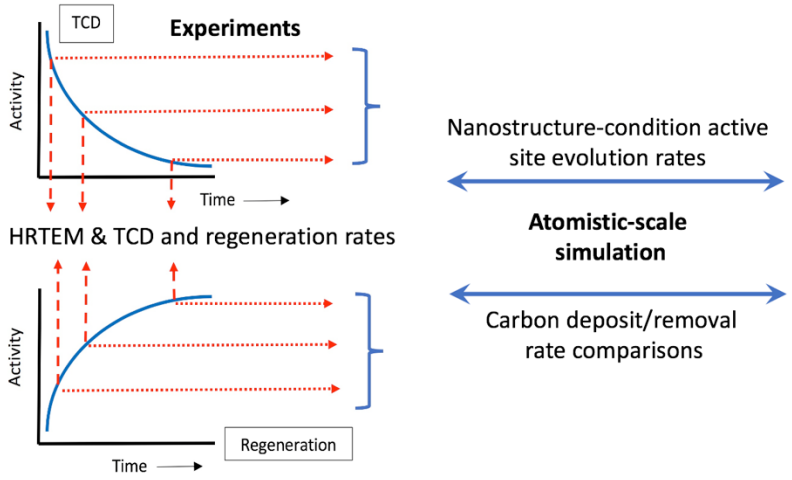

Figure 1 – Experimental – modeling connections.

References

1. Ashik, U. P. M., Daud, W. W., and Abbas, H. F. (2015). Production of greenhouse gas free hydrogen by thermocatalytic decomposition of methane–a review. *Renewable and Sustainable Energy Reviews*, *44*, 221-256.

2. Abbas, H. F., Daud, W. W. (2010). Hydrogen production by methane decomposition: a review. *International Journal of Hydrogen Energy*, *35*(3), 1160-1190.

3. Huang, C. H., and Vander Wal, R. L. (2016). Partial premixing effects upon soot nanostructure. *Combustion and Flame*, *168*, 403-408

4. Mao, Q., van Duin, A. C., Luo, K. H. (2017). Formation of incipient soot particles from polycyclic aromatic hydrocarbons: A ReaxFF molecular dynamics study. *Carbon*, *121*, 380-388.

Probing Nonvalence Excited States of Anions Using Photodetachment and Photoelectron Spectroscopy

Lai-Sheng Wang
Department of Chemistry, Brown University, Providence, RI 02912
Email: lai-sheng_wang@brown.edu

Program Scope

This program is aimed at providing energetic, electronic, and vibrational information about molecular species important in combustion using novel anion spectroscopic techniques. Negative ions do not possess Rydberg states, but highly diffuse nonvalence excited states can exist for anions as a result of long-range forces between an electron and a molecule, including charge-dipole, charge-quadrupole, or charge and induced-dipole interactions. A major goal of this project is to probe this class of anionic excited states that exist in polycyclic aromatic hydrocarbon (PAH) or functionalized PAH molecules. The weakly-bound nature of these nonvalence states implies that vibrational excitation in the neutral core can induce autodetachment via vibronic coupling. We have developed a high-resolution electrospray photoelectron imaging apparatus equipped with a cryogenically-controlled ion trap, which is ideal to probe this class of anionic excited states. Photodetachment spectroscopy is used to search the nonvalence excited states of cryogenically-cooled anions via resonant two-photon detachment or vibrational autodetachment. The autodetachment process is investigated by resonantly-enhanced photoelectron imaging. The combination of photodetachment spectroscopy and resonant photoelectron imaging can probe the dynamics of the vibronic interactions leading to autodetachment, as well as detailed energetic, electronic, and vibrational information about the underlying neutral radicals. Three types of anionic species are investigated: 1) O-containing PAH anions with dipole-bound excited states; 2) O- and/or N-functionalized PAH anions with quadrupole-bound excited states; and 3) PAH and fullerene anions with polarization-bound excited states.

Recent Progress

Photodetachment Spectroscopy and Resonant Photoelectron Imaging of the 2-Naphthoxide Anion via Dipole-Bound Excited States.[9] We investigated the 2-naphtoxide anion and 2-naphthoxy radical using photodetachment spectroscopy and resonant photoelectron imaging. A dipole bound state was observed 202 cm^{-1} below the detachment threshold of the 2-naphthoxide anion. The electron affinity of the 2-naphthoxy radical was measured accurately as 19,387(4) cm^{-1} or 2.4037(5) eV. Thirty-eight above-threshold resonances were observed in the photodetachment spectrum, which led to thirty-eight resonantly enhanced photoelectron spectra via vibrational autodetachment. A total of seventeen fundamental vibrational frequencies were measured for the 2-naphthoxy radical by combining the photodetachment spectroscopy and resonant photoelectron spectroscopy. Remarkably, seven bending vibrational modes were observed, including the two lowest frequency modes (ν_{48} and ν_{47}) with measured frequencies of 102 cm^{-1} and 171 cm^{-1}, respectively. The rich vibrational information would be valuable to calibrate theoretical methods aimed at understanding the vibrational properties of PAHs. This study demonstrated that the combination of photodetachment spectroscopy and resonant photoelectron spectroscopy is a powerful technique to obtain vibrational information for dipolar neutral radical species via vibrational autodetachment from dipole-bound excited states.

Polarization of Valence Orbitals by the Intramolecular Electric Field from a Diffuse Dipole-Bound Electron.[11] The diffuse electron in a dipole-bound state is spatially well-separated from the valence electrons and is known to have negligible effects on the molecular structure of the neutral core. Interestingly, we have obtained direct experimental evidence that the dipole-bound electron can have strong correlation effects with the valence electrons as a result of the electric field exerted by the distant dipole-bound electron. Photodetachment spectroscopy revealed a dipole-bound state (Fig. 1a) in the deprotonated 4-(2-phenylethynyl)-phenoxide anion (PEP^-), 348 cm^{-1} below its detachment threshold. Resonant two-photon detachment of the dipole-bound state was observed to be accompanied by a simultaneous shakeup process from the HOMO-2 valence orbital (Fig. 1c). This shakeup process was due to configuration mixing as a result of the polarization effect of HOMO-2 by the intramolecular electric field of the dipole-bound electron (Fig. 1b). This observation suggests that dipole-bound anions can serve as a new platform to probe how oriented electric fields influence the valence electronic structure of polyatomic molecules.

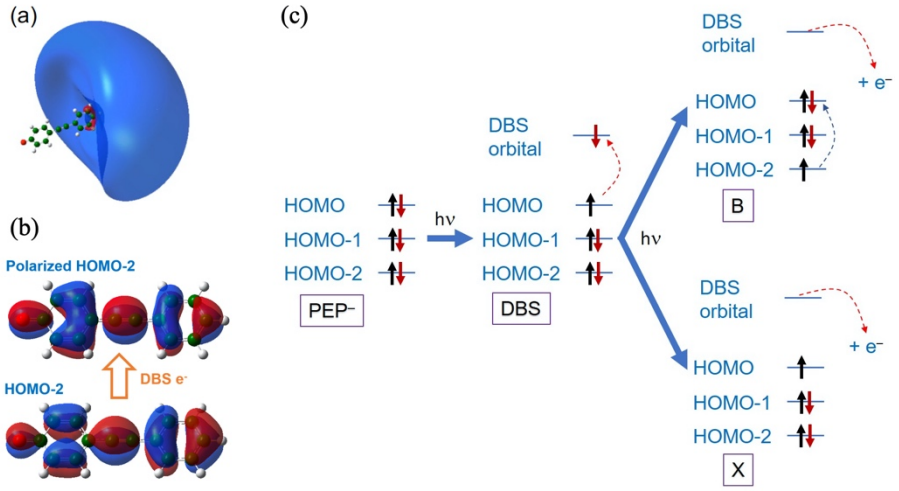

Fig. 1. (a) The dipole-bound orbital of the PEP^- anion. (b) The polarization of the HOMO-2 due to the electric field of the dipole-bound electron. (c) Excitation of PEP^- by the first photon to the dipole-bound state followed by detachment of the dipole-bound electron by the second photon to the ground state (X) of PEP and to the excited state (B) of PEP due to shakeup of a HOMO-2 electron to the HOMO.

Observation of a Symmetry-Forbidden Excited Quadrupole-Bound State.[12] The neutral 1,2,4,5-tetracyanobenzene (TCNB) molecule containing four polar –CN groups is a good electron acceptor and can form a stable valence-bound anion. Owing to its high symmetry (D_{2h}, see inset of Fig. 2), TCNB has no dipole or octupole moments, but a large quadrupole moment with only nonzero diagonal terms. We observed an excited quadrupole-bound state (QBS) in $TCNB^-$ using both photoelectron and photodetachment spectroscopies, but found that it was symmetry-forbidden (Fig. 2). The electron affinity of TCNB was accurately measured to be 2.4695 eV. Photodetachment spectroscopy of $TCNB^-$ revealed selected symmetry-allowed vibronic transitions to the QBS, but the ground vibrational state was not observed because the transition from the ground state of $TCNB^-$ (A_u symmetry) to the QBS (A_g symmetry) is triply-forbidden by the electric dipole, magnetic dipole, and the electric quadrupole. The binding energy of the QBS was found to be 0.2206 eV, which is unusually large due to strong correlation and polarization effects. A

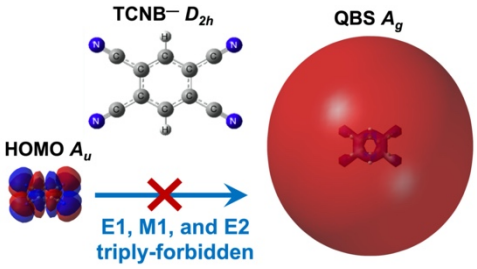

Fig. 2. Schematics showing the forbidden transition from the A_u ground state of $TCNB^-$ to its highly diffuse QBS (A_g).

centrifugal barrier was observed for near-threshold autodetachment, as well as relaxations from the QBS vibronic levels to the ground and a valence excited state of $TCNB^-$. The study showed a rare example where symmetry selection rules, rather than the Franck-Condon principle, governed vibronic transitions to a non-valence state.

Photodetachment Spectroscopy and Resonant Photoelectron Imaging of Cryogenically-Cooled 1-Pyrenolate.[13] We investigated the 1-pyrenolate anion (PyO^-) and the 1-pyrenoxy radical (PyO) (see inset of Fig. 3 for a structure model) using photodetachment spectroscopy and resonant photoelectron imaging. The electron affinity of PyO was measured to be 2.4772 eV (19,980 cm^{-1}). Photodetachment spectroscopy revealed a dipole-bound state for PyO^- 280 cm^{-1} below the detachment threshold (peak 0 in Fig. 3), as well as a broad and intense valence excited state (shape resonance) 1,077 cm^{-1} above the detachment threshold. The shape resonance with an excitation energy of 21,055 cm^{-1} was due to excitation of an electron from the HOMO of PyO^- to its LUMO in the continuum. Twenty-nine vibrational levels of the DBS were observed, including twenty-seven above-threshold vibrational levels (vibrational Feshbach resonances). Twenty-seven resonant photoelectron spectra were obtained by tuning the detachment laser to the vibrational Feshbach resonances, resulting in highly non-Franck-Condon photoelectron spectra and rich vibrational information. In total, the frequencies of twenty-one vibrational modes were obtained for the PyO radical by the combination of the photodetachment and resonant photoelectron spectroscopy, including thirteen out-of-plane bending modes.

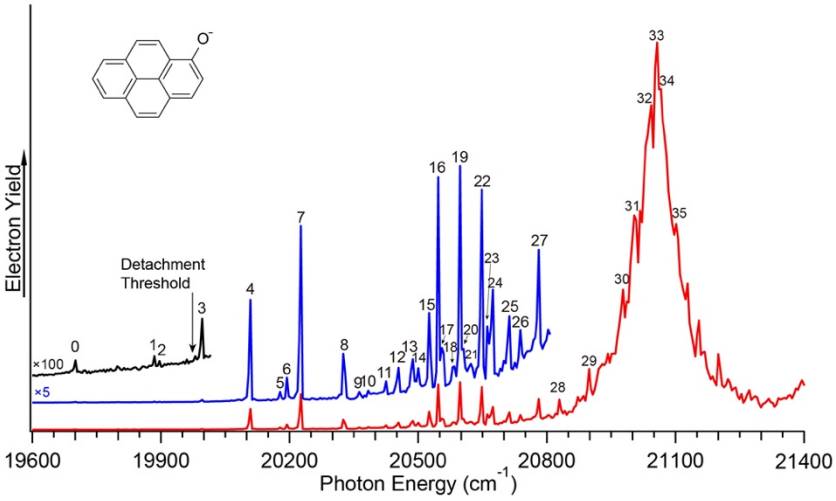

Fig. 3 The photodetachment spectrum of PyO^- (see inset) by measuring the total electron yield as a function of photon energy near the detachment threshold (indicated by the arrow). The broad peak at ~21,050 cm^{-1} is due an above-threshold valence excited state (i.e. a shape resonance) of PyO^-.

Future Plans

Experiments on dipole-bound excited states will be continued on O- and N-containing PAH anions. Specifically, we plan to move to larger PAH species containing 3 to 6 phenyl rings. We want to further examine systems with π-type dipole-bound states and search for QBS and correlation-bound states in large PAH anions. We will also investigate more complex O-containing PAHs, such as the C-linked multi-phenol oxide anions and phenoxide with complex substituents to examine the influence of the intramolecular electric field of the dipole-bound electron on the valence electrons.

Publications resulted from the BES-GPCP sponsored research (2018- present)

1. G. Z. Zhu, Y. Liu, Y. Hashikawa, Q. F. Zhang, Y. Murata, and L. S. Wang. Probing the Interaction between the Encapsulated Water Molecule and the Fullerene Cages in $H_2O@C_{60}^-$ and $H_2O@C_{59}N^-$. *Chem. Sci.* **9**, 5666-5671 (2018). (DOI: 10.1039/C8SC01031E)

2. G. Z. Zhu, C. H. Qian, and L. S. Wang. Dipole-Bound Excited States and Resonant Photoelectron Imaging of Phenoxide and Thiophenoxide Anions. *J. Chem. Phys*. **149**, 164301 (2018). (DOI: 10.1063/1.5049715)

3. G. Z. Zhu, C. H. Qian, and L. S. Wang. Tautomer-Specific Resonant Photoelectron Imaging of Deprotonated Cytosine Anions. *Angew. Chem. Int. Ed*. (2019). (DOI: 10.1002/anie.201903444)

4. J. Czekner, L. F. Cheung, G. S. Kocheril, and L. S. Wang. Probing the Coupling of a Dipole-Bound Electron with the Molecular Core. *Chem. Sci*. **10**, 1386-1391 (2019). (DOI: 10.1039/c8sc04771e)

5. G. Z. Zhu, L. F. Cheung, Y. Liu, C. H. Qian, and L. S. Wang. Resonant Two-Photon Photoelectron Imaging and Intersystem Crossing from Excited Dipole-Bound States of Cold Anions. *J. Phys. Chem. Lett*. **10**, 4339-4344 (2019). (DOI: 10.1021/acs.jpclett.9b01743)

6. C. H. Qian, G. Z. Zhu, and L. S. Wang. Probing the Critical Dipole Moment to Support Excited Dipole-Bound States in Valence-Bound Anions. *J. Phys. Chem. Lett*. **10**, 6472-6477 (2019). (DOI: 10.1021/acs.jpclett.9b02679)

7. G. Z. Zhu and L. S. Wang. High-Resolution Photoelectron Imaging and Resonant Photoelectron Spectroscopy via Noncovalent-Bound Excited States of Cryogenically-Cooled Anions. *Chem. Sci.* **10**, 9409-9423 (2019) (Invited perspective). (DOI: 10.1039/C9SC03861B)

8. D. F. Yuan, Y. Liu, C. H. Qian, Y. R. Zhang, B. M. Rubenstein, and L. S. Wang. Observation of a π-Type Dipole-Bound State in Molecular Anions. *Phys. Rev. Lett*. **125**, 073003 (2020). DOI: 10.1103/PhysRevLett.125.073003.

9. C. H. Qian, G. Z. Zhu, and L. S. Wang. Photodetachment Spectroscopy and Resonant Photoelectron Imaging of the 2-Naphthoxide Anion via Dipole-Bound Excited States. *J. Chem. Phys*. **152**, 214307 (2020). DOI: 10.1063/5.0011234.

10. Y. T. Wang, C. G. Ning, H. T. Liu, and L. S. Wang. High-Resolution Photoelectron Imaging and Photodetachment Spectroscopy of Cryogenically-Cooled IO^-. *J. Phys. Chem. A* **124**, 5720-5726 (2020). DOI: 10.1021/acs.jpca.0c04080.

11. D. F. Yuan, Y. Liu, C. H. Qian, G. S. Kocheril, Y. R. Zhang, B. M. Rubenstein, and L. S. Wang. Polarization of Valence Orbitals by the Intramolecular Electric Field from a Diffuse Dipole-Bound Electron. *J. Phys. Chem. Lett*. **11**, 7914-7919 (2020). DOI: 10.1021/acs.jpclett.0c02514

12. Y. Liu, G. Z. Zhu, D. F. Yuan, C. H. Qian, Y. R. Zhang, B. M. Rubenstein, and L. S. Wang. Observation of a Symmetry-Forbidden Excited Quadrupole-Bound State. *J. Am. Chem. Soc*. **142**, 20240-20246 (2020). DOI: 10.1021/jacs.0c10552

13. C. H. Qian, Y. R. Zhang, D. F. Yuan, and L. S. Wang. Photodetachment Spectroscopy and Resonant Photoelectron Imaging of Cryogenically-Cooled 1-Pyrenolate. *J. Chem. Phys*. **154**, 094308 (2021). DOI: 10.1063/5.0043932

14. D. F. Yuan, Y. R. Zhang, C. H. Qian, Y. Liu, and L. S. Wang. Probing the Dipole-Bound State in the 9-Phenanthrolate Anion by Photodetachment Spectroscopy, Resonant Two-Photon Photoelectron Imaging, and Resonant Photoelectron Spectroscopy. *J. Phys. Chem. A* , submitted (2021).

Experimental and Computational Study of Quantum Nuclear and Many-Body Effects in Water Network Formation and Water-Surface Interaction in PAH-Water Cluster Ions

J. Mathias Weber[1,2] (weberjm@jila.colorado.edu, PI)
Joel D. Eaves[2] (joel.eaves@colorado.edu, Co-PI)

[1]JILA, 440 UCB, University of Colorado Boulder, Boulder, CO 80309-0440
[2]Department of Chemistry, 215 UCB, University of Colorado Boulder, Boulder, CO 80309-0215

Program Scope

In this combined experimental and theoretical program, we aim to quantify interactions between water molecules and aromatic hydrocarbons (PAHs) at an unprecedented level of detail. Molecular clusters are excellent systems for theoretical and computational work, since they are sufficiently small for high-accuracy electronic structure calculations, and their spectroscopy can unveil important information about details of molecular interactions that remain obscured in the condensed phase. The precise control over experimental conditions in cryogenic cluster ion experiments, both through mass selection and cooling, dramatically reduces systematic uncertainties compared to analogous condensed phase work. Crucially, quantum nuclear effects that arise from non-classical, quantum behavior of protons in water often display modest effects in bulk liquid at room temperature. These effects are expected to be more pronounced in small water-PAH clusters, particularly at low temperatures. Thus, the proposed systems will allow us to explore several different treatments for including quantum nuclear and many-body effects in the computational description of water-PAH interactions.

PAHs are valuable model systems for both neutral and charged graphene and their chemical derivatives. The water-graphene interaction is of paramount importance in materials chemistry. Theoretical predictions and careful experiments have shown that the graphene wetting characteristics are highly sensitive to small changes in the chemistry on the graphene surface. For example, the application of small voltages applied to nanoporous graphene is predicted to increase water throughput in desalination applications, and the predicted water transport through such systems strongly depends on the details of the model for water-carbon interaction used. This implies that applications ranging from battery technology to electrocatalysis depend on interfacial phenomena that contemporary theoretical models only poorly describe. Experimentally probing the molecular level details of the interaction of single-layer graphene with water is also rather challenging, due to pitfalls in the preparation of clean single-layer graphene films and the size and shape heterogeneity of graphenic nanostructures synthesized in typical chemical preparations.

We will study the interaction of water molecules with charged PAHs in mass-selected cluster ions of the form $PAH^{+/-}\cdot(H_2O)_n$, using cryogenic infrared photodissociation spectroscopy, and compare the experimental results with theoretical predictions. From an experimental point of view, using mass-selected PAH ions allows us to precisely control the size and shape of the graphenic system, as well as the number of water molecules interacting with it. This strategy leads to exquisitely well-controlled experimental conditions because it removes fluctuations in the solvent environment and lets us study solvent interactions one molecule at a time.

In the theoretical/computational component of this project, we will parameterize the many-body intermolecular potential, and test both centroid and ring-polymer molecular dynamics approximations to relevant quantum time correlation functions associated with transitions between stable structures of the clusters and IR spectroscopy. Fully predictive molecular models for aqueous chemistry must account for complexities in both the nuclear potential energy surface and the dynamics on those surfaces. The potential energies have received the lion's share of attention. We pursue a complementary approach that focuses on the dynamics.

Recent Progress

The program is in its early days. In the experimental component of the program, we have modified an existing electrospray ionization (ESI) source to be able to safely work with organic solvents for PAH ion generation by ESI. The ions are transferred through a series of octopole ion guides into a cryogenic ion trap, which can be operated at temperatures from 15 K to room temperature. In this trap, we can condense water molecules on the PAH ions (at temperatures of 160 K – 185 K) or add N_2 molecules as messenger tags to molecular and cluster ions to enable infrared photodissociation spectroscopy. Mass selection and infrared photodissociation spectroscopy are performed in a tandem time-of-flight mass spectrometer, using a nanosecond-pulsed infrared optical parametric converter system with wavelength coverage in the range 15 μm – 2.5 μm (ca. 2 cm^{-1} bandwidth). Spectroscopy in the UV and visible range is also possible with this setup. The apparatus is shown in Figure 1.

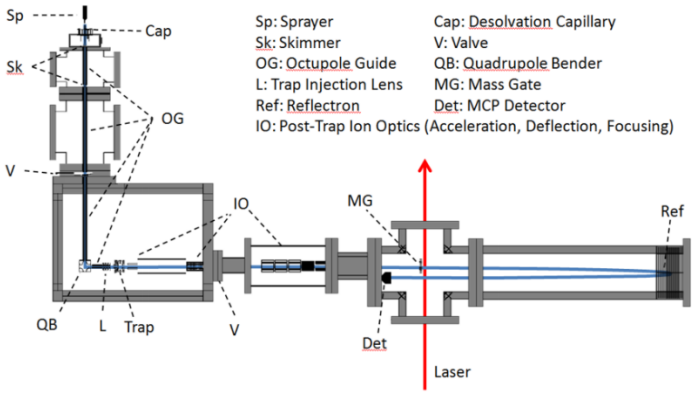

Figure 1: Schematic of the experimental apparatus (top view). The blue line shows the ion trajectory through the apparatus.

Using PAHs dissolved in various solvents (acetonitrile, *o*-dichlorobenzene, toluene), we have been able to prepare anionic deprotonation products of pyrene, tetracene, and indole. We also prepared pyrene carboxylate in hydrated clusters with up to three water molecules (see Figure 2).

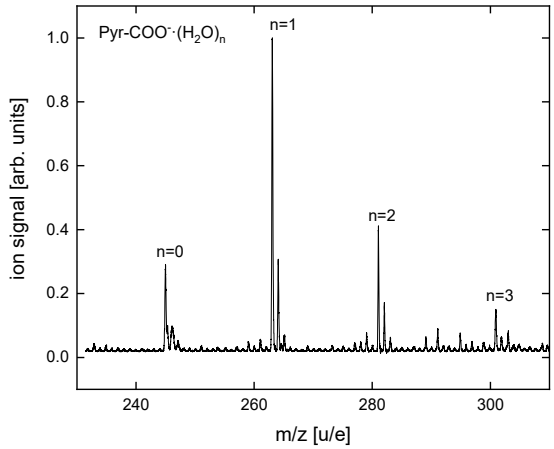

Figure 2. Mass spectrum of hydrated pyrene carboxylate anions, Pyr-$COO^{-}\cdot(H_2O)_n$ (n = 0-3). The mass spectrometer was optimized for preparation and detection of the water clusters, suppressing the intensity of bare Pyr-COO^{-}.

In the computational part of the program, we have started molecular dynamics simulations of the IR spectra of anionic hydrated naphthalene, $Np^{-}\cdot(H_2O)_n$ (n=2-6). The time correlation function formalism avoids many pitfalls with the conventional harmonic analysis one performs on the critical points of the many-body nuclear potential energy surface. Classical simulations of the IR spectrum in the OH stretch region give results for the IR spectrum that are surprisingly good given the simplicity of the potential function and the complete neglect of quantum nuclear effects. The simulations show that even in the smallest clusters the potential energy surface is complex, with structures trapped inside basins that are estranged from one another. Dynamics within those basins involve large-scale, anharmonic molecular motions that would be difficult to obtain using harmonic analysis, even in a presumably exact many-body potential.

Future Plans

The next steps in the experimental program are to acquire the first spectra of hydrated PAH cluster ions, first focusing on pyrene carboxylate, Pyr-$COO^{-}\cdot(H_2O)_n$, and deprotonated indole, $[Ind\text{-}H]^{-}\cdot(H_2O)_n$. In parallel, a solvent preparation ion trap is currently being implemented on a second molecular beam apparatus that is overall similar to the one described above. With this trap, we will be able to prepare water adducts before the final cooling step in the cryogenic Paul trap, enabling the preparation of PAH-water cluster ions at lower temperatures. Also in parallel, we are currently developing an ion source based on electron capture rather than ESI to enable the preparation of PAH radical anions (especially pyrene, tetracene, coronene) and their water clusters. Implementation of a second reflectron will allow hole burning spectroscopy in $(MS)^3$ experiments.

In the computational part of the program, we plan to explore how completely classical calculations of the IR spectra, using the time correlation function formalism, compare to those which include quantum nuclear effects, and we will compare how these different methodologies perform for the dynamics. Our early data on naphthalene-water clusters make the case that we may need a more sophisticated treatment of the electron in the anionic cluster as a quantum object, and so we may need to develop a pseudopotential for it. Many believe that quantum nuclear effects are absorbed into the parameterization of the potential, but that has not been easy to show rigorously. These studies aim to find which parts of the potential are hiding the effects of quantum nuclear motion in purely classical dynamical simulations. We will test both water-naphthalene anion clusters and water-pyrene carboxylate clusters and benchmark both potentials and dynamics methods against experimental results.

Fundamental chemical kinetics of siloxane and silicon compounds

DOE BES Grant #18SC503179
Margaret S. Wooldridge (PI)
University of Michigan, Department of Mechanical Engineering, 2350 Hayward St., Ann Arbor, MI, 48109-2125, mswool@umich.edu
Andrew B. Mansfield
Eastern Michigan University Mechanical, Engineering, College of Technology, Ypsilanti, MI, 48197, amansfi3@emich.edu,
Robert S. Tranter
Chemical Sciences and Engineering Division, Argonne National Laboratory, Argonne, IL, 60439, tranter@anl.gov

Program Scope

Siloxanes and other silicon compounds play significant roles as impurities in land-fill gas and as primary feedstock materials for high-value and large-volume products, yet the fundamental reaction chemistry of gas-phase silicon compounds remains largely unexplored. The proposed work integrates two complementary experimental efforts to significantly advance the science of gas-phase silicon reaction chemistry. The primary research focus is on the elementary thermal reactions of siloxanes and their decomposition products with a progression in the chemical structure of the compounds studied to elucidate the effects of bond structure. An additional area of interest is the interaction of gas-phase species with silica nanoparticles that are formed naturally as products of the thermal reactions of siloxanes and during oxidation.

Methodology

The experimental approach leverages the strengths of the University of Michigan (UM) rapid compression facility (RCF) and atmospheric burner, and the diaphragmless shock tube (DFST) and the high-repetition rate shock tube (HRRST) at the Argonne National Laboratory (ANL) for advancing understanding of siloxane chemistry. The combination of experimental approaches allows a broad and complementary range of state conditions to be studied with temperatures in the range of 700-2000 K and pressures of 0.1-50 bar. With the RCF studies, the past year focused on narrowline laser absorption measurements to measure the formation of the OH radical during ignition of H_2 and CO with and without the addition of trace amounts of trimethylsilanol. OH is the radical chain carrier in these ignition systems and the impact of trimethylsilanol on OH provides insight into the reaction pathways active during siloxane oxidation. The RCF experiments were complemented by atmospheric burner studies that were used to develop calibration strategies for gas-chromatography (that will be applied in future RCF experiments) and to characterize the composition of the nanoparticles created during siloxane oxidation (that will also be applied in future RCF experiments).

Together the UM and ANL data sets provide a foundation for developing an accurate understanding of gas-phase silicon chemistry over a wide range of state conditions. These are the first measurements to systematically address such a large spectrum of fundamental gas-phase silicon chemistry. Successful outcomes of this work include multiple categories of pioneering data, and directly address the two **DOE BES Grand Challenges** of *Synthesizing new forms of matter with tailored properties* and *Understanding and controlling material properties emerging from complex atomic and electronic interactions.*

Recent Progress

Autoignition delay times (τ_{ign}) and OH radical mole fraction time histories were measured in mixtures of H_2, CO, O_2, N_2 and Ar with and without the addition of 100 ppm of trimethylsilanol. Molar O_2 to inert gas ratios of 1:3.76 were used with H_2 to CO molar ratios of 3:7 (corresponding to air levels of dilution and a fuel to oxygen equivalence ratios of φ = 0.1). Pressures and temperatures of the experiments ranged from 4.3 to 5.1 atm and from 1000 to 1080 K, respectively. Quantitative OH time histories were obtained using differential narrowline laser absorption of the $R_1(5)$ line of the $A2\Sigma^+ \leftarrow X2\Pi i(0,0)$ band of the OH spectrum (ν_0 = 32606.56 cm^{-1}). Typical results for an autoignition experiment including pressure and OH data are provided in **Fig. 1**. The ignition delay times and maximum OH levels observed near the time of autoignition (i.e., peak OH) are compared in **Fig. 2** for mixtures with and without trimethylsilanol. Details on the experimental methods, including the laser absorption system and the analysis applied to convert fractional absorption to OH mole fraction are provided in Kim et al. (2021).

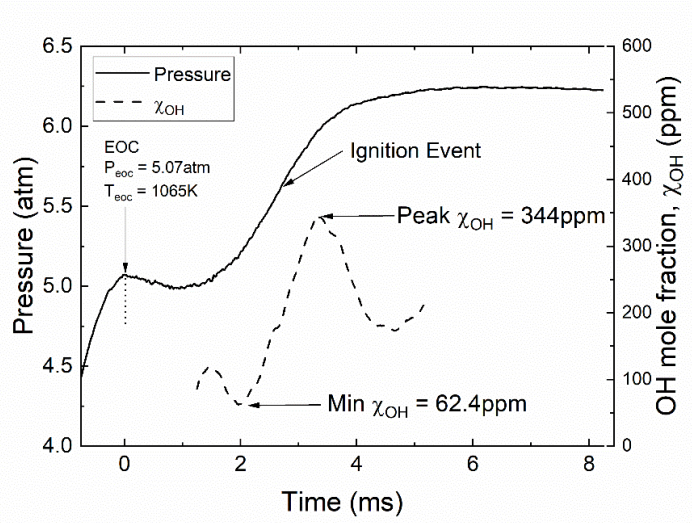

Fig. 1. Typical pressure and OH mole fraction time histories for an auto-ignition experiment in the UM-RCF at P = 5.03 atm, T = 1063 K with a mixture of 1.2% H_2/2.8% CO/20% O_2/8% Ar/68% N_2 by volume.

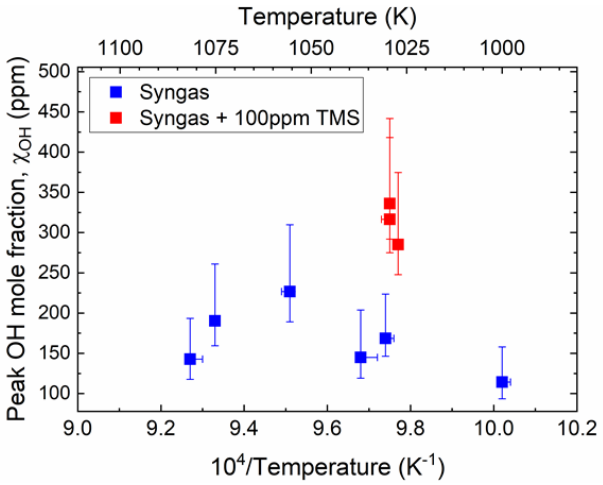

Fig. 2. Maximum OH mole fraction (χ_{OH}) as a function of inverse temperature for mixtures of syngas (H_2 and CO) with and without 100ppm TMS; Conditions of 5 atm with a mixture of 1.2% H_2/2.8% CO/20% O_2/8% Ar/68% N_2 by volume.

Addition of 100 ppm trimethylsilanol caused 14-40% decrease in the autoignition delay time at 5 atm. Furthermore, trimethylsilanol significantly increased the maximum observed OH mole fraction by ~50%. In previous work (Mansfield and Wooldridge, 2015; Schwind and Wooldridge, 2019), it was hypothesized that trimethylsilanol enhances the consumption of HO_2, thus increasing OH production for the mixtures and state conditions studied. The OH results of the current work support the hypothesis that the HO_2 chemistry is altered by the trimethylsilanol. Interestingly, it appears the increase in OH mole fraction of 100-200 ppm is of the same magnitude as the initial concentration of trimethylsilanol in the mixture, suggesting trimethylsilanol decomposition with a corresponding release of an OH radical could be a possible kinetic pathway explaining the observed trends. However, Schwind and Wooldridge (2020) considered the two mechanisms of influence and found OH production through a direct reaction with trimethylsilanol (e.g., trimethylsilanol +M → OH + products, or trimethylsilanol +A → OH + products) are not likely channels. Additionally, ALS experiments conducted last year indicate H2O is not eliminated from trimethylsilanol. Further experiments expanding the OH data at other conditions and for other mixtures are in progress, coupled with detailed modeling efforts to determine the reaction processes affected more precisely.

Current work in the past year has also included gas chromatography (GC) and GC mass spectrometry (MS) measurements using an atmospheric burner. Initial results indicate quantitative calibrations for several siloxanes, including trimethylsilanol, hexamethyldisiloxane (HMDSO) and other higher molecular weight siloxanes can be developed. The burner studies have also been used to develop protocols for sampling condensed-phase nanoparticles produced during oxidation of siloxanes and analyzing the surface properties of the particles. Application of these diagnostics for RCF autoignition studies of siloxanes will directly complement the OH measurements, providing additional insights into siloxane oxidation.

The DFST and HRRST were previously used to acquire time dependent data on the decomposition of hexamethyldisoloxane and trimethylsilanol. The HRRST experiments were conducted at the Advanced Photon Source with tunable VUV photoionization and photoionization spectra were obtained as well as mass spectra aiding the identification of species. The mass spectra present several challenges to interpretation, not least of which is that the primary ion from the parent molecules creates an extremely strong signal limiting resolution of other species. We have observed similar effects from a variety of siloxanes and trimethylsilanol suggesting that most Si species in moderate concentrations will produce intense signals. Surprisingly, the peak heights in the post-shock mass spectra are small apart from features associated with the reagent. This is not due to slow reaction but rather indicative of the rapid growth of Si containing molecules so that only low concentrations of gas-phase species exist at any time. Nonetheless, the ongoing analyses indicate several interesting points. First, while the highly reactive decomposition products 2-silaisobutene and dimethylsilanone that have been postulated,[1] as initial decomposition products and key promotors of molecular growth, are not observed there are indications of their co-products. Secondly, the DFST and HRRST experiments both show methane, acetylene and ethylene as the only hydrocarbon products. The lack of ethane indicates that loss of a methyl radical from hexamethyldisiloxane and trimethylsilanol, is at most a minor path; previously it has been suggested that methyl elimination would be important as the C-Si bond is the weakest one. Rather acetylene and ethylene are indicative of intramolecular eliminations, and these routes are being investigated further. Thirdly, molecular hydrogen is formed early in the hexamethyldisiloxane

[1] Almond, M. J., Becerra, R., Bowes, S.J., Cannady, J.P, Ogeden, J.S., Young, N.A., Walsh, R., A mechanistic study of the low pressure pyrolysis of linear siloxanes, Phys. Chem. Chem. Phys. 11 (2009) 9259–9267.

experiments but only late in the trimethylsilanol experiments. This suggests that trimethylsilanol decomposition results in the formation of siloxanes and that hydrogen is coming from further reaction of the siloxanes. Fourthly, a significant number of peaks with masses up to around 260 were observed in the trimethylsiloxane experiments. In contrast, almost no peaks heavier than the parent were observed in the hexamethyldisiloxane work. Fifthly, a method has been developed for subtracting spectral features due to the parent molecule (or products providing certain conditions are met) that has allowed weak features to be resolved and assigned to species., Lastly, hexamethyldisiloxane was consumed in the experiments, and a significant solid material was produced, suggesting siloxanes may undergo much more rapid molecular growth than silanols.

The analysis of the mass spectral studies is nearly complete and the combined HRRST and DFST studies have allowed a wide range of pressure (180 Torr to 12 bar) to be studied at similar temperature ranges. The use of both electron impact ionization and photoionization has also been helpful for understanding the mass spectra. The results are planned for submission for publication in the coming year.

Future Plans

The ANL DFST and HRRST and the UM RCF data are the first of their kind, and provide sound experimental bases for developing detailed understanding of siloxane reaction chemistry. We are developing methods of using low electron energy ionization and VUV-photoionization at ANL which will complement the studies at the ALS. We are also setting up a new shock tube that will be equipped for optical diagnostics including OH absorption. Studies in this tube will complement the RCF work. Our current work also includes translating the particle sampling methods from the atmospheric burner to RCF studies, and thermal decomposition experiments of siloxanes using the RCF to complement and expand on the DFST and HRRST studies.

We continue to work with Dr. Raghu Sivaramakrishnan (ANL) to develop siloxane thermochemistry to allow further insights into the elementary reactions controlling siloxane combustion. Additionally, Dr. Rachel Schwind, who worked with Tranter at ANL and LBNL on siloxane studies and completed her PhD dissertation at UM on siloxane chemistry is currently a post-doctoral scholar working with Prof. Franklin Goldsmith at Brown University. Prof. Goldsmith and Dr. Schwind are collaborating with us on additional development of the siloxane thermochemistry and interpretation of the experimental data from the prior shock tube studies.

DOE publications supported by this project

Kim, J. H., Mansfield, A. B., Burnett, M. A., Wooldridge, M. S., (2021) "An Experimental Study of OH During Auto-Ignition of Syngas with Trace Trimethylsilanol," 12th National Meeting of the U.S. Sections of the Combustion Institute.

Mansfield, A.B. Wooldridge, M.S. The effect of impurities on syngas combustion, Combust. Flame 162 (2015) 2286-2295.

Schwind, R. A., 2019, *Understanding the Combustion Chemistry of Siloxanes: Reaction Kinetics and Fuel Interactions*, Ph.D. Thesis, University of Michigan, Ann Arbor.

Schwind, R., Wooldridge, M. S., (2019) "Effects of Organic Silicon Compounds on Syngas Auto-ignition Behavior," *Combustion and Flame*, 212 pp. 234-241.

Schwind, R. A., Wooldridge, M. S., Sivaramakrishnan, R., (2019) "Understanding Siloxane Combustion Chemistry: Computational and Experimental Studies of Hexamethyldisiloxane (HMDSO)," 11th National Meeting of the U.S. Sections of the Combustion Institute, Paper No. 1A18, Pasadena, CA.

Spectroscopic and Computational Studies of Spin-Orbit Coupling of Lanthanide Oxides

Dong-Sheng Yang, University of Kentucky (Principal Investigator)
Mark S. Gordon, Iowa State University and Ames Laboratory (Co-Principal Investigator)
dyang0@uky.edu, mark@si.msg.chem.iastate.edu

Program Scope

Spin-orbit (SO) coupling makes it possible for spin forbidden transitions or reactions within non-relativistic quantum theory feasible. Thus, quantification of such interactions has important implications in photophysics and chemical catalysis. This work aims to quantify SO interactions using lanthanide (Ln) oxides as target molecular systems. Through these systems, we examine the impact on the SO coupling by electron configurations and 4f orbital occupancies of Ln elements and sizes of the metal oxides. By examining these factors, we explore how SO coupling is affected by the number of Ln 4f electrons for a given size of molecules and if the Ln 4f orbitals remain atomic in nature in these small clusters. Ln oxides are produced in laser ablation molecular beams, identified with time-of-fight mass spectrometry, and characterized with laser spectroscopy and relativistic quantum chemical computations. Spectroscopic measurements include mass-analyzed threshold ionization (MATI), zero electron kinetic energy, and slow electron velocity-map imaging spectroscopies. Relativistic computations treat scalar relativistic corrections, electron correlations, and SO interactions. The main results are SO terms and energies of the neutral molecules and singly charged cations, ionization energies of the neutral species, metal-metal and metal-oxygen vibrational frequencies of the ions and, in some cases, neutrals as well, and charge effects on the bonding and structures.

Recent Progress

Diatomic Ln oxide molecules. In the first year of the project, we focused on LnO (Ln = La, Ce, Pr, and Lu), where the Ln elements are in a single or predominantly single isotope and have fewer 4f electrons or holes (La, $5d^16s^2$; Ce, $4f^15d^16s^2$; Pr, $4f^36s^2$; and Lu, $4f^{14}5d^26s^1$) than those in the middle of the Ln series. The single or predominantly single isotope simplifies the separation of the ions produced by laser ionization from those generated by delayed-field ionization in the MATI experiments. The Ln elements with fewer 4f electrons or holes were thought to facilitate the theoretical treatment, though Lu was found to be an unexpected exception. The measured adiabatic ionization energies (IEs) are two-fold improvements over previously reported values where the comparison is available. The IE of the neutral molecule and vibrational frequencies in the neutral and ionized states quantify the charge effects on the metal-oxygen bonding, and the vibrational frequencies of these molecules in the gas phase also reveal the effects of low-temperature inert-gas matrices when compared with previous matrix-isolation infrared spectroscopic measurements. The SO terms and energies quantify the extent and strength of electron spin and spatial orbital mixing. In comparing with the measured spectroscopic constants, computations yield reasonable agreements for the ground states of the neutral and ionized molecules.

LaO and CeO. The spectrum of LaO displays a single vibronic band system with a very strong origin band, two vibrational intervals of the ion, and four intervals of the neutral molecule.

The single band system arises from the transition of the ground state ($^2\Sigma^+$) of the neutral molecule with the La($6s^1$)O($2p^6$) major valence configuration to the ground state ($^1\Sigma^+$) of the singly charged ion with the La($6s^0$)O($2p^6$) configuration. The measured adiabatic IE from the $^2\Sigma^+$ neutral state to the $^1\Sigma^+$ ion state is 42300 (5) cm^{-1} or 5.2445(6) eV. This represents a two-fold improvement over the literature value with the smallest reported uncertainty, 4.9(1) eV. From the four vibrational intervals observed for the neutral molecule, a quadratic polynomial fit yields ω_e = 814.23 ± 1.25 cm^{-1} and $x_e\omega_e$= 1.86 ± 0.30 cm^{-1}. The neutral frequency from the MATI spectrum is ~18 cm^{-1} higher than the value (796.7 cm^{-1}) of LaO deposited in a low-temperature Ar matrix. For the LaO^+ ion, the two vibrational intervals of the ion are measured to be 877 and 883 cm^{-1}, with the average of 880 cm^{-1}. The gaseous ion frequency is ~ 42 cm^{-1} higher than that (838.2 cm^{-1}) measured in the Ar matrix. The lower stretching frequencies of LaO and LaO^+ deposited in the low-temperature Ar matrix suggest that Ar is likely bound with the metal oxide via the metal atom or ion and that such bonding reduces the strength of the La-O bond and the reduction is more pronounced for the ion. The spectral intensity is not governed by the Franck-Condon (FC) principle. For example, the intensity of the first-quantum vibronic band relative to that of the origin band is measured to be ~ 7%, while the corresponding FC intensity is estimated to be ~ 37%. The calculated coupled cluster CCSD(T) vibrational frequencies of the neutral (808 cm^{-1}) and ion (871 cm^{-1}) and IE of the neutral molecule (5.32 eV) are satisfactory.

The MATI spectrum of CeO is much more complex than that of LaO. It consists of 11 vibronic band systems from transitions of low-energy SO levels of the neutral molecule to the lowest SO level of the ion and two bands from transitions of the two lowest SO levels of the neutral molecule to the first excited SO level of the ion. The 11 SO terms of the neutral molecules are identified in the order of 1Δ (0) < 1Φ (88 cm^{-1}) < 1Π (819 cm^{-1}) < 2Δ (912 cm^{-1}) < $2^3\Pi$ (1675 cm^{-1}) < 3Π (1873 cm^{-1}) < $1\Sigma^+$ (1920 cm^{-1}) < $2^3\Phi$ (2048 cm^{-1}) < 3Φ (2144 cm^{-1}) < 4Φ (2626 cm^{-1}) <3Δ (2771 cm^{-1}), and the two lowest SO term of the ion are $^2\Sigma_{5/2}$ (43015 cm^{-1}) and $^2\Sigma_{3/2}$ (43680 cm^{-1}). The electronic energies (T_0) of 1Π and 2Δ overlap with the first vibrational quanta of 1Δ and 1Φ, respectively. The SO terms are predicted by the SO multiconfiguration quasi-degenerate perturbation theory (SO-MCQDPT), where the terms without electron multiplicities are mixtures of Russell-Saunders (RS) singlet and triplet states. The main valence electron configurations are Ce($4f^16s^1$)O($2p^6$) for the neutral molecule and Ce($4f^1$)O($2p^6$) for the ion. The SO-MCQDPT predicted SO term energies are in very good agreement with the measured values. The adiabatic IE value of $^2\Sigma_{5/2} \leftarrow 1\Delta$ from the measurements is 43015 (5) cm^{-1} or 5.3332 (6) eV, which again is a two-fold improvement over the literature value with the smallest reported uncertainty. The IE of CeO is slightly higher than that of LaO, even though the IE of Ce (5.5387 eV) is a little lower than that of La (5.5769 eV). This observation suggests that the bond-energy difference between the ion and neutral molecule is slightly smaller for the Ce oxide (0.2055 eV) than for the La oxide (0.3323 eV). For the 1Δ and 1Φ terms of the neutral molecule, the harmonic frequency and anharmonicity are fitted as ω_e= 819.72 ± 0.27 cm^{-1} and $x_e\omega_e$ = 0.36 ± 0.06 cm^{-1} for the 1Δ level and ω_e= 823.81 ± 0.80 cm^{-1} and $x_e\omega_e$ = 0.93 ± 0.19 cm^{-1} for the 1Φ level. The vibrational intervals of the $2^3\Pi$, 3Π, $1\Sigma^+$, $2^3\Phi$, and 3Φ terms are averaged as 817 ± 2 cm^{-1}, while those of 4Φ and 3Δ are measured to be 832 and 826 cm^{-1}, respectively. For the ion, the vibrational frequency is 887 cm^{-1} for the $^2E_{5/2}$ level. Like LaO, the vibrational frequencies of LuO and LuO^+ in the gas phase are higher than those (808.4 and 849.5 cm^{-1}) of the neutral and ionized molecules deposited in an Ar matrix.

PrO and LuO. The MATI spectrum of PrO consists of the origin band at 43575 (5) cm^{-1} or 5.4026 (6) eV, two vibronic band systems separated by 215 cm^{-1} and an additional band at 2071 cm^{-1}. Each band system consists of two vibrational intervals of ~ 840 cm^{-1} and at least one satellite band at 75 cm^{-1} from each member of the band systems. The 840 cm^{-1} interval is the vibrational frequency of the neutral states, while the 75 cm^{-1} satellite bands are sequence bands, which yield the vibrational frequency of 915 cm^{-1} [(840 + 75) cm^{-1}] for the ion. The two vibronic band systems arise from the ionization of two SO terms of the $Pr(4f^26s^1)O(2p^6)$ configuration of the neutral molecule to the lowest-energy SO term of the $Pr(4f^2)O(2p^6)$ ion. The SO-MCQDPT calculations predict the separation of the two neutral SO terms with $\Omega = 4.5$ and $\Omega = 3.5$ to be 210 cm^{-1} and the adiabatic IE to be 43666 cm^{-1}. For the neutral molecule, the ground SO term is predominantly a RS quartet state, while the excited SO term is a mixture of RS quartet and doublet states. The 2071 cm^{-1} band does not belong to either of the progressions and is between the energy of Ω =1.5 (2005 cm^{-1}) and $\Omega = 5.5$ (2138 cm^{-1}) predicted by the SO-MCQDPT calculations. For the ion, the ground SO term is mainly a RS triplet state. The calculated vibrational frequencies at the level of density functional theory (B3LYP) are 828 cm^{-1} for the neutral molecule and 913 cm^{-1} for the ion.

The spectrum of LuO displays only a single vibronic system as in the case of LaO. The IE of LuO is measured to be 44696 (5) cm^{-1} or 5.5416 (6) eV, and the vibrational frequencies are 748 and 772 cm^{-1} for the neutral molecules and ion, respectively. However, the assignment of the observed spectrum turns out to be surprisingly challenging. In an attempt to rationalize the spectrum, we have performed extensive MCQDPT calculations, and preliminary results are summarized in Table 1. Good agreement is observed between the computed and previous experimental results for the ground state, while significant deviations occur for the excited states. In comparison with the current measurements, the observed transition could be due to the $X^1\Sigma^+ \leftarrow A^2\Sigma^+$ transition as the calculated transition energy (41558 cm^{-1}) is closer to the measured IE (44696 cm^{-1}) than that of any other predicted transitions so far. However, the computed anharmonic frequency for the $X^1\Sigma^+$ ion state (928 cm^{-1}) is unusually high compared with the experiment (772 cm^{-1}) by considering computational accuracies for the ground states of Ln-containing molecules.

Table 1. Equilibrium bond lengths (R_e, Å), harmonic (ω_h, cm^{-1}) and anharmonic (ω_a, cm^{-1}) vibrational frequencies, rotational constants (B_e, cm^{-1}), and 0-0 transitions from the ground state (T_e, cm^{-1}) of LuO and LuO^+.[a]

	Neutral			Cation			
	$X^2\Sigma^+$	$A^2\Sigma^+$	$B^2\Pi$	$X^1\Sigma^+$	$A^3\Pi$	$B^1\Pi$	$C^3\Sigma^+$
R_e	1.784	1.912	2.053	1.721	1.968	1.970	1.862
	(1.7904)	(1.8283)	(1.805)				
ω_h	865	674		939	661		746
ω_a	859	664	546	928	648	652	716
	(842.5)	(770)	(793)				
B_e	0.36139	0.31427	0.27279	0.38817	0.29687	0.29608	0.33144
	(0.35806)	(0.34411)	(0.3528)				
T_e	0	17301	34131	58859	70772	71197	73118
		(24403)	(19370)				

[a] Values in parentheses are taken from K.P. Huber and G. Herzberg, *Molecular Spectra and Molecular Structure. Iv. Constants of Diatomic Molecules*. (Van Nostrand-Reinhold: New York, 1979).

Thus, additional calculations are being performed that will consider the $^2\Delta$ state of the neutral molecule that is formed by singly occupying the degenerate Ln 5dδ orbitals as well as quartet states that are in the same energy range as the excited doublet states. Calculations of the quartet states and the $^2\Delta$ state will require the inclusion of the Ln 5dδ and/or 6pπ orbitals in the active space.

Software development. To meet the need of this project, we have implemented several new features in the GAMESS code originally developed in our group. These new developments include, but are not limited to, (1) support for relativistic integrals involving h and i functions for spin-orbit calculations. This is in addition to the support for scalar relativistic methods that was previously implemented. (2) a special case for diatomic molecules in the numerical Hessian code that reduces the number of energy evaluations from 108 to 4. This approach rotates the coordinates to realign the molecule along the principal axes after each displacement, thus preserving symmetry. This has the two-fold advantage of reducing the number of energy evaluations needed based on symmetry constraints while simultaneously allowing for the use of symmetry to aid in the optimization of excited state. (3) a special case for diatomic molecules that allows for the use of symmetry when computing excited states with the vibrational self-consistent field method. (4) parallelization of the computation of the transition density matrix in the spin-orbit code. (5) expanding support for the density-based bonding analysis to allow for the use of the graphical unitary group approach-based multireference methods. Previously, this functionality was limited to use of the occupation restricted multiple active space method. (6) support for effective core potentials (ECPs) that use a h-ul potential with a coefficient of zero. This allows for the use of the Stuttgart-Dresden ECPs and by extension the correlation consistent pseudopotential-based basis sets. The h-ul potential provides an upper limit (ul) for the angular momentum as well as a reference point for difference potentials that are computed based on the s, p, d, f, and g potentials provided in the input file. (7) support for the generation of valence virtual orbitals when using model core potentials.

Future Plans

We will investigate Ln oxide clusters containing two or three Ln atoms and various numbers of oxygen atoms. Experimental measurements will be focused on the search of vibronic spectra of the clusters of interest, and theoretical computations will be performed in coordination with the experiments. It is expected that the theoretical treatment of Ln cluster oxides will be more challenging due to the larger size of the systems and the possible coupling of the 4f electrons on separated Ln atoms. We thus will implement new functionalities in the GAMESS code to accomplish the task as specific needs become apparent in the course of this work.

Publications supported by the BES-GPCP program (8/2020-present)

W. J. Cao, Y. C. Zhang, L. Wu, and D. S. Yang, "Threshold Ionization Spectroscopy and Theoretical Calculations of LnO (Ln = La and Ce)," J. Phys. Chem. A **125**, 1941-1948 (2021). DOI: 10.1021/acs.jpca.1c00533.